VTT

beyond
the obvious

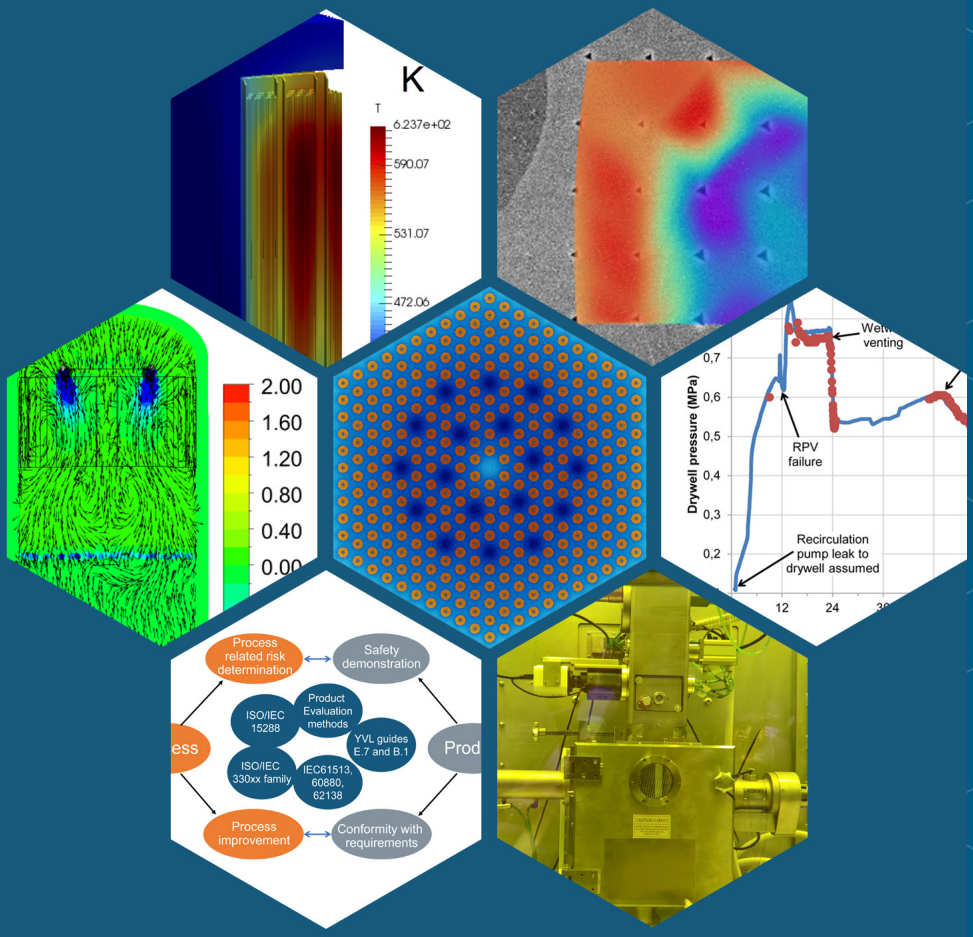

SAFIR2018 - The Finnish Research Programme on Nuclear Power Plant Safety 2015-2018

Final Report

Jari Hämäläinen | Vesa Suolanen (eds.)

VTT TECHNOLOGY 349

VTT TECHNOLOGY 349

SAFIR2018 - The Finnish Research Programme on Nuclear Power Plant Safety 2015-2018

Final Report

Jari Hämäläinen & Vesa Suolanen (eds.)

VTT

ISBN 978-951-38-8682-0

VTT Technology 349

ISSN-L 2242-1211
ISSN 2242-122X (Online)
DOI: 10.32040/2242-122X.2019.T349

JULKAISIJA – PUBLISHER

VTT
PL 1000
02044 VTT
Puh. 020 722 111
https://www.vtt.fi

VTT
P.O. Box 1000
FI-02044 VTT, Finland
Tel. +358 20 722 111
https://www.vttresearch.com

Preface

The Finnish Research Programme on Nuclear Power Plant Safety 2015–2018, SAFIR2018, continues a series of Finnish national research programmes in nuclear energy that started in 1989. The programmes were initially carried out separately in the fields of operational aspects of safety (YKÄ 1990–1994, RETU 1995–1998) and structural safety (RATU 1990–1994, RATU2 1995–1998, OHA 1995–1998), and then in combined programmes (FINNUS 1999–2002, SAFIR2003–2006, SAFIR2010 2007-2010, SAFIR2014 2011-2014). Simultaneously research has been carried out in the national nuclear waste management programmes (KYT2018 in parallel with SAFIR2018).

SAFIR2018 consisted of four main research areas: (1) Plant safety and systems engineering; (2) Reactor safety; (3) Structural safety and materials; and (4) Research infrastructure. Research was carried out annually in around 30 projects that were guided by six reference groups. The research results of the projects have been published in scientific journals, conference papers and research reports.

The programme management structure consisted of the Management Board, four steering groups managing the research areas, six reference groups, and programme administration. SAFIR2018 Management Board had representatives of the Radiation and Nuclear Safety Authority (STUK), the Ministry of Economic Affairs and Employment (MEAE), Fennovoima Oy, Fortum, Teollisuuden Voima Oyj (TVO), VTT Technical Research Centre of Finland Ltd (VTT), Aalto University (Aalto), Lappeenranta University of Technology (LUT), the Finnish Funding Agency for Innovation (Tekes), and the Swedish Radiation Safety Authority (SSM).

The research in the programme was carried out by VTT, LUT, Aalto, University of Oulu, Finnish Meteorological Institute (FMI), Finnish Institute of Occupational Health (FIOH), University of Helsinki (Institute of Seismology, ISUH), University of Jyväskylä, RISE Research Institute of Sweden, Risk Pilot AB, Finnish Software Measurement Association FISMA and IntoWorks. A few subcontractors also contributed to the work in the projects.

This report has been prepared by the programme management in cooperation with the project leaders and project staff. More information about SAFIR2018 can be found on the programme website http://safir2018.vtt.fi/. Finnish national research on nuclear power plant safety continues in SAFIR2022 programme for the years 2019–2022, see http://safir2022.vtt.fi/.

Contents

1. Introduction

1.1 SAFIR2018 and previous Finnish nuclear safety research

The Finnish Nuclear Power Plant Safety Research Programme 2015–2018, SAFIR2018, was a 4-year national technical and scientific research programme on the safety of nuclear power plants. The programme was funded by the Finnish State Nuclear Waste Management Fund (VYR), as well as other key organisations operating in the area of nuclear energy. The programme provided conditions for maintaining expertise needed for ensuring the continuance of safe use of nuclear power, for developing new expertise and for participation in international co-operation. Major part of Finnish public research on nuclear power plant safety during the years 2015–2018 was carried out in the SAFIR2018 programme.

In accordance with the Finnish Nuclear Energy Act, the objective of SAFIR2018 was to ensure that should new matters related to the safe use of nuclear power plants arise, the authorities possess sufficient technical expertise and other competence required for rapidly determining the significance of the matters.

The SAFIR2018 programme's planning group, nominated by the MEAE in March 2014, defined the following mission for national nuclear safety programmes:

> *National nuclear safety research develops and creates expertise, experimental facilities as well as computational and assessment methods for solving future safety issues.*

The vision of SAFIR2018 was defined as follows:

> *The SAFIR2018 research community is a vigilant, internationally recognised and strongly networked competence pool that carries out research on topics relevant to the safety of Finnish nuclear power plants on a high scientific level and with modern methods and experimental facilities.*

The Framework Plan [1] describes the research themes of SAFIR2018 that essentially also covered the themes of the preceding SAFIR2014 programme [2].

The total volume of the research projects in the SAFIR2018 programme in 2015-2018 was 29,6 M€ and 209 person years. The main funding organisations were the

Finnish State Waste Management Fund (VYR) with 17,7 M€ and VTT Technical Research Centre of Finland Ltd (VTT) with 6,4 M€. Research projects of SAFIR2018 were chosen on the basis of annual call for proposals and in 2018, research was carried out in 32 projects. The results are utilised by the Radiation and Nuclear Safety Authority (STUK), Teollisuuden Voima Oyj (TVO), Fortum and Fennovoima Oy, in addition to the research organisations carrying out the projects. However, international co-operation is involved in most of the projects and thus the results are more widely utilised.

In addition to the funding of the research projects, SAFIR2018 programme has involved special funding for the VTT Centre for Nuclear Safety (CNS). In 2015-2018, the research equipment investments were funded by 8,2 M€ (RADINFRA project) and laboratory facility by 4,6 M€ (RADCNS project). KYT2018 programme also funded the two projects with 4,0 M€. Thus the total volume of the SAFIR2018 programme in 2015-2018, including the research projects and infrastructure development, was 46,4 M€.

VYR funding is collected from the Finnish utilities Fennovoima, Fortum and TVO based on their MWth shares in Finnish nuclear power plants (units in operation, under construction, and in planning phase according to the decisions-in-principle). VYR funding was smaller in 2016 as compared with 2015 due to the suspension of Olkiluoto 4 (OL4) project in 2015 before entering the construction license phase, which made its funding proportion not to be available since 1.1.2016. In addition to VYR and VTT, other key organisations operating in the area of nuclear safety also funded the programme.

International co-operation was an essential part of the SAFIR2018 programme. Participation in several OECD Nuclear Energy Agency (NEA) projects was one of the key international activities. Further, international contacts included co-operation with several Swedish organisations as well as within the Nordic Nuclear Safety Research (NKS) and the Nordic Thermal-Hydraulic Network (Northnet), and participation in other international experimental research programmes. A Memorandum of Understanding (MoU) on scientific and technical co-operation in the area of nuclear safety research was signed between NUGENIA (Nuclear Generation II & III Association) and SAFIR2018 programmes and co-operation and research results exchange took place particularly in material research. Several Euratom Programme projects in Horizon 2020 also had connections to research carried out in SAFIR2018.

National research programmes on nuclear safety have had a significant role in the maintenance of expertise and the training of new experts. Since 1990 the programmes (YKÄ & RATU 1990–1994, RETU&RATU2 1995–1998, OHA 1995-1998, FINNUS 1999–2002, SAFIR 2003–2006, SAFIR2010 2007–2010, SAFIR2014 2011-2014 and SAFIR2018 2015-2018) have had a total volume of 172 M€ and 1 374 person years (Figure1, Table 1).

The programmes have produced 5 639 publications and reports in various categories as well as 63 Doctor, 20 Licentiate and 145 Master level academic degrees. Nuclear safety research continues in the SAFIR2022 programme during the years 2019–2022.

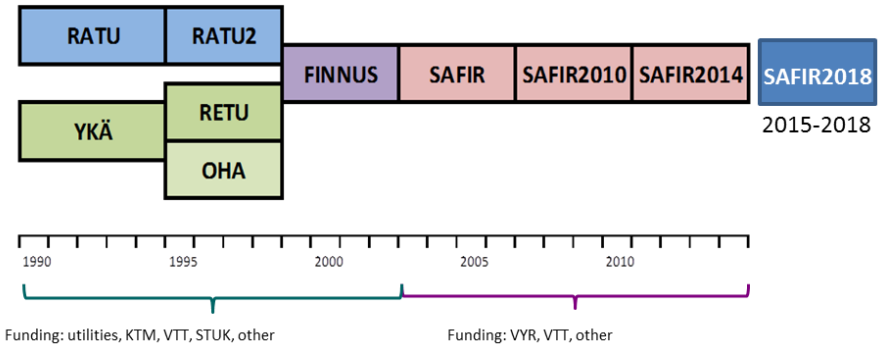

Figure 1. Finnish research programmes on nuclear power plant (NPP) safety.

Table 1. Finnish national research programmes on NPP safety in 1990-2018.

Programme	Volume, M€	Volume, person years	Total number of publications	Academic degrees		
				Dr.	Lic.	M.Sc.
YKÄ 1990-1994	15,4	168	318	6	5	10
RATU 1990-1994	8,2	76	322	1	3	3
RETU 1995-1998	9,8	107	405	3	2	2
RATU2 1995-1998	7,5	60	280	3	4	11
FINNUS 1999-2002	14,4	130	564	6	2	18
SAFIR 2003-2006	19,7	148	545	6	1	17
SAFIR2010 2007-2010	27,5	197	866	8	1	31
SAFIR2014 2011-2014	40,1	279	1244	12	2	27
SAFIR2018 2015-2018	29,6	209	1095	18	0	26
Total	**172,2**	**1374**	**5639**	**63**	**20**	**145**

1.2 Research areas and projects

Research in SAFIR2018 has been carried out according to the research needs described in the Framework Plan [1], the Annual Plans [5] and decisions of the Management Board. Guidance on programme practices was given in the Operational management handbook [3]. The research in many topics was based on results of SAFIR2014 programme [2].

SAFIR2018 has four main research areas: plant safety and systems engineering, reactor safety, structural safety and materials, and research infrastructure.

The plant safety and systems engineering research area considered topics of operational resilience in nuclear domain, management principles and safety culture, PRA methods including Defence-in-Depth (DiD), integrated safety assessment of nuclear power automation (I&C), and electrical systems. The goal of the work was to increase the understanding and management of issues significant to overall safety throughout the life cycle of nuclear power plants.

In *the reactor safety research area*, experimental and computational methods were developed for ensuring that the plant and its systems satisfy the safety requirements. The research focused on thermal-hydraulic problems, development and validation of computational fluid dynamics (CFD) methods, development of Monte Carlo based methods for reactor core safety analyses, fuel behaviour studies, reactor dynamics, severe accidents and fission product transport, and uncertainty and sensitivity analyses for reactor safety.

The aim of the research in *the structural safety and materials area* was to increase knowledge supporting the long-term and reliable use of nuclear power plants, particularly with respect to the integrity of barriers and material issues that affect safety. The aging phenomena of structures and equipment, experimental and numerical methods for external event assessment, and fire risk evaluation were important research topics.

In addition, *infrastructure related research* was funded in SAFIR2018 in order to ensure modern research facilities and equipment. Funding was allocated to the Centre for Nuclear Safety (CNS) at VTT, to national thermal-hydraulic experimental facilities at LUT, and to the participation in the Jules Horowitz Reactor (JHR) development. An activity was also started in co-operation with Swedish partners for the evaluation of embrittlement using material removed from a decommissioned reactor pressure vessel and CNS facilities.

The scientific results of the programme have been reported in the Annual Reports [4], in the Interim Seminar report [9] and in the publications.

Table 2 shows the actualised costs and volumes of SAFIR2018 research projects in 2015-2018.

In addition to the research projects, the Management Board could annually initiate small projects with the order procedure. The following small projects were carried out during the programme:

(1) Systems thinking for management and organizations in nuclear energy production – a feasibility study (Tampere University of Technology and VTT)
(2) Review on code validation matrices for identification of reproducible test cases (LUT)
(3) Overall safety conceptual framework (LUT)
(4) Research of electric systems of Finnish nuclear power plants (VTT, Aalto)
(5) Overall safety and organisations: institutional strength-in-depth and national actors (VTT, LUT)
(6) Seismic monitoring and corresponding safe shutdown criteria of NPPs in low/moderate seismicity areas (VTT)

(7) Survey of 3D printing in nuclear industry (VTT)
(8) Survey of competence in the nuclear energy sector 2017-2018 (VTT) [10].

The costs of the ordered small projects (1)-(7) were included in the SAFIR2018 administration project (ADMIRE). The survey (8) was also realised in the ADMIRE project.

Table 2. SAFIR2018 research projects in 2015-2018.

Project	**Acronym**	**Organisations**	**Costs (k€)**	**Person years**
SG1. Plant safety and systems engineering				
Crafting operational resilience in nuclear domain	CORE	VTT, FIOH	1118	9,1
Extreme weather and nuclear power plants	EXWE	FMI	1115	12,5
Management principles and safety culture in complex projects	MAPS	VTT, Aalto, Univ Oulu, Univ Jyväskylä	849	6,2
Probabilistic risk assessment method development and applications	PRAMEA	VTT, Aalto, Risk Pilot	1420	10,9
Integrated safety assessment and justification of nuclear power plant automation	SAUNA	VTT, Aalto, FISMA, Risk Pilot, IntoWorks	1733	13,7
Safety of new reactor technologies	GENXFIN[2]	VTT	302	1,8
Electric systems and safety in Finnish NPP	ESSI[3]	VTT, Aalto	236	2,3
Practical applications and further development of overall safety concept	ORSAPP[4]	LUT, VTT	69	0,5
SG2. Reactor safety				
Comprehensive analysis of severe accidents	CASA	VTT	960	6,4
Chemistry and transport of fission products	CATFIS	VTT	708	4,6
Comprehensive and systematic validation of	COVA	VTT	1069	7,7

independent safety analysis tools				
Couplings and instabilities in reactor systems	INSTAB	LUT	688	5,9
Integral and separate effects tests on thermal-hydraulic problems in reactors	INTEGRA	LUT	1367	11,6
Nuclear criticality and safety analyses preparedness at VTT	KATVE	VTT	797	6,5
Development of a Monte Carlo based calculation sequence for reactor core safety analyses	MONSOON	VTT	565	4,3
Neutronics, burnup and nuclear fuel	NEPAL15[1]	Aalto	96	1,0
Development and validation of CFD methods for nuclear reactor safety assessment	NURESA	VTT, LUT, Aalto	929	7,2
Physics and chemistry of nuclear fuel	PANCHO	VTT	1113	8,8
Safety analyses for dynamical events	SADE	VTT	463	3,5
Uncertainty and sensitivity analyses for reactor safety	USVA	VTT, Aalto	572	5,1
SG3. Structural safety and materials				
Experimental studies on projectile impacts against concrete structures	ESPIACS[1]	VTT	44	0,3
Experimental and numerical methods for external event assessment improving safety	ERNEST[2]	VTT	320	1,6
Fire risk evaluation and Defence-in-Depth	FIRED	VTT, Aalto	820	6,3
Analysis of fatigue and other cumulative ageing to extend lifetime	FOUND	VTT, Aalto	1592	10,5

Long term operation aspects of structural integrity	LOST	VTT	895	5,3
Mitigation of cracking through advanced water chemistry	MOCCA	VTT	538	2,9
Numerical methods for external event assessment improving safety	NEST[2]	VTT	334	2,0
Thermal ageing and EAC research for plant life management	THELMA	VTT, Aalto	1123	7,0
Non-destructive examination of NPP primary circuit components and concrete infrastructure	WANDA	VTT, Aalto	774	5,2
Condition monitoring, thermal and radiation degradation of polymers inside NPP containments	COMRADE[2]	VTT, RISE	574	2,3
Evolving the Fennoscandian GMPEs	EVOGY[4]	VTT, ISUH	161	1,5
SG4. Research infrastructure				
Development of thermal-hydraulic infrastructure at LUT	INFRAL	LUT	1215	8,8
JHR collaboration & Melodie follow-up	JHR	VTT	128	0,7
Radiological laboratory commissioning	RADLAB[5]	VTT	3193	18,9
Barsebäck RPV material used for true evaluation of embrittlement	BRUTE[4]	VTT	286	1,6
Programme administration				
SAFIR2018 administration project	ADMIRE	VTT	1386	4,3
Total			**29550**	**208,7**

The costs of ADMIRE are for the period 1.1.15-31.3.19. The costs include the costs of the small projects and value-added tax.

[1]) *Project carried out only in 2015*
[2]) *Project started on 1.1.2016 (ESPIACS and NEST continued as ERNEST)*
[3]) *Project started on 1.1.2017*

[4]) *Project started on 1.1. 2018*
[5]) *The statistics of REHOT[1] carried out in 2015 is included in RADLAB.*

1.3 Financial and statistical information

The total volume of the research projects in the SAFIR2018 programme in 2015-2018 was 29,6 M€ and 209 person years. The funding partners were VYR with 17,707 M€, VTT with 6,418 M€, Lappeenranta University of Technology with 0,819 M€, Aalto University with 0,704 M€, NKS with 0,601 M€, SSM with 0,493 M€, Halden Reactor Project in-kind with 0,459 M€, TVO with 0,352 M€, Fennovoima with 0,295 M€, Fortum with 0,128 M€, and several other partners with 1,575 M€. The funding proportions of the major funding partners are illustrated in Figure 1. One should note that the reported VYR funding is collected from TVO, Fortum and Fennovoima.

The costs structure of the projects is shown in Figure 2. The personnel costs make up the major share.

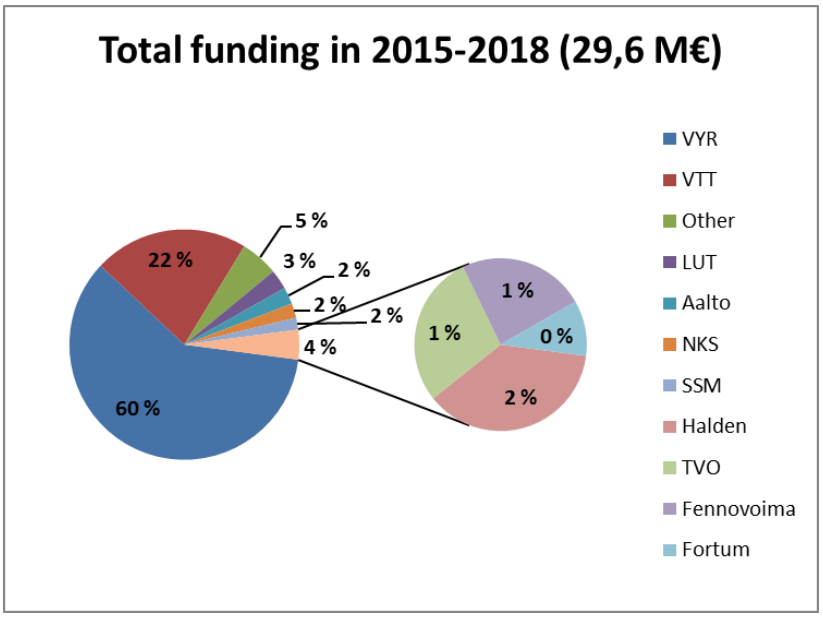

Figure 1. Funding of the SAFIR2018 programme in 2015-2018.

Figures 3-5 show the funding and volumes of SAFIR2018 research areas in 2015-2018. In the Structural safety and materials (SG3) and Research infrastructure (RG6) areas the shares of person-years were lower than the shares of total funding

(Figures 3-4). In SG1 and SG2 areas the shares of the person-years were bigger than the shares of the total funding, respectively.

The effect of the decrease in VYR funding in the beginning of 2016 can clearly been seen in Figure 5.

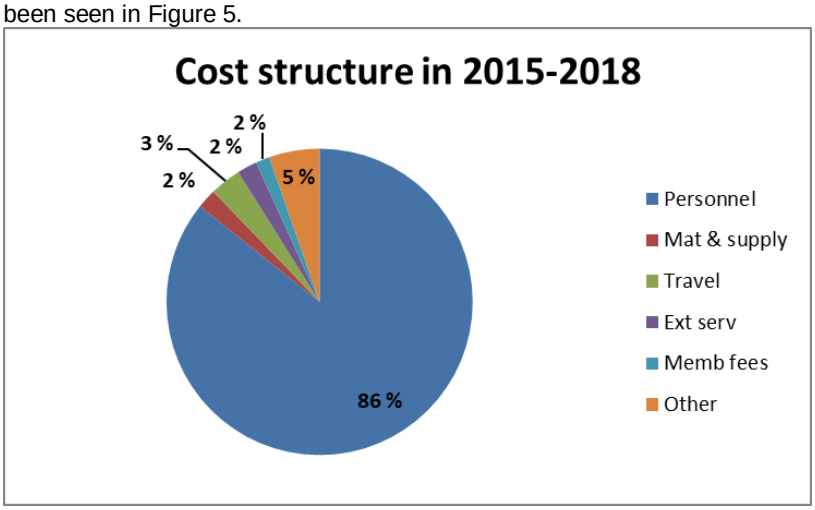

Figure 2. Cost structure of SAFIR2018 in 2015-2018.

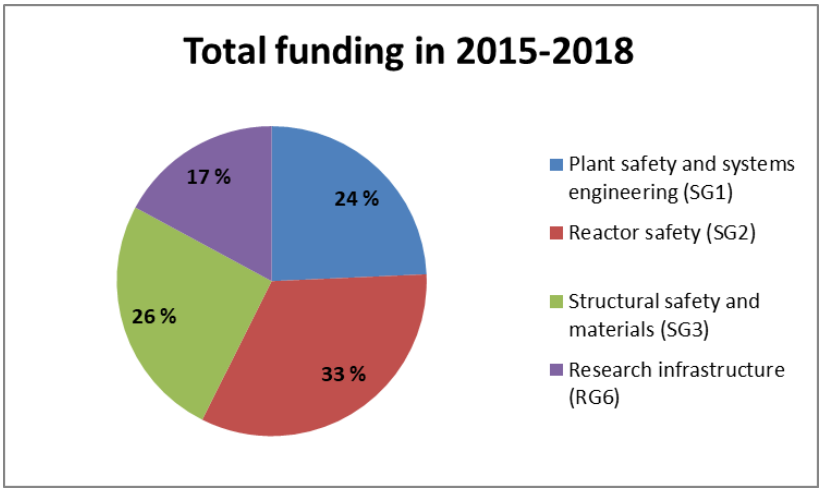

Figure 3. Funding by research area in 2015-2018.

The projects of the programme have produced 1 095 publications in 2015-2018 (Table 3). Major part of the publications consisted of public research reports and

conference articles. A total of 166 scientific journal articles were made. The average number of publications was 5,3 per person year, and the average number of scientific journal articles was 0,81 per person year (administration project excluded). The projects had different scopes and there were also clear differences in the number of publications between the projects even when the project volumes are taken into account. Some projects also mainly published the results as research reports that allow more extensive reporting and are useful for the end-users of the results in certain research areas.

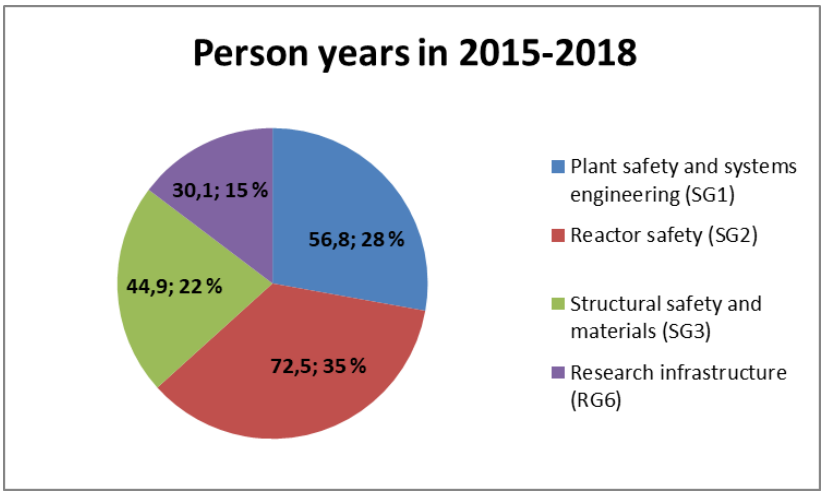

Figure 4. Person years by research area in 2015-2018.

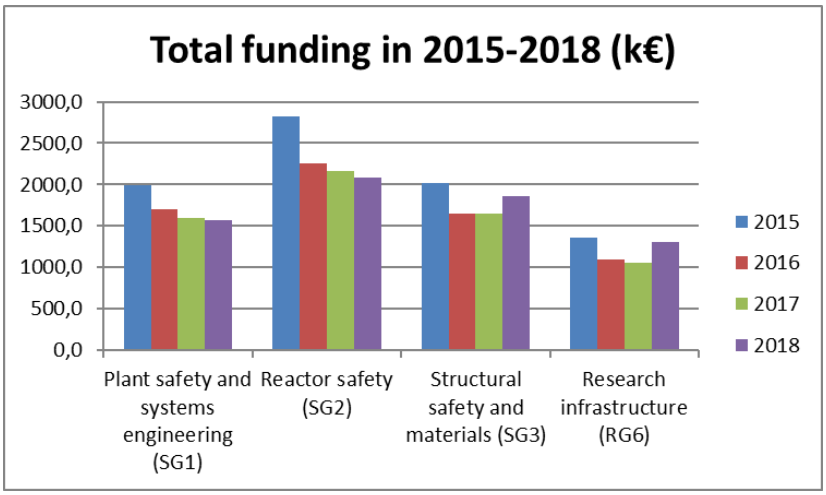

Figure 5. Total funding in the SAFIR2018 research areas in 2015-2018.

Table 3. Publications in the SAFIR2018 projects in 2015-2018.

Total Projects	Volume (person years)	Publications				
		Research reports	Scientific journal articles	Conference articles	Others	**Total** number of publications
Total	208,7	**453**	**166**	**236**	**240**	**1095**
CORE	9,1	11	4	30	18	**63**
EXWE	12,5	22	26	11	23	**82**
MAPS	6,2	5	9	15	11	**40**
PRAMEA	10,9	39	11	12	14	**76**
SAUNA	13,7	19	4	38	20	**81**
GENXFIN	1,8	7	1	1	10	**19**
ESSI	2,3	7	1	6	1	**15**
ORSAPP	0,5	1	0	0	0	**1**
CASA	6,4	21	3	5	17	**46**
CATFIS	4,6	12	11	9	10	**42**
COVA	7,7	24	1	0	1	**26**
INSTAB	5,9	15	6	2	2	**25**
INTEGRA	11,6	11	4	1	2	**18**
KATVE	6,5	18	6	8	5	**37**
MONSOON	4,3	8	10	10	5	**33**

NEPAL15	1,0	0	6	0	2	**8**
NURESA	7,2	27	4	2	3	**36**
PANCHO	8,8	21	6	6	16	**49**
SADE	3,5	7	8	5	6	**26**
USVA	5,1	7	4	5	6	**22**
ESPIACS	0,3	1	1	1	0	**3**
ERNEST	1,6	5	3	5	0	**13**
FIRED	6,3	9	8	3	4	**24**
FOUND	10,5	40	2	9	9	**60**
LOST	5,3	17	7	4	5	**33**
MOCCA	2,9	9	6	2	2	**19**
NEST	2,0	2	1	4	2	**9**
THELMA	7,0	15	6	13	18	**52**
WANDA	5,2	13	2	16	5	**36**
COMRADE	2,3	12	1	4	3	**20**
EVOGY	1,5	1	1	1	0	**3**
INFRAL	8,8	7	3	6	2	**18**
JHR	0,7	2	0	0	6	**8**
RADLAB*	18,9	24	0	2	10	**36**
BRUTE	1,6	6	0	0	0	**6**
ADMIRE	4,3	8	0	0	2	**10**

*) REHOT in 2015 included

Altogether 44 higher academic degrees were obtained in the research projects in 2015-2018: 18 Doctoral degrees and 26 Master's degrees (Table 4).

Table 4. Acedemic degrees obtained in the projects in 2015-2018.

Project	**Doctor**	**Master**
EXWE	4	1
MAPS		1
PRAMEA	1	
SAUNA	1	2
ESSI		2
CASA	1	1
CATFIS	2	
INSTAB		2*
INTEGRA		1
KATVE		2
MONSOON	2	1**

NURESA		1
PANCHO	4	
USVA		1
FIRED	1	
FOUND		2
LOST		1
THELMA	2	
WANDA		2
COMRADE		2
EVOGY		1
INFRAL		3
Total	**18**	**26**

Licentiate degrees were not obtained in SAFIR2018.
*) one Master's thesis jointly in INSTAB and INFRAL
**) one Master's thesis jointly in MONSOON and SADE

1.4 Administration, seminars and international evaluation

SAFIR2018 Management Board was nominated in September 2014. It consisted of representatives of STUK, Ministry of Economic Affairs and Employment (MEAE), Fennovoima, Fortum, TVO, VTT, Aalto University (Aalto), Lappeenranta University of Technology (LUT), and the Finnish Funding Agency for Innovation (Tekes). In 2015 the management board was completed with a representative of Swedish Radiation Safety Authority (SSM).

The four research areas were managed by the steering groups: SG1 Plant safety and systems engineering, SG2 Reactor safety, SG3 Structural safety and materials, and RG6 Research infrastructure (see http://safir2018.vtt.fi/ and [3]).

Research was carried out under the guidance of six reference groups:

RG1. Automation, organisation and human factors
RG2. Severe accidents and risk analysis
RG3. Reactor and fuel
RG4. Thermal hydraulics
RG5. Structural integrity
RG6. Research infrastructure.

The programme management bodies, the Management Board, four steering groups and six reference groups, met on regular basis three times annually. Several projects also has additional project specific meetings. The programme was operationally managed by the Programme Director, the Project Co-ordinator and the project managers of the individual research projects.

The progress of projects was communicated three times a year via project specific reports, the annual plans and reports of the whole programme and the SAFIR2018 website. Additional information was given in seminars organised by several research projects. The detailed scientific and technical results were published as articles in scientific journals, conference papers, and separate reports.

A major event was the SAFIR2018 Interim Seminar in March 2017 (see the interim report [9]) with some 200 participants. An international evaluation of the programme was carried out and in January 2017 the evaluation group followed project presentations, interviewed Management Board, steering and reference group members, gave a summary in the exit meeting and then finalised the evaluation report [6]. The evaluation also gave recommendations for the planning workshop of SAFIR2022 held in April 2018.

In addition to conducting the actual research according to the yearly plans, SAFIR2018 has been an efficient forum for information exchange with all organisations operating in the nuclear energy sector in Finland. It has also been an open discussion forum for participation in international projects and planning of new projects.

1.5 Structure of the report

The report contains presentation of the main scientific achievements of the projects. For more detailed information about research results and publications as well as programme organisation, reference is made to the Annual Reports that can be found on SAFIR2018 website.

1.6 Acknowledgements

The results of the SAFIR2018 programme have been produced by all who have been involved in the research projects. Their work is highly esteemed.

The contributions of project managers and researchers that form the essential contents of this report are acknowledged with gratitude.

The work of the persons in the Management Board, steering groups and reference groups that has been carried out at the expense of their own organisations is highly appreciated.

Jari Hämäläinen and Vesa Suolanen

References

[1] National Nuclear Power Plant Safety Research 2015-2018. SAFIR2018 Framework Plan. Publications of the Ministry of Employment and the Economy, Energy and the climate 34/2014. (in Finnish, an English version available on http://safir2018.vtt.fi/).

[2] Hämäläinen J. & Suolanen, V. (eds) SAFIR2014 - The Finnish Research Programme on Nuclear Power Plant Safety 2010-2014. Final Report. VTT Technology 213. Espoo 2015. 722 p. (http://safir2014.vtt.fi/).
[3] SAFIR2018 – The Finnish Research Programme for Nuclear Power Plant safety 2015-2018. Operational Management Handbook. 2015. 19 p + 26 app. (http://safir2018.vtt.fi/).
[4] Hämäläinen, J. & Suolanen, V. (eds) SAFIR2018 Annual Reports 2015-2017. Research Reports VTT-R-01745-16, VTT-R-02893-17 and VTT-R-02454-18. (http://safir2018.vtt.fi/).
[5] Hämäläinen, J. & Suolanen, V. (eds) SAFIR2018 Annual Plans 2015-2018. Research Reports VTT-R-02813-15, VTT-R-02463-16, VTT-R-02921-17, VTT-R-02884-18. (http://safir2018.vtt.fi/).
[6] SAFIR2018 Evaluation Report. Publication of the Ministry of Employment and the Economy, 5/2018, ISBN:978-952-327-325-2 (link on http://safir2018.vtt.fi/).
[7] National Nuclear Power Plant Safety Research 2015-2018. SAFIR2022 Framework Plan. Publications of the Ministry of Employment and the Economy, Energy and the climate 34/2014 (http://safir2022.vtt.fi/).
[9[Hämäläinen J. & Suolanen, V. (eds) SAFIR2018 - The Finnish Research Programme on Nuclear Power Plant Safety 2015-2018. Interim Report. VTT Technology 294. Espoo 2017. 387 p. (http://safir2018.vtt.fi/).
[10] Hämäläinen, J. & Suolanen, V., Survey of Competence in the Nuclear Energy Sector 2017-2018 (Ydinenergia-alan osaamisselvitys 2017-2018; in Finnish, an English version to appear). VTT Technology 344. Espoo 2018. 66 p + 6 app. (https://www.vtt.fi/inf/pdf/technology/2018/T344.pdf).

2. Automation, Organisation and Human Factors

2.1 Electric systems and safety in Finnish NPP (ESSI)

Seppo Hänninen[1], Riku Pasonen[1], Anna Kulmala[1], Antti Alahäivälä[1,2],Matti Lehtonen[2], Ismet Tuna Gürbüz[2], Deepak Subedi[2], Jan-Erik Holmberg[3]

[1]VTT Technical Research Centre of Finland Ltd
P.O. Box 1000, FI-02044 Espoo

[2]Aalto University
P.O. Box 11000, FI-00076 Aalto

[3]Risk Pilot AB
P.O.Box 72, 02101 Espoo

Abstract

The project researched phenomena, impacts and mitigation methods for possible common cause faults in electrical systems caused by open phase conditions (OPC), large lightning strikes and flexible operation of nuclear power plant (NPP). Unbalances of voltages and currents and temperature evolution in motors were measured with different transformer connections in different OPC cases. Effects of OPCs on NPP electrical components and the related protection of components were mapped. Simulation models were developed to study the lighting surges. Surge arrestor, capacitors and external conductive grounding cables parallel to the protected signal cables are very effective at damping fast transient overvoltages. Areas of concern and risks for flexible operation of NPP are thermal system, turbine, control room and personnel, financial profitability and grid stability in low inertia case. A risk analytic approach to assess options for flexible operation was outlined.

Introduction

Open phase condition (OPC) is a situation where one or two phases of the feeding network are disconnected and the voltages become unbalanced. Generators are relatively sensitive to unbalance and they are easily tripped by unbalance relays. In directly connected motors, sustained operation with unbalanced supply voltage leads to either tripping of the motor protection, or in the worst case, damaging of the machine due to overheating. If unbalance sustains for a longer time, transformers

and cables may be overheated due to excessive load currents. In case of converters, the uninterruptible AC power system functionality can be impacted. The project investigated the preparedness of Finnish NPPs against OPC.

Lightning overvoltages can be caused in NPP power and automation systems via two different mechanisms: If lightning strikes in the phase of the 400 kV (or 110 kV) transmission line connected to the NPP, an overvoltage can be transmitted through the transformers to the lower voltage levels. The second mechanism is lightning strike to the grounded parts of the NPP, causing ground potential rise (GPR) and potential differences between grounded parts and insulated power, communication and instrumentation circuits. The project examined the impact of higher lightning currents on the NPP electrical and automation systems.

Adaptive operation of NPP is expected in future flexible power system due to fluctuating renewables power. It is also possible in Finland that periodically the NPPs have to adapt to the consumption and run at decreased power level after all new NPP units are taken in the use. The potential safety issues of electrical systems related to the operation of nuclear power plants in the load following mode were researched.

Open Phase Conditions (OPC)

A comprehensive analysis of OPC impacts on an induction motor was provided. Several transformer connections with single or double line OPC on their primary-side were investigated analytically as well as with simulations. Of particular interest was to understand the required reaction speed needed to protect the motor. For that purpose, a motor was measured under OPC and the motor temperature was reported. Measurements were done to validate the calculations using 1.5 kW, three-phase, two-pole, squirrel-cage induction motor. The studied motor had an insulation class F, for which the maximum temperature of 155 °C is allowed.

The Table 1 summarizes the measured phase voltages and currents for each case. It shows the values when motor was not loaded during the fault, when the loading was reduced, and when the loading was nominal. The connection of the transformer feeding the motor has a strong impact on fault severity. In the case of YNd11 and a single OPC, only minor voltage unbalance was seen by the motor, whereas the most severe situation was with Dyn11. When double OPCs were considered, all the studied cases showed severe unbalances. The influence of the condition on the motor is strongly affected by the load dynamics. Measurements indicated that the motor is likely to stall, if the motor loading is not reduced under OPC. On the other hand, if the motor continues rotating, the increased currents tend to heat up the motor. Temperature rise during a one minute fault was measured for different fault cases. The fastest temperature rise was measured in the YNyn double OPC (approx. 2°C/10 s), but also in this case, the highest measured temperature remained far from the allowed 155 °C. Therefore, it can be concluded that short-term OPCs will not cause overheating of induction motors. It should be, however,

noted that the measurements do not reveal whether the maximum allowed temperature would be reached, if the OPC would remain for a long time. (Alahäivälä and Lehtonen 2018).

Table 1. Measured phase voltages and current when motor was not loaded, when the loading was reduced from nominal, and when loading was nominal.

		U_a[V]	U_b[V]	U_c[V]	I_a[A]	I_b[A]	I_c[A]
No load	Single phasing	165	228	229	0,0	3,4	3,4
	YNyn S	202	231	222	1,0	3,0	2,7
	Dyn11 S	174	206	157	2,1	4,0	2,2
	YNyn D	221	164	176	4,1	2,4	2,0
Reduced loading	Single phasing (70 %)	87	228	223	0,0	6,4	6,4
	YNyn S (100%)	190	227	223	2,7	4,8	4,2
	Dyn11 S (40 %)	138	199	153	3,1	5,7	2,7
	YNyn D (50%)	221	157	140	6,4	3,2	3,3
Nominal (Stalls)	Single phasing	117	221	214	0,0	13,5	13,5
	YNyn S	-	-	-	-	-	-
	Dyn11 S	80	160	80	5,6	11,2	5,6
	YNyn D	210	82	80	13,8	7,0	6,9

Detection of OPCs is not straightforward, because transformers and motors regenerate voltage and the unbalances can remain at a level which is not detected by protection. It is harmful to the NPP operation if lasting for a long time. Transformers between the faulted point and the point of interest affect significantly the observed voltages and currents. The level of regeneration depends on the winding configuration and grounding as well as sometimes core construction (Alahäivälä and Lehtonen 2018). Table 2 presents the effect of several transformer types on voltage and current unbalances. The most severe locations for OPC are the main generator bus, primary side of the unit transformer and primary side of the standby transformers. From OPC detection point of view, the most challenging OPC occurs when the NPP is supplied from the off-site grid, the main generator is disconnected i.e. transformer loading is low and the single open phase is on the primary side of the unit or standby transformer.

Table 2. Effect of transformer connection and grounding on voltage and current imbalances under OPC (Christensson and Lingärde 2014, Norouzi 2013).The considered transformers are three-legged core type.

Transformer	OPC	Primary unbalance		Secondary unbalance		Zero Current	Comments
		Voltage	Current	Voltage	Current		
YNd	Single	Low	High[1]	Low	Low[2]	Close to positive	1) One phase current missing 2) Increases if induction motor load
	Double	Moderate[1]	High[2]	Moderate[1]	High[3]	Same as positive	1) All phases regenerated, unbalance high with only resistive load 2)Two phase current missing 3) One phase current missing
YNy, YNyn	Single	Low	High[1]	Low	Low[2]	Close to positive	1) One phase current missing 2) Increases if induction motor load
	Double	Moderate[1]	High[2]	Moderate[1]	High	Same as positive	1) With only resistive load, unbalance worse 2) Phase current missing
Dy	Single	Moderate[1]	High[2]	Moderate[1]	High	No grounding	1) With only resistive load, unbalance worse 2) Phase current missing
	Double	High[1]	High[3]	High[2]	High[3]	No grounding	1) Phases are in the same potential 2) No voltage on the secondary 3) No currents
Yy	Single	Moderate[1]	High[2]	Moderate[1]	High[2]	Zero	1) With only resistive load, unbalance worse 2) Phase current missing
	Double	High[1]	High	High	High[1]	Zero	1) Phases are in the same potential

The resulting unsymmetrical system affects the different NPP electrical system components in various ways (IAEA 2015, Alahäivälä and Lehtonen 2018) which is summarized in Table 3. The table also presents the potential NPP component protection functions that might operate in OPC situations. Several alternative methods for OPC detection exist and the selection of the most suitable methods for a particular NPP depends on the NPP characteristics. The preparedness of Finnish NPPs against OPC can be considered good and no critical safety risks were identified during this research (Kulmala and Alahäivälä 2019).

Table 3. Effects of OPCs on NPP electrical components and the related protection of the components.

Component	Effects	Protection
Main generator	Negative sequence currents heat the rotor and can lead to damage of the generator if the unbalance situation remains for a too long time. There is also a risk of a pole slip.	• Negative sequence current relays with inverse time characteristics • Undervoltage protection • Pole slipping protection
Induction motor	If voltages are unbalanced, problems related to overheating and increasing vibrations can occur. A motor may also stall and it may not start-up with unbalanced voltages.	• Some critical motors have negative sequence current protection • Some motors have undervoltage protection • Overload protection • Some motors have temperature measurements with alarms
Power electronics (converters)	Unbalanced voltages can cause synchronization difficulties for some power electronic devices. Undervoltage and/or voltage unbalance protection can be quite sensitive and devices can disconnect easily. Possibly connects automatically back when voltage normalized.	• Differential current protection • Ground fault protection
Transformers	Not considered as the most vulnerable component during OPC. Overheating can occur in some loading conditions.	• Differential current protection • Ground fault protection

Lightning overvoltage.

Direct stroke to the phase conductor of the connected line and back flashover resulting from the lightning stroke to the transmission tower or shield wire inject wave current with high amplitude to the phase conductors and eventually through the transformer. The voltage rise at the secondary of each connected transformer at different voltage levels in a house load network of a power generation plant was analyzed. Protective measures were analyzed to mitigate the transferred overvoltage at the far end and ensure the overvoltage is within the basic insulation level (BIL) of the connected equipment. The study ensured whether the equipment connected to the medium and low voltage side of the system are within the protection limits. Simulations using different combination of protective surge arrestors have been done with EMTP-ATPDraw. The presence of the 400 kV surge arrestor that is connected on the system has significantly limited the transferred transient voltage peak at this voltage level during direct stroke and back flashover. For the protection of the generator 15.75 kV (having BIL of 68 kV) surge arrestor and a surge capacitor is required at the 15.75 kV side as the presence of these protective equipment has reduced the voltage well below the BIL. In order to ensure the protection of the connected equipment (having BIL of 29kV) at the 6 kV voltage network, the installation of the surge arrestor at the 400 kV and 15.75 kV side has a very strong positive impact. The voltage at the 6 kV side has been reduced significantly and is well

below the basic insulation level. The combination of 400 kV and 15.75 kV surge arrestors are enough to protect the generator against 20 kA lightning as the transient voltage is significantly reduced. If larger surges are to be expected, the rating of the surge arrestor should also be higher. It is a subject for further research to investigate how likely is that 26.6 kA surge enters the phase conductor (Subedi and Lehtonen 2018).

The impacts of lightning strike on low voltage power electronic devices and their protection were simulated with PSCAD transient simulator. Metal oxide protector, three phase rectifier load and clamp style protection device with over-current protection and a battery were simulated. Metal oxide protector was effective to limit over voltage, but a rise in DC bus voltage was noticed. The connection of power electronic load solely limited the overvoltages in LV AC points near the load due to capacitance in the load to buffer the rectifier voltage. The capacitors are very effective at damping fast transient overvoltages. Most DC rectifiers are based on active bridge technologies, it is a small effort to also include protective functionalities such as overvoltage and over-current protections. Mechanical breakers are effective devices, but they have operational delay for noticing the fault and acting. Therefore some passive protective methods could be used such as clamp type protection or additional capacitors. Battery also dampened the overvoltage so much that clamp type protection did not even activate. There is uncertainty of battery behaviour in very fast transient phenomena as most of measurements and models do not focus on this, but it is very clear that dampening effect is considerable (Pasonen 2018b)

The three-dimensional finite-difference time- domain (FDTD) method has been enployed to study the performance of the large-scale grounding system (LSGS) against a lightning strike with different lightning surge propagation properties and how to improve transient protection for control equipment. The study emphasized how a nearby sea influences the ground potential rise on large- scale grounding system considering soil ionization. Two case studies were conceived regarding the position of the nearby sea, where it is located on the y+ and x+ sides of the LSGS, see Figure 1. In addition, two striking scenarios were considered where the lightning strikes the first and the second tower. One example of simulation results is in Figure 2, corresponding to Figure 1 case.

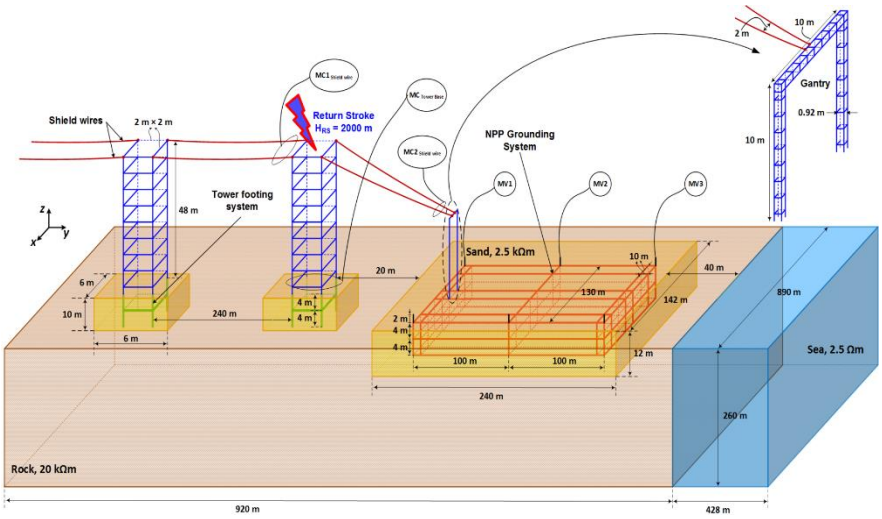

Figure 1. Physical grounding system model used in simulation. The figure corresponds the case where the sea is located on y+ side and the lightning strikes the first tower.

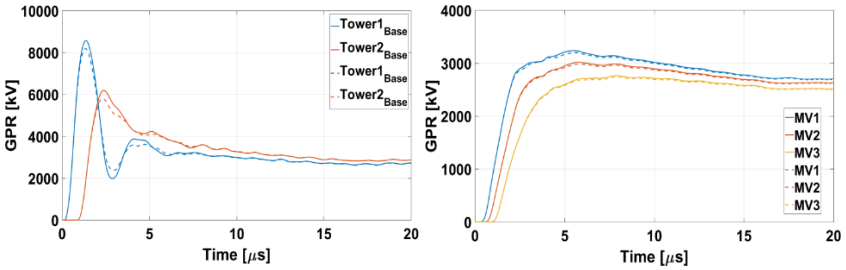

a) b)

Figure 2. Ground potential rise: a) in tower bases and b) in three different points of grounding system, solid line without ionization and dash line with ionization. The lightning current has a peak value of 100 kA, the rise time of strike is 4 μs and the resistivity is 20/2.5 kΩm for rock/sand.

The results showed that the magnitude of ground potential rise (GRP) at different points of LSGS is strongly influenced by sea. In addition, the extent that soil ionization affects the ground potential rise is dependent on the distance between tower and the large-scale grounding system. Soil ionization causes a decrease in the soil resisitivity and subsequently, in the computed GPR. The farther the tower is from LSGS the ionization impact on the GRP and currents waveforms becomes more significant (Gürbüz 2018). The potential differences on different parts of the grounding system may damage the connected wiring and equipment, depending on how grounding connections are made. For example, control devices can be grounded locally or grounded via the cable shield only since both cases can be encountered

even in the same plant. Figure 3 shows simulation results of voltage differences between phase and local ground in the aforementioned two grounding cases.

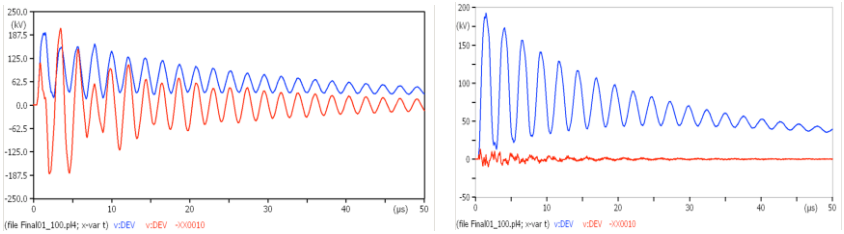

a) b)

Figure 3. a) Voltage differences between phase and local ground (red; maximum amplitude 205.3 kVp) as well as remote ground (blue; maximum amplitude 193.3 kVp) in the case no equipotential bonding system is present. b) Voltage differences between phase and local ground (red; maximum amplitude 12.7 kVp) as well as remote ground (blue; maximum amplitude 191.9 kVp) in the case an equipotential bonding system is present. In Figure 3: x-axes Time (μs), y-axes: Voltage (kV).

In the case of large wide area grounding system and high soil resistivity, the ground potential rise may cause high voltage stress in the connected equipment. One of the critical situations is the lightning strike to the gantry or adjacent transmission tower of a large power generating station. A large lightning current may cause huge potential differences between different grounded parts of the electrical systems. In the extreme case, these differences may cause excessive stress to the insulation of the signal cables of the automation and control systems. These voltage stresses may be mitigated by adding to the grounding system external conductive cables parallel to the protected signal cables. In addition, surge protective devices may be needed in most critical locations. Planning such a protection requires a detailed analysis of the grounding system and electrical system lay out, as well as investigation of the different routes along which the lightning current may enter the plant. It might be necessary to limit the possible lightning entering routes by using lightning rods (Lehtonen et al 2018).

Flexible operation of NPP

The project focused to study risks caused by flexible operation of NPP to electric systems and to control inside stabilization of national grid. It is expected that the disturbance sensitivity of the electrical components and ICT systems can increase. The load-following operation has some influence on the ageing of certain operational components and thus one can expect an increase in maintenance and surveillanve. The research based on a literature study survey and interviews of Fennovoima, Fortum, Teollisuuden Voima, Fingrid and Radiation and Nuclear Safety Authority (STUK). The Swedish Centre for Nuclear Technology was also contacted. The requirements of flexible operation for Finnish NPPs were studied.

For the time being, there are no plans to apply load-following for any of the plants in Finland. Some units have only manual power controls possbility and new automation system would be needed for automatic control of load-following. Some operators have personnel experience with flexible operation, but investments in knowledge and additional personnel would be needed for actual operation. New units will be capable of flexible operation, but that is not currently a target for practical operation. Areas of concern for flexible operation that came up in discussion were: thermal system & turbine, control room and personnel and financial profitability. No issues regarding electric system were pointed out. STUK sees load-following as a technical issue and not as an issue that is limited by the regulation.

Flexible operation is actively used in Germany, France and a couple of other countries. France uses flexible operation, because plants have to be designed to provide 70% of electric power in the national power system. In Germany nuclear power plants operate in load-following mode due to high percentage of renewables. In this regard Finnish power system is different and balanced compared to these countries, but situations can change during the long lifetime of nuclear power plants. Basic problem with this is that NPPs are high capital and low running costs type of units. For this reason and reactor physics, savings in fuel costs in load-following are smaller with nuclear power plants when compared to traditional power plants. If flexibility in Finnish power system becomes an issue, nuclear units will compete with bio based units and also with other flexibility resources for their share on the ancillary service markets. (Pasonen 2017).

Balancing possibilities in frequency containment reserve for normal operation (FCR-N) market was estimated with an assumption of 4.6% additional cost of flexible operations. Using market data from 2016, there were 1144 hours when flexible operation could have been profitable. In this case, 4.6% increase was calculated with respect to Nordpool SPOT price, but in reality there is plant specific operation cost. With that, the decrease of the capacity factor per plant was estimated to be only 0.5% with two months of measured frequency data with 1 s interval. Figure 4 shows an example of the simulation results. The following assumtions were done: the simulated power plant size is 1300 MW, all power plants in the Nordic power systemwould take part in automatic frequency regulation, the minimum production capacity in Nordic power system is 10000 MW, maximum change of power 3 %/min from nominal power, power response setting or slope of the droop is 0,5.

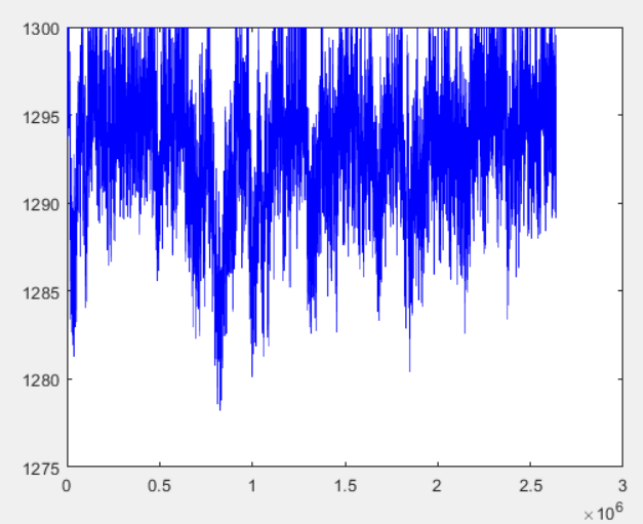

Figure 4. Simulation of 1300 MW power plant participation in frequency containment control for normal operation (FCR-N) in about 1 month period. X-axes: time in seconds (one month period), Y-axes: power on MW.

Fingrid sees that 2020 onwards rotating generation will be more limited in the power system, and there will also be less controllable power plants. This means that price variations might be large. The discussion are ongoing, but the energy producers all of them currently have better resources than NPPs for balancing purposes. There has not been instances that Fingrid had to demand nuclear power plant to reduce power or demand disconnection. Market based solutions have been enough for now. For voltage control however there has been more requests to change reactive power injection / voltage setpoint. The call to change output power would go from Fingrid control center straight to the operator of the nuclear power plant. When grid frequency is outside normal operation region, the grid code demands power plant to be controlled lower or higher output linearly respect to deviations in frequency.

Instead of bidirectional balancing, nuclear power plants could serve better in down regulation reserve in cases for system over-frequency and normally leave bids to down regulation balancing market. This practice would guarantee down regulation capacity even if NPPs would never win the bids to actually activate. It should be noted that Frequency Containment Reserve for Disturbances (FCR-D) for disaster situations is only defined for situations when there is lack of power in the system (and not for over-frequency). For system stability respect, there are no large risks in NPP participating to balancing. The most obvious risk to system stability is that if large nuclear plant is taking major role in system balancing and plant disconnects from grid when there is low inertia in the grid (summer time). For risk analysis perspective, the role of the single plant in balancing should be limited. It is likely that pressures on all generation to participate more actively on system balancing will

increase, and it is very likely that new units will be required to take part at some point of their long operation life cycle (Pasonen 2018a)

The project outlined a risk analytic approach to assess options for flexible operation. The optimization of operational strategies of NPPs is both a multi-criteria task and an issue for multiple stakeholders. Just looking at from a single unit point of view is not sufficient, but it should be analysed from the portfolio of generating units point of view. It is suggested that the assessment can be divided into three major categories: 1) grid system risks, 2) economical risks (of the plant owner), and 3) NPP reactor safety risks. These categories can be broken down into subcategories that can be assessed separately, see Figure 5. This approach leads to a multi-attribute decision analysis framework, which also allows to take uncertainties into consideration (Holmberg 2018).

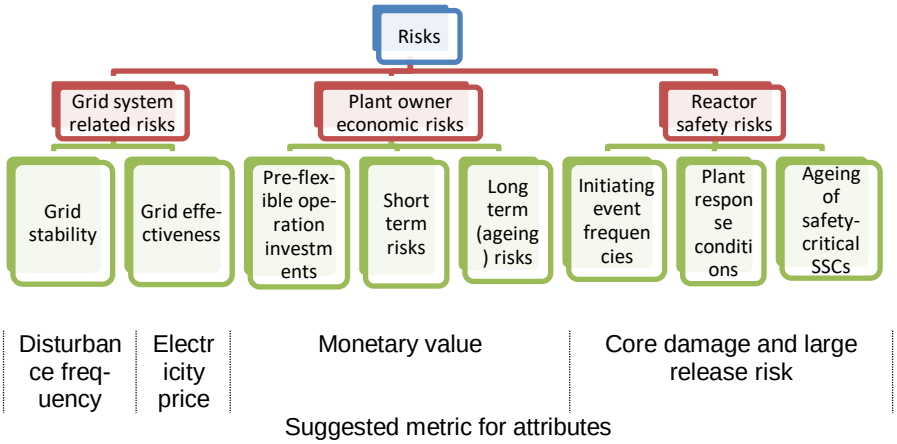

Figure 5. Multi-attribute decision making structure.

Summary and conclusions

The project researched the possible risks of open phase conditions, large lightning strikes and adaptive operation of nuclear power plant (NPP) to electrical systems of Finnish NPP.

OPC results in component overloading. In the case of single OPC of motors, only moderate unbalance is observed with YNd and YNyn transformer connection, whereas the highest phase current occurs with Dyn connection. From OPC detection point of view, the most challenging OPC occurs when the NPP is supplied from the off-site grid, the main generator is disconnected i.e. transformer loading is low and the single open phase is on the primary side of the unit or standby transformer. The preparedness of Finnish NPPs against OPC can be considered good and no critical safety risks were identified during this research.

Simulation models were developed to study the lighting surges which can transferred to NPP via phase conductors or via grounding system. Surge arrestor at the 400 kV and 15.75 kV, together to 15.75 kV surge capacitor,have significantly limited the transferred transient voltage peak at these voltages level during direct stroke and back flashover. The capacitors are very effective at damping fast transient overvoltages on low voltage power electronic devices. One of the critical situations is the lightning strike to the gantry or adjacent transmission. A large lightning current may cause ground potential rise leading to huge potential differences between different grounded parts of the electrical systems. In the extreme case, these differences may cause excessive stress to the insulation of the signal cables of the automation and control systems. These voltage stresses may be mitigated by adding to the grounding system external conductive cables parallel to the protected signal cables. In addition, surge protective devices may be needed in most critical locations.

For the time being, there are no plans to apply load-following for any of the units in Finland. New units will be capable of flexible operation but old units have only manual power controls possbility and new automation system would be needed for automatic control of load-following. Areas of concern and risks for flexible operation are: thermal system & turbine, control room and personnel and financial profitability. STUK sees load-following as a technical issue and not as an issue that is limited by the law. The most obvious risk to system stability is that if large nuclear plant takes the major role in system balancing and plant disconnects from grid when there is low inertia in the grid (summer time). A risk analytic approach to assess options for flexible operation were outlined divided into three major categories: 1) grid system risks, 2) economical risks (of the plant owner), and 3) NPP reactor safety risks.

Acknowledgement

The authors gratefully acknowledge the valuable information obtained through interviews of the Finnish utilities (Fortum, TVO, Fennovoima), the Radiation and Nuclear Safety Authority and the Finnish transmission system operator Fingrid.

References

Alahäivälä, A. and Lehtonen, M. 2018. Analysis of open phase condition influence on an induction motor. 19th International Scientific Conference on Electric Power Engineering (EPE), Brno, Czech Republic, May, 16-18.2018. 6 p.

Christensson, A., Lingärde, E. 2014. Transformatorers beteende vid fasavbrott i matande spanning. Lund, Sweden. MSc thesis, Lund University.

Gürbüz, I. T. 2018. Lightning Induced Over-voltages in Nuclear Power Plants. Espoo, Finland. MSc thesis, Aalto University, School of Electrical Engineering. 11 + 91 p.

Holmberg, J.-E. 2018. Preliminary risk analysis for adaptive operation of NPP. Espoo. Risk Pilot Report 17141_R001. 13 p.

IAEA Safety Report. 2015. Impact of open phase conditions on electrical power systems of nuclear power plants.

Kulmala, A., Alahäivälä, A. 2019. Methods for detection of the OPC condition and recommendations to improve safety of NPPs in the case of OPC. Espoo: VTT. VTT Research report VTT-R-000020-19. 22 p.

Lehtonen, M., Schürhuber,R., Pichler, M. 2018. Ground potential rise and lightning overvoltages in control systems of large powerplants under high soil resistivity. Espoo. SAFIR 2018 deliverable D2.3. 4.p

Norouzi, A. 2013. Open phase conditions in transformers analysis and protection algorithm. Proc. 66th Annual Conference for Protective Relay Engineers, College Station, TX, USA.

Pasonen, R. 2017. Finnish Perspectives for Flexile Nuclear Power Plant Operation. Espoo: VTT. VTT Research report VTT-R-06514-17. 19 p.

Pasonen, R. 2018 a. Risks of adaptive control of NPP electrical systems and stability of the grid. Espoo: VTT. VTT Research report VTT-R-04700-18. 15 p.

Pasonen, R. 2018 b. Power plant lightning overvoltage protection of low voltage power electronics. Espoo: VTT. VTT Research report VTT-R-06945-18. 21 p.

Rizk, M., Lehtonen, M., Baba, Y., Abulanwar, S. 2018. Performance of the large-scale grounding system in thermal power plants against lightning strikes to nearby transmission towers. IEEE Transactions on Electromagnetic Compatipility, accepted for publicayion in a future issue. 8 p.

Subedi, D., Lehtonen, M. 2018. Lightning Overvoltages in Electrical Power System of a Power Plant. 2018 IEEE International Conference on High Voltage Engineering and Application (ICHVE 2018). Athens, Greece on September 10-13, 2018 7 p.

2.2 Management principles and safety culture in complex projects (MAPS)

Nadezhda Gotcheva[1], Kaupo Viitanen[1], Marja Ylönen[1], Sampsa Ruutu[1], Pertti Lahdenperä[1], Jaakko Kujala[2], Kirsi Aaltonen[2], Farzad Pargar[2], Karlos Artto[3]

[1]VTT Technical Research Centre of Finland Ltd
P.O. Box 1000, FI-02044 Espoo

[2]University of Oulu
P.O. Box 4610, FI-90014 Oulu

[3]Aalto University
P.O. Box 15500, FI-00076 Espoo

Abstract

MAPS project aimed at enhancing nuclear safety by supporting high quality execution of complex nuclear industry projects. The results advance knowledge on key dimensions of governance for safety in inter-organizational project networks and suggest a novel approach for self-assessment based on the governance framework. Insights from the empirical case studies point to importance of enahancing non-technical capabilities, such as communication and collaboration, and aligning fragmented viewpoints. Leading methodical change of safety culture in dynamic and networked organizations requires a systemic approach. System dynamics modelling resulted in an interactive simulation game to support decision-makers in gaining a holistic perspective on patterns of dynamics interrelations in project contexts.

Introduction

Complex projects are large-scale temporal undertakings, marked by high levels of uncertainty with major financial, environmental, political and social implications for stakeholders and society. In the nuclear industry, there is increasing interest towards understanding how to successfully manage and implement such projects. Previous research indicates that inability to manage the increasing complexity in projects plays a significant role in deficient project performance (Flyvbjerg et al., 2003). A recent report on lesson-learning in nuclear construction projects by the World Nuclear Association highlights the need to enhance *collaborative ways of working* by stating that “standard contractual arrangements may not be sufficient to ensure this and appropriate procurement arrangements and project delivery models are needed to support such a mode of collaborative working” (WNA, 2018).

Project governance emphasizes collaborative arrangements for aligning multiple diverse project stakeholders’ interests to work together towards shared goals

(Turner & Sinister, 2001). Such approach is much needed in the nuclear industry nowadays, when projects are increasingly carried out by a multinational network of companies in conditions of changing regulatory requirements and contextual factors. Some of the project parties might have little experience with specific national nuclear regulatory requirements or nuclear industry practices in general. In this context, it is challenging to ensure that the safety and quality requirements are adequately understood and fulfilled by every organization involved in the project network throughout the project lifecycle. *Project management* has not been much within the radar of safety research because delays have largely been seen as economic issues. However, safety cannot be separated from other performance issues when a *systemic approach* is applied, that is, when human, technological, organizational and cultural factors are seen as interrelated elements (Reiman & Rollenhagen, 2014; IAEA, 2014). *Safety* is an emerging property of the sociotechnical system, continuously created in daily activities (Hollnagel 2009; Reiman & Oedewald, 2009; Oedewald et al., 2011).

As temporary organizations, projects can be characterized according to four main areas (Bakker, 2010): *time* (existence within predetermined and limited timeframe); *task* (motivation for creating the temporary organization); *team* (emergence of unique team and group interdependence dynamics); and *context* (relations between temporary organization and its more stable environment). From a safety perspective, these orientations may lead to strong focus on task performance, short-term focus, difficulties of building relationships and shared approaches, multiple loyalties, communication and lessons learned challenges or trust issues. *Safety culture* is an organization's potential for safety, or the ability and willingness of organizations to *understand* safety and hazards, and the ability and willingness to *act* on safety and actively prevent hazards from actualizing (Reiman & Oedewald 2009, Oedewald et al. 2011). The characteristics of nuclear industry projects and experienced safety culture challenges triggered previous research to focus on *safety culture in a network of companies*, where interactions and relationshops between parties and therefore the network management strategies and practices are considered important factors (Oedewald & Gotcheva, 2015).

Thus, there is research and practical need to clarify the principles for developing, changing and managing safety, and steer collaborative processes and structures in inter-organizational nuclear industry project networks.

Objectives of MAPS project

The overall *research question* of the MAPS project is: what are the safety management principles that should be applied in managing complex projects in the nuclear industry, and how these principles can be implemented in practice? Fig.1 presents the ultimate *goal of MAPS project* (2015-2018) and specific objectives formulated according to this goal.

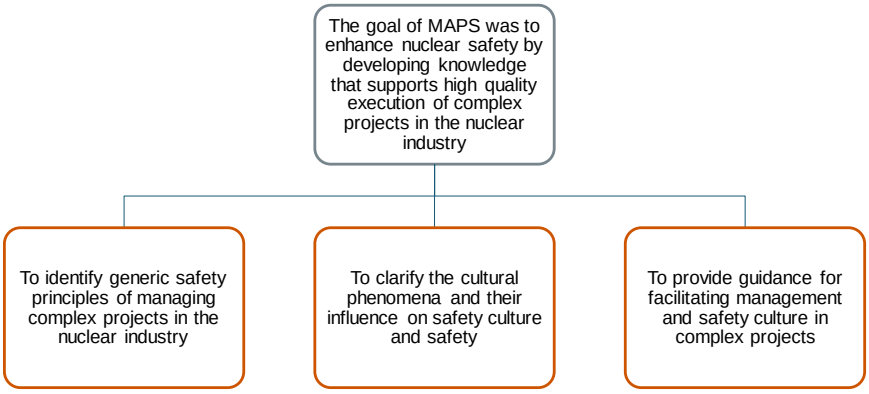

Figure 1. The goal and objectives of MAPS project (2015-2018).

The project brought together expertise in safety culture and organizational factors, project governance, societal research on safety regimes, system dynamics modelling and complexity. It integrated theories and concepts from these disciplines to advance knowledge and provide practical guidance for nuclear industry community. Methods included systematic literature reviews, document analysis, empirical case studies, information exchange with companies, and workshops with practitioners.

Supporting high-quality execution of complex projects by linking project governance and safety: Generic principles

Based on a systematic review of project governance literature, we developed a framework that summarizes the key principles of governance in inter-organizational project networks (Kujala et al., 2016). The framework categorizes *governance in project networks* under six key dimensions: goal setting, rewarding, monitoring, coordination, roles and decision-making power, and capability building (Fig. 2):

- *Goal setting* to create shared performance goals for the project that are understood by all project actors.
- *Monitoring* to raise awareness of risks or potential for unwanted events in the future; to ensure that stakeholders understand this and behave as expected.
- *Roles and decision-making* to ensure decisions are made promptly based on up-to-date information by most releant experts and effect of decisions to overall performance is taken account.
- *Rewarding* to align stakeholders' goals with project goals by means of incentives, linked to joint performance goals, conditional future payments and work prompting a life-cycle approach.
- *Coordination* to align behavioral patterns of stakeholders to effectively work together, based on adapting tools and compatible work processes.
- *Capability building* to ensure that project stakeholders have adequate capabilities and resources to meet performance expectations.

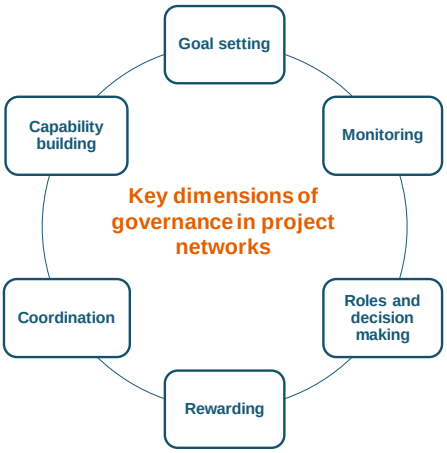

Figure 2. Key dimensions of governance in inter-organizational project networks (adapted from Kujala et al., 2016).

In addition, the applicability of governance approaches related to project alliancing and its influence on safety in nuclear industry projects was studied. *Project alliancing* is a particular type of project delivery method based on strong inter-organizational integration (Lahdenperä, 2012). A key feature of project alliancing is *effective collaboration* and creating and developing a *common best-for-project mindset and culture* (Walker, 2016). The nature of incentive is "painshare/gainshare" with added focus on committed relationships and early involvement of contractors.

A Master's thesis was successfully completed on evaluating how different project governance mechanisms are related to safety in the context of nuclear industry projects (Starck, 2016). The results indicated that a project was rather seen as carried out by each of the project actors, and not as a shared entity consisting of multiple actors. A shared project culture was seen as something to strive for. The findings also indicated that the key dimensions of project governance exist also in the safety literature, and two additional sub-dimensions were found: coordination tools and informal roles. The findings also highlighted the importance of a project organization, leaders' participation in safety related issues, and sharing a common view of safety in the project network.

To further bridge project governance and safety research, we analysed how governance mechanisms influence coordination and organizing in project networks, and highlighted the importance of paying attention to and developing relationships and other inter-organizational factors to enhance nuclear safety in projects (Gotcheva et al., in press). An empirical study on perceived project complexity identified the need to pay more attention to non-technical aspects of complexity (e.g. organizational, emergent, institutional arrangements) and their implications for safety in projects (Gotcheva et al., 2015). Furthermore, we studied the sensemaking related to introducing a new safety-related method during the project's design phase. The empirical analysis resulted into nine distinct storylines, which describe

a wide range of perceptions and interpretations about the adoption of an innovation in the project. These findings point to the fragmented nature of sensemaking in complex projects and the need to understand, monitor and manage ambiguities and their potential effects on nuclear safety (Aaltonen et al., 2017; forthcoming).

Knowledge on governance of safety and management of complex projects was advanced also by *benchmarking the Norwegian oil & gas industry* by studying both the regulatory and the industry perspectives. Criteria for comparison between Finnish and Norwegian regulatory regimes were the following: safety philosophy, stakeholder involvement, regulatory practices and the role of inspectors. Findings indicate that Norwegians have adopted safety philosophy that includes also economic aspects, including national interest in oil revenues and safeguarding profit. Still, political and economic issues could potentially undermine existing trust between parties and influence the climate of cooperation. In Finland, economic aspects are excluded from safety regulation (Ylönen & Engen, 2016). The Norwegian regulatory regime is risk-informed, function-based, trust and dialogue-based. Although the Finnish regime has similar features, it can be characterized as a command and control type of regulation. The industry level benchmarking analysis indicated that Norwegian oil companies have mostly adopted hands-on strategy in managing relationships with contractors due to problems experienced with hands-off strategy (i.e. giving freedom to contractor to realize the project) (Ylönen, 2017).

Clarifying the cultural phenomena and their influence on safety culture and safety: How to assure and improve safety culture in complex projects?

To clarify the cultural phenomena pertinent to dynamic and networked organizations, we studied their generic characteristics. To understand their influence on safety culture and safety, we applied systems thinking. The NKS SC_AIM study focused on safety culture improvement and assurance methods in complex projects. We carried out literature reviews of safety culture improvement methods and temporary organizations, empirical case studies in nuclear power companies and information exchange with power companies. The predominant approaches for safety culture development are based on the assumption that the context is stable and relatively homogeneous, which often does not apply to dynamic project networks. Although a variety of approaches was identified in the literature, practical methods intended specifically for project environments are scarce (Viitanen, Gotcheva & Rollenhagen, 2017).

Three empirical case studies in Nordic nuclear industry organizations were conducted as a part of this study. The main case study focused on Safety Culture Ambassadors group as a method. It was found that this method could influence safety culture through multiple mechanisms. Furthermore, the flexibility of this method can potentially balance some of the challenges posed by the project environment, and even benefit from them. The findings indicated that the Safety Culture Ambassadors group could facilitate the development and assurance of safety culture by improving

the information flow, enabling bidirectional communication, encouraging and facilitating participation of personnel and ensuring that safety is taken into consideration in various activities in the project. Benchmarking information exchange with another power company was also carried out. Based on the findings, a *guideline for implementing a safety culture ambassadors group* was produced (Viitanen, et al. 2018).

Other case studies focused on a safety-oriented project management seminar as a method and information exchange sessions with human and organizational factors experts, which provided additional insights into the current challenges and opportunities of safety culture improvement in projects.

Twelve principles that summarize the essential good practices of leading safety culture change of safety culture change were developed (Viitanen et al. 2018a, 2018b). The principles represent a systemic approach to leading safety culture change, which is based on a variety of contemporary views of safety science and organizational management (Fig. 3).

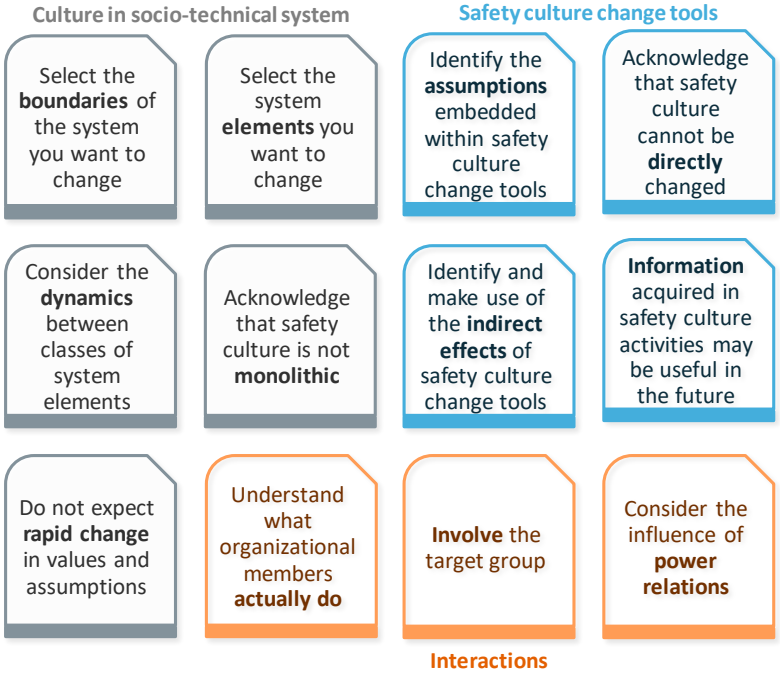

Figure 3. Twelve principles for methodical safety culture change (Viitanen et al., 2018).

The principles cover topics that include explicating the nature of sociotechnical systems and how culture forms and changes in them, how goals are set in complex, nested and conflicted systems, how various types of interactions can be leveraged for safety culture change, and how different time scales manifest when initiating culture change. The principles can be utilized to support various practical endeavours at safety-critical organizations such as nuclear power plants. For example, the

principles can support practitioners in helping steer safety culture change activities, in identifying the leverage points in the system that drive positive change in safety culture, or in identifying the prerequisites that are required for successful implementation of safety culture tools or methods. In essence, complex projects induce various challenges to safety culture change activities and these are insufficiently addressed by current safety culture methods or improvement paradigms. The safety culture change principles appear to be applicable also in dynamic and networked organizations. They have the potential to raise awareness about issues to be considered and opportunities to be leveraged.

Practical tools for facilitating management and safety culture: Project governance self-assessment tool and applying system dynamic modelling in complex projects

Project governance self-assessment tool provides structure to describe the project context and specific questions or statements for discussion (Fig. 4), based on the conceptual governance framework. Its first version was designed with the following objectives:

- To create shared language, understanding and learning, as well as to form and maintain relational capital throughout the lifecycle of a project.
- To increase understanding of how the context may influence effectiveness of different management practices.
- To raise awareness that in inter-organizational project networks all organizations in the network, their relationships and actions influence safety.
- To explore possibilities for various applications throughout a nuclear industry project lifecycle (training, regulatory oversight support, etc.).

The self-assessment process includes planning, conducting and discussion on utilization of results and next steps. Planning the self-assessment includes the following steps: 1) identification and description of goals of the self-assessment, 2) planning of self-assessment timetable, scope and cycle, 3) assigning the responsibilities for the self-assessment process (process owner) an ensuring commitment from management, 4) deciding the target group, and 5) creating description of the project context in a preparatory workshop (project management or external facilitator). Conducting the self-assessment includes a) project evaluation (individually or in a joint workshop) by using evaluation scale 1-5 and place for free comments; and b) synthesis of the self-assessment results for the consensus meeting/workshop by the self-assessment process owner.

Discussion on utilization of results and next steps includes a) consensus meeting to agree on the status of the project and to identify and agree on areas that need improvement, planning of Improvement actions (facilitated); b) follow-up of improvement actions (project management), and c) ensuring continuity of the self-assessment.

The tool can be piloted and used in different project contexts (e.g. smaller modernization projects or large-scale new build projects), as well as in different lifecycle

stages of a NPP project, ranging from pre-project to decommissioning. Development of the tool and associated methodology needs further research.

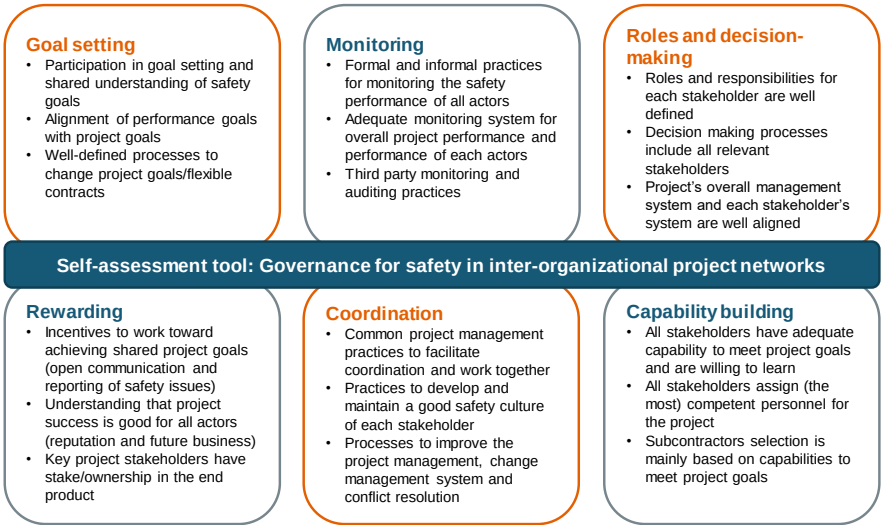

Figure 4. Project governance self-assessment: key dimensions and statements examples.

Another area of practical guidance concerns *system dynamics modelling* as a methodology for modelling complex systems: the focus is on dynamic behaviour over time of the system, not on individual events. To understand the dynamic behaviour over time, the structure of the system (e.g. feedback mechanisms, time delays, accumulations) need to be clarified. Diagramming tools such as causal loop and stock/flow diagrams can help in enhancing holistic understanding of a system. In non-linear systems, simulations can reveal e.g. tipping points in which the behaviour of a system changes qualitatively after a certain threshold.

We conducted a literature review of the use of system dynamics modelling of complex safety critical projects (Ruutu, 2015). The review indicated that although there are many existing studies of applying system dynamics to project management, and the key feedback mechanisms have been discovered (Lyneis & Ford 2007), governance of multiple stakeholders is not typically studied. Furthermore, safety issues in existing models are not taken into account explicitly.

The study identified two ways, in which the simulation modelling can be of practical relevance. First, the modelling can be done interactively within a workshop setting, which means that the models can be used as boundary objects to get people to form a common understanding of a complex issue. Second, the models can be used for theory building and generation of insights based on which practical policy recommendations for companies can be drawn.

Interactive workshops were held with experts involved in nuclear industry projects in Finland to support the simulation modelling. The focus was on delays in creating and handling design documents: this is a topical issue since small delays and disruptions in document handling processes can cause complex projects to suffer massive cost and time overruns. The causal loop diagram of how governance and safety aspects related in a nuclear industry project has been prepared. Efficient document management system and processes are both crucial and challenging due to the huge amount of documents and potential safety implications if design-related information is lost, unclear or incomplete, e.g. during plant maintenance. The results indicated that to evaluate and mitigate the cumulative impact of delays in complex projects, a system dynamics perspective is beneficial for proactively understanding reinforcement over time of delays and disruptions (Tuovinen & Gotcheva, 2017).

After a system dynamics model was created, it was developed further into an interactive simulation game. In the game, users can experiment how project resourcing and scheduling of two interacting work phases affect the performance of a project. The web user interface is shown in Figure 5. The simulation game was piloted in a workshop with nuclear industry company representatives.

Figure 5. Web user interface of the developed interactive simulation game (https://forio.com/app/sruutu/maps/)

Acknowledgements

MAPS project was funded by the Finnish Nuclear Waste Management Fund (VYR) and other organizations operating in the field of nuclear energy through SAFIR2018, the Finnish Research Programme on Nuclear Power Plant Safety (2015-2018), the Nordic Nuclear Safety Research (NKS) and VTT. The authors are grateful to the regulator STUK and the nuclear power companies for their cooperation.

References

Aaltonen, K., Gotcheva, N., Kujala, J. & Artto, K. 2017. Making sense of an innovation in a project network: A megaproject case study from the nuclear power industry. IRNOP, International Research Network on Organizing by Projects Conference, 11-14 June, Boston, USA.

Aaltonen, K., Gotcheva, N., Kujala, J. & Artto, K. (forthcoming). Making sense of an innovation in a safety-critical megaproject. Under review in *International Journal of Managing Projects in Business.*

Bakker, R. M. 2010. Taking stock of temporary organizational forms: a systematic review and research agenda: temporary organizational forms. *International Journal of Management Reviews* 12: 466-486.

Flyvbjerg, B., Bruzelius, N. & Rothengatter, W. 2003. *Megaprojects and Risk: An Anatomy of Ambition*. Cambridge University Press.

Gotcheva, N., Ylönen, M., Kujala, J. and Aaltonen, K. 2015. Characteristics of complex projects in the Finnish nuclear industry: Interview study of three cases. Research report.

Gotcheva, N., Aaltonen, K. & Kujala, J. (in press). Governance for safety in inter-organizational project networks, *Safety Science Research: Evolutions, Challenges and New Research Directions*, J-Ch. Le Coze (Ed.), Routledge.

Hollnagel, E. 2009. The four cornerstones of resilience engineering. In Nemeth, C., Hollnagel, E., Dekker, S. (Eds.) *Resilience Engineering Perspectives*, Volume 2. Preparation and Restoration. Ashgate.

IAEA, 2014. IAEA Report on Human and Organizational Factors in Nuclear Safety in the Light of the Accident at the Fukushima Daiichi Nuclear Power Plant International Experts Meeting 21-24 May 2013, Vienna, Austria.

Kujala, J., Aaltonen, K., Gotcheva, N. & Pekuri, A. 2016. Key dimensions of project network governance and implications for safety in nuclear industry projects, European Academy of Management (EURAM), 1-4 June 2016, Paris, France.

Kujala, J., Aaltonen, K., Gotcheva, N. & Pekuri, A. 2016. Key dimensions of project network governance and implications for safety in nuclear industry projects, European Academy of Management (EURAM), 1-4 June 2016, Paris, France.

Lahdenperä, P. 2012. Making sense of the multi-party contractual arrangements of project partnering, project alliancing and integrated project delivery, Construction Management and Economics, 30:1, 57-79.

Lyneis, J. & Ford, D. 2007. System dynamics applied to project management: a survey, assessment, and directions for future research, System Dynamics Review, 23 (2-3),157-189.

Oedewald, P., Pietikäinen, E. & Reiman, T. 2011. A Guidebook for Evaluating Organizations in the Nuclear Industry – an example of safety culture evaluation, SSM: The Swedish Radiation Safety Authority, 2011: 20.

Oedewald, P. & Gotcheva, N. 2015. Safety culture and subcontractor network governance in a complex safety critical project, Reliability Engineering and System Safety, Special Issue “Resilience Engineering”,141, 106-114.

Reiman, T. & Rollenhagen, C. 2014. Does the concept of safety culture help or hinder systems thinking in safety? Accident Analysis and Prevention, 68, 5-15.

Reiman, T. & Oedewald, P. 2009. Evaluating safety critical organizations: focus on the nuclear industry. Swedish Radiation Safety Authority, Research Report 2009:12.

Ruutu, S. 2015. System dynamics modelling of complex safety critical projects. VTT Research Report, VTT-R-05827-15, Espoo, 2015.

Starck, M. 2016. Key dimensions of project governance and their relation to nuclear safety - An explorative study of nuclear industry projects, Master’s thesis, Department of Management and Organization, Hanken School of Economics, Helsinki.

Tuovinen, J. & Gotcheva, N. 2017. Delays in creating and handling design documents: A case study of a complex nuclear industry project. VTT Research Report, VTT-R-00892-17, Espoo.

Turner J.R. & Sinister S. 2001. Project contract management and a theory of organization. *International Journal of Project Management* 19(8): 457-464.

Viitanen, K., Gotcheva, N. & Rollenhagen, C. 2017. Safety Culture Assurance and Improvement Methods in Complex Projects – Intermediate Report from the NKS-R SC_AIM, NKS-381. http://www.nks.org/en/nks_reports/view_document.htm?id=111010214063661

Viitanen, K., Gotcheva, N., Rollenhagen, C. & Reiman, T. 2018a. Safety Culture Assurance and Improvement Methods in Complex Projects – Final Report

from the NKS-R SC_AIM. NKS, NKS-405.http://www.nks.org/en/nks_reports/view_document.htm?id=111010214694225

Viitanen, K., Reiman, T., Rollenhagen, C. & Gotcheva, N. 2018b. Mapping Methodical Change in Safety Culture, Proceedings of PSAM14, The Probabilistic Safety Assessment & Management, September 16-21, 2018, CA, USA.

World Nuclear Association. 2018. *Lesson-learning in Nuclear Construction Projects*, April 2018. Report No. 2018/002, World Nuclear Association.

Ylönen, M. & Engen, O. A. 2016. Sociotechnical aspects in safety regulation in the high-risk industries. In Walls, L., Revie, M.,Bedford, T. (Eds). Risk, Reliability and Safety. Innovating theory and practice: Proceedings of ESREL 2016, Glasgow, Scotland, 25-29 September.

Ylönen, M. 2017. Licensee's relationship with the suppliers – Simple rules, lessons learned, in M. Cepin & R. Bris (Eds.) Proceedings of 27th European Safety and Reliability Conference, ESREL 2017, Slovenia, 18-22 June 2017.

2.3 Crafting operational resilience (CORE)

Jari Laarni[1], Hannu Karvonen[1], Jussi Korpela[2], Hanna Koskinen[1], Timo Kuula[1], Marja Liinasuo[1], Kristian Lukander[2], Satu Pakarinen[2], Markus Porthin[1], Vuokko Puro[2], Henriikka Ratilainen[2], Marika Schaupp[2], Laura Seppänen[2], Anna-Mari Teperi[2], Maria Tiikkaja[2,] Jari Torniainen[2], Kaupo Viitanen[1], Mikael Wahlström[1]

[1]VTT Technical Research Centre of Finland Ltd
P.O. Box 1000, FI-02044 Espoo

[2]Finnish Institute of Occupational Health (FIOH)
P.O. Box 40, FI-00251 Helsinki

Abstract

The CORE project aimed to identify the key characteristics of operational resilience at three defence levels of prevention, preparation, and consequence management and to study how these characteristics are manifested in operator behaviour and how they can be operationalized and measured. More specifically, we developed 1) tools and practices for gathering positive operating experiences from challenging operational situations; 2) training interventions and guidance to promote reflective thinking and learning and effective interruption management and troubleshooting among operators; 3) interventions and guidance for the management of acute stress and fatigue; and 4) guidance for the promotion of communication and coordination of activities in emergency exercises. In addition, a safety management procedure, Human Factors tool, was developed to analyse human contribution to nuclear safety.

Introduction

The aim of the CORE project was to improve safe operation of nuclear power plants (NPPs) by developing guidance, training interventions, and other practical solutions that promote resilience for the three general defence levels of prevention, preparation, and consequence management. Regarding prevention, we developed new Human Factors (HF) guidelines, models and tools and interventions that were tested and examined in simulated test environments and in workshops. Regarding preparation, we investigated the effects of acute stress on operator performance in simulated accident situations and collected operating experiences from successful actions and decisions and analysed the lessons learned from these experiences. Regarding consequence management and recovery, we developed methods and tools for crisis management that help stakeholders with different responsibilities to coordinate their actions to achieve a common operational picture. The chapter presents the findings of the research conducted in each work package of the project.

Learning from successes in nuclear power plant operation to enhance organizational resilience

Operating experience activities at nuclear power plants primarily consist of analysing adverse events and providing corrective action plans and lessons learned to avoid their recurrence. Modern developments in safety science, such as Resilience Engineering, have questioned the efficiency of failure-oriented approaches to learning and safety management and have presented alternatives. Complementary to the traditional approaches that emphasize avoiding things that "go wrong", it is proposed that in order to sustain safety effectively, the organisation also needs to ensure that things "go right", i.e. an organisation should focus on understanding the reasons behind successful activities (Hollnagel, 2014). We propose that promoting deliberate learning from success is important to (e.g., Hollnagel, 2014):

- Understand how normal daily work maintains nuclear safety
- Create new opportunities for learning and development of activities
- Avoid the formation of unwanted, potentially unnoticed tendencies such as taking successes for granted or misinterpreting failures as successes.

This work package focused on examining how learning from successes could be included in nuclear operating experience activities.

We carried out a literature review in the fields of safety science, organizational learning, leadership and management literature to identify theories that define success and provide insight into learning from successful experiences. Two empirical case studies were carried out at two Nordic NPPs. These findings are reported in more detail in a research report (Viitanen et al., 2016), several conference papers (Skjerve et al., 2017; Viitanen et al., 2017; Viitanen, Koskinen, et al., 2016) and a journal article (in preparation).

Success is a complex and multidimensional concept that can take many forms. Viewing success as just a "non-failure" may mean that many important and potentially informative aspects to success would be overlooked. Within the context of this study, we defined success as matching, exceeding or returning to an expected performance level. In order to capture successes, a range of metrics was identified. These were associated with processes, management (i.e., cost, budget, and scope), task/project output acceptance, organization (e.g., creating financial, technological, social or structural benefit for the organization), preparation for future scenarios, socio-affective impact, as well as lagging and leading safety metrics. Success can also have properties such as time and situation-dependence, and it relates to the objective or subjective expectations of multiple stakeholders.

We found that successes are often less salient and less likely to trigger intentional learning processes than failures. We also observed similar tendencies in normal situations where a task had been executed as expected: further investigation into how exactly the success was achieved (to create lessons) was often not found motivating – the successes were "business as usual". Facilitating learning from success is thus likely to require deliberate effort, such as its formal inclusion into existing practices for collecting or analysis purposes.

We observed that there was clear interest in successes at nuclear power plants: existing methods, albeit not very refined, were already in place that could be utilized to learn from successes in a more systematic way. For example, various types of staff meetings often included a success item - either formally or informally - thus potentially serving knowledge management functions such as knowledge acquisition and sharing (e.g., identifying and reflecting successful experiences), knowledge creation (e.g., joint innovating) and storage (e.g., minutes of meetings) (Viitanen et al., 2017). Often, however, more profound analysis of successes appeared to be less prevalent, which may create a risk of confirming unwanted practices: deliberate effort by operating experience personnel could be in a central role in identifying and counteracting these tendencies.

To summarize the overall findings of the study and to provide guidance to practitioners, we produced a guideline that proposes eight basic principles on how to learn from successes. The guideline also describes a step-by-step process for implementing it in practice. The guideline was reported as a conference paper for academic audience (Skjerve et al., 2017) and as a research report for practitioners (Skjerve et al., 2018). The purpose of this guideline was to provide insights to practitioners working at safety-critical organizations on how to promote learning from successes and to help develop practical tools to achieve this goal.

Developing work-based learning in the NPP domain

We assume that an important aspect in system resilience is the quality of operators' work practices. More specifically, as suggested by Savioja et al. (2014), being able to consider situations *interpretatively* in NPP operations provides a good basis for handling various kinds of challenges, even unexpected situations, and interpretation also supports the correct use of procedures. Being interpretative entails, for instance, a profound understanding of the plant dynamics as well as consideration of various information sources and dialogue within the operator crews prior executing operating procedures. According to Savioja et al. (2014), there are differences between operator crews in the interpretativeness of their work practices. In order to reduce these differences and to refine operators' work practices, operator training has to be improved.

However, we have identified challenges in the existing training practices, which can be seen as being at odds with generating interpretive workers (Wahlström & Kuula, 2016). For example, at one specific NPP, training is performed tightly in accordance of the official training curriculum, while more time would be needed for freely "playing" with the simulator; allowing understanding of plant dynamics holistically as considered necessary by the operators themselves. To allow the proliferation of good practices between the work shifts, the crews would also need opportunities to witness and exchange the practices with other crews. Furthermore, in terms of learning, it is problematic that the current safety procedures determine operator activity in detail – capability to handle new kinds of situations is not, thus, efficiently developed in the emergency training where these procedures are applied. Overall,

training is a top-down guided process, while exchange and creation of good work practices should be emphasized. Transition from the kind of training where learners are more or less “passive objects” to active and critical subjects is necessary. It is possible that some of these challenges are typical to the nuclear power plant work, because of safety critical and hierarchical nature of the domain (Wahlström & Kuula, 2016). Recently, however, more freeform simulator training has been taken into use at the plants, i.e., the operators have to solve a certain incident without procedures.

We assume that new training methods for the NPP domain could be developed by drawing from the Finnish Change Laboratory tradition (Engeström et al., 2014) and from the French Activity Clinic approach (Clot, 2009). To simplify, some of the main ideas of these approaches can be summarized as follows:

1. Double-stimulation: in dialogical workshops with workers, certain problem area or question can be considered with a new kind of presentation (or “stimulus”), such as, map or model; this technique enhances problem solving, concept formation and worker agency (Engeström et al., 2014)
2. Simple self-confrontation: the worker reviews sequences of his/her work activity together with the researcher, by using video material or other means of representation (Clot, 2009).
3. Crossed self-confrontation: a group or duo of workers review sequences of their work activity and discuss this together, with the guidance of a researcher (Clot, 2009; Seppänen et al., 2016).

More specifically, for enhancing simulator training, we have generated a self-evaluation method that aims to disseminate good practices by the means of guided dialogue among the operators. It consists of 1) personal evaluation, 2) group evaluation and 3) inter-group learning. Two questionnaires were constructed for self-evaluation in first two phases, including simulator task performance related open-ended questions and statements with rating scales. The group discussions were recorded for later analysis.

The operator crews’ reflections on the simulator tasks have been analysed. In short, reflection here indicates an activity in which the operators are analysing or commenting on themes prompted by their simulation experience or by the self-evaluation guideline. Reflection is expressed as uncertainty or doubt, dilemmatic speech, expressions of challenges, evaluation or questioning, and expressions of feelings (Heikkilä & Seppänen, 2014). As a result on the method introduced, we have found that reflection was quite abundant, consisting of more than a half of all discussions. In this sense, self-evaluations were efficient in enhancing operators’ reflection: they involved dialogue and reflection among operator crews about their own work practices and capability in emergency situations. Overall, findings portray a vivid discussion among the operator shifts encompassing the following themes: work practices, collaboration, plant dynamics and stress at emergency situations.

In future, new digital technologies could also be used in a post-simulator self-study: automatically created video representation of the performance can be imagined, including video clips synchronized with time-line of simulator events. This would require a synchronization of a video-observation system with the simulator system. With the various current software applications, audio could be represented

visually for indicating collaboration. With this kind of media representation of the simulator performance, the operators could be able to better reflect and compare activity in discussion after simulator sessions.

Supporting operational resilience in complex and dynamic environments

We studied the impact of multitasking and interruptions/distractions on work performance in safety-critical domains by preparing a literature review, and developed a method for the identification and classification of distractions in operator work, which tested in the analysis of simulated accidents. According to the literature review, interruptions and distractions that divert attention away from the task at hand to another task have typically a detrimental effect on performance (Laarni et al., 2016). We observed main control room operators' work in order to investigate the effects of interruptions and task switching in simulated accident management situations and the management of multiple parallel tasks (Laarni et al., 2016). It was found that the shift supervisors were interrupted somewhat more often than the other operators in loss-of-coolant accident (LOCA) simulation runs (Laarni et al., 2016). On the other hand, the interruptions were longer for reactor operators than for the other operators. Tasks that were most often interrupted were screen monitoring and procedure handling activities and panel operations (Laarni et al., 2016). A response to an interruption was typically immediate, indicating that the operators considered it necessary to respond immediately to the interrupter so that the latter does not need to wait for a long time. In general, external interruptions were caused by alarms, phone calls and other operators' comments. The shift supervisors interrupted reactor and turbine operators by asking questions or providing updates about important issues more frequently than the other way around (Laarni et al., 2016).

A review of the role of cognitive heuristics in process control work was prepared, and heuristics, biases and rules of thumb were collected by analysing debriefing interview sessions that has been collected in simulator settings (Laarni, in press). Because we have no direct access to people's thought processes, it is difficult to say what role cognitive biases play at the shop floor level, and how we could prevent them. Even though various kinds of de-biasing techniques are available, a quite common view is that it is very difficult to fight against cognitive biases, especially if they are based on automatic thinking processes.

There is evidence that control room operators have problems in diagnosing complicated events and multiple simultaneous events in process industry. Even though there is a lot of research on finding faults in complex incident situations, there is quite little knowledge of the problem solver's cognitive strategies, states and activities in troubleshooting situations. We conducted a literature review on diagnostic reasoning and troubleshooting in process industry. With regard to nuclear domain, better methods have to be developed to study diagnostic reasoning and trouble-

shooting in simulator or plant environments. For example, the process tracing approach has to be tailored to suit better the analysis of team collaboration and cooperation in incident and accident situations.

One of our main aims in the CORE project has been to develop new modelling tools for the analysis of distributed cognition in general and collaborative troubleshooting in particular. To that aim, we developed a modelling approach suitable for analysing collaborative diagnostic reasoning and troubleshooting of a NPP control room crew which is based on existing methods and tools. The approach describes the progress and evolution of a CR operator crew's knowledge states and communication throughout the critical sections of a simulator run. The model would be useful, for example, in the analysis of operator collaborative fault-finding behaviour in the Human Factors validation of CR systems.

Supporting operator performance in extreme stress

It is well known that acute stress affects cognition and performance roughly according to an inverted U-shaped function. Whereas low-to-moderate amounts of stress may improve cognitive performance, high stress typically has an impairing effect: attention is more focused but narrower (e.g., Skosnik et al, 2000), working memory capacity decreases (Hsu et al., 2003) and encoding to and retrieval from long-term memory becomes impaired (de Quervain et al., 2000).

Typically, stress is evaluated by collecting self-reports of experienced stress. Objective and unobtrusive measurements of workload and stress levels are needed to provide more accurate information on the state of the individual within the desired time frame, without disturbing the primary task. Once this is achieved, the evaluation of the effects of stress on operator performance becomes more reliable.

We conducted a literature review on the effects of stress on cognition and performance, with the applied focus on NPP operator work and some examples from other safety critical domains such as mining and aviation. We have disseminated the findings to the NPP personnel in the form of a research report and several lectures at both TVO Olkiluoto and Fortum Loviisa facilities.

One of the main goals of our study has been to quantify the stress of NPP operators during simulated incident and accident scenarios. The scenarios selected for the simulations were 1) malfunction of an oil pressure sensor, 2) fire and 3) radioactive steam leakage. We quantified the level of stress of 22 NPP operators during these simulated scenarios by questionnaires and ambulatory measurements of electrocardiography (ECG) and electrodermal activity (EDA). We also used accelometers to separate the effects of stress on physiology from the effects of physical activity, i.e., operators moving in the simulator. All the measures, namely self-reports and the physiological recordings of mean heart rate (HR), heart rate variability (HRV), and skin conductance response (SCR) indicated that the operators' stress was mild to moderate during the malfunctioning oil pressure sensor incident, and moderate to high during the accident scenarios of fire and radioactive gas leak-

age. The perceived and physiologically measured stress were low after the scenarios and during normal operation. We also detected signs of pretest excitement in the cardiac signal during the baseline period preceding the simulations. (Pakarinen et al., 2016; Pakarinen et al., 2018; Torniainen et al., 2016)

Before the simulations were carried out, we also built a model of the predicted stress from the operator instructor's rating on the stressfulness of the task and our assumption that the baseline periods and normal run would not be stressful. Further, we examined the relationship between predicted stress, and the physiological stress response of operators during the simulated scenarios. Interestingly, the predicted stress better matched the physiological responses of the operators, than did the operators' self-evaluated stress, apparently because of some operators' self-reports were in conflict with their physiological results.

In order to examine the association between stress and crew performance, the variability in two performance measures, the performance time and the operator instructor's evaluation of the performance, were modelled with the cardiac and physical activity of the operator crews. After each simulated incident and accident scenario the primary operator instructor evaluated the performance of the crew from four perspectives: 1) information seeking, 2) diagnosis and corrective actions, 3) use of emergency operations procedures and 4) collaboration and communication. We also calculated the overall score as a mean of the 1–4. Performance time was calculated as the time between the occurrence of the fault and the time it was completely resolved. We hypothesized that the stress levels of the crew would be associated with the crew performance in a way that those crews with the highest stress levels would show the poorest performance and those with the highest performance would exhibit the least stress.

From the six measures of operator crew performance only the information seeking performance and the performance time were associated with the physiological measures of operator stress. Both these performance measures were predicted by the cardiac indices of operator stress. The movement of the operator, as measured with the accelerometers was associated only with the information seeking aspect of performance, not with the performance time. As hypothesized, increased level of stress was associated with poorer performance, as well as with longer performance time. Otherwise, crew performance was robust, as the diagnosis and corrective actions, use of emergency operations procedures, and collaboration, were only weakly associated with the stress physiology.

The association between information seeking performance and stress might be explained by the larger requirement for cognitive processing at the information gathering phase of the task. These results show that psychophysiological measurements of stress and activity can provide valuable information on stress and its association with cognitive performance at work. The results also suggest, that the operator cognition and therefore performance may be more vulnerable to negative effects of stress in the diagnostic phase when the degree of structural support is low and the identification of the problem relies mainly on operators' cognition. On the positive side, is also suggests that the effects of stress may be effectively mitigated with support from EOPs.

Supporting resilience in emergency management

Vital functionalities of the society need to be secured in case of emergency. Emergency preparedness means readiness to act in case of emergency, supported by precautionary measures. Emergency exercises are an important part of such measures, maintaining and developing preparedness for emergencies which could have devastating consequences.

We studied emergency exercises from a theoretical (resilience), regulatory (e.g., YVL guides) and practical points of view, as realised in the Finnish operating nuclear power plants. Studies in the field, about practices and conceptions related to emergency exercises, have been performed by observing communication in an emergency exercise, by conducting key-person interviews, and by a survey among nuclear professionals (Loviisa and Olkiluoto personnel as well as STUK personnel).

Emergency exercises, in accordance with all activities in the nuclear domain, are to be conducted according to regulation. In Finland, emergency exercise activity is described in YVL C.5 4.3. We found out that these requirements are well fulfilled; the emergency organisations are established, the exercises conducted and evaluated as required by regulation in the both operating NPPs in Finland. NPPs organise also training to support effective emergency management. Emergency exercises are organised in three-year periods so that a regular exercise takes place once a year in minimum, whereas a large emergency exercise with several participating organisations takes place every third year.

We identified several development needs. The main developmental need identified was the lack of clearly defined objectives for the exercises. With such objectives, exercises could be planned and evaluated in a systematic way. In this way, the participating personnel would know what they are expected to do and eventually, the performance in exercises and consequently in a potential emergency situation as well would improve.

The developmental needs can be scrutinized from the perspective of resilience. To start with, resilience can be defined as features of safe and flexible socio-technical system. In the preparedness related system, the social part is the share of personnel which is nominated with vacancies, each vacancy possessing specific responsibilities during an emergency. The technical share is the technology used and affecting emergency related activities; part of the technology being used in normal daily routines and part is dedicated to emergencies only. Vacancy owners are given training and the functioning of the procedures and workflows as well as technology is tested and verified during emergency exercises. The basis for preparedness is thus set but it also can be improved.

The ability to learn from experience is the aspect of resilience the nuclear organisations seems to have the weakest point. The learning from experience is specifically supported by YVL guide, in the form of demanding that the licencees identify and report the defects or development areas and actions decided based on them. Thus, this is taken care of at least in the orgainsational level. However, exercise participants easily lack true feedback to learn. Personnel competence is vital, along with well-defined procedures and workflows. If something unexpected happens, and

if an emergency took place it would probably be unexpected, the readiness of each relevant role to act in that situation is crucial.

Feedback is related to the evaluation of emergency exercises. With no systematic evaluation, including feedback about the appropriateness of each action performed in the emergency exercise, it is hard to develop the preparedness in personal level. The building of relevant procedures and workflows partly compensate that, but there is always the share of human factor left, in the form of error or success. False conceptions and biases in performance are worth correcting, and the new ideas and especially successful performance are the cornerstones for better performance. This is important in the personal and also in the organisational level. The organisational level is reached by delivering and utilising this information more widely than among the people whose performance is the basis for this information.

Applying a HF tool to learn to analyse human contribution to nuclear safety

The latest debate concerning Human Factors (HF) in safety has stressed a need to a new perspective in safety management, in which people are seen as solutions to harness and presence of positive capacity (so called Safety-II), in contrary to traditional view (Safety-I), in which people are seen as source of failures and safety as a bureaucratic accountability (Hollnagel, 2014).

Also nuclear safety guidelines recommend incorporating systematic methods in the management system in order to identify and manage HF affecting safety. Competence should be developed in the management of HF, to identify the strengths, weaknesses, and areas for improvement of the safety culture especially in connection with operational events (OEs).

In our study in 2015-2018, we identified the current HF conceptions, practices and tools used by the nuclear safety organisations in the two NPPs and by Radiation and Nuclear Safety Authority (STUK). We then modified and tested a new HF tool for OE analyses and evaluated the prerequisites for its implementation in safety management practices The data was collected with document analyses (e.g. YVL guide, guidelines at each NPP), 22 interviews at NPP and STUK, and with intervention material from eight workshops with safety experts of two NPPs, NPP project and STUK. During the project, we modified, trained, tested, and implemented nuclear HF-tool version to include basic and refresher training, detailed tool for gathering investigation data from HF perspective (HF-fan), and designing combination of Accimap and HF-tool (HF-map) for OE analysis. The HF tool was used by safety experts of two NPPs, to recognize and analyse both positive (successes) and negative (risks, errors) contributing factors to OEs, thus aligning the latest safety debate (Hollnagel, 2014).

As results, the conceptions regarding HF were individual and error based and the safety procedures, reporting and analysis of OEs mainly focused on technical and risk aspects, indicating traditional safety thinking. HF remained abstract and there were no concrete tool in use, for learning and analysing HF in OEs. There was a

clear need to concretize HF, as well as to improve holistic knowledge of HF. Based on the HF tool testing, the HF tool was regarded as clear and easy-to-use, and it was considered a useful tool especially at OE analysis, reporting and training as well as to self-evaluation and for monitoring safety trends. It was found to offer a more accurate picture of the analysed OEs and HFs affecting OEs including the success factors, than current OE analysis methods (Teperi et al., 2017; 2018).

The implementation of HF tool had features of participative planning and design thinking, which would be useful in nuclear energy industry, to balance the technical-driven burden of the nuclear energy field. Although the HF-tool use had promising results, the future implementation would demand more systematic work with evaluating the quality of analysis and corrective actions based on findings with HF focused OE analysis, conducted by NPPs. Furthermore, collecting more accurate OE data would be a prerequisite for proper analysis of the real outcome. This would demand more HF competence and awareness not only by safety experts in NPPs, but also by the authority, top and middle management and supervisors in NPPs, operative personnel, to renew practices in safety management. For this kind of future work, we defined strategic guideline for HF implementation, reported as a part of CORE final report.

Conclusion

The CORE project developed operational practices that promote resilience in different levels of defence and that can be utilized by design organizations, NPPs and regulatory bodies. We developed guidelines for prevention, preparation and consequence management at the operational level and training interventions and tools that complement the existing guidance and training procedures. The project provides solutions and practices for better management of severe unanticipated accidents and challenging incident situations. The results will hopefully improve nuclear safety at the national level by improving ability to respond, monitor and anticipate to potentially disruptive situations at the operational level.

References

Clot, Y. 2009. Clinic of activity: the dialogue as an instrument. In A. Sannino, H. Daniels, & K. Gutiérrez (Eds.), Learning and expanding with activity theory (pp. 286–302). Cambridge: Cambridge University Press.

de Quervain D.J., Dominique, J. F., Roozendaal, B., Nitsch, R. M., McGaugh, J. L., & Hock, C. 2000. Acute cortisone administration impairs retrieval of long-term declarative memory in humans. Nature neuroscience, 3(4), 313-314.

Engeström, Y., Sannino, A., & Virkkunen, J. 2014. On the methodological demands of formative interventions. Mind, Culture, and Activity, 21(2), 118–128.

Heikkilä, H., & Seppänen, L. 2014. Examining developmental dialogue: the emergence of transformative agency. Outlines: Critical Practice Studies, 15(2), 5–30.

Hollnagel, E. 2014. Safety-I and Safety–II: The Past and Future of Safety Management. Farnham, Surrey: Ashgate.

Hsu, F. C., Garside, M. J., Massey, A. E., & McAllister-Williams, R. H. 2003. Effects of a single dose of cortisol on the neural correlates of episodic memory and error processing in healthy volunteers. Psychopharmacology, 167(4), 431-442.

Laarni, J. Cognitive heuristics and biases in process control and maintenance work. In press.

Laarni, J., Karvonen, H., Pakarinen, S., & Torniainen, J. 2016. Multitasking and interruption management in control room operator work during simulated accidents. In: Proceedings of HCI International 2016, Toronto, Canada, July 17 - 22, 2016.

Pakarinen S, Korpela J, Torniainen J, Laarni J, Karvonen H. 2016. Control room operator stress and cardiac activity in simulated incident and accident situations. In: Proceedings of the 39th Enlarged Halden Research Project Meeting, Fornebu, Norway, May 9th – 12th, 2016.

Patrick, J. 1999. Analysing operators' diagnostic reasoning during multiple events. Ergonomics 42, 493-515.

Savioja, P., Norros, L., Salo, L., & Aaltonen, I. 2014. Identifying resilience in proceduralised accident management activity of NPP operating crews. Safety Science, 68, 258–274. http://doi.org/10.1016/j.ssci.2014.04.008.

Seppänen, L., Kloetzer, L., Riikonen, J., & Wahlström, M. 2016. A developmental perspective to studying objects in robotic surgery (pp. 229–245). http://doi.org/10.1007/978-3-319-49733-4_14.

Skjerve, A. B., Viitanen, K., Axelsson, C., Bisio, R., Koskinen, H., & Liinasuo, M. 2017. Learning from successes in nuclear operations – A Guideline. Presented at the ESREL2017, Portorož, Slovenia.

Skjerve, A. B., Viitanen, K., Koskinen, H., Liinasuo, M., & Axelsson, C. 2018. Learning from successful operating in nuclear power plants - a guideline (No. IFE/E-2018/001). Institute for Energy Technology.

Skosnik, P. D., Chatterton, R. T., Swisher, T., & Park, S. 2000. Modulation of attentional inhibition by norepinephrine and cortisol after psychological stress. International Journal of Psychophysiology, 36(1), 59-68.

Teperi, A.-M., 2012. Improving the mastery of human factors in a safety critical ATM organization. Cognitive Science, Institute of Behavioural Sciences, Faculty of Behavioural Sciences, University of Helsinki, Finland. Doctoral dissertation.

Teperi, A.-M., Leppänen, A., Norros, L., 2015. Application of the HF tool in the air traffic management organization. Safety Science, 73, 23-33.

Torniainen J, Korpela J, & Pakarinen S. 2016. Control room operator stress and electrodermal activity in simulated incident and accident situations. In: Proceedings of the 39th Enlarged Halden Research Project Meeting, Fornebu, Norway, May 9th – 12th, 2016.

Viitanen, K., Bisio, R., Axelsson, C., Koskinen, H., Liinasuo, M., & Skjerve, A. B. 2016. Learning from Successes in Nuclear Power Plant Operation - Intermediate Report from the NKS-R LESUN (No. NKS-354). NKS. Retrieved from. http://www.nks.org/en/nks_reports/view_document.htm?id=111010213330253

Viitanen, K., Koskinen, H., Axelsson, C., Bisio, R., Liinasuo, M., & Skjerve, A. B. 2016. Learning from successful experiences: An undeveloped potential in the nuclear industry? Presented at the Enlarged Halden Programme Group Meeting, Fornebu, Norway.

Viitanen, K., Koskinen, H., Skjerve, A. B., Axelsson, C., Bisio, R., & Liinasuo, M. 2017. Modelling Organizational Learning from Successes in the Nuclear Industry – Staff Meetings as Forums of Knowledge Sharing and Acquisition. Presented at the 7th Resilience Engineering Symposium, Liège, Belgium.

Wahlström, M., & Kuula, T. 2016. Organizational self-determination and new digital self-study applications as means for developing nuclear power plant operation training. International Conference on Learning and Collaboration Technologies. Retrieved from http://link.springer.com/chapter/10.1007/978-3-319-39483-1_59.

2.4 Institutional strength-in-depth in the context of decommissioning and learning from incidents (ORSAPP)

Marja Ylönen

VTT Technical Research Centre of Finland Ltd
P.O. Box 1000, FI-02044 Espoo

Abstract

The goal of the study is to examine the robustness of Finnish nuclear community in the context of decommissioning and robustness of license holder in the context of incident investigations. The concept of institutional strength-in-depth, introduced by the IAEA (2017) refers to the openness, transparency and questioning attitude, in core organizations in the nuclear sector. The concept is a reference point when examining the robustness in the inter-organizational and organizational contexts.

The findings of decommissioning case show that Finnish nuclear community is relatively robust as regards institutional strength-in-depth and its characteristics, namely openness and transparency. However, the stakeholders' respect of each others' roles and responsibilities may hinder the questioning attitude, another characteristic of institutional strength-in-depth. Furthermore, there is no comparison whether VYR funding is sufficient. In order to enhance the robustness of nuclear community in the phase of decommissioning, it would be important to develop risk management towards taking better into account qualitative risks and critical points, such as organizational and motivational aspects.

Incident reports show that the instrumental rationality is licensee organization's principal way to handle and govern incidents and learn from them. Accimaps and use of pre-job briefings can be good tools but they remain inadequate to address broader social and organizational context related issues. Therefore, in order to improve the handling of and learning from incidents, and particularly the handling of communication and organizational factors related aspects, adoption of reflexive responsive rationality is recommended.

Introduction

Overall safety is topical in the Finnish nuclear community's parlance and this overall safety and robustness are approached from organizational factors' and institutional strength-in-depth (ISiD) perspectives. The study consists of two tasks. The first task deals with the robustness of Finnish nuclear community in the context of decommissioning that is relevant as regards overall safety. The analysis provides insights into strengths and possible weaknesses in the preparatory phase of the decommissioning and indicates how the robustness could be developed further in organizational aspects. The second task examines the robustness of licensee in the context

of incident investigations and learning from them. The study examines incident reports and their underlying rationality, on the basis of which the licensee organization approaches the incidents and learns from them. The latter analysis illuminates organizational rationality in the context of incident investigation and contributes to the organization's possibility to learn more.

Theoretical framework consists of application of theories of governance (Dean 1999). This emphasizes understanding the rationality, on the basis of which stakeholders approach and deal with decommissioning.

The research questions are the following:

- How robust is the Finnish nuclear community from the perspective of ISiD?
- What do the collaboration, expectations towards other organizations, as well as meanings related to decommissioning, reveal from the Finnish nuclear community's robustness in terms of institutional strength-in-depth?
- How is the collaboration between the core organizations?

The second task orientates from the concept of ISiD and leadership and management studies, where a distinction has been made between the instrumental rationality and the rationality based on reflexive responsive processes (Stacey 2012). This distinction is exploited in the study. The role of incident reports as a relevant source of learning at organizational context has been questioned by safety and organizational studies (Maslen and Hayes 2016). It is argued that incident reports often provide thin information and knowledge with regard to organizational learning (mt.). Thus, this aspect motivates this study together with the concept of ISiD (INSAG-27 2017).

The research questions are the following:

- What kinds of rationality guides the identification, handling and learning from incidents?
- What do the identification, handling and learning of incidents tell about ISiD?
- How could organization learn more?

The data and method of analysis

The data of the decommissioning case consist of decommissioning reports (Ylönen 2019) and 6 interviews with experts from the Radiation and Nuclear Safety Authority (STUK), representatives from the Ministry of Economic Affairs and Employment (MEAE), and experts from a power company. The duration of interviews was 1-1,5 hours. Despite the small number of interviewees, the study provides a sectional view over the decommissioning and the relationships between the organizations.

Thematic interviews were exploited as method of data gathering in the decommissioning case. Themes cover the main challenges related to decommissioning, cooperation between the organizations, expectations related to other organizations, funding mechanisms, attitudes concerning participation in commercial decommissioning. Interviews were first transcribed into files, then they were classified based

on the themes. After that, meanings related to the decommissioning were analysed, and underlying rationality of each theme was examined. Interpretations of interviews draw on studies on governance and the concept of ISiD. Qualitative content analysis was exploited as a method of analysis (Krippendorf 2004).

The data of incident investigation case consist of 19 incident reports, and interviews with 3 experts from the power company. The goal of the licensee organization is to collect information also about less important incidents and to learn from them. Therefore, incident reports provided by the company concerned cases, which were minor in terms of safety.

The incident reports were analysed based on the content analysis (Krippendorf 2004). First, all reports were written in the form of table and classified based on the following criteria: operation condition, safety class, safety effect, immediate cause of the incident, contributing factors, description of the event, lessons learned. Second, the main reasons for incidents were collected from the reports. Third, the underlying rationality related to incident investigations and learnings from incidents, particularly related to handling of communication and organizational factors, was examined. This underlying rationality affects sense-making of a situation, and what knowledge is regarded relevant, not to mention learning from incidents. Analysis and interpretations draw on studies on governance and leadership and management (Dean 1999, Stacey 2012).

Case 1: Decommissioning

The Ministry of Economic Affairs and Employment (MEAE) acts as an enabler in the decommissioning. MEAE is in charge of regulation of nuclear power by participating in updating the Nuclear Energy Act. MEAE takes part in preparation of decisions related license approval. It approves the license holder's waste management plans. The national funding for nuclear waste management (VYR), works under the MEAE. Furthermore, the MEAE is promoting the mutual collaboration of actors who are responsible for waste management. Moreover, the MEAE participates in international collaboration as regards decommissioning.

The Radiation and Nuclear Safety Authority (STUK) acts as a control authority as regards radiation and nuclear safety. STUK is in charge of updating the regulations and guidelines related to radiation and nuclear safety. Similarly, STUK provides guidance via requirements e.g. what can be done within the operation license and within the decommissioning license.

License holders are obliged to take care of waste management. They are obliged to prepare the decommissioning plan and gradually develop it to a more detailed direction. The updated decommissioning plan is sent to the MEAE every sixth year, but the updating work is continuous. License holder's duty is to apply for decommissioning license and to be in charge of decommissioning and dismantling of the plant. In addition, license holder is responsible for the final disposal of the nuclear spent

fuel and wastes. Furthermore, license holders are encouraged to develop decommissioning services and participate in commercial decommissioning projects as service provider together with other companies. This is one way to tackle the images of sunset area or funeral procession associated with the decommissioning.

Summary and conclusions concerning decommissioning

Meanings related to decommissioning are relevant because they tell about motivation of actors as regards decommissioning. Experts of the MEAE emphasized reputation and credibility of Finland as a country of high technology and Posiva as the world's first disposal for spent nuclear fuel. These factors create pressure to succeed in decommissioning. Furthermore, representatives of the MEAE associated successful handling of decommissioning with public acceptability of nuclear power. The MEAE aims to create positive image about the decommissioning by referring to abovementioned aspects and Finnish sense of responsibility and possibility to participate in decommissioning business.

Experts of STUK approached decommissioning from the pragmatic viewpoint. They stressed continuous learning process, need to update the requirements and need to create own solutions and decision-making as recards decommissioning due to the lack of common guidelines for decommissioning in the international level. Difficulties to create common international guidelines for decommissionin is due to the fact that each country has its own practices and ways to implement decommissioning.

Representatives from one power company were interviewed that means that the meanings are indicative, not representative to all power companies. The power company expressed its active and responsible role in planning of decommissioning It stressed its good preparedness for decommissioning, and it trusted in its own organization and plans.

MEAE, STUK and license holders have clear roles and territories that each stakeholder respects. Furthermore, stakeholders trust in each other. These factors provide good preconditions for safe and successful decommissioning. Collaboration has been supported via work groups, (JETI, VYR) and mutual cooperation between the power companies. Furthermore, collaboration is under development. These contribute to openness that is relevant feature of institutional strength-in-depth thinking.

Finnish nuclear community can be interpreted to be relatively robust as regards the following aspects: high technology that is manifested in the final disposal of spent nuclear fuel storage; planning of decommissioning has been started early; legislation regarding decommissioning has been updated; funding mechanism is unique and power companies invest yearly in VYR fund; apart from spent nuclear fuel, the radioactive wastes of operating plants will be placed on the site that makes process straightforward; collaboration between the stakeholders is relatively easy and flexible. Finnish nuclear community is relatively robust also as regards institutional strength-in-depth and its characteristics, namely openness, transparency. However, the stakeholders respect of each others' roles and responsibilities, may

hinder the questioning attitude that is another characteristic of institutional strength-in-depth.

From the point of view of overall safety there is a danger that knowledge related to the critical points and factors in decommissioning is shared by small group of people but that knowledge is not spread throughout the organization. There is a need for holistic understanding of decommissioning and better integration of different expertise into planning of decommissioning. For instance, economy, safety, technical and organizational aspects shall be dealt with as intertwined factors. This is important from the overall safety perspective. In the final report recommendations are provided as regards organizational aspects in decommissioning.Similarly, from the overall safety perspective, the comparison of cost estimations with the foreign decommissioning projects is seen relevant in order to evaluate the sufficiency of VYR funding.

In order to enhance the robustness of Finnish nuclear community in the preparatory phase of decommissioning, it would be important to develop risk management towards taking better into account qualitative risks and critical points such as, organizational and motivational aspects. For instance phases, through which the operating organization transforms to decommissioning organization, the size of organization in the decommissioning phase, maintaining motivation of the personnel, and improving the competence of personnel as regards decommissioning would be important to deal with thoroughly and well before the decommissioning phase. Furthermore, in order to enhance robustness of the Finnish nuclear community, it would be important that all stakeholders share similar understanding about the broad meaning of decommissioning relating to the image of Finland as a country of high technology and to the future prospects of the nuclear energy. This way stakeholders could be motivated to act in concert, for safer and successful decommissioning.

License holders are encouraged by the MEAE to develop decommissioning services and participate in decommissioning projects as service provider together with other companies. This is one way to tackle the images related to sunset area or funeral procession associated with the decommissioning, and to learn from decommissioning as well as to keep personnel motivated.

Finally, due to that fact that there are different ways to implement decommissioning and the international guidelines for decommissioning are lacking, the role Finnish nuclear community, and all stakeholders are emphasized. Therefore, stakeholders' mutual cooperation is important.

Case 2: Underlying assumptions concerning incidents and learning from them

In the licensee organization, incident reports were still in the beginning of 2000 concise, maximum 2 pages long and technically oriented. Reports did not address decision-making chain or different phases that had led to incident. In the earlier days the requirements concerning incident reports were not so specific as currently and

therefore reporting style varied. For these reasons learning from incident reports remained poor.

Gradually incident reporting have become more thorough, thanks to tighter requirements. Reporting started to change from a component and worker focused thinking towards organization's impacts on incidents. In 2012 investigation of incidents were expanded so that an own operation experience group was established in the company. Documents changed into e-format in 2013 and reports became more wide in 2014. Especially more demands were targeted to the content of reports and efforts have been put on human and organizational aspects. Furthermore, attention has been paid also to less important incidents that can be seen as a good sign and willingness to learn. From 2016 onwards, the incident reports include also positive aspects. The goal of reporting is to take into account also success factors.

The incident reporting has gone through a development trend from concise technically oriented incident reports towards broader, organizational factors including reports, and from failure orientation towards positive factors. Similarly, methods, such as accimap, have contributed to identification of causes and effects, and understanding of the incidents. Accimap method has brought systematic structure and uniform quality to the incident reports, however, it is not ideal for illustrating organizational aspects. Thus, there are things that requires further attention in incident reporting.

Challenges related to incidents investigation are resources. There are resources in use, but thorough investigation requires lot of resources. Challenges include also identification of incidents. Despite that the operating experience unit has different technical expertise in their use, when they investigates incidents, it does not include all technical areas. In addition, even though organizational aspects are more broadly taken into account, it is not clear how deeply and adequately organizational aspects are approached and handled in the organization. Experts' education and frameworks also circumscribe incident reports.

Another challenge relates to learning. There are relevant stakeholders involved in incident investigations, and among them learning occurs, but how well the message spreads throughout the organization is another thing. Hence, there is a big field of work as regards improving learning from incidents.

Summary and conclusions concerning incident investigations

Robustness of organization i.e. its institutional strength-in-depth can be assessed in relation to organization's approaches to incident investigations and ability to learn from incidents. Incident reports show that the instrumental rationality is organization's principal way to handle and govern incidents and learn from them. Instrumental rationality manifests itself in the form of procedures, such as accimap, which provides a general framework for investigations. Accimap focuses on causes and effects, but is not ideal for illustrating organizational aspects. Similarly, tools like fonetic alphabets are good practical tools but they do not help if there are deeper

problems related to social interaction in organization. Therefore, if organization aims at deeper and broader learning, Instrumental rationality is not an adequate approach. By resorting to instrumental rationality, incident reporting and learning from them remains thin. Inadequate learning from incidents is noticed in the studies on safety critical organizations in general (Meslen and Hayes 2016). Focus on minor incidents does not contribute to learning, if rationality and assumptions on the basis of which organization identifies, investigates and learns from incidents, are not broad enough.

In order to improve the handling of and learning from incidents, and particularly the handling of communication and organizational factors related aspects, the reflexive responsive rationality would be needed. In instrumental rationality approach communication is often seen as a transfer of information from a sender to receiver and efforts are made to make the transfer of information efficient and clear. Instead, reflexive responsive rationality would mean taking into account broader social context within which communication occurs. Communication would be approached as a form of social interaction that is affected by social context, power relationships, cultural frameworks, experts' frameworks or meaning constitutive boundaries. More nuanced understanding of interaction in organization context would be beneficial for learning from incidents.

The benefit of adoption of reflexive responsive rationality would be that deeper causes of incidents and deficiencies in communication are illuminated, and this would mean that better means to govern and prevent some incidents could be developed. Adoption of reflexive responsive rationality would require competences to open up the social and organizational relationships and this would require experts in social sciences. Improvement of incident investigation towards reflexive responsive rationality would require attitudinal and resource-based support from organization.

There has occurred some recent developments towards reflexive responsive rationality in incident investigation. The license holder organization addresses the background factors of incidents that refer to organization's structures and leadership. However, it is much easier to resort to instrumental rationality -based corrective measures, such as purchasing a new adjustable wrench to a fitter than to address that there would be something to be corrected in the supervision of work and leading. License holder has actively developed its incident investigation practices and learning from incidents. Willingness to learn from minor incidents shows license holder's ambition and motivation. Instrumental rationality way of governing incidents is prevailing and it has provided good pragmatic tools. However, instrumental rationality cannot identify patterns that would require understanding of broader social context. Therefore, new perspectives and approaches, such as reflexive responsive rationality, would be needed alongside with the instrumental rationality, to improve incident investigation. In the final report recommendations and checklist are provided as regards organizational aspects and reflexive responsive process in incident investigation.

References

Dean, M. 1999. Governmentality. Power and Rule in Modern Society. London: Sage.

INSAG-27. 2017. Ensuring Robust National Nuclear Safety Systems – Institutional Strength in Depth. A report by the International Nuclear Safety Group. IAEA.

Krippendorff, K. 2004. Content Analysis: An Introduction to its Methodology. Second Edition. Sage Publications, London.

Maslen, S. and Hayes J. 2016. Preventing Black Swans: incident reporting systems as collective knowledge management. Journal of Risk Research, 19, 10: 1246-1260

Stacey, R. 2012. Tools and Techniques of Leadership and Management. Meeting the challenge of complexity. Routledge, Taylor and Francis Group. London, New York.

Ylönen, M. 2019. Institutional strength-in-depth in the context of decommissioning and learning from incidents (ORSAPP). SAFIR final report. VTT-R-00139-19.

2.5 Integrated safety assessment and justification of nuclear power plant automation (SAUNA)

Antti Pakonen[1], Jarmo Alanen[1], Kim Björkman[1], Igor Buzhinsky[2], Jan-Erik Holmberg[4], Hanna Koskinen[1], Jari Laarni[1], Joonas Linnosmaa[1], Risto Nevalainen[3], Nikolaos Papakonstantinou[1], Tero Tyrväinen[1], Eero Uusitalo[5], Janne Valkonen[1], Timo Varkoi[3], Valeriy Vyatkin[2]

[1]VTT Technical Research Centre of Finland Ltd
P.O. Box 1000, FI-02044 Espoo

[2]Aalto University, Department of Electrical Engineering and Automation
P.O. Box 15500, FI-00076 Aalto

[3]Finnish Software Measurement Association FiSMA ry
Tekniikantie 14, FI-02150 Espoo

[4]Risk Pilot AB Suomen sivuliike
P.O. Box 72, FI-02101 Espoo

[5]IntoWorks Oy
Liitintie 14, FI-90630 Oulu

Abstract

Our general objective in SAUNA (2015-2018) has been to develop integrated methods and tools for safety assessment and transparent safety demonstration of nuclear power plant instrumentation and control (I&C) systems. Due to the multidisciplinary nature of the nuclear power plant as a whole, I&C safety assessment calls for an overall safety point-of-view. We have worked towards that goal by 1) specifying model-based Systems Engineering approaches for I&C, 2) developing concepts and models for analysing Defence-in-Depth issues in I&C architectures, 3) integrating existing methods and finding novel tools for analysing overall safety (with particular focus on formal verification), and 4) developing model-based ways for attesting conformity in the I&C qualification process.

Introduction

The key challenge in assessing the overall plant safety of nuclear power plant instrumentation and control systems (I&C) is to account for all types of hazards, all the different disciplines and types of system elements (technical, human, environmental…) and all the life-cycle phases and activities.

Accordingly, the overall objective of SAUNA (2015-2018) has been to create integrated methods and tools for safety assessment and transparent safety demonstration of nuclear I&C systems. While focusing on I&C systems and their human users, we have considered the power plant and the people involved in its development, licensing and maintenance as a complex sociotechnical system. As the basis for integrating different aspects and disciplines of safety into a consistent framework, we have tried to adapt good Systems Engineering practices to the needs of the domain.

To facilitate collaboration, we have developed common terminologies, documentation practices and information models. Specific focus has been on the Defence-in-Depth architectures. A key example of a shared model is the virtual plant developed (primarily to support probabilistic risk assessment) first with Nordic partners, and then in the OECD working group project DIGMAP.

For the assessment of overall safety, we have 1) integrated and co-used existing, established methods and tools, as well as 2) investigated novel methods and tools particularly tailored for multidisciplinary analysis. Particular focus in integration has been on finding new ways to apply a formal verification method called model checking. Examples of novel approaches have been System-Theoretic Process Analysis (STPA) and Architecture Description Languages (ADL).

Finally, we have, together with Nordic partners, developed guidelines and practices for argumenting the safety of I&C systems in a structured, model based way. We have also demonstrated how our model for conformity assessment can be used to support qualification of I&C.

Safety Systems Engineering

Model-based I&C safety engineering

ISO/IEC/IEEE 42010 defines a model as follows: “M is a model of S if M can be used to answer questions about S.” In that sense, all kinds of typical engineering artefacts (work products) that are created to specify or describe a system are models. This would make all systems engineering to be model-based systems engineering. To make the difference, we use the definition by INCOSE for model-based systems engineering: “Model-based systems engineering (MBSE) is the formalized application of modelling to support system requirements, design, analysis, verification and validation activities beginning in the conceptual design phase and continuing throughout development and later life cycle phases.” (INCOSE 2007). The difference here to the traditional SE is in the use of formalised or semi-formalised, machine readable, models or virtual engineering artefacts instead of text processing documents to specify and describe the system-of-interest. This does not mean that documents are not used in MBSE, but it means that MBSE is not based on documents but on formalised, semi-formalised, or visual models. As a consequence, the role of documents changes: in MBSE, the documents are a means to present infor-

mation (including models) instead of being containers of information. This fact encourages using automatic or semiautomatic document generation, which is not possible in traditional SE.

The goal was to promote moving from document centric systems engineering towards MBSE also on engineering management level. Hence we created an engineering process constructs model – or, in fact, enhanced the one presented in ISO/IEC/IEEE 15288. Our process constructs model is depicted in Figure 1.

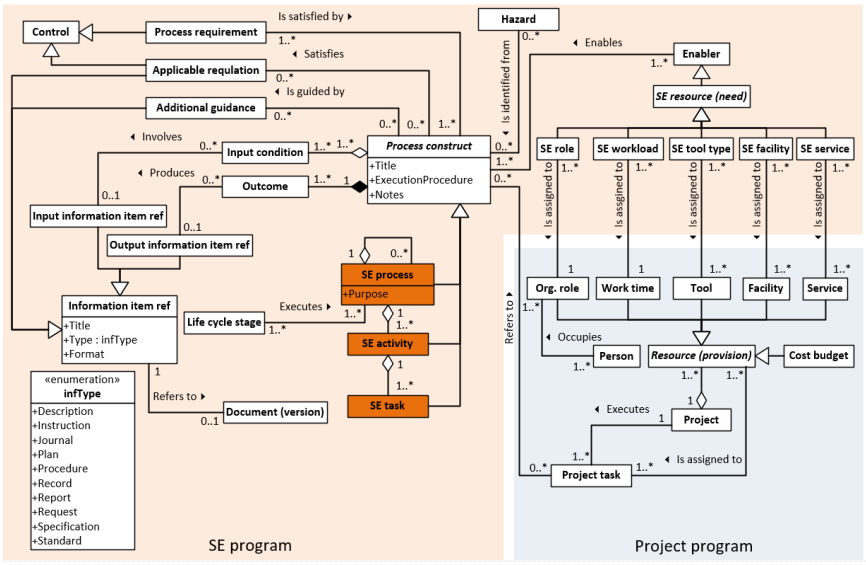

Figure1. Engineering process and project constructs model. Also the main project artefacts are added to illustrate the interface between the SE program and project program (Alanen & Tommila 2016).

The process construct model in Figure 1 provides some additional elements compared to the ISO/IEC/IEEE 15288 model (and omits the Note element). The main advantages of the new elements are that the engineering processes can thus systematically be traced (facilitated by a suitable software tool) to life cycle stages, process requirements, outcomes and process hazards. Furthermore, the model facilitates database-oriented implementation of engineering process descriptions. This has several advantages, for example the possibility to automatically generated process description documents and the possibility to use forms to capture the necessary information. Forms allow provision instructions about what should be input and even narrow the input information, in some cases, to a forced list of possible selections; this makes information from different engineers more consistent and concise.

Traditionally, the IAEA and the STUK (Säteilyturvakeskus; Radiation and Nuclear Safety Authority) regulations do not recognise systems engineering as such

but state requirements on the management system of the Nuclear Power Plant (NPP) organisations and their safety-significant suppliers. In our study (Alanen & Salminen 2016), we prove that most of the management system process requirements of IAEA and STUK can be satisfied by applying the systems engineering processes of ISO/IEC/IEEE 15288. Hence we created a prototype management system using Microsoft SharePoint platform such that the engineering process constructs model elements in Figure 1 were implemented as SharePoint lists. The information in the SharePoint lists were then dynamically imported into the engineering process descriptions realised by SharePoint wiki pages. An example of such process description can be found in (Alanen & Salminen 2016). The process descriptions include, among others, the execution procedure descriptions to describe the flow of activities. In addition, in this case we applied MBSE to make the procedure descriptions more formal. An example procedure description of *Stakeholder needs and requirements definition process* using SysML activity diagram notation is provided in (Alanen & Tommila 2016). The particular procedure description is dynamic, for example, the process requirements depicted in the procedure diagram are not written to the diagram but are dynamically retrieved from the SharePoint list that stores all the process requirements.

Systems engineering starts with creating a Systems Engineering Management Plan (SEMP). In our work (Alanen & Salminen 2016), we exploited the model based process descriptions to create a SEMP template for NPP I&C systems. The SEMP table of contents is presented in (Alanen & Salminen 2016).

Modelling and analysing defence-in-depth

Defence in depth (DiD) is a key design principle of complex systems for enabling overall safety. Our first focus was to establish the state of the art in DiD, based on literature and on interviews with power utilities and STUK. Our effort then focused on developing methods to support the early assessment of DiD attributes (such as redundancy, isolation, diversity, etc.) in complex systems.

One of the crosscutting topics in the SAUNA project is overall safety which, when looked from the safety engineering perspective, is concretized in the plant-level DiD architecture. A second main topic in SAUNA, instrumentation and control (I&C), has a major role in the DiD implementation. Therefore, the design decisions concerning DiD and I&C architecture, for example independence of DiD levels and redundancies, are critical and should be verified as early as possible.

In order to provide a basis for modelling and model-based safety assessment, we started by reviewing the principles, challenges, terminology and assessment methods related to DiD (Tommila & Papakonstantinou 2016). We learned that DiD continues to be a major design principle for nuclear power plants. Partly due to the Fukushima disaster, there is a debate going on its scope and interpretations concerning, for example, human and organisational factors and extreme conditions. The concrete challenge is to find good technical solutions and practices for development and assessment. Moreover, many terms related to DiD (e.g. physical separation and functional isolation) and failure behaviour (active failure, failure mode,

etc.) would still need clarification to provide a good basis for computer tools. As a complement to Probabilistic Risk Analysis (PRA) of digital automation (see below), also other kinds of models and simulation and reasoning algorithms would be needed for analysing the DiD solutions at early stages of development. With this in mind, as described in the sections below, we have explored various approaches and proposed methodologies for the analysis of hidden dependencies and failure propagation paths.

Failure propagation between redundant systems

We developed a method for estimating the failure propagation risk between uncoupled systems in constructed environments (O'Halloran et al. 2015). The system components are given 3D coordinates (placed in the environment) and a list of potential failure modes and related probabilities is generated. We developed a software tool called Uncoupled Failure Flow State Reasoner (UFFSR) which traverses through all the components and based on the nature of the failure mode (e.g. water leak, steam leak, explosion) and the location it calculates the propagation probability of that fault through the environment to a component belonging to a redundant subsystem. The UFFSR tool provides a report of the failure propagation paths and a total risk estimation for the design.

Cable routing when redundant systems are present

In complex systems with multiple redundancy (e.g., 4 redundant systems), it may not be possible to completely isolate the cabling required for the redundant systems. This introduces a risk of failure propagation. We proposed the Cable Routing Function Failure Analysis (CRFFA) functional model based method for cable routing aiming to minimize this risk of failure propagation between redundant systems (O'Halloran et al. 2016). This method calculates all the possible arrangements of cable bundles, rejects the ones that lead to risk higher than a set threshold and ranks the acceptable routing solutions.

Model driven approach for early assessment the reliability of Emergency Operating Procedures

Human factors are an important aspect when considering complex system safety. We proposed the early Model-based HRA (eMHRA), an early safety assessment method for Emergency Operating Procedures (EOPs) (Papakonstantinou et al., 2016). We developed a metamodel that can be used to model EOPs with the addition of SPAR-H Human reliability attributes. These EOPs can be automatically assessed and the total Human Error Probability can be calculated using a software tool.

A model driven approach for assisting the generation of fault trees, extension for generating hybrid fault and threat trees.

A multidisciplinary dependency model of a complex system contains significant amount of information that can be used to model potential propagation of failures initiated by faults or by security threats. We developed a method for extracting fault tree statements that can be compiled into fault trees from a High Level Interdisciplinary Model (HLIM) of the complex system under study (the case study used to demonstrate the method was a spent fuel pool cooling system) (Papakonstantinou et al., 2018). The dependency model was then extended with malicious actors to allow the method to produce statements that include also security threats as basic events. This lead to the generation of hybrid threat/fault tree statements that could be combined to produce trees (see Figure 2) (Papakonstantinou et al., 2019).

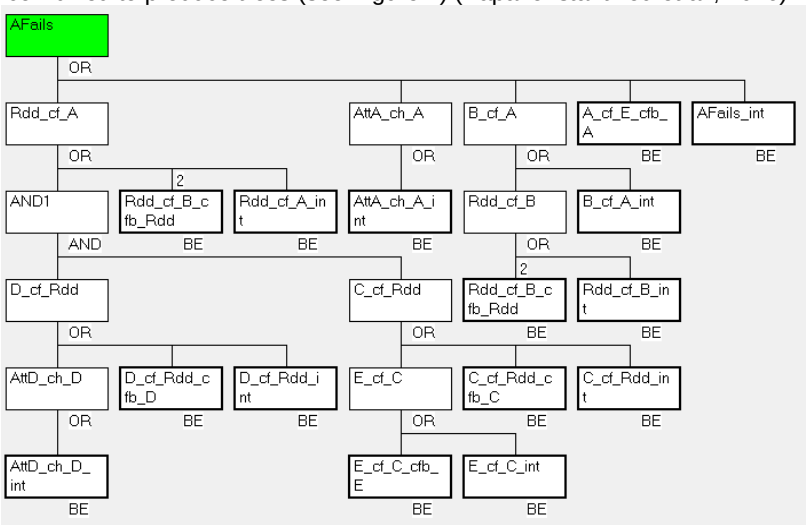

Figure 2. An example of a hybrid threat and fault tree of a system with five components (A to E), four attackers and one redundancy Rdd between components C and D. The basic events are either security related (e.g. AttD_ch_D_int=Attacker D causes harm to component D because he has internal motives) or reliability related (e.g. E_cf_C_cfb_E=Component E causes component C to fail which then causes E to fail).

Model driven early assessment of Defence in depth

The practical early application and assessment of DiD is a challenging task. Based on the state of the art report on DiD we proposed a metamodel for creating High Level Interdisciplinary Models (HLIMs) which also include DiD attributes which help the assessment of the design (Papakonstantinou et al. 2017). A HLIM is a dependency model that captures the human factors, electrical, automation, process and environment aspects of a complex system. We developed a set of DiD guidelines

which should be followed early on in the design process. A software tool can parse the HLIM and assess these rules. The results can be used to improve the design until it is acceptable.

Modelling of digital automation systems

Challenges with modelling of digital automation systems in the context of probabilistic risk assessment (PRA) comprises of both functional and physical complexity of automation systems relevant to safety, multitude of failure modes that may need to be considered and scarcity of representative reliability data, which is needed for quantification. All these are culminated in software systems but a proper consideration of hardware is also relevant for PRA.

With regard to modelling, an example model was developed in the previous NKS DIGREL project, representing a fictive BWR NPP with four redundant safety systems and a diversified four redundant reactor protection system (RPS) (Authén et al. 2015, Holmberg 2016). We have utilized this DIGREL model in further studies such as assessment of defence-in-depth (DiD), analysis of spurious actuations, comparison with model checking and in an international benchmark study. As the I&C architecture itself with multiple I&C systems has safety significance, we also created a roadmap to expand the DIGREL model with a reference I&C architecture and took the first steps, ending where cross-disciplinary design inputs (i.e. functions) are required (Uusitalo & Koskela 2015).

With regard to software reliability analysis, we have studied the confidence building in the method to estimate application software failure probability (Authén et al. 2016). The impact of pooling data from high and low demand systems is discussed. Also the principle of the probability estimation has been adjusted from the approach developed in the DIGREL project (Bäckström et al. 2015). A solution for the software complexity assessment was prepared.

I&C failure data is one of the information sources proposed to be used for the assessment of I&C reliability. Vendors of digital I&C have shown to be potential data sources as they typically have access to experience data from many plants, have needed insight on the software development processes and are capable to analyse the causes of the detected failures. The OECD/NEA ICDE (International Common Cause Failure Data Exchange) project has started collection of digital I&C related failure data in 2015. ICDE's primary focus is on understanding of failure causes and ways of prevention, and reliability quantification is not pursued. Thus, the digital I&C related failure data collected by ICDE does not likely support PRA in the best possible way. International collaboration and discussions are still needed in order to forward the use of I&C failure data in PRA.

Spurious actuation is a functional failure mode when a component performs a function without a real demand. Spurious actuations are of special interest for I&C due to complex effects via system dependences and due to a huge number of possible failure locations. There is a need to develop a reasonable but comprehensive

approach both for deterministic (Pakonen & Björkman 2017) and probabilistic analyses. We have compiled requirements to analyse spurious actuations, prepared an analysis approach and outlined a generic failure modes taxonomy based on von Wright's theory on concept of action (Authén et al. 2016).

Working Group on Risk Assessment (WGRISK) of OECD Nuclear Energy Agency initiated a project called DIGMAP (Digital I&C PSA - Comparative application of digital I&C modelling approaches for PSA) in 2017 to compare digital I&C modelling approaches used in different countries (Porthin 2018). Participating countries include Republic of Korea, Switzerland, Finland, Germany, France, The Netherlands, United Kingdom and Czech Republic. We have participated in the coordination of the project. In the project, a simplified boiling water reactor plant design and a generic digital RPS architecture have been developed based on the DIGREL model previously developed in SAFIR and NKS projects (Authen et al. 2015, Holmberg 2016). Fictive failure data have also been provided along with the plant and system description. The modelling will focus on a loss of main feed water scenario. The modelling work has been started in 2018, but not finished yet. The modelling approaches of different participants will be compared in 2019. The comparison will particularly focus on challenging issues, like fault tree modelling of fault-tolerant techniques and software, and selection of level of detail and common cause failure groups.

We have developed a tentative version of a PRA model to be included in the comparison (Tyrväinen & Porthin 2019). The selected modelling approach is close to the previous model of the DIGREL project, employing small fault trees as building blocks (Authen et al. 2015). I&C component failures have been divided into detected failures and undetected failures. Significant portion of the contribution of the RPS related risk comes from application software failures, along with undetected hardware failures. On the other hand, detected hardware failures in the RPS have insignificant contribution to the core damage risk, likely because spurious actuations have not been analysed. The importance of automatic testing and periodic testing as fault tolerant techniques to reduce the risk of undetected hardware failures was recognized in the sensitivity studies. Some of the results however depend a lot on modelling assumptions that are based on a quite broadminded system description. The results should not be assumed applicable to real life systems as such.

One of applications areas of PRA is to assess the defence-in-depth (DiD) concept of the design (Authén et al. 2016, Holmberg et al. 2017). DiD requirements can be grouped into four categories: 1) deterministic plant condition category related requirements, 2) probabilistic plant condition category related requirements, 3) independence requirements between DiD levels and 4) individual DiD level strength requirements. Deterministic and probabilistic safety assessments (DSA, PRA) rely on the identification and assessment of a number of scenarios which form the so-called design basis of the plant. DSA and PRA should be carried out in an integrated manner to save analysis resources as well as to reach a common and broad understanding on issues important to safety. The logic model of PRA provides a powerful tool to complement the deterministic assessments.

The assessment of DiD and diversity is in principle straightforward for PRA, e.g., risk metrics can be used to evaluate DiD levels 3, 4 and 5. A PRA model always includes uncertainties, which needs to be accounted for and argumented, especially when comparing with deterministic assessment. Regarding digital I&C, the focus of the assessment is on the DiD levels 1, 2 and 3. DiD level 4 (severe accident management) can be also assessed, but it is quite simple from the I&C point of view. An important question is how detailed the logic model and simulation models should be. Generally, a failure analysis of I&C is a demanding task. Previous research work has given guidance for the definition of failure modes but there are still open issues in this task (Authén et al. 2015). Failure propagation can be analysed only in limited manner following on some analysis assumptions. A crucial issue is which common cause failures (CCF) should be postulated and how CCF should be defined.

As an example, we have studied the assessment of preventive safety functions, which belong to the defence-in-depth level 2 (Holmberg et al. 2017). DiD level 2 is interesting since it overlaps with DiD level 1 and 3 both functionally and with regard to system arrangements. Secondly, the role of DiD level 2 has been somewhat diffuse both in DSA and PRA, and there are, e.g., some differences in the design requirements for DiD level 2 functions and systems. In current PRA models, only a fraction of DiD level 2 functions and associated systems are included. Based on the example it is evident that the preventive safety function of DiD level 2 can be implemented in PRA models. For PRA event trees, the implementation is a quite straightforward procedure. The main challenges are expected in the initiating event analysis and system analysis parts of PRA modelling.

Another application of PRA that we have studied is the risk-informed safety classification of structures, systems and components, especially related to electric and automation systems (Holmberg 2018). The safety classification shall basically follow the functional importance of the items. One challenge with the nuclear safety classification is that different classification systems are used in different countries and standards. Even if certain classification scheme can be agreed upon, it is not straightforward how the classification should be carried out for various components. At higher plant and system level, the safety importance of functions can be defined directly, but the classification of smaller components requires further assessments. In principle, a component's safety class follows its functional importance. Downgrading is possible if mitigative factors and reliability arguments can be shown. The importance of finding correct safety class is that it determines the quality assurance requirements for the component. We have outlined a risk-informed safety classification approach for the components, based on both probabilistic and deterministic assessments. Emergency diesel generator system was used as an example.

Formal verification methods

User-friendly model checking

To apply model checking in industrial practice (Pakonen et al. 2017), experts need profound knowledge and experience. This is caused by the need to apply many complex, non-automated steps, including the following ones:

1. Preparing the formal model of the system to be verified and simplifying it in order to make model checking computationally feasible.
2. Formalizing natural language specifications into the form suitable for model checkers, such as temporal logics.
3. Interpreting the results of formal verification, which are often represented in the form of counterexamples – model behaviours showing that the formal specification is violated.

The necessary level of knowledge and expertise is difficult to obtain. Even experts may also exclude important system behaviours from consideration, miss certain software faults due to erroneous formal specifications, or interpret the results of verification incorrectly.

In SAUNA, in order to increase the level of automation of steps (2) and (3), we worked on making model checking more user-friendly. The current practice of performing step (2) is completely manual: natural language requirements are formalized into temporal languages, such as linear temporal logic (LTL) or property specification language (PSL). First, we focused on the observation that in the nuclear automation field temporal properties of particular types, or patterns, prevail. We found (Pakonen et al. 2016) that more than 90% of all temporal properties that were model-checked in VTT's customer projects belong to as few as ten patterns, such as invariance or request-response. In parallel, we studied existing user-friendly formal specification languages, especially visual ones, and evaluated (Buzhinsky 2016) their applicability to specify the requirements belonging to the most frequent patterns. In the report (Buzhinsky 2016), we chose five visual specification languages as candidates to be applied as is, or to be used as a basis for a potentially new visual language that would be most suitable for nuclear I&C model checking. Yet, we did not develop such a language.

Continuing the work on simplifying the creation of formal requirements, in (Buzhinsky 2019) we reviewed research on automatic requirements formalization. Due to the ambiguity of natural languages, this problem can hardly ever be solved in a way requiring no manual post-processing of generated formal requirements; yet, generation of an at least an approximation of these requirements would reduce

manual work. We have found that approaches that are based on formal grammars may be potentially adapted to the nuclear I&C domain.

As for the step (3), the practice prior to SAUNA was to interpret the counterexamples generated by model checker NuSMV manually. The MODCHK tool (Pakonen et al. 2017) facilitated this task by highlighting signal values from counterexamples in the model for each time instant.

In SAUNA, we first investigated existing approaches of counterexample visualization and explanation. Among the reviewed approaches, the one by Beer et al. (2012) was capable of finding pairs of variables and time instants such that these variables at these time instants were sufficient to cause (i.e. explain) the overall false result of verifying the considered temporal property. We improved this approach and implemented it in a software tool that accepts counterexamples in the NuSMV format as input. The tool (Figure 3) not only finds the aforementioned pairs, but also visualizes them on the temporal property and allows the user to interactively explore the causes of values of all subformulas of the temporal property, at all time instants.

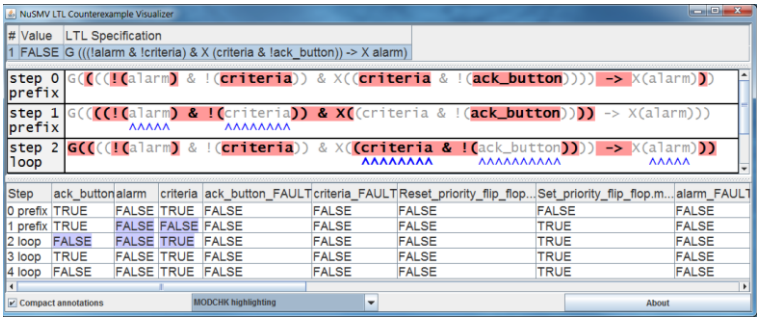

Figure 3. Counterexample visualization tool (Pakonen et al. 2018).

Closed-loop model checking

For the last ten years (Pakonen et al. 2017), model checking has been applied to nuclear I&C systems in open loop – that is, during verification, the automation logic was provided with free, unconstrained inputs. However, in this case the plant, or the environment where the controller operates, is disregarded. Thus, the controller is checked for correctness under the presence of plant behaviours (represented as input sequences) that are impossible in real life. This can result in irrelevant counterexamples generated by the used model checker. Moreover, with explicit-state model checkers, having too many inputs to the controller leads to the “state explosion” problem. In contrary, in closed-loop model checking, the plant and the controller models are composed into a closed-loop system, which eliminates the aforementioned problems. Thus, we decided to investigate the application of this technique in the nuclear automation industry.

As a case study for our work, we used the generic pressurised water reactor (PWR) model provided by Fortum Power and Heat Oy, which is implemented in the Apros continuous process simulator and contains basic components of an NPP. We manually prepared the formal models of several I&C (controller) subsystems of the PWR model in the MODCHK tool (Pakonen et al. 2017) and exported them into the format of the NuSMV symbolic model checker.

Following a similar approach to account for plant models was computationally infeasible due to the complexity of the plant, which is significantly larger compared to a single I&C subsystem. The solution was to prepare a simplified model. Since doing it manually required solid domain expertise, we explored the possibility of using automatic model generation approaches. Typically, such approaches use behaviour examples, or traces, as input data. However, there were no plant model generation approaches specifically for the purpose of subsequent closed-loop model checking, and thus we developed several approaches of our own: an approach to generate plant models from behaviour traces and temporal properties (Buzhinsky & Vyatkin 2017a); two approaches to generate plant models as a concise system of constraints and as an explicit state machine (Buzhinsky et al. 2017b); and an approach of modular plant model generation (Buzhinsky & Vyatkin 2017b).

We collected behaviour traces from the generic PWR model and applied these approaches to construct plant models for eight I&C subsystems thereof. The overall results are controversial. On one hand, closed-loop verification of nuclear I&C systems became possible. From the computational point of view, constraint-based models (Buzhinsky et al. 2017b) were more suitable for symbolic verification (e.g. in NuSMV), and explicit-state models (Buzhinsky et al. 2017b) were more efficient in explicit-state verification (Buzhinsky et al. 2017a). However, regardless of this choice, open-loop verification in NuSMV appeared to be faster. On the other hand, adding the plant model filters out unrealistic behaviour scenarios, but it also introduces a safety threat: relevant behaviours may also be missed. Future work may focus on keeping such behaviours of the closed-loop model present.

Hardware aspects in software model checking

In practice, model checking has so far been used to verify I&C application logic as if the logic was operating “in a vacuum”. In SAUNA, we experimented with an approach that also accounts for hardware aspects of I&C (Pakonen & Buzhinsky 2019). This was done by explicitly considering the allocation of function block I&C diagrams to physical divisions, modelling the following phenomena:

1. Presence of faults. According to the so-called N+2 or N+1 requirement, safety systems must be tolerant to any single failure. We accounted for communication failures and failures within any of acquisition and processing units (APUs) and actuation logic units (ALUs).

2. Presence of communication delays and asynchrony. Since different parts of each safety system operate on different devices located in different buildings, synchronous modelling commonly applied to individual I&C systems is not sufficient.

Previous research already considered asynchrony (Lahtinen et al. 2012) and fault modelling (Lahtinen 2014), but these works faced scalability issues. We achieve betters scalability due to the following:

3. Unlike (Lahtinen et al. 2012), our approach is based on symbolic verification in NuSMV and MODCHK (Pakonen et al. 2017). Our fault model is simpler than in (Lahtinen 2014) but nevertheless rather general.
4. We utilize the symmetry of the problem of verifying a system of four semi-redundant divisions. In particular, this allows us to leave only one ALU (e.g. the one in division 1) in the overall formal model: verifying the output of this ALU is only meaningful when the fault is located outside of this ALU. What is more, from the point of view of this ALU, faults in different divisions are equivalent, and thus we can fix the division where the fault occurs. This approach is illustrated in Figure 4, where the ALU of division 1 is verified and the fault is located in division 2.

As a case study, we used the reactor protection system of the proposed U.S. version of the European Pressurized Water Reactor (EPR) nuclear plant. We modelled a single I&C safety subsystem in MODCHK. Single failure tolerance of this subsystem was based not only on using four independent divisions, but also on coupling all signals with their Boolean validity values that were accounted for within APUs and ALUs. We successfully verified the requirements for this subsystem assuming single failure tolerance and asynchrony with bounded model checking (BMC).

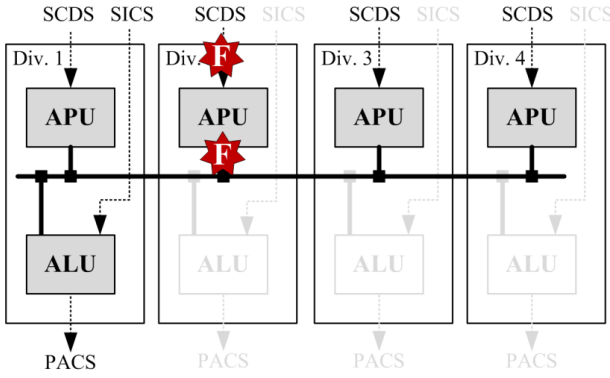

Figure 4. Simplifying the hardware and software verification problem by using symmetry (Pakonen & Buzhinsky 2019)

We also studied another way to simplify the hardware / software verification problem by using PRA to identify the most critical locations where failures can occur. The

idea of the developed approach (Lahtinen & Björkman 2016) is to restrict the model checking analysis based on PRA results, deemed most import, potentially improving scalability of model checking.

PRA is used to compute the relevant minimal cut sets. For example, minimal cut sets can be computed from a single fault tree representing a safety function. From model checking perspective, the basic events of a minimal cut set represent a combination of hardware (or software) failures events that are relevant for the analysis. A basic event in a minimal cut set specifies the location of a failure (and also the failure mode). Model checking is used to thoroughly analyse the system behaviour under the failures specified by a minimal cut set.

In (Björkman & Pakonen 2019), we studied the applicability of the coupling approach by performing a case study using an example system, based on a fictitious reference model of a boiling water nuclear reactor. Compared to unrestricted model checking analysis, the computation times decreased considerably when the analysis was restricted. Still, the overall process for introducing the failures requires a lot of manual labour, and needs to be automated.

Multidisciplinary safety assessment

Process assessment

The foundation for our work is the Nuclear SPICE process assessment model (PAM) that was already developed in SAFIR2014. However, as ISO/IEC 15288 was largely renewed in 2015, the existing software engineering oriented PAM could not sufficiently address the systems engineering approach. Also, the SAFIR2018 Framework Plan for Plant safety and systems engineering research area emphasizes the analysis “from the perspectives of the system (ISO 15288) and its operating environment”.

Our aim was that the Nuclear SPICE method will be based on the newest international standards and represents the strictest approach in process assessment. The method aims to ensure trustworthy systems development by identifying the risks related to the development processes, and to increase confidence and trust between acquirers, suppliers and regulators. The overall goal was to establish a domain specific interpretation of process quality that sustains achievement of safety goals in systems engineering.

The Nuclear SPICE PAM is a two-dimensional model of process quality. The process performance dimension describes each process with name, purpose and a set of outcomes. The process quality dimension presents the process attributes and quality levels. Nuclear SPICE applies process capability as the quality measure as defined in the standard ISO/IEC 33020. The assessment results are expressed as achieved capability levels for each assessed process.

The main effort was to develop a new PAM based on the ISO/IEC 15288:2015 standard. The revised ISO/IEC 15288 standard provides the process reference

model (Figure 5) including activities, tasks and information products as assessment indicators. In addition, we supplemented the process assessment process with a conformity evaluation activity. Based on our assessment experiences, we defined example process sets for two typical applications: supplier selection and project evaluation. These applications improve the usability of the Nuclear SPICE method.

Qualification in the nuclear domain is traditionally product or system centric. The achievement of product safety needs to be explicit, evidenced and quantified. Process approach is required in many guides and standards (Varkoi and Nevalainen 2017) but is less used in practice. Nuclear SPICE highlights the relevance of the development process in software intensive system qualification. The use of process and product centric methods should be integrated and balanced (Figure 6).

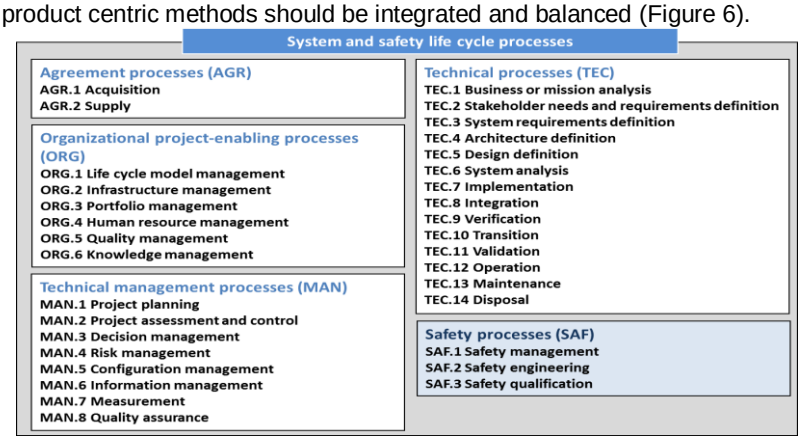

Figure 5. Nuclear SPICE systems and safety engineering processes.

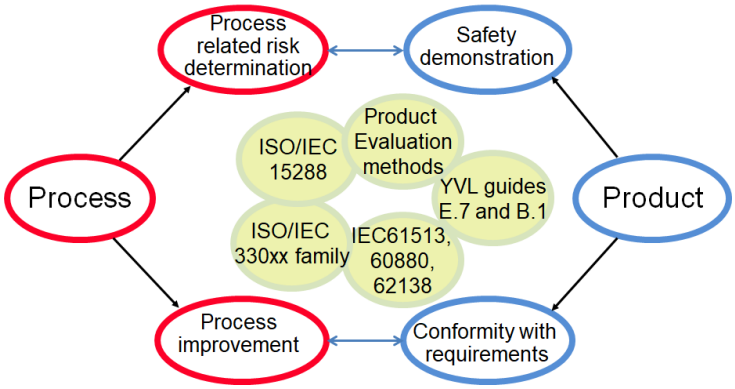

Figure 6. The main use cases of Nuclear SPICE.

The Handbook (published as FiSMA report 2018-1 Nuclear SPICE Handbook 1.0) describes the Nuclear SPICE process assessment method, defines a process

assessment model for performing systems engineering process assessments primarily in the nuclear industry domain and describes the process assessment process. The process assessment process ensures repeatability and reliability of the assessment results.

International collaboration had a high priority. Conference attendances provided valuable feedback on the research ideas and offered contacts to other safety experts. In addition to the three FiSMA reports that describe the contents of the Nuclear SPICE, we published seven conferences papers related to safety-focused process assessment. In the last paper, we validated usefulness of the Nuclear SPICE process assessment method in compliance evaluation (Varkoi et al. 2018).
As the main outcome, Nuclear SPICE provides a cost-efficient way to address the acquirer/supplier interface, to reduce risks in deliveries and to systematically collect evidence for system qualification. The Nuclear SPICE method has already been used productively with several system development projects.

System-Theoretic Process Analysis (STPA)

According to Regulation STUK Y/1/2018, the safety of a NPP and its safety systems shall be assessed analytically, and the analyses must be maintained and revised throughout the plant's life cycle.

The fast technological change, and increasing complexity and coupling of systems have stretched traditional safety engineering. Hazard analysis methods such as FMEA or FTA are mainly based on reliability theory, where accidents are seen as a chain of component failures. However, accidents could also be caused by component interactions where no components have failed but the system design has. On the basis of systems theory, a new hazard assessment technique called Systems-Theoretic Process Analysis (STPA) has been created (Leveson 2011).

We evaluated the use of STPA in a safety-critical design process of a reactor service bridge (RSB), or refuelling machine. System context, process model and operating conditions for RSB, fixed structures, overall system requirements and operations performed were defined. Next, accidents, system level hazards, system level safety constraints and the overall safety control structure of the RSB were identified. Analysis of mitigation chances of system level hazards was then made.

With this basis, we were able to start the two steps of STPA safety-critical design process: Identifying unsafe control actions and mitigating them as part of the design, and then identifying causal factors leading to those unsafe control actions.

Our findings from the use of STPA as part of safety-critical design process were as follows. Top-down reasoning with systemic approach provides a stepwise design path, where every decision in every stage of the design has a clear trace upward back to related hazards and accidents. The required safety functions are constructed according to unsafe control actions, which can also be traced back to hazards. Design decisions are made so that requirements of the safety functions are fulfilled. Safety classification can be made and justified accordingly.

We found STPA based safety guided design provides traceable justifications for the design decisions of safety-related components and functions. The traceability also promotes assessment by external parties.

As STPA needs only the systems engineering foundation and a concept of the system, and early analysis of functionality can be performed. Another strength is that the results are easy to refine when more details are added to the system or system modifications are made during operations (Hirvonen 2016).

Architecture Description Languages (ADL)

In 2018 we introduced a new task to expand our previous work towards model-based approach of I&C architecture modelling by studying architecture description languages (Linnosmaa et al., 2019). We see them as a possible way of combining hardware and software components of different levels to a same model, making it possible to analyse them all together. Another possibility with ADLs could automatic generation of assurance case material, as referenced above or in (Hawkins et al. 2015); (Gacek et al. 2014). First, we needed to get familiar with ADLs and the features they offer. We took a closer look at two of the most interesting languages from analysis and safety demonstration point of view: AADL (Architecture Analysis & Description Language) and SysML.

Based on a literature review we studied the analysing possibilities they offer, mostly used in other safety critical domains. We found out that possible analyses included modelling fault propagation, failure behaviour of individual components as well as failure behaviour of a system in terms of component failure behaviour, thereby facilitating automation of fault impact, fault tree, and reliability analysis. It looks like there is an active research community outside the nuclear industry working on producing methods and tools for modelling and analysing architecture with model-based engineering, which could be utilized for nuclear safety. Another part of the task was to do some hands-on architecture modelling with AADL and SysML in an exploratory case study modelling a piece of APR1400 reactor protection system. We based it on a linear system description from a real applicant's design control document.

Based on our literature review and the experience while modelling the system, we concluded that architecture description languages can offer benefits over the use of natural language in both ambiguity and traceability. However, modelling large and complex systems takes notable amounts of time and effort, at least without proper modelling expertise. To use SysML and AADL effectively, in-depth and multidisciplinary insight into the target system is required. Both languages seemed to be quite mature and able to model the system architecture on its own. We found SysML to be more suitable for conceptualization, while supporting functional analysis. On the other hand, we think AADL could be more suitable for the more detailed "component" level and non-functional analysis of the target system. Compared to current practice, for example natural text and block diagrams, model-based approaches have much higher learning curve. The initial step to start learning and

using them can be rather difficult. For ADL based safety demonstration to be practical, both the designer and the regulator would need to agree on some common ground.

Safety Demonstration of control room systems

Development of a new method for safety demonstration of control rooms

We have developed a Systems Usability Case (SUC) approach suitable for stepwise verification and validation of nuclear power plant control-room systems (e.g., (Koskinen et al. 2017)). The SUC approach has been applied in the analysis of the results of validation tests at the Fortum Loviisa NPP. Recently, we have focused on constructing an overall assessment of the SU of the CR systems which is based on reasoning within a SUC. The main aim of the SUC is to accumulate evidence throughout different design stages of the system and build a convincing documented body of evidence about the quality and acceptability of the system. The SUC consists of two main parts, the goal structure and the claim structure parts. The goal structure is developed before the validation test and the claim structure afterwards to organize the results of the validation to derive an assessment. Since validation of a complex system is a temporarily extended activity, the SUC should be a living document requiring updating after each validation or human performance monitoring activity.

We have participated in the task group of the Working Group on Human and Organisational Factors (WGHOF) of OECD NEA in which a general approach for multi-stage validation have been developed and a report entitled “Multi-Stage Validation of Control Room Designs and Modifications” have been prepared. Our ideas of the SUC has been presented in “Integrating results and drawing conclusions” – section of the report.

Developing a High Fidelity Virtual Control Room for Human Factors Evaluations in Nuclear Power

Two tests have been conducted to explore the applicability of a virtual reality control room (VR CR) for CR evaluations (e.g., (Bergroth et al. 2018)). Each operator is sitting in front of a physical workstation, wearing headset and using controller, keyboard and mouse to interact with the VR CR. A multiuser functionality enables several operators to be located and to collaborate in the virtual CR environment at the same time. In our first test, we studied how an immersive VR environment may augment and advance the evaluation of safety-critical nuclear power plant CR systems. Overall, the operators were able to execute individual monitoring and control tasks successfully, and their comments were quite positive. Operators experienced a moderate level of spatial presence, their symptoms of simulator sickness were low, and according to the Systems Usability questionnaire, they thought that the VR system was promising and suitable for CR V&V tests.

In our second test, an integrated system validation was conducted in a virtual control room with three operator crews. Twenty design deficiencies were identified, related to deficiencies in HSIs, procedures and operational concept. Operators were surprised of how compelling the VR user experience was, and their overall opinion was that the VR CR is well suitable for CR validations provided that some critical (e.g., resolution) fidelity problems are corrected.

Safety demonstration methods and practices

One of the goals of the SAUNA project was to identify development needs and possible solutions in the design and safety assessment of nuclear I&C systems. We published the collected insights in (Valkonen et al. 2016a), (Valkonen et al. 2016b) and (Valkonen et al. 2017).

Developing an understandable, transparent, convincing and complete safety demonstration in a cost-effective way is a difficult task, especially in the context of complex systems and varying regulatory environment. From the viewpoint of safety authorities, submittals of licensing documentation for regulatory review and approval could have more explicit argumentation, better traceability and clearer structure. From the licensee viewpoint, it has been a problem to collect and understand a complete set of requirements and to demonstrate compliance to them.

Challenges of safety justification can be summarised as follows:

1. Assuring safety of complex system is difficult in principle
2. The amount of information is large
3. Variations in standardization and regulatory practices.

The nuclear power industry would benefit from more structured, systematic and harmonised practices in engineering I&C systems and justifying their safety.

Possible solutions for improved safety demonstrations

Systems Engineering principles: Systematic and multi-disciplinary approach is needed. Utilization of Systems Engineering principles and related standards and guidelines can provide an overall framework also for the design of nuclear I&C.

Document and information management: Design documentation, safety analysis and V&V results, safety demonstrations, as well as the underlying regulations and standards, are a knowledge asset that must be communicated and maintained throughout the system life cycle. The solutions available today include, for example, good practices of technical writing and drawing, document and configuration management systems and design and plant databases. Irrespective of any formal structure for safety argumentation, these methods can be applied for preparing better safety demonstrations.

Harmonization and standardization: There is a need for further harmonisation and standardisation. Already now, there are many international and national groups sharing information and exploring opportunities for convergence of requirements

and practices. Besides harmonisation, standardisation bodies are moving towards electronic publication, online databases, modularisation and formalisation.

Assurance case approach: Similar to a safety demonstration, an assurance case (ISO/IEC 15026-2: 2015) includes one or more top-level claims for properties of a system, argumentation regarding truth of the claims, and evidence and assumptions used as the basis of the argumentation. Multiple levels of sub-claims and argumentation connect the top-level claims to the evidence. While being internally traceable, an assurance case/safety demonstration should be also linked to all relevant engineering artefacts used, for example, as evidence.

Model-based approaches: One attractive solution is to move from documents based design and safety justification towards Model-Based Systems Engineering (MBSE) which can be defined as the formalised application of modelling to support system requirements, design, analysis, verification and validation activities beginning in the conceptual design phase and continuing throughout development and later life cycle phases. Models can be used to guide designers in their work, and to enable design automation and computer-assisted system analysis, such as formal verification (e.g. model checking) and simulation-assisted I&C testing. Moreover, structured models help to link I&C specifications and PRA models.

Model-based safety demonstration

Qualification of a Nuclear I&C architecture and I&C systems is a crucial activity to attest conformity to the regulatory safety requirements. It is crucial both from the safety point of view and from the qualification costs point of view. In our work, we studied the potential of Model-Based Systems Engineering (MBSE) to perform qualification in a cost-effective way. The study focused on two main subjects: modelling of the qualification process and modeling of the input and outcome artefacts of the conformity assessment and qualification processes (the latter being a special case of an attestation process); the development and determination artefacts were defined in an early study (Tommila & Alanen 2015). We define thus the development activities to consist of four tiers, development, determination[1], conformity assessment and attestation.

We define qualification process to consist of two conformity assessment loops, 1st party conformity assessment and 3rd party conformity assessment, which we also call attestation (attestation in this model has two special cases, certification and qualification; certification was not covered by our study). Both the loops are depicted in Figure 7. The 1st party conformity assessment consists of Verification and Validation (V&V) activities of the organization that provides the system-of-interest. We

[1] Determination means "*Activity to find out one or more characteristics and their characteristic values"* [source: ISO 9000:2015]. Here we consider it to include activities such as testing, analysis, demonstration, inspection, similarity comparison, measurement, assessment, exercise, simulation, sampling, calculation, review, check, interview, examination and audit, or similar activity to observe the actual properties of the system-of-interest.

do not define V&V to include testing, analysis, etc. activities; such activities are included in the determination activities; only claiming and providing arguments and objective evidence is considered to be covered by V&V activities.

We try to promote MBSE, i.e. to avoid document centric systems engineering, by defining a structured data repository for engineering process descriptions (see the Section 'Model-based I&C safety engineering') and process input and output artefacts. The qualification process model is based on the engineering process constructs model illustrated in Figure 1 in the Section 'Model-based I&C safety engineering**Error! Reference source not found.**' above.

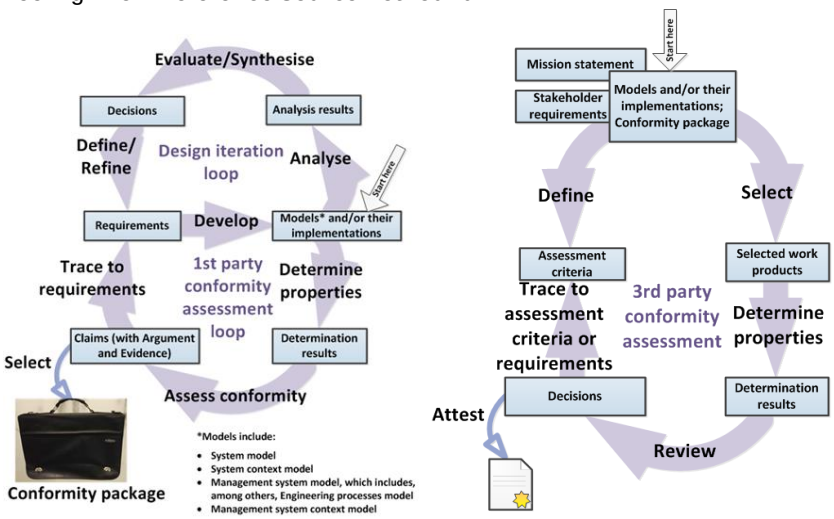

Figure 7. 1st party conformity assessment loop (to the left) and 3rd party conformity assessment loop (to the right); arrows denote activities, rectangles denote engineering artefacts (Alanen et al. 2017).

.

Six activities within the qualification process were identified (performer of the activity given in parentheses):

5. Create qualification process template (licensee);
6. Create qualification plan (licensee);
7. Perform qualification (licensee);
8. Assess qualification artefacts (licensee);
9. Assess safety case (in Safety Class 2 only; external assessor);
10. Create qualification report (licensee);
11. Attest (overview, review and approval by the regulator).
12. The details of the core activities are described in (Alanen & Tommila 2016).

We modelled the qualification execution procedure using the Business Process Model and Notation (BPMN) (Version 2.0) diagrams. The qualification process description was implemented using Microsoft SharePoint lists and wiki pages based on the process constructs model illustrated in Figure 1. Because the wiki pages can reflect data from the MS SharePoint lists, the process descriptions can be semi-automatically generated after the process descriptions, outcomes, process requirements, etc. are recorded into the SharePoint lists. An example of such a qualification process description is presented by Alanen & Tommila (2016).

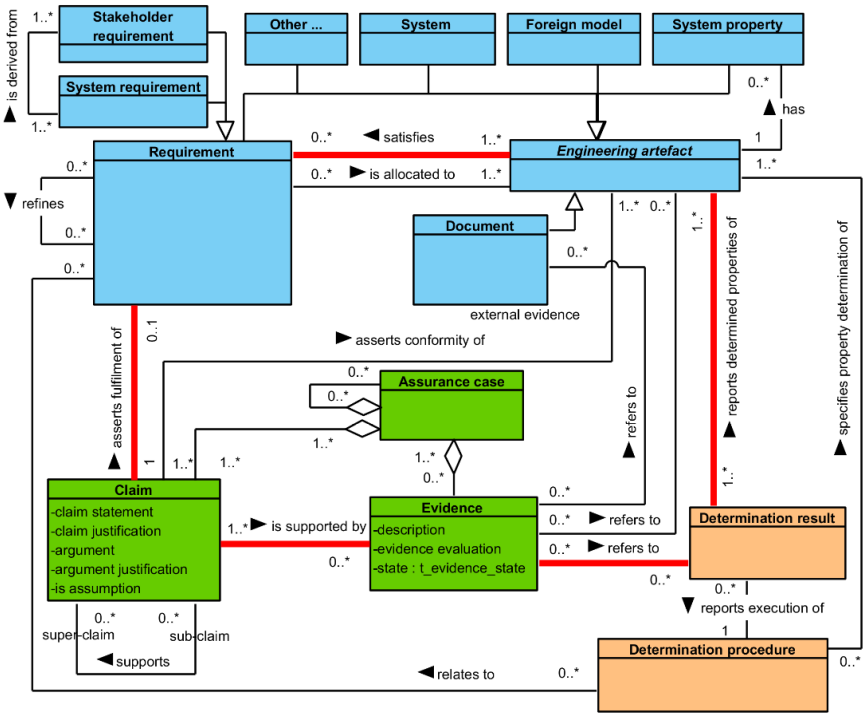

Figure 8. Our suggested data model for the main development artefacts (blue rectangles), determination artefacts (orange rectangles) and conformity artefacts (green rectangles) (stripped down version of (Alanen et al. 2017)).

The main input for the qualification process is the conformity package. The conformity package includes the safety demonstration. We provide a structured model for the conformity package data, i.e. the artefacts that constitute the core input for the qualification process. Such artefacts include, among others, requirements, system models, reports from tests, analyses, simulations etc., conformity claims, conformity arguments and conformity evidences. The artefacts model is shown in Figure 8. Furthermore, we provide a model for the attestation artefacts that include, among others, criteria and decisions (see Figure 9).

The conformity assessment part (the green rectangles in Figure 8) of the data model is based on the structured assurance case model of ISO/IEC 15026-2, i.e. the Claim-Argument-Evidence model. To optimise the assurance case structure for easy implementation, we included the Argument element into the Claim element as one of its attributes; this is justified by the fact that typically, the relationship between Claim and Argument is a one-to-one relationship, and Claim and Argument have the same lifecycle. Our suggestion is that the relevant development artefacts, requirements, system models (or at least their surrogates), and the determination artefacts (at least the determination procedures and results) are included into the safety demonstration. The key idea of our model is to integrate the safety demonstration with the other systems engineering artefacts, especially requirements, design and implementation artefacts and with determination (test, analysis, demonstration, etc.) artefacts into an engineering data repository to facilitate provision of evidence of the traceability of the artefacts.

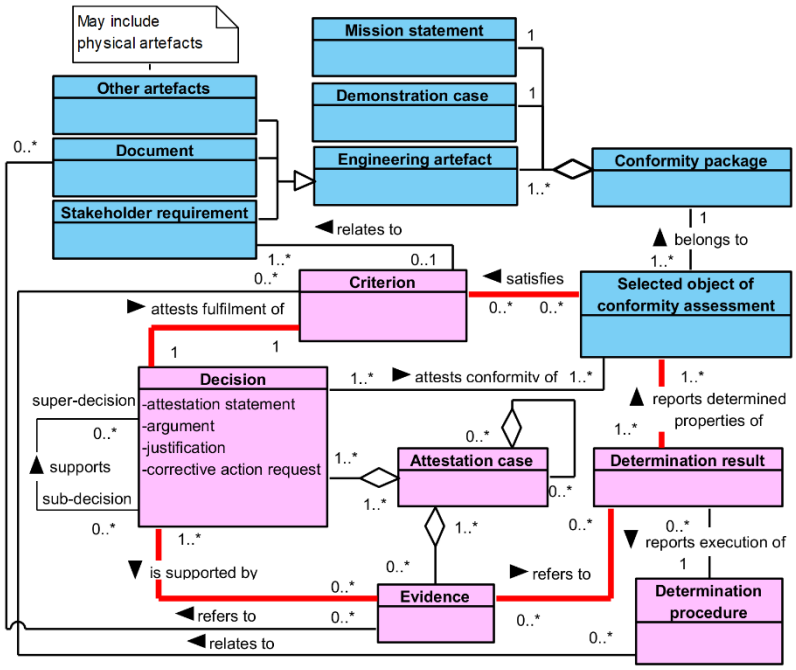

Figure 9. Our suggested data model for the attestation artefacts (the pink rectangles) (stripped down version of (Alanen et al. 2017)).

The artefact models we present in Figure 8 and Figure 9 are simple to implement compared, for example, to the ISO 10303-233 systems engineering data model. We demonstrated the artefacts model in Figure 8 using the Polarion Application Lifecycle Management (PLM) tool by Siemens by implementing a case to manage the traceability and conformity claiming of a diversity requirement of a spent fuel cooling

pool. The demonstration was successful with acceptable configuration effort. From previous experience, e.g. (Tommila & Alanen 2015), we know that such artefacts models can be implemented with other software tools that provide structured data repository and traceability management.

References

Alanen, J., Linnosmaa, J. & Tommila, T. 2017. Conformity assessment data model. Finland: VTT Technical Research Centre of Finland. Research report: VTT-R-06743-17. 34 p.

Alanen, J. & Salminen K. 2016. Systems Engineering Management Plan template - V1. Espoo: VTT. Research Report: VTT-R-00153-16. 78 p. + app. 12 p.

Alanen, J. & Tommila, T. 2016. A reference model for the NPP I&C qualification process and safety demonstration data. Research Report: VTT-R-00478-16. 43 p. + app. 21 p.

Authen, S., Holmberg, J.-E., Tyrväinen, T. & Zamani, L. 2015. Guidelines for reliability analysis of digital systems in PSA context - Final report. Roskilde: Nordic Nuclear Safety Research. NKS-330. 63 p. + app. 37 p.

Authén, S., Bäckström, O., Holmberg, J.-E., Porthin, M. & Tyrväinen, T. 2016 Modelling of DIgital I&C, MODIG — Interim report 2015, NKS-361, Nordic nuclear safety research (NKS), Roskilde.

Beer, I., Ben-David, S., Chockler, H., Orni, A. & Trefler, R. 2012. Explaining counterexamples using causality. Formal Methods in System Design 40(1), 20–40.

Bergroth, J.D., Koskinen, H.K. & Laarni, J.O. 2018. Use of Immersive 3-D Virtual Reality Environments in Control Room Validations. Nuclear Technology 202, 278-289.

Buzhinsky I. 2016. Visual formalisms applied to temporal logic property patterns in the nuclear automation domain. Technical report. Espoo: Aalto University. 40 p.

Buzhinsky I. 2019. Formalization of natural language requirements into temporal logics: a survey. Submitted to 17th IEEE International Conference on Industrial Informatics (INDIN).

Buzhinsky, I., Pakonen, A. & Vyatkin, V. 2017a. Explicit-state and symbolic model checking of nuclear I&C systems: A comparison. 43rd Annual Conference of the IEEE Industrial Electronics Society (IECON). October 29 – November 01, 2017, Beijing, China, pp. 5439–5446.

Buzhinsky, I., Pakonen, A. & Vyatkin, V. 2017b. Scalable methods of discrete plant model generation for closed-loop model checking. 43rd Annual Conference of the IEEE Industrial Electronics Society (IECON). October 29 – November 01, 2017, Beijing, China, pp. 5483–5488.

Buzhinsky, I. & Vyatkin, V. 2017a. Automatic inference of finite-state plant models from traces and temporal properties. IEEE Transactions on Industrial Informatics 13(4), 1521–1530.

Buzhinsky, I. & Vyatkin, V. 2017b. Modular Plant Model Synthesis from Behavior Traces and Temporal Properties. 22nd IEEE Conference on Emerging Technologies & Factory Automation (ETFA). September 12–15, 2017, Limassol, Cyprus. IEEE.

Björkman, K. & Pakonen A. 2019. Coupling model checking and PRA – a case study. Submitted to: 29th European Safety and Reliability Conference (ESREL 2019), September 22–26, 2019, Hannover, Germany.

Bäckström, O., Holmberg, J.-E., Jockenhövel-Barttfeld, M., Porthin, M., Taurines, A. & Tyrväinen, T. 2015. Software reliability analysis for PSA — Final report. NKS-341, Nordic nuclear safety research (NKS), Roskilde.

Common position 2014. Licensing of safety critical software for nuclear reactors – Common position of international nuclear regulators and authorised technical support organisations. Revision 2014.

Gacek, A., Backes, J., Cofer, D., Slind, K. & Whalen, M. 2014. Resolute: an assurance case language for architecture models. ACM Conference on High Integrity Language Technology HILT 2014, Portland, Oregon, USA, 18-21 October.

Hawkins, R., Habli, I., Kolovos, D., Paige, R. & Kelly, T. 2015. Weaving an Assurance Case from Design: A Model-Based Approach. 16th IEEE International Symposium on High Assurance Systems Engineering HASE 2015, Daytona Beach Shores, FL, USA, 8-10 Jan. pp. 110–117.

Hirvonen, A. 2016. Implementing systems-theoretic process analysis (STPA) in safety-critical system design. Master's Thesis, University of Oulu / IntoWorks. 112 p.

Holmberg, J.-E. 2016. DIGREL example PSA model description, Report 14127_R001, Risk Pilot AB, Espoo.

Holmberg, J.-E., Helminen, A. & Porthin M. 2017. Using PSA to assess defence-in-depth — case study on level 2 of defence-in-depth, Report 14127_R002, Risk Pilot AB, Espoo.

Holmberg, J.-E. 2018. Risk-informed safety classification of components of auxiliary systems for emergency diesel generators in nuclear power plants. In: S. Haugen et al. (eds.) Safety and Reliability – Safe Societies in a Changing

World: Proceedings of ESREL 2018, June 17-21, 2018, Trondheim, Norway, Taylor & Francis Group, London, Pp. 1589−1597.

INCOSE 2007. INCOSE Systems Engineering Vision 2020. Version 2.03. San Diego: International Council on Systems Engineering. INCOSE-TP-2004-004-02. 32 p.

Koskinen, H., Laarni, J., Liinasuo, M., Norros, L. & Savioja, P. 2017. Systems Usability Case in Stepwise Control Room Validation. In: Proceedings of the 10th International Topical Meeting on Nuclear Plant Instrumentation, Control, and Human-Machine Interface Technologies (NPIC & HMIT 2017), San Francisco, CA, June 11-15, 2017.

Lahtinen, J. 2014. Hardware failure modelling methodology for model checking. Espoo: VTT. VTT Technology VTT-R-00213-14. 36 p.

Lahtinen, J., Launiainen, T., Heljanko, K. & Ropponen, J. 2012. Model checking methodology for large systems, faults and asynchronous behaviour. SARANA 2011 work report. Espoo: VTT. VTT Technology 12. 84 p.

Lahtinen, J. & Björkman, K., (2016) Integrating model checking and PRA: a Novel Safety Assessment Approach for Digital I&C Systems, in 26th European Safety and Reliability, ESREL 2016, 25 - 29 September 2016, Glasgow, UK Risk, Reliability and Safety: Innovating Theory and Practice, Walls, Lesley etc. eds.. CRC Press (2016), 486, 2016.

Leveson, N., 2011. Engineering A Safer World. MIT Press. ISBN:9780262016629

Linnosmaa, J., Valkonen, J. Karpati, P., Hauge, A., Sechi, F. & Gran, B. A. 2019. Towards model-based specification and safety assurance of nuclear I&C systems – Applicability of SysML and AADL. 11th Nuclear Plant Instrumentation, Control and Human-Machine Interface Technologies NPIC&HMIT 2019, Orlando, FL, USA, 9-14 February.

O'Halloran, B., Papakonstantinou, N. & L. Van Bossuyt, D. 2015. Modeling of Function Failure Propagation Across Uncoupled Systems, Reliability and Maintainability Symposium (RAMS) 2015, Palm Harbor, FL, January 26–29, 2015.

O'Halloran, B., Papakonstantinou, N. & L. Van Bossuyt, D. 2016. Cable Routing Modeling in Early System Design to Prevent Cable Failure Propagation Events, Reliability and Maintainability Symposium (RAMS) 2016, Tucson, AZ, USA, January 25–28, 2016.

Pakonen, A. & Björkman, K. 2017. Model checking as a protective method against spurious actuation of industrial control systems. In: M. Cepin, & R. Bris

(Eds.), Safety and Reliability: Theory and Applications. Proceedings of ESREL 2017. CRC Press, pp. 3189-3196.

Pakonen, A. & Buzhinsky, I. 2019. Verification of fault tolerant safety I&C systems using model checking. 20th IEEE International Conference on Industrial Technology (ICIT). February 13-15, 2019, Melbourne, Australia.

Pakonen, A., Buzhinsky, I. & Vyatkin, V. 2018. Counterexample visualization and explanation for function block diagrams. In 16th IEEE International Conference on Industrial Informatics (INDIN). July 18–20, 2018, Porto, Portugal, pp. 747–753.

Pakonen, A., Tahvonen, T., Hartikainen, M. & Pihlanko, M. 2017. Practical applications of model checking in the Finnish nuclear industry, 10th International Topical Meeting on Nuclear Plant Instrumentation, Control and Human Machine Interface Technologies (NPIC & HMIT 2017), 11 - 15 June, 2017, San Francisco, CA, USA, pp. 1342-1352.

Pakonen, A., Pang, C., Buzhinsky, I. & Vyatkin, V. 2016. User-friendly formal specification languages — conclusions drawn from industrial experience on model checking. 21st IEEE Conference on Emerging Technologies & Factory Automation (ETFA). IEEE, pp. 1–8.

Papakonstantinou, N., Porthin, M., O'Halloran, B. & L. Van Bossuyt, D. 2016. A model-driven approach for incorporating human reliability analysis in early emergency operating procedure development, Reliability and Maintainability Symposium (RAMS) 2016, Tucson, AZ, USA, Jan 25–28 2016.

Papakonstantinou, N., Tommila, T., O'Halloran, B., Alanen, J. & L. Van Bossuyt, D. 2017. A Model Driven Approach For Early Assessment Of Defence in Depth Capabilities Of Complex Sociotechnical Systems, ASME 2017 International Design Engineering Technical Conferences & Computers and Information in Engineering Conference (IDETC/CIE 2017), Cleveland, Ohio, USA, August 6-9 2017.

Papakonstantinou, N., Alanen, J., Linnosmaa, J. & O'Halloran, B. 2018. Automatic fault tree generation from multidisciplinary dependency models for early failure propagation assessment, ASME 2018 International Design Engineering Technical Conferences & Computers and Information in Engineering Conference IDETC/CIE 2018, Aug 26-29, 2018, Quebec City, Canada.

Papakonstantinou, N., Alanen, J., Linnosmaa, J. Bashir, A. Z., O'Halloran, B. & L. Van Bossuyt, D. 2019. Early hybrid safety and security risk assessment based on Interdisciplinary dependency models, IEEE Reliability and Maintainability (RAMS), Annual Symposium, Jan 28-31, 2019, Orlando, FL, USA.

Porthin, M. 2018. Progress of WGRISK digital I&C benchmark study DIGMAP in 2017 (D1.3.2). VTT Technology VTT-R-06873-17. 4 p. + app. 20 p.

Tommila, T. & Alanen, J. 2015. Conceptual model for safety requirements specification and management in nuclear power plants. Espoo: VTT.

Tommila, T. & Papakonstantinou, N. 2016. Challenges in defence in depth and I&C architectures, Research Report, VTT-R-00090-16, VTT 2016, 54 p. + app. 5 p.

Tyrväinen, T. & Porthin, M. 2019. Probabilistic risk model of digital reactor protection system. Espoo: VTT. VTT Technology VTT-R-06631-18. 27 p.

Uusitalo, E. & Koskela, M. 2015. Towards a functional nuclear I&C reference architecture based on the DIGREL plant model, IntoWorks research report, IW2015-001. 25 p.

Valkonen, J., Tommila, T., Linnosmaa, J., Karpati, P. & Katta, V. 2017. Demonstrating and Argumenting Safety of I&C Systems – Challenges and Recent Experiences, 10th International Topical Meeting on Nuclear Plant Instrumentation, Control, and Human-Machine Interface Technologies NPIC & HMIT 2017, San Francisco, CA, USA, June 11-15, pp. 568-580

Valkonen, J., Tommila, T., Linnosmaa, J. & Varkoi, T. 2016a. Safety demonstration of nuclear I&C - an introduction, VTT Technical Research Centre of Finland Ltd, VTT Research Report, VTT-R-00167-16, p. 38.

Valkonen, J., Tommila, T., Alanen, J., Linnosmaa, J. & Varkoi, T. 2016b. Views on safety demonstration and systems engineering for digital I&C, Proceedings of the 39th Enlarged Halden Programme Group Meeting EHPG 2016, 8 - 13 May, Fornebu, Norway p. 13.

Varkoi, T., Mäkinen, T., Cameron, F. & Nevalainen, R. 2018. Validating Effectiveness of Compliance Evaluation in Safety-Critical Process Assessment. In: Larrucea X et al. (Eds.): Systems, Software and Services Process Improvement. EuroSPI 2018, CCIS 896, pp. 181–192, Springer 2018.

Varkoi, T. & Nevalainen, R. 2017. Process Assessment in Supplier Selection for Safety-Critical Systems in Nuclear Domain. In: Tonetta S et al. (Eds.): SAFECOMP 2017 Workshops, LNCS 10489, pp. 298–308, Springer 2017.

3. Severe Accidents and Risk Analysis

3.1 Extreme weather and nuclear power plants (EXWE)

Kirsti Jylhä, Havu Pellikka; Ari Karppinen, Ari Viljanen, Jan-Victor Björkqvist, Carl Fortelius, Hilppa Gregow, Otto Hyvärinen, Milla Johansson, Terhi Laurila, Ulpu Leijala, Anna Luomaranta, Anniina Korpinen, Rostislav Kouznetsov, Matti Kämäräinen, Antti Mäkelä, Taru Olsson, Jenni Rauhala, Mikhail Sofiev, Jani Särkkä, Peter Ukkonen and Andrea Vajda

Finnish Meteorological Institute (FMI)
P.O. Box 503, FI-00101 Helsinki

Abstract

The general objective of EXWE was to give better estimates of probabilities of extreme geophysical events that affect the design principles of nuclear power plants (NPPs) and may pose external threats to the plants. Extreme incidents in weather, sea level events and space weather, as well as atmospheric dispersion were considered. Various observations, modelling and machine learning approaches were utilized. A significant positive trend in Finland over the past 40 years was detected in a traditionally-used predictor of thunderstorms. If in any of the three NPP sites, the probability of severe freezing rain might increase in Hanhikivi in the future. Simulations of four past coastal snowfall cases with a numerical weather prediction system revealed similarities in their patterns. Flow patterns in summertime sea-breeze circulation and their impacts on atmospheric dispersion of potential releases were also realistically simulated, provided that a sufficiently high resolution is used in the meteorological and dispersion simulations. Improved coastal flooding risk estimates were made by examining the joint effect of high sea level and wind waves. The availability of local wave measurements is a limiting factor in calculating accurate flood risk estimates that take into account the effect of waves. Other sea level research topics included meteotsunamis, sea level and wave model validation as well as mean sea level scenarios on the Finnish coast over the 21st century.

Introduction

Major nuclear accidents are typically low-probability–high-consequence events. The overall safety management over the life cycle of a nuclear power plant (NPP) requires, among others, evaluation of external events that are not directly connected with the operation of the NPP but could influence its safety. Geophysical phenomena, such as extreme weather and sea level events affect the design principles of NPPs and may pose external threats to the plants. On the other hand, transport and

dispersion of emissions from a source located on the seashore, such as the Finnish NPPs, are subject to specific coastal atmospheric phenomena.

In order to support regulatory decision making in NPPs through the use of probabilistic risk assessment (PRA), harsh weather and other external risks have been examined in Finland since the early 1990s, and the preparedness against extreme natural phenomena is continuously being improved (Himanen et al., 2012; Sandberg & Vuorio, 2014; Paillère et al., 2014; Jänkälä, 2016). Despite these already-taken measures, further research needs to be conducted. This is because estimates of frequencies of vary-rare weather-related and sea-level-related hazards, corresponding to return periods of thousands or millions of years, are subject to considerable uncertainties. Moreover, the patterns of extreme events, both in frequency, extremity, and magnitude, are likely to alter in the course of time because of the global climate change. Therefore, a hazard curve evaluated from time series of past measurements needs to be regularly updated.

A recent paper gave an overview on meteorological and marine studies in EXWE since 2007 to support nuclear power plant safety in Finland (Jylhä et al., 2018). In the current report, main results achieved during the period 2015-2018 are summarized.

Main objectives

The purpose of EXWE in SAFIR2018 was to support PRA of new and existing NPPs and the design phase of new infrastructures by enhancing scientific understanding of the environmental conditions of the NPP locations and predicting how they can change. Three themes were studied during the whole four-year period of SAFIR2018: 1) extreme weather incidents, 2) extreme sea level events, and 3) atmospheric dispersion. In addition, 4) extreme space weather and its effects were considered during the first two years.

The specific topics included: severe warm-season convective weather events; intense sea-effect snowfall; severe freezing rain; strong winds; extreme sea levels, high waves and their co-occurrence; meteotsunamis and other short-period sea-level events; sea level and wave modelling; global sea level rise and its effect on mean sea level on the Finnish coast; solar storms and geomagnetic disturbances; and nesting of high-resolution weather and dispersion modelling.

Regarding the weather and sea-level events, the objective was to deliver better estimates of their frequencies and trends near the Finnish coast. The work focusing on atmospheric dispersion modelling aimed to provide a modern platform for assessing consequences of accidental releases at multiple transport and time scales.

To achieve the objectives, a spectrum of different sources of information was utilized as the research material. Observational-based data sets included eyewitness observations, a range of instrumental records, gridded observational data, as well as global assimilation-based reanalysis data sets that have been constructed by merging weather station data, radiosonde soundings and satellite information with the aid of a numerical weather prediction model. Model data included, in turn,

high-resolution atmospheric modelling, sea level and wave modelling, data assimilation, and output from climate models. Besides, the research team covered a wide range of scientific expertise, and the know-how was transferred from more experienced researchers to new experts.

Extreme convective weather in summer

Extreme convective weather (ECW) is characterized by thunderstorms that produce heavy rain, large hail, intense lightning, strong wind gusts (i.e., downbursts) or tornadoes (termed as waterspouts over sea, and in Finnish “trombi” or “vesipatsas”). In the warm season, ECW can be caused by detached thunderclouds, derechos (in Finnish “syöksyvirtausparvi”) and other mesoscale convective systems”), or by convective elements in extra-tropical cyclones. Increasing observation density owing to the use of weather radars, satellites and lightning-location sensors has revealed that ECW is more common in northern Europe than generally expected. All of these thunderstorm-related ECW phenomena may be harmful to infrastructure, the severity of the impacts depending on the intensity and location of occurrence of the events. Among other impacts, ECW may result in flash floods and coastal flooding, including also meteotsunamis.

Lightning is an essential element of a thunderstorm. While the data set of lightning in Finland is robust and long, dating back in time to 1887, the time series of the other ECW phenomena, especially those needing human observations (tornadoes and large hail), are likely to miss observations. An important question is how well the occurrence of lightning can be used as a proxy for the other hazardous ECW events related thunderstorms (and for atmospheric conditions favouring them). According to Mäkelä et al. (2016) and Laurila et al. (2016), lightning and rainfall are correlated (the more lightning, the more intense the precipitation; and the higher average lightning flash density, the higher annual number of heavy rainfall cases). Instead, a correlation between lightning and the formation of large hail is weaker, and tornadoes may occur in Finland without any lightning. Heavy wind gusts are practically always involved in thunderstorms, but their intensity, extent and height of occurrence vary. Based on a study by Rauhala et al. (2017), atmospheric conditions and synoptic-scale circulation patterns favouring significant hail can be categorized into four distinct classes, two of which have similarities with the patterns observed in Finland in tornado situations (Rauhala et al., 2017). Mesoscale and synoptic scale features of a derecho that occurred in north-eastern Europe on 8 August 2010 was studied in detail by Rauhala (2018). By looking into the observations and comparing them to previous research it was found that the derecho case was a linear mesoscale convective line that can be called a squall line.

Thunderstorm occurrence was efficiently identified from reanalysis data using neural networks (NN) (Ukkonen et al., 2017, Ukkonen and Mäkelä, 2017). NN is a machine learning method where high-quality observations of e.g. lightning and precipitation are used to train the NN model and complex relationships can be learned from data.

Recent findings by Ukkonen and Mäkelä (2018a) indicated that the NN and boosted decision tree methods provide improved forecasting of thunderstorms over different climatological regions. They compared these methods against traditional thunderstorm forecasts that are based on the use of a measure of atmospheric instability, so-called convective available potential energy (CAPE). The comparisons over Scandinavia, Central-Europe and Sri Lanka in the tropics showed that the NN overcomes the CAPE-based forecasts especially in the tropics where the CAPE appeared not to have useful skill at all. Output from NN and boosted decision trees had a very high correlation (r> 0.94) with monthly mean thunderstorm occurrence in all the domains considered.

To assess how the Northern European thunderstorm environments are affected by changing climate, Ukkonen and Mäkelä (2018b) examined a state-of-the-art atmospheric reanalysis data (ECMWF ERA5). A significant positive trend in CAPE over the past 40 years (1979-2018) was detected (Fig. 1). Furthermore, the annual variation in CAPE appeared to strongly correlate with the annual amount of lightning in Finland. It was concluded that the increase in atmospheric instability is likely to continue and manifest in substantial future increases in flash density and thunderstorm days and/or in the increase in the intensity of the thunderstorms (to the extent that the regional climate continues to warm).

Regarding the safety operations of nuclear power plants, lightning peak current is one of the most frequent parameter against which special attention should be paid. Because a large fraction of the extremely high-peak current strokes detected by lightning location systems are not reliable, specific filtering methods need to be used. Results using extreme value theory and millions of strokes in the data set (i.e., either a large spatial domain and/or a long time series) suggest that the extreme natural lightning peak current seems to be approximately in 500-600 kiloamperes (kA).

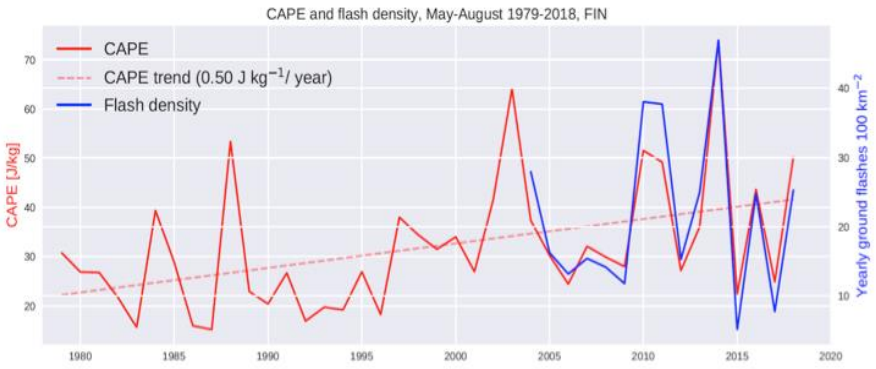

Figure 1. The time series of mean summertime CAPE (solid red line) and its linear trend (dotted red) over Finland from 1979 to 2018, derived from ERA5. Also shown is the flash density for ground flashes beginning from 2004, when the lightning detection network began to differentiate between ground and cloud flashes and whereafter the detection efficiency is high and relatively homogenous over Finland.

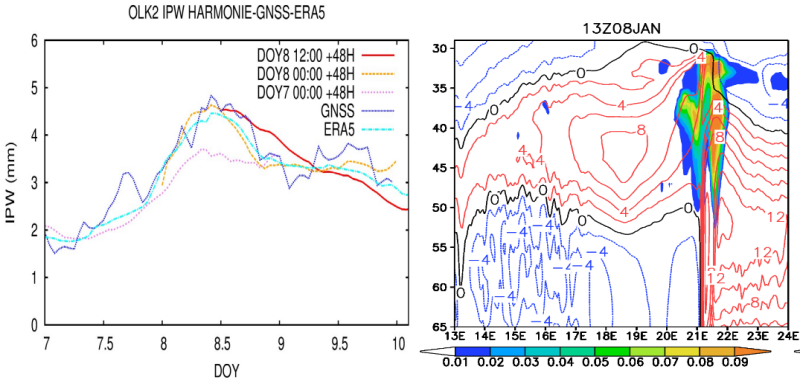

Figure 2. Left: Total amount of water as precipitable rain (IPW, mm) in an atmospheric column as a function in the Olkiluoto GNSS site on 7-10 January 2016. The time series are extracted from GNSS receivers, ERA5 reanalyses and three HARMONIE-AROME simulations, initiated at different times (00 UTC at 7 Jan 2016, and 12 UTC and 00 UTC at 8 Jan 2016, pink, yellow and red, respectively). Right: Vertical cross-section (up to ~700 hPa) of cloud water and ice (g/m^2) and meridional wind speed (m/s, southerly in red, northerly in blue) along 62°N as simulated by HARMONIE during the most intense snowfall at the coast (13 UTC on 8 Jan 2016). DOY stands for day of the year. (Based on Figs. 5 and 7 of Olsson et al. 2018a.)

Sea-effect snowfall

Typical conditions of sea-effect snowfall, as a wintertime convective weather phenomena, include 1) ice-free sea surface which acts as a constant source of energy and moisture into the atmosphere, 2) cold air mass over the sea and 3) wind which blows from a suitable direction over the sea. When these prerequisites are met, the vertical temperature difference and the moisture flux from the sea surface generate strong rising air motion and convective precipitation (Olsson et al. 2017 and references therein). Depending on the mean wind direction, excess sea-effect coastal snowfall may occur. This was experienced in Merikarvia on 8 January 2016, when up to 73 cm of new snow accumulated in less than a day. This new national snowfall record in Finland distinctly exceeded the previous record, 50 cm, measured in a nearby coastline city, Rauma, 100 kilometres to the south on 21 November 1971.

Assessments of the probability of intense coastal snowfall on the Finnish coast is of relevance for NPP safety, since they might lead to a blockage of ventilation air intakes and emergency diesel generator combustion air intakes in the NPPs (Table 1 in Jylhä et al., 2018). Besides, rapidly decreasing road surface friction and reduced visibility due to intense snowfall events increase the probability of severe accidents in road traffic (Juga et al., 2012).

Studies about sea-effect snowfall were initiated in EXWE in 2014. At first, a list of past sea-effect snowfall cases prior to the year 2001 was created using manual recordings of weather codes (Kämäräinen and Jokinen, 2014). In order to include the years 2001–2014 into the list, a new identification method was developed in 2015 that utilizes, among others, information in reanalysis data about convectivity of precipitation, i.e., the portion of snowfall as convective (Luomaranta et al. 2016).

The Merikarvia case in 2016 has been studied in detail by Olsson et al. (2017, 2018a). In the first study, a preliminary simulation was conducted with HARMONIE-AROME, a high-resolution non-hydrostatic numerical weather prediction model, without any assimilation of weather radar reflectivity data. Verification of the outcomes with weather radar images indicated that the simulation was able to capture the overall situation quite well, although this may not be true for other intense snowfall events (Olsson et al. 2017).

Subsequently, Olsson et al. (2018a) simulated the Merikarvia case by running HARMONIE-AROME both with and without assimilation of radar data and using three different initiation times (Fig. 2, left). ERA5 reanalysis and Global Navigation Satellite System (GNSS) observations were additionally used to study the basic characteristics of the snowband. The results were encouraging towards the use of ERA5 data in identification of historical sea-effect cases and their frequency. The time series of precipitable water (IPW, if all the water in the above atmospheric column would precipitate as rain) showed good agreement between ERA5, the GNSS method and HARMONIE-AROME simulations (Fig. 2, left). The convergence zones near the coastline, associated with the intense snowfall, can be seen distinctly in the model data (Fig. 2, right).

In addition to the Merikarvia event, three additional coastal snowfall incidents were simulated by Olsson et al. (2018b): 20-23 December 2011, 1-4 February 2012 and 8-9 November 2016. The first case was identified by the method documented by Luomaranta et al. (2016), and the second episode severely worsened traffic safety in Helsinki (Juga et al. 2014). The four cases showed similar characteristics: the wind speed was mainly over 8 m/s, the wind shear stayed below 60° during the snowbands, the temperature difference between the surface and 850 hPa levels was higher than the critical threshold value of 13 °C, and the boundary layer height was distinctly higher than the required value of 1000 m.

In Finland, wind direction enabling snowbands to hit the coast range from easterlies to southwesterlies along the southern coastline and from southwesterlies to northwesterlies along the western coastline. A difficulty in developing and using algorithms to detect sea-effect snowfall cases is that meteorological conditions can vary distinctly over a small spatial area since, for example, between eastern and western parts of the Gulf of Finland. This is worth keeping in mind if a sea-effect snowfall detection method is applied to reanalysis data or climate model data. The simulations with the weather forecast model HARMONIE-AROME, discussed above, give an upper estimate of how reliable model-based assessments can be concerning the occurrence and characteristics of sea-effect snowfall.

Severe freezing rain

Freezing rain (FZRA) is supercooled liquid precipitation which freezes on contact with solid objects, forming a coating of ice. In NPPs, FZRA might hamper ventilation air intakes and emergency diesel generator combustion air intakes. An optimal vertical temperature profile for freezing rain consists of sub-zero temperatures near the ground and a melting layer aloft. Climatological information about the occurrence of FZRA can be produced by applying a precipitation typing algorithm that is based on vertical profiles of relative humidity and temperature. The algorithm was developed by Kämäräinen et al. (2017a) and was first applied to ERA-Interim, a widely used reanalysis data set. In order to assess the effects of climate change on FZRA in Europe, the algorithm was then applied to output from simulations by seven EURO-CORDEX regional climate models (Kämäräinen et al., 2018). Two emission scenarios were considered, RCP4.5 representing moderate and RCP8.5 unregulated global future CO_2 emissions in the future. According to the results, there will be a general increase in the occurrence of freezing rain in northern and northeastern Europe and a decrease in western, central, and southeastern Europe.

At the coastal sites of the Finnish NPPs, however, no common trends could be found for severe FZRA, having all-year-round probabilities of less than 10^{-5} (Kämäräinen et al., 2017b; Jylhä et al. 2018). In Olkiluoto, based on the multi-model means, the projections for the most intense FZRA cases showed future shifts towards smaller rather than larger probability levels for accumulations periods of 6 h, 24 h and 72 h. In Loviisa, the projected sign of the change depended on the emission scenario and the accumulation period. The largest chance for potential increases in very severe FZRA appeared in Hanhikivi.

Continuing the analysis, Hyvärinen and Vajda (2018) examined the co-occurrence of freezing rain and high wind speeds at the Finnish NPP sites (Fig. 3). Gale winds (17–20 m/s) rarely co-occur with FZRA, but precipitation during FZRA is somewhat more intense than in non-FZRA precipitation. The further interpretation of results is difficult without knowledge of any specific thresholds of combinations of wind speed and FZRA intensities that might be critical to the structure, especially for the NPP safety.

Qualitative speaking, in future, precipitation of non-FZRA is expected to increase somewhat, but it is unclear if there is more increase in precipitation amounts during FZRA. No change in the wind distribution is apparent either in FZRA or non-FZRA, as the number of events is rather small and results therefore somewhat noisy. However, more quantitative results would need more research. The distributions differ quite a lot from simple theoretical distributions, such as Gaussian or Gamma distributions, and so a non-parametric method, the kernel density estimation with normal kernels, was used in the present study. However, this is a rather coarse method for quantitative analysis, and therefore probabilities smaller than 0.001 were not considered.

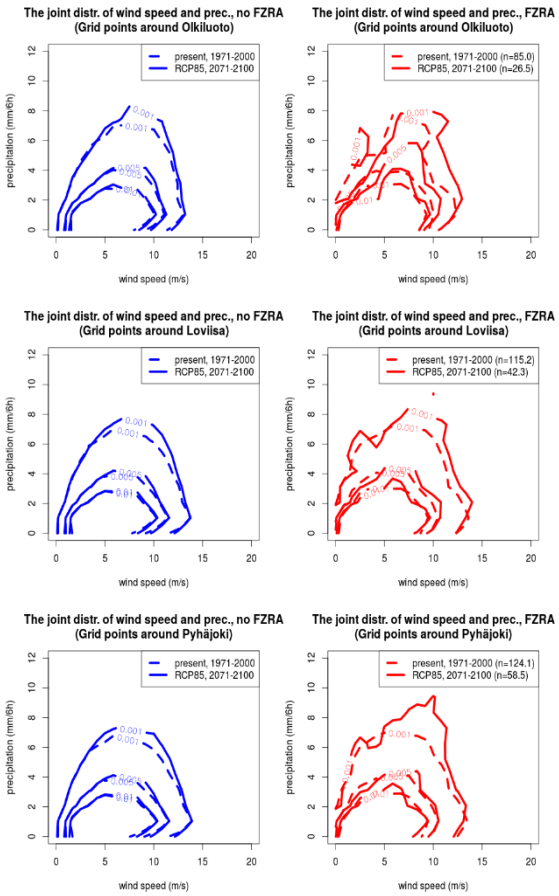

Figure 3. Changes in the joint distribution of wind speed and precipitation in liquid form (column on left) and freezing rain (column on right) by 2071-2100, according to the RCP8.5 scenario, in Olkiluoto (top), Loviisa (middle) and Hanhikivi (bottom).

Strong winds

Investigations on strong winds have focused on the occurrence of large scale windstorms in Europe and on dynamical aspects of storm Mauri in Finland in 1982. Based on analyses of 56 large scale windstorms that occurred in western, central and northern Europe in 1951-2010, Gregow et al. (2017) demonstrated that the year 1990 represented a change-point in windstorm damages. Since then, windstorm induced large scale forest damages have increased by a factor of three in Europe. The seasonal occurrence of the most severe windstorms has also changed, shifting from September-November in the 1960's and 1970's to December-February in the 1990's and onwards. Gregow et al. (2017) also found that the severe large scale

winter storms correlate with North Atlantic Oscillation (NAO) whereas the storms occurring during autumn do not correlate with NAO. They discussed the possible linkages between Arctic climate change and autumn storminess and considered that as a topic that should be further investigated.

A detailed dynamical analysis was performed about storm Mauri that occurred in northern Finland on 22 September 1982, causing two fatalities and 3 Mm^3 of forest damage. By using ERA-Interim reanalysis data, Laurila (2016) found a connection between storm Mauri and the extratropical transition of Hurricane Debby. Ongoing research with the aid of numerical model simulations has preliminarily indicated that the linkage between Debby and Mauri was complex and that the interaction with another extratropical cyclone was essential for transitioned Debby to travel to Finland and lead to damaging winds (Laurila et al., 2019, in preparation).

Joint effect of high sea level and high waves

Extreme sea level events have been an important research topic in EXWE since 2008, as all Finnish NPPs are located on the coastline. The efforts have mainly concentrated on improving the estimates of probabilities of coastal flooding in the current and future climate.

Leijala et al. (2018) combined the probability distributions of three different components: (1) long-term mean sea level change, (2) short-term sea level variations and (3) wind-generated waves, using a method based on the probability of the sum of two independent random variables. With this approach, a single probability distribution for the total water level was obtained in contrast to earlier estimates, in which a fixed, location-specific wave action height was added to account for the effect of waves. The method can be used to estimate flooding probabilities in the present conditions as well in the future.

The method was developed and tested using data from the Helsinki archipelago, but it is applicable to any location on the Finnish coast as long as sufficient information on sea level variations and waves is available to form the probability distributions. Sea level variations are well recorded by the Finnish tide gauge network, but wave observations are more limited. Wave conditions are highly location-dependent, and open-sea observations are generally not representative of the wave field close to the shore. Leijala et al. (2018) used data from short nearshore measurement campaigns to define attenuation factors which can then be used to estimate nearshore wave conditions based on the much longer time series of open sea observations. Similar local measurement campaigns are recommended for any location where accurate flood risk estimates are needed. The limited spatial coverage of the measurements can be augmented with results from a validated numerical wave model.

Theoretical considerations of Leijala et al. (2018) showed that the effect of waves cannot generally be quantified by a wave action height that is independent of the risk level (events/year) considered. This is especially true if the height of the wave run-up is clearly dominant compared to the background sea level variations. Nevertheless, if the wave run-up is small relative to other water level variations—such as

in the case of a sheltered coastline—the additional effect of the waves in a specific location is almost constant for all risk levels that are typically considered.

Leijala et al. (2018) assumed that sea level and wave height are independent random variables. The method was refined further by examining the dependency between the two parameters in the follow-up study of Särkkä et al. (2018). They used 27 years of sea level observations from Helsinki; the significant wave height during this period was modelled using wind observations and validated against wave buoy measurements. The analysis suggested some correlation between the two variables. The correlation depends on wind direction, reflecting the effect of local topography on the interplay of wind, waves, and sea level surges. Särkkä et al. (2018) constructed the joint distribution of sea level and waves using a bivariate Weibull distribution, but as the variables are not clearly Weibull-distributed, a more flexible copula approach will be applied to further analyse the effect of the dependency on the total water level distributions.

Meteotsunamis

Meteotsunamis are long, tsunami-like waves caused by air pressure disturbances, such as thunderstorms, moving over the sea. When the speed of the disturbance coincides with the speed of a tsunami wave in the sea, the resonance between atmosphere and ocean leads to the amplification of the wave. Virtually nothing was known about the occurrence of this phenomenon in Finland before the work around the topic started in EXWE in 2012, prompted by several eyewitness observations of such waves in 2010 and 2011.

Extensive research efforts have produced a unique century-long time series of meteotsunami occurrence in the Gulf of Finland (Fig. 4; Pellikka et al. 2018). Dozens of meteotsunamis have been identified in sea level observations, both in the archived paper recordings of the tide gauges and in high-resolution digital sea level data. This has enabled us to sketch first estimates of exceedance probabilities of meteotsunami heights on the Finnish coast (Pellikka et al. 2016).

Typical meteotsunami heights recorded by the tide gauges are 10–30 cm, while the eyewitnesses have reported oscillations of up to 1 m (Pellikka et al. 2014). The eyewitness observations represent events in which the wave is locally amplified through resonance mechanisms related to coastal bathymetry. The probability distributions of meteotsunamis were extended towards stronger events by a simple scaling, backed with refraction model results. Such scaled distributions, however, are based on rather crude assumptions and have large uncertainties.

New insights have also been gained regarding the atmospheric conditions that create meteotsunamis. Comparing the meteotsunami occurrence with lightning observations revealed that meteotsunamis on the Finnish coast are strongly connected to thunderstorms (Pellikka et al. 2018). Pellikka et al. (2017) analysed the 1-min sea level data available from 2004 onwards to see what kind of meteorological conditions created the strongest events of rapid sea level oscillations. Synoptic conditions differed clearly between the summer and winter seasons: Summer events were generally caused by cold fronts or mesoscale convective systems propagating

over the sea with a resonant speed. Winter events were related to cold fronts, and storm winds were frequently present. Sea level oscillations were generally slower than during the summer events, indicating that the events were small storm surges rather than meteotsunamis.

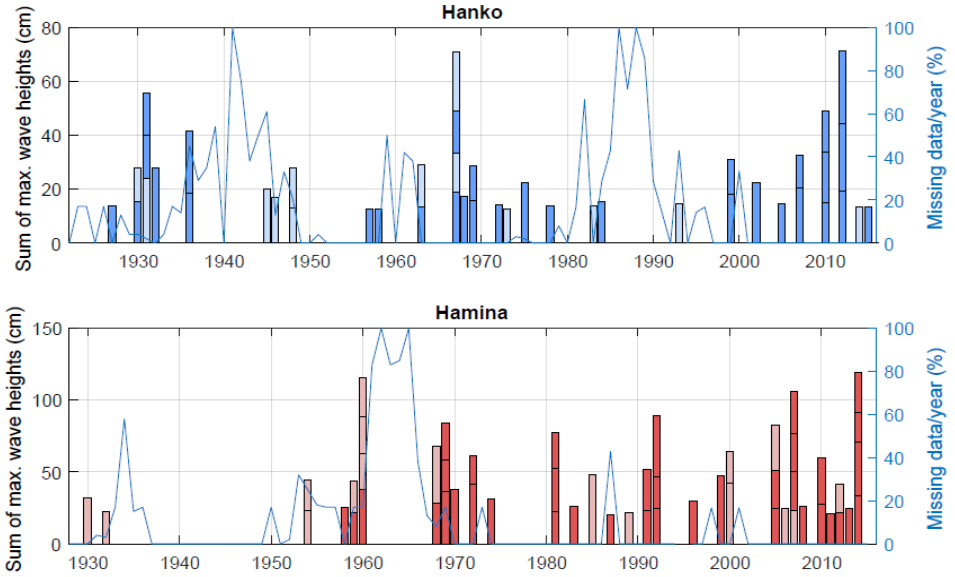

Figure 4. Meteotsunamis identified in the sea level records of Hanko and Hamina. The height of the columns represents maximum wave height, and the events recorded each year are stacked. The events plotted with dark colour have been confirmed from air pressure observations, while the atmospheric origin of the light-coloured events is uncertain. The blue curves show the proportion of missing data per year.

Advances in sea level and wave modelling

Sea level and wave models are useful tools for estimating the probabilities of extreme sea level events. Model data can be used to complement observations where they are sparse or non-existent, and extending the observational time series with simulated data allows estimates of rare sea level events. Modelling can also deepen our understanding of the factors that cause extreme sea level events and trends in the extremes. Validating the simulations against observations is essential for estimating the reliability of the models.

Two model validation studies were performed in EXWE during the SAFIR2018 period. Särkkä and Johansson (2018) simulated Baltic Sea level over the period 1900–2010 using a two-dimensional hydrodynamic model to calculate internal var-

iations within the Baltic Sea basin, while water volume variations due to water exchange in the Danish Straits were simulated using a statistical model based on wind speeds. The wind and air pressure forcing was taken from the atmospheric reanalysis dataset ERA-20C produced by the European Centre for Medium-Range Weather Forecasts.

Simulated sea levels agreed well with tide gauge observations from Finland and Sweden, but highest sea level extremes were underestimated because of the insufficient resolution of the atmospheric forcing data. Positive trends in sea level maxima after 1960 were identified at all tide gauges. Simulated sea levels were divided in 1) the storm surge component caused by local short-term sea level variations and 2) the water balance component caused by variations in the total water amount of the Baltic Sea. Despite the positive trends in total sea level, the study found opposing trends in the storm surge component: positive trends on the Finnish coast and negative trends in Sweden. This might be caused by an eastward shift of the tracks of low pressure systems in the region (Särkkä and Johansson 2018).

The complex Finnish coastline with thousands of small islands poses challenges for nearshore wave modelling, and more research is needed before the wave models can reach the same accuracy close to the shore as has been demonstrated on the open sea. Björkqvist et al. (2017) compared the performance of three wave models (WAM, SWAN and WAVEWATCH III) in the Helsinki archipelago by validating them against observations from nine wave buoys. The three models simulated the significant wave height equally well in the archipelago, but small differences between the models still affected the estimates of e.g. the dominant wave period.

Mean sea level scenarios

Global mean sea level rise (SLR) is a hot topic in sea level science, given the large uncertainties in SLR predictions and their significance for coastal adaptation and flood protection. New studies are published regularly, and it is important to update the flooding risk estimates calculated for the Finnish coast regularly with the latest information. Pellikka (2016) reviewed recent literature on SLR scenarios and Antarctic ice sheet instability, which is the largest uncertainty in the predictions. At that time, worst-case scenarios were close to 2 m during the 21st century, but since then, Le Bars et al. (2017) extended the upper limit to 2.9 m, illustrating the large uncertainties in the low-probability, high-impact upper tail of the distribution.

Pellikka et al. (2019) calculated new scenarios for mean sea level on the Finnish coast based on an ensemble of recent predictions, including Le Bars et al. (2017). The most important difference compared to earlier estimates is that the scenarios were calculated separately for three Representative Concentration Pathway (RCP) scenarios, representing different climate change mitigation policies. Thus, more information is now available about the effect of the future carbon emission pathway to mean sea level on the Finnish coast. Results for the NPP sites are summarized in Table 1.

Table 1. Projected mean sea level change in 2000–2100 at the Finnish NPP sites for the three Representative Concentration Pathway (RCP) scenarios and different probability levels (Pellikka and Johansson, 2019).

	Hanhikivi			**Olkiluoto**			**Loviisa**		
	RCP2.6	RCP4.5	RCP8.5	RCP2.6	RCP4.5	RCP8.5	RCP2.6	RCP4.5	RCP8.5
1%	-88	-80	-65	-67	-59	-44	-28	-19	-3
5%	-81	-71	-54	-61	-51	-33	-21	-10	8
50%	-61	-47	-22	-41	-26	-1	0	15	42
95%	-37	-1	59	-16	22	84	25	64	129
99%	-23	29	108	-2	54	135	39	97	181

Extreme space weather and its effects

Normal operation of technological conductor systems, such as high-voltage power grids, can be disturbed by geomagnetically induced currents (GIC) that are quasi-DC currents compared to the AC frequency of 50 Hz (Molinski, 2002). GIC are driven by geoelectric fields at the Earth's surface that are caused by time variations of the geomagnetic field.

Globally, there have been only a few big GIC events per decade (Boteler et al., 1998). Before 1989, GIC has evidently caused only short terminations in power distribution. An extensive blackout occurred in Québec, Canada, in March 1989 (Bolduc, 2002), and a transformer in New Jersey, USA, was permanently damaged (Kappenman and Albertson, 1990). In October 2003, there was a blackout in Malmö (Pulkkinen et al., 2005). One of the largest GIC events in Finland occurred on 24 March 1991, during which GIC up to 200 A were recorded at the Rauma 400 kV station, however, without harmful impacts.

The number of direct observations of the geoelectric field in the Nordic countries is small. The largest values up to about 4-5 V/km are known from Sweden (Wik et al., 2009). It can be indirectly estimated that the peak maximum geoelectric fields in Finland have been at most some V/km.

Based on space plasma simulations with hypothetical solar wind input, Ngwira et al. (2014) concluded that geoelectric fields larger than twice those produced by March 1989 or the October 2003 storms could occur. Ngwira et al. (2013) considered the July 2012 event when a strong solar wind burst was observed at the Earth's orbit, but aside our planet. A direct hit could have produced slightly larger electric fields than those during the March 1989 or the October 2003 storms.

Extreme geoelectric fields can also be assessed from the measured magnetic field and ground conductivity models. Viljanen (2016) performed a test using 1-min magnetic data from Nurmijärvi (1975-2015) and Sodankylä (1980-2010) and a simple 2-layer ground model. In that test, the largest storms appeared to be 13 July 1982 and 30 October 2003. At Nurmijärvi, the modelled July 1982 storm is about 1.5 times larger than the second largest one. The electric field reached equally large values at Nurmijärvi as at Sodankylä, under the assumption of identical ground conductivity models.

Using North European magnetometer data in 1993-2006 as input in their model of the electric field, Pulkkinen et al. (2012) found that a 1-in-100 year extreme value could be about twice the maximum in 1993-2006. Based on a similar analysis for Norway, Myllys et *al.* (2014) found the 100-year maximum geoelectric field to be about twice the peak in 1994-2011 and close to the modelled electric field on 13-14 July 1982. Wintoft et al. (2016) indicated that the largest possible electric fields might already have occurred at northern latitudes during the latest 20-30 years. However, we can still expect two times larger values within 50-150 years, or even more frequently in Central and Southern Europe.

The longest high-resolution time series of modelled peak geoelectric fields, one for Victoria and another for Ottawa, Canada, have been used by Nikitina et al. (2016) for extreme value analysis (Fig. 5a). The 1-in-50 years and 1-in-100 years return level estimates in Fig. 5a were normalized by Viljanen (2016) with respect to the largest modelled geoelectric field that was calculated using the measured magnetic field at Canadian observatories. The results shown in Fig. 5b suggest that at observatories with data for at least 39 years, the extreme value is in nearly all cases only 10-20% larger than what would have been observed within the period covered by data. At other stations (17-31 years of data), a relatively larger extreme electric field is expected. So we concluded that a time series of about 40 years already contains an event close to the one expected to occur once in 100 years. On the other hand, time series of 30 years or shorter yield overestimated values for a once in 100 year's event.

Attention to GIC problems has mostly concentrated on immediate impacts. However, Gaunt and Coetzee (2007) found increased levels of dissolved gases at South African high-voltage transformers after large storms in 2003, and suggested this to be the reason for that some transformers had to be removed from service after the stormiest period. Schrijver et al. (2014) analysed insurance claims for equipment losses and related business interruptions in North American commercial organizations that are associated with problems in electrical and electronic equipment. They found elevation of claim rates with increased geomagnetic activity.

GIC amplitudes as such do not provide a direct measure to assess risks, but we need to consider the tolerance of high-voltage transformers. Although currents up to 200 A have been measured in Finland, and larger values have probably occurred, there have been no harmful impacts. This is due to the special design of the Finnish high-voltage power grid (Elovaara, 2007; Lahtinen and Elovaara, 2002). Based on a transformer test and modelled GIC statistics, Lahtinen and Elovaara (2002) do not

consider GIC as a significant risk in Finland. However, they note that the risk depends on the transformer design. Consequently, when installing new transformers, GIC is still one factor to be taken into account.

Nearly all studies of space weather effects on power grids consider only GIC. Molinski (2002) mentions that space weather affects ground-based communication systems, communication satellites and propagation of navigation signals reflected from or going through the ionosphere. He does not refer to any consequent impacts on power grids. However, Svenska Kraftnät (2012) recommends measures to be taken to ensure precise time information at substations, which could be endangered in case of GPS problems.

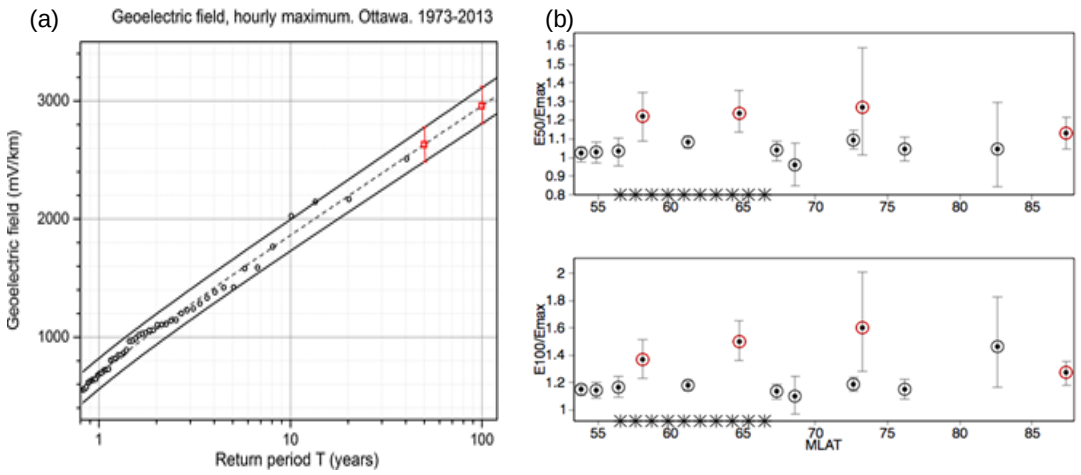

Figure 5. (a) Fitting of the modelled peak geoelectric fields (circles) in Ottawa to an extreme value distribution (dashed line) with 99% confidence intervals (solid lines). The predicted values once per 50 years and once per 100 years are denoted by red squares (Nikitina et al., 2016, Fig. 7). (b) Estimated 1-in-50 years (top) and 1-in-100 years (bottom) geoelectric field normalised by the maximum value modelled from magnetic data at Canadian observatories. Data coverage of 17-31 years is denoted by red and 39-42 years by black. Vertical bars indicate the 99% confidence intervals. The horizontal axis shows the geomagnetic latitude. Asterisks indicate the geomagnetic location of Finland. The plot is based on Nikitina et al. (2016, supporting information, Table S3).

High-resolution meteorological and dispersion modelling

The dispersion calculations performed for nuclear safety assessments are typically based on Gaussian dispersion modelling. However, this assumption limits such studies to the range of 10–20 km from the site, and moreover, the Gaussian models

are not well suited for simulating dispersion driven by coastal wind systems, such as sea-breeze circulation, low-level jets, and air flows between a marine atmospheric boundary layer and a coastal one. Meanwhile, Lagrangian and Eulerian dispersion models, such as the FMI's SILAM model (Sofiev et al., 2006, 2015), have been developed for operational use in combination with numerical weather prediction (NWP) models. In parallel, NWP modelling, using e.g., the HARMONIE-AROME model already referred to before (Fig. 2), has progressed to a stage where coastal meteorological conditions can be properly assessed and fed into the dispersion modelling system.

Operational weather prediction systems covering the Finnish domain employ a horizontal grid stepping of 2500 m at best, which was too coarse to be applicable in the kilometre-scale dispersion modelling targeted within EXWE. Therefore, a version of the HARMONIE-AROME numerical weather prediction system, suitable for providing input for high-resolution dispersion modelling on a kilometre-scale, was set up and executed on a domain of about 300 km x 300 km, with a grid having a spacing of only 500 m in the horizontal. For that purpose, in order to correctly represent important air-surface interaction, adequate methods to aggregate and interpolate topographic data (terrain-elevation, distribution and properties of water or land surfaces, land use, vegetation covers, built-up areas, etc.) were essential (Kurzeneva et al., 2016).

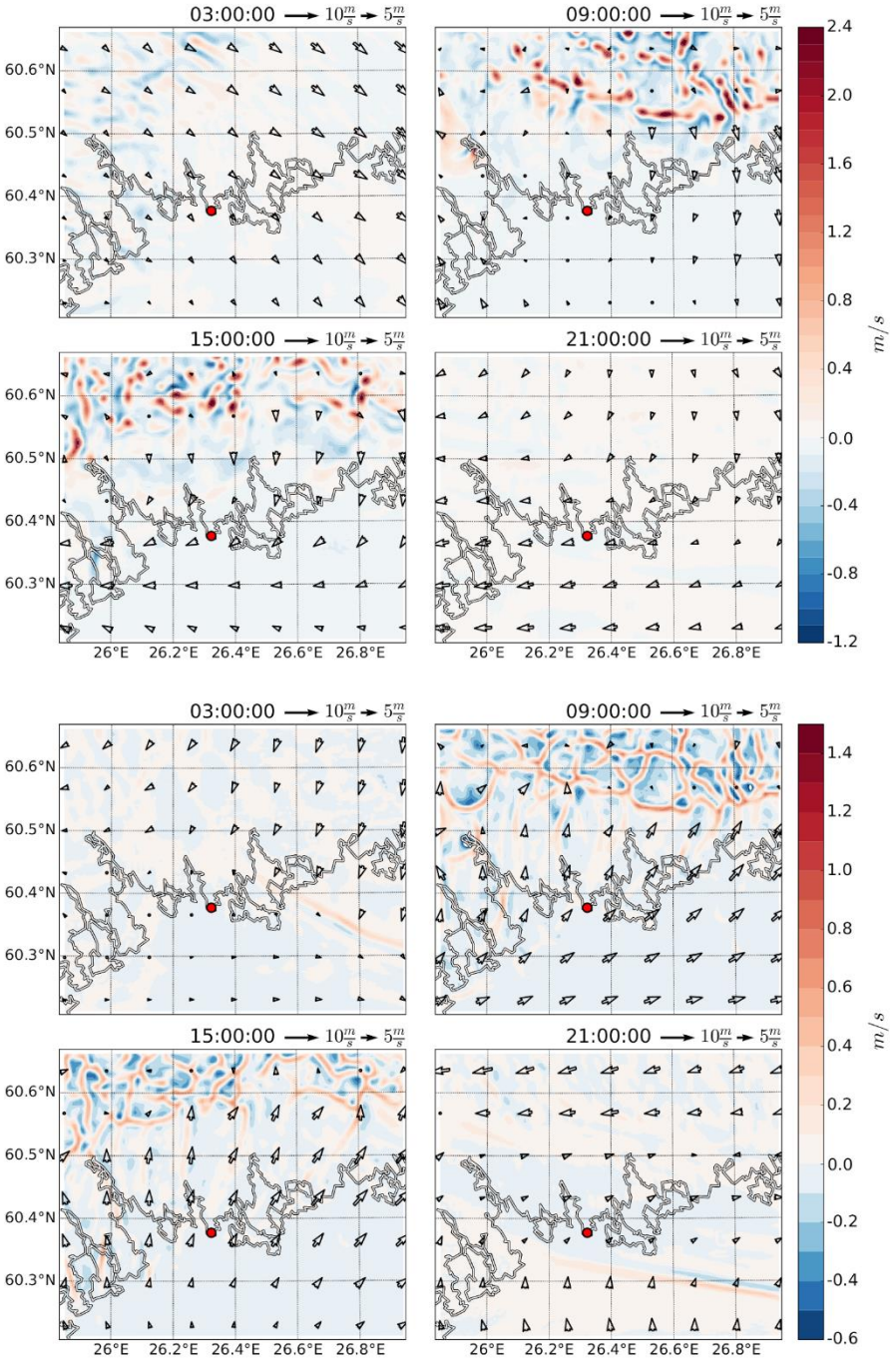

Figure 6. Horizontal distribution of the predicted vertical velocity (color-shading) and horizontal wind (arrows) in a developing sea-breeze circulation on the 17th of May 2015 at 1300 m above ground (top) and 100 m above ground (bottom).

The very high resolution (500 m) HARMONIE-AROME model version was used to generate hind-casts for the Loviisa NPP site in April and May 2015. The simulated meteorological data, with a temporal resolution of one hour, were compared to a rich set of measurements available at that time (Jurvanen, 2015). The comparisons confirmed that HARMONIE-AROME was able to respond to the thermal and mechanical contrast between land and sea in a realistic manner. Results for 3-6 May, presented in Jylhä et al. (2017, Fig. 10), show that variations in wind direction were well predicted by HARMONIE-AROME from the surface up to the maximum LIDAR measurement height of 200 m. In particular, variations in wind direction and speed associated with the sea-breeze circulation developing in response to differential heating over land and sea on the cloudless afternoon of 4 May, turning the low level wind from a roughly westerly direction into southwest, was well simulated by the model.

An example of the transition from a marine boundary layer structure to a coastal one is seen in the profiles of potential temperature from HARMONIE-AROME on 15 UTC on 4 May, extracted along a line passing the Loviisa NPP from south to north (Fig. 11 in Jylhä et al., 2017). It can be clearly seen how the cold surface temperature and stably stratified marine boundary layer, found over the Gulf of Finland, gradually gives way to a heated surface and a convective well-mixed over the inland. As the distance from the coast increases, so does the temperature and the depth of the well mixed layer.

The ability of HARMONIE-AROME to generate realistic flow-patterns in a developing sea-breeze is demonstrated in Fig. 6, taken from Korpinen (2018). As the sea-breeze circulation develops during the morning hours, rising motions over land close to the surface are organized into open cells and these merge into convective plumes at higher altitudes.

The examples above suggest that forecasts generated by the HARMONIE-AROME system are likely to become a valuable data source for dispersion modelling and dispersion forecasting. In order to demonstrate that, the high-resolution meteorological fields were supplied to SILAM, which was, for the first time, applied at 500 m spatial resolution. The simulations indicated that there are no principal unsolved problems in running the model with such a resolution. The simulations showed the development of intermittent 3-D plumes, their sharp uplift due to convection over terrestrial part of the domain, with examples shown in Figure 7. For additional examples, see Fig. 8 in Jylhä et al. (2018).

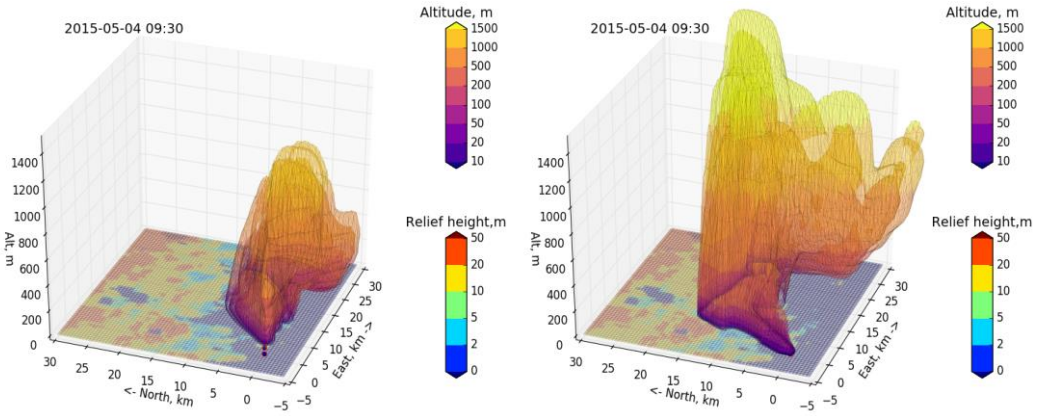

a) Source height 500 m b) Source height 10 m

Figure 7. Position of the plume after 2.5 hours since the start of the release with two different heights of the source. Panel a) high source at 500 m above the ground, panel b) low source, 10 m above the ground.

Considering Figure 7, one can see that the position of the plume released from the near-ground source is *higher* than that of the plume released from the high source (500 m). The reason is quite straightforward: near the ground, a low-level jet brings the plume ashore, where it is picked by a convective turbulence. As a result, within just 2.5 hours the top of the initially low-level plume exceeds 1500m, while the plume initially released at 500 m height barely reaches 1000 m.

This case study, purely accidental in tiny details of the plume behaviour, shows, however, how complex the behaviour of the coastal meteorological systems and their impacts on dispersion can be. Accounting them for the evaluation of specific episodes is the only way to obtain a realistic pattern. Simplified approaches would lead to large and poorly quantifiable errors. The situation for longer-term average fields can be much less dramatic: details of individual episodes will average out and, e.g., monthly or annual distribution of concentrations is much less sensitive to the above peculiarities. But for accidental releases it is the episodes that matter.

Apart from the high-resolution simulations and connection to HARMONIE-AROME, new radioactive dose calculation models were integrated to SILAM (mostly using the FMI own funding, but also usable for the EXWE purposes). Work was done within the major update of the SILAM dose module, which interface is now embedded into the main SILAM core. This work laid down the foundation of the SILAM interface towards the impact assessment applications. Sofiev et al. (2017) documented in detail the current user interface for SILAM v5 chemical transport model.

Conclusions

The general objective of EXWE was to give better estimates of probabilities of occurrence and magnitude of extreme geophysical events that affect the design principles of NPPs and may pose external threats to the plants. A spectrum of different sources of information was utilized as the research material, and the methods included various modelling and machine learning approaches. The main findings of EXWE in 2015-2018 are given below:

- Extreme convective weather (ECW) phenomena are caused by mesoscale convective systems (such as derechos), detached thunderclouds or convective elements in extratropical cyclones. Notable cross correlations were found between i) thunderstorm days, lightning and heavy rainfall, ii) heavy rainfall and tornadoes and iii) large hail and tornadoes. Atmospheric conditions and synoptic-scale circulation patterns favouring significant hail in Finland were compared to tornado situations. Thunderstorm occurrence was efficiently identified from reanalysis data using neural networks (NN). The NN and boosted decision tree methods were found to improve forecasting of thunderstorms over different climatological regions. A measure of atmospheric instability (CAPE) showed a significant positive trend over the past 40 years (1979-2018) in Finland.
- While summertime ECW is more likely to occur, wintertime sea-effect ECW occasionally develops over ice-free sea areas. Depending on the mean wind direction, excess coastal snowfall may occur, as happened in Merikarvia on 6 January 2016, with 73 cm of new snow. Simulations with the non-hydrostatic convection-permitting HARMONIE-AROME numerical weather prediction model were used to examine four past sea-effect snowfall cases at the coasts of Finland. The model was able to capture the timing and the location of the snowstorms. Favourable conditions for sea-effect snowfall to occur were assessed from these simulations. Results from a detailed study of the Merikarvia case results were encouraging towards the use of ERA5 reanalysis data in identification of historical sea-effect cases and their frequency.
- After calibrations against SYNOP weather station observations in Europe, a method for estimating the occurrence of freezing rain (FZRA) in gridded atmospheric datasets was used together with reanalysis data and output from regional climate models. In Olkiluoto, the projections for the most intense FZRA cases showed future shifts towards smaller probability levels for accumulations periods. In Loviisa, the projected sign of the FZRA change depended on the emission scenario and the accumulation period. The largest chance for potential increases in very severe FZRA appeared in Hanhikivi. The co-occurence of freezing rain and high wind speeds at the Finnish NPP sites showed no conclusive results.

- The year 1990 was found to represent a change-point after which large scale forest damages induced by windstorms have increased by a factor of three in Europe. Also the seasonal occurrence of the most severe windstorms has changed in time. A detailed dynamical analysis of storm Mauri (22nd September 1982) in Finland was performed. Besides the windstorm climate, the impacts of the storms depend on environmental conditions (decrease in soil frost, increase in forest growth), urbanization, and increased dependence on electricity and communication networks.
- An improved method to estimate coastal flooding probabilities as a joint effect of sea level and wind waves was developed. The method is applicable to any location on the Finnish coast as long as sufficient information on sea level variations and waves is available to form the probability distributions. Because wave observations are usually the limiting factor, local wave measurement campaigns are highly valuable for accurate flood risk estimation.
- A century-long time series of meteotsunami occurrence in the Gulf of Finland has been produced, enabling us to sketch first estimates of exceedance probabilities of meteotsunami heights. Meteotsunami occurrence on the Finnish coast is strongly linked to thunderstorms.
- Sea level and wave models are useful tools for estimating the probabilities of extreme sea level events, and validating the simulations against observations is essential. High-resolution atmospheric forcing data is needed for accurate simulation of sea level extremes.
- Recent worst-case predictions of global mean sea level rise during the 21st century are higher than previous estimates, extending up to 2.9 m. New scenarios calculated for the Finnish coast give more information on the effect of the future carbon emission pathway to mean sea level change at the NPP sites.
- Although no serious effects have occurred in Finland, large geomagnetically induced currents must be taken into account when installing new transformers or power lines affecting the operation of NPPs.
- Introduction of high resolution weather prediction systems opens up opportunities for high resolution dispersion modelling which resolves explicitly both mesoscale (convection, land-sea breezes) and large scale meteorological features. Simulations with the HARMONIE-AROME numerical weather prediction (NWP) system of a few past sea-breeze circulation cases showed that the flow patterns and coastal heterogeneity in atmospheric conditions can be realistically simulated, provided that a sufficiently high resolution is used.
- The high-resolution meteorological fields from the NWP system were supplied to the SILAM dispersion model, which was, for the first time, applied at 500 m spatial resolution. The case study demonstrated how complex the

behaviour of the coastal meteorological systems and their impacts on dispersion can be in an episode of accidental releases.

- New radioactive dose calculation models have been integrated to SILAM, which laid down the foundation of the SILAM interface towards the impact assessment applications.

Acknowledgement

In addition to the funding granted by the State Nuclear Waste Management Fund in Finland, this work has been partly finalized by the Swedish Radiation Safety Authority, the Finnish Meteorological Institute, the European Union's Seventh Programme for research, technological development and demonstration under the RAIN project (Risk Analysis of Infrastructure Networks in response to extreme weather; http://rain-project.eu/; grant agreement no. 608166) and the EU funded Copernicus Climate Changes Service Clim4Energy project (http://clim4energy.climate.copernicus.eu/). We acknowledge Fingrid for long-term collaboration in studies of geomagnetically induced currents in the Finnish high-voltage power grid.

References

Björkqvist, J.-V., Vähä-Piikkiö, O., Alari, V., Kuznetsova, A., & Tuomi, L. 2017. WAM, SWAN and WAVEWATCH III in the Finnish archipelago — The effect of spectral performance on bulk wave parameters. SAFIR2018/EXWE deliverable D2.2.1 in 2017.

Bolduc, L., 2002. GIC observations and studies in the Hydro-Québec power system. J. Atmos. Sol.-Terr. Phys., 64, 1793-1802, doi:10.1016/S1364-6826(02)00128-1.

Boteler, D.H., Pirjola, R.J. & Nevanlinna, H. 1998. The effects of geomagnetic disturbances on electrical systems at the earth's surface. Adv. Space Res., 22, 17-27, doi:10.1016/S0273-1177(97)01096-X.

Bolduc, L. 2002. GIC observations and studies in the Hydro-Québec power system. J. Atmos. Sol.-Terr. Phys., 64, 1793-1802, doi:10.1016/S1364-6826(02)00128-1.

Elovaara, J. 2007. Finnish experiences with grid effects of GIC's. In: Space Weather - Research Towards Applications in Europe (ed. J. Lilensten), Astrophysics and Space Science Library, 344, 311-326.

Gaunt, C.T. & Coetzee, G. 2007. Transformer failures in regions incorrectly considered to have low GIC-risk. Proceedings of the IEEE Powertech Conference, July 2007, Lausanne, Switzerland, paper 445, 6 pp, doi: 0.1109/PCT.2007.4538419.

Gregow, H., Muzaffer, E. A. & Laaksonen, A. 2017. Increasing large scale windstorm damage in Western, Central and Northern European forests, 1951-2010. Scientific Reports. (http://rdcu.be/q66j)

Himanen, R., Julin, A., Jänkälä, K., Holmberg, J.E. & Virolainen, R. 2012: Risk-Informed regulation and safety management of nuclear power plants - On the prevention of severe accidents. Risk Analysis, 32, 1978–93. https://doi.org/10.1111/j.1539-6924.2012.01904.x

Juga, I., Hippi, M., Moisseev, D. & Saltikoff, E 2012. Analysis of weather factors responsible for the traffic 'Black Day' in Helsinki, Finland, on 17 March 2005. Met. Apps, 19: 1-9. doi:10.1002/met.238

Juga, I., Hippi, M., Karsisto, V. & Nurmi, P. 2014. Weather factors triggering the massive car crashes on 3 February 2012 in the Helsinki metropolitan area, in: Proceedings of the 17 th SIRWEC conference, 30 January-1 February 2014, La Massana, Andorra.

Jurvanen, J.-P. 2015. Sekoituskerroksen korkeuden arviointi eri menetelmin Loviisan ydinvoimalaitoksen läheisyydessä. Master's thesis, University of Helsinki, Department of physics (in Finnish).

Jylhä K., Björkqvist, J.-V., Fortelius, C., Gregow, H., Heinonen, S., Hongisto, M., Hyvärinen, O., Johansson, M., Karppinen, A., Korpinen, A. Kurzeneva, E., Kämäräinen, M. Laurila, T., Lehtonen, I., Leijala, U., Mäkelä, M., Olsson, T., Pellikka, H., Perttula, T., Rauhala, J., Sofiev, M., Särkkä, J., Vajda, A., Venäläinen, A. & Viljanen, A. 2017. Extreme weather and nuclear power plants (EXWE). In J. Hämäläinen & V. Suolanen (eds.): SAFIR2018 – The Finnish Research Programme on Nuclear Power Plant Safety 2015–2018 Interim Report. VTT Technology 294, ISBN 978-951-38-8524-3, https://www.vtt.fi/inf/pdf/technology/2017/T294.pdf, p. 104-124.

Jylhä K, M. Kämäräinen, C. Fortelius, H. Gregow, J. Helander, O. Hyvärinen, M. Johansson, A. Karppinen, A. Korpinen, R. Kouznetsov, E. Kurzeneva, U. Leijala, A. Mäkelä, H. Pellikka, S. Saku, J. Sandberg, M. Sofiev, A. Vajda, A. Venäläinen, & J. Vira, 2018. Recent meteorological and marine studies to support nuclear power plant safety in Finland. Energy, 165 (A), 1102-1118. https://doi.org/10.1016/j.energy.2018.09.033

Jänkälä, K.E. 2016. Analysing and decreasing external event risks of Loviisa NPP. 13th International Conference on Probabilistic Safety Assessment and Management (PSAM 13), http://www.psam13.org/. p. A-204.

Kappenman, J.G. & Albertson, V.D. 1990. Bracing for the geomagnetic storms. IEEE Spectrum, March 1990, 27-33.

Korpinen, A. 2018. Rajakerroksen simulointi heterogeenisellä alustalla. Master's thesis, University of Helsinki, Institute for Atmospheric and Earth System research. (In Finnish)

Kurzeneva, E., Fortelius, C., Karppinen A., & Sofiev, M. 2016. HARMONIE code update for preparation of high-resolution physiography data files. EXWE/SAFIR2018 project report, FMI.

Kämäräinen, M. & Jokinen, P. 2015. Severe winter weather in Finland: Part II: Freezing rain and lake-effect snowfall. EXWE/SAFIR2014 project report 2014, Finnish Meteorological Institute.

Kämäräinen, M., Hyvärinen, O., Jylhä, K., Vajda, A., Neiglick, S., Nuottokari, J. & Gregow, H. 2017a. A method to estimate freezing rain climatology from ERA-Interim reanalysis over Europe, Nat. Hazards Earth Syst. Sci., 17, 243-259, doi:10.5194/nhess-17-243-2017.

Kämäräinen, M., Jylhä, K., Hyvärinen, O. & Vajda, A. 2017b. Present-day and future probabilities of severe freezing rain at the nuclear power plant sites in Finland. EXWE/SAFIR2018 deliverable D1.3.1 in 2017, Finnish Meteorological Institute.

Kämäräinen M, Hyvärinen O, Vajda A, Nikulin G, Meijgaard E, Teichmann C, Jacob D, Gregow H, Jylhä K., 2018: Estimates of present-day and future climatologies of freezing rain in Europe based on CORDEX regional climate models. Journal of Geophysical Research: Atmospheres, 123, 13291-13304. https://doi.org/10.1029/2018JD029131

Lahtinen, M. & Elovaara, J., 2002. GIC Occurrences and GIC Test for 400 kV System Transformer. IEEE Trans. Power Delivery, 17, 555-561.

Laurila, T. K., 2016. Extratropical transition and characteristics of storm Mauri in September 1982. Master thesis, Univ. of Helsinki, Department of Physics, 51 p.

Laurila T. K., J. Rauhala, T. Olsson, A. Mäkelä, & K. Jylhä, 2016. Historical time series of extreme convective weather. EXWE/SAFIR2018 project report 2016, Finnish Meteorological Institute.

Laurila T. K., Sinclair, V. A, & Gregow, H. 2019: Transition of Hurricane Debby and its re-development into an intense windstorm in Finland. (in preparation)

Le Bars, D., Drijfhout, S. & de Vries, H., 2017. A high-end sea level rise probabilistic projection including rapid Antarctic ice sheet mass loss. *Environmental Research Letters* 12 (4), 044013.

Leijala, U., Björkqvist, J.-V., Johansson, M.M., Pellikka, H., Laakso, L. & Kahma, K.K., 2018. Combining probability distributions of sea level variations and wave run-up to evaluate coastal flooding risks. *Natural Hazards and Earth System Sciences* 18 (10), 2785–2799.

Luomaranta, A., Kämäräinen, M., Laurila, T. K. & Jylhä K., 2016. Severe winter weather in Finland, Part III: Past sea-effect snowfall cases and predictors

of extreme cold-season convective weather. EXWE/SAFIR2018 project report 2015, Finnish Meteorological Institute.

Molinski, T.S. 2002. Why utilities respect geomagnetically induced currents. J. Atmos. Sol.-Terr. Phys., 64, 1765-1778, doi:10.1016/S1364-6826(02)00126-8.

Myllys, M., Viljanen, A., Rui Ø.A. & Ohnstad, T.M. 2014. Geomagnetically induced currents in Norway: the northernmost high-voltage power grid in the world. J. Space Weather Space Clim., 4, A10, doi: 10.1051/ swsc/2014007.

Mäkelä, A., J. Rauhala, A.-J. Punkka, J. Tuovinen, & K. Jylhä 2016. Past cases of extreme warm season convective weather in Finland. EXWE/SAFIR2018 project report 2015, FMI.

Ngwira, C.M., Pulkkinen, A., Leila Mays, M., Kuznetsova, M.M., Galvin, A.B., Simunac K., Baker, D.N., Li, X., Zheng Y. & Glocer, A. 2013. Simulation of the 23 July 2012 extreme space weather event: What if this extremely rare CME was Earth directed? Space Weather, 11, doi:10.1002/2013SW000990.

Ngwira, C.M., Pulkkinen, A., Kuznetsova, M.M. & Glocer, A. 2014. Modeling extreme "Carrington-type" space weather events using three-dimensional global MHD simulations. J. Geophys. Res. Space Physics, 119, 4456-4474, doi:10.1002/2013JA019661.

Nikitina, L., Trichtchenko, L. & Boteler, D.H. 2016. Assessment of extreme values in geomagnetic and geoelectric field variations for Canada. Space Weather, 14, doi:10.1002/2016SW001386.

Olsson, T., Perttula, T., Jylhä, K. & Luomaranta, A. 2017. Intense sea-effect snowfall case on the western coast of Finland, Adv. Sci. Res., 14, 231-239 https://doi.org/10.5194/asr-14-231-2017.

Olsson, T., Post, P., Rannat, K., Keernik, H., Perttula, T., Luomaranta, A., Jylhä, K., Kivi, R. & Voormansik, T. 2018a. Sea-effect snowfall case in the Baltic Sea region analysed by reanalysis, remote sensing data and convection-permitting mesoscale modelling, Geophysica, 53(1), 65-91.

Olsson, T., Luomaranta, A. & Jylhä, K. 2018b. Detecting the atmospheric conditions favoring the development of sea-effect snowfall on the Finnish coast from HARMONIE simulations. . EXWE/SAFIR2018 deliverable D1.2.1 in 2018, Finnish Meteorological Institute.

Paillère, H., Cameron, R., Caneill, J. & Syri, S. 2014. Climate Change: Assessment of the Vulnerability of Nuclear Power and Cost of Adaptation. The 19th Pacific Basin Nuclear Conference (PBNC 2014). [http://www.pbnc2014.org/proceedings/html_files/2325.html].

Pellikka, H. 2016. Recent results on future sea level rise and ice sheet instability. Literature review. SAFIR2018/EXWE deliverable D2.3.1 in 2016, Finnish Meteorological Institute.

Pellikka, H. & Johansson, M. 2019. Mean sea level change at the Finnish NPP sites by 2100 under the RCP scenarios. SAFIR2018/EXWE deliverable D2.2.2 in 2018, Finnish Meteorological Institute.

Pellikka, H., Rauhala, J., Kahma, K.K., Stipa, T., Boman, H. & Kangas, A. 2014. Recent observations of meteotsunamis on the Finnish coast. Natural Hazards 74, 197–215.

Pellikka, H., Kahma, K., Karjalainen, A. & Boman, H. 2016. Meteotsunami probabilities at the Finnish NPP sites. SAFIR2018/EXWE deliverable D2.1 in 2015, Finnish Meteorological Institute.

Pellikka, H., Šepić, J., Lehtonen, I. & Vilibić, I. 2017. Synoptic features of high-frequency sea level oscillations in the northern Baltic Sea. SAFIR2018/EXWE deliverable D2.2.1 in 2016, Finnish Meteorological Institute.

Pellikka, H., Laurila, T., Boman, H., Björkqvist, J.-V. & Kahma, K.K. 2018. Historical analysis of meteotsunami occurrence in the Gulf of Finland. SAFIR2018/EXWE deliverable D2.3.1 in 2017, Finnish Meteorological Institute.

Pellikka, H., Johansson, M.M., Nordman, M., Bilker-Koivula, M. & Ruosteenoja, K. 2019. Probabilistic projections for regional sea level rise in Finland by 2100. SAFIR2018/EXWE deliverable D2.2.1 in 2018, Finnish Meteorological Institute.

Pulkkinen, A., Lindahl, S., Viljanen, A. & Pirjola, R., 2005. October 29-31, 2003 geomagnetic storm: geomagnetically induced currents and their relation to problems in the Swedish high-voltage power transmission system. Space Weather, 3, S08C03, doi: 10.1029/2004SW000123.

Pulkkinen, A., Bernabeu, E., Eichner, J., Beggan, C. & Thomson, A.W.P. 2012. Generation of 100-year geomagnetically induced current scenarios. Space Weather, 10, S04003, doi:10.1029/2011SW000750.

Rauhala, J. 2018. Mesoscale factors contributing to a derecho event in northeastern Europe on 8 August 2010. EXWE/SAFIR2018 deliverable D1.1.3 in 2017, Finnish Meteorological Institute.

Rauhala J., T. K. Laurila, A. Mäkelä & K. Jylhä, 2017. Atmospheric conditions and circulation patterns favouring severe convective storm weather in Finland: synoptic setting of significant hail. EXWE/SAFIR2018 deliverable D1.1.4 in 2016, Finnish Meteorological Institute.

Sandberg, J. & Vuorio, U. 2014. The role of external events PSA in the Finnish regulatory approach. Probabilistic Safety Assessment (PSA) of Natural External Hazards Including Earthquakes - Workshop Proceedings, NEA/CSNI/R(2014)9, p. 365–6.

Schrijver, C.J., Dobbins, R., Murtagh, W. & Petrinec, S.M. 2014. Assessing the impact of space weather on the electric power grid based on insurance claims for industrial electrical equipment. Space Weather, 12, doi:10.1002/2014SW001066.

Sofiev, M., Siljamo, P., Valkama, I., Ilvonen, M. & Kukkonen, J. 2006. A dispersion modelling system SILAM and its evaluation against ETEX data. Atmospheric Environment, 40, 674–85. https://doi.org/10.1016/J.ATMOSENV.2005.09.069

Sofiev, M., Vira, J., Kouznetsov, R., Prank, M., Soares, J. & Genikhovich, E. 2015. Construction of the SILAM Eulerian atmospheric dispersion model based on the advection algorithm of Michael Galperin, Geosci.Model Developm. 8, 3497-3522, doi:10.5194/gmd-8-3497-2015.

Sofiev M., Soares, J. & Kouznetsov, R. 2017. SILAM User-interface. EXWE/SAFIR2018 deliverable D4.2.1 in 2016, Finnish Meteorological Institute.

Svenska Kraftnät, 2012. Skydd mot geomagnetiska stormar - Elektromagnetisk påverkan på kraftsystemet (in Swedish), Dnr: 2011/805, 30 March 2012.

Särkkä, J. & Johansson, M., 2018. Sea level extremes simulated from atmospheric reanalyses in the Baltic Sea. SAFIR2018/EXWE deliverable D2.1.1 in 2018, Finnish Meteorological Institute.

Särkkä, J., Björkqvist, J.-V., Leijala, U., Johansson, M.M. & Kahma, K.K. 2018. Mutual dependence of wind waves and sea level variations on the coast of the seasonally ice-covered Gulf of Finland. SAFIR2018/EXWE deliverable D2.1.1 in 2017, Finnish Meteorological Institute.

Ukkonen, P. & Mäkelä, A. 2017. Using machine learning and reanalyses for constructing a multi-decadal convective climatology for Finland Part 1: Development and testing of method. EXWE/SAFIR2018 deliverable D1.1.1 in 2017, Finnish Meteorological Institute.

Ukkonen P., Manzato A. & Mäkelä, A. 2017. Evaluation of thunderstorm predictors for Finland using reanalyses and neural networks. J. Appl. Meteor. Climatol., 56, 2335–2352, https://doi.org/10.1175/JAMC-D-16-0361.1

Ukkonen P. & Mäkelä, A. 2018a: Evaluation of machine learning classifiers for predicting deep convection. Submitted to Journal of Advances in Modeling Earth Systems.

Ukkonen P. & Mäkelä, A. 2018b: Climate change impacts on summer convection in Finland. SAFIR2018/EXWE deliverable D1.1.2. in 2018, Finnish Meteorological Institute.

Viljanen, A., 2016. Extreme space weather effects on nuclear power plants. EXWE/SAFIR2018 deliverable D3.1.1 in 2016, Finnish Meteorological Institute

Wik, M., Pirjola, R., Lundstedt, H., Viljanen, A., Wintoft P. & Pulkkinen, A., 2009. Space weather events in July 1982 and October 2003 and the effects of geomagnetically induced currents on Swedish technical systems. Ann. Geophys., 27, 1775-1787.

Wintoft, P., Viljanen, A. & Wik, M., 2016. Extreme value analysis of the time derivative of the horizontal magnetic field and computed electric field. Ann. Geophys., 34, 485-491, doi:10.5194/angeo-34-485-2016.

3.2 Probabilistic risk assessment method development and applications (PRAMEA)

Ilkka Karanta[1], Kim Björkman[1,] Teemu Mätäsniemi[1], Tero Tyrväinen[1], Marja Liinasuo[1], Terhi Kling[1], Jan-Erik Holmberg[2]; Alessandro Mancuso[3], Ahti Salo[3]

[1]VTT Technical Research Centre of Finland Ltd
P.O. Box 1000, FI-02044 Espoo

[2]Risk Pilot AB
P.O. Box 72, FI-02101 Espoo

[3]Aalto University, Systems Analysis Laboratory
P.O. Box 11100, FI-00076 Aalto, Finland

Abstract

The goal of PRAMEA project has been to develop methods and use of probabilistic risk analysis (PRA), covering most of its currently topical subfields.

A literature survey concerning human reliability analysis (HRA) in advanced control rooms (CR) revealed that there are significant differences in human errors and performance shaping factors between conventional and advanced CRs. Preparation of an IAEA safety report on HRA has been participated. A new framework for the conduct of site level PRA has been created in co-operation with Nordic partners. Dynamic containment event tree modelling techniques have been studied and guidance provided for performing uncertainty analysis in that context. Substantial new features have been implemented to PRA software FinPSA, including integration of PRA levels 1 and 2, a risk integrator for level 2, and a task file for time-dependent analysis. In level 3 PRA, a guidance document has been written in cooperation with Nordic partners, among other things. Novel methods for conducting risk management actions cost-efficiently and in a risk-informed manner, and a method for selecting mitigation actions against cyber threats to electric power systems have been developed.

Introduction

Probabilistic risk analysis (PRA) is a methodology aimed at identifying and quantitatively assessing risks and main contributors to risk of a system, and uncertainties involved. Its main focus is in the accident risks of technical systems. The multitude of possible hazards, complexity of systems involved (humans and organizations,

physical systems, computers and other technical systems interacting), diversity of methods and variety of possible sources of data contribute to the diversity and interdisciplinarity of PRA as a field.
The objective of PRAMEA project was to develop methods and tools for PRA. It covered much of the scope of contemporary active PRA research, including human reliability analysis, site-level PRA, dynamic PRA, PRA of severe accidents, and quantitative risk management. The project was responsible of carrying out most of the PRA research in SAFIR2018.

Human reliability analysis

Human reliability analysis (HRA) is a research field of assessing and predicting the impacts of human performance and error on risk. The main function of HRA is to estimate the probability of human error to perform a task required in a given accident sequence or, from a more qualitative perspective, to identify the causes and sources of human errors and provide them a numeric estimate in the form of likelihood of their realization. HRA typically includes three phases: the identification, the modelling and the quantification of errors.

Requirements for HRA for advanced control rooms

Digital human-system interfaces (HSIs) are becoming common in nuclear power plants (NPPs) through modernisations and new-builds. NPP control rooms with modern digital HSI are commonly referred to as advanced control rooms, and are characterised by integrated information systems, soft controls and computer-based procedures. Most of the HRA methods commonly used today do not properly account for the induced changes in the work of the operator.

In (Porthin et al. 2016), we performed a literature survey that focused on recent development related to HRA in NPPs using digital HSI. The use of digital HSI changes the working environment of the operator, induces new tasks, and modifies group dynamics and communication. This improves crew performance and reduces workload. Negative effects include declined primary task performance due to attention shift to interface management, and sub-optimal use of the HSI in high workload situations due to minimized capability to focus on interface management tasks. Only two known HRA methods, HuRECA and MERMOS, are applicable to digital HSIs. In recent years there has also been some further methodological progress in the field mainly by Korean and Chinese researchers, including proposals for new performance shaping factors and typical error types when using soft controls.

In (Porthin et al. 2017) we examined the use of performance shaping factors (PSFs) in human reliability analysis (HRA) methods when assessing the human error probability (HEP) in post-initiator situations in the main control room, with focus on advanced control rooms. The PSFs of commonly used traditional HRA methods can in general be grouped into nine categories: stress level, action type, experience, time constraints, places where operator actions are taken, procedures, training, HSI

and team factor. In general, first generation HRA methods typically do not address all these PSF categories, whereas many second generation methods address all, or most of, the categories in one way or another. The flexibility and versatility of computerized systems enable both improved support and possibilities for task tailored information to the operator, but at the same time increase the complexity of the user interface and possibilities for new types of errors. It can be concluded that whereas the main categories for PSFs for analogue control rooms are still valid in digital settings, their interpretation and detailed definitions as well as effects on the HEP may be different.

We carried out a case study (Liinasuo & Kling 2019) to identify possible human errors related to accident management. In the study, we focused on human performance with the procedures for primary to secondary leaks (PRISE) in a hybrid control room. Three operators (Shift Supervisor, Reactor Operator, Turbine Operator) of a nuclear power plant were interviewed separately on their experiences and conceptions with PRISE management. The purpose of these interviews was to find out all possible human errors, including unlikely but possible errors. The results show that errors could occur much more often when using analogue user interfaces than the digital user interfaces. However, in most of the cases, the same error could occur with both types of user interfaces. This means that the possibility of an error is not dependent on the type of the user interface. Furthermore, the cause behind the apparently same error may be different, which may affect its probability. More detailed qualities of the user interface should be known to estimate what kind of error is possible to make with a specific user interface. To conclude, the mere "analogueness" or digitality do not determine whether the user interface in question makes the human operator prone to errors.

Benefits from qualitative analysis

(Liinasuo & Porthin 2016) concentrate on qualitative HRA, including the identification of the sources of human error and the modelling of these errors as part of a systemic analysis. In the report, the qualitative human reliability analysis (HRA) related data-gathering methods are scrutinised from various points of view: the commonly used methods in HRA context, recommendations about HRA methods as well as the suitability of validation methods in HRA context. After scrutinising the various types of methods mentioned, it was concluded that the methods used in human factors validation are applicable and possibly also included among those which are used as HRA methods. Familiarising in the practise of validation methods may also broaden the methodology to be used for HRA purposes.

The actual and recommended qualitative HRA methods extended by those used in human factors validation were concluded to be applicable not only for HRA or validation but also for other purposes related to developing operations in the nuclear domain: in operator training, when developing present or new emergency operating

procedures or when evaluating the details of the concept of operations for control-room operators.

Awareness of these possibilities would add knowledge and save resources in the nuclear field. When data gathering is planned for any of the above mentioned purposes, it would be valuable to broaden the perspective and include also other purposes and data gathering methods in the study in question when needed. This requires flexibility and cooperation among various professionals and sections of a nuclear power plant organisation and possibly also new processes.

Dependencies in HRA

Accounting for dependencies has been identified as a problem area for HRA. Dependencies in HRA generally refer to the probabilistic relationship between two or more human interactions analysed and modelled in PRA

There are several types of dependencies that may need to be accounted in HRA:

- Dependencies between category A human errors (errors made before an initiating event causing latent unavailabilities in safety systems). For instance, alignment errors in redundant system trains are a critical issue. Inter-system and procedural dependencies are often ignored but may be important.
- Dependencies between category B human errors (errors causing an initiating event and its recovery). Treatment of these dependencies depends heavily on the level of analysis details and the meaning of recovery.
- Dependencies between category C human actions (actions made after an initiating event). This includes a large range of dependencies, e.g.,
    - Context dependency
    - Dependencies between level 1 and 2 PRA actions.
    - Time-constrained actions with limited resources. The more time is spent in one action, the less time there is for the following action.
    - Dependencies between distributed actions, coordination between control room actions and local actions (e.g. fire scenarios)
    - Dependencies in multi-unit scenarios.

We performed two case studies to evaluate existing methods and develop supplementary guidance for a new method for the assessment of dependencies in HRA and the need for additional method development.

In the first case study on category A action dependences (Porthin 2015), we examined the probabilistic assessments of dependency between multiple pre-initiator actions in Fortum's HRA as part of Loviisa 1 and 2 PRA. The chosen case example was the calibration error of two redundant thermostats due to a common cause failure (CCF) leading to loss of certain cooling systems in emergency situations due to no actuation of auxiliary air conditioning. Fortum's dependency model has been developed based on the Technique for Human Error Rate Prediction

(THERP) method, from which it has been somewhat modified to better meet Fortum's needs. It can be concluded that the model gives similar results as THERP, seems reasonable and differentiates between different situations. The clearly defined questionnaire for determining the dependency level adds transparency and reproducibility to the method.

In the second case, the analysis of dependences of post initiating event operator actions was demonstrated (Holmberg & Jacobsson 2015). Loss of coolant accident (LOCA) during shutdown in a boiling water reactor is used as an example of a complex scenario. The main focus is in the qualitative analysis of the scenario where the relevant operator actions and their interdependences are identified. Quantification of dependences is demonstrated using one commonly applied method.

The main challenge in the analysis of complex sequences is to identify and define operator actions in a meaningful way that fits in the PSA model environment. The proposed analysis approach focuses mainly on qualitative analysis. It is structured into the following steps:

1. Analysis of main safety objectives.
2. Analysis of tasks related to the main safety objectives. (task analysis)
3. Sequence analysis
4. Quantification of the basic events (human failure events).

In the dependency assessment the attention is on the cases where judgement between no and fully dependency is needed. It should be noted that there are also many evident dependences implied by the sequence, where there is no need to make judgements since the latter (dependent) action is needed only because the preceding action has either failed or succeeded. As an example the action "immediate isolation of the LOCA" divides the LOCA scenarios into two different branches. The following actions depend obviously on the isolation action success, but the outcome from the isolation effort can be included in the definition of the context of the following human failure event (HFE).

In the example, the interesting cases are related to the various methods to recover residual heat removal from the reactor core. In top-LOCA, there is a several hour time window to establish a cooling method. However, the actions are presumably performed by the same crew and guided by the same emergency operating procedure and have common cues.

Quantification example shows that high/moderate dependency instead of full dependency can reduce the core damage frequency for this initiating event by a factor 7, which is considerable difference. It can be hard to justify whether full dependency is a conservative assumption or high/medium dependency is an optimistic assumption. If shutdown top-LOCA is a significant initiating event, a sensitivity analysis of the case should be included in PRA. It is also important to include a systematic qualitative analysis of possible actions related to the scenario.

HRA outside the PSA: State-of-the-practice survey

PRA typically only makes use of the quantitative Human Error Probability (HEP) that is produced by the HRA, meaning that the detailed qualitative analyses that underpin this calculation and the knowledge that is produced in the activity are not utilised outside of the HRA. However, qualitative HRA can provide valuable insights into the individual, workplace and organisational factors that drive human performance and errors, and may be useful for a range of risk-informed applications beyond the PRA.

A questionnaire was carried to how HRA has been used outside PRA and what potential HRA has to widen its scope in the nuclear domain (Holmberg & Liinasuo 2017). This questionnaire was sent to Nordic PRA/HRA organisations. In Finland and Sweden, HRA is used in great majority of cases for PRA purposes only. The lack of broader experience of the area seems to be one reason for that as in the replies, the need for guidance was emphasised. The counterpart for this lack of expertise is the lack of respect towards HRA from the part of organisations which are to utilise the HRA originating results. These forces strengthen each other: without understanding the value of HRA, resources are not distributed to develop HRA and HRA expertise, and without proper resources, less HRA can be done.

A reasonable way to solve this problem would be to strengthen HRA from inside of the HRA community. That can be done in PRA and non-PRA context. Regarding the usage of HRA in non-PRA purposes, many possibilities can be identified. Part of them are realised but a lot can still be done. SAFIR programme provides one possibility to strengthen HRA from various perspectives.

IAEA Safety Report on Human Reliability Assessment for Nuclear Installations

IAEA initiated an effort to prepare a Safety Report on Human Reliability Assessment (HRA) for Nuclear Installations in 2016. Risk Pilot AB has participated in the expert group that has prepared the report. The objective of the publication is to provide assistance to the Member States for the HRA implementation.

- to collect the different practices on HRA
- to provide a harmonised framework on HRA
- to provide well-structured and detailed description of HRA procedures (overall methodology) and factors to be considered in the HRA process
- to provide examples.

In addition, the document contains a brief overview of number of HRA methods used in nuclear power plant PRA context. The publication is intended to be used by a broad spectrum of analysts (e.g. PSA practitioners, human factor engineers) from regulatory bodies, utilities, research institutes, technical support organisations and designers of nuclear installations. The finalization of the publication was in progress in January 2019 (IAEA 2019).

Site level PRA

The Fukushima Daiichi accident in March 2011 pointed out that the risk of external events affecting multiple NPP units is significant. Consequently, interest in multi-unit PRA has also increased. A large part of the nuclear power sites house more than one NPP and/or other nuclear facility such as a spent fuel pool.

Currently, multi-unit risks have not typically been adequately accounted for in risk assessments. Due to possible dependencies between the units at a site the question of several simultaneous reactor accidents is not one of possibility but rather one of probability. Based on a literature study (Björkman & Tyrväinen 2015), a large part of the research seems to focus on identifying and accounting for different kinds of dependencies and on external hazards. We outlined a method for preliminary multi-unit PRA (Tyrväinen et al. 2017). This work was further developed in the Nordic SITRON project.

The SITRON project

The SITRON (SITe Risk Of Nuclear installations) project has searched for practical approaches for Nordic utilities to assess the site level risk. Starting point of SITRON work has been the fact that the Nordic utilities already have good unit-specific PRAs. Therefore, the question is what additional efforts are needed to obtain a site level risk assessment. Practically, it means two tasks: 1) to identify relevant inter-unit dependences, and 2) to quantify the site level risk. Inter-unit dependences consist of multi-unit initiating events, shared systems, structures and components, dependences in human actions, identical components, and plant operating state combinations.

Figure 1 illustrates the scope of various risk assessments with respect to the concepts “site”, “unit” and “source” (or fuel location) for a hypothetical site with two reactor units and an interim storage for spent fuel. “Site” covers all units and fuel locations at the site. “Unit” refers to each facility at the site, which has an operating license of its own. In this example, there are three units/facilities at the site. “Source” refers to each point at the site where spent fuel can be located and for which a separate risk assessment can be carried out.

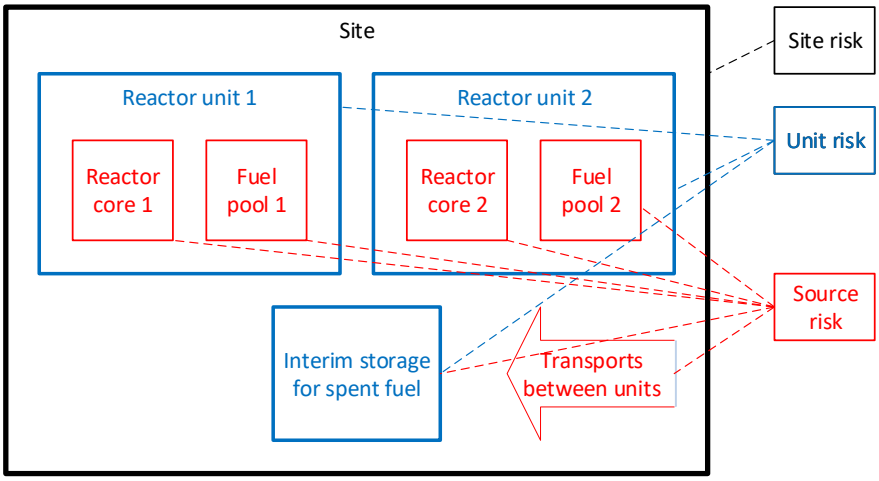

Figure 1. Illustration of concepts “site”, “unit” and “source” from the PRA scope point of view.

SITRON project has considered risk metrics from the point of view of Nordic conditions (Holmberg 2017). Both in Finland and Sweden, the requirement is to perform full scope level 1 and 2 PRA, but there is no requirement to perform level 3 PRA. There is also no requirement to quantify site level risk metrics.

There are several options for site level risk metrics, i.e., metrics for various double, triple and quadruple combinations of units (fuel locations) at the site. When accounting for combinations, it is important to notice that there is a principal difference between level 1 risk metrics and level 2 risk metrics. The level 1 risk metrics are based on binary conditions (fuel damage happens vs. does not happen), while level 2 risk metrics are derived by partitioning a “continuous” property (magnitude and timing of release) into a limited number of classes by threshold values. Thus, the level 1 risk metrics concern the number of damaged units, but level 2 risk metrics are defined by the release magnitudes regardless of the number of units involved.

SITRON provides guidance how to perform the identification of dependences and how to select relevant dependences for quantification (screening). Quantification of site risk can be performed quite straightforwardly, given that the quality of the single-unit PRAs is sufficient (Bäckström et al 2019). The estimation of inter-unit CCF probabilities and human error probabilities in multi-unit scenarios however contains significant uncertainties, and conservative approaches, such as use of single-unit CCF data, are recommended.

The method development has been driven by two practical pilot studies — one for the Forsmark nuclear power station (Cederhorn et al. 2018, Holmberg 2018) and second for the Ringhals nuclear power station (Bäckström et al. 2018a & 2018b). Both pilot studies concern an assessment of a two-unit combination. Therefore, the developed method assumes a two-unit case, but it could be generalized to a site risk analysis with more units.

Besides general method development, procedures are needed for documenting the site PRA, managing possible modifications made to the single-unit PRA models, and managing the data and computation. (Tyrväinen & Björkman 2019) provides guidance for the model management.

SITRON project has also included a survey on the role of Emergency Response Organisation (ERO), often referred to as the Technical Support Centre (TSC) in accident management (Massaiu 2019). Based on responses from four plants in Finland and Sweden, SITRON has investigated different implementations of EROs with respect to possible impact on operational decisions in severe accident and multi-unit scenarios. The human role in severe accidents differs markedly: new decision makers (ERO and TSC rather than main control room); different instructions (guidelines rather than procedures); different decisions (involving trade-offs, novel actions, and strategies contrary to conventional knowledge); inter-unit influences; unreliability of instrumentation; and long time windows for actions.

Dynamic flowgraph methodology

Dynamic flowgraph methodology (DFM) is method for the reliability analysis of dynamic systems with time-dependencies and feedback loops. As in fault tree analysis, the aim of DFM is to identify which conditions can cause a top event, which can be, for example, the system's failure. DFM has most often been applied to different digital control systems. One reason for this is that a DFM model can represent the interactions between a control system and the controlled process. Components of DFM models are analysed at discrete time points and they can have multiple states. DFM can more accurately represent system's evolution in time than traditional methods, such as fault tree analysis.

We performed a literature survey (Tyrväinen 2017a) on the applications of DFM. Application areas include digital control and safety systems in nuclear power plants, space systems, hydrogen production plants, human performance, networked control systems and field programmable gate arrays. In most applications, DFM has been used to analyse how control system failures can cause some physical variable, e.g. water level or pressure, to have too low or high value. Generally, DFM has been found useful within the application areas. Most of the presented models have been quite moderately sized, though larger models exist too.

We studied solving DFM models using fault trees of the FinPSA software (Tyrväinen 2017b). To enable this, we developed the minimal cut set solving algorithm of FinPSA to take into account non-coherent logic of DFM models. We developed a preliminary implementation that solved a simple DFM model correctly.

Level 2 PRA and FinPSA

Level 2 PRA studies how a nuclear power plant accident progresses after core damage, and how frequent and large radioactive releases are. FinPSA is a PRA software tool that was originally developed by STUK, and is currently maintained and

developed by VTT. In the previous SAFIR programme, we implemented dynamic containment event trees (CETs) in FinPSA, and the parametric model specified by containment event tree programming language (CETL) underlying the CETs. We have developed level 2 computation of FinPSA further, introducing also new features. In our level 2 analyses, we have utilized both pre-existing features and new developments (Tyrväinen et al. 2016).

Severe accident modelling

We prepared a summary on previous research performed on integrated deterministic and probabilistic safety assessment of severe accidents at VTT (Tyrväinen & Silvonen 2015). It covered case studies on steam explosions, passive autocatalytic hydrogen recombinators, passive containment cooling system and ex-vessel debris coolability. In the studies, both probabilistic and deterministic analyses were performed. Especially, it was demonstrated how the results of deterministic simulations can be incorporated into a containment event tree model. Knowledge on severe accident phenomena and modelling capabilities were gathered. The analysis and modelling principles are quite similar regardless of which phenomenon and plant type is analysed.

We studied factors that affect the height and temperature of radioactive releases (Tyrväinen & Karanta 2017). The height and temperature have typically not been included in level 2 PRA, even though they are needed as inputs for level 3 PRA. Release height is usually the height of the location where the reactor building leaks (which depends on the containment failure mode), or the height of the chimney if the release is controlled. In an uncontrolled accident case, both the containment failure location and the flow path of radionuclides in the reactor building need to be analysed to determine the release height. The temperature of release from containment is in most cases close to 100°C, but the temperature of radionuclides can potentially change during their migration in the reactor building. Higher temperatures can be caused by fires and explosions. There are computer codes that can be used to analyse radionuclide flows in reactor building and determine the release heights and temperatures.

We have also studied hydrogen explosions in boiling water reactor (BWR) nuclear power plant (Tyrväinen & Karanta 2017). Hydrogen explosions can occur in a nuclear power plant containment if hot zirconium reacts with steam producing significant amount of hydrogen during severe accidents. These explosions have potential to be powerful enough to break the containment and cause a large early release. Hydrogen explosions in BWR plants have been studied little because inerting of containment - filling the containment with a non-flammable gas (usually nitrogen) - prevents explosions with certainty. However, an accident can also occur when the containment is not inert, e.g. during start-up or shut-down. Hydrogen explosions outside containment are considered more likely, but they have usually not been modelled in PRA because they presumably would not break the containment

and cause radioactive release. However, those hydrogen explosions can break the reactor building and increase the releases to environment, like in Fukushima.

We have developed a simplified PRA model for BWR plant with PRA levels 1 and 2 as integrated (Tyrväinen & Karanta 2018). The development has focused mainly on the level 2 part, which was based on a CET model that was developed in the previous SAFIR programme. We identified that there were no uncertainty distributions specified for probability parameters in the original model. Therefore, we developed complete uncertainty analysis for the model in (Tyrväinen & Karanta 2017). In the process, we identified problematic issues and good practises for performing uncertainty analysis in FinPSA level 2. The original model was heavily based on computation with physical parameters, whereas in the new version, the focus is on probabilistic modelling. The mean values of the probability distributions used in the new model were derived from the original model and its results. In (Tyrväinen & Karanta 2018), we extended the model with four new CETs. We demonstrated how emergency core cooling system recovery probability in level 2 can be calculated automatically based on level 1 results and how the risk contributions of level 1 events can be seen in level 2 results. The example model has been and can be utilised in further studies, demonstrations, training and FinPSA testing.

We have also studied ex-vessel steam explosions in (Tyrväinen & Karanta 2018). Probabilistic modelling of steam explosions is very challenging because uncertainties related to the phenomenon are very high. Pressure impulses of explosions can be calculated quite well using deterministic software tools, but the probability that an explosion occurs in the first place cannot be properly estimated based on current knowledge. Currently, it is good practice to use conservative probabilities in PRA.

In (Tyrväinen & Karanta 2019), we have studied modelling of timings and uncertainty analysis in dynamic CETs. We have used simple emergency core cooling system recovery case to demonstrate different options to model the recovery time and the effects of different timings. Epistemic and aleatoric uncertainties have been separated in the case study, and two-phase uncertainty analysis has been performed. The case study demonstrates the need to separate epistemic and aleatoric uncertainties in dynamic accident modelling to analyse uncertainties in a consistent manner. We have also developed a high pressure melting containment event tree of the previously developed simplified BWR model further, e.g. by modelling timings of depressurization, emergency feedwater system recovery, emergency core cooling system recovery and lower drywell flooding explicitly. The upper part of the CET is presented in Figure 2.

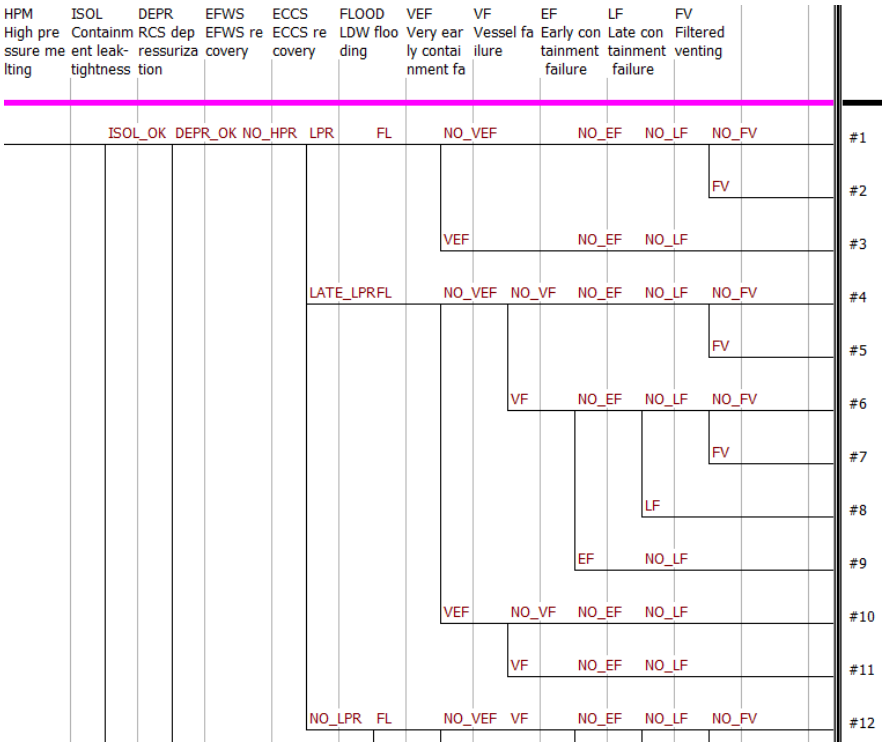

Figure 2. The upper part of the high pressure melting containment event tree.

Method support for PRA level 2

To monitor level 2 simulation and point value computations in FinPSA we implemented a variable viewer (Björkman 2017). The variable viewer shows the values of global variables at a given place (branch) in the CET model. FinPSA supports three ways to monitor variables during simulation and point value computation: 1) by computing the point values up to a branch in the CET, 2) by using Halt() command in CETL code 3) by setting break points for branches in the CET.

To combine PRA level 2 analysis results a risk integrator was implemented. The risk integrator computes total PRA results from the results of multiple CETs. CETs included in the analysis are speficied separately. In risk integration of a release category, the results from all sequences leading to the release category are combined. For each variable, a sum value weighted by sequence frequencies is calculated in each simulation cycle. Then, based on those weighted values statistical analyses are performed.

Results of all variables can be inspected in total results and in a selected release category. The results of a variable include a header section (with information such as model name, number of simulation rounds, participating event trees etc.), contributions of different CETs, density function, statistical numbers, correlation between

a variable and frequency, complementary cumulative distribution, and contributions of CET sequences and branch functions. CET contributions tell how different CETs contribute to the combined results. The CET fractions for frequency weighted and non-weighted (raw) values are provided (Fig. 3).

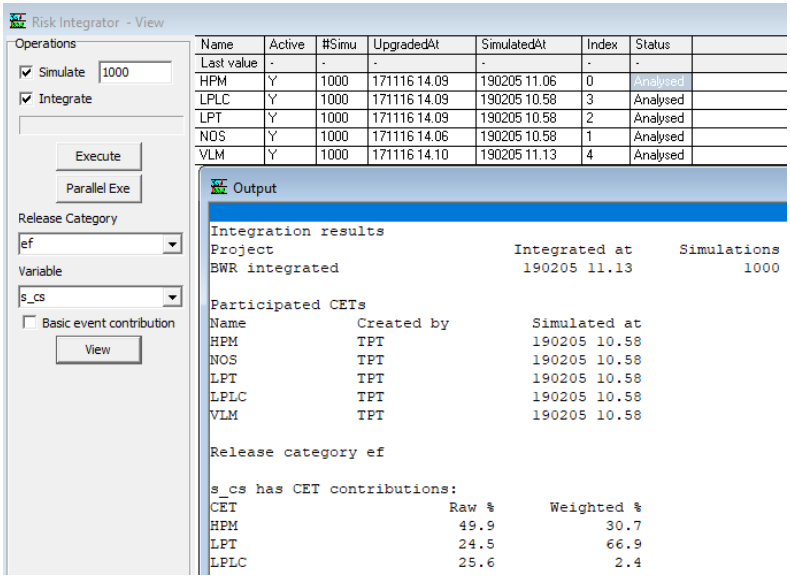

Name	Active	#Simu	UpgradedAt	SimulatedAt	Index	Status
Last value	-	-	-	-	-	-
HPM	Y	1000	171116 14.09	190205 11.06	0	Analysed
LPLC	Y	1000	171116 14.09	190205 10.58	3	Analysed
LPT	Y	1000	171116 14.09	190205 10.58	2	Analysed
NOS	Y	1000	171116 14.06	190205 10.58	1	Analysed
VLM	Y	1000	171116 14.10	190205 11.13	4	Analysed

Figure 3. Frequency weighted and non-weighted CET fraction values

Density function depicts how frequency weighted values of a variable are distributed over simulation cycles. The frequency weighted values represent total result over all sequences belonging to a release category (Fig. 4).

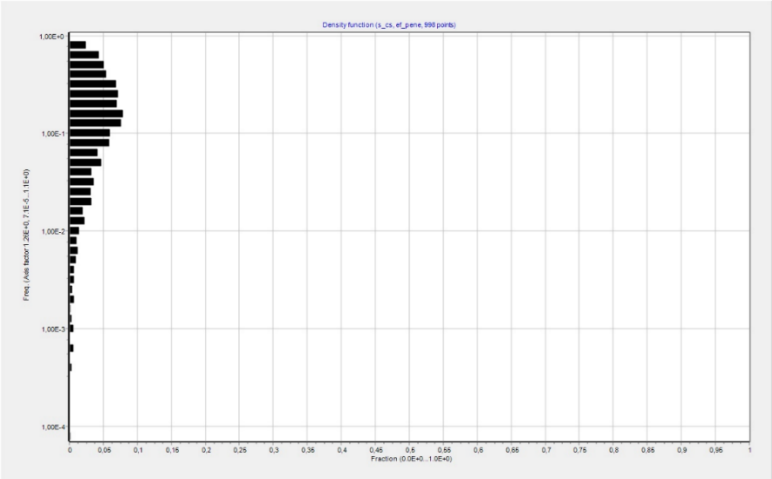

Figure 4. Density function

The following statistical numbers are calculated for a variable: mean, standard deviation, minimum, maximum and percentile values. Correlation between a variable and frequency is presented in two different kinds of scatter plots. The first one is based on frequency weighted values of the variable (one value from each simulation cycle). The second scatter plot (Fig.5) contains raw values (multiple values from each simulation cycle if there are multiple sequences leading to the release category). Both scatter plots are discrete. In other words, a mark in a plot can present several hits on a value range.

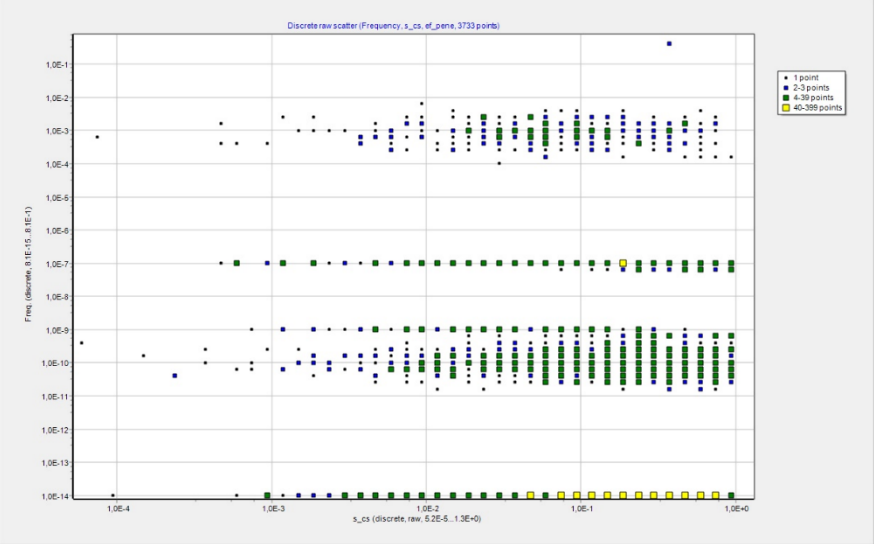

Figure 5. Correlation between a variable and frequency

Complementary cumulative distribution (Fig 6) shows how often the variable has a value above a particular level. For example, in Fig 6, ruthenium releases exceed 10% of the core inventory approximately with frequency 1E-8/year.

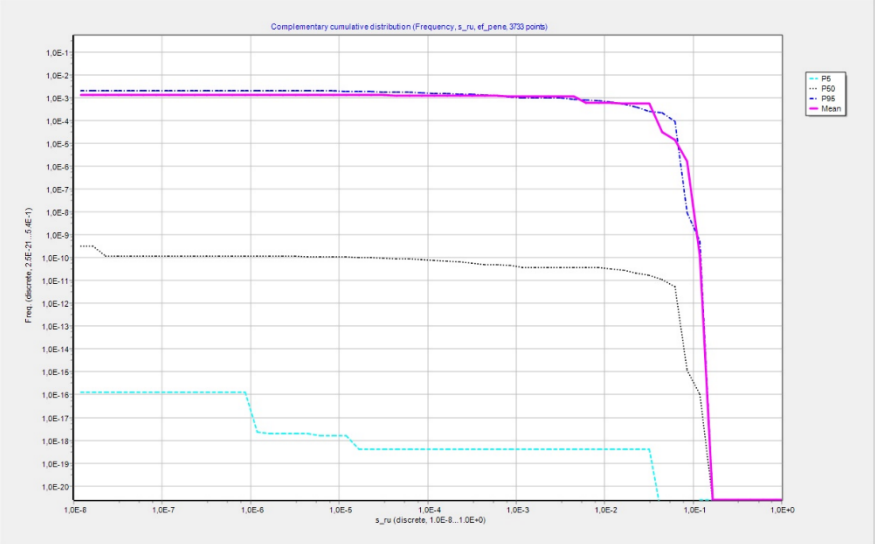

Figure 6. Complementary cumulative distribution

Contributions of CET branch functions to frequencies of release categories represent risk importances (Fussell-Vesely) of severe accident management actions, such as core cooling recovery and depressurization. In addition, contributions of CET sequences and branch functions are calculated with regard to source variables (amounts of released radionuclides). The contributions to a source variable weighted by accident sequence frequencies represent contributions to the total risk (of the radionuclide type represented by the source variable).

In addition, the risk integrator implements ability to control operations such as simulation of CETs and overall management of CETs. The simulation of active CETs was implemented as a background activity which coordinates parallel CET simulations and combines PRA results after successfull simulations.

Method support for levels 1 and 2 tight integration

PRA is most accurate when dependencies between levels 1 and 2 are modelled, and all the relevant information is passed from level 1 to level 2. In FinPSA, analyses of levels 1 and 2 are performed using different methods, which complicates the integration. Figure 7 presents different phases of FinPSA analysis including both levels 1 and 2.

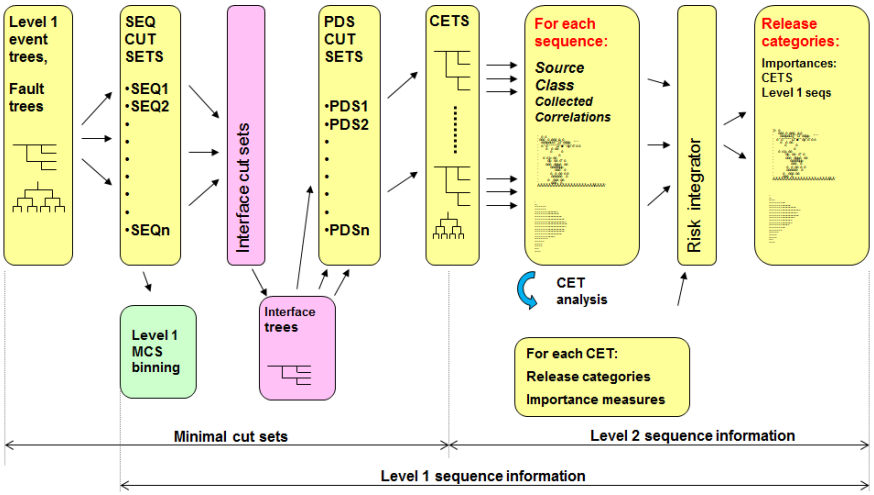

Figure 7. FinPSA analysis phases.

We have developed tight integration of PRA levels 1 and 2 in FinPSA (Björkman 2017, Mätäsniemi 2017). There are two main areas in tight integration (Tyrväinen 2016):

1. How level 1 information is incorporated and utilised in level 2 models
2. How level 1 accident sequences and basic events are seen in level 2 results

There are typically many level 1 accident sequences leading to the same PDS. Different accident sequences can affect later severe accident progression differently. Therefore, it is possible to define categories for level 1 sequences inside a PDS in the corresponding CET model. In the CET, it is then possible to calculate the conditional probability of a level 1 sequence category, e.g. in order to calculate the probability of a CET branch. It is also possible to reduce the level 1 sequence list of the PDS so that only specific sequences contribute to specific level 2 sequences. In addition, it is possible to calculate the conditional probability, i.e. Fussell-Vesely value, of a level 1 basic event in level 2.

It can be calculated how level 1 sequences, basic events and initiating events contribute to the values of level 2 variables, namely frequencies of level 2 sequences and release categories, and values of source variables. These contributions represent the importances of level 1 events with regard to level 2 results. This way level 2 results can be traced back to level 1.

Time-dependent analysis

We have developed a new time-dependent calculation feature in FinPSA (Tyrväinen 2018, Mätäsniemi & Tyrväinen 2019). The user can specify events, such as maintenance activities or tests, parameter changes and configuration changes to a time line in a task file, and FinPSA automatically calculates and draws the time-dependent risk curve based on that information, existing minimal cut sets and data. Figure

8 presents a time-dependent task file and the resulting risk curve. More detailed analyses, e.g. computation of importance measures, can also be performed for selected time points. The time-dependent analysis has been demonstrated with three simplified analysis cases in (Tyrväinen 2018).

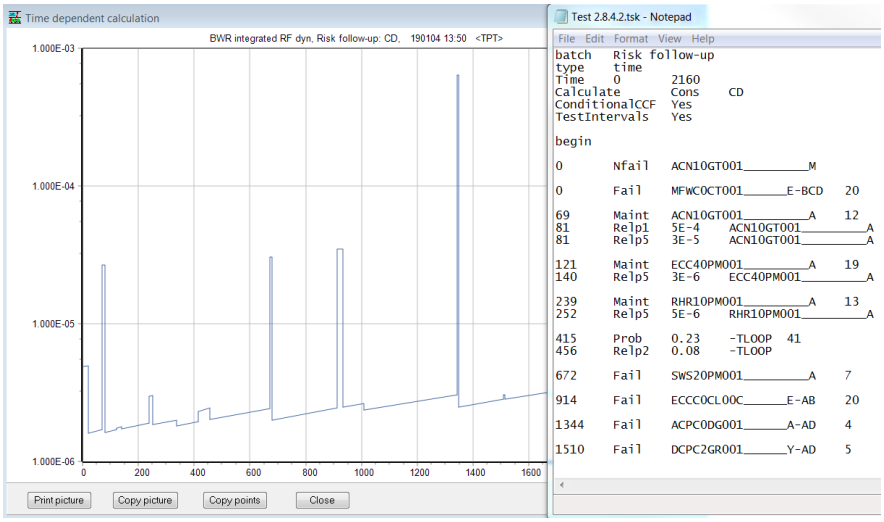

Figure 8. Time-dependent task file and the resulting risk curve.

Level 3 PRA

Level 3 PRA concerns with the consequences of a radionuclide release. Research in level 3 was carried out on several fronts: literature review, method development, pilot development, and guidance development.

L3PSA project

We participated in a Nordic cooperation project "Addressing off-site consequence criteria using Level 3 PSA" (L3PSA) together with Lloyd's Register, ÅF Konsult, Risk Pilot AB and Vattenfall. The project had started earlier, but during PRAMEA, the main activities were improving pilots that had been created earlier, and writing a guidance document on level 3 PSA, with a special view of Nordic conditions.

We improved a method, developed in the earlier PRADA project, for organizing level 3 analyses. In it, the possible accident progressions starting from a radionuclide release are represented as an event tree (ET). The initiating event of the tree is a single release (source term). The ET layers of the tree consist of weather factors (one layer for wind direction, one for wind speed, one for rain) and countermeasures (one layer for evacuation success, and one for shielding success). The branching probabilities of weather factors are obtained from meteorological statistics, and the branching probabilities of countermeasures were assessed as functions of time

available. We used dynamic event trees of FinPSA (Tyrväinen et al. 2016) in the modelling demonstrating how the method is applicable also in areas other than level 2 PRA. The consequences of each branch in the event tree were estimated with a consequence analysis code (ARANO). The main improvements to the model were that wind speed was treated as a continuous variable, drawn from a Weibull distribution in Monte Carlo simulation, and that source term uncertainties were taken into account; also the handling of evacuation was improved slightly.
We participated in the writing of a guidance document on level 3 PSA (Wallin Caldwell et al. 2017). The document has a focus on Nordic conditions. Its purpose is to help in creating a common understanding of the usability of consequence analysis and its benefits and limitations, and to ensure that scenarios and results from one plant can be compared with those of another. The document goes through the regulatory framework both in the Nordic and the international context, international guides and standards, and available software. The objectives, value and benefits of level 3 PSA are explicated, as well as its limitations. The main elements of analysis are described from risk criteria to representation of results. Recommendations are given throughout, partly based on the pilot studies conducted in the project.

Other level 3 PRA activities

Population dose assessment is about assessing the dose of ionizing radiation that a population get from a radionuclide release through different pathways (ingestion and inhalation of radionuclides, radiation from radionuclides in the air etc.). The dose assessment methods used in modern computer codes applicable to level 3 analyses (VALMA, SILAM, RODOS, MACCS2) and in recent level 3 and consequence assessment studies (SOARCA, UNSCEAR study of the Fukushima accident) were reviewed (Karanta 2017). The Finnish codes VALMA and SILAM combine advanced methods of atmospheric dispersion computation with dose assessment. Relatively little progress in dose assessment methods has been made in the last 20 years.

There are many seasonal factors that may affect nuclear accident consequences and level 3 PRA results significantly. For example, snow, ice cover and frost may affect the transport of radionuclides. There are also contextual factors, specific to certain (but not all) accidents, that may change consequences significantly; an example is that large areas in the Fukushima prefecture were depopulated at the time of radionuclide releases due to the tsunami and consequent evacuation, and thus population dose from the accident remained very small. Neither seasonal nor contextual factors are taken into account systematically in contemporary level 3 PRA. We have laid groundwork for a systematic treatment by making an overview of such factors and their potential impacts on accident consequences and their systematic incorporation in level 3 analysis (Karanta 2018). These factors affect many important level 3 phenomena such as aquatic dispersion, transport of radionuclides in the environment and biosphere, population demography and behaviour, and atten-

uation of ionizing radiation. These, in turn, affect level 3 analyses concerning population dose, evacuation, sheltering and distribution of radionuclides in the environment. We also conducted a survey among the Finnish NPP companies and STUK on the current status and future prospects of seasonal and contextual factors in level 3 and related analyses (Karanta 2019). It turned out that the Finnish stakeholders do not consider that there would be significant research needs on these factors on level 3. However, studying the effect of SCFs on level 1 and level 2 PRA results was judged to be relevant, and there was also some interest on integrated analysis covering PRA levels 1-3.

Reliability analysis of defence-in-depth in organizations

We have developed novel methodologies to support decisions for improving safety and reliability of technical systems, based on the formulation of optimization problems for (i) risk-based inspection strategies, (ii) safety of nuclear systems and (iii) security of cyber-physical systems.

First, we have developed of a novel risk-based methodology to optimize the inspections of large underground infrastructure networks (Mancuso et al., 2016). The risk assessment of such networks is typically based on incomplete information about the network components. Our methodology has been motivated by and developed in the context of a real case study for a civil pipe network; but it can be extended to and is applicable to nuclear systems. The risk of each pipe has been assessed through Multi-Attribute Value Theory (MAVT), which provides a systemic approach for evaluating decision alternatives with regard to multiple objectives. Risk is evaluated in terms of (i) failure likelihood and (ii) impact on the network disruption so that *likelihood* depends on pipe features, past events and local circumstances, whereas *impact* quantifies the effect of a pipe failure on the network and on the surroundings. Cost-efficient strategies for pipe inspections are determined by adapting Aalto University's previous results on Robust Portfolio Modelling. .

Second, we have developed a a systemic approach to determining the optimal portfolio of safety measures that minimizes the risk of the system (Mancuso et al. 2017; Mancuso et al. 2019a); thus, it provides an alternative to using risk importance measures for guiding the selection of safety measures. The alternative scenarios leading to system failure are represented through Bayesian networks, which can be derived from traditional Fault Trees and are expressive enough to encode event dependencies and multi-state failure behaviours. We also developed an optimization algorithm to identify which portfolios of safety measures minimize the risk of system failure subject to budget and technical constraints. We have illustrated our methodology by revisiting the Design Basis Accident that occurred in the airlock system of a CANDU nuclear power plant in 2011. The comparison of results with those of choosing safety measures based on risk importance measures showed that our approach leads to considerably lower residual risk of system failure.

The final outcome of accident scenarios can depend on the *order*, *timing* and *magnitude* of the component failures. If the risk analysis does not account for the

dynamic evolution of failures, it may fail to consider severe accident scenarios. For this reason, we have extended the methodology to support the selection of cost-efficient portfolios for dynamic systems. This model captures the dynamics of accident scenarios through the temporal evolution of component failures. In this framework, the alternative scenarios leading to system failure have been represented through Dynamic Bayesian Networks. Then, an optimization model selects all Pareto optimal portfolios of safety measures, which are cost-efficient in minimizing the residual risk of the system. We have illustrated our methodology by revisiting the accident scenario of a vapour cloud ignition occurred at Universal Form Clamp in Illinois, U.S. on 14 June 2006. The results are shown for different budget levels, which provides further insights. Future research will further extend this methodology to account for safety measures that can be dynamically activated or deactivated depending on the specific states of the system components.

Finally, we have proposed a systemic analysis based on Bayesian networks to quantify the risks of cyber threats to electric power systems (Mancuso et al., 2019b). Electric power systems extensively rely on cyber-physical systems, making them vulnerable to cyber threats with frequent and costly impacts worldwide. For instance, in 2015 a cyber-attack to an electric grid caused a power outage in Ukraine. These episodes show the need for an efficient resource allocation to reduce the risk of cyber threats. Standard approaches guide the selection of mitigation actions by prioritizing the cyber threat scenarios through a qualitative assessment. These approaches consider cyber threat scenarios separately, thus they possibly result in sub-optimal resource allocations for the system. By constrast, our methodology is based on a multi-objective optimization model for identifying the cost-efficient portfolios of security measures that minimize the risk of cyber threats, subject to relevant budget and technical constraints. We have illustrated the methodology by analyzing the cyber threat scenarios concerning the advanced metering infrastructure of an electric power grid. The results have shown that a systemic analysis of multiple cyber threat scenarios is helpful in the selection of security measures.

References

Björkman, K. & Tyrväinen, T. 2015. Multi-Unit PRA — Literature Review. Espoo: VTT. VTT Technology VTT-R-04580-15. 11 p.

Björkman, K. 2017. FinPSA – Software design – Tight integration of levels 1 & 2. Espoo: VTT. VTT-R-04831-16. 13 p.

Björkman, K. 2017. FinPSA – User guide – Monitoring containment event tree computation. Espoo: VTT. VTT Technology VTT-R-05137-17. 5 p.

Bäckström, O., He, X., Holmberg, J.-E., Tyrväinen, T. 2019a. SITRON — WP2 — Method development. Site level risk assessment. Report 212634-R-001, Lloyd's Register Consulting, Sundbyberg.

Bäckström, O. & He, X. 2019. SITRON – Pilot study Ringhals 3&4, Report 212634-R-002, Lloyd's Register Consulting, Sundbyberg.

Cederhorn, E., Holmberg, J.-E. Sunde, C. 2018. SITRON — Pilot study Forsmark 1 and 2. Report 14124_R007, Risk Pilot AB, Espoo.

Holmberg, J.-E. 2017. SITRON — Risk metrics. Report 14124-R005, Risk Pilot AB, Espoo.

Holmberg, J.-E. 2018. SITRON — Pilot study Forsmark 1 and 2 2018. Report 14124_R010, Risk Pilot AB, Espoo.

Holmberg, J.-E. & Jacobsson, M. 2016. Dependencies in human reliability analysis — case study on shutdown LOCA, Report 14124_R001, Risk Pilot AB, Espoo, 34 p.

Holmberg, J.-E. & Liinasuo, M. 2016. Non-PSA applications of HRA, Report 14124_R003, Risk Pilot AB, Espoo, 25 p.

IAEA. 2019. Human reliability analysis for nuclear installations, International Atomic Energy Agency, Vienna. Draft (to be published in IAEA Safety Reports Series).

Karanta, I. 2017. Dose assessment in level 3 PRA - a review of recently used methods. Espoo: VTT. VTT Technology VTT-R-00738-17, 14 p.

Karanta, I. 2018. Seasonal and contextual factors in level 3 PSA. Espoo: VTT. VTT Technology VTT-R-00221-18, 19 p.

Karanta, I. 2019. Seasonal and context factors in level 3 PRA - survey of status in Finland. Espoo: VTT. VTT-R-00142-19, 14 p.

Liinasuo, M. & Kling, T., 2019. Human error analysis for a hybrid control room − A case study. Espoo: VTT-R-00143-19, 16 p.

Liinasuo, M. & Porthin, M., 2016. Qualitative HRA and human factors validation – methods and application areas. Espoo: VTT-R-00564-16, 18 p.

Mancuso, A., Compare, M., Salo, A., Zio, E. and Laakso, T., 2016. Risk-based optimization of pipe inspections in large underground networks with imprecise information. Reliability Engineering & System Safety, 152, pp.228-238.

Mancuso, A., Compare, M., Salo, A. and Zio, E., 2017. Portfolio optimization of safety measures for reducing risks in nuclear systems. Reliability Engineering & System Safety, 167, pp.20-29.

Mancuso, A., Compare, M., Salo, A. and Zio, E., 2019a. Portfolio optimization of preventive safety measures for time-dependent accident scenarios. Forthcoming on Reliability Engineering & System Safety.

Mancuso, A., Zebrowski, P. and Couce-Vieira, A., 2019b. Risk-based selection of mitigation strategies for cybersecurity of electric power systems. Under review for IEEE Transactions on Dependable and Secure Computing.

Massaiu, S. 2019. Decision-making during severe and multi-unit accidents: Technical Support Centers and Emergency Response Organizations at Nordic Countries, IFE/F-2018/189, Institute for Energy Technology, Halden.

Mätäsniemi, T. & Tyrväinen, T. 2019. FinPSA – Software testing – Verification and validation report for time-dependent task file. Espoo. VTT. VTT Technology VTT-R-00084-19. 78 p.

Mätäsniemi, T. 2017. FinPSA – Software testing – Verification and validation plan and results for tight integration. Espoo. VTT. VTT Technology VTT-R-00552-17. 79 p. + app. 7 p.

Porthin, M. 2015. Methods for handling of dependencies in HRA: Fortum case study, VTT-R-05397-15, Espoo.Porthin, M., Kling, T. & Liinasuo, M., 2017. D2.3.2 Performance shaping factors for advanced control room HRA. Espoo: VTT-R-00905-17, 25 p.

Porthin, M., Liinasuo, M. & Kling, T., 2016. HRA of digital control rooms: Literature review. Espoo: VTT-R-00434-16, 21 p.

Tyrväinen, T., Björkman K. 2019. SITRON — Site PSA model management, VTT-R-06885-18, VTT, Espoo.

Tyrväinen, T., Häggström, A., Bäckström, O. & Björkman, K. 2017. A methodology for preliminary probabilistic multi-unit risk assessment. Espoo: VTT. VTT Technology VTT-R-00086-17. 20 p. + app. 9 p.

Tyrväinen, T. & Karanta, I. 2017. Level 2 PRA studies – Source term characteristics and hydrogen explosions. Espoo: VTT. VTT Technology VTT-R-00354-17. 19 p. + app. 2 p.

Tyrväinen, T. & Karanta, I. 2018. Level 2 PRA studies – Steam explosions and integration of PRA levels 1 and 2. Espoo: VTT. VTT Technology VTT-R-00191-18. 26 p.

Tyrväinen, T. & Karanta, I. 2019. Dynamic containment event tree modelling techniques and uncertainty analysis. Espoo: VTT. VTT Technology VTT-R-06892-18. 31 p.

Tyrväinen, T., Silvonen, T. & Mätäsniemi, T. 2016. Computing source terms with dynamic containment event trees. Seoul, Korea: 13th International Conference on Probabilistic Safety Assessment and Management (PSAM 13). 10 p.

Tyrväinen, T. & Silvonen, T. 2015. Summary on integrated deterministic and probabilistic safety assessment development and case studies. Espoo: VTT. VTT Technology VTT-R-04473-15. 31 p.

Tyrväinen, T. 2016. FinPSA – User guide – Tight integration of PRA levels 1 and 2. Espoo: VTT. VTT Technology VTT-R-03893. 11 p. + app. 1 p.

Tyrväinen, T. 2017a. Dynamic flowgraph methodology and its applications. Espoo: VTT. VTT Technology VTT-R-03364-16. 18 p.

Tyrväinen, T. 2017b. Solving dynamic flowgraph models with FinPSA. Espoo: VTT. VTT Technology VTT-R-04628-17. 13 p. + app. 2 p.

Tyrväinen, T. 2018. Time-dependent probabilistic risk assessment in FinPSA. Espoo: VTT. VTT Technology VTT-R-04119-18. 25 p. + app. 1 p.

Wallin Caldwell, A., Olsson, A., Georgiadis, A., Jošek, R., Johanson, G., Holmberg, J.-E., Karanta, I. & Fritioff, K. Level 3 PSA Guidance for Nordic Conditions. NPSAG Report 29-001:11, March 2017.

3.3 Safety of new reactor technologies (GENXFIN)

Tuomo Sevón[1], Mikko Ilvonen[1], Jarno Kolehmainen[1], Sami Penttilä[1], Ville Tulkki[1], Antti Rantakaulio[2], Jaakko Ylätalo[2], Rasmus Karell[2]

[1]VTT Technical Research Centre of Finland Ltd
P.O. Box 1000, FI-02044 VTT

[2]Fortum Power and Heat Oy
P.O. Box 100, FI-00048 FORTUM

Abstract

The GENXFIN project investigated safety issues of advanced reactor concepts, mainly SMRs. Various international forums and working groups on advanced reactor concepts were participated and the information was distributed to the SAFIR reference group. The project organized a national SMR seminar.

The licensability of the passive safety systems of the NuScale SMR design was investigated. The key issues are probably the independency of the defense in depth levels, and the severe accident management systems. Doses caused by a hypothetical radioactive release from a NuScale reactor were calculated. With conservative release estimates, sheltering could be needed within 5–12 km of the plant, and evacuation could be needed within 2–8 km.

Modeling methods of passive safety systems were developed by calculating PANDA isolation condenser experiments with the MELCOR code. When compared with earlier calculations with other codes, MELCOR gave about equally good results as the APROS code and better results than the RELAP5 code. As an in-kind contribution to the GENXFIN project, Fortum shared a report of their APROS modeling work of the NuScale and Yanlong SMRs.

Introduction

The main objective of the GENXFIN project was to increase knowledge on safety issues of advanced reactor concepts and to coordinate participation in various international forums and working groups, as well as to disseminate information to Finnish stakeholders. The emphasis of the project was on SMR (Small Modular Reactor) designs that could be deployed in Finland in the near future.

In addition to the normal VYR and VTT funding, TVO and Fennovoima directly funded the project. As an in-kind contribution, Fortum shared reports of its own SMR research to the SAFIR reference group.

Licensability of NuScale cooling systems in Finland

The GENXFIN project investigated the passive safety features of the NuScale SMR design and their licensability in Finland. The work was made in co-operation by VTT and Fortum (Kolehmainen et al. 2018). SMRs differ from large reactors, among other things, by placing all the primary circuit components in the reactor pressure vessel. Thanks to their smaller power, SMRs contain less radioactive materials than large reactors. The key issues in NuScale licensing in Finland are probably the independency of the defense in depth levels and severe accident management systems, which Finland requires for all reactors.

In publicly available NuScale documents, the Decay Heat Removal System, the Emergency Core Cooling System, and the Containment Heat Removal System are all credited at three or four different defense in depth levels. This may indicate non-compliance to Finnish regulations. However, it might be possible to allocate the Decay Heat Removal System solely to level 2 and the Emergency Core Cooling System solely to level 3. This could partially solve the problem of non-independent defense in depth levels. However, defense level 4 seems to be missing from the NuScale design, since Kolehmainen et al. (2018) found no severe accident management systems for heat removal in public NuScale documents.

Emergency preparedness zones required for SMR sites

A review of international developments in sizing of emergency preparedness zones was made, with a focus on SMRs. Since the fission product inventory in SMRs is smaller than in large reactors, also the environmental consequences of a severe accident are expected to be smaller. In addition, the lower decay heat and the use of passive safety systems may reduce both the probability of a severe accident and the probability of a containment failure. Thus, SMRs could be located closer to cities, which would allow them to be used for district heating. On the other hand, if several SMRs are located on the same site, the possibility of a multi-unit accident due to a common cause needs to be taken into account. (Ilvonen 2018, 2019)

In the GENXFIN project, doses caused by a hypothetical radioactive release from a NuScale reactor were calculated with VTT's VALMA code. The fission product inventory was calculated with the Serpent code. Conservatively, it was assumed that the release fractions are the same as those that would cause a 100 TBq Cs-137 release from a 1 600 MW EPR. In effect, credit was taken of the smaller inventory, but not of the possibly smaller accident probability or the possibly smaller release fraction. A statistical analysis was performed using one-year weather data provided by the Finnish Meteorological Institute. The assumed release location was Olkiluoto. With these assumptions, sheltering could be needed within 5–12 km of the plant, and evacuation could be needed within 2–8 km. (Ilvonen 2018)

An ideal procedure to determine the size of an emergency preparedness zone would involve a full-scope level 3 PRA. However, this would require very large resources. Still, the definition of an acceptable risk would remain a political question: “How safe is safe enough?”

A practical starting point is proposed: Select some SMR types that could be viable alternatives for Finland. Study their fission product inventories and accident mitigation systems on the basis of public sources. Then, choose some possible sites for district heat generation and study their environment in detail (population distribution, schools, hospitals, etc.) Calculate doses to the population using some justified fractions of the fission product inventory released to the atmosphere in accidents. Then check if STUK dose limits would be exceeded and how the protective measures could be carried out in practice. (Ilvonen 2019)

Modeling of PANDA isolation condenser experiments with MELCOR

Many SMR designs include passive safety systems for removing decay heat from the reactor. The SMART design has the Passive Residual Heat Removal System, and the NuScale design has the passive Decay Heat Removal System. Both systems have a vertical heat exchanger immersed in a water pool. Steam, coming from the steam line, flows through the heat exchanger tubes and condenses there. The condensed water flows back to the feedwater pipe. Passive condensers with vertical heat exchange tubes are also used in the AES-2006 steam generator passive heat removal system.

In the GENXFIN project, PANDA Isolation Condenser experiments (Dreier et al. 1998) were modeled with the MELCOR code (Sevón 2019). The work was a continuation of earlier research, in which experiments on steam condensation in vertical tubes were calculated with MELCOR (Sevón 2013). In the earlier work, it was found that in some cases MELCOR significantly underestimates the condensation rate in vertical tubes, when using default heat transfer parameters, both with pure steam and with steam–air mixtures. The problem was fixed by changing the condensate film Reynolds number limits from the default values to literature values (Incropera & DeWitt 2002), using MELCOR’s sensitivity coefficients. The Reynolds number limits are used for classifying the condensate film flow as laminar or turbulent. The PANDA experiments calculated in the GENXFIN project were performed at higher pressure than the earlier work, and the pure steam tests were performed so that all the steam condensed in the tubes and only water flowed out.

MELCOR nodalization of the PANDA isolation condenser is presented in fig. 1. The condenser was immersed in a water pool at the saturation temperature and atmospheric pressure. Steam, air and helium were fed to the upper drum through the supply line. The steam condensed in 20 vertical tubes with inner diameter of 51 mm and length about 2 m. The condensed water flowed from the lower drum to the drain line. In tests with non-condensable gases, the air, helium and remaining steam flowed through the vent line to the wetwell, which was kept at a constant

pressure. In pure steam tests, the vent line was closed and the condenser settled itself to an equilibrium pressure, in which all the steam condensed.

In the MELCOR model, the 20 heat exchange tubes were divided into four groups. Each group represented five tubes of equal length. Each tube group was divided into three control volumes (CV) of equal length in the vertical direction.

The water pool at the secondary side of the condenser was divided to five CVs in the vertical direction, in order to model the effect of the hydrostatic pressure on the saturation temperature. At first, it was attempted to model both water flow downwards and steam flow upwards with a single flow path between each pair of pool CVs on top of each other. However, the counter-current flow of water and steam through the same flow path lead to heavily oscillating flow rates and very short time steps. The problem was solved by modeling the water and steam flows with separate flow paths, with the steam paths leading from the top of each CV to the top of the whole pool. Modeling the pool as a single CV was also tested.

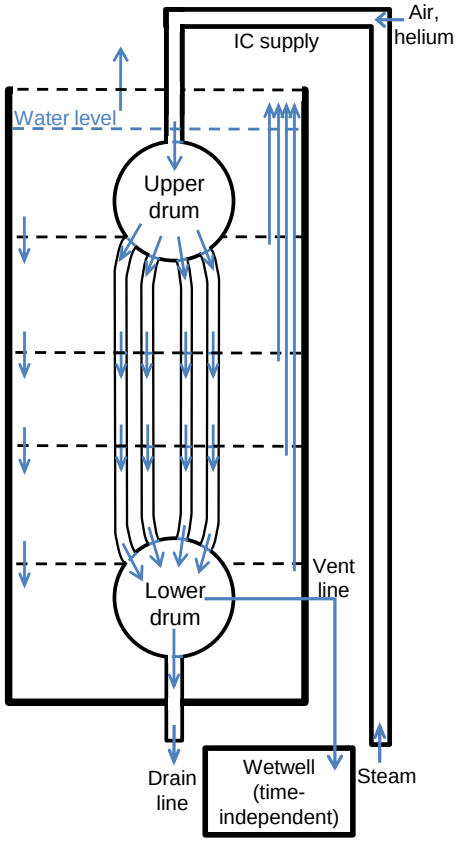

Figure 1. MELCOR model of the PANDA isolation condenser. The blue arrows are flow paths.

The calculations were made with MELCOR version 2.2 revision 11932. Four variants of the MELCOR model were used. The water pool on the secondary side was modeled either as five CVs stacked in the vertical direction, or as a single CV. Both default and modified condensate film Reynolds number limits were tested.

MELCOR underestimated the equilibrium pressure in the pure steam tests (fig. 2). The average underestimation was 12 % with the five CV pool model and modified Re limits. Underestimating the pressure in these tests means overestimating the condensation. As a result, the best results were obtained with the five CV pool model with the default Re limits because it gave the lowest condensation rate. This is in contrast to the (Sevón 2013) calculations, in which the default Re limits underestimated the condensation rate but the modified limits gave good results. The main difference is that all the steam condensed in the PANDA pure steam tests, while in the tests calculated in (Sevón 2013), the flow rate was so high that some of the steam did not condense.

MELCOR underestimated the condensation rate in the mixture tests (fig. 3). The average underestimation was 5 % with the five CV pool model and modified Re limits. The best results were obtained with the single CV pool model and modified Re limits. However, the difference between the five CV and single CV pool models was very small in the mixture tests because the main heat transfer resistance is inside the tubes, due to the non-condensable gases, and the heat transfer model on the outer surface is less important.

Using the modified condensate film Re limits can still be recommended because they give better results in all the condensation experiments calculated so far by VTT, except the PANDA pure steam tests in which the vent line was closed. Dividing the water pool into several CVs in the vertical direction may be beneficial in pure steam cases because accuracy of the heat transfer model on the outer surface of the tubes is more important than with steam – non-condensable gas mixtures. Division of the pool into several CVs requires careful definition of the flow paths between the CVs, in order to avoid oscillating steam flow that causes unacceptably short time steps and slow calculation.

The MELCOR results are compared with earlier RELAP5 and APROS calculations in figures 2 and 3. MELCOR gives about equally good results as the APROS code. The MELCOR results are better than the RELAP5 results.

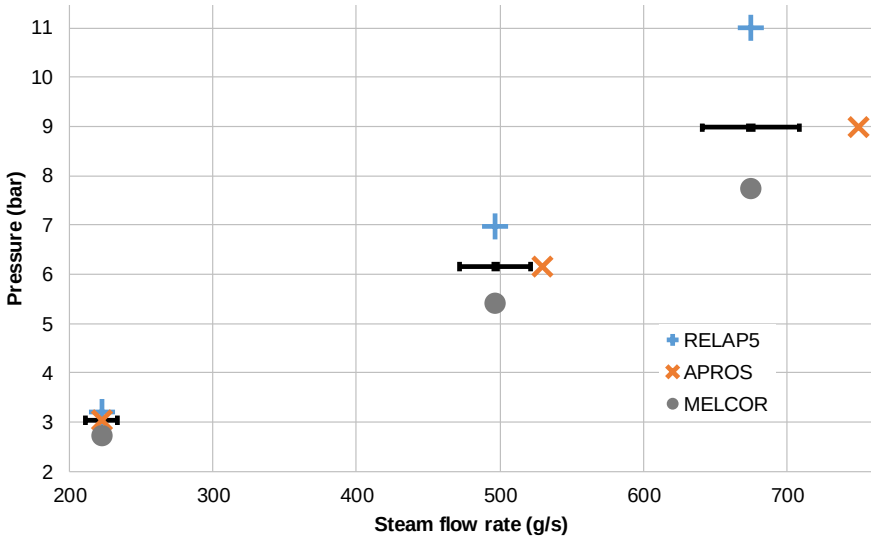

Figure 2. Results of pure steam tests in the PANDA isolation condenser. The measurements are shown with the black error bars. RELAP5 results from (Dreier et al. 1998), APROS results from (Hillberg 2012), and MELCOR results from (Sevón 2019) using the 5 CV pool with modified Re limits.

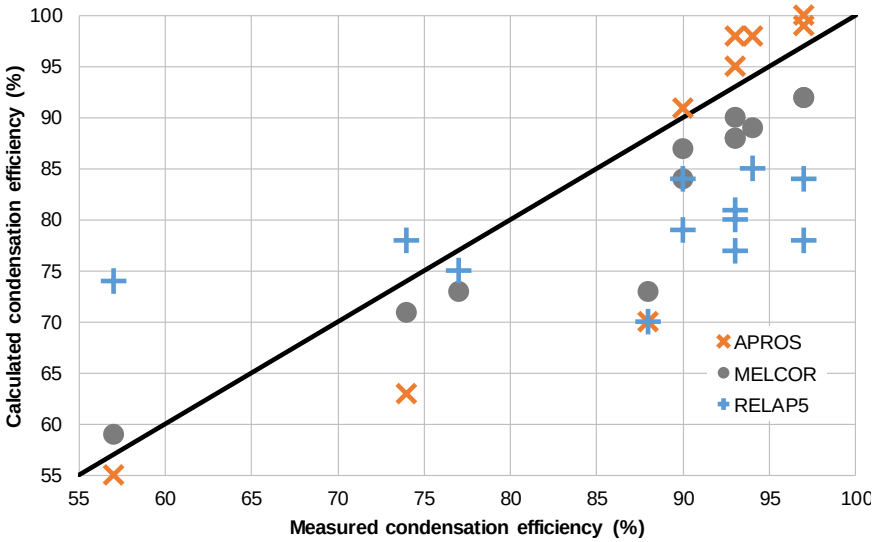

Figure 3. Results of steam – non-condensable gas mixture tests in the PANDA isolation condenser. RELAP5 results from (Dreier et al. 1998), APROS results from (Hillberg 2012), and MELCOR results from (Sevón 2019) using the 5 CV pool with modified Re limits.

Modeling of NuScale and Yanlong reactors with Apros

As an in-kind contribution to the GENXFIN project, Fortum shared a report of its SMR modeling with the Apros code (Ylätalo 2018). Two reactor types were modeled, NuScale and Yanlong. Both models are based on publicly available design data. The objectives were to test the capabilities of Apros to model helicoil steam generators and connection of an SMR to a district heating network.

In the NuScale model, two 160 MW_{th} reactors were connected to a single turbine and to a district heating network. The model demonstrated that SMR combined heat and power plants can be modeled with Apros. The simulated values are very close to NuScale design values at full power. The evaluated heat transfer rate of the helicoil steam generators is 10 % lower than in the design. The difference has to be compensated in the model either by increasing the secondary mass flow rate or the heat transfer area. Some instability was noticed in the behavior of the steam generator. If the intake pressure drops below a critical limit, in this case 1 bar below the design pressure, the steam generator start to pulsate. The cause of the phenomenon is still under investigation.

The second SMR study investigated the Chinese Yanlong 400 MW district heating reactor. The reactor is located in a 25 m deep water pool. The pool surface is at the atmospheric pressure, and the core is pressurized by the hydrostatic pressure. The model was tested at full power operation with the district heating network connection. It was concluded that the reactor concept is very robust due to its simplicity and the large amount of water.

Participation in international forums

A major part of the GENXFIN project was participation in various international forums and working groups on advanced reactor concepts, and disseminating the information to the SAFIR reference group. Meetings organized by IAEA, Generation IV International Forum, American Nuclear Society, and Canadian Nuclear Laboratories were participated. Topics of the meetings included SMRs, supercritical water reactors, district heating reactors, accident tolerant fuels, and emergency preparedness and response. During 2017 and 2018, ten travel reports were written.

SMR seminar

In order to enhance national collaboration and information exchange on SMRs, the GENXFIN project organized a seminar in Espoo on 20 November. 24 people participated the seminar. Presentations were given by VTT, STUK, Fortum, and LUT. Discussion topics included the potential of district heating with SMRs in Finland, the possibility of unmanned remote-operated reactors, siting requirements of SMRs, application of defense in depth in SMRs, and the necessity of changes to Finnish legislation and YVL guides to facilitate SMR licensing.

References

Dreier, J., et al. 1998. PANDA test results and code assessment for investigations of passive decay heat removal from the core of a BWR. 6th International Conference on Nuclear Engineering (ICONE-6463), San Diego, California, 10–14 May 1998.

Hillberg, S. 2012. PANDA steady state isolation condenser experiments with APROS. VTT Technical Research Centre of Finland. (Research report VTT-R-01259-12)

Ilvonen, M. 2018. Off-site radiological consequences from a SMR unit. VTT Technical Research Centre of Finland. (Research report VTT-R-00651-18)

Ilvonen, M. 2019. Considerations in EPZ sizing of SMR plants. VTT Technical Research Centre of Finland. (Research report VTT-R-06998-18)

Incropera, F.P. & DeWitt, D.P. 2002. Fundamentals of Heat and Mass Transfer. John Wiley & Sons, fifth edition, pp. 615–620.

Kolehmainen, J., Rantakaulio, A. & Karell, R. 2018. Application of system engineering approaches to evaluate the heat removal strategies of NuScale Power Module. VTT Technical Research Centre of Finland & Fortum. (Research report VTT-R-00608-18)

Sevón, T. 2013. Modeling of ESBWR passive containment cooling system with MELCOR. 22nd International Conference Nuclear Energy for New Europe, Bled, Slovenia, 9–12 September 2013. http://www.nss.si/proc/nene2013/pdf/NENE2013_405.pdf

Sevón, T. 2019. Modeling of PANDA isolation condenser experiments with MELCOR. VTT Technical Research Centre of Finland. (Research report VTT-R-00021-19)

Ylätalo, J. 2018. Fortum SMR modelling 2018. Report.

3.4 Fire risk evaluation and Defence-in-Depth (FIRED)

Jukka Vaari[1], Anna Matala[1], Topi Sikanen[1], Antti Paajanen[1], Simo Hostikka[2], Deepak Paudel[2]

[1]VTT Technical Research Centre of Finland Ltd
P.O. Box 1000, FI-02044 VTT

[2]Aalto University
P.O. Box 11000, FI-00076 AALTO

Abstract

A significant proportion of the overall core damage risk in nuclear power plants is associated with internal fires. The computational tools that are used for assessing the fire risks have developed significantly over the last ten years: the deterministic analyses are now solely based on CFD, and probabilistic analyses using Monte Carlo –simulation have been carried out. Maintaing the computational infrastructure requires continuous investments, and significant research efforts are still needed to enable predictive engineering simulations of fire spreading. The main themes covered by the FIRED project were fire risks of cables during the plant life cycle, fire Defence-in-Depth, and modelling tool development and validation. In addition, active participation in OECD PRISME 2 –project was continued.

Introduction

The main objective of the FIRED project was to develop the tools for fire risk evaluation and create a new methodology for assessing the Defence-in-Depth in the context of fire safety. To meet this main objective, a number detailed objectives were set out for the project.

Developing pyrolysis modelling capability for new flame retardants is required in order to predict their performance. New ingredients e.g. nanofillers / nanocomposites (organoclays, mesoporous silicate particles, layer-by-layer technologies) are now emerging to the market, but the understanding of their flame retardant mechanisms on the level of modelling capability, and thus the competence for safety assessment is practically non-existent. In FIRED, we pro-actively built a future competence for analysing the new flame retardants by carrying out fundamental studies of their performance and modelling.

Quantification of the agein effect on modern cables remains an issue. The current understanding is that the traditional PVC cables can actually become less flammable during the years of use, as the flammable softeners and other additives slowly escape from the polymer matrix. However, detailed ageing studies combining small scale experiments (micro-scale combustion calorimeter, thermogravimetry and cone calorimeter) and the flame spread tests with pyrolysis modelling have not been

found. Furthermore, an interesting question is how the ageing affects the efficiency of the modern flame retardants that are now being installed (metal hydroxides) or those that are just emerging on the market (nano-fillers).

Further developments are required in our a capability to predict the fire resistance of a barrier element with the Fire-CFD. Structural fire protection, which is the most traditional form of fire protection engineering, has the strong tradition of relying of fire resistance classifications, and this has delayed the development of engineering methods for barrier performance assessment, including the computational tools and, most importantly, the acceptance criteria. More work is needed to enable efficient assessment of structural and barrier performance within the fire simulation environment that is already commonly used for other purposes.

Numerical modelling remains an important tool for assessing fire risk at nuclear power plants. Continuous improvement of existing models is necessary to improve the reliability an accuracy of the modelling results. At the same time, the range of models available for making these predictions is expanding, and efforts should be allocated in evaluating new and complementary modelling approaches to existing ones. In FIRED, reactive molecular dynamics was introduced as a new potential approach to gain molecular level insight into pyrolysis of polymeric materials.

Fire risks during cable life cycle

Arguably the most difficult part in setting up a fire-CFD simulation involves the description of the burning materials. In the context of fire-CFD, the pyrolysis of solid materials is typically modelled using a one-dimensional heat conduction solver, based on the finite difference method, with source terms modelling the effects of chemical reactions and internal radiation. Only few of the pyrolysis model parameters can be directly measured. The others must be estimated from experimental data (Matala 2013). If the material cannot be tested for some reason, the remaining option is to estimate the thermal and kinetic properties from constituent-level material simulations.

Molecular-level modelling of the mechanisms of fire retardancy requires the description of chemical reactions, i.e. the forming and breaking of chemical bonds. Reactive Molecular Dynamics (RMD) offers a trade-off between the efficiency of classical MD and the accuracy of ab initio quantum chemistry methods.Our hypothesis is that state-of-the art RMD methods can yield sufficiently accurate descriptions of the thermal degradation chemistry of fire retardants and polymeric base materials. This hypothesis was tested in a proof of concept demonstration for a fire retardant compound that is relevant for electrical cabling applications.

We carried out reactive molecular dynamics simulations based on the ReaxFF reactive force field to study the effect of aluminium (tri)hydroxide on the thermal decomposition of polyethylene. The simulations reproduced the endothermic decomposition of aluminium (tri)hydroxide into alumina and water. Other known mechanisms of flame retardancy, such as heat absorption by the filler and its residue,

were reproduced with reasonable accuracy. The simulations also revealed a chemical interaction between polyethylene and aluminium (tri)hydroxide, in which hydroxyl radicals released by the aluminium (tri)hydroxide abstracted hydrogen from the surrounding polyethylene, resulting in enhanced water production and enhanced charring of polyethylene (Vaari & Paajanen 2018).

Furthermore, we analysed the data in order to obtain kinetic parameters for the pyrolysis model of the Fire Dynamics Simulator. Specifically, a set of thermal decomposition simulations using linear heating rates in the range 0.3 - 5 K/ps were performed for model systems of pure aluminium trihydroxide (modelled as gibbsite), pure amorphous polyethylene, and a composite of PE+ATH. The simulations can be regarded as a set of atomistic scale thermogravimetric experiments. Kinetic parameters for the decomposition reaction of each system were extracted from the data using two model-free isoconversional methods, where 'model-free' means that no assumptions need to be made on the reaction model. It was enough to assume an Arrhenius-type behaviour for the reaction rate constant, and to derive the associated pre-exponential factor A and activation energy E_a from the isoconversional analysis. Examples of results are shown in Figure 1 for pure polyethylene.

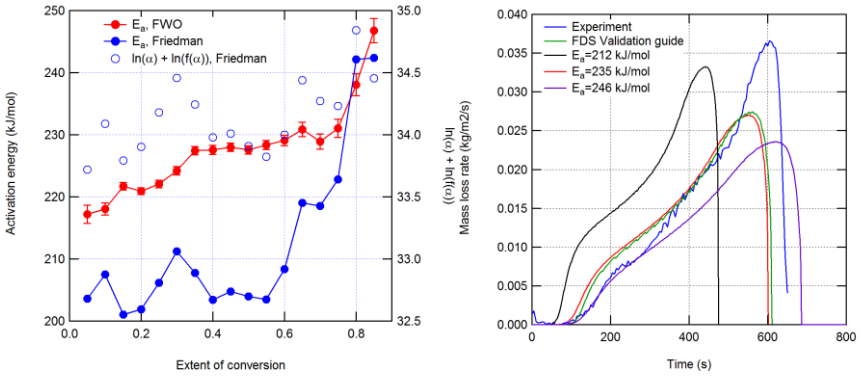

(a) (b)

Figure 1. (a) Kinetic parameters for polyethylene decomposition from isoconversional analysis of RMD data. (b) FDS simulation of the cone calorimeter experiment under nitrogen atmosphere using the kinetic parameters form RMD.

Thermal ageing of cables during the NPP lifetime has been studied by literature and experimentally. Different polymers and additives behave in very versatile manners during decades at elevated temperatures. In earlier studies it was observed that the fire performance of a PVC cable may actually improve during ageing, while some other flame retardants evaporate and leave the polymer less protected.

Two flame retardant cable types from actual NPP were aged by means of accelerated ageing. The ageing time and temperature were determined from very slow (0.3-3 K/min) TGA tests. While these results were not unambiguous, they indicated the order of magnitude for setting up the parameters for accelerated ageing. The cables were placed in a furnace at 105 °C for 1-2 months' time. These conditions

correspond to service time of 40-60 years at 40 °C. After ageing, the cables were tested using MCC and cone calorimeter methods. In addition, a flame retarded (FRNC-B) cable was aged by radiation to correspond approximately over 45 years of service time. The possible changes in the fire safety of the cable were studied via small and bench scale experimental methods.

For the thermally aged cables, the results showed that no significant changes in fire behaviour could be observed between new and aged cables. Due to lack of sample material and other resources, the testing had to be limited to five cone calorimeter experiments per cable. The conclusions made from these tests could be improved by adding repeated tests, heat fluxes and allowing longer ageing times. For the radiation aged cable, in small scale (TGA and DSC) the differences between cables were minimal, but in cone calorimeter some differences were observed, warranting further studies on the subject.

Fire-barrier performance assessment

Computation of heat conduction and pyrolysis of solid materials is commonly needed in the context of numerical fire simulations. Examples of such simulations include the computation of fire spreading on polymeric materials, such as electrical cables, and the response of structural fire barriers on heat exposure. The current solid-phase solver of Fire Dynamics Simulator (FDS) software is based on the finite difference (FD) formulation. It works relatively well for many applications, but in the case of pyrolysing materials, the numerical fluctuations of the temperature and pyrolysis rate solutions can cause large uncertainties or stability problems in simulations.

We developed a new, Finite Element Method -based solver for the heat conduction in a pyrolyzing material in the form of a stand-alone Matlab-code, with an option to be implemented later in FDS. This model has been applied in 1D heat transfer calculations of concrete and stone-wool fire barriers in order to obtain an alternative result to the FDS heat transfer calculation. The model has also been used as part of studies involving uncertainty propagation which represent the main focus of our fire-barrier related work.

All numerical models have a certain modeling inaccuracy; i.e. the model cannot capture the actual physical phenomenon perfectly. For a particular output, the modeling inaccuracy should be quantified in a meaningful way. In fire safety engineering, the most common practice is to express it as a measure of systematic and random deviation from the experimentally observed value. For example, in the validation guide of FDS, the modeling uncertainty is presented for various output quantities. The data obtained from numerous fire experiments are compared with the corresponding model simulations and the model uncertainty is quantified in terms of systematic bias and the second central moment of random errors. These two parameters represent the trending error property of the model, hence can be used to estimate the prediction inaccuracy resulting from using the tool.

The possible uncertainty or distribution of the input variables can be taken into account by manually varying the inputs within allowable and rather narrow limits. This is mathematically a fairly well-posed problem, and a rough range of error can be established for the target function by carrying out a fairly small number of such calculations. If more complete information of the error distribution is needed, stochastic methods sich as Monte Carlo should be used. In Monte Carlo, a large number of samples is randomly chosen from the input space and mapped through the system into the target distribution. In demanding error analyses this has been a standard technique for some time (Hostikka & Keski-Rahkonen 2003).

The problem not addressed by the above-mentioned and similar other studies is that the stochastically inferred output uncertainty is inevitably a combination of both input and modeling uncertainties, being possibly very different from the true output uncertainty. We have developed an uncertainty model that can be used to obtain the true output uncertainty from the stochastically simulated one (Paudel & Hostikka 2019). This requires *a priori* knowledge of the modelling error.

To demonstrate the capability of the new approach, use was made of a series of fire tests carried out at VTT Building Technology with aim to produce a set of data for validation of fire models. The tests were conducted in a compartment, 10 x 7 x 5 m^3, having one door opening to the surrounding large test hall (Figure 2). Systematic variations in fire size and locations were made to determine their effects on the fire environment. Thermocouples and heat flux gauges were placed at various locations to measure gas and wall temperatures and heat fluxes. Altogether 20 tests were conducted.

The wall temperatures were modelled by a coupled CDF+FDM approach (FDS simulations), where wall temperature was predicted based on the mass loss rate of the fuel (heptane) and gas temperatures measured during the experiment. In addition, the standalone 1D heat transfer model was used to simulate the wall heat transfer based on either the experimentally measured heat flux or the heat flux prediction from FDS.

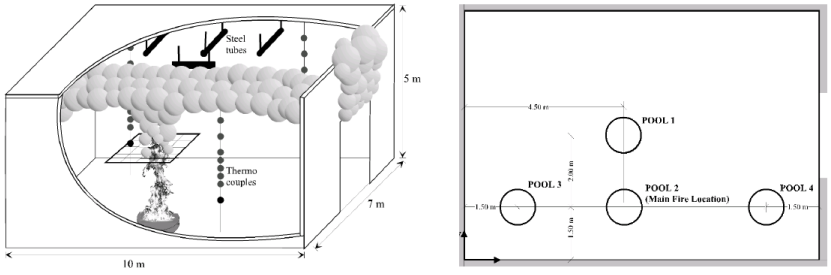

Figure 2. schematic diagram representing the fire experiment and the fire pool locations.

Table 1 shows the predicted ($\widetilde{\sigma_M}$) and measured ($\widetilde{\sigma_E}$) uncertainties, and systematic bias (δ) in various output quantities. It also compares of the values obtained from the current study with the the one reported in the FDS validation guide. The

values obtained from the current experiment were closely matching with the one reported in the validation guide, except for the gauge heat flux. The gauge heat fluxes in this study were over-predicted.

Table 1. Comparison selected temperature measurements to simulation results.

	Current Experiment			Validation Guide		
Output Quantity	$\tilde{\sigma}_E$	$\tilde{\sigma}_M$	Bias	$\tilde{\sigma}_E$	$\tilde{\sigma}_M$	Bias
HGL Temperature	0.05	0.05	0.91	0.07	0.07	1.05
Ceiling Jet Temperature	0.06	0.06	0.93	0.07	0.14	1.05
Plume Temperature	0.07	0.12	0.90	0.07	0.16	1.18
Adiabatic Surface Temperature	0.07	0.13	1.02	0.07	0.13	1.04
Gauge Heat-Flux	0.11	0.60	1.13	0.11	0.22	0.99
Wall Temperature	0.07	0.14	1.07	-	-	-

Using the predicted and measured uncertainties from of Table 1 (“current experiment” values) as the *a priori* information of the modelling error, it was possible to convert any simulated output quantity into an estimate of the true output quantity. For example, failure of a fire barrier can be associated with a temperature exceeding a given threshold value. The upper part of Figure 3 shows the predicted, measured, and corrected wall temperatures at three different times in all tests. It is seen that when prediction and measurement were apart, the corrected value was usually closer to the measurement. The bottom part probability that the wall temperature exceeds a given threshold in a given time. The predicted probabilities were higher than the measured ones, due to the positive bias in temperature estimation. The corrected probabilities were closer to the measured ones.

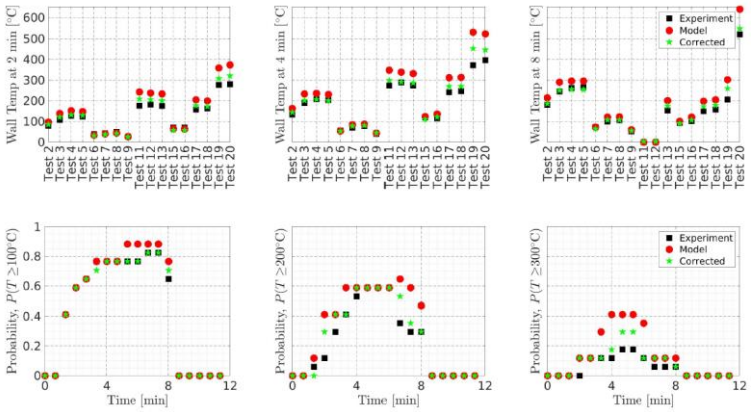

Figure 3. Top: predicted, measured, and corrected wall temperatures at 2, 4, and 6 minutes in all tests. Bottom: probability that the wall temperature exceeds a given threshold in a given time.

Fire simulation development, maintenance and validation

Numerical modelling remains an important tool for assessing fire risk at nuclear power plants. Continuous improvement of existing models is necessary to improve the reliability an accuracy of the modelling results. Improvements regarding simulations of liquid pool fires, liquid fire spreading, and cable fire spreading, were achieved. In addition, the Pyroplot tool for identifying pyrolysis model paramaters was replaced by a Python-based code, PyroPython.

Liquid pool fires are a significant hazard to industrial facilities. The liquids could originate e.g. from leaking transformers, generators or other machinery. Knowing the fire burning rate is the starting point of any fire safety analysis. The factors affecting the burning rates of liquid pool fires in open atmosphere are well known for a wide variety of liquids. However, many fire scenarios, especially in nuclear facilities, involve fires in confined spaces.

The burning rates in confined spaces, possibly coupled with mechanical ventilation, can be significantly different from the ones measured in open atmosphere. These differences are caused by e.g. air vitiation and heat radiation from hot walls and the hot gas layer. An international research program PRISME was conducted between January 2006- June 2011 to study fires in air-tight mechanically ventilated compartments. Results from this program have been previously used in validation of CFD codes for compartment fire scenarios.

In this work, we investigated modelling the liquid evaporation rate from the first principles (Sikanen & Hostikka 2017a). The benefit of our approach is that the burning rates can also be predicted for fuels for which the experimental data is not available. On the other hand, much more detailed information about the thermophysical properties of the fuels is needed. We focussed on 0.4 m^2 pool fires. First the model predictions were compared against experimental data from open air experiments. We looked at both the burning rate predictions and the temperatures within the liquid. After this we turned to under-ventilated fires, and looked at predicted burning rates and extinction times as a function of ventilation rate.

Predictive simulations of liquid pool fires were conducted using a CFD solver coupled with a detailed model for liquid evaporation. The results (see Figure 4) showed that code is capable of predicting the steady state burning rates of the TPH pool fires in compartments within 15% of the experimental value. The characteristic dependence between the ventilation rate and the burning rate was correctly captured.

In some simulations, the predicted burning rate showed strong oscillations that were not observed in the experiments. Similar oscillations have been observed in other experiments conducted in the same enclosure, though. The appearance of the oscillations was found to depend on the details of the geometry, grid resolution and the combustion modelling options.

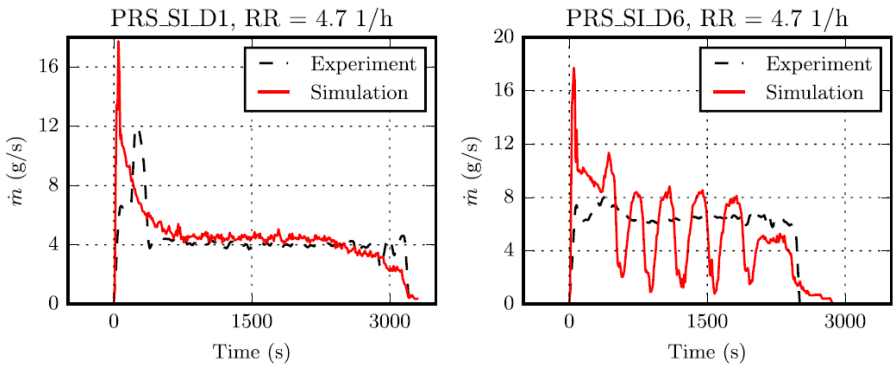

Figure 4. Comparison of predicted and simulated burning rates for a 0.4 m^2 TPH pool fire at an air renewal rate of 4.7 h^{-1}. Left: inlet in high position. Right: inlet in low position.

The 1D heat transfer model employed in this work could not reproduce the temperature gradient in the liquid phase. It is possible, that the gradual rise seen in burning rates of open atmosphere pool fires could be explained by enhanced heat transfer within the liquid phase by, e.g., lateral convection. The effect of non-gray radiation transport should also be investigated in the future.

Safety analyses of nuclear power plants (NPPs) have long included aircraft impacts. Initially, the impact was envisioned to be from a small aircraft or possibly a fighter plane. Following the September 11 terrorist attacks on the World Trade Center in 2001, these analyses have been extended to assume the impact of a large commercial aircraft.

Such an aircraft can damage safety-related structures and components through mechanical impact and fire. Fires induced by an aircraft impact may influence the NPP by three different mechanisms. First, a large fireball is created by the fuel cloud erupting from the breaking fuel tanks, resulting in high thermal radation levels. Second, only a fraction of the fuel carried by the plane will burn in the initial fireball, and the remaining fraction of the fuel will accumulate and burn in pools near the aircraft impact position. Third, fuel may penetrate inside the plant through openings.

The objective of this work was to develop and validate a CFD methodology for predicting the spreading and combustion of liquid fuel released upon an aircraft impact (Sikanen and Hostikka 2017b). The model for liquid release is based on the experimental work of Hostikka et al. (2015). The experimentally determined droplet sizes and spray velocities were used to determine realistic spray boundary conditions for liquid insertion. We focused on the threat posed by the initial fireball and amount of fuel that collects on the target surfaces. The subsequent combustion of the pools was not considered.

Figure 5 qualitatively compares the flame and smoke spread patterns for two different wind directions.

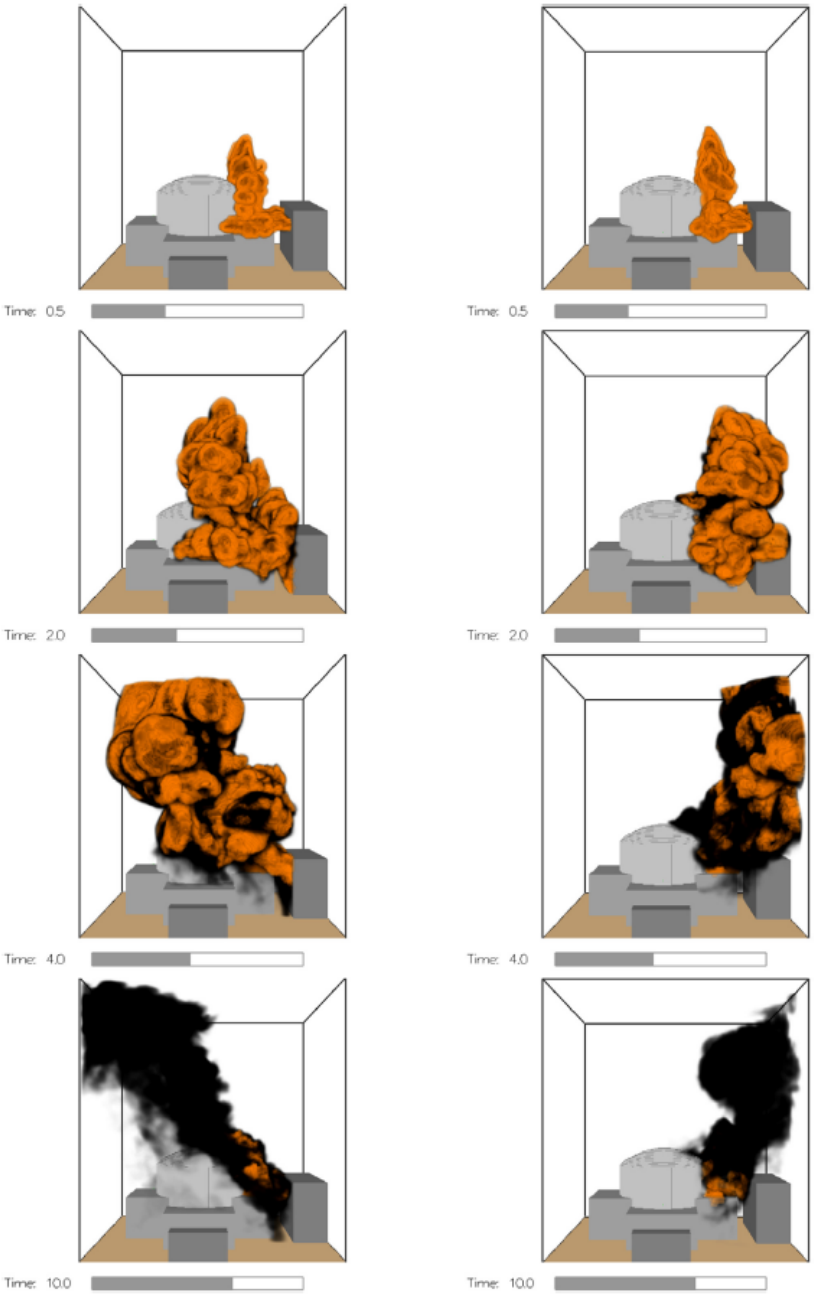

Figure 5. Qualitative comparison of the flame and smoke spread patterns at 0.5, 2.0, 4.0, and 10.0 s after impact for two different wind directions.

At 0.5 s from the impact, the flame shape was still dominated by the spray pattern. One second after impact, the wind started to bend the flame to the downwind direction, which significantly affected the portion of the plant geometry that was engulfed in flames. About 4 s after impact, the flame developed to the lift-up phase, and the wind effect was mainly limited to the extent of the smoke spreading. Later, the flames were only visible above the pool fire that formed below the impact position, and their movement was mainly dominated by the large-scale turbulence. Smoke spreading is strongly influenced by the wind. The horizontal distance of the flame influence was estimated to be less than 50 m.

The simulated fireballs resulted in locally high temperatures, velocities, and pressures but for only a short duration. Up to 20% of the fuel involved in the crash accumulated on the surfaces of the target building. The subsequent burning of this fuel may then be a significant hazard to the safety of the NPP and should not be ignored. Droplet size and the geometry surrounding the impact location had a significant effect on the pooling fraction. Lower impact location and larger average droplet size lead to larger pooling fractions.

One of the efforts in to achieve a good FDS description of a spreading fire in a cable tray has involved describing the cables as Lagrangian particles instead of solid obstacles. In FIRED, work was done to implement the aerodynamic resistance provided by the cables for the flow field. We proposed a method of modeling the drag of cable trays based on correlations developed for use in heat exchangers. The method was verified by comparing the predicted pressure drops of tube banks with results from the literature. The drag coefficients calculated using this method improved the flame spread predictions but did not affect the slow initial flame spread.

Furthermore, we identified deficiencies in the way current FDS algorithm handles the absorption and emission of thermal radiation by sub-grid scale elements such as cables. The default model in FDS underestimates the incident heat flux on sub-grid scale particles. The results in this report suggest that this leads to slower flame spread than experimentally observed.

We proposed an alternative method for determining the effective absorption coefficient used in the solution of the RTE. The proposed method produced more realistic flame spread in the initial phase of the simulations. However, after the initial flame spread phase, the simulations showed unphysically high temperatures. This was attributed to the self-absorption of emitted radiation by the sub-grid scale particles. The conclusion was that better treatment of radiation absorption is necessary for correct prediction of flame spread. However, it is unclear how the radiation absorption should be modeled, and further work is required.

A new tool called PyroPython was developed as a successor to the Pyroplot tool devloped in earlier SAFIR projects. The motivation for writing a new tool was to make it faster and more accessible. Python was chosen as the programmingn lanquage of the project due to the rich open source scientific computing ecosystem available for Python.

Unlike Pyroplot, which used genetic algorithms for optimizing the model parameters, PyroPython aims to be agnostic to the choice of the optimizer. Currently, the

software supports Bayesian Optimization (BO), optimization by multistart method using a derivative-free optimization algorithm (Nelder-Mead), differential evolution, and random sampling. Usage of BO for parameter identification is a novel aspect of the PyroPython tool. It involves fitting a response surface model to model evaluations and using the response surface to explore promising solution candidates.

Several optimization methods were tested on a very challenging 16 parameter pyrolysis model fitting problem. It was found that, at least for the present optimization problem, the traditional optimization methods, Nelder-Mead simplex and differential evolution have better performance than the Bayesian Optimization methodology. This conclusion may, however, change if the optimization problem at hand would be more costly to evaluate, say a long cone calorimeter experiment or a bench scale experiment.

References

Hostikka, S. and Keski-Rahkonen, O. 2003. Probabilistic simulation of fire scenarios. Nuclear Engineering and Design 224, 301-311.

Hostikka, S., Silde, A., Sikanen, T., Vepsä, A., Paajanen, A., Honkanen, M., 2015. Experimental characterisation of sprays resulting from impacts of liquid containing projectiles. Nuclear Engineering and Design 295, 388–402.

Matala, A. 2013. Methods and Applications of Pyrolysis Modelling for Polymeric Materials. Dissertation. Espoo: VTT. VTT Science 44. 85 p + app. 87 p.

Paudel, D., Hostikka, S. 2019. Propagation of modeling uncertainty in stochastic heat-transfer simulation using a chain of deterministic models. Accepted for publication in International Journal for Uncertainty Quantification. doi:10.1615/Int.J.UncertaintyQuantification.2018027275.

Sikanen, T. and Hostikka, S. 2017a. Predicting the heat release rates of liquid pool fires in mechanically ventilated compartments. Fire Safety Journal 91, 266-275.

Sikanen, T. and Hostikka, S. 2017b. Numerical simulations of liquid spreading and fires following an aircraft impact. Nuclear Engineering and Design 318, 147-162.

Vaari, J. and Paajanen, A. 2018. Evaluation of the reactive molecular dynamics method for Research on flame retardants: ATH-filled polyethylene. Computational Materials Science 153, 103-112.

3.5 Comprehensive analysis of severe accidents (CASA)

Anna Korpinen, Mikko Ilvonen, Jukka Rossi, Tuomo Sevón, Magnus Strandberg, Veikko Taivassalo, Eveliina Takasuo

VTT Technical Research Centre of Finland Ltd
P.O. Box 1000, FI-02044 Espoo

Abstract

Overall understanding of the progress and mitigation of severe accidents was strengthened by simulating the Fukushima accidents. When determining the post-dryout behaviour of the debris beds, the friction model effects notably the level the temperature stabilizes. VTT's modelling framework for hydrogen combustion works reasonably as the maximum pressure is close to the experimental result and the pattern of the flame front propagation is similar enough. MELCOR simulations are in a good agreement with the pool scrubbing experiments for non-soluble aerosols whereas ASTEC results were in a good comparison with the experiments for soluble aerosols. The offsite dispersion and dose assessment codes VALMA and ARANO typically predicts smaller dose values than widely validated MACCS.

Analysing Fukushima accidents

The Fukushima accident provides a unique opportunity for gaining more information on the progress of severe accidents and their prevention and mitigation. Finland participated phase 2 of the OECD NEA BSAF (Benchmark Study of the Accident at Fukushima) project. The objectives in analysing the accidents are 1) improving expertise in severe accident modelling, using data from a real full-scale reactor accident; 2) gaining a better understanding of the events in the Fukushima reactors; 3) getting insights into the capabilities and weaknesses of the integral codes in simulating severe accidents.

VTT has MELCOR models for all three units that have been updated when new plant data has been obtained (Sevón 2015; Sevón 2016; Sevón, 2017a; Sevón, 2017a). The current unit 1 model reproduces the measured pressures well as indicated for the containment drywell in Figure 1. Leaks from the recirculation pump seals were assumed because otherwise the measured containment pressure would have been underestimated. It was assumed that the seawater injections during the calculated time period (five days) failed because starting and stopping of the injection would have caused large changes to the reactor and containment pressures, but such changes do not exist in the measured pressures. The earlier freshwater injections were assumed successful. Reactor Pressure Vessel (RPV) lower head

penetration failure and debris ejection to the containment was calculated to occur at around 12 h.

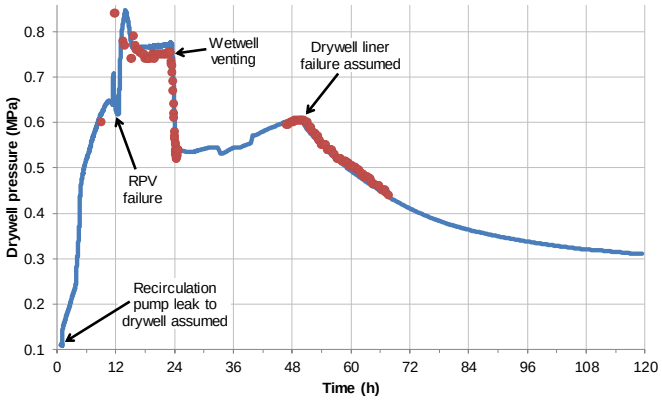

Figure 1. Fukushima unit 1 pressure in the containment drywell during the accident. The red dots are measured values and the blue curve is the result from the MELCOR simulation.

The unit 2 model reproduces the measured pressures in the reactor and in the containment well during the first 81 h. This required manual adjustment of the RCIC system flow rates and flooding rate of the torus room, so that a good match to the measurements is obtained. According to the calculation, the core was uncovered for 14 h. The actual time may have been longer because the calculation underestimates the reactor pressure between 83 and 89 h and therefore the water injection rate with the fire engine may be overestimated.

In Unit 3 the reactor was cooled by the RCIC and HPCI systems for the first 36 hours. In the model the RCIC and HPCI flow rates were manually adjusted so that the measured water level and pressure in the reactor are reproduced. The rise of the containment pressure accelerated after 6 h. This might be caused by stratification of the wetwell water, but it could not be reproduced by a simple stratification model. A small leak from the recirculation pump seal to the drywell was assumed, starting at 6 h 20 min, in order to reproduce the measured pressure increase.

Debris bed coolability

Coolability of corium should be ensured in all of its locations and forms. Previously the effect of the debris bed geometry and flooding mode on the dryout heat flux were analysed experimentally and analytically to evaluate the coolability of an ex-vessel debris bed (Takasuo, 2015; Takasuo, 2016a; Takasuo, 2016b) . However, the coolability limit based on the minimum dryout heat flux might be overly conservative, since the temperature may remain on an acceptable level even in the dry zone. Instead of the dryout heat flux, it has been proposed that the coolability limit

should be based on the increase of the particle temperature. To analyse this, the post dryout behaviour of conical debris beds was studied by performing MEWA simulations examining the influence of the bed particle size, heating power and porosity (Taivassalo & Takasuo, 2017). Due to the lack of experimental data that could be directly used for code validation, the MEWA results were compared to the DECOSIM results by Yakush & Kudinov (2014).The simulation results were not in agreement. The transient behaviour of the maximum particle temperature was in most cases nearly similar, but the temperatures stabilized to different levels.

The effect of heat transfer models available in MEWA did not explain the differences compared to the KTH's DECOSIM results and therefore the influence of the friction model in post-dryout conditions was analysed (Taivassalo, 2018). As MEWA does not feature the same friction model used in DECOSIM, it was added into the Fluent implementation of the debris bed coolability models. The usage of the same friction model improved the agreement with the DECOSIM results.

The validation of the Fluent implementation with the same friction model as in DECOSIM were continued with truncated-cone debris beds as the flow field close to the tip with the conical beds may hamper qualitative comparison of Fluent results with MEWA and DECOSIM (Taivassalo, 2019). The differences between the Fluent and DECOSIM results showed the same characteristics as obtained previously in the conical bed cases.

Implementing the friction model applied in DECOSIM also into MEWA improved the correspondence of the results notably. In order to obtain the same saturation temperature reported to be in the DECOSIM simulations, the pressure on the top surface was reduced from 3 bar (documented to be used in the DECOSIM simulations) to 1.3 bar. The MEWA results for the reduced pressure agree reasonably with the DECOSIM results in all analysed cases as illustrated in Figure 2 for the truncated-cone debris beds.

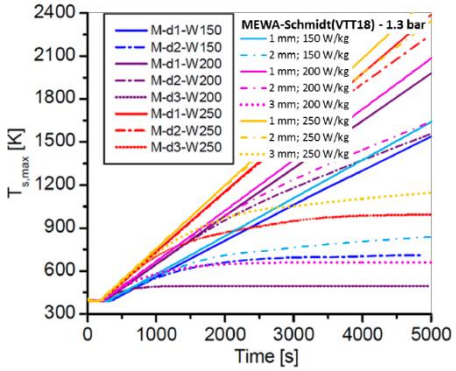

Figure 2. Comparison of the time evolution of the maximum solid particle temperature for the truncated-cone debris beds in the MEWA simulations of this study and in the DECOSIM simulations (Yakush & Kudinov 2014). In the MEWA simulations, the top surface pressure is 1.3 bar.

Ex-vessel steam explosion analyses with MC3D

Preserving of knowledge of steam explosions is important still today, since the risk of steam explosions during a severe nuclear accident cannot be excluded in our current nuclear power plants. The steam explosion loads in a Nordic BWR containment were assessed with the MC3D code studying the sensitivity of the results for some key input parameters (Strandberg, 2016). The main focus of the analysis was on the dynamic loads on the cavity wall imposed by the explosion.

The sensitivity analysis was done for melt temperature, coolant subcooling, cavity water level and melt drop size. Simple MELCOR calculations were made to find realistic boundary condition limits for the parameters. Based on the sensitivity analysis, the droplet size has the largest and most predictable impact on both explosion strength and probability. When assuming larger droplets, explosion becomes more probable and also stronger.

Also the effect of RPV breaking location was analysed (Strandberg, 2017). During the analysis of the results, it became clear that the calculations suffer from stability issues during the explosion part that caused the calculations to stop before the defined end time. This in turn makes analysing the pressure peaks at the wall difficult as it becomes uncertain if the maximum is reached before the calculations end. However, the resulting explosions were stronger in comparison to the previous 2D central break cases.

Hydrogen combustion

The common tools for hydrogen combustion modelling and especially those which are applicable in a containment-scale are strongly simplified models for complicated combustion-related processes occurring in complex geometries. Therefore, it is essential to evaluate critically the performance of the simplified tools. Especially valuable is to validate the models against experiments comparable to realistic containment geometries.

The ENACCEF2 facility at the Institut de Combustion Aérothermique Réactivité et Environnement (ICARE) of the Centre National de la Recherche Scientifique (CNRS) in Orléans (France) can be equipped with obstacles accelerating the flame propagation as in real containment rooms. An international double blind validation benchmark was participated simulating the flame propagation in three experiments (Bentaib et. al., 2018). The model predictions were computed with a CFD-based combustion model developed at VTT for lean hydrogen mixtures. The combustion model is implemented as user defined functions in the CFD-code Fluent. The applicability of alternative modelling approaches was tested by computing the first experiment and the most promising ones were chosen. The uncertainties of model parameters are commonly significant in terms of the flame propagation speed. The flame speed was also found to be sensitive especially to the modelling approach for the flame-front propagation and to some extent to the mesh density as well as time

step. However, the maximum pressure is less influenced by the computational parameters. The computed and measured flame speeds are compared in Figure 3. The overall agreement is good.

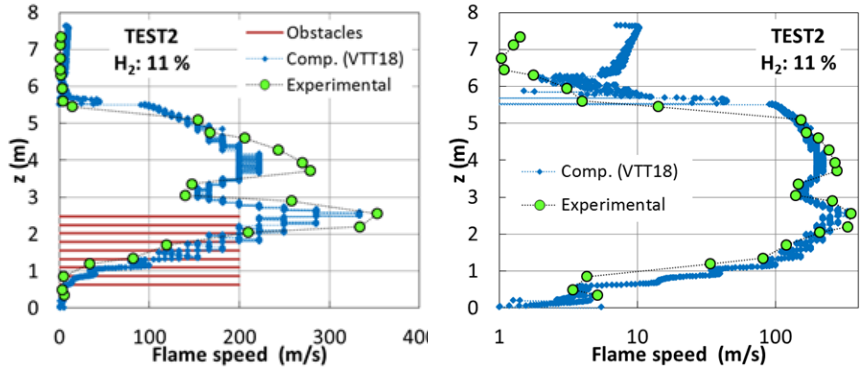

Figure 3. Computed and experimental flame speed in Test 2 of the Etson-Mithygene benchmark a) with and b) without obstacles.

Also the THAI-3 blind benchmark on hydrogen combustion and flame propagation in the two-compartment system, the HD-44 experiment, was participated (Taivassalo, 2019). The hydrogen combustion model of VTT was developed further by extending the Zimont model for lean hydrogen mixtures and by assuming the flame speed to be determined by the dominating phenomenon of laminar burning, flame instabilities, buoyancy and flow turbulence. Furthermore, the influence of the flame thickness on the burning velocity is taken into account for flames with instabilities.

The performance of the revised modelling framework was demonstrated by reproducing experimental results of several tests with downward and upward flame propagations. The computational results are mainly in satisfactory agreement with experimental results. The comparison of the blind predictions of the HD-44 results to the preliminary experimental data shows that the computational results are in a reasonable agreement with the experimental data. The maximum pressure is close to the experimental one and the pattern of the flame front propagation is similar enough (the blind-predicted flame arrival time is shown in Figure 4). However, the flame speed was underestimated by about a factor of 2. The difference is not that unexpected regarding the uncertainties of the models determining the flame speed in these conditions: the Zimont correlation for the turbulent burning velocity is very simple approximation and it utilises turbulent quantities estimated with the almost simplest turbulence model, the standard kε model.

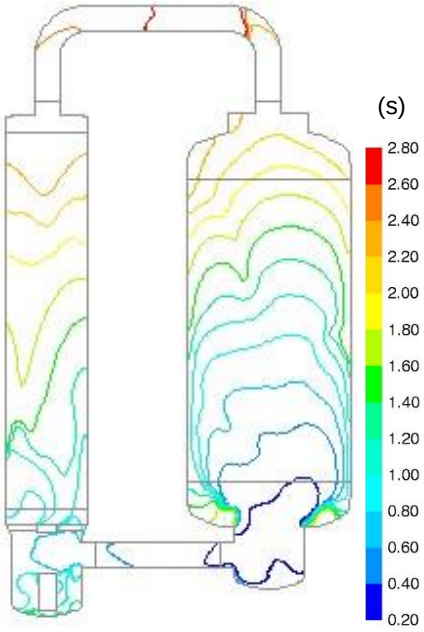

Figure 4. Blind prediction of the flame arrival time for the HD-44 experiment. The flame propagates also in the lower connection pipe against the gas flow and upward also in the smaller PAD vessel. In the upper part of the PAD vessel, the flame propagates faster than in the bigger THAI test vessel. The two flame fronts meet in the upper connection pipe above the THAI test vessel.

Pool scrubbing

Pool scrubbing experiments performed in the SAFIR2018 CATFIS project provide excellent validation data for the integral codes. The medium-scale pool scrubbing experiments with non-soluble aerosols were analysed with ASTEC and MELCOR (Strandberg et. al., 2018; Korpinen et. al., 2019) for different pool temperatures and inlet airflow rates. Since in the experiments two different measurement devices were used, it was possible to study also the effect of the aerosol size on the Decontamination Factor. However it should be noticed that SMPS tells the geometric diameter, whereas ELPI measures the aerodynamic diameter. The results are in Figure 5.

ASTEC results notably smaller Decontamination Factor (DF) values than recorded in the experiments or resulted by MELCOR for pool temperatures clearly below the boiling point. The effect of the particle size on ASTEC DFs seems to be almost negligible with small DF. With 20 °C pool temperature, MELCOR DF values match very well with the experimental results for all air flow rates. With 70 °C pool temperature the deviation is bigger but more or less at the same range with both particle sizes.

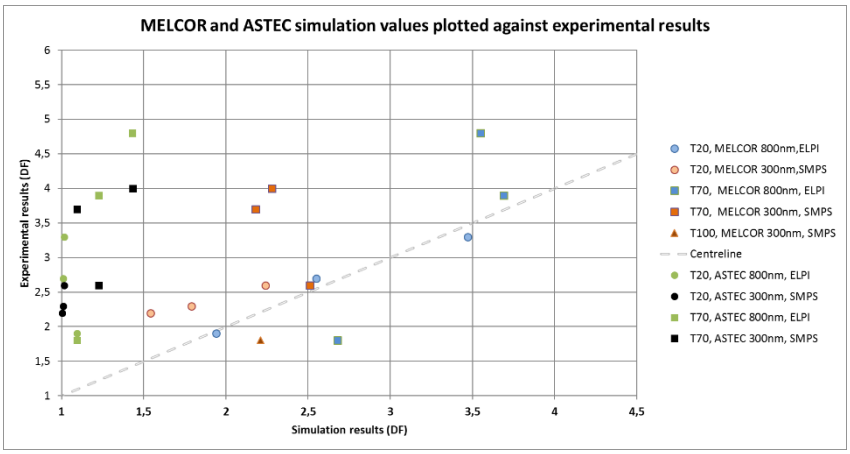

Figure 5. Comparison of simulated and experimental results. The T100, 300nm value for ASTEC is not included, as it is out of range.

ASTEC analyses were also performed for medium-scale experiments with soluble CsI with four different pool depths (30cm, 50cm, 70cm and 90cm) and three different inlet flow rates for N2 (26.9 l/min, 14.1 l/min and 7.7 l/min). The DF values produced by ASTEC were in a good agreement with the experimental results (Figure 6.) Both in the experiment and in the analyses, DF increases with decreasing N2 inlet flow rate and with increasing pool depth. Aerosol balances were also analysed, and it was noticed that the amount of aerosols accumulated in the facility gas phase was notable with lower inlet flow rates.

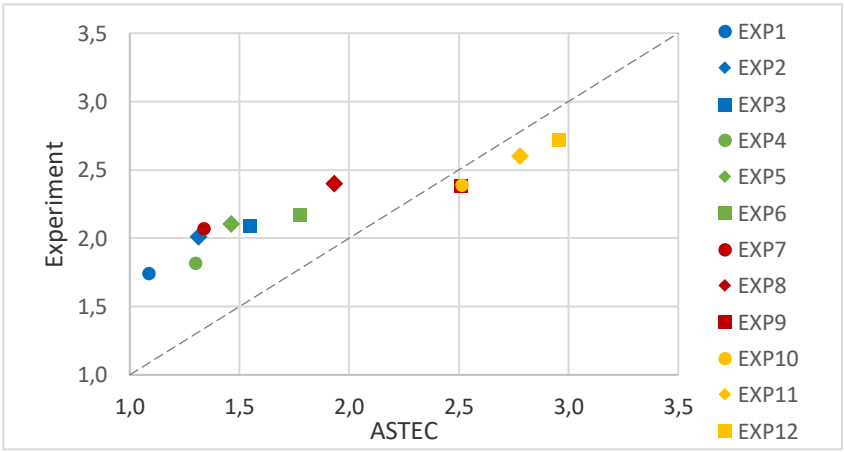

Figure 6. Comparison of ASTEC results to the experimental values in the case of non-soluble CsI. Same colour indicates the same pool depth that increases when proceeding to the next phase. Inlet flowrates decrease when proceeding to the next phase for a pool depth.

Passive Containmnet Cooling System (PCCS)

Modelling practices that can be used in safety analyses of reactors equipped with a PCCS were developed modelling the LUT PCC-10 experiment including aerosol injection to the experimental facility (Strandberg, 2019). The experiment was conducted at four different stages, with cooling and ventilation in between and therefore, the MELCOR analysis was split into four separate calculations. The results of the first stage overestimated the pressure and the cooling ability of the system as illustrated in Figure 7. As the facility heated up in the following phases, the analytical results improved and showed even lower pressures than in the experiments. The MELCOR results also indicated that the PCCS is able to capture aerosols, but further experiments as well as analyses are needed to verify how effective it is.

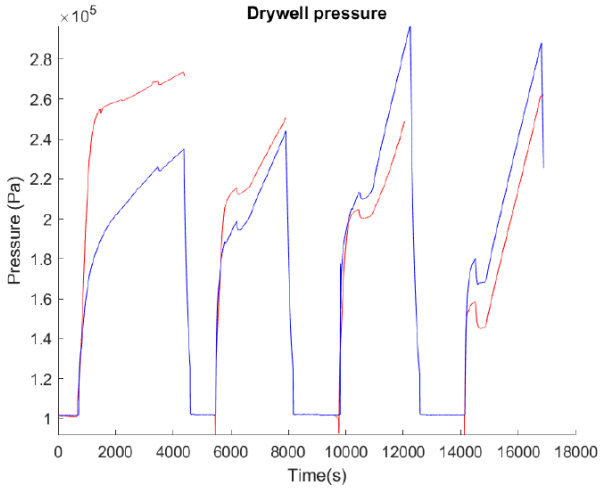

Figure 7. Comparison of the drywell pressure, MELCOR resuts in red and experimental results in blue.

Environmental consequences

There are two in-house models at VTT available to assess the environmental consequences from atmospheric releases for emergency preparedness purposes and level 3 PSA. ARANO is based a short and medium range dispersion model to handle a single or large number of weather conditions. In ARANO weather remains the same until the plume exits the computation area, but in VALMA weather conditions can change during dispersion. VALMA is especially a long-range dispersion and dose assessment code purposed originally to serve as an emergency preparedness tool but was extended later to enable calculation of a large number of weather conditions. ARANO can use weather data only from the release point but VALMA is able to use many kinds of weather data.

VALMA was further developed (Ilvonen & Rossi, 2017) by implementing there the ingestion dose pathways (green vegetables, grain, root vegetables, cow milk and cow meat) based on coefficients acquired from the AGRID nutrition dose model. Also the calculation of acute and late health effects of radiation doses was implemented in VALMA incorporating the fortran-coded functions returning the probabilities of certain health effects when the corresponding radiation dose is given (Ilvonen & Rossi, 2018).

After previous years' developments, the validity of VALMA-calculated doses at long distances was evaluated (Ilvonen & Rossi, 2019) comparing them not only to ARANO but also to MACCS, that is a widely validated code developed by Sandia National Laboratories. MACCS was developed as a general-purpose tool applicable to diverse reactor and non-reactor facilities.

The calculated cases dealt with offsite doses without countermeasures in a single weather condition as well as with the probabilistic approach employing annual weather data. Calculation results indicate significant differences in some single atmospheric dispersion cases, but differences are reduced if annual weather is used and fractile (percentile) values are presented as in Figure 8. Then ARANO typically predicts smaller dose values than MACCS. Also comparable dose estimates of VALMA predict smaller dose values than MACCS. The results may indicate that MACCS, a code with long history, was coded with some conservatism in mind.

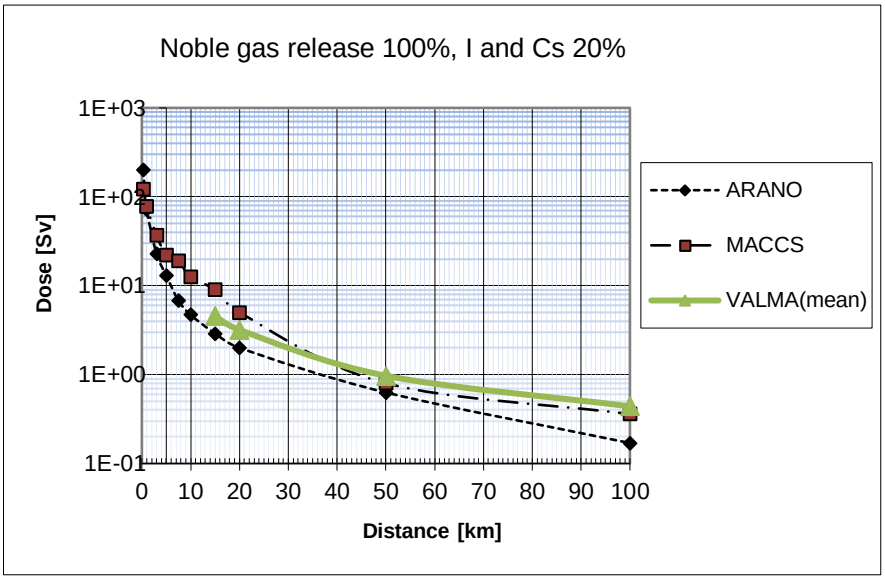

Figure 8. The dose of 95% fractile as a function of distance from the power plant. Integration time is one year for external radiation from the ground.

References

Bentaib, A., Chaumeix, N., Grosseuvres, R., Bleyer, A., Gastaldo, L., Maas, L., Jallais, S., Vyazmina, E., Kudriakov, S., Studer, E., Dehbi, A., Halouane, Y., Schramm, B., Taivassalo, V., Frankova, M., Kotsuba, O., Holler, T., Kljenak, I., Maruyama, Y., Nuri, T., Sato, M., Murgatroyd, J., Povilaitis, M., 2018. ETSON-MITHYGENE benchmark on simulations of upward flame propagation experiment in the ENACCEF2 experimental facility. 12th International Topical Meeting on Nuclear Reactor Thermal-Hydraulics, Operation and Safety (NUTHOS-12). Qingdao, China, October 14-18, 2018.

Ilvonen, M. & Rossi, J. 2017. VALMA extension with ingestion doses assessment. Espoo: VTT. VTT Research Report VTT-R-00695-17. 42 p. + app. 42 p.

Ilvonen, M. & Rossi, J. 2018. Radiological health effects in models ARANO and VALMA. VTT Research Report VTT-R-00885-18. 52 p.

Ilvonen, M. & Rossi, J. 2019. Comparison of MACCS, ARANO and VALMA. VTT Research Report VTT-R-00136-19. 18 p. + app. 9 p.

Korpinen, A., Strandberg, M., Sevón, T., Kärkelä, T. & Hokkinen, J. 2019. Retention of fission products in a containment pool - Parts A and B. VTT Research Report VTT-R-00152-19. 43 p. + app. 12 p.

Nieminen, A. 2018. Analysis of WH-24 experiment with ASTEC. OECD/NEA THAI-5 PRG5 meeting. October 1–2, 2018, Frankfurt, Germany.

Sevón, T. 2015. A MELCOR model of Fukushima Daiichi Unit 1 accident. Annals of Nuclear Energy, Volume. 85, p. 1–11.

Sevón, T. 2016. Fukushima Unit 2 Accident Modeling with MELCOR, Version 2. Espoo: VTT. VTT Research Report VTT-R-00829-16. 49 p.

Sevón, T. 2017a. Fukushima Unit 3 Accident Modeling with MELCOR, Version 2. Espoo: VTT. VTT Research Report VTT-R-00461-17. 50 p.

Sevón, T. 2017b. Fukushima Unit 1 Accident Modeling with MELCOR, Version 3. VTT Research Report VTT-R-04046-17. 43 p.

Strandberg, M. 2016. Ex-Vessel Steam Explosion Analysis with MC3D. Master's Thesis. 68 p. + app. 15 p.

Strandberg, M. 2017. Ex-vessel steam explosion with non-central break location. VTT Research Report VTT-R-05270-17. 12 p.

Strandberg, M.. 2019. Simulating passive containment cooling with MELCOR. VTT Research Report VTT-R-00146-19. 14 p.

Strandberg, M., Nieminen, A., Sevón, T., Hokkinen, J. & Kärkelä, T. 2018. Retention of fission products in a containment pool. VTT Research Report VTT-R-00974-18. 26 p. + app. 12 p.

Taivassalo, V. & Takasuo, E. 2017. Predicting debris bed behaviour in post-dryout conditions. Espoo: VTT. VTT Research Report VTT-R-00762-17. 28 p.

Taivassalo, V. 2018. Comparison of friction models for debris beds in post-dryout conditions. VTT Research Report VTT-R-01003-18. 63 p.

Taivassalo, V. 2019. Comparison of simulations for debris bed behaviour in post-dryout conditions. VTT Research Report VTT-R-00223-19. 47 p.

Taivassalo, V & Strandberg, M. 2019. Blind simulation of a hydrogen deflagration test in the two-vessel THAI+ facility. VTT Research Report VTT-R-00181-19. 59 p.

Takasuo, E. 2015. Coolability of porous core debris beds: Effects of bed geometry and multi-dimensional flooding. VTT Science 108. Teknologian tutkimuskeskus VTT Oy. Juvenes Print, Tampere 2015. ISBN 978-951-38-8344-7. 112 p. + app. 72 p.

Takasuo, E. 2016a. An experimental study of the coolability of debris beds with geometry variations, Annals of Nuclear Energy, Volume 92, p. 251-261.

Takasuo, E. 2016b. A summary of studies on debris bed coolability and multidimensional flooding. . Espoo: VTT. VTT Research Report VTT-R-00432-16. 27 p.

Yakush, S. & Kudinov, P., 2014. A model for prediction of maximum post-dryout temperature in decay-heated debris bed. In 22nd International Conference on Nuclear Engineering. July 7-11, 2014, Prague, Czech Republic.

3.6 Chemistry and transport of fission products (CATFIS)

Teemu Kärkelä[1], Mélany Gouëllo[1], Jouni Hokkinen[1], Karri Penttilä[1], Tommi Kekki[1], Petri Kotiluoto[1]

[1]VTT Technical Research Centre of Finland Ltd
P.O. Box 1000, FI-02044 Espoo

Abstract

The aim in the CATFIS project during 2015-2018 was to investigate the transport and chemistry of gaseous and particulate fission products in severe accident conditions. The main focus was on the behaviour of iodine and ruthenium which are highly radiotoxic and the mitigation of their possible source term is of utmost importance. It was observed that the fission product deposits on the reactor coolant system surfaces act as an important source of gaseous iodine, which can enhance the iodine source term. In air ingress conditions, the oxidizing air radiolysis products had a significant impact on the formation of gaseous ruthenium, which was observed to exist even at the low temperatures of containment building. Similarly, airborne CsI reacted with ruthenium oxides and increased the gaseous ruthenium fraction. The understanding on fission products retention in the water pools of containment due to pool scrubbing was improved. The phenomenon was studied with experiments and simulations. The follow-up of OECD/NEA STEM-2 and BIP-3 projects was carried out.

Introduction

In Fukushima Daiichi nuclear plant cooling of the reactor cores at units 1, 2 and 3 was lost due station black out. Since the cooling could not be restored in time, fuel damage took place in all three reactors and fission products were partly released from the core. As expected in a such severe accident, the highest contribution to the source term to the environment was from iodine isotopes. In case of the Chernobyl accident, a high release of fission products to the environment took place and fission products (FPs) were spread e.g. across the continent of Europe. In this accident, a fall-out of radioactive FPs containing also ruthenium was detected as far away as in Finland [Pöllänen, 1997].

Traditionally, it has been assumed that in a severe accident most iodine would be released from the fuel. Release to the containment would take place mostly as aerosol particles with gaseous fraction of about 5%. Concerning studies on iodine chemistry in the primary circuit, it is typically assumed that caesium iodide is the main iodine compound formed in the reactor coolant system. This assumption leads to a low release of gaseous iodine into the containment, because the current severe accident (SA) integral codes do not take into consideration the effect of FP deposits

chemical reactions on the primary circuit surfaces. Also, the previous studies have mainly focused on the reactions taking place in the gas phase [Gouëllo, 2013; Grégoire, 2012]. However, the importance of surface reactions as a source of volatile iodine is even increased at the late phase of accident when the thermalhydraulic conditions of the circuit are changing.

Along with iodine, low-volatile ruthenium is released from the fuel in oxidizing conditions. The most important volatile forms of ruthenium are RuO_3 and RuO_4. Currently, the fraction of ruthenium which can be transported to the containment atmosphere in gaseous form is not well-known. VTT´s previous studies [Kärkelä, 2014] indicated that the gaseous fraction can be significantly higher than what is expected based on thermodynamic equilibrium calculations. In general, the experimental work on international level has focused on pure air or air-steam atmospheres. The effect of oxidizing air radiolysis products and airborne aerosols on the chemistry of ruthenium and on the formation of gaseous Ru compounds has not been studied in detail. Nevertheless, most ruthenium in a severe accident would be expected to transport mainly as RuO_2 aerosol e.g. as a consequence of a reactive condensation of RuO_3 at ca. 1000 K.

Pool scrubbing is an important phenomenon in mitigating the source-term to the environment by retention of fission products passing through water pools of containment building. The majority of the experimental studies related to pool scrubbing have been conducted in 1980s and 1990s in order to establish suitable models for predicting the pool decontamination efficiency under reactor-typical conditions. Results from past research on pool scrubbing showed that both experimental data on fission products retention in water pools as well as related model predictions were affected by large uncertainty bands, which make application to reactor cases questionable. Particularly, the retention of fission products in pools at high temperatures and high gas flow rates through the pool are not well-understood.

The follow-up of OECD/NEA STEM-2 (Source Term Evaluation and Mitigation Issues) and OECD/NEA BIP-3 (Behaviour of Iodine) projects, which both began in January 2016, is being conducted. The four-year STEM-2 project is focused on the transport of ruthenium in the primary circuit conditions and on the reactions of particulate iodine on the painted and metal containment surfaces. The three-year BIP-3 project is focused on the behaviour of gaseous inorganic and organic iodine on the painted containment surfaces, especially the adsorption and desorption phenomena.

Primary circuit chemistry of iodine

After fission products have been released from the overheated and molten fuel, they are transported through the reactor coolant system and FPs will reach areas at lower temperature. As a consequence, vapour condensation and particle nucleation processes takes place in the gas flow. If vapour condensation takes place close to the surfaces of primary circuit, a layer of condensate can be formed on it. Particles in the gas flow may also deposit on the circuit surfaces together with control rod and

structural materials. The study on the release of gaseous iodine from precursor mixtures simulating deposits in primary circuit conditions have been performed with EXSI-PC facility [Kärkelä, 2009; Kalilainen, 2011] and the results of years 2017-2018 have been summarized in [Gouëllo, 2017; Gouëllo, 2018]. The set-up of the experimental EXSI-PC facility used for experiments is presented in Figure 1. Inactive materials have been used to simulate fission products. The precursor materials were CsI and MoO_3 and they were placed into an alumina crucible. The choice of the crucible material, non-representative of primary circuit surface, was selected because the purpose of the following experiments is to study reaction between the precursor materials at the surface of the crucible and not with the surfaces of the crucible. Since it was previously shown that the CsI precursor reacts with iron oxide layer on the stainless steel crucible surface [Kalilainen, 2011], it was preferred to work with an alumina crucible.

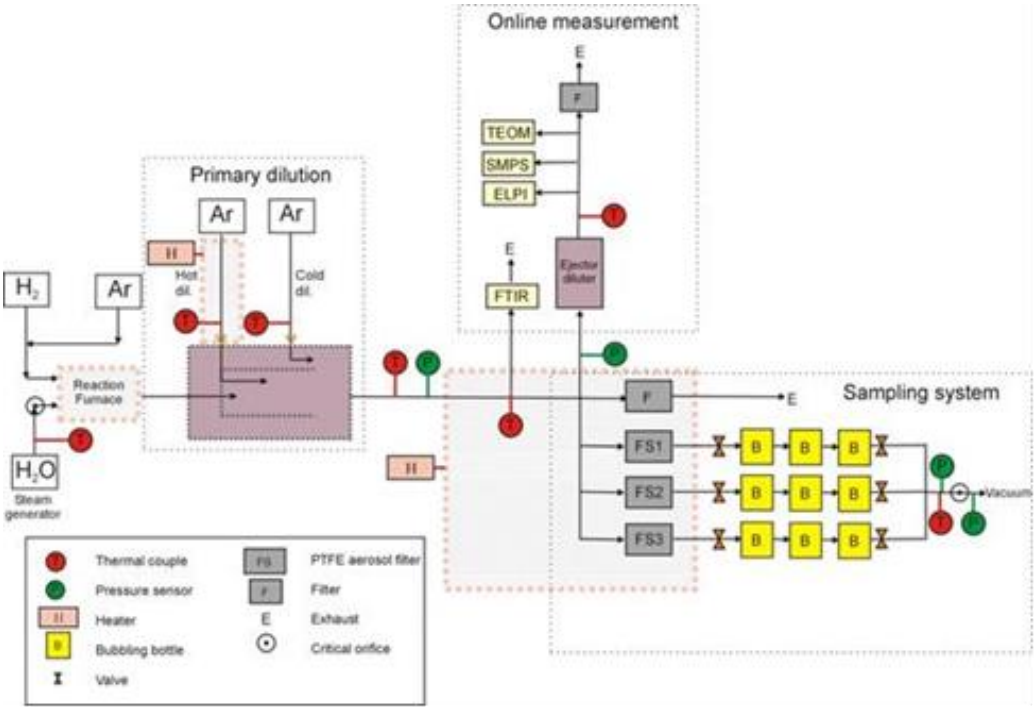

Figure 1. Schematics of the experimental EXSI-PC facility.

The evaporation crucible containing the precursor material(s) is placed in a tube inside the reaction furnace. The furnace tube used in the experiments was made of stainless steel (AISI 304), which was pre-oxidized before the experiment. The furnace is heated to 700 °C. The carrier gas is then fed into the heated furnace, where the source materials react with each other, with gas and with the surface of the crucible. The oxygen pressure in the gas phase above the crucible is monitored with

a MicroPoas probe (GENAIR). Reaction products are then transported with the gas flow into the primary diluter where the sample mixture is diluted and cooled down to 120 °C. The sampling furnace contains three sampling lines, each is equipped with a polytetrafluroethylene (PTFE) membrane filter (hydrophobic, poral grade 5.0 µm, 47 mm, Mitex®) and two glass scrubbers assembled in series (0.1 M NaOH and 0.02 M $Na_2S_2O_3$ water solution. Additional toluene trap was used in some experiments. The elemental composition of both samples was analysed with Inductively Coupled Plasma Mass Spectrometer (ICP-MS). A list of the recently conducted experiments is presented in Table 1. Experiments included three or four different gaseous atmosphere conditions, with different fractions of steam, argon, hydrogen and air, shown in Table 2.

Table 1. Experiments conducted on primary circuit chemistry of iodine during the past two years.

Exp.	Precursor	Precursor mass [g]	Initial Mo/Cs molar ratio	Carrier gas composition*
Mo-1	CsI	2.497	5.08	A
	MoO_3	7.019		
Mo-2	CsI	2.501	5.06	D
	MoO_3	7.01		
Mo-3	CsI	2.502	1.61	A
	MoO_3	2.234		
Mo-4	CsI	2.501	1.61	D
	MoO_3	2.235		
Mo-5	CsI	2.51	3.06	A
	MoO_3	4.256		
Mo-6	CsI	2.504	3.06	D
	MoO_3	4.247		
Mo-7	CsI	1.441	5.05	A
	MoO_3	4.027		
Mo-1bis	CsI	2.5	5.06	A
	MoO_3	7.011		
Mo-2bis	CsI	2.5	5.08	D
	MoO_3	7.025		

* The composition of atmosphere is explained in Table 2.

Table 2. Volume percentage of gases fed to the reaction furnace.

		Atmosphere composition			
		A	B	C	D
Gas vol-%	Argon	86.7	83.9	76.1	86.7
	Steam	13.3	13.5	13.4	0
	Hydrogen	0	2.6	10.5	0
	Air	0	0	0	13.3

The work performed during the past two years has been particularly focused on determining how significant effect the presence of molybdenum on the primary circuit surfaces can have on the physical and chemical form and on the transport of iodine and caesium, under different gas composition.

The addition of molybdenum to caesium iodide resulted in a higher gaseous iodine fraction in an atmosphere composed of argon and air (Figure 2). For all the studied parameters (initial Mo/Cs ratio and initial precursor mass), the gaseous iodine release was higher when the oxygen partial pressure was higher (i.e. for Ar/Air atmosphere). The formation of caesium molybdate was identified in the crucible after the experiments, confirming that the reaction between caesium and molybdenum is the reason for the observed formation of gaseous iodine. Gaseous molecular iodine (I_2) was clearly identified as the main gaseous iodine species formed during the reaction (> 68 %). On the other hand, the addition of caesium hydroxide to caesium iodide resulted in a notable decrease in the gaseous iodine fraction in both argon/steam and argon/air atmospheres.

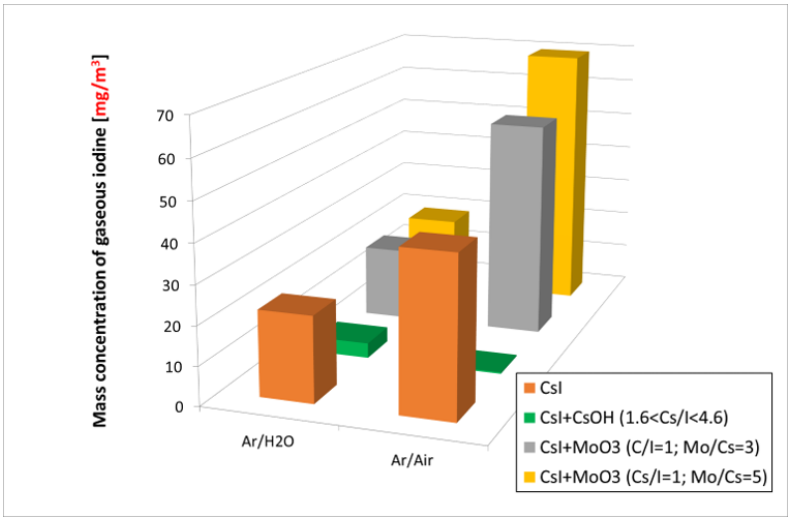

Figure 2. Gaseous iodine transport as a function of the precursor and carrier gas compositions. The experiments were performed at 650 °C [Gouëllo 2018].

In the Mo-7 experiment, which was performed with a smaller initial total mass of precursors, interesting observations were made. All recorded values (Raman spectra, particle number size distribution, mass concentration, Mo/Cs and Cs/I ratios on filters) were similar to the ones performed with a higher amount of precursors, except the amount of released gaseous iodine, which was higher by a factor of 1.7 (Figure 3).

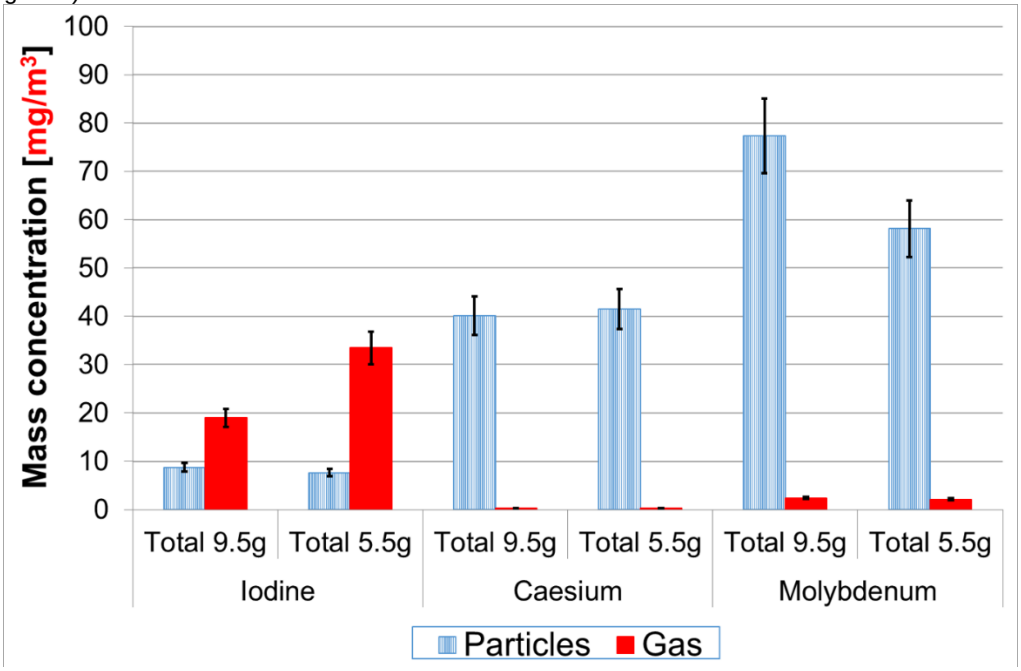

Figure 3. Transported iodine, caesium and molybdenum mass concentrations (particles and gas), vaporised at 700 °C in an atmosphere composed of Ar/H_2O. Transport results were determined from the collected particles on filter and trapped gases in bubblers with ICP-MS after the vaporisation of $CsI+MoO_3$ (Mo/Cs~5; Cs/I~1) precursor mixtures with total masses of 9.5 g (Mo-1bis) and 5.5 g (Mo-7) [Gouëllo 2018].

Primary circuit chemistry of ruthenium

Most of the international experiments on the transport of ruthenium through a reactor coolant system have been conducted in a flow of pure air and/or steam with Ru oxides [Kärkelä, 2014]. The focus in the CATFIS project was to find out the effect of other components, such as aerosols and air radiolysis products, on the transport of gaseous and particulate ruthenium species through a model RCS in air ingress conditions. Thus this study gave a possibility to study the speciation of ruthenium in more realistic conditions. The study was performed in collaboration with Chalmers

University of Technology (Sweden) within SAFIR2014/SAFIR2018 and Nordic Research on Nuclear Safety NKS-R (ATR activity) programs. This collaboration received also travel assistance from NUGENIA for researcher mobility between the organisations. The results of this collaboration are summarized in scientific publications [Kajan, 2017] and [Kärkelä, 2017].

The work was conducted with “VTT´s Ru transport facility” simulating a primary circuit. The configuration of the facility for the experiments can be seen in Figure 4. The main component of the facility was the horizontal, tubular flow furnace (Entech, ETF20/18-II-L), which was used to heat the anhydrous RuO_2 powder (99.95 %, Alfa Aesar). The furnace was 110 cm long and it had two heating sections, each 40 cm long. These zones were separated by a 38 mm layer of insulation. At both ends of the furnace, there was 131 mm of thermal insulation. The furnace tube was made of high purity alumina (Al_2O_3, 99.7 %) and its inner diameter was 22 mm. The alumina crucible (length 20 cm) with the RuO_2 powder (mass. 1 or 2 g depending on the temperature used in the experiment) was placed in the beginning of the second heated zone of the furnace. As a new feature in these experiments, inside the furnace tube was inserted a second alumina tube (Al_2O_3, 99.7 %, outer diameter 6 mm with a wall thickness of 1 mm), which outlet was located directly after the crucible. The RuO_2 powder was heated to 1300 K, 1500 K or 1700 K in an oxidizing flow in order to produce gaseous ruthenium oxides.

The total flow rate through the facility was 5.0 l/min (NTP; NTP conditions 0 °C, 101325 Pa, measured with Thermal Mass Flowmeter TSI 3063, TSI Incorp.). Half of the total flow was directed through the inner furnace tube and the rest of the flow was passing through the furnace tube. The pressure inside the facility ranged from 102 to 104 kPa. The air flow (2.5 l/min, NTP) directed to the furnace tube was fed through an atomizer (TSI 3076). The air flow transported the water droplets (Milli-Q, ultrapure water, resistivity of 18.2 MΩ·cm at 25 °C) produced by atomizer via the heated line (120 °C) into the inlet of the furnace. Water evaporated when the droplets were heated and thus it led to an increase in the steam concentration within the furnace. A flow of N_2O, NO_2 or HNO_3 gases (2.5 l/min, NTP) was fed through the inner furnace tube. NO_2 was diluted with N_2 to obtain a similar concentration of precursor as in case of N_2O. As HNO_3 was fed with an additional atomizer (located then before the inlet of inner furnace tube, not presented in Figure 4), a carrier gas of nitrogen was used to transport HNO_3 droplets (solution of HNO_3 and Milli-Q water) via the heated line (120 °C) into the inlet of the inner furnace tube. CsI additive was also fed with an atomizer, but the inner furnace tube was removed in those experiments.

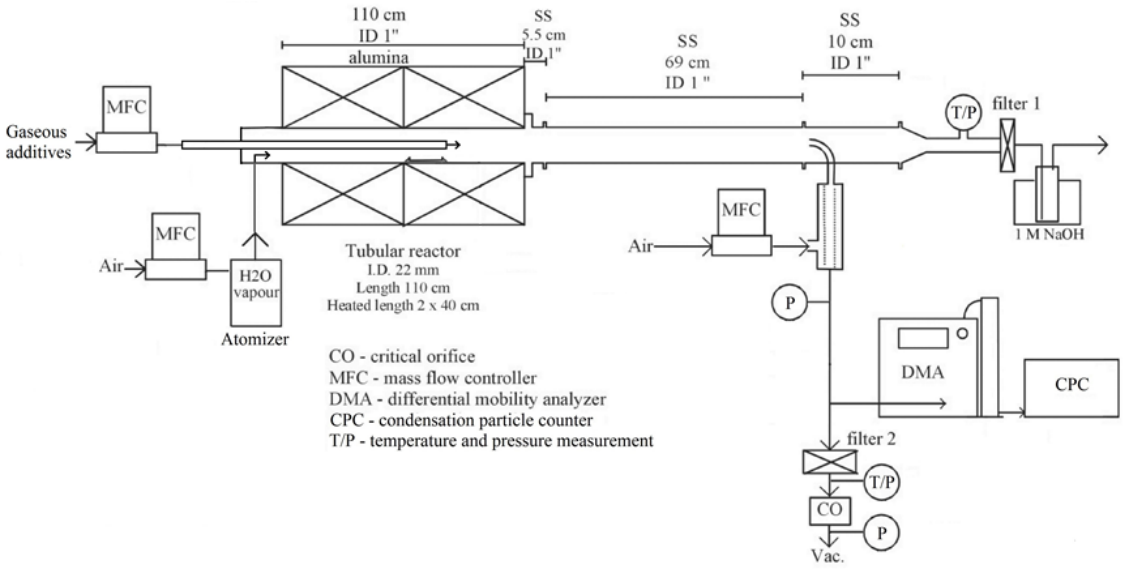

Figure 4. Schematics of the experimental facility for ruthenium transport studies.

After the vaporization of Ru and the following reactions within the gaseous atmosphere, the gaseous and particulate reaction products were trapped in a NaOH solution and collected on planer filters, respectively (see Figure 5). The diameter, number concentration and the number size distribution of particles was analysed online with a combination of DMA and CPC. The experimental matrix is presented in Table 3.

(a) (b)

Figure 5. (a) Gaseous ruthenium trapped in two sequential bubblers with NaOH solution. (b) A SEM micrograph of the typical, crystalline, needle-shaped form of RuO_2 particles.

Table 3. Matrix of Ru transport experiments (air atmosphere; 1300 to 1700 K).

Exp	T [K]	Precursor	Gas phase	Additive precursor conc.	Humidity
1	1300	RuO_2	Air	-	dry
2	1500	RuO_2	Air	-	dry
3	1700	RuO_2	Air	-	dry
4	1300	RuO_2	Air	-	humid
5	1500	RuO_2	Air	-	humid
6	1700	RuO_2	Air	-	humid
7	1300	RuO_2	Air+NO_2	50 ppmV NO_2	humid
8	1500	RuO_2	Air+NO_2	50 ppmV NO_2	humid
9	1700	RuO_2	Air+NO_2	50 ppmV NO_2	humid
10	1300	RuO_2	Air+N_2O	50 ppmV N_2O	humid
11	1500	RuO_2	Air+N_2O	50 ppmV N_2O	humid
12	1700	RuO_2	Air+N_2O	50 ppmV N_2O	humid
13	1300	RuO_2	Air+HNO_3	5 ppmV HNO_3	humid
14	1500	RuO_2	Air+HNO_3	5 ppmV HNO_3	humid
15	1700	RuO_2	Air+HNO_3	5 ppmV HNO_3	humid
16	1300	RuO_2	Air+CsI	4 wt.% of CsI solution	humid
17	1500	RuO_2	Air+CsI	4 wt.% of CsI solution	humid
18	1700	RuO_2	Air+CsI	4 wt.% of CsI solution	humid

Experiments were conducted at 1300 to 1700 K with air as the carrier gas which was mixed with steam, air radiolysis products (NO_2, N_2O, HNO_3) or CsI particles. The quantification of ruthenium transport showed significant impact of the experimental conditions on both the absolute amount as well as on the partitioning of the transported ruthenium between gaseous and aerosol compounds (see Figure 6). In general, the increase in temperature resulted in higher release of ruthenium from the precursor and also to higher transport of ruthenium downstream the furnace. The gaseous fraction of transported ruthenium was significantly increased under all temperatures due to NO_2. At temperatures of 1300 and 1700 K the overall transport

of ruthenium was significantly increased when compared to the humid air atmosphere. The diameter of particles seemed to increase in the course of experiments, whereas the particle number concentration was low. It is suggested, that part of the formed gaseous Ru compounds was condensing on the surface of the existing particles and thus increased the particle diameter. Introduction of N_2O into the gas phase led to a decrease of gaseous ruthenium transport through the facility as well as to an increased fraction of ruthenium transported in form of aerosols. Nearly 100% increase in the total amount of transported ruthenium was detected at temperature of 1500 K when compared to the humid air atmosphere. An interesting observation was also done in the experiments with HNO_3 in the humid air flow. The transport of gaseous ruthenium increased at all studied temperatures. However, the overall transport of ruthenium was fairly similar than in humid air atmosphere. Thus, the partitioning of ruthenium to gaseous and aerosol compounds was influenced by the fed HNO_3. Likely, the concentration of HNO_3 was too low in order to observe a higher increase in ruthenium transport. The feed of CsI into the flow of ruthenium oxides had a significant effect on the thermodynamic equilibrium of Ru species. The transport of gaseous ruthenium increased from 0.2 % up to 16 % and 6 % at 1500 K and 1700 K, respectively, whereas the aerosol transport of ruthenium decreased significantly. This is the highest amount of Ru ever observed in gaseous form in the experiments with this facility. At 1300 K the transport of ruthenium was rather similar to that in an air atmosphere, as it has been reported previously. At all studied conditions (Table 3), most of the released ruthenium was deposited inside the facility.

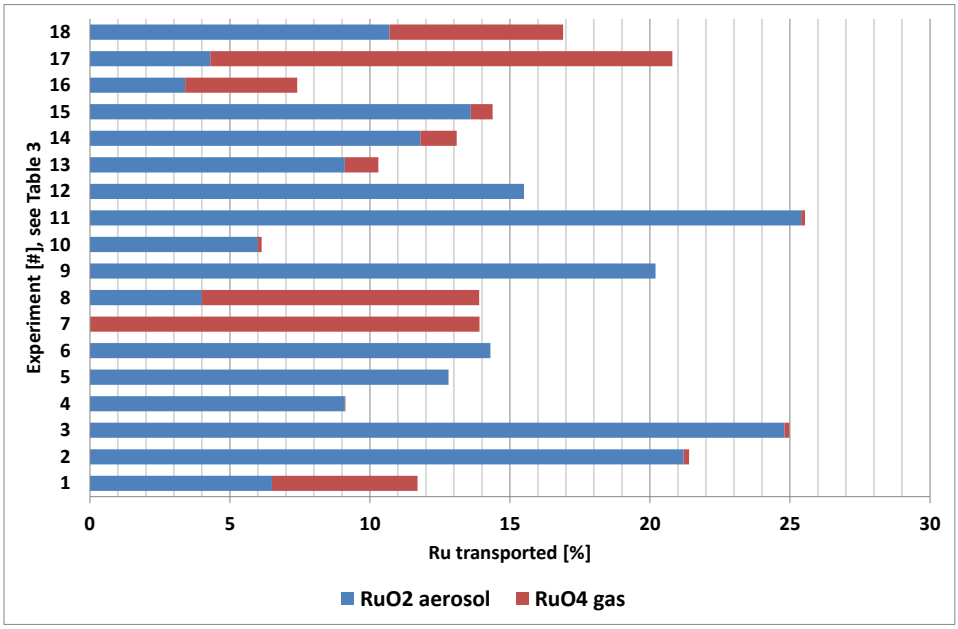

Figure 6. Ruthenium transport as aerosol and gaseous compounds through the experimental facility. Note the numbering of experiments on y-axis (see Table 3).

The effect of air radiolysis product NO_2 on ruthenium transport is also a research topic in the ongoing international OECD/NEA STEM-2 programme (see below). The STEM / START experimental facility is very similar to the facility of VTT, shown in Figure 4. CATFIS project was asked to perform complementary experiments for the STEM-2 programme. As part of experiments, the increased transport of gaseous RuO_4 was studied in more detail. The evolution of RuO_4 transport rate during the experiment was obtained with the UV-Vis analysis method, see Figure 7.

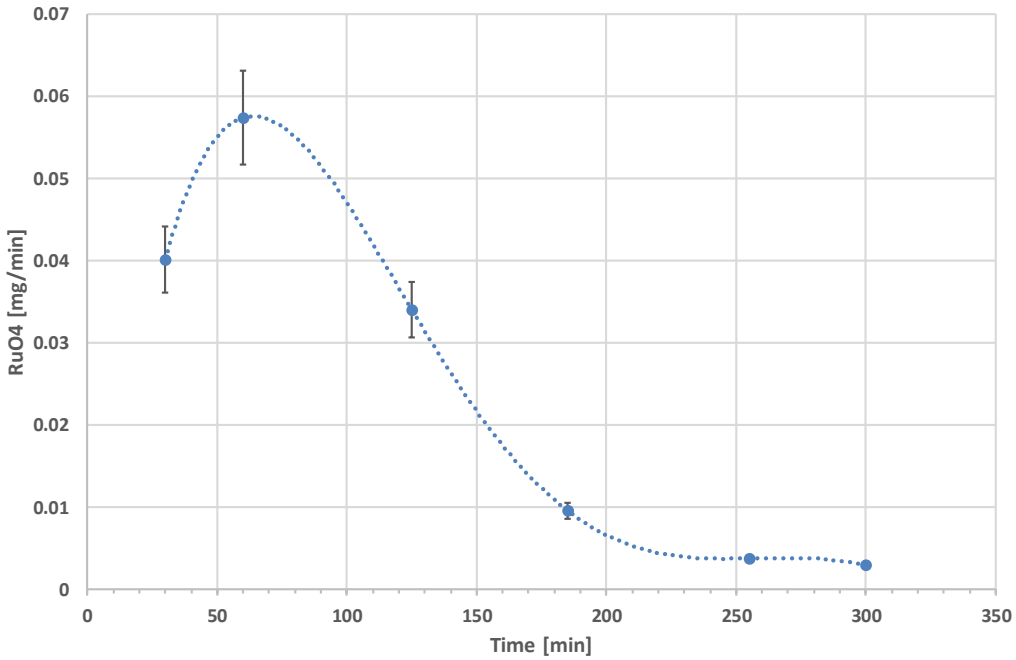

Figure 7. Ruthenium transport as gaseous RuO_4 through the experimental facility. RuO_2 precursor in an evaporation crucible was oxidized at 1500 K in air with 50 ppmV NO_2 gas. The air flow (in total 2.2 l/min, lower than in the previous experiments) was saturated with water at 298 K. The formation of RuO_4 was increased and the transport maximum was ca. 60 minutes after the beginning of experiment, when the revaporisation from the RuO_2 surface deposits in a temperature gradient tube was also the highest. Afterwards, most of the RuO_2 precursor was already vaporised and the main source of RuO_4 were the surface deposits. In total 8% of the released ruthenium from the evaporation crucible transported as gaseous RuO_4 through the experimental facility to the area of sampling at 298 K.

Pool scrubbing

The topic of pool scrubbing is of major relevance both in Boiling Water Reactors (BWR) and Pressurized Water Reactors (PWR) as it plays a vital role in mitigating the source-term to the environment by retention of fission products passing through water pools. The aim in the CATFIS project was to investigate experimentally and analytically the retention of fission products (gas and aerosol) in the pools of NPP containment in case of a severe accident. At this stage, the work was focused on the suppression pool conditions and on the retention of soluble CsI, non-soluble TiO_2 aerosols and gaseous CH_3I [Kärkelä, 2019]. Two experimental setups simulating small and medium-scale pools (both in laboratory-scale) were built. Decontamination factors for particle and gaseous compounds removal by the pool were derived. The aerosol experiments were simulated with severe accident analysis codes ASTEC and MELCOR by the CASA project and the obtained decontamination factors were compared with the experimental results.

In the medium-scale facility, the pool was composed of two identical, cylindrical tubes with an inner diameter of 0.2 m and a height of 1.1 m. When both parts are combined, the maximum pool height is 2.2 m. The material of tubes was stainless steel. Thus, for example, the temperature and pressure of pool can be varied in a wide range. The “downcomer” tube was vertical going through the pool surface towards the pool bottom and the nozzle was located 0.2 m above the pool bottom. The nozzle inner diameter was 4.4 mm. The medium-scale facility was equipped with several online measurement devices, such as Scanning Mobility Particle Sizer (SMPS) and Electrical Low Pressure Impactor (ELPI) for the aerosol number size distribution measurements, Tapered Element Oscillating Microbalance (TEOM) for the aerosol mass concentration measurement and Fourier Transform InfraRed (FTIR) for the identification and concentration measurement of gaseous compounds.

The retention of CsI aerosol in a water pool with a height of 0.1, 0.3, 0.5 and 0.7 m from the nozzle to the pool surface was examined at 20 °C. The geometric mean of the fed CsI aerosol mass size distribution was 0.2 µm with a geometric standard deviation of 1.85. The gas flow rate to the pool ranged from 7.7, 14.1 to 26.9 l/min (NTP). The preliminary DF results of these experiments are presented as a function of flow rate in Figure 8. The trends are visible, DF seemed to decrease due to increasing flow rate through the pool. On the other hand, the deeper pool was resulting in a higher DF. This study has produced basic information on the pool performance at moderate conditions. The work will be continued in the coming years and a deeper understanding on various phenomena effecting on the pool scrubbing, as well as on the uncertainties in the measurements and analysis, will be gained.

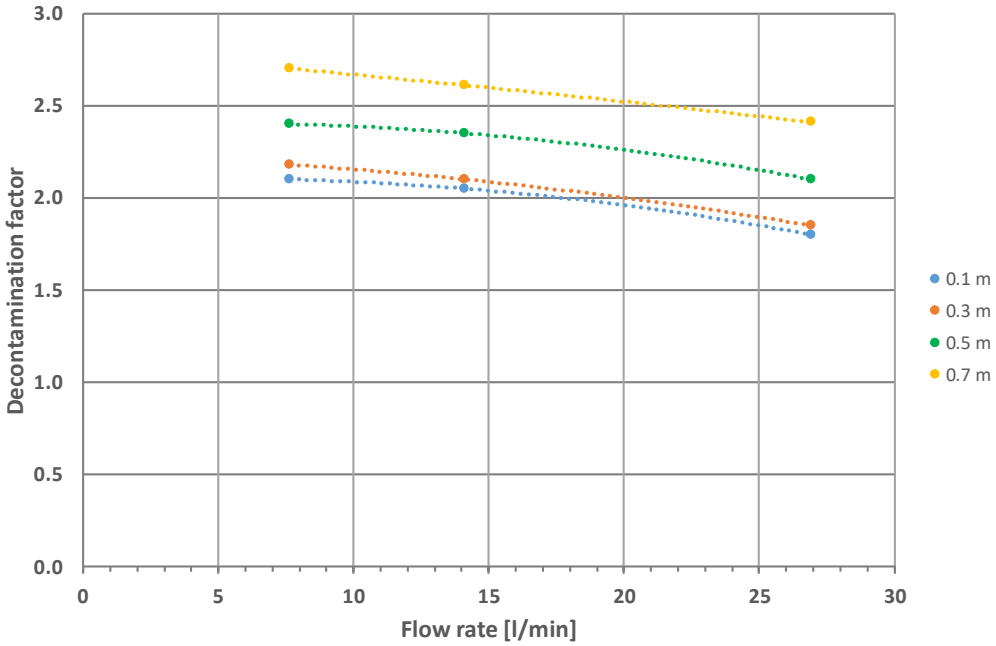

Figure 8. Preliminary decontamination factor results for CsI aerosol on mass basis as a function of flow rate through the pool with various pool heights from the nozzle to the pool surface. The nozzle was located 0.2 m above the pool bottom. The results are based on the measurement data without considering aerosol lossess on surfaces or aerosol re-entrainment from the pool.

The follow-up of OECD/NEA STEM-2 and BIP-3 projects

The follow-up of both OECD/NEA STEM-2 and BIP-3 projects [OECD, 2017] is performed as part of CATFIS. Both projects started in 2016 and the duration of STEM-2 is four years and BIP-3 three years. The experimental work is ongoing currently. The OECD/NEA STEM-2 project composes of two experimental main topics: ruthenium transport in primary circuit conditions (as described above) and behaviour of particulate iodine on containment surfaces. The OECD/NEA BIP-3 project focuses especially on the adsorption and desorption phenomena of gaseous inorganic and organic iodine on the painted containment surfaces. Both projects include analytical working groups to simulate the experiments with various computer codes by the participating countries/organisations and to discuss about a comprehensive analysis of the results obtained and extrapolation to the reactor case. CATFIS has presented the experimental results on ruthenium and iodine chemistry in the follow-up meetings of these projects.

Conclusions

The main focus in the CATFIS project is study the transport and chemistry of fission products in a severe accident. The emphasis is on the phenomena, which are poorly-known internationally or not considered in the current severe accident analysis codes due to the lack of information. In 2015-2018, the effect of FP deposits chemical reactions on the primary circuit surfaces to the release of gaseous iodine from the deposits was investigated. It seemed that molybdenum reacted with caesium iodide forming caesium-molybdate compound. As a result, iodine was released from the surface deposit as gas, especially in an atmosphere with high oxygen partial pressure. On the other hand, additional CsOH seemed to partially bind the formed gaseous iodine. As part of CATFIS the formation of air radiolysis products and their effect on the transport of FPs has been investigated. A significant increase in the fraction of gaseous RuO_4 was detected due to air radiolysis product NO_2. Additionally, CsI compound seemed to react with gaseous Ru oxides and thus a remarkable transport of gaseous ruthenium compound was observed. Recently, a study on the retention of fission products in the water pools of containment has been launched. The experimental facilities have been set-up and first decontamination factor results have been obtained. The work will be continued in the coming years.

The OECD/NEA STEM-2 and BIP-3 projects produce new data on the chemistry of iodine and ruthenium in severe accident conditions. Part of that experimental work will complement and verify the observations made in the CATFIS project and in the previous CHEMPC and TRAFI projects of the SAFIR2010 and SAFIR2014 programs.

The experimental results produced in the CATFIS project (2015-2018) will increase the knowledge on the behaviour of fission products during a severe accident. The experimental data can be used for PSA level 2 analysis of the existing nuclear power plants.

Acknowledgement

The financial support of VTT Technical Research Centre of Finland Ltd, The Finnish Research Programme on Nuclear Power Plant Safety (SAFIR2018), Nordic Nuclear Safety Research Programme (NKS-R) and NUclear GENeration II & III Association (NUGENIA) is acknowledged.

References

Gouëllo, M., Hokkinen, J. 2017. Experimental Study on the Behaviour of CsI on Primary Circuit Surfaces of a Nuclear Power Plant: Effects of Molybdenum on Iodine Transport at 700 °C, Research report VTT-R-04041-17.

Gouëllo, M., Hokkinen, J. 2018. Experimental Study on the Behaviour of CsI on Primary Circuit Surfaces of a Nuclear Power Plant: Effects of Molybdenum on Iodine Transport: part II, Research report VTT-R-04457-18.

Grégoire, A.-C., Mutelle, H., Experimental study of the [Mo, Cs, I, O, H] and [B, Cs, I, O, H] systems in the primary circuit of a PWR in conditions representative of a severe accident, In the proceedings of NENE2012 conference, Ljubljana, Slovenia (2012).

Kalilainen, J., Kärkelä, T., Rantanen, P., Forsman, J., Auvinen, A. & Tapper, U. 2011. Chapter ”Primary circuit chemistry of iodine”, SAFIR2010, The Finnish Research Programme on Nuclear Power Plant Safety 2007-2010, Final report, pp. 312-320.

Kajan, I., Kärkelä, T., Auvinen, A., Ekberg, C. 2017. Effect of nitrogen compounds on transport of ruthenium through the RCS, Journal of Radioanalytical and Nuclear Chemistry 311(3), 2097-2109.

Kärkelä, T., Auvinen, A. 2009. Experimental Study on Iodine Chemistry (EXSI) - Facility for Primary Circuit experiments. Espoo, Finland, Research report VTT-R-02791-09.

Kärkelä, T., Vér, N., Haste, T., Davidovich, N., Pyykönen, J. & Cantrel, L. 2014. Transport of ruthenium in primary circuit conditions during a severe NPP accident. Ann. Nucl. En. 74, 173-183.

Kärkelä, T., Kajan, I., Tapper, U., Auvinen, A., Ekberg, C. 2017. Ruthenium transport in a RCS with airborne CsI, Progress in Nuclear Energy 99, 38-48.

Kärkelä, T., Korpinen, A., et al. 2019. Retention of fission products in a containment pool - Parts A and B, Research report VTT-R-00152-19.

OECD: https://www.oecd-nea.org/jointproj/ , 2017.

Pöllänen, R., Valkama I. & Toivonen, H. 1997. Transport of radioactive particles from the Chernobyl accident. Atmospheric Environment 31(21), 3575-3590.

3.7 Experimental and numerical methods for external event assessment improving safety (ERNEST)

Ari Vepsä[1], Kim Calonius[1], Alexis Fedoroff[1], Ludovic Fülöp[1], Vilho Jussila[1], Arja Saarenheimo[1], Piritta Varis[1], Markku Tuomala[2]

[1]VTT Technical Research Centre of Finland Ltd
P.O. Box 1000, FI-02044 Espoo

[2]Consultant of VTT

Abstract

Aircraft impact is one of the external threats that nuclear power plant structures might undergo. WTC terrorist attacks showed that also deliberate crashes with large passenger aircrafts are possible. These impacts and their consequences can be analyzed with sophisticated computational tools. However, in order to be reliable, these tools must be validated against relevant experimental data.

The main purpose of ERNEST project has been to carry out selected medium scale impact tests with reinforced concrete slabs, to develop modelling tools used at VTT for analyzing this type of events and to validate these tools against experimental test data. The tests have been carried out with VTT's own testing apparatus.

Development of a concrete material model has been a major part of the modelling tool development. The material model has been implemented into Abaqus finite element code and it enables more realistic behavior of concrete under impact loading. The tools, including the material model, have been validated mainly against test data collected from tests carried out at VTT.

Introduction

Phenomena related to aircraft impact against reinforced concrete (RC) structures has been studied extensively at VTT for example within SAFIR2006, SAFIR2010, SAFIR2014 and SAFIR2018 programmes. An experimental testing platform has been built and over 120 medium scale tests with different types of RC structures carried out with it within different projects. The results have been utilized in development and validation of computational tools and models, an activity that has also been carried out at VTT for a long time. With validated tools, assessment of the severity of a real scale aircraft impact against, for example, a reactor building of a nuclear power plant, can be carried out with increased level of reliability. Correct modelling of the behaviour of concrete is of high importance in these assessments. This topic has been paid special attention during the last two project years of ERNEST.

In addition to impact testing and computational model validation, the first two project years included also modelling of impact loading by a wide body passenger

aircraft (Boeing 777-300), numerical studies on ageing of pre-stressed RC containment and earthquake source modelling to support NPP safety in Finland. These work packages have already been reported in an article by Vepsä et al (Vepsä et al., 2016), published in the SAFIR2018 interim report. Since these work packages were not continued during the last two project years, they are not covered here.

Impact testing

Experimental test data is needed for validation of computational models. The tests should yield relevant and reliable data. In addition, the tests yield interesting information about the phenomena that arise in an aircraft crash and how these phenomena are affected by different factors. VTT has an advantage that it owns an apparatus with which medium scale impact tests can be carried out (Kärnä et al., 2004). This enables tailoring the tests to be carried out for the particular needs of models and tools to be validated.

Altogether five impact tests were carried out within ERNEST projects. Two of these tests were carried out with semi-hard projectiles with the target response being combination of bending damage and shear punching damage. The three remaining tests were carried out with hard projectiles with the target response being punching failure.

The two combined bending and punching response tests were carried out with 250 mm thick square RC slabs with simple supporting in both directions with the span width being 2 metres. The reinforcement was made out of D10 mm B500B rebars in both directions and on both faces with spacing of 90 mm in one slab (E1) and 45 mm in the other (E2). Concrete cover was 25 mm and no shear reinforcement was used.

Concrete used to cast the slabs was subjected to static material testing. The unconfined compression strength was 78.7 MPa when tested with cubes (side dimension 150 mm) and 69.9 MPa when tested with cylinders (D150mm, h300mm). The splitting tensile strength was 3.70 MPa and Young's modulus 31.54 GPa.

The projectiles that were used in the combined bending and punching tests were made out of stainless steel pipes, typically used in process industry, with a cap welded at the front. Main information about the projectiles are compiled in Table 1. The projectile types and impact velocities were chosen so that test E1 would emphasize the bending response of the target while test E2 would stress the punching response.

Table 1. Main information about the projectiles used in tests E1 and E2.

Parameter	Test E1	Test E2
Projectile outer diameter [mm]	260	219.1
Projectile body wall thickness [mm]	5.0	6.35
Outer radius to wall thickness ratio [-]	26	17.3
Projectile material	Steel EN 1.4432	Steel EN 1.4432
Projectile mas [kg]	49.90	50.04
Impact velocity [m/s]	124.0	150.6

The tested slabs were instrumented with strain gauges glued on the reinforcement bars of the slab as well as on the front surface of the slabs and displacement sensors. In addition, support forces were measured on the four horizontal supports of slab-frame system. The impacts were also documented with high shutter speed video cameras.

The tested slabs were sawn into quartiles after the test. Vertical cross sections of the lower left quartiles are shown in Figure 1. The figure clearly demonstrates the difference in the damage caused for the slabs by the impacts. It can be seen that test E5 resulted in a shear cone, which is almost completely detached from the surrounding medium.

(a) (b)

Figure 1. Vertical cross sections of the tested slabs sawn into quartiles. (a) Test E1. (b) Test E2.

Strains measured with strain gauges glued on selected vertical reinforcement bars are shown in Figure 2. The strains look very similar the first 3 ms of the impact. After that, most of the gauges (or their wiring) break in test E2. Since this breaking occurs at quite low strains, it is reasonable to assume that this breaking is not due to bending damage. In test E1, the gauges 1 and 2, closest to the hit point, show large amounts of plastic deformations. In test E1, the strains measured with gauge 1 stay at relatively low level.

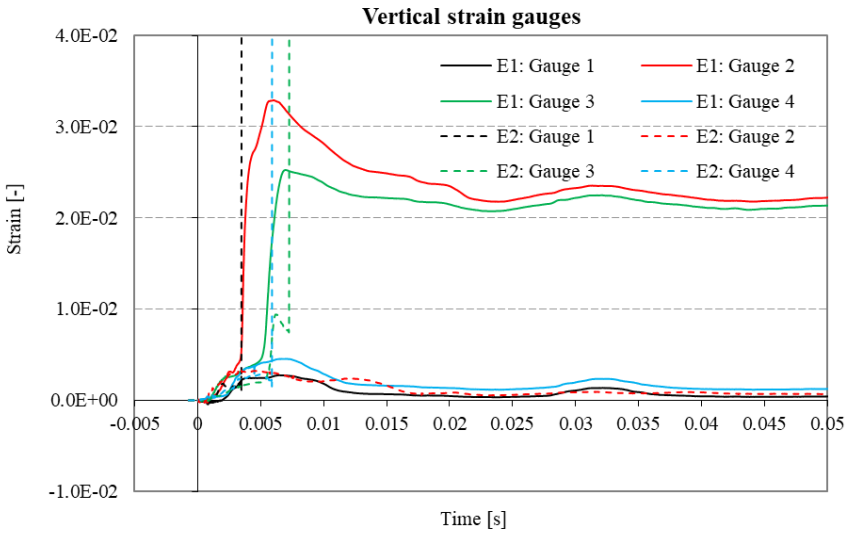

Figure 2. Strains measured with strain gauges on selected vertical reinforcement bars.

The other three tests were carried out with so-called hard projectiles that are much less deformable than the targets they impact against. The projectile type is shown in Figure 3. Together with the high-speed video footage, the aluminium pipe at the rear of the projectile was used to determine the velocity of the projectile after it has perforated the slab. The in-plane dimensions of the test were the same than in tests E1 and E2. The slab thickness was 300 mm in test E3 and 250 mm in tests E4 and E5.

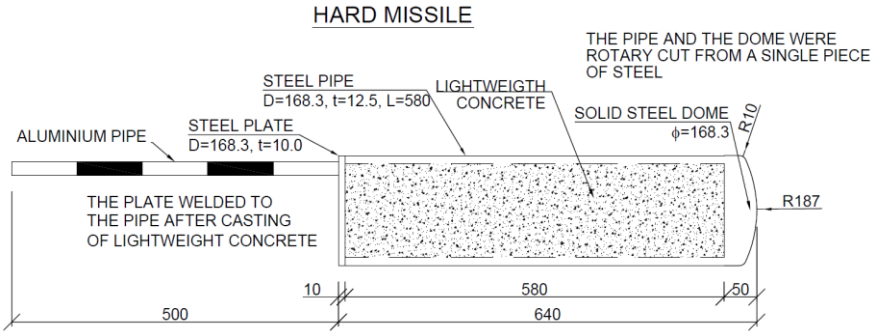

Figure 3. Hard projectile type used in tests E3 - E5.

In test E3, there was a 50 mm thick 1 m * 1 m sheet of expandable polystyrene (EPS) at the centre of the slab, dividing it into two 125 mm thick halves. The purpose was to study the punching resistance of this type of separated double-slab structure compared to a similar single slab with the same total thickness and reinforcement ratio.

The slabs E4 and E5 were reinforced only at the edges so that a ~1 * 1 m square area at the centre of the slab contained only concrete. The slabs were cast with concrete having maximum aggregate grain size of 8 mm (E4) and 32 mm (E5). Otherwise, the target was to keep the static mechanical properties of the slabs as similar as possible. The purpose of the tests was to study how the grain size of the concrete aggregates affects the punching resistance of slabs cast with otherwise similar concretes.

The realized input and output values from tests E3 - E5 are compiled in Table 2. The main output parameters of interest are the residual velocity of the projectile after it has perforated the slab and the areas at the front and rear surfaces from which the concrete has scabbed off. The just perforation velocity was estimated using the methodology by Kar (Kar, 1979). Photographs of the vertical cross sections of the sawn slab quartiles are shown in Figure 4.

Table 2. Main input and output parameters from impact tests E3 - E5.

Parameter	**Test E3**	**Test E4**	**Test E5**
Projectile mass [kg]	47.58	47.60	47.58
Impact velocity [m/s]	102.6	104.9	104.0
Concrete compression strength [MPa] Cube/Cyl.	57.7/55.5	57.5/51.8	57.5/49.9
Concrete splitting tensile strength [MPa]	3.35	2.77	3.26
Residual velocity [m/s]	41	42	49
Scabbing area [m^2]	0.65	0.52	0.89
Mass of detached concrete [kg]	58	67	141
Estimated just perforation velocity [m/s]	81	82	36

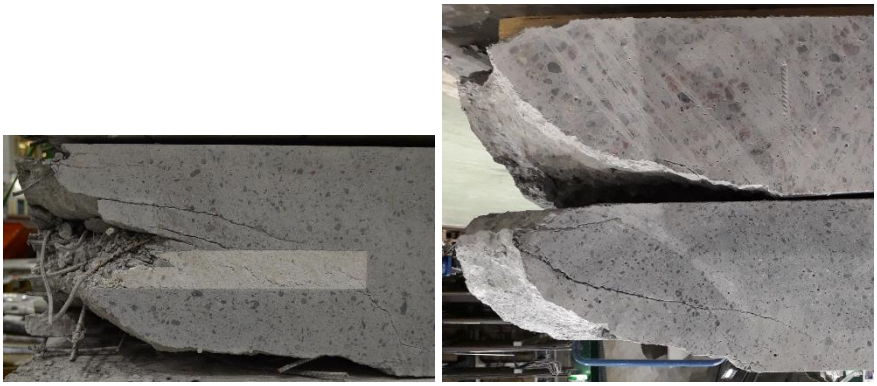

(a) (b)

Figure 4. Vertical cross sections of the tested slabs sawn into quartiles. (a) Test E3. (b) Test E5 (top) and test E4 (bottom).

Compared to a similar single slab (the same reinforcement ratio, the same ovelall thickness, the same concrete strength), test slab E3 had significantly weaker punching resistance. The result indicates that a double wall system is not a feasible option to increase the punching resistance against hard impacts. More feasible would be to build a single wall with the same total thickness and reinforcement ratio.

The results of tests E4 and E5 indicate that, contrary to what was expected, increasing the grain size of aggregates while keeping the static mechanical properties the same does not necessarily increase the punching resistance of the slab. Since only one test was carried out with concretes having 8 mm and 32 mm maximum aggregate size, the results cannot be generalized without further tests.

All the tests can be considered as successful. They fulfilled the purposes they were designed to and resulted in wealth of measurement data. The main benefit of the tests is that they provided valuable experimental data for validation of computational models. The tests are discussed more thoroughly in the work by Vepsä (Vepsä, 2017, 2018, 2019).

Material model development

The understanding and assessment of accidental crash scenarios on RC structures is of high interest for safety issues. Although experimental research on this topic has already a long and successful history, there are many issues waiting to be solved as far as numerical simulations are concerned.

The Abaqus Concrete Damage Plasticity (CDP) material model, as documented in the Abaqus user and theory manuals, (Simulia, 2016), is based on two damage-plasticity theory building blocks. The first building block is a modified Drucker-Prager yield surface with Rankine tension cut-off together with a non-associative Drucker-Prager hyperbolic flow potential. The second building block is a bi-isotropic strain hardening behaviour, which depends on the evolution of two scalar internal hardening variables: the compressive and tensile equivalent plastic strains. On the top of this elastic-plastic material behaviour there is a possibility to couple scalar damage, i.e. stiffness degradation. The single scalar damage variable is defined to be directly dependent on the internal hardening variables. Historically, the yield surface and the non-associative flow potential that is characteristic to the CDP model was first proposed by Lubliner and his co-workers in the so-called “Barcelona” model, (Lubliner et al., 1989). However, the bi-isotropic hardening and the scalar stiffness degradation properties were introduced in the works of J.H. Lee and G. Fenves, (Lee, 1996) (Lee and Fenves, 1998).

The Abaqus CDP model can be used in its standard form, by providing in the model definition the two hardening curves and a few input parameters that control the shape of the yield surface and the flow potential. However, there is also a possibility in the CDP model to apply user defined field variable dependency on any of the material parameters. For example, confined uniaxial compressive experiments

show a strong dependency of the axial stress-strain curve on the hydrostatic confining pressure, (Gabet, 2006) (Vu, 2013), and the Eurocode proposes a dependency of the concrete strength mean values on the confinement ratio, (CEN, 1992). Likewise, there are experiments, (Klepaczko and Brara, 2001), that show a dependency of the tensile axial stress and fracture energy on the loading rate. It is worthwhile to note that especially in hard missile impact simulations these field variable dependencies of compressive and tensile hardening are necessary, (Rodriguez et al., 2013) (Fedoroff et al., 2017). Combined bending and punching tests were simulated with three different forms of CDP model (Calonius, 2018).

In order to use the Abaqus CDP material model in simulations of RC structures under impact loads, one has to understand the effect of various parameters of the material model. Although most of the material parameters can be determined from standard concrete tests, some need more advanced tests to be determined. In impact simulations, one often has only limited material data available, and it makes therefore sense to study the parameter sensitivity of the material model in order to fix realistic parameter values. In this project, the sensitivity of the simulation response with respect to two model parameters was studied first: the dilation angle and the tensile to compressive meridian ratio. The sensitivity study was performed in three simple but representative stress states: the uniaxial tension state, the confined uniaxial compressive state and the pure shear state. Finally, a concrete removal criterion based on pure shear failure was proposed. This was reported with theoretical background in a scientific article manuscript to Rakenteiden Mekaniikka (Journal of Structural Mechanics) (Fedoroff et al., 2019). The effect of some input parameters was preliminarily studied also in a VTT research report by Fedoroff (Fedoroff, 2017).

Another manuscript about the using of this material model in impact simulations was sent to the same journal (Fedoroff and Calonius, 2019). After the abovementioned sensitivity study, some particularities of the Abaqus CDP model were investigated with the purpose of using efficiently the CDP model in impact loaded RC structure simulations. In particular, the sensitivity of the simulation response with respect to angle of dilatation and element size was studied. The simulation response, in particular with respect to the performance of the proposed element deletion algorithm, was compared to measurements from benchmark impact tests on RC plates.

Four distinct tests, E4 and E5 tests from SAFIR ERNEST project, A11 from VTT IMPACT phase I and A12 from VTT IMPACT phase II project were considered as candidates for model validation purposes, (Lastunen and Hakola, 2009) (Vepsä et al., 2012) (Vepsä et al., 2016). The expected failure mechanism is local shear together with small global displacements. Tests E4 and E5 are described above in the previous chapter. There was a perforation in all tests except A11. The missile and slab are similar in each test, but there is no reinforcement in the impact area in E4 and E5. The finite element (FE) model is shown in Figure 5.

The benchmark simulations were carried out using Abaqus with explicit central difference time integration. A quarter of the model is considered, as shown in Figure 5. The concrete slab is bounded by steel channels in order to withstand the contact

pressure from the steel rods on both sides of the slab. These steel rods are attached to the frame that holds the slab in place. In these simulation models, the steel frame is not modelled at all. The steel rods, which are assumed to simulate hinged boundary conditions, are modelled as rigid bodies and they are rigidly fixed to the frame of reference.

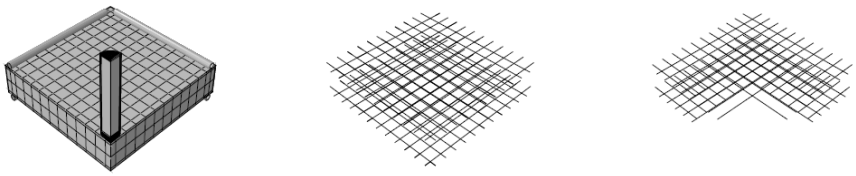

(a) (b) (c)

Figure 5. The quarter model used in the simulation of all benchmark cases (a). Steel reinforcement for A11 and A12 tests (b). Steel reinforcement for E4 and E5 tests (c).

Only simulation results of test E4 are described here. Figure 6 shows the projectile velocity in test E4 and corresponding FE simulations with two different mesh sizes (L is either 5 mm or 10 mm) and values of dilation angle (psi is either 30 or 35). The maximum element size above which various local physical phenomena cannot be described accurately is approx. 10 mm. On the other hand, 5mm (50 elements through the thickness of the slab) is a minimum element size from computational cost point of view. In this case, since the element size is only slightly affecting the results, 10 mm can almost be considered as an adequate size, although a smaller size is recommended for more detailed results. Lower dilation angle yields a higher residual velocity, i.e. decreases the punching capacity of the slab. The dotted black curve representing test result has been obtained from the high-speed videography. Especially the beginning of the curve is not very accurate, but it can be reliably said that the missile decelerates somewhat slower in the test than in the simulations. One reason seems to be the fact, that the missile did not hit the slab in direct angle and the pipe walls were more in contact with the concrete during the impact.

Figure 7 shows on the left the back surface of E4 slab after the test and on the right the deformed FE model shape 4 ms after the start of the impact with SDV4 (a field variable indicating progress of the failure mode) magnitude represented with different colours for the case with dilation angle of 30 degrees and element size of 5 mm.

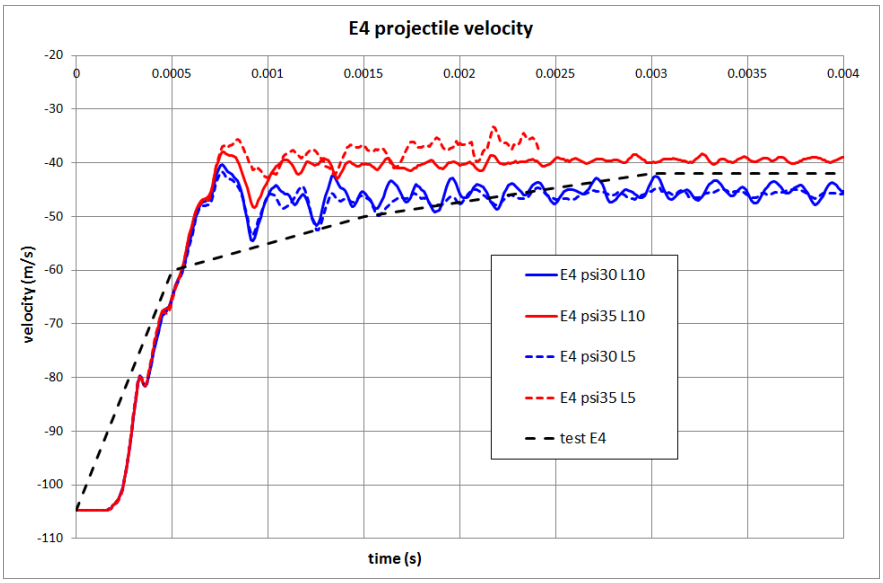

Figure 6. Projectile velocity in test E4 and corresponding FE simulations with two different mesh sizes and values of dilation angle (the first 4 ms).

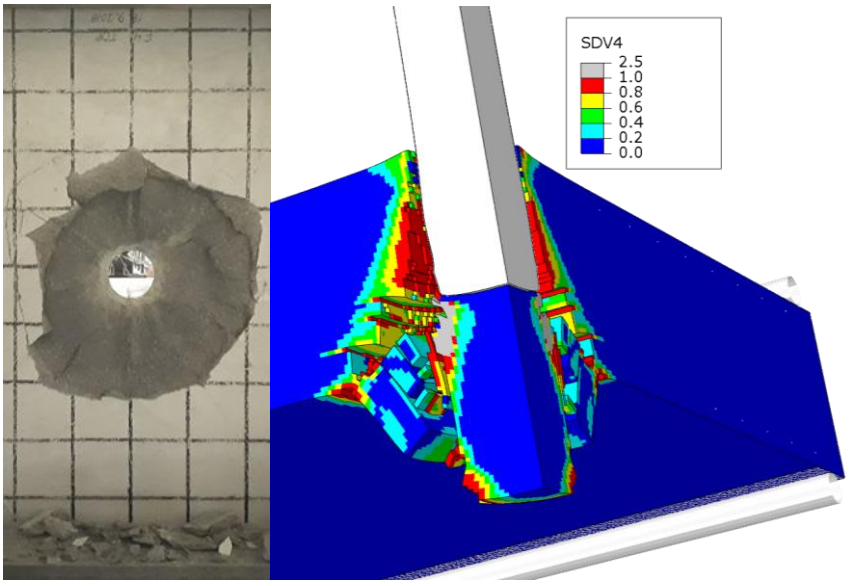

Figure 7. Left: Back surface of E4 slab after the test. Right: Deformed FE model shape after 4 ms with SDV4 magnitude represented with different colours (E4, dilation angle 30, element size 5 mm).

The first conclusion is that the proposed material model and the element removal algorithm is mesh size independent. The second conclusion is that the material

model and the element removal algorithm is sensitive to the variation of a particular material parameter, namely the angle of dilation. Therefore, particular care should be paid in impact simulations to the choice of that parameter. Validation of the proposed material model and element removal algorithm against experimental results yields rather satisfactory conclusions for the selected benchmark tests. Nevertheless, it must be acknowledged that the range of benchmark tests should be widened in order to generalize these conclusions to arbitrary impact simulations.

Acknowledgement

The financial support of VTT Technical Research Centre of Finland Ltd and Nuclear Waste Management Fund of Finland is acknowledged.

References

Calonius, K. 2018. FE simulations of combined bending and punching tests, VTT Research report VTT-R-05644-17, 42 p.

CEN European Committee for Standardization. 1992. Eurocode 2 - Design of concrete structures. Finnish Standards Association SFS.

Fedoroff, A., Kuutti, J. and Saarenheimo, A. 2017. A physically motivated element deletion criterion for the concrete damage plasticity model. In SMiRT-24 transactions. International Association for Structural Mechanics in Reactor Technology

Fedoroff, A. 2017. Continuum damage plasticity for concrete modeling. VTT reports, VTT-R-00331-17.

Fedoroff, A. & Calonius, K. 2019. Using the Abaqus CDP model in impact simulations. Rakenteiden Mekaniikka (Journal of Structural Mechanics). Manuscript under review.

Fedoroff, A., Calonius, K. & Kuutti, J. 2019. Behavior of the Abaqus CDP model in simple stress states. Rakenteiden Mekaniikka (Journal of Structural Mechanics). Manuscript under review.

Gabet, T. 2006. These: Comportement triaxial du beton sous fortes contraintes: influence du trajet de chargement. Universite Joseph Fourier, Grenoble.

Kar, A.K. 1979. Residual velocity for projectiles, Nuclear Engineering and Design, Vol 53, pp. 87-95. Elsevier

Klepaczko, J.R. and Brara, A. 2001. An experimental method for dynamic tensile testing of concrete spalling. International Journal of Impact Engineering.

Kärnä, T., Saarenheimo, A. and Tuomala, M. 2004. Impact loaded structures. In the Interim report of SAFIR The Finnish Research Programme on Nuclear Power Plant Safety 2003-2006. Espoo. VTT. pp. 113-123.

Lastunen, A. and Hakola, I. 2009. Pre-stressed concrete walls under impact loading. VTT reports, VTT-R-02904-09.

Lee, J.H. 1996. Theory and implementation of plastic-damage model for concrete structures under cyclic and dynamic loading. PhD dissertation, University of Berkley, California.

Lee, J.H and Fenves, G. 1998. Plastic-damage model for cyclic loading of concrete structures. Journal of Engineering mechanics, 124(8):892–900.

Lubliner, J., Oliver, J., Oller, S. and Onate, E. A plastic-damage model for concrete. Int.J. of Solids and Structure, 25(3):299–326, 1989.

Rodriguez, J., Martinez, F. and Marti, J. Concrete constitutive model, calibration and applications. 2013 SIMULIA Community Conference, 2013.

Simulia. Abaqus Manual. Dassault Simulia, 2016.

Vepsä, A., Saarenheimo, A., Tarallo, F., Rambach, J.-M. and Orbovic, N. 2012. Impact tests for iris 2010 benchmark exercise. Journal of Disaster Research, 7(5), 619-628, 7(5):619–628, 2012.

Vepsä, A., Calonius, K., Fedoroff, A., Fûlöp, L., Jussila, V., Saarenheimo, A., Varis, P., Fälth, B., Lund, B. and Tuomala, M. 2016. Experimental and numerical methods for external event assessment improving safety (ernest). In SAFIR2018 The Finnish Research Programme on Nuclear Power Plant Safety 2015-2018: interim report. VTT, Technical Research Centre of Finland.

Vepsä, A. 2017. Impact Espoo: VTT. VTT Research report VTT-R-00267-17. 63 p. p. p.

Vepsä, A. 2018. Hard impact punching behaviour structure. Espoo: VTT. VTT Research report VTT-R-05780-17. 44 p. p.

Vepsä, A. 2019. Two punching resistance tests of plain concrete slabs with different maximum aggregate sizes. Espoo: VTT. VTT Research report VTT-R-00040-19. 42 p.

Vu, X.D. 2013. Vulnerabilite des ouvrages en beton sous impact: Caracterisation, modelisation, et validation. Universite Joseph Fourier, Grenoble.

4. Reactor and Fuel

4.1 Development of a Monte Carlo based calculation sequence for reactor core safety analyses (MONSOON)

Jaakko Leppänen[1], Ville Valtavirta[1], Antti Rintala[1], Ville Sahlberg[1], Heikki Suikkanen[2]

[1]VTT Technical Research Centre of Finland Ltd
P.O. Box 1000, FI-02044 Espoo

[2]LUT University
P.O. Box 20, FI-53851 Lappeenranta

Abstract

The MONSOON project continued the development of the Serpent Monte Carlo code, with the specific goal of establishing a complete and independent calculation sequence for the safety analyses of Finnish power reactors. During the first years the work covered development of methodologies for spatial homogenization, which forms the first part of the traditional multi-stage calculation scheme applied to core physics calculations. The focus was later shifted to the development of a new nodal neutronics code Ants as part of the new Kraken computational framework.

The work on Serpent development was started during the previous SAFIR programmes, and the KÄÄRME project in SAFIR2014 provided a proof-of-concept type demonstration for the use of the continuous-energy Monte Carlo method for spatial homogenization. The purpose of the MONSOON project was to proceed from feasibility studies to practical applications. Serpent development is carried out in close collaboration with a large international user community. The code is currently used in more than 200 organizations in 42 countries around the world

Introduction

Nuclear reactor safety analyses involving coupled full-scale fuel cycle and transient calculations currently rely on a two-stage calculation scheme, in which the neutron transport physics at the fuel assembly level is first reduced into a set of representative group constants, which are then used as the input data for a reduced-order steady-state or dynamic full-core calculation. Group constant generation involves a procedure called spatial homogenization, which essentially implies the solution of the heterogeneous transport problem at the local fuel assembly level. The procedure is repeated for different assembly types, burnups and reactor operating conditions, and the result is a complete data library, providing the sufficient building blocks for the coupled full-scale calculation.

Managing this calculation scheme as a whole is an important part of reactor core analysis, and profound understanding of the methods, theory and underlying physics is absolutely essential for the safe and reliable utilization of nuclear energy. The MONSOON project aimed to enhance the knowledge basis needed for performing independent safety analyses for Finnish power reactors, relying on a novel approach using the continuous-energy Monte Carlo method for spatial homogenization. The work extended the methodologies applied in the calculation scheme to state-of-the-art and beyond. The primary calculation tool was the Serpent Monte Carlo code (Leppänen, 2015), which has been developed for reactor physics applications at VTT since 2004 (Leppänen, 2007).

The MONSOON project essentially continued the work started in the KÄÄRME project of SAFIR2014. The success of the previous work was recognized in the SAFIR2018 Framework Plan (SAFIR2018), where it was explicitly stated that the Serpent code has proven to be an international success, and that its development should be continued and the range of application targets broadened. It was also pointed out that the work connects to a broader goal of developing a fully independent reactor physics calculation system, accompanied by fundamental, source-code level understanding of the underlying computational methodology.

Encouraged by the recognition and positive feedback, the original project plan for MONSOON was drafted with ambitious goals. The primary objective was to develop the methodology for Monte Carlo based spatial homogenization into a practical computational framework for routine nuclear reactor safety analyses. In other words, to proceed from proof-of-concept type studies to practical applications. The major tasks and goals included in the original project plan can be summarized as follows:

1. Complete the methodological development in the Serpent code that was started in SAFIR2014
2. Establish the systematic procedures required for producing the full set of homogenized group constants for different reactor types (VVER, PWR, BWR) and applications (fuel cycle simulations and transient analyses)
3. Perform extensive validation for the developed computational methodology involving the most relevant calculation codes used at VTT (ARES, TRAB3D, HEXBU-3D, HEXTRAN, Apros, PARCS, Simulate, DYN3D, etc.)
4. Study new approaches and methodologies for Monte Carlo based spatial homogenization and nodal diffusion calculations (3D methods, coupled calculations, etc.)
5. Maintain contacts and enhance collaboration with Serpent users and the international reactor physics community

Unfortunately, the planned project volume was considerably reduced in 2015 and 2016. The applied volume in 2015 was 23.5 person-months and 275 k€. The realized volume was 12.7 pm and 148 k€. In 2016 the volume was further reduced to only 7.8 pm and 100 k€. With one third of the original funding it became apparent

that accomplishing the planned tasks would not be possible, and most of the ambitious goals had to be dropped early on. At that time the project was essentially reduced to completing the work carried over from SAFIR2014.

The funding situation improved in 2017-2018, and during the course of the work it was also discovered that the accuracy of existing core simulator and transient codes was seriously limited by methodological factors. The methods used in VTT's nodal diffusion codes originate from the 1970's, and they no longer represent the state-of-the-art in reactor analysis. The accuracy of legacy codes is compromised in particular near sharp material discontinuities, such as the core-reflector boundary, near control rod tips, and in modern fuel types with axial profiling.

To overcome this problem, the development of a new nodal neutronics solver called Ants was started in 2017. The code relies on Serpent-generated group constants and modern AFEN-FENM methodology, and will be capable of handling both square and hexagonal lattice geometries in steady-state and transient conditions. The work is connected to the renewal of VTT's computational system for reactor core safety analyses, which was started in mid-2017 when a new research professorship was established in the field of reactor safety. In practice, the Ants code forms the neutronics solver in a reduced-order calculation sequence of the new Kraken computational framework.

Selected highlights of the MONSOON project are introduced in the following sections with some example results.

Serpent-Ares calculations (2015-2016)

During the first two years the work was focused on the Serpent-ARES code sequence with the purpose of 1) verifying the methodology used in Serpent for group constant generation, and 2) demonstrating that the continuous-energy Monte Carlo method is a viable option for spatial homogenization.

ARES is BWR/PWR core simulator, developed at the Finnish Radiation and Nuclear Safety Authority (STUK), and used at VTT mostly for research purposes. The neutronics model in ARES solves the two-group steady-state diffusion equations in rectangular geometry, using the analytical function expansion nodal model (AFEN). The homogenized group constants for ARES were produced using the standard methodology available in Serpent 2 (Leppänen, 2016a).

The test case for the Serpent-ARES code sequence was the MIT BEAVRS benchmark (Horelik and Herman, 2013), which was originally established for the purpose of validating high-fidelity core analysis methods against experimental reactor physics measurements. The benchmark model consists of a detailed description of a commercial 1000 MW Westinghouse PWR core, with assembly loading patterns and operating histories covering the first two core cycles. The detailed benchmark specification allowed constructing a very precise 3D model of the core for reference Serpent calculations. This way the Serpent-ARES results could be compared not only to experimental data, but also to a high-fidelity Monte Carlo solution. This type

of comparison is extremely valuable for the validation of reduced-order methodologies, since all uncertainties from nuclear interaction data and experimental measurements are reduced to zero, and the comparison truly reflects how well the computational sequence preserves the physics of the heterogeneous transport solution.

The first part of the study involving hot zero-power (HZP) state of the initial core was completed in the KÄÄRME project of SAFIR2014 (Leppänen, 2014). The work carried out in the MONSOON project extended the calculations to hot full-power (HFP) state and fuel cycle simulations (Leppänen, 2016b). Producing the full set of group constants for ARES required a very large number of calculations, taking into account parametrization with respect to fuel temperature, moderator temperature and density, coolant boron concentration and insertion of control rods. Covering all assembly types and reactor operating conditions required running the Monte Carlo transport simulation 11,868 times, not counting the transport solutions run during fuel depletion. Each simulation involved 10 million neutron histories. The branch variations were invoked using a built-in automated calculation sequence in the Serpent code (Leppänen, 2016a), and the manual effort required for preparing the input files remained moderate.

The calculations were run in VTT's computer cluster, "The Doctor", which allowed handling multiple burnup histories simultaneously. The liming calculation case took 46 hours to complete. Since the procedure of group constant generation has to be performed only once, this test case can be taken as a practical demonstration that the continuous-energy Monte Carlo method can be used for spatial homogenization at an acceptable computational cost.

The calculations performed for the study involved the evaluation of critical boron concentrations and control rod bank worths for various configurations, comparison of HFP core power distributions to reference Serpent 3D results and calculation of boron dilution curve for the first core cycle. Both the critical boron concentrations and control rod bank worths showed good agreement with the experimental reference results. Hot full-power calculations were performed for the fresh core at 3411 MW fission power, assuming zero concentrations for fission product poisons. The differences in assembly powers generally remained below 1%, with the notable exception of assembly types with asymmetrically positioned burnable absorber pins.

Fuel cycle simulations for core cycle 1 were run with ARES. Reactor power was kept constant at 3411 MW, and the cycle length was set to 326 days with 30 intermediate steps as listed in Table 21 of (Horelik and Herman, 2013). All control rods were withdrawn from the core, and equilibrium iteration was applied for fission product poisons ^{135}Xe and ^{149}Sm. The measured and simulated boron let-down curves are compared in Fig. 1. The results are in good agreement. The critical concentration is systematically under-predicted by ARES, but the differences remain below 25 ppm. The simulation is terminated when the boron concentration reaches zero at 324.8 days, which means that the overall cycle length falls short by only 29 hours.

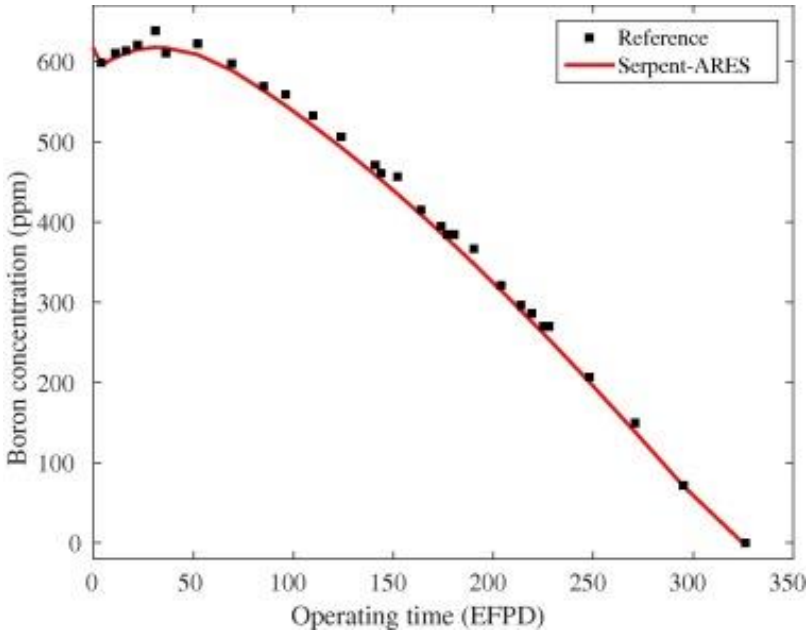

Figure 1. Boron let-down curve for cycle 1 calculated by Serpent-ARES compared to experimental reference data.

Development of a new nodal diffusion solver (2017-2018)

During work in the SADE project in the SAFIR2018 programme, the existing nodal neutronics solvers were compared to 3D full core Serpent calculations. From this, it was discovered that notable inaccuracies existed both near axial discontinuities, such as control rod tips or axial profiling, and near the radial reflectors. Several approaches to attenuate these problems were tested, but they only worked well for single core states. Therefore, a new methodology for nodal neutronics was needed to further improve the accuracies of burnup calculations and transient safety analyses.

A hybrid AFEN-FENM methodology was chosen as the solution algorithm for the new nodal neutronics solver. It is based on a subset of analytic solutions to neutron diffusion equation in three dimensions. Based on existing scientific literature, the use of analytic solutions greatly decreases inaccuracies near discontinuities such as the radial reflector or axial profiling. In addition, such a scheme requires less approximations, meaning that the resulting tool is more generalizable to both different reactor types and different core states. This is relevant for example for modelling small reactors or exotic core states for transient safety analyses.

The development of actual nodal neutronics program Ants started with developing a proof-of-concept rectangular geometry nodal diffusion solver. The methodology of the solver was reported together with results of IAEA 3D PWR benchmark (Sahlberg, 2018). The development continued with hexagonal geometry diffusion solver applicable to for example VVER type reactors. The first results of the hexagonal geometry solver were reported with multiple hexagonal geometry results in (Rintala, 2018b). With the solvers of both geometries, satisfying results were obtained.

Ants is currently capable of solving steady state diffusion problems in the mentioned three-dimensional geometries. Ants supports a simplified one state point group constant format and the HEXBU-3D/MOD5 group constant format (Rintala, 2018a). With the HEXBU-3D/MOD5 group constant format, in addition to the effective multiplication factor, also the boron concentration criticality parameter and equilibrium xenon and samarium states are supported. The reflectors are modeled with reflector nodes instead of albedos. The geometry input of the program is currently node-wise. Ants supports modeling of multi-part control elements with control bank support.

The feature development of Ants will continue so that together with Kraken, Ants will be capable of performing steady state, including cycle simulations, and transient simulations with all features required for safety analysis. Together with Ants, also the group constant models and group constant generation features of Serpent will be further developed. In addition to the feature development, also nodal neutronics methodology development will be performed.

International collaboration

The Serpent code has been in public distribution since 2009. When the MONSOON project started in 2015, the number of users was around 380. At the time of this writing the user community had grown to almost 900 users in 216 organizations around the world. Serpent is most commonly used by university students for academic research and thesis work, but the code has an extensive user basis in various research organizations as well. In recent years Serpent has also been adopted by the nuclear industry and small businesses working on innovative reactor designs.

The strong emphasis in academic research is reflected in the number of publications. A total of 720 peer-reviewed scientific journal articles and conference papers and 175 theses have been published on Serpent-related topics since the beginning of code development in 2004. In Finland, Serpent development and applications have provided topics for seven doctoral and 33 M.Sc. and B.Sc. theses and special assignments at Aalto University and Lappeenranta University of Technology. The number of Serpent users and publications since 2005 is presented in Figures 2 and 3.

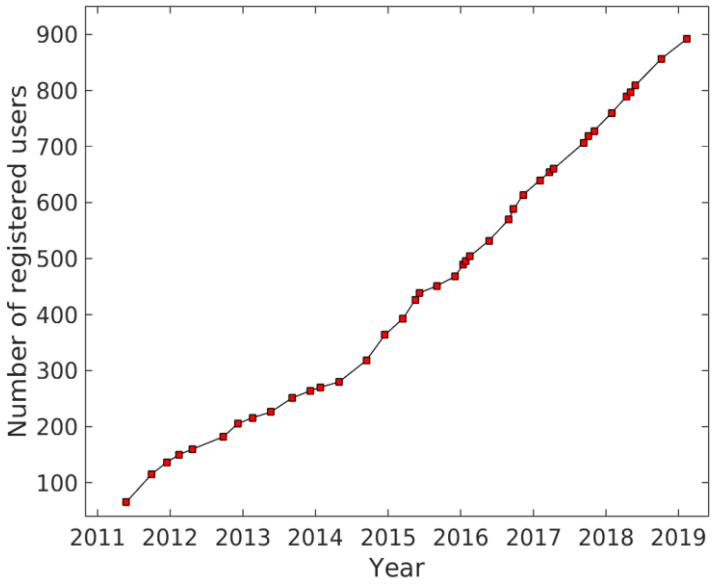

Figure 2. Number of registered Serpent users since 2011.

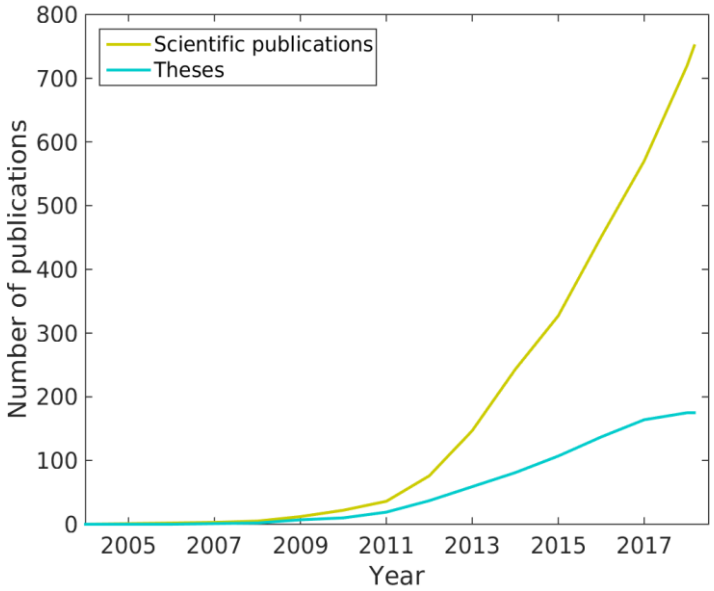

Figure 3. Number of Serpent-related publications since 2005.

Active communication with Serpent users is maintained in various ways. Serpent has an official website (http://montecarlo.vtt.fi), an interactive discussion forum (http://ttuki.vtt.fi/serpent), and a Wiki-based on-line user manual (http://serpent.vtt.fi/mediawiki). Annual international user group meetings have been hosted together with Serpent user organizations since 2011. The 8th international UGM was hosted by Aalto University in Espoo, Finland in May 2018. The meeting brought together 40 Serpent enthusiasts from 22 organizations in 11 countries around the world.

Other results

The multi-physics developments for Serpent started in the Academy of Finland Numerical Multi-Physics (NUMPS) project were continued in MONSOON. The capability for Serpent to use multi-physics feedbacks from external or internal solvers in burnup calculations was implemented using a stochastic approximation based approach.

These capabilities were used in estimating the effects of homogenized fuel temperature distributions in the history calculations of group constant generation via comparisons to calculations using accurate fuel temperature distributions provided on a pin-by-pin basis by the externally coupled ENIGMA fuel performance code.

The differences were tracked from nuclide distributions via the generated group constants all the way to the results of the ARES core simulator for the initial cycle of the EPR reactor (Valtavirta, 2017b).

LUT University participated MONSOON in 2018 with a task to assess the performance of a new detector type, the functional expansion tally (FET), recently implemented into Serpent. This work was motivated by the possibility to utilize FETs especially in coupled calculations, such as between Serpent and the fuel performance code TRANSURANUS; a coupling developed at LUT within another project but also slightly improved within MONSOON.

FETs can be used for obtaining continuous reaction rate distributions as, instead of scoring events in spatially discretized bins, events are scored on an orthogonal basis of polynomial functions. Previous studies (Wendt, 2018) have shown that using FETs in place of conventional bin-based tallies can reduce the computational effort required, e.g., to obtain pin power distributions, at least in cases in which low-order FETs are sufficient to capture the correct form of the distribution.

The work performed in MONSOON, however, showed that accurately capturing the power distribution in more challenging cases, such as for a pin located next to a partially inserted control rod (see Figure 4), will require increasing the FET order, thus significantly increasing the number of FET coefficients and subsequently the effort to expand the functions. Due to the nature of the underlying polynomial functions, the distributions obtained with FETs can exhibit oscillatory behavior with amplitude decreasing with increasing FET order. This can even lead to unrealistic negative values in some cases, such as shown in Figure 4. Thus, it was concluded that using FETs properly will require some experience from the user.

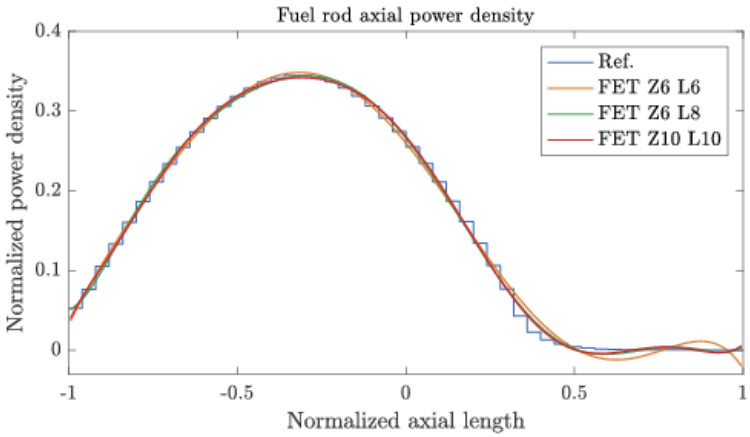

Figure 4. Axial power density distribution for a fresh UO2 rod located next to a partially inserted control rod. FET solutions obtained using different orders for the Zernike (Z) and Legendre (Z) polynomials.

Summary and future plans

The MONSOON project focused on the development of the Serpent Monte Carlo code, for the purpose of producing homogenized group constants for deterministic core simulator and transient analysis codes. The project also initiated the development of a new nodal solver Ants, which is together with other state-of-the-art physics solvers is intended to replace the legacy in-house codes used at VTT for LWR safety analyses. The functional modules form a new computational framework Kraken, the development of which is continued in the LONKERO project of SAFIR2022.

References

Horelik, N. and Herman B. 2013. Benchmark for Evaluation and Validation of Reactor Simulations rev. 1.1.1 MIT Computational Reactor Physics Group (2013).

Leppänen, J. 2007. Development of a new Monte Carlo reactor physics code. D.Sc. Thesis, Helsinki University of Technology, 2007.

Leppänen, J., Mattila, R. and Pusa, M. 2014. Validation of the Serpent-ARES code sequence using the MIT BEAVRS benchmark - initial core at HZP conditions. Ann. Nucl. Energy, 69 (2014), pp. 212–225.

Leppänen, J., et al. 2015. The Serpent Monte Carlo code: Status, development and applications in 2013. Ann. Nucl. Energy, 82 (2015) 142-150.

Leppänen, J., Pusa, M. and Fridman, E. 2016a. Overview of methodology for spatial homogenization in the Serpent 2 Monte Carlo code. Ann. Nucl. Energy, 96 (2016) 126-136.

Leppänen, J. and Mattila, R. 2016b. Validation of the Serpent-ARES code sequence using the MIT BEAVRS benchmark – HFP conditions and fuel cycle 1 simulations. Ann. Nucl. Energy, 96 (2016) 324-331.

Leppänen, J. et al. 2017. Renewal of VTT's calculation system for nuclear reactor core physics analyses. VTT-R-00707-17. VTT Technical Research Centre of Finland, 2017. (confidential)

Rintala A. 2018a. Implementation of HEXBU-3D/MOD5 group constant model in Ants. VTT-R-03315-18. VTT Technical Research Centre of Finland Ltd, 2018.

Rintala A. and Sahlberg V. 2018b. Extension of nodal diffusion solver of Ants to hexagonal geometry. In proc. 28th Symposium of AER on VVER Reactor Physics and Reactor Safety, 2018.

Rintala, A. 2017. Serpent – HEXBU-3D calculation chain in case of a hot zero power VVER-1000 initial core. VTT-R-00580-17, VTT Technical Research Centre of Finland, 2017.

SAFIR2018 Planning group. National Nuclear Power Plant Safety Research 2015-2018, SAFIR2018 Framework Plan.

Sahlberg, V. 2015. Validating Pin Power Reconstruction Module with Serpent 2 – TRAB3D Code Sequence. Special assignment, Aalto University, 2015.

Sahlberg, V. 2016a. Modelling of axial discontinuities in reactor cores with Serpent 2 - TRAB3D code sequence. M.Sc. Thesis, Aalto University, 2016.

Sahlberg, V. 2016b. Recalculating the steady state conditions of the V-1000 zero-power critical facility at Kurchatov Institute using Monte Carlo and nodal diffusion. In proc. 26th Symposium of AER, Helsinki, Finland, Oct. 10-14, 2016.

Sahlberg, V. and Rintala, A. 2018. Development and First Results of a New Rectangular Nodal Diffusion Solver of Ants. In proc. PHYSOR 2018: Reactor Physics paving the way towards more efficient systems. 2018.

Valtavirta, V. and Leppänen, J. 2017a. Coupled Neutronics–Fuel Behavior Burnup Calculations Using the Serpent 2 Monte Carlo Code. Ann. Nucl. Energy (in review).

Valtavirta, V. and Leppänen, J. 2017b. Estimating the effects of homogenized fuel temperature in group constant generation using Serpent 2. Ann. Nucl. Energy, 105 (2017) 79-94.

Wendt, B. 2018. Functional expansions methods: Optimizations, characteri-zations, and multiphysics practices. PhD Thesis, Idaho State University, 2018.

4.2 Neutronics, burnup and nuclear fuel (NEPAL15)

Pertti Aarnio[1], Jarmo Ala-Heikkilä[1], Olli Hyvönen[1], Aarno Isotalo[1,2], Markus Ovaska[1]

[1]Aalto University School of Science, Dept. of Applied Physics
P.O. Box 15100, FI-00076 Aalto

[2]Current affiliation: Teollisuuden Voima Oyj

Abstract

This project was a direct one-year continuation of the NEPAL project of the SAFIR2014 programme. Our main focus area has been accurate burnup calculations that aim at finding rare but potentially problematic nuclides like strong absorbers or other reactor-physically important nuclides. New burnup calculation methods have been developed, implemented mainly in the Serpent code, and thoroughly evaluated. Evaluations show significant improvements in accuracy without additional computational resources. The work has been published in open scientific literature and at conferences. In these projects, we have also developed a novel mesoscopic model of the thermal creep failure of fuel pellets. The model includes damage accumulation from radiation-induced fission gas buildup and the behaviour of the gases themselves. Additionally, optimal reconstruction parameters for cross section libraries of Serpent have been investigated.

Introduction

The Fission and Radiation Physics Group at Aalto University School of Science has concentrated on developing calculation methods for reactor physics, modeling basic physical and chemical phenomena in nuclear fuel, and researching new fuel cycles and next generation nuclear reactors. The activities seamlessly combine education and research of nuclear engineering. The essential field of know-how of the group covers physics-based analyses and numerical computation, especially development of Monte Carlo codes.

The objective of NEPAL15, a direct continuation of the NEPAL project in the SAFIR2014 programme, was to increase our knowledge on burnup calculations on one hand and nuclear fuel behaviour on the other hand. We explored new methods in an academic manner, but we have practical applications in sight for the longer term.

A central goal of NEPAL15 was education of new experts in the field. In the preceding NEPAL project, one DSc thesis, one MSc thesis and one BSc thesis were

produced, and all by different authors. In NEPAL15, one of the deliverables was a BSc thesis.

Objectives

The contents and results of the NEPAL project have been summarized in the SAFIR2014 final report available at http://safir2014.vtt.fi/. In the burnup calculation task, we sent our postdoc Aarno Isotalo to work at Oak Ridge National Laboratory (ORNL) in June 2014 to develop various methods of mutual interest. These included the advanced depletion coupling schemes developed by us and the CRAM solver developed at VTT. Additionally, runtime and memory enhancements were investigated and implemented in various codes. This visit lasted until December 2015, a total of 19 months, and produced a number of scientific publications listed in the References.

In the task on mesoscopic fuel model, the objective was to further increase the realism in our thermo-mechanical model. In order to produce quantitative predictions more information and models were needed on the percolation threshold, growth rate of damages and thermal creep failure. The simulation results were to be compared to empirical measurements. This work was planned as a Bachelor's thesis or special assignment, but we did not manage to recruit a summer student for the task.

In RG meeting 1/2015 it was agreed that NEPAL15 funding would be used for another Bachelor's thesis where a BSc student optimized cross section libraries for Serpent 2 under the supervision of DSc Tuomas Viitanen (VTT). It had been observed that the cross section libraries in Serpent 1 were not accurate enough for all reactor systems. On the other hand, the memory consumption had to be kept under control, so the accuracy should be increased sensibly. This optimization was done in a BSc thesis under NEPAL15.

Burnup calculation methodology

In the first part of DSc A. Isotalo's work at ORNL (see References), he implemented a CRAM depletion solver to the ORIGEN module of SCALE. The new CRAM solver is superior to the old solver of ORIGEN in every way, and should eventually replace the old solver in all applications.

In addition to implementing CRAM, A. Isotalo developed three new capabilities for it. The first of these is a way to include a source term in the calculations, which has previously not been possible with CRAM. This allows CRAM to be used for modeling systems, such as molten salt reactors and reprocessing facilities, with material flows. The new method can even handle source terms with general polynomial time-dependence. Using a time dependent source term of any kind has previously not been possible with any depletion algorithm capable of handling the full system of nuclides.

The second new capability is internal substepping which further improves the already remarkable accuracy of CRAM with only a modest effect on running times. Even decay problems, where there have previously been concerns about the accuracy and reliability of CRAM, can now be solved with ten correct digits for all nuclides with atomic fraction above an arbitrary limit.

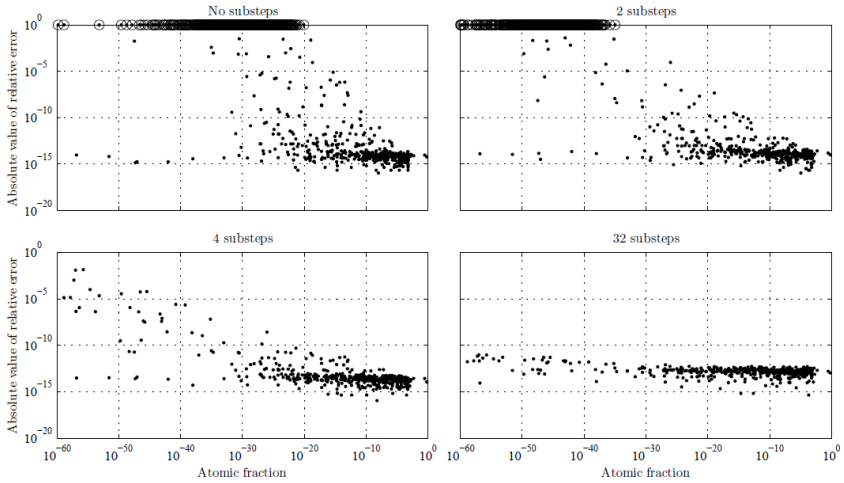

Figure 1. Relative errors with different numbers of internal substeps when old fuel is decayed for 365 days. Circles indicate errors that have been reduced to 1 for plotting. [Isotalo, Pusa 2016]

Finally, A. Isotalo developed a new method for calculating the time-integrals or averages of any and all quantity that are weighted sums of the atomic densities as a part of a single depletion solution with CRAM. Examples of such quantities are time-average atomic densities, the number of fissions, and the amount of energy released during a depletion step. The new method is fast and extremely accurate, which enables these quantities to be used in ways that have not previously been realistic.

A. Isotalo also participated in developing and implementing an internal burnup calculation capability for the new high performance Monte Carlo transport code called Shift. In particular, he implemented the higher order neutronics-depletion coupling schemes developed as a part of his PhD research. The capability has been completed and is being tested. A conference paper was written that describes the implemented burnup calculation capabilities.

In addition to regular code development activities, A. Isotalo used Shift to study the use of flux renormalization in constant power burnup calculations to further improve the implemented burnup calculation methodology. This includes developing a new renormalization method that leverages the new CRAM capabilities, a comparison of different renormalization strategies, and scoping on how much of a difference renormalization actually makes.

Mesoscopic modelling of nuclear fuel

During the four-year NEPAL project in the SAFIR2014 programme, M. Ovaska developed a computational model for simulating the microstructural evolution of nuclear fuel [Ovaska, Alava 2015]. The model includes damage accumulation from thermal creep deformation and from fission gas buildup within the pellet. Damage accumulation is linked with increasing porosity of the fuel, as microcracks and gas bubbles are formed. Diffusion of fission gases is simulated from the viewpoint of percolation theory: gas flows through interlinked pores, and can only reach the surface of the pellet through continuous pore pathways.

In NEPAL15, it was our plan to continue this modeling as a Bachelor's thesis or special assignment under supervision of M. Ovaska. Due to manpower limitations, this plan was not realized.

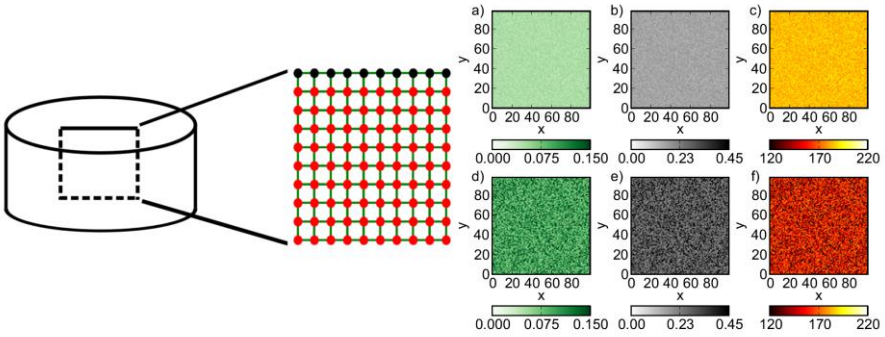

Figure 2. On the left: Schematic of the simulation system: A rectangular cross-section from a pellet. Gas nodes (red) are interconnected through bonds (green). Fission gas is released through the top boundary (black nodes). On the right: Example snapshots of porosity (a & d), damage (b & e) and Young's modulus in GPa (c & f). The top row (a-c) corresponds to the initial state, and the bottom row (d-f) shows a later stage when creep and radiation damage have weakened the pellet. [Ovaska, Alava 2015]

Processing cross section libraries for Serpent 2

In O. Hyvönen's BSc thesis, optimal reconstruction parameters for cross section libraries used with neutron transport calculation code Serpent 2 were sought. The nuclear data processing system NJOY, operated with a wrapper code SFFER by

DSc Tuomas Viitanen, was used to generate the cross section libraries. The essential reconstruction parameters in question were *err*, *errint* and *errmax* of NJOY's *RECONR* module.

Accuracy of the generated libraries was tested with Serpent 2 using simplified models of two thermal (HTGR, PWR) and one fast reactor (LFR). Fresh fuel calculations were used to establish a fundamental baseline for accuracy, and depleted fuel calculations were performed to examine if the presence of hundreds of different nuclides in the fuel affects how the reconstruction parameters should be chosen. Results of a simulation were compared to the reference result of the same simulation, calculated with highly accurate libraries.

As a result, the suggested reconstruction parameters for optimal thermal libraries are *err* = 0.005, *errint* = $2.5 \cdot 10^{-7}$ and *errmax* = 0.05. However, a library used for fast reactor simulations should not be generated with these values, as the integral thinning property they enable in the *RECONR* module impairs the accuracy of the library with fast reactors. However, it seems that the Serpent default library reconstructed with *err* = 0.01 and with integral thinning disabled by choosing *errmax* = *err* is accurate enough.

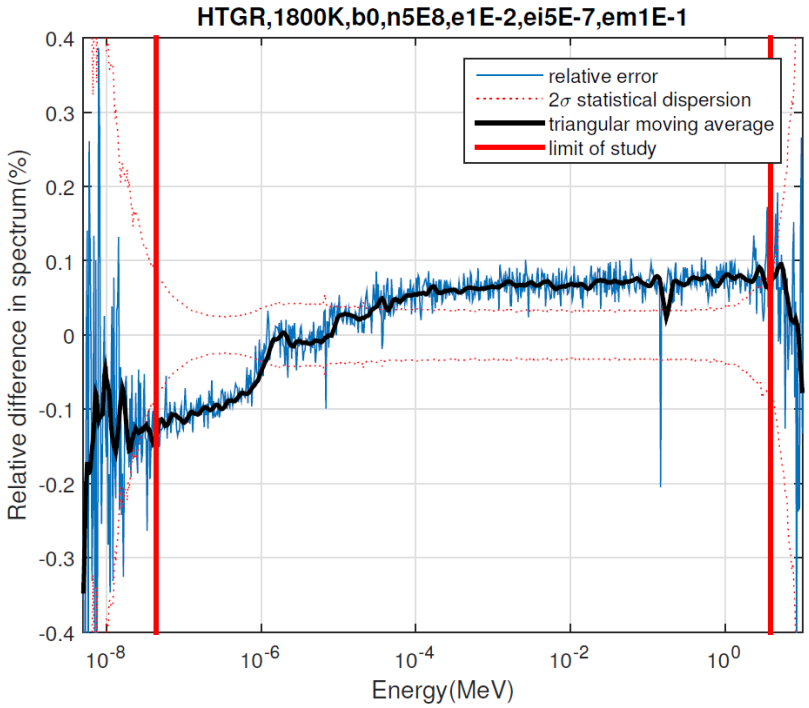

Figure 3. A relative difference neutron spectrum utilized in the parameter optimization. The title contains all relevant information about the simulation: case (HTGR), temperature (1800 K), fuel burnup (b0 = 0 MWd/kgU), number of neutron histories (n5E8 = $5 \cdot 10^8$), *err* (e1E-2 = 0.01), *errint* (ei5E-7 = $5 \cdot 10^{-7}$) and *errmax* (em1E-1 = 0.1). [Hyvönen 2015]

Conclusions

The objectives of the NEPAL and NEPAL15 projects can be defined primarily as new calculation methods and scientific publications documenting them. Moreover, the new expertise in the field and the new experts themselves are important deliverables of the project. One DSc thesis, one MSc thesis and two BSc theses were produced in these projects, and all by different authors, so we can conclude that the projects have reached their main objective. As of this writing, these young experts have continued their careers in other organizations in the nuclear field, thus completing the delivery.

These projects show that it is possible to contribute to the publicly-funded nuclear safety research in a university environment. Our scientifically oriented basic research is not necessarily applicable at the regulator and utilities in the short term, but it is instrumental in keeping the research at a high level and educating new experts to the field.

Acknowledgement

We acknowledge the fruitful collaboration of VTT and Oak Ridge National Laboratory. We also acknowledge the computational resources provided by the Aalto Science-IT project.

References

Isotalo, A.E., Davidson, G.G., Pandya, T.M., Wieselquist, W.A., Johnson, S.R., Flux renormalization in constant power burnup calculations, Annals of Nuclear Energy 96 (2016) 148-157. http://dx.doi.org/10.1016/j.anucene.2016.05.031

Isotalo, A.E., and Pusa, M., Improving the Accuracy of the Chebyshev Rational Approximation Method by Using Substeps. Nuclear Science and Engineering 183 (2016) 65-77. http://dx.doi.org/10.13182/NSE15-67

Isotalo, A.E., Calculating Time-Integral Quantities in Depletion Calculations. Nuclear Science and Engineering 183/3 (2016) 421-429. http://dx.doi.org/10.13182/NSE15-119

Davidson, G.G., Pandya, T.M., Isotalo, A.E., Johnson, S.R., Evans, T.M., Wieselquist, W.A, Nuclide depletion capabilities in the Shift Monte Carlo code, Proceedings of Physics of Reactors 2016, PHYSOR 2016: Unifying Theory and Experiments in the 21st Century, Sun Valley 1-5 May 2016.

Isotalo, A.E., Sahlberg, V., Comparison of Neutronics-Depletion Coupling Schemes for Burnup Calculations. Nuclear Science and Engineering 179/4 (2015) 434-459. http://dx.doi.org/10.13182/NSE14-35

Isotalo, A.E., Comparison of Neutronics-Depletion Coupling Schemes for Burnup Calculations 2. Nuclear Science and Engineering 180/3 (2015) 286-300. http://dx.doi.org/10.13182/NSE14-92

Isotalo, A.E., Wieselquist, W.A., Method for Including External Feed in Depletion Calculations with CRAM and Implementation to ORIGEN. Annals of Nuclear Energy 85 (2015) 68-77. http://dx.doi.org/10.1016/j.anucene.2015.04.037

Ovaska, M., Alava, M.J., Joint modeling of thermal creep and radiation damage interaction with gas permeability and release dynamics: the role of percolation. Physica A 436 (2015) 538-546. http://dx.doi.org/10.1016/j.physa.2015.05.068

Hyvönen, O., Finding optimal reconstruction parameters for cross section libraries used with Serpent 2, Bachelor's thesis, Aalto University School of Science, Sep 13, 2015.

4.3 Safety analyses for dynamical events (SADE)

Elina Syrjälahti, Ville Hovi, Anitta Hämäläinen, Hanna Räty, Ville Sahlberg, Veikko Taivassalo

VTT Technical Research Centre of Finland Ltd
P.O. Box 1000, FI-02044 Espoo

Abstract

Capabilities to model transients and accidents have been improved in the SADE project. The focus has been in the VVER modelling, with two parallel development branches: tools for practical safety analyses and more ambitious approach to use CFD-type 3D thermal-hydraulics in reactor dynamics modelling. During this four year project the coupling between VTT's reactor dynamics code HEXTRAN and system code SMABRE was extended with the new internally coupled simulation mode, which can be now used for routine safety analyses. Several improvements have been done to the neutronics modelling and also to the whole safety analyses calculation sequence. Group constants created with Serpent-2 have been taken into use in VTT's reactor dynamics codes that makes it possible to use independent, domestic calculation tools for the all phases of the safety analyses. Breakthrough was achieved when first truly coupled transient simulations were done using CFD code for reactor pressure vessel, the HEXTRAN code for core neutronics and SMABRE for the rest of the reactor coolant system.

Introduction

SADE was a four year project whose aim has been to model transients and accidents in such a way, that we can give more reliable answers to the safety requirements set in the YVL guides. The goal has been to have at VTT a fully self-developed, independent calculation system which can be used for the whole calculation sequence from basic nuclear data to coupled 3D transient analyses. SADE project has had two parallel development branches: tools for practical safety analyses, and high-fidelity branch, in which modelling capabilities have been improved by coupled use of the CFD-type thermal-hydraulics solver and the reactor dynamics codes. Developing and maintaining our own codes and in-depth understanding of them enables the best possible expertise on safety analyses.

The project had two main research areas. The objective of the first work package was to enhance the core modelling, especially neutronics modelling, of VTT's 3D reactor dynamics codes HEXTRAN and TRAB3D. Need for the more detailed neutronics modelling as well as for revision of the the whole safety analyses methodology was recognized to get the full benefit on the improved accuracy of the thermal-hydraulics modelling. Development of the solution methods and analysis of the methods versus accurate reference results has been also an efficient way to study

nodal codes in depth. A pin power reconstruction module has been implemented to TRAB3D, VTT's code for quadratic assembly PWRs and BWRs, to improve the resolution at which power distribution can be analysed. The reconstruction module utilizes the full core solution from TRAB3D and an additional pre-calculated assembly-wise input from the reactor physics code Serpent 2. Neutronics model of the HEXTRAN code has been further developed so that it can more reliably model transients of reactor cores with modern fuel assemblies. During the SAFIR2018 work has been done also to enable use of the group constants created with the reactor physics code Serpent 2 in the reactor dynamics codes TRAB3D and HEXTRAN.

The second work package focused on whole core transient analyses, especially on cases where mixing in reactor pressure vessel or open core geometry play an essential role. VTT's main tools for this kind of transient and accident simulations of VVERs are reactor dynamics code HEXTRAN and system code SMABRE. Modelling and development has had two parallel branches: development of the internally coupled HEXTRAN-SMABRE that can be routinely used for safety analyses already now, and modelling of transients with CFD-style codes that have more detailed description. Internal coupling implemented in the SADE project improves modelling of the cores consisting of fuel assemblies without boxes, as is the case with VVER-1000 and AES-2006 reactors. As a most remarkable achievement of the project first truly coupled transient simulations have been done using CFD code for reactor pressure vessel, the HEXTRAN code for core neutronics and SMABRE for the rest of the reactor coolant system.

Neutronics, system code and CFD

An up-to-date reactor analysis framework was developed by coupling VTT's reactor dynamics code for VVER-reactors HEXTRAN and the system code SMABRE with two CFD solvers, the PORFLO and OpenFOAM codes. The new dynamic analysis tool combines a 3D neutronics calculation and system code simulation with CFD modelling.

In the beginning of the project the one-way coupling between the VTT-developed porous-CFD code PORFLO and the core neutronics code HEXTRAN was created. The one-way coupling was tested in VVER-440 and VVER-1000 transients. In the second phase, full couplings of the codes HEXTRAN and SMABRE with the PORFLO code were implemented. The main communications between the codes are visualized in Fig. 1 with the primary quantities transferred. Typically a CFD mesh covers a pressure vessel or a major part of it and a SMABRE nodalization the rest of a plant. HEXTRAN thus communicates with PORFLO but not with SMABRE. Data transfer between PORFLO and HEXTRAN or SMABRE is handled through the TCP/IP sockets. 2-way coupling routines were developed for information exchange between the codes. Some significant modifications were also necessary in the coupled codes themselves. In addition, new parameters controlling the coupling were added in the inputs.

The 2-way coupling of HEXTRAN and PORFLO provides more realistic neutronics calculations. The 3D neutronics computation in HEXTRAN is based on 3D core thermodynamic data sent by PORFLO. After receiving a new 3D field for the coolant heating power, PORFLO updates the thermo-dynamic data and returns it to HEXTRAN. Converged solution is thus obtained by iteration within a time step. Furthermore, the VTT-developed fuel behaviour module FINIX can optionally be used with HEXTRAN and/or PORFLO.

The PORFLO code is also fully coupled with the system code SMABRE. The main quantities transferred between the codes are given in Fig. 1. In the coupled SMABRE-PORFLO simulations, a converged and consistent solution is also obtained by iteration within a time step.

The applicability of the new coupled HEXTRAN-SMABRE-PORFLO simulation framework for nuclear power plants was tested in five transients. For VVER-1000 reactors three variants of main steam line break (MSLB) accidents and one main coolant pump (RCP) transient were simulated. For VVER-440 reactors, the 7th dynamic AER benchmark for the start-up of an inoperable cold loop was successfully computed with the PORFLO-coupled code system.

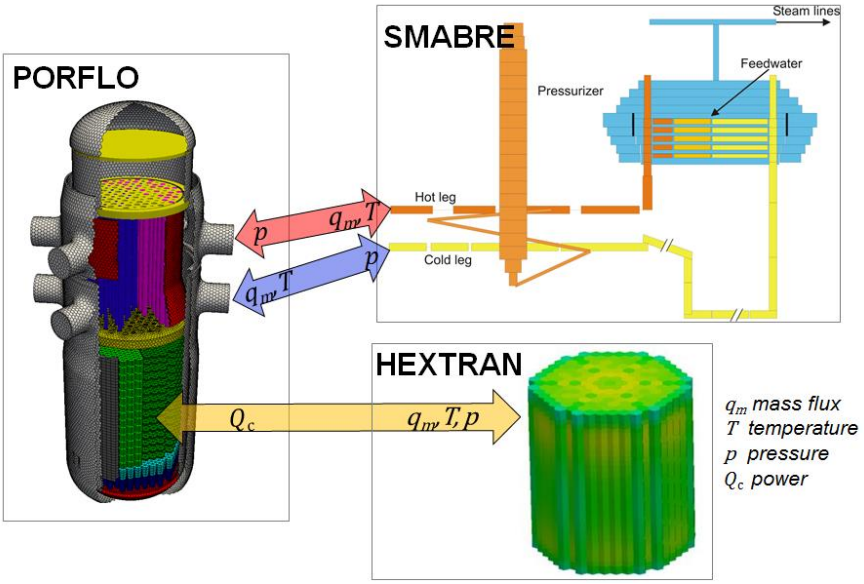

Figure 1: Coupling and data transfer between the neutronics code HEXTRAN, system code SMABRE and CFD-style PORFLO code in a VVER-1000 simulation. All four loops are modelled with SMABRE, but only one loop is shown in this figure.

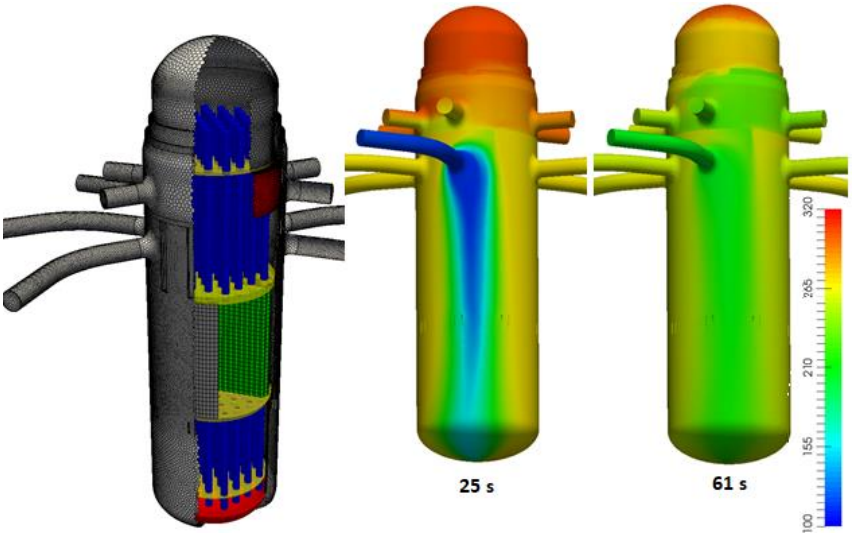

Figure 2: Computational mesh (left) and the coolant temperature (°C) in reactor pressure vessel in the coupled HEXTRAN-SMABRE-PORFLO simulation of the 7th dynamic AER benchmark for the start-up of an inoperable cold loop in a VVER-440 reactor.

In the first stage of VVER-440 modelling, the computational domain in CFD modelling consisted of a part of the primary circuit from the main isolation valves in the cold legs to the lower end of the core (Hovi et al., 2016; Hovi et al., 2017). The mesh consisted of 165 000 cells, most of which were hexahedra and prisms. The SMABRE model covered the rest of the plant. In this case, PORFLO communicated only with SMABRE, which provided coolant properties for HEXTRAN. In the second stage, the computational domain comprised the whole coolant volume of the pressure vessel, same parts of the cold legs as in the previous mesh and small parts of the hot legs. 7th dynamic AER benchmark was computed with the fully coupled HEXTRAN-SMABRE-PORFLO simulation framework. The created polyhedral mesh of 720 000 cells and coolant temperature in reactor pressure vessel after the start-up are visualized in Fig. 2. CFD-coupled simulations pointed out the significance of the modelling of control rod follower guide tubes in lower plenum. This has lead to the changes in the system code models.

In the VVER-1000 analyses, the computational domain covers whole fluid volume of the pressure vessel with small parts of cold and hot legs. A computational mesh was created (Fig. 1) and it consists of 870 000 polyhedral cells. Fully CFD-coupled HEXTRAN-SMABRE-PORFLO computations were performed for OECD/NEA V1000CT-2 main steam line break benchmark Variant a of Scenario 1 (1a) and Variants a and b of Scenario 2 (2a and 2b) of Exercise 3 (NEA 2010). Core inlet temperature and assembly-wise fission power at time of maximum fission power during return-to-power phase with different coupling methods are compared in Fig. 4. With CFD-coupling, temperature distribution at core inlet is more realistic and the peak power is higher than in the HEXTRAN-SMABRE results.

The coupling routines of PORFLO with HEXTRAN and SMABRE were implemented also in an OpenFOAM solver. VVER-1000 MSLB benchmark Scenario 2a of Exercise 3 was computed as a test case with the both CFD codes. Fig. 3**Error! Reference source not found.** shows the computed coolant temperature in reactor pressure vessel with HEXTRAN-SMABRE-OpenFOAM coupling at time of maximum power during return-to-power phase. Fission power and hot leg 4 temperature as a function of time with the results of other codes are also shown in Fig. 3. The deviation from the HEXTRAN-SMABRE curve results from smaller dispersion.

The applicability of the CFD-coupled simulation framework was also tested with the OECD/NEA Kalinin-3 benchmark concerning switching off one main coolant pump (RCP) of working four RCPs. In Fig. 7 the computed total fission power is compared to the HEXTRAN-SMABRE simulation.

The first coupled simulations demonstrated the feasibility and advantages of coupling 3D thermal hydraulics with 3D neutronics and system codes. The results emphasise the importance of realistic 3D thermal hydraulics modelling of the pressure vessel providing more realistic and reliable computational results for nuclear power plants. Coupled simulations with 3D neutronics and CFD-level representations for pressure vessels will likely bring out new information on the behaviour of the reactors during transients. Furthermore, the simulations provided more realistic novel reference results for the benchmarks.

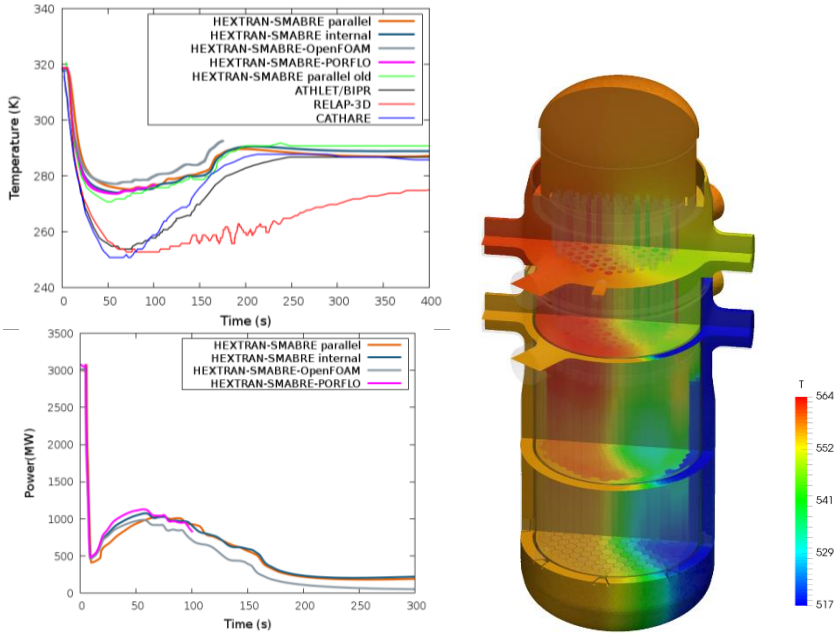

Figure 3: Fission power and hot leg #4 temperature during VVER-1000 MSLB accident and RPV temperature [K] on 55s after break in the coupled HEXTRAN-SMABRE-OpenFOAM simulation (V1000CT-2 - Exercise 3 - Scenario 2a).

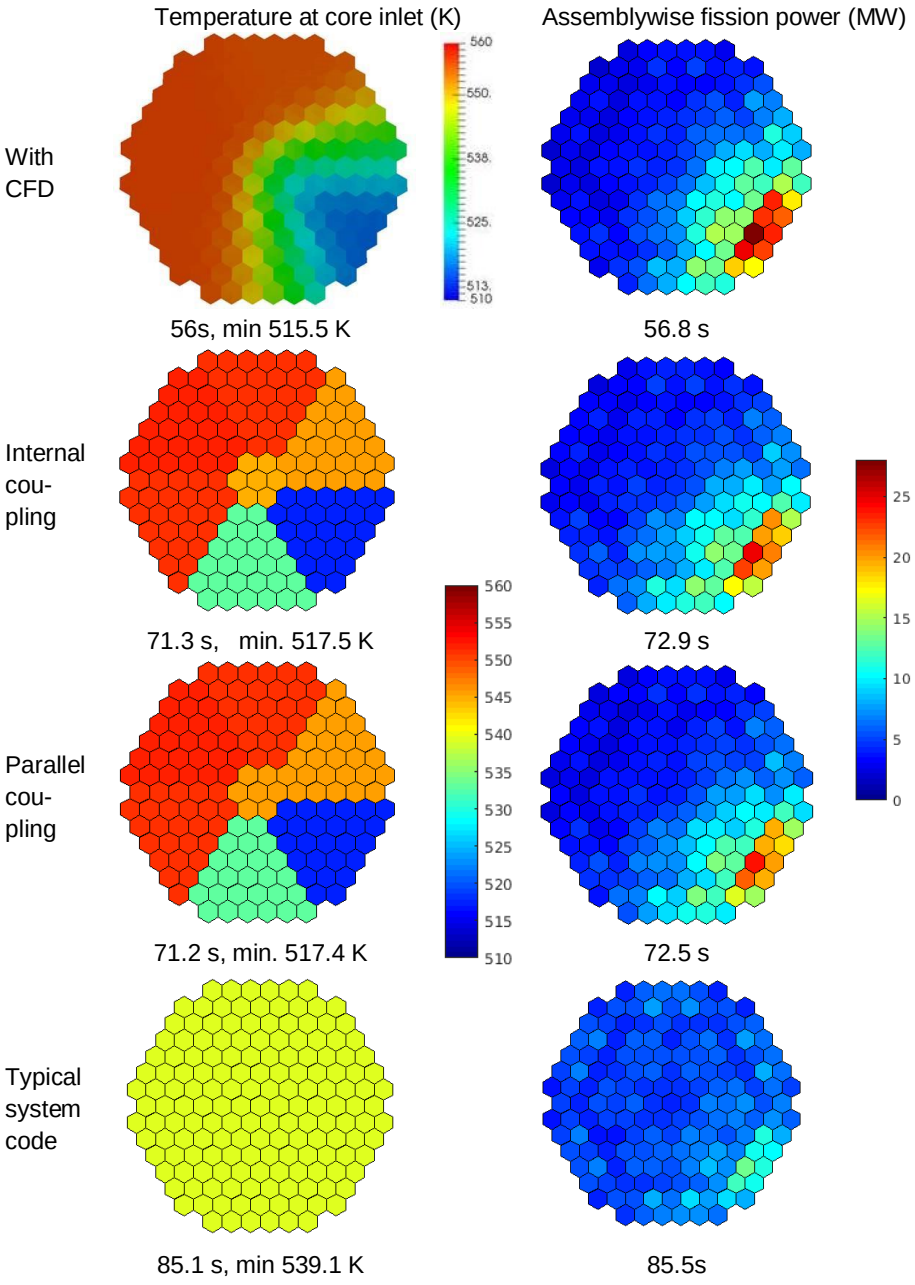

Figure 4: Core inlet temperature at time of minimum temperature, and assembly-wise fission power at time of maximum fission power during the main steam line break of VVER-1000 reactor with distinct coupling methods between HEXTRAN, SMABRE and PORFLO. OECD/NEA V1000CT-2 benchmark, Exercise 3 case 2a.

Internally coupled HEXTRAN-SMABRE

VTT's reactor dynamics code for VVER-reactors HEXTRAN and system code SMABRE has long been used together for transient and accident analyses. Coupling between the codes has been so called parallel coupling, which means that SMABRE has calculated whole thermal hydraulics of the loops and the core usually in a sparse geometry and additionally HEXTRAN has performed the more detailed thermal hydraulics and fuel transfer calculation in every fuel assembly.

In 2015, first version of the internally coupled HEXTRAN-SMABRE was implemented. New code version includes both coupling methods, parallel and internal, that enables use of both coupling methods with same SMABRE inputs only with minor modifications. In internally coupled simulations HEXTRAN solves the core neutronics and heat transfer in fuel rods and SMABRE the thermal hydraulics of the whole circuit using same nodalization in the core than HEXTRAN. Internal coupling enables use of more versatile nodalization in reactor cores thus improving modelling of the open core geometry used for example in VVER-1000 and AES-2006 reactors. Internal coupling has also been the basis for CFD coupled code.

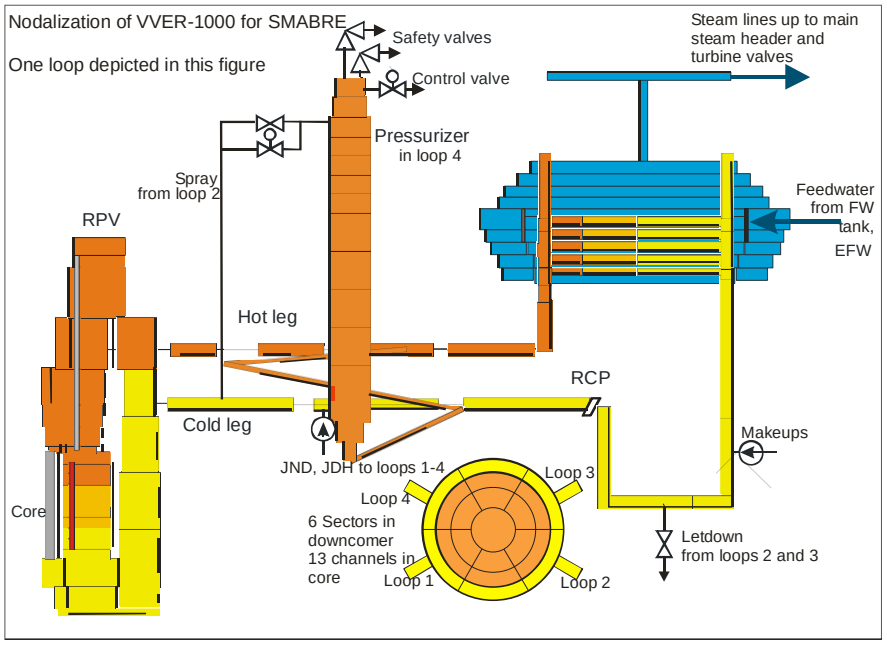

Figure 5: Overview of the primary side nodalization of Kalinin-3 VVER-1000 for SMABRE.

The new HEXTRAN-SMABRE version was first tested with VVER-440 control rod ejection (CRE) and main steam line break (MSLB) cases, in which already preliminary version of the code showed good agreement between the internally and parallelly coupled simulation modes as well as with earlier parallelly coupled code versions (Syrjälahti 2016). After two years pause development and validation of the code was continued in 2018 as a focus in VVER-1000 modelling (Syrjälahti, 2018b). Main validation cases for VVER-1000 have been OECD/NEA benchmarks V1000CT-2 concerning hypothetical main steam line break (MSLB) accident at Kozloduy-5 NPP (Fig. 4), and K3 based on measured data from a test at Kalinin-3 NPP where one main coolant pump (RCP) was switched off.

New HEXTRAN-SMABRE model was created for the Kalinin-3 NPP. Model is based on existing VVER-1000 plant model and overview of the primary side nodalization is shown in Fig. 5. The model has been described specific model report (Syrjälahti 2018a) in such a way that model can be later used for other purposes, e.g. in the OECD/NEA uncertainty analysis benchmark UAM-LWR. Power distribution in reactor core is shown in Fig. 6. Discrepancy between internally and parallelly coupled simulations is mainly due to slightly different mass flow distribution at core inlet. Mass flow to the central area of the reactor is slightly higher with internal simulation mode, because mass flow is distributed between channels in slightly different way with parallel simulation mode. Axial power distribution at the initial state and during the transient is very similar with both coupling modes as shown in Fig. 7 Also behaviour during the transient is very similar.

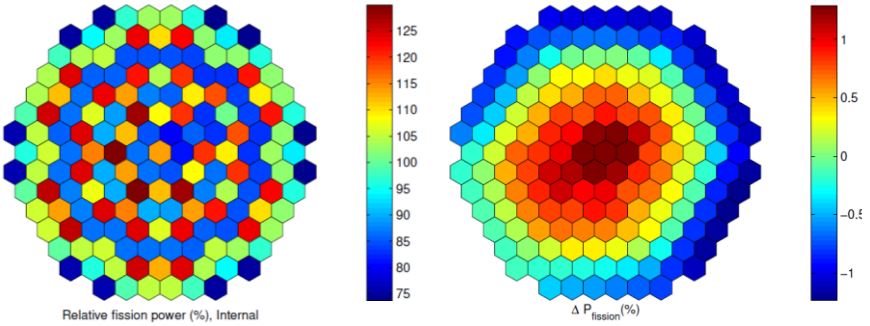

Figure 6: Steady state power distribution of Kalinin-3 core with HEXTRAN-SMABRE using internal coupling (left) and relative difference to parallelly coupled simulation (right).

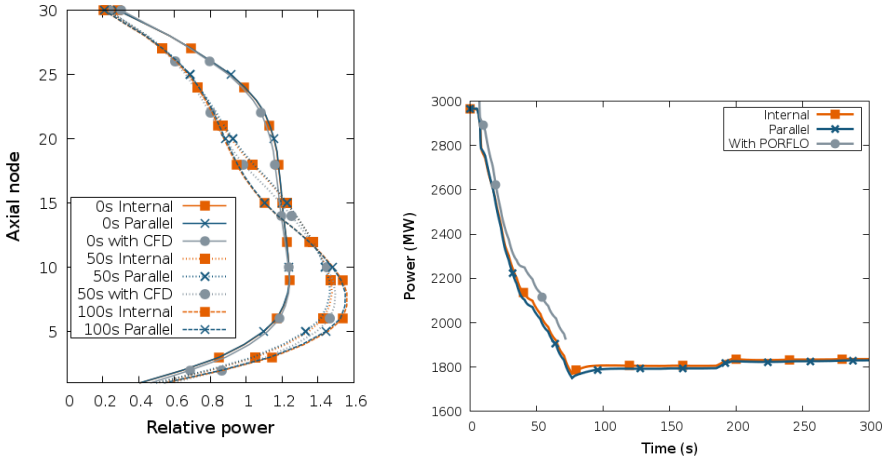

Figure 7: Axial power distribution (left) and total fission power (right) during Kalinin-3 benchmark transient with internally, parallelly and CFD coupled HEXTRAN-SMABRE.

Neutronics and reactor core

The neutronics and reactor core -task in SADE achieved the following:

- further refinements in the accuracy of the neutronics of the reactor dynamics codes TRAB3D and HEXTRAN produced the initial discovery on how to develop neutronics models with significantly higher resolution of output information - this led to the development of the solver “Ants” as a part of the Kraken computational framework
- updated coupling of fuel behavior module FINIX to the neutronics solver
- adopting Serpent 2 as a practical tool for group constant generation
- adoption of group constants generated with Serpent 2 into use with TRAB3D and HEXTRAN

During the project, the Finnish Monte Carlo reactor physics code Serpent was adopted into practical use with the reactor dynamics codes TRAB3D and HEXTRAN. For TRAB3D, Serpent 2 was used both to produce input quantities as well as a development and analysis tool. A pin power reconstruction routine was implemented to TRAB3D, and Serpent 2 was used to generate pin power profiles it requires as an input (Sahlberg 2015). Serpent 2 was also used to verify the pin power reconstruction routine. This required producing two-group group constants with Serpent 2 as input parameters for TRAB3D as well as producing a 3D full core reference solution with Serpent 2.

With HEXTRAN, Serpent 2 was used to generate the two-group group constants and albedo boundary conditions required as an input for reactor analyses. This was demonstrated by modelling the V-1000 zero power facility at Kurchatov Institute using Serpent-HEXTRAN calculation chain (Sahlberg 2017 and 2017b).

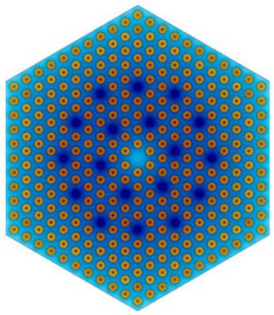

Figure 8: Serpent-generated plot of one of the 2D assembly geometries used for group constant generation for the V-1000 calculation case.

In addition, the modelling of axially heterogeneous fuel in TRAB3D was enhanced by developing a methodology to generate axial discontinuity factors and by implementing a corresponding axial discontinuity model into TRAB3D. A master's thesis was completed on the generation and use of these axial discontinuity factors (Sahlberg 2016). The analysis performed during the thesis work led to the discovery of alternative solutions for neutronics solvers. These alternative approaches were deemed more easily generalizable for issues such as axially heterogeneous fuel or small reactor cores than previous solutions. This discovery led to the beginning of the development of "Ants" reduced-order neutronics solver module for the Kraken computational framework (Sahlberg, Rintala 2018b).

The modelling of axially profiled fuel in HEXTRAN was also improved. Although axial profiling is not common in VVER-type reactors, it is relevant in cases such as modelling the first fuel load of a new, modern VVER power plant. Originally, HEXTRAN had been developed to assume axially homogeneous fuel composition, excepting axial burnup distribution. Therefore, modelling such cases called for the modifications to HEXTRAN.

The modification requirements to HEXTRAN were mapped (Sahlberg 2018), the required changes were implemented and a large portions of the implemented modifications were already verified during the project (Sahlberg 2019).

In addition to neutronics, some development and validation work has been done for fuel rod modelling. Fuel behaviour module FINIX was coupled with both TRAB3D and HEXTRAN during SAFIR2014. In SADE project this coupling has been renewed and early FINIX version has been replaced with the structurally fully renewed FINIX (Räty 2018). Several transients have been calculated in the SADE project in order to show performance of the FINIX-HEXTRAN coupling. Current version of the HEXTRAN code is also capable to model burnup-induced fuel rod deformations (Syrjälahti et al 2018c).

International co-operation

The cooperation and information exchange on VVER safety within the AER framework together with other countries that use VVER reactors has been continued.

SADE project has been at VTT responsible for official communication with AER including participation to scientific council. Two conference papers of SADE project have been presented in the AER symposium held in Helsinki in 2016 (Hovi et al. 2016; Sahlberg 2016). Achievements of the project has presented also in the annual meetings of the AER working group D on VVER safety analyses.

Participation in the OECD Nuclear Energy Agency (NEA) working groups and benchmarks has been one of the most important ways of validating the methods and codes used in reactor analysis. SADE project has included the participation in the meetings of the NEA Working Party on the Scientific Issues of Reactor Systems (WPRS) and its expert groups. WPRS is responsible for the organization of the reactor dynamics benchmarks among other activities. In the frame of the SADE project VTT continued participation in the OECD/NEA BWR stability benchmark (O2), in which main modelling effort was done during the SAFIR2014, and in 2018 participated to the kick-off meeting of the new Rostov-2 benchmark.

In the beginning of the project, some resources were reserved also to the reporting the research results of the predecessors of the SADE project and to minor development work, the need of which arises during the project. With these resources it was possible to present our reactor dynamics modelling in journals (Ikonen, et al., 2015; Ikonen, et al., 2016) and in conference papers (Syrjälahti, et al. 2015; Ikonen, et al., 2015b).

Summary

This paper summarizes achievements of the four-year SADE project, in which capabilities to model transients and accidents have been improved. We have developed tools for practical safety analyses and parallelly combined high-fidelity tools to conventional transient analysis methods. During this four-year project the coupling between VTT's reactor dynamics code HEXTRAN and system code SMABRE was extended with the new internally coupled simulation mode, which can be now used for routine safety analyses. Group constants created with Serpent-2 have been taken into use in VTT's reactor dynamics codes that makes it possible to use independent, domestic calculation tools for the all phases of the safety analyses. Several improvements have been done also to the neutronics modelling. In the SADE project, we have developed coupling between neutronics, plant modelling and CFD. We have simulated several transients and accidents using true two-way coupling between CFD code and reactor dynamics and system code.

References

Hovi, V., Taivassalo, V., Hämäläinen, A., Syrjälahti, E., & Räty, H. (2016). Start-up of a cold loop - the 7th AER benchmark calculation with Hextran-Smabre-Porflo. Proceedings of the 26th Symposium of AER, pp. 369-389. 10-14 October 2016, Helsinki, Finland.

Hovi, V., Taivassalo, V., Hämäläinen, A., Räty, H. & Syrjälahti, E. 2017. Start-up of a cold loop in a VVER-440, the 7th AER benchmark calculation with HEXTRAN-SMABRE-PORFLO. Kerntechnik 82(2107)4 page 426-435 DOI 10.3139/124.110820

Ikonen, T., Loukusa H., Syrjälahti E., Valtavirta V., Leppänen J. & Tulkki V. 2015a. Module for thermomechanical modeling of LWR fuel in multiphysics simulations. Annals of Nuclear Energy 84 (2015) 111–121. doi:10.1016/j.anucene.2014.11.004.

Ikonen, T., Syrjälahti, E., Valtavirta, V., Loukusa H., Leppänen, J. & Tulkki, V. 2015b. Multiphysics simulation of fast transients with the FINIX fuel behaviour module In: TopFuel 2015, 13-17 September 2015, Zurich, Switzerland, paper A0110. https://www.euronuclear.org/events/topfuel/topfuel2015/transactions/topfuel2015-transactions-oral-1.pdf. ISBN 978-92-95064-23-2.

Ikonen, T., Syrjälahti, E., Valtavirta, V., Loukusa, H., Leppänen, J. & Tulkki, V. 2016. Multiphysics simulation of fast transients with the FINIX fuel behaviour module. EPJ Nuclear Sci. Technol., 2 (2016) 37 DOI: http://dx.doi.org/10.1051/epjn/2016032

NEA (2010), VVER-1000 Coolant Transient Benchmark: Phase 2 (V1000CT-2), Final Specifications of the VVER-1000 MSLB Problem, NEA/NSC/DOC(2006)6, OECD/NEA, Paris.

Räty H. 2018. Coupling the fuel behaviour module FINIX-0.17.12 to the three-dimensional reactor dynamics code HEXTRAN 4.0, Research report VTT-R- 06735-18

Sahlberg V. 2015. Validating Pin Power Reconstruction Module with Serpent 2 – TRAB3D Code Sequence", special assignment, Research report VTT-R-04065-15

Sahlberg, V. 2016. Recalculating the steady state conditions of the V1000 zero power facility at Kurchatov Institute using Monte Carlo and nodal diffusion. Proceedings of the 26th Symposium of AER, pp. 485-497. 10-14 October 2016, Helsinki, Finland.

Sahlberg, V., 2016b. Modelling of axial discontinuities in reactor cores with Serpent 2 - TRAB3D code sequence, Master's Thesis, Aalto University. 59+6 p.http://urn.fi/URN:NBN:fi:aalto-201608263123

Sahlberg V. 2017. Recalculating the steady state conditions of the V-1000 zero-power facility at Kurchatov Institute using Monte Carlo and nodal diffusion codes. Kerntechnik September 2017, Vol. 82, No 4. Pages: 420–425. https://doi.org/10.3139/124.110810

Sahlberg V. 2017b. Calculating V-1000 Core Model With Serpent 2 - HEXTRAN Code Sequence", M&C 2017 International Conference on Mathematics & Computational Methods Applied to Nuclear Science and Engineering, Jeju, Korea, April 16-20, 2017. Paper P260S06-03SahlbergV.

Sahlberg V. 2018. Modifications to axial material models in HEXTRAN. Research report VTT-R-00844-18

Sahlberg V. 2019. Changelog and report on notable changes to the HEXTRAN code for heterogeneous fuel modelling. Research report VTT-R-00045-19

Sahlberg V. & Rintala, A. 2018b. Development and preliminary verification of a new rectangular nodal diffusion solver of ANTS. Physor 2018, April 22 – 26, 2018 Cancun, Q.R., Mexico

Syrjälahti E., Valtavirta V., Kättö J., Loukusa H., Ikonen T., Leppänen J. and Tulkki V. 2015. Multiphysics simulations of fast transients in VVER-1000 and VVER-440 reactors. In: 11th International Conference on WWER fuel performance, modelling and experimental support. 26 September – 03 October 2015, Golden Sands Resort, Bulgaria

Syrjälahti, E. 2016.HEXTRAN-SMABRE version 4060 with internal coupling between the HEXTRAN and SMABRE codes, Research report VTT-R-00457-16

Syrjälahti E. 2018a. Kalinin-3 -- Model report and simulation of the benchmark problem. Research report VTT-R-06914-18. 29p.

Syrjälahti E. 2018b. HEXTRAN-SMABRE development and validation of the internally coupled simulation mode in 2018. Research report VTT-R-06913-18. 27 p.

Syrjälahti, E., Ikonen, T. & Tulkki, V.. 2018c. Modeling burnup-induced fuel rod deformations and their effect on transient behavior of a VVER-440 reactor core, Annals of Nuclear Energy,Volume 125,2019,Pages 121-131,ISSN 0306-4549, https://doi.org/10.1016/j.anucene.2018.10.039.

4.4 Nuclear criticality and safety analyses preparedness at VTT (KATVE)

Pauli Juutilainen[1], Eric Dorval[1], Toni Kaltiaisenaho[1], Jaakko Leppänen[1], Antti Räty[1], Risto Huhtanen[1], Silja Häkkinen[1], Mika Jokipii[1], Petri Kotiluoto[1], Juho Peltola[1], Karin Rantamäki[2], Ville Valtavirta[1], Riku Tuominen[1], Tuomas Viitanen[2]

[1]VTT Technical Research Centre of Finland Ltd
P.O. Box 1000, FI-02044 Espoo

[2]VTT at the moment of contribution

Abstract

Developing the capabilities in criticality safety, radiation shielding, activation analysis, dosimetry and dry storage modelling has been the main objective in the KATVE project. The development consists of both code and method development as well as educating new experts. The work on criticality safety has mostly consisted of assembling the validation package for fresh fuel criticality analysis and creating competence to utilize burnup credit in the spent fuel criticality safety studies. Photon transport routines have been developed to the Serpent Monte Carlo code in order to expand its applicability from reactor physics and burnup calculation to various radiation shielding applications. Dry storage cask has been a new research subject in the Finnish scope. The heat transfer in such a cask has been computed to determine the peak cladding temperature of the stored fuel pins as a function of time. The information was used to evaluate the fuel integrity in the cask. The activation analysis and dosimetry capabilities have been maintained: the MAVRIC code has been taken into use and new experts have been educated to use the dosimetry calculation chain.

Introduction

The KATVE project covers a group of research themes that are at least loosely connected to reactor physics, in addition to which a new research subject, dry storage facility, has been part of the project. The project aims at improving the analysis preparedness in the selected fields, which requires both code development and educating new experts.

Criticality safety is one of the subjects that has been neglected at VTT in the recent history, but during the SAFIR2014 programme it was addressed more strongly than earlier. For example, the work to construct a proper validation package restarted after a hiatus of more than a decade and it was continued throughout the latest programme. Constructing such a package is a long-lasting task and can

hardly ever be judged fully completed, but significant progress has been made. As a goal, it should provide the correct bias of the computational system and thus enable the criticality safety analysis fulfilling the international standards.

Development of photon transport functionalities to the Serpent Monte Carlo code has been another major topic in the project. These functionalities enable the code to be used for radiation shielding analyses. When expanding the scope of the code from reactor physics to radiation transport, new particle interaction models are required and have been developed. For computational efficiency, variance reduction methods are necessary. They have, therefore, been an important part of the work.

Neutron dosimetry and activation analysis comprise the third topic included in the project. Dosimetry is used to estimate the damage caused by the fast neutron irradiation to the structures inside the reactor pressure vessel. During the programme, the main focus in the task, however, was in educating new experts following personnel changes in the field, but simultaneously new codes were taken into use and old manuals and scripts updated and clarified.

The safety of dry storage casks was chosen to be a part of the studies in KATVE. Used fuel rods from nuclear power plants have to be contained in interim storage facilities for approximately 40 years before the final disposal, even though longer periods up to 100 years have been suggested. Storage pools have been the established solution to the problem in Finland, but the idea of dry storage has also raised some interest. The safety aspects for such storage include radiation shielding, criticality safety, containment and structural safety and heat removal capacity. The whole chain includes analysis of heat decay rate of used fuel, heat transfer and temperature estimate of the cask and fuel at selected time and analysis of integrity of fuel rods under these conditions over the whole storage history. The computing chain was demonstrated in the KATVE project.

Criticality Safety

The work of improving criticality safety analysis capabilities has consisted of developing the criticality safety validation package and acquiring general understanding about the requirements and international practicalities related to the usage of burnup credit (BUC) in spent fuel storage configurations. The criticality safety analyses in general is preferably performed with continuous-energy Monte Carlo codes. The bias of the computing platform that consists of the software, cross-section library, operating system and hardware needs to be carefully defined through calculations against well-documented, high-quality critical experiments. The defined bias is used in the criticality safety analyses as an extra safety margin in addition to the standard subcriticality margin set by the regulator. The progress has been annually reported as VTT reports. The last of these (Juutilainen, 2019) provides a somewhat larger summary on the whole package, in addition to the description of the activities in the reported year 2018.

The validation package has been assembled for the MCNP (Goorley, 2012) and Serpent (Leppänen, 2015a) Monte Carlo codes at VTT over the recent years. In the

end of the SAFIR2018, the package contains 208 critical experiments for MCNP and 507 for Serpent, all documented in the International Handbook of Evaluated Criticality Safety Benchmark Experiments.

A significant fraction of these are based on the MCNP inputs that VTT obtained from the Dutch NRG in 2016. Out of the more than 2000 inputs received, 365 are suitable for the validation package. These have been beneficial also for the package of Serpent with the help of a conversion script. However, according to the general instructions of the validation processes, the inputs obtained from elsewhere need to be reviewed before used, due to which the above-mentioned numbers of inputs in the package is smaller than the number of inputs available. Additionally, 180 Serpent inputs were obtained from Czech collaborators in the end of the programme. These could be later verified and added to the package.

The number of the critical inputs modelled to the package could be sufficient in principle. However, the mere number of cases does not prove the sufficiency, but the neutronic properties of the critical experiments used in validation have to be similar to the target configuration. Additionally, the independency between the modelled experiments should be considered. Majority of the modelled experiments have been performed at relatively few facilities, which somewhat limits the effective extent of the package. Therefore, new critical experiments may have to be modelled.

The first sets of experimental series added to the package were VVER-440 and VVER-1000 type configurations, whose most distinct feature is the core consisting of hexagonal fuel assemblies. These experiments have been mostly performed at the Hungarian ZR-6 reactor, Czech LR-0 and Russian SF-9 and facility P, located at Kurchatov Institute. The package has later been extended to square-lattice experiments, performed mostly at CEA Valduc in France or at Pacific Northwest Laboratory (PNL) in the USA.

The large number of inputs has to be run and analysed automatically, for which a validation script has been and is still developed. Running the calculations and performing the statistical analyses based on the calculated k_{eff} values and the related computational as well as experimental uncertainties are the key functions of the script to determine the systematic bias of the computing platform. The statistical analysis is based on the instructions presented in the validation guide by Dean & Tayloe (Dean, 2001).

The script currently calculates the bias for both MCNP and Serpent, but for a proper validation report it is also important to include trend analysis of various parameters affecting the neutronics, such as uranium-235 enrichment, boron concentration in the moderator, lattice pitch and fuel-to-moderator ratio. The required function has been implemented to the script, but it can work only if the parameters are given in a standardised manner, either in the code input or in separate file. For Serpent, the parameters are given in the inputs, even though not in fully consistent manner, but the MCNP inputs do not contain any parameters yet.

The package described above is related to criticality safety analyses with fresh fuel assumption. When spent fuel storage and transportation systems are considered, the capability to take into account the decreased reactivity as a consequence of fissile fuel depletion - the concept known as burnup credit (BUC) - has become

essential. However, the capability has not been built at VTT as much as it should have, but within KATVE project some preliminary steps were taken in order to improve the situation. At first, a literature survey was conducted to explore the international and national standards and practicalities related to the topic. As the next step, the burnup functionality of Serpent was tested against the OECD/NEA Burnup Credit Benchmark Phase VI with experimental PIE data on spent VVER-440 fuel assembly. These studies have provided some new information on the code's performance and a little on the impact of various computational parameters, but further studies are required.

Photon transport and variance reduction in Serpent

The implementation of a photon transport mode in the Serpent code started outside the KATVE project, originally for the purpose of accounting for gamma heating in coupled multi-physics simulations (Leppänen, 2015b). The photon transport mode was introduced in 2015 (Kaltiaisenaho, 2016) and have been further developed since (Kaltiaisenaho, 2019a). The capability to model photons in addition to neutrons, however, enabled broadening the scope of Serpent applications beyond reactor physics. The focus in the KATVE project has been in radiation shielding and transport applications, but the methodology can be applied to other fields as well, such as fusion research. In addition to implementing the physics routines for photon transport, the KATVE project has involved work related to the production of radioactive source terms and variance reduction. The work has also involved implementing special detector types for photon transport calculations, such as dose and pulse-height detectors.

The photon physics model is capable of simulating photon interactions with the elements from Z=1 to 99 over the default energy range from 1 keV to 100 MeV. The four main photoatomic interaction mechanisms – the photoelectric effect, Rayleigh scattering, Compton scattering and electron-positron pair production – are modeled with detailed state-of-the-art interaction models. Bremsstrahlung photons emitted by secondary electrons and positrons are treated with a so-called thick-target bremsstrahlung (TTB) approximation. Fluorescence photons emitted as a result of the photoelectric effect and Compton scattering are also included. For storing photon cross section and interaction data, Serpent uses the Photon, Atomic relaxation and Electron library (PAELib) which was developed in the MONSOON project. PAELib supports multiple different data libraries; the currently recommended data library is mostly based on the EPDL97 photoatomic (Cullen, 1997) and EADL91 atomic relaxation (Perkins, 1991) libraries. Validation of the photon transport mode was started in 2017 (Valtavirta, 2017) by calculating a set of MCNP photon transport benchmark problems (Whalen, 1991). Good agreement was obtained between Serpent and MCNP6.1, but moderate differences between experimental data and both codes were observed. The validation work will be continued in the RACSA project of SAFIR2022.

In addition to the photoatomic reactions mentioned above, treatment of photonuclear reactions was also developed in Serpent (Kaltiaisenaho, 2019b). The capability to simulate photoneutron production is needed for applications such as neutron shielding, neutron source generation, beryllium reflectors and heavy water moderated reactors. Data-based approach is used for simulating photonuclear reactions, which utilizes the same reaction sampling methods that are used for neutrons in Serpent, with the exception of relativistic collision kinematics and frame-of-reference transformation (Caro, 2016) required for photons. Because photonuclear reaction probabilities are always low (less than 5%), a variance reduction technique known as forced collisions was implemented which produces photoneutrons on every photon interaction whenever possible.

A radioactive decay source mode was developed in Serpent in order to perform radiation transport calculations involving radioactive materials. Serpent reads radioactive decay data from ENDF format data libraries and forms the source term by combining the compositions of radioactive materials to nuclide-wise emission spectra. The decay source is set by simply defining the composition of the radioactive material, which is done automatically after a neutron activation or burnup calculation. The decay source mode can simulate the emission of gammas, neutrons and bremsstrahlung emitted by beta particles and internal conversion electrons. Beta spectra are calculated with a built-in model (Kaltiaisenaho, 2018) from the ENDF format decay data, or alternatively ICRP-107 beta spectrum data (Eckerman, 2008) can be used, and bremsstrahlung photons are created with the TTB approximation mentioned above. The most relevant application for the radioactive decay source mode in KATVE is a shielding calculation performed for a spent fuel transport or storage cask, in which the irradiated material compositions are obtained from Serpent burnup calculations. The methodology has also been applied for the calculation of shut-down dose rates in a fusion reactor (Sirén, 2016; Leppänen, 2016). Even though this study was part of an effort to broaden the scope of Serpent applications to new fields, the challenging test case made it very relevant considering methods developed within the KATVE project..

Radiation shielding applications involve calculation of dose rates in locations isolated from the source by physical barriers. This type of geometry is challenging for the Monte Carlo method, and in practice requires efficient use of variance reduction techniques. Serpent was originally developed as a reactor physics code, and variance reduction for shielding applications is therefore a new topic and challenge. The implemented approach is based on the use of weight-windows on a super-imposed Cartesian or cylindrical mesh (Leppänen, 2017). The importance map can be read from standard WWINP format files used by the MCNP code (Pelowitz, 2013). This enables the use of state-of-the-art variance reduction tools, such as ADVANTG (Mosher, 2013) or MAVRIC (Peplow, 2011). An alternative approach is to calculate the importances using a light-weight built-in solver based on the response-matrix method. The development of the internal solver was completed in 2017-2018. The methodology supports multiple detectors and provides a global variance reduction scheme for deep-penetration problems. A comprehensive methodological description is provided in a paper submitted to Nuclear Technology. The variance reduction

capabilities are currently being applied to shielding calculations involving the hot-cell facilities at VTT's Centre for nuclear safety.

Neutron dosimetry and activation analysis

In-core neutron flux calculations are required at VTT mainly as input quantities for dosimeteric calculations to study the effect of neutron irradiation on material properties. The calculations cases are often so complicated that deterministic codes are preferred to heavier Monte Carlo methods, however, a combination of the two can also be a valid option in some cases. Adopting new codes and educating new experts due to changes in personnel were the key features in the field during the project.

Discrete ordinates codes DORT and TORT (DOORS, 2017) (Rhoades, 1997) have been used earlier, but they are no longer developed or updated and contain some outdated features. Therefore the MAVRIC (Monaco with Automated Variance Reduction using Importance Calculations) code (Peplow, 2011) was chosen to possibly replace these codes gradually. MAVRIC is under constant active development and is also integrated into the SCALE code package (ORNL, 2017) that has been used in VTT for a long time. It combines deterministic and Monte Carlo in order to utilize the strengths of both methods, that is, to provide a coarse solution with fast deterministic calculation and use the data in a more detailed Monte Carlo calculation. MAVRIC was introduced at VTT through training and testing it with two separate calculation cases: the Kobayashi benchmark (Kobayashi, 2000) and dosimeter samples irradiated at Loviisa power plant (Räty, 2015; Räty 2017). These exercises provided valuable information about the strengths and deficits of the code.

The Loviisa case was also calculated with Serpent as one of the first test cases for the newly developed variance reduction methods (Viitanen, 2016). Figure 1 depicts the importance map used in the case. The variance reduction technique decreased the calculation time requirement by factor 100–700.

LSL-M2 code in neutron dosimetry

The neutron adjustment program LSL-M2 (Stallman, 1986) has been used in dosimetry work at VTT for several years. Along the history of use of this program, several users have been responsible for dosimetry work, in addition to numerous changes in the computer architecture and operating systems used. These changes pose challenges from the point of view of knowledge retention; use of best practices; and software portability.

Research report (Viitanen, 2015) provides a concise hands-on guide for the use of LSL-M2 with particular emphasis on the processing of input data for the code, which is an aspect not readily available in the program documentation. The processing of data is clearly divided into two parts: the generation and migration of multi-group cross section data among different group structures, and the estimation of relative covariances.

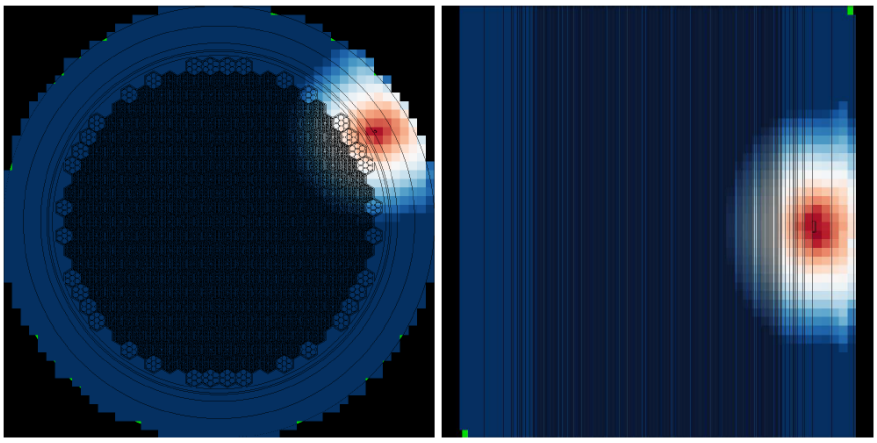

Figure 1. Importance map used in the variance reduction. White color corresponds to importance of 1, red means high importance and blue is for low importance.

This work was instrumental in identifying shortcomings and bottlenecks in data processing. The codes PREPRO (Dermott, 2015) and NJOY (NJOY, 2013) were put to use in the generation of multi-group dosimetry XS data. This work also included the development of scripts for rigorous estimation of activity correlation matrices. The resulting research report included an overall description of the steps involved in a spectral unfolding problem, with experimental data from the FiR research reactor. This report was also a valuable guide for the new successor who took over the next KATVE dosimetry task.

On the use of VTT's dosimetry tools

This work was undertaken by the new dosimetry practitioner, and was focused around the use of most of VTT's dosimetry tools, including the Serpent model of the Loviisa reactors. In order to better understand the generation of weight windows with the built-in importance solver in Serpent, and compare the performance against other ways of calculating weight windows, a duplicate model was developed in MCNP. Whereas the values obtained using either set of weight windows were comparable within statistics, the use of the importance maps generated by Serpent lead to better computational performance.

Predicted specific dosimeter activities were compared against experimental data and also against results of the PREVIEW code, and several of the modeling assumptions were studied in detail. In particular, it was observed that the effect of the irradiation history on short-lived activation products could be significant (Figure 2), and therefore several transport runs should be carried with Serpent.

In spite of the improved computational efficiency of Serpent, a detailed irradiation history encompassing several operation cycles is still too demanding. However, one of the conclusions of this work (Dorval, 2017) highlights that Serpent can be used

for the generation of kernel data for PREVIEW. In this way, the accuracy of Serpent can be combined with the speed of the (deterministic) PREVIEW code.

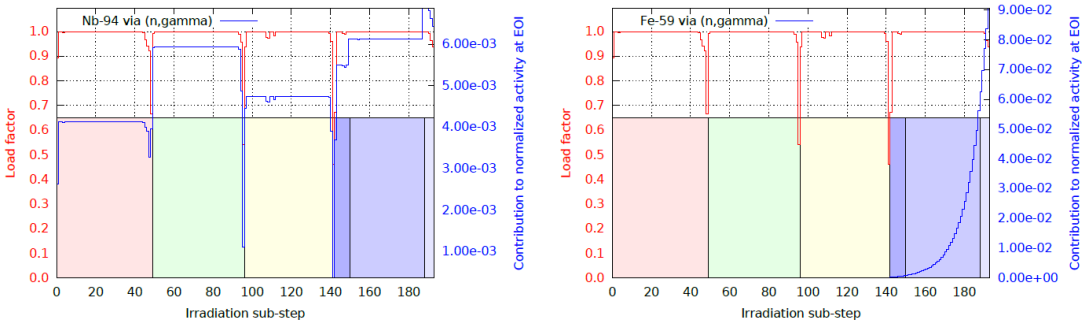

Figure 2. Time-step-wise load factors and contributions to final calculated specific activities of ^{94}Nb (left) and ^{59}Fe (right) at the end of the last cycle. Reaction rates were calculated with Serpent once per cycle. Cycles are depicted by colored boxes. Shades of blue in the last box indicate further refinement in the last cycle, where three transport calculations were conducted.

Generation of dosimetry libraries for spectral adjustment

This work (Dorval, 2018) entailed a thorough revision of all the steps involved in the generation of a traceable set of input data files and programs to be used for a practical spectral adjustment exercise. The main results consisted of a "roadmap" (Figure 3) for the production of traceable, consistent input data for LSL-M2, as well as a vast number of processing scripts and functions to produce such input data in an automated fashion. Some of the scripts were based on previous work.

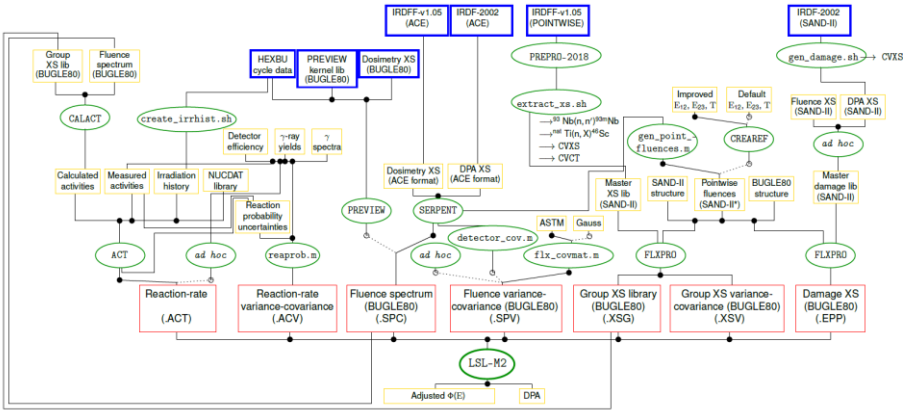

Figure 3. Most relevant input data files and programs/scripts involved in the solution of a spectral adjustment problem with the LSL-M2 computer code.

Amongst others, the scripts allow the user to adopt the latest dosimetry XS data from IRDF-2002 and IRDFF (Zsolnay, 2012) for the production of problem-dependent cross section libraries, including the cross sections' associated correlation matrices.

With regards to flux correlation matrices, four different formalisms (Figure 4) were tested, including a novel proposal that relies entirely on statistical correlations obtained through a modified version of Serpent plus post-processing tools.

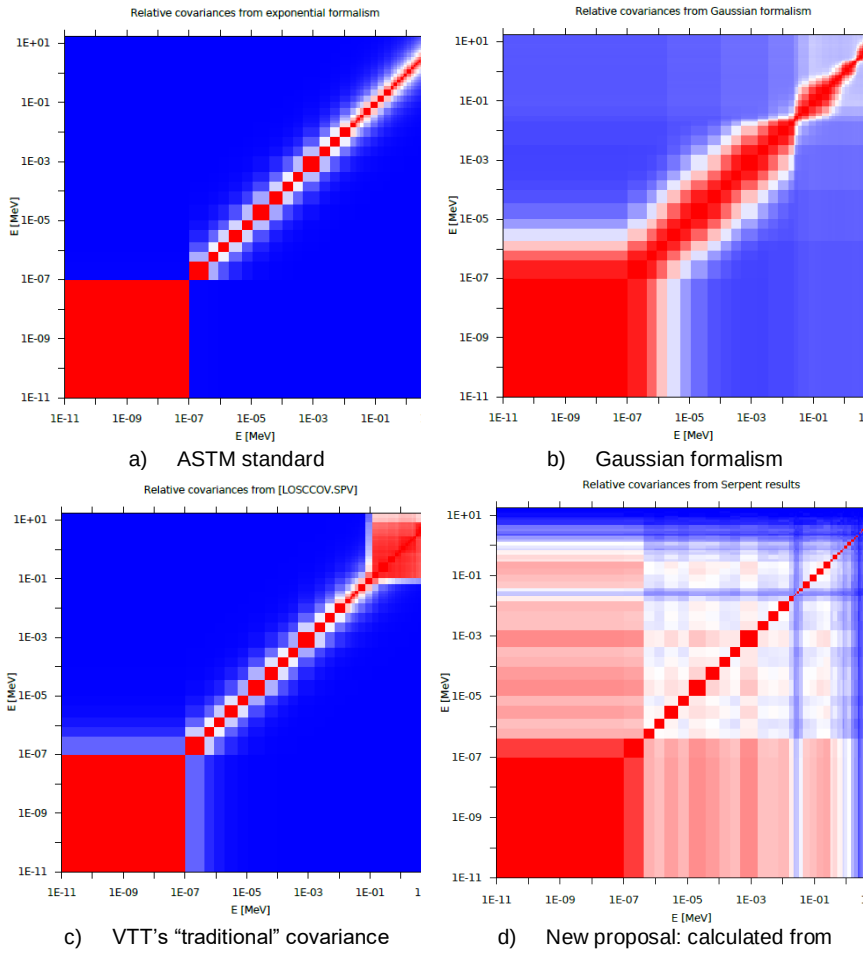

a) ASTM standard

b) Gaussian formalism

c) VTT's "traditional" covariance matrix

d) New proposal: calculated from Serpent runs

Figure 4. Different flux correlation coefficient matrices studied.

The similar group structures and file formats shared between the dosimetry libraries of LSL-M2 and PREVIEW results in that the tools generated in this work are also readily applicable to the creation of dosimetry libraries for PREVIEW, too.

All the work conducted in the dosimetry task of KATVE allowed the education of a new practitioner in several aspects. In this way, competences were retained at VTT and further developed, including the use of tools developed in-house. Gaining expertise in all possible aspects of reactor dosimetry is a long term goal. KATVE was instrumental in addressing the main priorities and developmental needs for future reactor dosimetry work. It is expected that international cooperation will strengthen and that the work proposed for the next SAFIR programme shall benefit greatly from the work conducted in KATVE.

CFD and fuel integrity analysis of spent fuel in dry storage cask

Air-cooled dry storage of spent nuclear fuel is widely used abroad but not applied in Finland. Prior to this project, no domestic experience on the thermal hydraulic analysis of cooling of such facilities existed. As the first step of the project, the heat transfer and peak cladding temperature (PCT) of spent fuel rods were investigated in a single dry storage cask (Huhtanen et al. 2016a) for fuel after seven years of cooling in a water pool. Computational Fluid Dynamics (CFD) heat transfer calculations were performed with OpenFOAM version 3 (OpenFOAM Foundation, 2015). The spent 17x17 PWR fuel was assumed to be stored in a helium-filled Castor® V/21 cask (Dziadosz, 1986), shown in Figure 5.

As a boundary condion for the CFD, the decay heat was calculated according to the instructions of the BEAVRS benchmark (Horelik, 2013) with the Serpent Monte Carlo reactor physics burnup code. Some simplifications were made in the burnup calculation, but the model can be considered representative regarding irradiation of an average assembly in a reactor core.

The CFD analysis was found to be consistent with the experimental results, although the experimental setup was not exactly the same as simulated here. In the next phase (Huhtanen, 2016b), the model was slightly improved and the calculations were extended to cover a longer period up to 300 years.

The obtained PCT history was then used as a boundary condition when studying the fuel rod cladding integrity in interim dry storage (Arkoma et al., 2018). The analysis was performed with VTT-ENIGMA fuel performance code (Kilgour et al., 1992), the main parameters of interest being the cladding creep hoop strain and stress in dry storage. Dry storage creep correlations from open literature had been implemented into VTT-ENIGMA in SAFIR2014 SPEFU project. Later on, the risk of hydride induced cladding failure in the same case was evaluated (Arkoma, 2018) with the BISON fuel performance code (Newman et al., 2009). BISON has been augmented (Courty et al., 2014; Stafford, 2015) with hydride modelling capabilities: hydrogen diffusion, precipitation into hydrides, and dissolution.

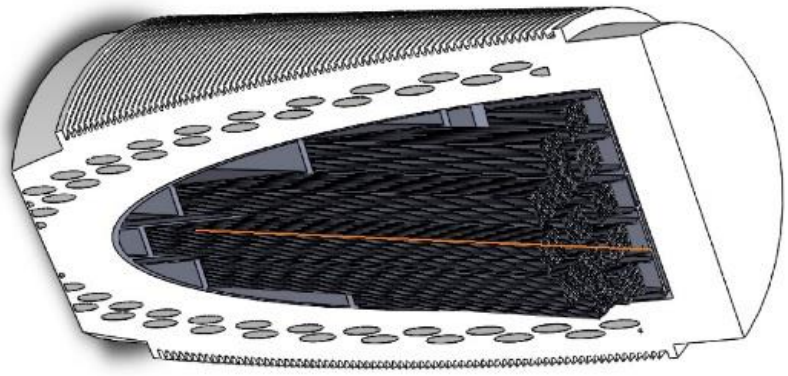

Figure 5. Dry storage cask layout with fuel assemblies, basket inside the cask, and absorber rods. The cask height and diameter are 4.9 m and 2.4 m, respectively. Figure reproduced from Arkoma et al. (2018) with permission.

Within this task, Serpent – OpenFOAM – VTT-ENIGMA calculation chain for dry storage analysis was demonstrated, and complementary hydride induced cladding failure study with BISON conducted. An average burnup of 50 MWd/kgU was applied at all successive stages of the calculation chain.

Results

The total heat rate in dry storage depends on the fuel irradiation history and the duration of the preceding wet storage. Fuel assemblies are kept in storage pools for several years, and the activity reduces exponentially during that time. The heat source of one rod after various cooling times is shown in Figure 6a, as calculated with Serpent. The total heat of a cask with 21 fuel assemblies is shown in Figure 6b.

The CFD simulations were performed as steady state analyses with each instant of time having its own heat load. The heat load changes so slowly that the flow at each instant of time can be considered as quasi-steady.

In order to make the analysis conservative with respect to the cladding maximum stress and creep in dry storage, the pool storage period was limited so that the temperature at the beginning of dry storage would reach approximately 400 °C, a limit temperature used in the USA (U.S.NRC, 2010). To achieve this, the heat rate profile at four years of pool storage was increased by 20%. This represents the situation approximately at 3.4 years. The resulting cladding temperature profiles at different cooling times are shown in Figure 7, as well as the general temperature field at four years. The cooling air flows upwards of the assemblies and the cooling

rate is best at the bottom of an assembly, leading to minimum temperatures being at the bottom of the rods.

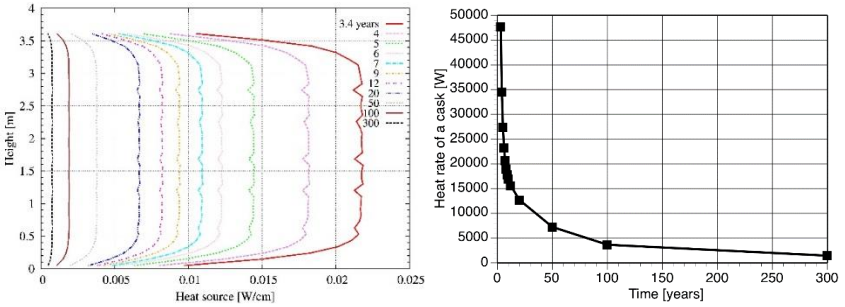

Figure 6. a) Heat release rate along a single rod as calculated with the Serpent code. b) Total heat rate in a cask with 21 fuel assemblies. Figures reproduced from Arkoma et al. (2018) with permission.

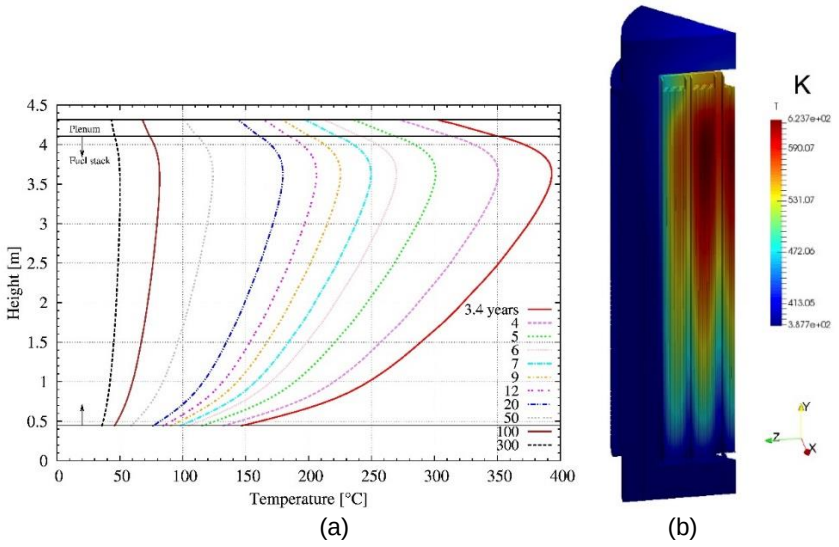

Figure 7. a) Cladding temperature profiles at the location of maximum temperature after various cooling times according to the CFD simulations. Location of the maximum temperature is in the same rod and height up to 100 years. At 300 years the location of maximum temperature moves to the middle assembly, but the temperature difference between the locations is very small. The graph gives the temperature profile at 300 years at the original 'hot spot'. b) Temperature field at four years after unloading from the reactor. Figures reproduced from Arkoma et al. (2018) with permission.

Evolutions of cladding creep and circumferentially averaged cladding hoop stress are shown in Figure 8. The two creep correlations produce consistent results compared to each other. Creep is well below 1%, a safety level considered in some countries, and thus the cladding is not likely to fail in this case due to creep.

The stress required for hydride radial reorientation in irradiated cladding is not well known. The maximum calculated cladding stress (95th percentile), 74 MPa, is close to some reorientation thresholds found in literature (Daum et al., 2005, 2006), and thus the cladding could potentially be susceptible to hydride reorientation and consequently brittle failure. However, it is unlikely that the hydride content calculated with BISON (Figure 9) is high enough to lead to a through-wall cladding failure. The maximum hoop stress during dry storage according to BISON was 78 MPa.

BISON results are typical and consistent compared to the hydrogen/hydride phenomena. Hydrogen and hydride evolutions during base irradiation, wet and dry storage are shown in Figure 9a. Steep and relatively narrow hydride rim is formed close to the colder cladding outer surface when hydrogen precipitates into hydrides during dry storage, Figure 9b.

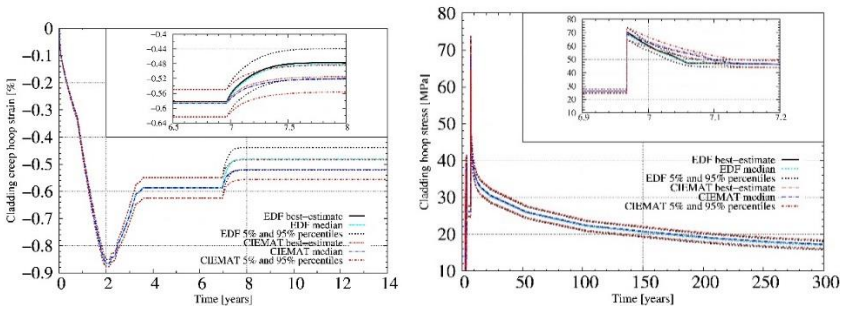

(a) (b)

Figure 8. a) Cladding creep and b) circumferentially averaged hoop stress calculated with VTT-ENIGMA. Figures reproduced from Arkoma et al. (2018) with permission.

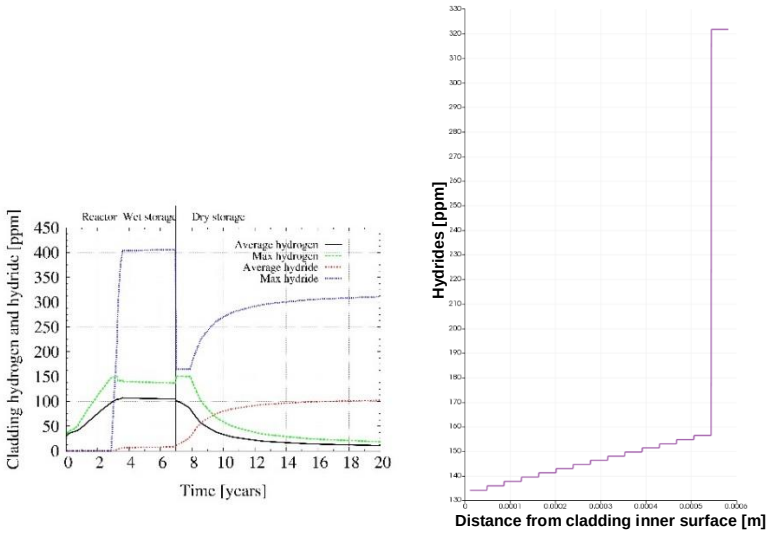

(a) (b)

Figure 9. a) Hydrogen and hydride evolutions during base irradiation, wet and dry storage, as calculated with BISON (Arkoma, 2018). b) Cladding radial hydride distribution at 40 years, counting from the start of the irradiation (Arkoma, 2018). This figure is plotted from the location of peak axial hydrogen/hydride content.

References

Arkoma, A., 2018. Modelling cladding hydrides in interim dry storage. VTT Research report, VTT-R-05604-18, Nov. 2, 2018, 18 p.

Arkoma, A., Huhtanen, R., Leppänen, J., Peltola, J., Pättikangas, T., 2018. Calculation chain for the analysis of spent nuclear fuel in long-term interim dry storage. Annals of Nuclear Energy, Vol. 119, pp. 129–138

Caro, E. 2016. Relativistic kinematics for photoneutron production in Monte Carlo transport calculations, Annals of Nuclear Energy, Vol. 96, 170-175, 2016

Courty, O., Motta, A.T., Hales, J.D., 2014. Modeling and simulation of hydrogen behavior in Zircaloy-4 fuel cladding. Journal of Nuclear Materials, Vol. 452, pp. 311-320

Cullen, D. E., Hubbell, J. H. and Kissel L. 1997. EPDL97: the Evaluated Photo Data Library '97 Version. UCRL-50400, Vol. 6-Rev. 5, Lawrence Livermore National Lab, 1997.

Daum, R.S., Majumdar, S., Liu, Y., Billone, M.C., 2005. Mechanical testing of high-burnup Zircaloy-4 fuel cladding under conditions relevant to drying operations and dry-cask storage. In proceedings of: 2005 Water Reactor Fuel Performance Meeting, Kyoto, Japan, Oct. 2-6, 2005

Daum, R.S., Majumdar, S., Liu, Y., Billone, M.C., 2006. Radial-hydride embrittlement of high-burnup Zircaloy-4 fuel cladding. Journal of Nuclear Science and Technology, Vol. 43, pp. 1054–1067

Dean, J. C. and Tayloe, R. W. 2001. Guide for Validation of Nuclear Criticality Safety Calculational Methodology. Technical report, U.S. Nuclear Regulatory Commission, 2001.

Dermott, E. C. E., 2015. E. C. E. Dermott, *PREPRO 2015, 2015 ENDF/B Pre-processing Codes,* IAEA-NDS-39, 2015

DOORS 2017. One, Two- and Three-Dimensional Discrete Ordinates Neutron/Photon Transport Code System, RSICC web page, http://www-rsicc.ornl.gov/codes/ccc/ccc6/ccc-650.html

Dorval, E. 2017. On the use of VTT's dosimetry tools, VTT Reseearch report VTT-R-03566-17, 2017.

Dorval, E. 2018. Generation of problem-dependent, traceable dosimetry libraries for reactor fluence spectral adjustment, VTT Research report VTT-R-04159-18, 2018.

Dziadosz, D. & Moore, E. V. 1986. The Castor-V/21 PWR Spent-Fuel Storage Cask: Testing and Analyses. EPRI NP-4887. November 1986. 262 p.

Eckerman, K. and Endo, A. 2008. ICRP Publication 107. Nuclear decay data for dosimetric calculations, Annals of the ICRP, Vol. 38(3), 7-96, 2008

Evans T. M. 2010. DENOVO: A New Three-Dimensional Parallel Discrete Ordinates Code in Scale, Nuclear Technology 171 (2010), pp. 171–200

Goorley, T. et al. 2012. Initial MCNP6 Release Overview. Nuclear Technology, 180 (2012) 298–315.

Horelik, N. & Herman, B. 2013. BEAVRS. Benchmark for Evaluation And Validation of Reactor Simulations. Release rev. 1.1.1. MIT Computational Reactor Physics Group. October 30, 2013. 163 p.

Huhtanen, R., Peltola, J. & Leppänen, J. 2016a. Heat transfer in dry storage cask. VTT Research report, VTT-R-00810-16. 26p.

Huhtanen, R., Peltola, J. & Leppänen, J. 2016b. CFD analysis of varying cooling times for the fuel. VTT Research report VTT-R-05236-16. 22p

Juutilainen, P. and Valtavirta, V. 2019. Status of the criticality safety validation package in 2018. VTT Research report VTT-R-00228-19. 28 + 4 p.

Kaltiaisenaho, T. 2016. Implementing a photon physics model in Serpent 2, Master's thesis, Aalto University, 2016

Kaltiaisenaho, T. 2018. Implementing a beta bremsstrahlung source in Serpent, Tech. rep., VTT Research Report VTT-R-00953-18, VTT Technical Research Centre of Finland Ltd, 2018.

Kaltiaisenaho, T. 2019a. Photon transport physics in Serpent 2 Monte Carlo code. Submitted to Radiation Physics and Chemistry, 2019

Kaltiaisenaho, T. 2019b. Photonuclear reactions in Serpent 2 Monte Carlo code. Extended summary submitted to the M&C2019 conference to be held in Portland, OR, August 25-29, 2019.

Kilgour, W.J., 1992. The ENIGMA fuel performance code, users guide, version 5.8d. Berkeley Nuclear Laboratories, TD/NS/REP/0034

Kobayashi, K., Sugimura, N. & Nagayay, Y. 2000. 3-D Radiation Transport Benchmark Problems and Results for Simple Geometries with Void Regions, Organisation for Economic Co-operation and Development Nuclear Energy Agency

Mosher, S. et al. 2013. ADVANTG – An Automated Variance Reduction Parameter Generator. ORNL/TM-2013/416, Oak Ridge National Laboratory (2013).

Newman, C., Hansen, G., Gaston, D., 2009. Three dimensional coupled simulation of thermomechanics, heat, and oxygen diffusion in UO2 nuclear fuel rods. Journal of Nuclear Materials, Vol. 392, pp. 6–15

Leppänen, J., Pusa, M., Viitanen, T., Valtavirta, V. & Kaltiaisenaho, T. 2015a. The Serpent Monte Carlo code: Status, development and applications in 2013. Annals of Nuclear Energy, 82 (2015) 142–150

Leppänen, J., Hovi, V., Ikonen, T., Kurki, J., Pusa, M., Valtavirta, V. and Viitanen, T. 2015b. The Numerical Multi-Physics project (NUMPS) at VTT Technical Research Centre of Finland. Ann. Nucl. Energy, 84 (2015) 55-62.

Leppänen, J. and Kaltiaisenaho, T. 2016. Expanding the Use of Serpent 2 to Fusion Applications: Shut-down Dose Rate Calculations. In proc. PHYSOR 2016, Sun Valley, ID, May 1-6, 2016.

Leppänen J., Viitanen T., Hyvönen O. 2017. Development of a Variance Reduction Scheme in the Serpent 2 Monte Carlo Code, M&C 2017 - International Conference on Mathematics & Computational Methods Applied to Nuclear Science & Engineering, Jeju, Korea, April 16–20, 2017

NJOY 2013. The NJOY Nuclear Data Processing System, Version 2012. Los Alamos National Laboratory, LA-UR-12-27079 Rev, 2013.

OpenFOAM Foundation2015. OpenFOAM 3.0.1, http://www.openfoam.org, OpenFOAM Foundation, 2015.

ORNL 2017. Oak Ridge National Laboratories, SCALE – A Comprehensive Modelling and Simulation Suite for Nuclear Safety Analysis and Design, http://scale.ornl.gov/

Pelowitz, D. (editor). 2013. MCNP6 User's Manual: Appendix C Mesh-Based WWINP, WWOUT, and WWONE File Format. LA-CP-13-00634, Los Alamos National Laboratory (2013).

Peplow, D. E. 2011. MAVRIC: Monaco with Automated Variance Reduction Using Importance Calculations, Oak Ridge National Laboratories ORNL/TM-2005/39, version 6.1

Perkins, S. T., Chen, M. H., Cullen, D. E. and Hubbell, J. H. 1991. Tables and graphs of atomic subshell and relaxation data derived from the LLNL Evaluated Atomic Data Library (EADL), Z=1-100, Lawrence Livermore National Laboratory, UCRL-50400, Vol. 30, 1991

Rhoades, W.A. 1997. The TORT Three-Dimensional Discrete Ordinates Neutron/PhotonTransport Code. Oak Ridge National Laboratories, ORNL/TM-13221, 1997

Räty, A. 2015. Kobayashi benchmark MAVRIC-ohjelmalla, VTT tutkimusraportti VTT-R-06333-15. 2015. 20 p. + app. 2 p. (in Finnish)

Räty, A., 2017. Calculating the cumulative flux of VVER-440 dosimeters with MAVRIC and KENO, VTT Research Report VTT-R-00380-17

Sirén, P. and Leppänen, J. 2016. Expanding the use of Serpent 2 to Fusion Applications: Development of a Plasma Neutron Source. In proc. PHYSOR 2016, Sun Valley, ID, May 1-6, 2016.

Stafford, D.S., 2015. Multidimensional simulations of hydrides during fuel rod lifecycle. Journal of Nuclear Materials, Vol. 466, pp. 362-372

Stallman, F. W. 1986. LSL-M2: A Computer Program for Least-Squares Logarithmic Adjustment of Neutron Spectra, NUREG/CR-4349, Oak Ridge National

Laboratory. 1986. (Additional unpublished manual provided with version 2.0)

Tuominen, R., Valtavirta, V. & Juutilainen, P. 2017. Kriittisyysturvallisuuden validointipaketin tilanne 2016. VTT Tutkimusraportti VTT-R-00749-17 2017. 19 p. (in Finnish)

U.S.NRC 2010. Standard review plan for spent fuel dry storage systems at a general licence facility. NUREG-1536, revision 1. U.S.NRC Final report. July 2010. 424p

Valtavirta, V. and Tuominen, R. 2017, Validation and verification of the photon transport capabilities in Serpent 2.1.27, VTT Research Report, VTT-R-00494-17, VTT Technical Research Centre of Finland Ltd, 2017.

Viitanen, T. 2015. On adjustment of neutron spectra using LSL-M2 program. VTT Research report VTT-R-06065-15. 2015. 39 p.

Viitanen T, Leppänen J. 2016. Calculating neutron dosimeter activation in VVER-440 surveillance chains with Serpent, 27th Symposium of AER on VVER Reactor Physics and Reactor Safety, November 2016, Helsinki, Finland

Whalen, D. J., Hollowell, D. E. and Hendricks, J. S. 1991. MCNP: Photon Benchmark Problems, Technical Report LA-12196, Los Alamos National Laboratory, 1991.

E. Zsolnay, et al. 2012. Summary Description of the New International Reactor Dosimetry and Fusion File (IRDFF release 1.0), Technical Report INDC(NDS)-0616, IAEA, 2012.

4.5 Physics and chemistry of nuclear fuels (PANCHO)

Asko Arkoma[1], Janne Heikinheimo[1], Timo Ikonen[1], Joonas Kättö[1], Henri Loukusa[1], Emmi Myllykylä[1], Jussi Peltonen[1], Rami Pohja[1], Ville Tulkki[1], Ville Valtavirta[1]

[1]VTT Technical Research Centre of Finland Ltd
P.O. Box 1000, FI-02044 Espoo

Abstract

PANCHO has been the essential platform for the ongoing development of FINIX fuel behaviour module and its accompanying automatic validation system. FINIX has been published through the OECD/NEA Data Bank, and has been licensed by several institutions around the world. The studies on fuel behaviour in accident conditions have been framed within the international projects, where the accident simulation codes have been tested and validated. A coupling between SCANAIR and GENFLO codes has been developed in the project.

The chemical experiments on nuclear fuel materials aimed to investigate characteristics of initial dissolution of crystalline ThO_2 by adding ^{229}Th tracer into the aqueous phase, and were conducted for total 534 days. The experimental campaign on cladding creep demonstrated that the VTT equipment is capable of performing suitable transient tests which support modelling efforts.

Three DSc theses were finalized based on the ongoing cladding creep modelling work, the modelling of fuel behavior in design basis accidents and fuel pellet dissolution experiments. One Master's thesis is to be finalized from the work performed in this project.

Introduction

The project PANCHO – Physics and Chemistry of nuclear fuels investigates the integral fuel behaviour as well as combines the experimental and the modelling approaches in studying several topical features of nuclear fuel behaviour. These topics are the the chemistry of the fuel pellet and the mechanical response of the cladding.

Nuclear fuel both produces the energy in nuclear power plants and acts as the first two barriers to the spread of radioactive fission products. The UO_2 matrix of the fuel pellets contains approximately 99% of the born radionuclides, while the cladding tube contains the rest. Therefore the integrity of the fuel during normal operation and accidents is of utmost importance. Traditionally fuel performance has been analysed with integral fuel codes that contain semi-empirical correlations deduced from experiments. These correlations and models become more and more mechanistic as the understanding and the demands increase.

These models are often empirical, and therefore understanding the domain of validity of the codes is of great importance. The models are often validated for a certain set of conditions, with different models used for describing behaviour at different conditions. The code validation is performed against large databases of experimental data. The experiments on nuclear fuel are complex and expensive. Therefore they require international consortiums which are vital for the transfer of in-formation and expertise. The current European experimental facilities include Halden Reactor in Norway and Osiris in France. The CABRI reactor has been reworked to facilitate experiments in a water loop and is nearing operational condition, while the future Jules Horowitz Reactor is being built in France. PANCHO has served as a framework for Finnish collaboration with the Halden Reactor as well as the CABRI International Project.

In PANCHO, the Finnish fuel code FINIX is developed and validated for simulations of the fuel behaviour across a wide range of scenarios, such as loss of coolant accidents and reactivity insertions. FINIX can be then implemented in a wide range of codes to provide systematic description of fuel behaviour.

The tools and expertise to analyse reactor safety during loss of coolant and reactivity initiated accidents in Finnish reactors are improved via strong international co-operation. Phenomena pertaining to LOCA and RIA are studied and the understanding is transferred to Finnish experts and tools.

In PANCHO the fuel pellet investigations concentrate on the chemical leaching beahaviour of fuel materials and physical properties arising from the vacancy-type defect evolution in the pellets. As for the cladding investigations the issue of transient creep is studied both theoretically and experimentally. The produced data combined with the more accurate creep strain models can be utilized to improve the tools used in the estimation of fuel cladding tube behaviour and lifetime.

FINIX development and validation

In SAFIR2014, the FINIX fuel behaviour module was developed within the PALAMA project. FINIX is a general purpose fuel behaviour module for thermal and mechanical fuel behaviour in multi-physics simulations, and has been integrated into VTT's Serpent 2 reactor physics code and reactor dynamics codes (Ikonen et al, 2015). In PANCHO, further development and validation of the FINIX fuel behaviour module was a major goal during 2015-2018.

As FINIX is intended for multiphysics simulations, it is important that the code is easy to couple with other simulation programs. Therefore in the beginning of PANCHO, the data structures were redesigned and an improved interface for coupled simulations was developed.

During the PANCHO project, several models have been implemented in FINIX with the goal of increasing accuracy of FINIX predictions both compared to temperature measurements from Halden but also in verification against other fuel performance codes. The first new model was time-independent plastic deformation in the cladding. Previously, only elastic deformation of the cladding was modelled. Time-

independent plastic deformation is very important when describing the behaviour of fuel under reactivity-initiated accident (RIA) conditions. In a RIA, the fuel expands rapidly, pushes against the cladding and plastic deformation occurs if the yield stress of the cladding is exceeded.

During the project, several models required for modelling long irradiation periods were implemented. These included models for cladding creep, fuel swelling and densification and fission gas release, and additionally new steady-state heat equation solver was developed. The combined effect of cladding creep inwards to the pellet and swelling of the pellet due to fission product accumulation lead to closing of the pellet-cladding gap. The new models were preliminarily validated with good results. This version was also released through the OECD/NEA Data Bank.

The final version published in the PANCHO project is 1.19.1 (Loukusa et al., 2019), which includes a cladding oxidation model for Zircaloy-4 and a rewritten coolant heat transfer model for standalone purposes. A better coolant model was decided to be implemented to yield more accurate cladding oxidation predictions, as FINIX could not previously model, for example, the axial rise in coolant temperature. A Master's thesis is currently being finalized based on the cladding oxidation and coolant models in FINIX. The latest version of FINIX predicts fuel temperatures within 6.6 % of experimentally measured values (Peltonen 2019), which is comparable to other fuel performance codes. The temperature validation results are shown in upper figure in figure 1.

In addition, FINIX-1.19.1 was used to model loss-of-coolant accidents for the first time. Even though the cladding mechanical models are insufficient for large strain deformation modelling, interesting and promising results to guide future development were obtained. Especially the inclusion of finite strain modelling, improvements in rod failure predictions and an update of the plenum temperature model were thought to be of most importance. In some cases, very good agreement with FRAPTRAN was obtained, such as in the fuel temperatures and rod internal pressure. The rod internal pressure predictions of FINIX are compared with FRAPTRAN in the lower figure in figure 1.

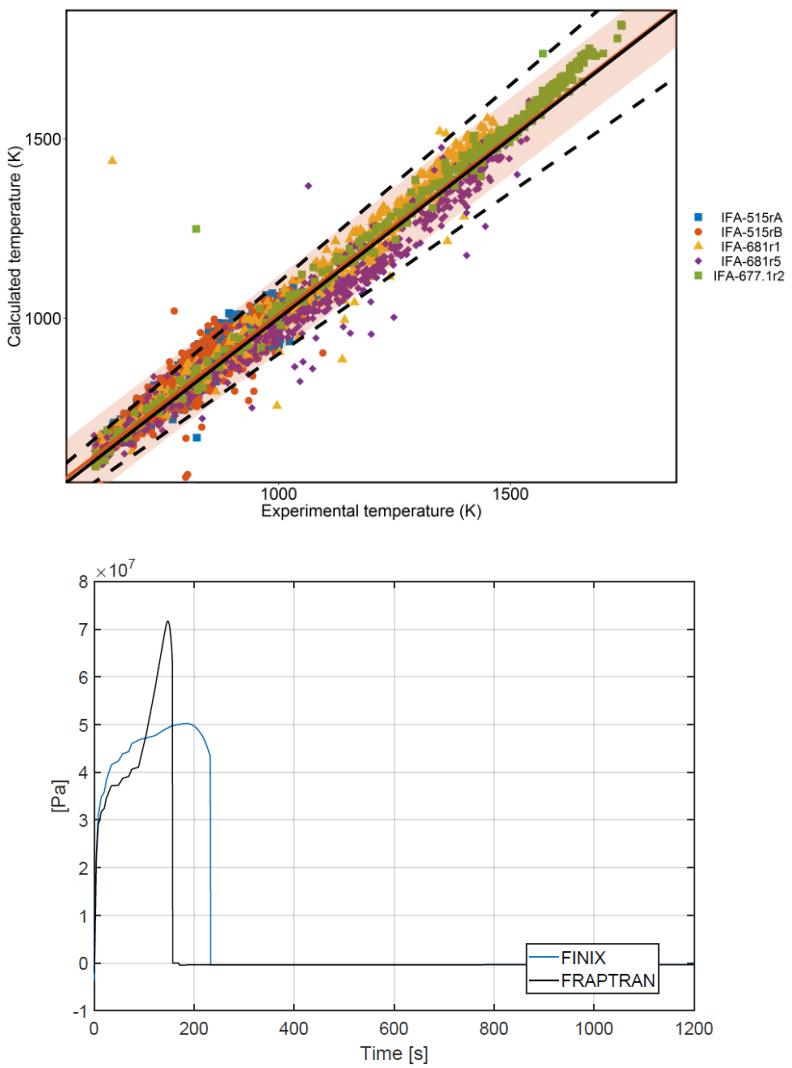

Figure 1. Temperature validation results of FINIX in selected Halden irradiations (upper) and .rod internal pressure predictions of FINIX in the IFA-650.5 LOCA test compared to FRAPTRAN (lower).

Validation system

Validation is an important step in software and model development. When nuclear fuel performance codes are developed and updated, their simulation results are compared against experimental data or reference program simulation data. In a proper validation process a large number of simulations are performed, and the results from each simulation run are compared to a large amount of data. This kind of

validation is time-consuming and error-prone when performed manually. The SPACE validation tool is a program that automates the validation process and makes the validation of fuel performance codes easier, more reliable and more efficient.

In 2016 the SPACE validation tool was completely rewritten based on the software development plan that was created in 2015 (Kättö 2017). The new validation tool is composed of a relational database and a piece of software for simulation program validation. The redesigned database contains all the data that are needed to construct the simulation program input files. It also contains the experimental data to which the simulation results can be compared. As the data is stored in a relational database, it is possible to run SQL queries against the data. This has several advantages, such as finding the fuel rods that meet the certain criteria and running the validation by using these rods only. It is also easier to manage a relational database than a flat-file database that was the database solution in the earlier SPACE versions.

SPACE allows the user to compare the simulation results of one or two simulation programs against the reference data. The reference data can be either experimental data or simulation data produced by a validated simulation program. As the validation tool runs a large number of simulations and compares the simulation results against the reference data, it will be easy to assess the validity of the simulation program or a single model of the program. The new version of the SPACE validation tool has been designed to be a general-purpose tool for fuel performance code validation, which means that the system is not tailored for any single simulation program. The current version supports FINIX and FRAPTRAN, but adding a support for a new simulation program is straightforward. In 2018, the SPACE validation tool was used in the validations of FINIX versions 1.18.9 and 1.19.1. The SPACE validation tool continues to be updated, and due the simplicity of its use it is possible to perform a validation for each published code version.

Fuel behavior during loss of coolant accidents

The goal in the loss of coolant accident (LOCA) research during the years 2015-2018 is to improve the picture of nuclear fuel behaviour in the accident conditions. Participation in international research program allows sharing good principles and data on the subject. The knowledge gained in the international program will be implemented in the VTT's in-house code FINIX in the future.

To meet the goal, VTT participated in an IAEA coordinated research project (CRP) called "Fuel Modelling in Accident Conditions (FUMAC)" that was launched in 2014. The aim of the project is to support the participants from different countries in their efforts to develop reliable tools for modelling of fuel behaviour during accidents. This task will be tackled by simulating predetermined experiments and by comparing the simulation results between the participants. VTT's contribution in the first phase was to calculate a set of AEKI separate effect tests and an intergral VVER LOCA test IFA-650.11 performed at Halden reactor. The code used in the

calculations was FRAPTRAN 1.4 - GENFLO. In the second phase, VTT calculated Halden IFA-650.10 and IFA-650.11 tests applying precalculated boundary conditions for coolant. In addition, the Studsvik test No. 192 was simulated. At the beginning of the second phase, the FRAPTRAN code was upgraded to the version 2.0 and put to use in VTT.

During the FUMAC CRP, VTT's simulations of AEKI ballooning tests with hollow Zircaloy-4 tubes showed slightly irregular behaviour with FRAPTRAN 1.4. Halden tests 650.10 and 650.11 were quite accurately predicted, both with FRAPTRAN 1.4 - GENFLO and with FRAPTRAN 2.0 - SOCRAT combinations. Figure 2 shows a good agreement between the experimental and simulated inner gas pressure in the Halden experiments. In addition, the Stusvik 192 experiment was successfully simulated with FRAPTRAN 2.0. The FUMAC project also included participation in three research coordination meetings (RCM) that allowed good networking and sharing of results in the global context. The results of the CRP FUMAC will be published in the IAEA TECDOC series.

VTT's in-house fuel performance module FINIX was tested against the data sets applied in the FUMAC CRP with good results. However, some crusial physical models have not been implemented yet, such as high temperature greep and plasticity of the cladding. This remains to be done in the future.

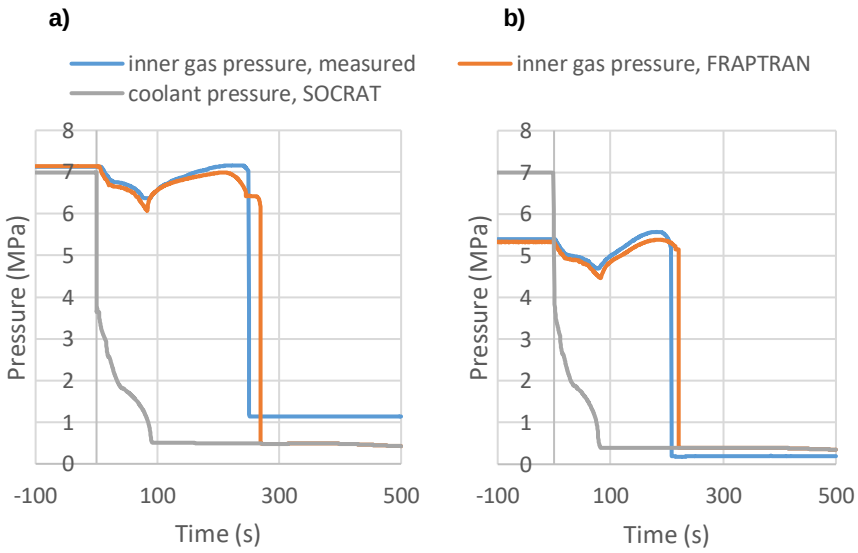

Figure 2. LOCA simulations with FRAPTRAN 2.0 with precalculated boundary conditions for coolant in Halden experiments IFA-650.10 (a) and IFA-650.11 (b).

Fuel behavior during reactivity initiated accidents

Fuel behaviour analyses of reactivity initiated accidents (RIA) had two topics in PANCHO project: uncertainty and sensitivity analyses of RIA modelling, and BWR RIA thermal hydraulics (TH) modelling. Uncertainty and sensitivity analyses were done in OECD Nuclear Energy Agency (NEA) RIA fuel codes benchmark Phase 2 and 3 with the SCANAIR code. SCANAIR is developed by IRSN specifi-cally for fuel performance analyses of RIAs.

SCANAIR's own TH model is not able to take the bulk boiling in BWRs into account, and therefore an interface between SCANAIR and a TH code was defined in SAFIR2014 PALAMA project. The work was continued in PANCHO in 2015 with verification (Arkoma, 2016) and in 2016 with preliminary validation (Arko-ma, 2017b) of a coupling between SCANAIR and VTT's subchannel TH code GENFLO (Figure 3). The results were published in a journal article (Arkoma, 2017a), and included to a doctoral dissertation partly funded by the PANCHO project (Arkoma, 2018).

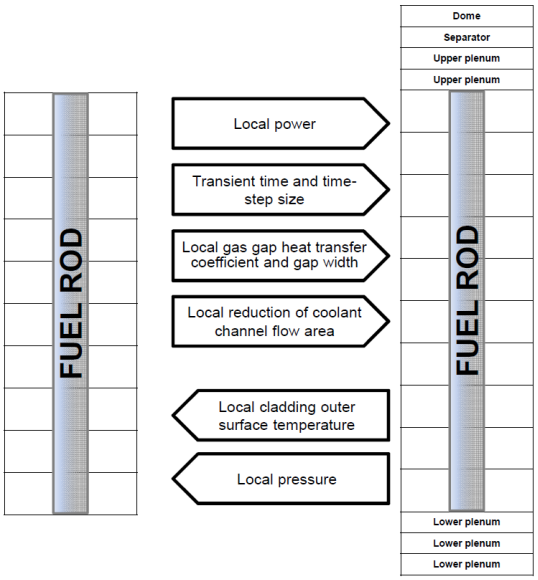

Figure 3. Coupling between SCANAIR and GENFLO. Figure reproduced from Arkoma (2017a) with permission.

OECD/NEA RIA fuel codes benchmark Phase 2 and 3

As a follow-up of the OECD/NEA RIA fuel codes benchmark that VTT participated (NEA/CSNI, 2013), Phase 2 of the benchmark was organized. It was divided into two parts: in Activity 1 (years 2014-2015), ten simplified (fabricated) RIA cases were simulated (NEA/CSNI, 2016) in order to understand the differences in modelling in

various codes. In Activity 2 (2015-2016), uncertainty and sensitivity analyses were done for a selected fresh fuel (but no pellet-cladding gap) PWR case from Activity 1 (NEA/CSNI, 2017). The number of uncertainty runs per participant was 200. Various influential input parameters were identified by using partial rank correlation coefficients. The results of Phase 2 cannot be extrapolated to cover irradiated fuel, and therefore, in Phase 3, a real RIA test with irradiated fuel was analysed with the methodologies agreed in Phase 2. Due to the large discrepancies regarding RIA thermal hydraulics modelling found in Phase 1 and 2, the uncertainty simulations considered CABRI International Programme (CIP) test CIP0-1 performed in a sodium loop. An example of sensitivity study results obtained at VTT is shown in Table 1 (Arkoma, 2019). A synthesis of participants' results and the conclusions of Phase 3 will be published in an NEA report in 2019.

Table 1. An example of sensitivity study conducted in RIA benchmark Phase 3 by calculating the partial rank correlation coefficients at the time of maximum power pulse (Arkoma, 2019). Blue colour indicates coefficients with absolute value at or above 0.25, and red colour at or above 0.75 (range being from zero, i.e., no significance, to one).

	Output				
	Thermal behaviour		Mechanical behaviour		Fission gas release
Input parameter	Fuel	Cladding	Fuel	Cladding	
Pellet-cladding radial gap					
Cladding roughness					
Fuel roughness					
Cladding outer oxide thickness					
Injected energy in the rod					
Radial power profile					
Power pulse width					
Fuel thermal conductivity model					
Fuel thermal expansion model					
Fuel enthalpy					
Cladding thermal expansion					
Cladding yield stress					

SCANAIR-GENFLO coupling

So far, demonstration of the coupled code has been done on two RIA benchmark Phase 2 cases considering PWR hot zero power initial conditions, with and without boiling during an RIA (Arkoma, 2017a), a hypothetical BWR RIA case starting from

hot full power (Arkoma, 2017a), and two actual RIA tests on BWR fuel performed in NSRR pool test reactor in stagnant water, room temperature and atmospheric pressure (Arkoma, 2017b).

The demonstration cases showed that the coupling works as expected. In benchmark case without boiling, cladding temperatures were comparable with the stand-alone SCANAIR (Figure 4, left). In benchmark case with boiling, the cladding temperatures of SCANAIR-GENFLO matched reasonably well with the stand-alone SCANAIR if similar assumptions and heat transfer correlations were used (Figure 4, right). The lack of GENFLO regarding RIA modelling is that the code's heat transfer models are not specifically fitted for fast transient conditions of an RIA.

Further validation of the coupled code against experimental results is necessary in the future.

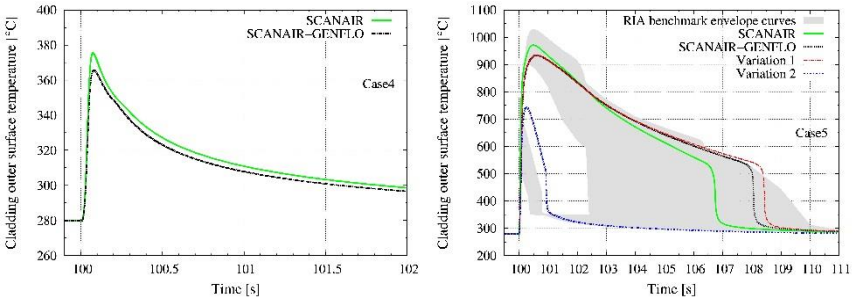

Figure 4. Cladding outer surface temperature in SCANAIR-GENFLO vs. stand-alone SCANAIR in RIA benchmark Phase 2 PWR case with (right) and without (left) boiling. Figures reproduced from Arkoma (2017a) with permission.

Leaching of thoria fuel

The experimental section of chemistry investigations concentrate on the leaching beahaviour of fuel materials in the storage conditions of defective fuel rod. The aim is to produce data for validation of models. The experiments were started in 2015 with the dissolution studies with crystalline ThO_2 with similar microstructure to UO_2 fuel matrix which continued the work performed in EURATOM FP7 project REDUPP (Reducing Uncertainty in Performance Prediction).

The experiments, aiming to investigate characteristics of initial dissolution of crystalline ThO_2 by adding ^{229}Th tracer into the aqueous phase, were started during the REDUPP and continued within the first year of the PANCHO for total 534 days. In addition, leached pellets were analysed with alpha spectrometry to study layer precipated on the surface of ThO_2 pellets during the leaching period. The experiments showed that ^{232}Th was released from the solid $^{232}ThO_2$ samples into the aqueous phase, eventhough the solution contained excess of ^{229}Th compared to the solubility limit of thorium. This indicated that early stage of the dissolution was rather controlled by the stability of surfaces than by the chemical equilibrium. Previous results

(Corkhill et al) showed that during the early stage, the dissolution took most probably place on grain boundaries and crystallographic defects, which can be defined as “high energy surface sites”. As the leaching proceeds the thorium concentration level drops down, but the isotopic ratio continues to decrease, which shows that the dissolution/precipitation reactions continue at the surfaces even though the chemical equilibrium is achieved, as can be seen from Figure 5. The ^{229}Th tracer experiments and their results are reported more detail in (Myllykylä et al. 2017)

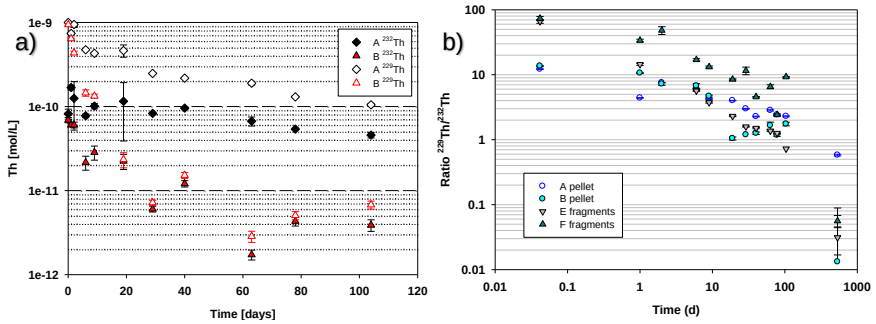

Figure 5. Evolution of thorium concentrations (a) and isotopic ratio ^{229}Th/^{232}Th (b) (measured with sector field ICP-MS) in dissolution experiments conducted with ThO_2 pellets (A and B) and fragments (E and F) in 0.01 M NaCl under anaerobic conditions.

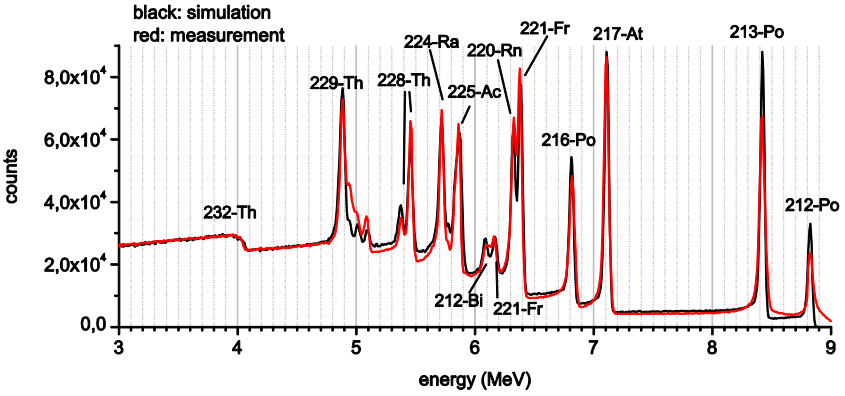

Figure 6. Measured (red) and simulated (black) spectra of the $^{232}ThO_2$ pellet A with the concentrated layer of ^{229}Th on top of the pellet.

The direct alpha spectrometric measurements of leached ThO_2 pellets accompanied with Advanced Alpha Spectrometric Simulation (AASI) suggested a formation of thin layer (< 0.1 µm) onto the $^{232}ThO_2$ pellet. According to the measured spectrum (see Fig. 6) the layer contained inceased amount of ^{229}Th and dauhgter

nuclides from both ^{232}Th and ^{229}Th decay series. The existence of of step like characterics of ^{229}Th and its daughters in the spectrum indicate their intrusion also below the thin surface layer into the bulk $^{232}ThO_2$. Due to energetically less stable nature of the grain boundaries, they are most probable intrusion route into the bulk pellet (Myllykylä et al 2017b).

During the PANCHO project, new dissolution experiment of ThO_2 pellets were conducted in clear MilliQ-water at 80°C under anaerobic conditions to simulate the storage conditions of a detective fuel rod. Higher temperature did not have increasing effect on the solubilty of thorium pellets under the used conditions. The chemical history indicated to have more effect on solubility than the temperature, as the "fresh" intact pellets released more thorium into solution than those already leached in the previous experiments. This supports the hypothesis of the relatively rapid initial dissolution, which occurs at "the high energy surface sites", like the crystallographic defects and grain boundaries.

Vacancy cluster evolution in ceria

Vacancies, starting from single missing atoms with low concentrations, specify many of the important physical properties of the oxide ceramics, such as thermal conductivity and gas diffusion coefficients (Khafizov et al. 2014, Catlow 1980). In nuclear fuel, thermal conductivity is closely related to the reactor safety and the energy conversion efficiency. Volatile element diffusion, in turn, ultimately determines fission gas release in the fuel rod, which is an important safety aspect affecting the rod design.

In some cases, it is reasonable to overcome the challenges caused by radioactivity and licensing of the samples via study and comparison of a non-radioactive surrogate material for nuclear fuel. CeO_2 is a widely used non-radioactive surrogate material for UO_2 and PuO_2 having the same fluorite structure.

This project aims to characterize vacancy-type defect evolution in proton-irradiated CeO_2 at 600 °C and connect it to the physical properties of the sample, such as thermal conductivity. So far the project includes fabrication of the samples, irradiation of the samples, and X-ray diffraction characterization at SCK-CEN Belgium, positron annihilation characterization and DFT calculations at Aalto University, and thermal conductivity measurements at Ohio State University, Columbus, United States, the latter studies being ongoing. Work in this subject performed in PANCHO has concentrated on research coordination and scientific article preparation.

Cladding creep

The cladding creep task builds on the previous modelling work on the creep phenomena, the LCSP model and the viscoelastic model that have been developed in past SAFIR projects and in the IDEA project funded by the Academy of Finland. In 2015 and 2016 the LCSP model was further developed and a possibility to apply

the LCSP modelling approach for creep transient response was investigated (Pohja 2015, Pohja et al 2016). Furthermore, a doctoral thesis “Modelling nuclear fuel behaviour and cladding viscoelastic response” was prepared and defended (Tulkki 2015).

The development of creep modelling of cladding materials benefits from experimental transient creep data at both in-reactor and ex-reactor conditions. Certain amount of transient creep data is available, but especially data including temperature and/or load drops, which is valuable for building the understanding of recovery phenomena in zirconium alloys during creep, is scarce in open literature. To gain additional transient creep data at ex-reactor conditions, which can be produced by using the VTT biaxial creep testing facilities, an experimental campaing to support the aforementioned modelling activities was planned.

To study the capabilities of VTT’s equipment for transient experiments, an experimental campaign using available materials and experimental facilities was initiated in 2015. At first stage, a temperature transient test with internal pressure and additional axial load was performed for a cold worked E110 zirconium alloy specimen.The internal pressure of the specimen and the additional axial pull load was applied to the specimen so that the axial to hoop stress stress ratio equaled 1 (α = 1). The stress level remained the same troughout the test, but a temperature transient (from 360°C to 400°C) was introduced after 500 hours. At the second qualification test, an E110 specimen was exposed to several stress transiens (load increases and drops) and the hoop to axial stress ratio was altered during the test. Based on the results of these tests, the VTT equipment is capable of performing suitable transient tests which support the modelling activities, but the performance of certain measurement units should be further improved to maximally utilize the results of test planned for Zircaloy-4 alloy.

The doctoral thesis “Modelling nuclear fuel behaviour and cladding viscoelastic response” was prepared and defended (Tulkki 2015). The scope of the thesis consisted of two main themes. The first was the uncertainty and sensitivity in fuel behaviour modelling and the tools required for its propagation to the rest of the nuclear reactor calculation chain. The second was the analysis and modelling of cladding response to transient stresses. Propagation of uncertainties through the nuclear reactor calculation chain is an international on-going effort, and the complex interactions in the fuel rods make them challenging to analyze. In the thesis uncertainty and sensitivity of fuel behaviour codes was investigated and the development of a fuel module suitable for propagation of the uncertainties was detailed. In the thesis a simple methodology for predicting fuel cladding macroscopic response to stresses and imposed strains was developed by taking anelastic behaviour into account. The model was shown to perform well in describing both creep and stress relaxation experiments.

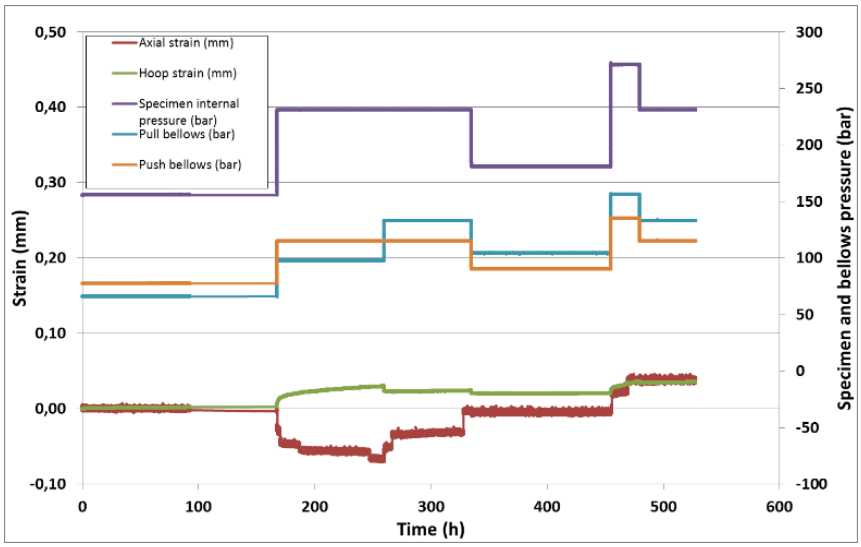

Figure 7. The curves for axial strain, hoop strain, specimen internal pressure, pull bellows and push bellows in a transient creep test.

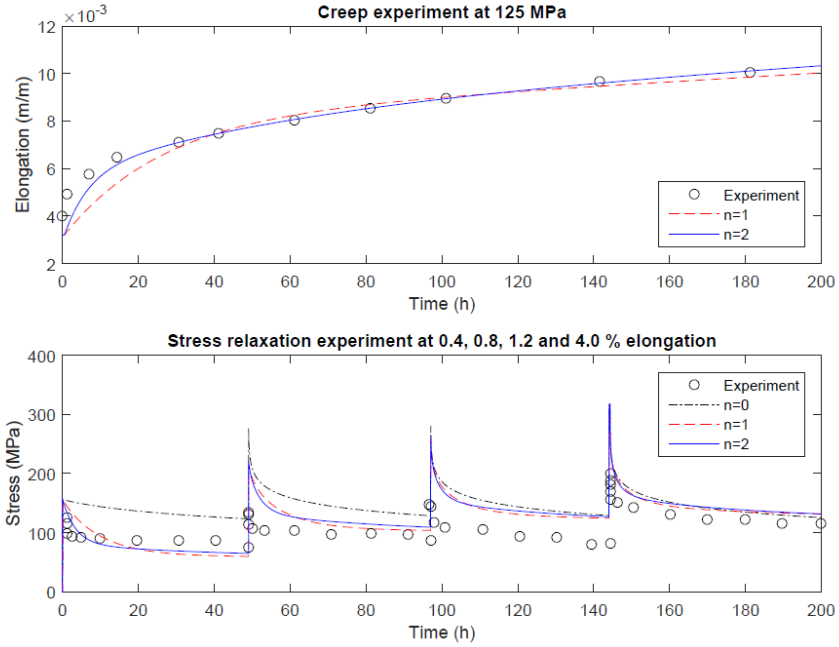

Figure 8. Demonstration of spring-dashpot model in modelling creep and stress relaxation experiments.

Three-dimensional nuclear fuel modelling

During the PANCHO project, the three-dimensional fuel performance code BISON developed at the Idaho National Laboratory (US) was taken into use at VTT. The investigations at VTT centered on general use of the code. A three-dimensional fuel performance code has not previously been in use at VTT, and several procedures in applying such codes had to be developed. The main challenge is the generation of computational meshes when the user wishes to calculate nonstandard geometries. Figure 9 shows a simulation approximating a missing pellet surface defect. In the figure, the central pellet effectively has a smaller radius than the surrounding pellets. As can be seen, the von Mises stress peaks at the pellet-pellet interfaces in the cladding.

The workflow in setting up BISON simulations and the generation of meshes has been refined at VTT, and the BISON code has been successfully installed to the VTT Linux cluster Potku2. This preparatory work eases future simulations of advanced fuels and claddings where either the geometry of the fuel is complex or several material layers are present, such as in coated claddings.

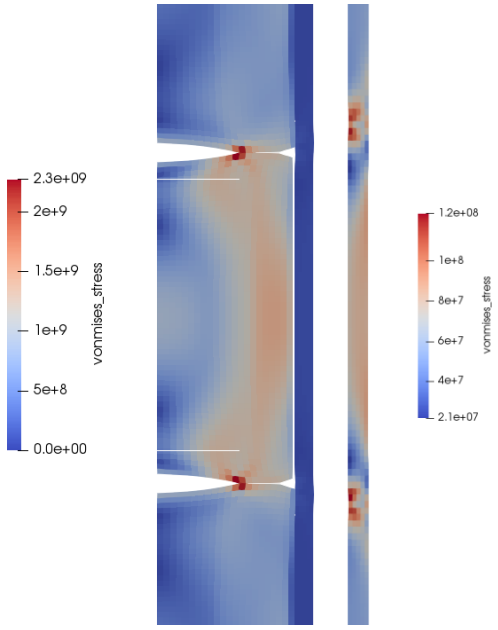

Figure 9. Two-dimensional simulation approximating a missing pellet surface defect, with the von Mises stress plotted on the computational mesh. The figure on the left shows the stresses in the pellet, which at maximum are an order of magnitude higher than the stresses on the right shown for the cladding.

References

Arkoma, A., 2019. WGFS RIA Fuel-Code Benchmark Phase 3 – SCANAIR uncertainty and sensitivity studies on CABRI CIP0-1 test. VTT Research Report, Jan. 31, 2019. VTT-R-00149-19

Arkoma, A., 2018. Modelling design basis accidents LOCA and RIA from the perspective of single fuel rods, Aalto University publication series, doctoral dissertations 26/2018, VTT Science 170, ISBN 978-952-60-7846-5 (printed), ISBN 978-952-60-7847-2 (pdf), http://urn.fi/URN:ISBN:978-952-60-7847-2 (accessed Feb. 7, 2019)

Arkoma, A., 2017a. Extending the reactivity initiated accident (RIA) fuel performance code SCANAIR for boiling water reactor (BWR) applications. Nuclear Engineering and Design, Vol. 322, pp. 192–203

Arkoma, A., 2017b. Validation status of SCANAIR-GENFLO coupling – Revision 1. VTT Research Report, Sep. 27, 2017. VTT-R-05272-17

Arkoma, A., 2016. Verification of the SCANAIR-GENFLO coupling. VTT Research Report, Jan. 31, 2016. VTT-R-00777-16

Catlow, C., Theory of fission gas migration in UO_2, Radiation Effects 53, 1980, 127-132.

Claire L. Corkhill, Emmi Myllykylä, Daniel J. Bailey, Stephanie M. Thornber, Jiahui Qi, Pablo Maldonado, Martin C. Stennett, Andrea Hamilton, and Neil C. Hyatt, Contribution of Energetically Reactive Surface Features to the Dissolution of CeO_2 and ThO_2 Analogues for Spent Nuclear Fuel Microstructures, ACS Applied Materials & Interfaces, 2014, 6, 12279−12289

Ikonen, T., Syrjälahti, E., Valtavirta, V., Loukusa, H., Leppänen, J., & Tulkki, V. (2016). Multiphysics simulation of fast transients with the FINIX fuel behaviour module. EPJ Nuclear Sciences & Technologies, 2, 37. https://doi.org/10.1051/epjn/2016032

Khafizov, M. et al., Thermal conductivity in nanocrystalline ceria thin films, Journal of the American Ceramic Society 97 (2), 2014, 562-569.

Kättö, J, SPACE - Validation tool for simulation software - User's guide for version 2.0.0, VTT Research Report, VTT-R.00204-17, 2017.

Loukusa, H., Ikonen, T., Räty, A., Tulkki, V. Thermochemical Modelling of the Oxygen Potential of Uranium Oxide Fuel Pellets Under Irradiation, Topfuel 2015, 13-17 September 2015, Zurich, Switzerland.

Loukusa, H., Ikonen, T., Valtavirta, V., Tulkki, V. Thermochemical modeling of nuclear fuel and the effects of oxygen potential buffers, Journal of Nuclear Materials, 2016, 440, 101-110.

Loukusa, H., Peltonen, J., Valtavirta, V. FINIX - Fuel behavior module and interface for multiphysics applications - Code description for version 1.19.1. VTT-R-00053-19, 2019.

Myllykylä, E., Tiina Lavonen, Lauri Koivula, Kaija Ollila, Marja Siitari-Kauppi: Dissolution of Crystalline ThO_2: study of dissolution process with initial ^{229}Th spike, Journal of Radioanalytical & Nuclear Chemistry, 2017, 311(1): 225-235

Myllykylä, E., Lauri Koivula, Merja Tanhua-Tyrkkö, Kerttuli Helariutta, Tiina Lavonen, Kaija Ollila, Marja Siitari-Kauppi: Direct alpha spectrometry for analysing the leached ThO_2 pellets, Journal of Nuclear Materials, 2017, 493:69-76.

NEA/CSNI, 2017. Reactivity-initiated Accident Fuel-rod-code Benchmark Phase II: Uncertainty and Sensitivity Analyses. NEA/CSNI/R(2017)1

NEA/CSNI, 2016. Reactivity Initiated Accident (RIA) Fuel Codes Benchmark Phase-II, Volume 1: Simplified Cases Results, Summary and Analysis. NEA/CSNI/R(2016)6/VOL1

NEA/CSNI, 2013. RIA Fuel Codes Benchmark, Volume 1. NEA/CSNI/R(2013)7

Peltonen, J. FINIX - Fuel behavior module and interface for multiphysics applications - Validation of version 1.19.1. VTT-R-00135-19, 2019.

Pohja, R. LCSP creep strain model performance of zirconium based fuel cladding materials in steady state and transient creep conditions, VTT Research Report VTT-R-06036-15, 2015.

Pohja, R., Huotilainen, S. Report on an experimental campaign on cladding transient behaviour, VTT Research Report VTT-R-00799-17.

Pohja, R., Tulkki, V., Ikonen, T., Moilanen, P., Rantala, J., Huotilainen, S., Ehrnstén, U.: Creep performance of fuel cladding, Proceedings of Baltica X conference

Loukusa, H., Peltonen, J., Valtavirta, V. FINIX - Fuel behavior module and interface for multiphysics applications - Code description for version 1.19.1. VTT-R-00053-19, 2019.

Tulkki, V. “Modelling nuclear fuel behaviour and cladding viscoelastic response”, D.Sc. (Tech) thesis, Aalto University School of Science, 2015.

Tulkki, V and Ikonen, T. “Modelling anelastic contribution to nuclear fuel cladding creep and stress relaxation”, Journal of Nuclear Materials, 465, 34–41 (2015). 2015a.

Tulkki, V and Ikonen, T. “Modelling cladding response to changing conditions”, Top-fuel 2015, 13-17 September 2015, Zurich, Switzerland. 2015b.

4.6 Uncertainty and sensitivity analyses for reactor safety (USVA)

Asko Arkoma[1], Torsti Alku[1†], Timo Ikonen[1†], Maria Pusa[1†], Elina Syrjälahti[1], Márton Szógrádi[1], Ville Valtavirta[1], Aarno Isotalo[2†], Aapo Taavitsainen[2†], Risto Vanhanen[2†]

[1]VTT Technical Research Centre of Finland Ltd
P.O. Box 1000, FI-02044 Espoo

[2]Aalto University School of Science
P.O.Box 11000, FI-00076 Aalto

[†]currently working elsewhere

Abstract

In USVA project, multidisciplinary uncertainty and sensitivity studies in reactor safety have been conducted. The most important accomplishments of the project include a thorough comparison of statistical sensitivity analysis methods in the context of fuel behavior modelling (Ikonen, 2015, 2016), sensitivity analysis of local uncertainties in a multicode calculation chain of a large break loss of coolant accident (LB-LOCA) (Arkoma and Ikonen, 2016a,b), development of an automated uncertainty analysis calculation system for the CASMO-4 – SIMULATE-3 calculation chain (Pusa, 2016; Pusa and Isotalo, 2017), and initial developments of uncertainty analysis for the group constant generation with Serpent (Valtavirta et al. 2018, Valtavirta 2018). Two publications of USVA were used in a doctoral dissertation (Arkoma, 2018c). A Master's thesis was finalized on the combined uncertainty analysis of coupled neutron transport and fuel behaviour codes (Taavitsainen, 2016).

Introduction

The general goal of USVA project was to develop methods and practices in uncertainty and sensitivity analyses of multiphysics problems and calculation sequences in reactor safety. The goal supports the long-term aim of establishing a comprehensive methodology for uncertainty and sensitivity analysis for the entire reactor safety field. The project built on the existing expertise in uncertainty and sensitivity analysis at VTT and Aalto University, and gathered the on-going research activities under one project. Also new experts in this area were trained. USVA promoted activities at the interfaces of different disciplines in reactor safety.

USVA had a high scientific level with a total of ten peer-reviewed scientific papers, including both journal and conference articles (Ikonen, 2015, 2016; Arkoma,

2018b; Arkoma and Ikonen, 2016a,b; Pusa, 2016; Pusa and Isotalo, 2017; Syrjälahti et al., 2019; Valtavirta et al., 2018; Vanhanen and Pusa, 2015). Two of these papers (Arkoma and Ikonen, 2016a,b) were used in an article based doctoral dissertation (Arkoma, 2018c). In addition, a Master's thesis (Taavitsainen, 2016) and a special assignment (Taavitsainen, 2015) were completed. Other deliverables of the project included seven research reports (plus one memorandum), and numerous travel reports and conference presentations.

Many of the tasks in USVA were related to the topics of OECD Nuclear Energy Agency (NEA) Benchmark for Uncertainty Analysis in Modelling (UAM) for the Design, Operation and Safety Analysis of LWRs. The members of USVA have had an active participation in this benchmark.

In the following, the various research topics studied in USVA are elaborated item by item.

Analysis of fuel rod failures in LB-LOCA

An LB-LOCA in an EPR type power plant was previously analysed with statistical methods (Arkoma et al., 2015). In that analysis, coupled FRAPTRAN-GENFLO fuel behaviour – subchannel thermal hydraulics code was used to estimate the percentage of failing rods in 59 global scenarios of the accident. Each of the global scenarios involved calculating boundary conditions for the accident with APROS. In each of the global scenarios, 1 000 FRAPTRAN-GENFLO simulations were performed, and in the worst scenario with respect to the number of failing rods, all the 63 865 rods were simulated. This data was used in sensitivity analyses in USVA (Arkoma, 2018a; Arkoma and Ikonen, 2016a,b). Also, a comprehensive literature review on internationally applied uncertainty and sensitivity analysis methods in fuel modelling was done (Arkoma, 2016).

Sensitivity analysis of uncertainties in LB-LOCA simulations

In Arkoma et al. (2015), the contributing factors of fuel rod failures were left undetermined. In USVA, importance of various local parameters, i.e., the location related parameters and the sampled fuel manufacturing parameters, to the outcome of chosen output parameters was studied in the worst global scenario (Arkoma and Ikonen 2016a,b). Later, sensitivities of global factors were included (Arkoma, 2018a).

The data originated from a multicode calculation chain: SIMULATE-3 (steady-state power histories), FRAPCON (steady-state fuel behaviour), APROS (transient power and thermal hydraulics), and FRAPTRAN-GENFLO (transient fuel behaviour). Due to complexity of the data, as a first step the relevant input parameters for the sensitivity analysis had to be specified. Data visualization with a cobweb graph (Fig. 1a) was used for the screening. Then, selected sensitivity measures (Fig. 1b) were calculated between the chosen input and output parameters. The sensitivity indices were Borgonovo's delta measure, first order Sobol' sensitivity index, and

squared Pearson correlation coefficient. The first mentioned is a novelty in this context. As an outcome, the most relevant parameters with respect to the cladding integrity were determined to be decay heat power during the transient, thermal hydraulic conditions in the rod's location in the reactor, and the steady-state irradiation history of the rod as represented in this analysis by the rod burnup. Meanwhile, the tolerances in fuel manufacturing parameters were found to have negligible effect on cladding deformation. The outlined analysis procedure is general, and could be useful in analysing other types of complicated calculation sequences or simulations that produce correlated and sparse data.

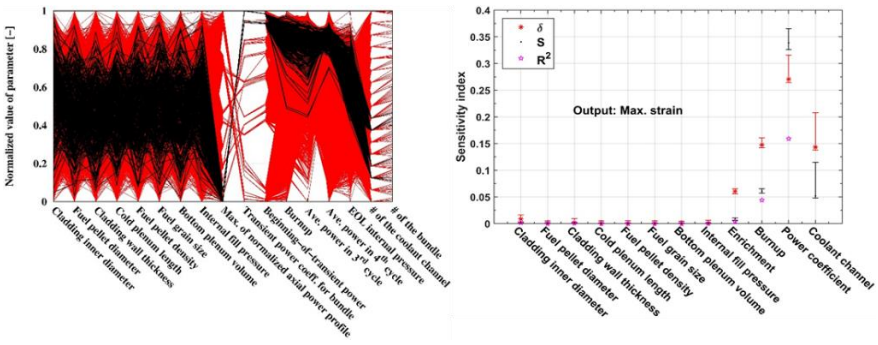

(a) (b)

Figure 1. a) Cobweb graph used for screening the most important input parameters. b) Calculated sensitivity indices. Arkoma and Ikonen (2016a).

Support Vector Machines

As a part of the EPR LOCA analysis (Arkoma et al., 2015), the applicability of neural networks to predict the number of failing fuel rods was tested. A network was trained using the 1 000 simulations from the worst global scenario. Network predictions were then comparated to FRAPTRAN-GENFLO simulations results of all the rods in the reactor. It was discovered that the rods calculated by FRAPTRAN-GENFLO to survive were well predicted by the network to survive. However, a significant number of rods calculated to fail were not correctly predicted by the network. This can be understood by the fact that the number of failing rods used in teaching the network was very limited.

An alternative way to produce predictions from the existing data is to apply support vector machines (SVMs), which were expected to have better performance in classification. The problem of imbalanced data sets was tackled by introducing an iterative method (Arkoma, 2017): an SVM was trained with the existing small number (1 000) of simulations, and then it was used in predicting a new set of rods that would be susceptible to ballooning in LOCA. These rods are simulated with the fuel performance code, and the resulting additional data is included to the training set of

an SVM. With this procedure, the accuracy of the predictions was shown to improve (Arkoma, 2017) when classifying rods into failing and non-failing rods with the SVM.

In order to extend the sensitivity analysis from the worst global scenario into all the other global scenarios, SVMs were used for generating additional data needed for the sensitivity analysis. In order to test the applicability of artificial data, the sensitivity analysis results produced with the help of SVMs in the worst global scenario were compared to the sensitivity analysis results from FRAPTRAN-GENFLO simulations (Arkoma and Ikonen, 2016a). Reasonable accuracy of SVMs was noted (Arkoma, 2018b). Then, a new SVM was fitted for each global scenario (Arkoma, 2018a). Sensitivity indices between global parameters and a relevant output quantity, selected to be the cladding maximum hoop stress, were calculated, and that way the importance of global input parameters was studied. The varied global parameters included APROS input parameters, and FRAPCON and GENFLO model parameters. In order to produce continuous output, SVM was used in regression mode, in which negligible improvements by the above described iterative scheme were noted (Arkoma, 2018b). Therefore, oversampling of high cladding hoop stress rods was used instead (Arkoma, 2018a). The results showed that the global parameters had actually negligible effect compared to the local parameters on maximum hoop stress in LB-LOCA.

Methodology for determining input uncertainties in thermal hydraulics simulations

In the OECD/NEA PREMIUM benchmark, it was distinquished that the medhods for the uncertainty assessment of thermal hydraulics codes' models needs to be further studied. Particularly, identification of uncertain input parameters and defining their probability density functions for the physical models that the thermal hydraulic safety codes rely on, is challenging. These models have been built based on fitting to experimental data and laws of physics. The existing methods used to quantify the uncertainty in thermal hydraulics codes were studied in literature reviews (Alku, 2017; Syrjälahti, 2018b; Szógrádi, 2018). In addition, methods used in other disciplines were considered and their applicabity to nuclear safety codes were studied. The objective was to be able to identify the most promising approaches and to set up guidelines on the research for the upcoming years.

Sensitivity analysis of fuel behavior

The influence of uncertainties in fuel performance simulations was studied (Ikonen, 2015, 2016). Based on previous experience, there was a need to review the various commonly used and also novel statistical methods that could be used to extract sensitivity information from the computational model. Several global sensitivity analysis methods were compared to assess their efficiency and applicability to nuclear fuel performance simulations. The implications of high input uncertainties and complex models were analysed. Such a comparison was done on an existing data set

of steady-state FRAPCON simulations, revealing several intricacies in the data. Depending on the considered output, the required fidelity varies. Hence, relying on a simple analysis method is not advisable. Instead, as a result of the work, a strategy is proposed that uses a mixture of various methods efficiently, so that comprehensive information can be extracted at a modest computational cost.

Method for the uncertainty analysis of nuclear fuel and neutronics

In the framework of coupled code systems, the objective was to study the combined uncertainty analysis of coupled neutron transport and fuel behaviour codes for a simple test case. A Master's thesis was written on the subject (Taavitsainen, 2016). Firstly, a computational system coupling the fuel behaviour code FINIX and the reactor physics code DRAGON was set up and applied to the PWR pincell test case of UAM benchmark. A special assignment was completed on constructing the FINIX-DRAGON calculation system (Taavitsainen, 2015). Secondly, the nuclear data code NJOY was coupled to the calculation system to allow uncertainty analysis. The most important aspect was to find out if the uncertainties in nuclear fuel modelling and neutronics modelling may be handled separately. As an outcome, these may indeed be propagated separately.

A methodology named "CFENSS-SRS" (Coupled Fuel Behaviour and Neutronics Stochastic Sampling with Simple Random Sampling) was developed for the purpose of this work. The method applies the statistical uncertainty analysis to univariate nuclear fuel parameters and correlated neutron cross sections (Taavitsainen, 2016). The result of a single average cross section perturbation is presented in Fig. 2.

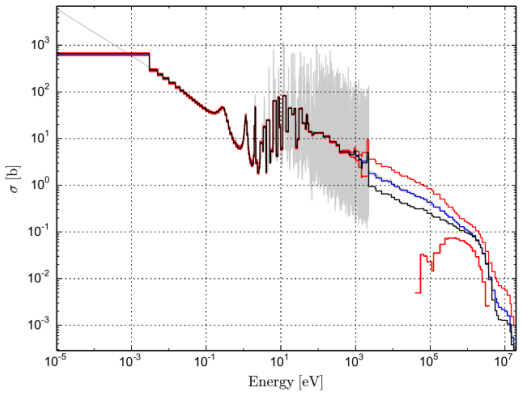

Figure 2. Nuclear data random sampling for the capture cross section of U-235. The red curves bound a 95% normal distribution confidence interval on both sides of the blue best estimate average curve. The black curve represents the perturbed average cross sections while the whitened background curve is for the pointwise data. Occasionally the lower red curve disappears by dropping to negative values and outside the used scale. Taavitsainen (2016).

Nuclear data uncertainty propagation in full-core calculation sequences

In the context of calculation sequences, the work carried out in the CRISTAL project of SAFIR 2014 was continued. Adjoint-based sensitivity and uncertainty analysis capability had previously been implemented to the assembly-level reactor physics code CASMO-4. In USVA, the implementation enabled the uncertainty analysis of assembly constants that were then passed on to codes simulating a full reactor core. In order to be able to propagate uncertainty through core-level simulations in a consistent manner, the methodology was extended to reflector regions. An automated calculation system was developed for propagating nuclear data uncertainty through assembly-level homogenization calculations with CASMO-4 in fresh fuel cases. Nuclear data uncertainty was propagated through the CASMO-4 – SIMULATE-3 (see Fig. 3) and CASMO-4 – TRAB3D calculation sequences with application to the PWR TMI-1 scenario (Pusa, 2016). The differences between covariance libraries were studied (Vanhanen and Pusa, 2015). In addition, one objective was to test the methodology for a transient simulation with TRAB3D (Fig. 4).

As explained above, the previously implemented uncertainty analysis capability CASMO-4 – SIMULATE-3 calculation sequence was based on the two-step approach. Namely, the adjoint-based method is used to compute the sensitivity profiles of assembly constants after which the corresponding uncertainties are propagated statistically through core-level simulations. The two-step method was further compared with a statistical approach. In the statistical approach, a large number of cross-section libraries were generated with Serpent using random samples of nuclear data. The two approaches were found to produce consistent best estimates, but unexplained deviations still remained in the uncertainties. An article on CASMO-4 – SIMULATE-3 uncertainty propagation sequence was finalized but without the Serpent results (Pusa and Isotalo, 2017).

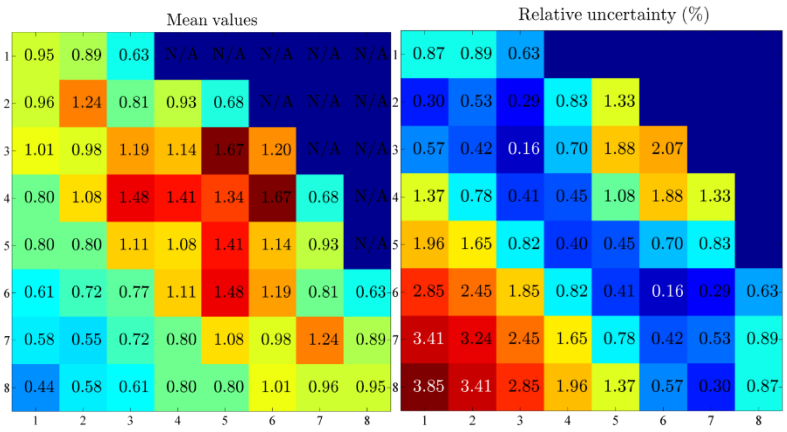

(a) (b)

Figure 3. (a) Radial power distribution, and (b) respective uncertainties for a PWR modelled using CASMO-4 – SIMULATE-3 uncertainty analysis sequence. Pusa (2016).

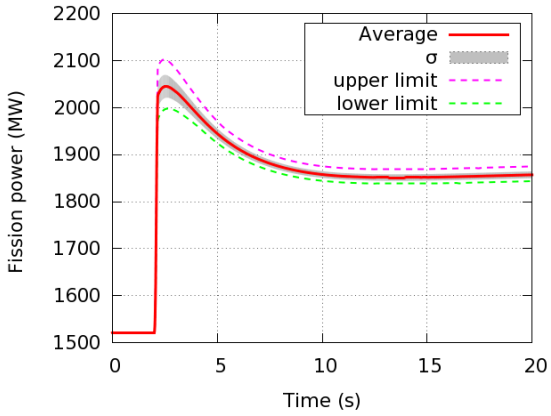

Figure 4. PWR control rod ejection transient simulated with TRAB3D using CASMO-4 neutronics data with propagated uncertainties.

Nuclear data uncertainty propagation to group and time constants generated with Serpent

One of the main applications of the Serpent Monte Carlo reactor physics burnup code is the generation of homogenized group and time constants for reactor simulator codes. The generation is a process that uses pre-processed evaluated nuclear data as an input for a transport code, and it produces a multitude of constants describing neutron interaction in a specific target system. As the evaluated nuclear data used as input in the process is obtained through a combination of experimental and theoretical work, it contains uncertainties. While some of these uncertainties are still unknown, the uncertainty evaluation and their listing as evaluated nuclear covariance data is ongoing.

If one can assess the sensitivity of some quantities of interest (such as group constants) to perturbations in nuclear data, one can propagate the uncertainty from the available nuclear covariance data evaluations to the quantities of interest. Such sensitivity calculation capabilities were implemented into Serpent 2.1.29 (Valtavirta et al., 2018) to be part of the official Serpent 2 distribution. This novel collision history based methodology was first implemented to an extended Serpent version by Aufiero et al. (2015). Serpent was further extended (Valtavirta, 2018) to enable reading, processing and interacting with the multi-group nuclear covariance data. This data was applied with the above mentioned sensitivity calculation capabilities to propagate nuclear data uncertainties into several different group constants that can be expressed as reaction rate or detector tally value ratios. The capabilities were demonstrated in calculations where detectors were set up to tally reaction rates, and fluxes and the group constants were calculated as a post processing step. As an example, Fig. 5 shows the contributions to the total uncertainty of the homogenized one group fission cross section in a hot-full-power pin cell for the Three Mile Island (TMI) 1 fuel type from UAM. In the future, a sampling based method should be used to verify the propagated nuclear data uncertainties.

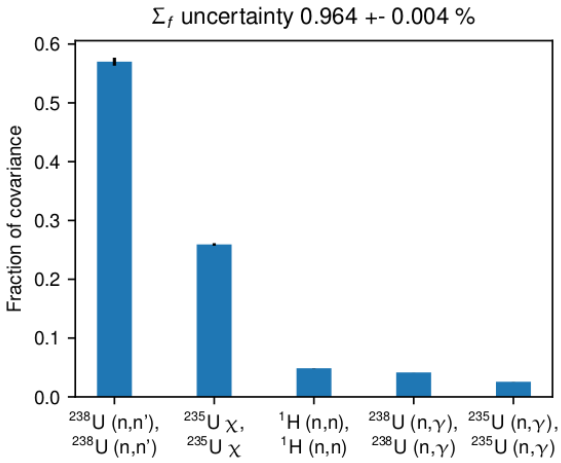

Figure 5. Top contributors (as a fraction of the total covariance) to the uncertainty of the macroscopic fission cross section homogenized by Serpent in a TMI1 (PWR) pin-cell.

Reducing the uncertainty in coupled fuel performance – reactor dynamics simulations

In safety analyses conducted with reactor dynamics simulations, conservativity of widely used simple fuel correlations is not obvious. To tackle this problem, a simplified model for burnup-induced fuel rod deformations was created (Syrjälahti et al., 2019). Purpose of the model is to provide fuel rod related information for multiphysics simulations, in which the use dedicated fuel performance codes is not always possible or reasonable. The developed model can be integrated, for instance, into coupled neutronics – thermal hydraulics codes that are used for simulation of plant transients. Comparison of the new model and FRAPCON-3.4 results showed that the simple model simulates pellet and cladding displacements very accurately. With the new model, the reliability of reactor dynamic simulations is thus improved. The new model has been integrated into VTT's reactor dynamics code HEXTRAN and has been applied to full-core simulation of VVER-440 control rod ejection transient.

Uncertainties and sensitivities in reactor dynamics simulations

The UAM benchmark is dedicated for various aspects of uncertainty analysis of reactor systems: quantifying the uncertainties in each stages of a multiphysics calculation chain (neutronics, thermal hydraulics, fuel), and combining these uncertainties. The benchmark is moving to a phase in which coupled analyses are done for

different reactor types: VVER, PWR and BWR. The final specifications for this phase have not been finalized but the group constant data containing propagated uncertainties has already been prepared for the VVER case. Preliminary simulations with this data were done in USVA (Syrjälahti, 2018). For this work, the HEXTRAN-SMABRE model of Kalinin-3 VVER-1000 plant was utilized, and 500 simulation runs of the benchmark problem, i.e., switching off one main coolant pump (MCP) of working four MCPs, were completed (Fig. 6). Additionally, the effect of nodalization of the pressure vessel on coolant mixing was studied.

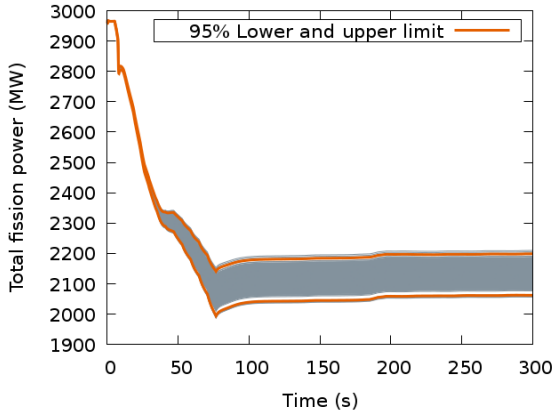

Figure 6. HEXTRAN-SMABRE simulation of Kalinin-3 benchmark, switching off one main coolant pump (MCP) of working four MCPs using 500 separate group constant sets.

References

Alku, T., 2017. Methods for the quantification of uncertainties related to Apros' physical models, VTT Research Report, VTT-R-00571-17, Jan. 31, 2017, 18 p.

Arkoma, A., 2018a. Sensitivity analysis of global uncertainties in large break loss-of-coolant accident (LB-LOCA) simulations. VTT Research Report, VTT-R-00137-19, Dec. 7, 2018, 18 p.

Arkoma, A., 2018b. Predicting fuel rod failures and their contributing factors with surrogate support vector machines in statistical LOCA analysis. In proceedings of: ANS Best Estimate Plus Uncertainty International Conference (BEPU 2018), Lucca, Italy, May 13-19, 2018, Paper 281

Arkoma, A., 2018c. Modelling design basis accidents LOCA and RIA from the perspective of single fuel rods, Aalto University publication series, doctoral dissertations 26/2018, VTT Science 170, ISBN 978-952-60-7846-5

(printed), ISBN 978-952-60-7847-2 (pdf), http://urn.fi/URN:ISBN:978-952-60-7847-2 (accessed Feb. 7, 2019)

Arkoma, A., 2017. Applying support vector machines (SVMs) to predict fuel failures in LOCA. VTT Research Report VTT-R-00964-17, Feb. 21, 2017, 11 p.

Arkoma, A., 2016. Uncertainty and sensitivity analysis methods in nuclear fuel modelling – a literature review. VTT Research Report, VTT-R-05086-16, Nov. 22, 2016, 17 p.

Arkoma, A., Hänninen, M., Rantamäki, K., Kurki, J., and Hämäläinen, A., 2015. Statistical analysis of fuel failures in large break loss-of-coolant accident (LB-LOCA) in EPR type nuclear power plant, Nuclear Engineering and Design Vol. 285, pp. 1–14

Arkoma, A., Ikonen, T., 2016a. Statistical and sensitivity analysis of failing rods in EPR LB-LOCA. In proceedings of: TopFuel 2016, Boise, Idaho, U.S.A., September 11-16, 2016, Paper no. 17570

Arkoma, A., Ikonen, T., 2016b. Sensitivity analysis of local uncertainties in large break loss-of-coolant accident (LB-LOCA) thermo-mechanical simulations, Nuclear Engineering and Design Vol. 305, pp. 293-302. http://dx.doi.org/10.1016/j.nucengdes.2016.06.002

Aufiero, M., Bidaud, A., Hursin, M., Leppänen, J., Palmiotti, G., Pelloni, S., Rubiolo, P., 2015. A collision history-based approach to sensitivity/perturbation calculations in the continuous energy Monte Carlo code SERPENT. Annals of Nuclear Energy Vol. 85, pp. 245-258

Ikonen, T., 2016. Comparison of global sensitivity analysis methods – Application to fuel behavior modelling. Nuclear Engineering and Design Vol. 297, pp. 72-80 http://dx.doi.org/10.1016/j.nucengdes.2015.11.025

Ikonen, T., 2015. Global sensitivity analysis in fuel performance modelling. In proceedings of: TopFuel 2015, Zurich, Switzerland, Sep. 13-17, 2015

Pusa, M., 2016. Uncertainty analysis of assembly and core-level calculations with application to CASMO-4 and SIMULATE-3. In proceedings of: PHYSOR 2016, Sun Valley, Idaho, USA, May 1-5, 2016

Pusa, M., Isotalo, A., 2017. Uncertainty analysis of assembly and core-level calculations with application to CASMO-4E and SIMULATE-3. Annals of Nuclear Energy Vol. 104, pp. 124–131 http://dx.doi.org/10.1016/j.anucene.2017.01.042

Syrjälahti, E., 2018a. Preliminary simulations of the Kalinin-3 benchmark problem for uncertainty and sensitivity analyses. VTT Research report, VTT-R-06972-18, Dec. 20, 2018, 16 p.

Syrjälahti, E., 2018b. Status report of the USVA project task 1.2: Development of a generic methodology for determining input uncertainties in nuclear safety codes. Memorandum, Feb. 26, 2018, 6 p.

Syrjälahti, E., Ikonen, T., Tulkki, V., 2019. Modeling burnup-induced fuel rod deformations and their effect on transient behavior of a VVER-440 reactor core, Annals of Nuclear Energy Vol. 125, pp. 121-131 https://doi.org/10.1016/j.anucene.2018.10.039

Szógrádi, M., 2018. Methodology for determining input uncertainties of Apros. VTT Research Report, VTT-R-04148-18, Aug. 24, 2018. 48 p.

Taavitsainen, A., 2016. CFENSS-SRS method for the uncertainty analysis of nuclear fuel and neutronics. Thesis for the degree of Master of Science in Technology, Aalto University, School of Science. 77 p. http://urn.fi/URN:NBN:fi:aalto-201606172584

Taavitsainen, A., 2015. Coupled FINIX-DRAGON Calculation Chain for an LWR Pin Cell Case. Special Assignment, Aalto university

Valtavirta, V., 2018. Nuclear data uncertainty propagation to Serpent generated group and time constants. VTT Research Report, VTT-R-04681-18, Oct. 9, 2018, 42 p.

Valtavirta, V., Aufiero, M., Leppänen, J., 2018. Collision-history based sensitivity/perturbation calculation capabilities in Serpent 2.1.30. In proceedings of: ANS Best Estimate Plus Uncertainty International Conference (BEPU 2018), Lucca, Italy, May 13-19, 2018, Paper 240

Vanhanen, R., Pusa, M., 2015. Survey of prediction capabilities of three nuclear data libraries for a PWR application. Annals of Nuclear Energy Vol. 83, pp. 408-421 http://dx.doi.org/10.1016/j.anucene.2015.03.044

5. Thermal hydraulics

5.1 Comprehensive and systematic validation of independent safety analysis tools (COVA)

Hillberg Seppo, Karppinen Ismo, Silde Ari, Hiittenkivi Jarno, Kurki Joona, Leskinen Joona, Szogradi Marton, Dorval Eric, Lauerma Sampsa, Alku Torsti, Airaksinen Robert, Hovi Tatu, Skipnikov Dmitri

VTT Technical Research Centre of Finland Ltd
P.O. Box 1000, FI-02044 Espoo

Abstract

Apros is a system-scale safety analysis tool developed at VTT in cooperation with Fortum since 1986. Apros is used for safety analyses of light water reactors, and thanks to addition of new advanced features in the recent years, it can also be utilized in analysing generation IV nuclear reactors. As a commercial code Apros has a rigorous and extensive version-validation process whose purpose is to ensure that no unwanted changes or error have been introduced in any of the application areas while introducing the new features or changes of existing features and corrections of detected errors into the new released version.

The overall objective of the COVA project was to improve the state of Apros' validation through a systematic and rigorous approach to the validation process, and also to promote this kind of approach to the validation process. The process enhanced the expertise in thermal hydraulic area of Generation II and III LWR reactors and included, as an essential part, training of new experts to this relevant area of reactor safety. While main effort was carried out using Apros, as it has higher national interest as a self-developed independent and versatile safety analysis tool, U.S. NRC's TRACE was also used in the analyses.

Critical assessment of thermal-hydraulic and containment models' validation

The project started in 2015 with an assessment of Apros's thermal-hydraulic and containment models' validation by compiling databases of the calculated validation cases and then by comparing them to the OECD/NEA's separate effect test [1,2] and containment [3] validation matrices. This work formed a foundation [4,5] on which much of the work done in COVA during its four-year period was based.

Validation assessment of Apros' thermal-hydraulic model

Assessment of Apros' TH model was commenced by gathering a list of all validation cases calculated with Apros throughout its development history, including information on what code version was used for each analysis and what kind of results was obtained. All available analysis reports on these calculations were gathered so that new simulation results could be later compared to earlier results if the same cases are chosen for recalculation. In the next stage OECD NEA's thermal hydraulic validation separate effects test matrix [1,2] (a part of the table is presented in Figure 1) was used to craft a comprehensive set of validation cases that, when analysed, would ensure the best possible validation of the code for all safety relevant nuclear power plant scenarios.

0. Basic Phenomena	1. Evaporation due to Depressurisation 2. Evaporation due to Heat Input 3. Condensation due to Pressurisation 4. Condensation due to Heat Removal 5. Interfacial Friction in Vertical Flow 6. Interfacial Friction in Horizontal Flow 7. Wall to Fluid Friction 8. Pressure Drop at Geometric Discontinuities 9. Pressure Wave Propagation
1. Critical Flow	1. Breaks 2. Valves 3. Pipes
2. Phase Separation / Vertical Flow with and without Mixture Level	1. Pipes / Plena 2. Core 3. Downcomer

Figure 1. Phenomena identified in the OECD SET –matrix [1,2] were used in categorizing the current Apros validation base (only a part of the table is shown – a full table contains 25 different phenomena divided into subcategories).

Recommendations for code assessment in each phenomenon were listed and recommendation was given that further validation work should be started with filling the gaps and extending the validation base in assessment of the basic phenomena. Among those, the interfacial friction in vertical flow was identified as one of the most important ones, since it affects other phenomena, like heat transfer in two phase flow (e.g. core cooling in accident conditions).

Apros' validation of separate effect phenomena was found to be quite comprehensive and most of the phenomena being covered. However, room for improvement was still found as some of the phenomena were assessed with only a single experiment in one test facility. Assessment of some combined phenomena was seen benefit from dedicated validation and the assessment base of the code was recommended to be extended.

Validation assessment of Apros' containment model

Validation assessment of Apros' containment package [5] covered a total of 43 tests, of which 21 were separate effect tests. In addition, 7 benchmark exercises were assessed. The validation cases covered the most common light water reactor containment types, such as BWR suppression pool containment, PWR large dry containment, PWR ice condenser containment, eastern type PWR bubble condenser containment, BWR containment with internal or external passive cooler, and German 1300 PWR containment. The range of pressure, gas and liquid water temperature and steam/light gas concentrations in the calculated experiments covered acceptably the typical containment conditions in design basis accidents (DBAs).

The assessment showed that Apros is capable in calculating the general containment behaviour (such as pressure, gas temperatures, steam-gas –mixture composition, flow paths etc.) in DBAs and did not reveal any severe deficiencies that could prevent from using Apros for DBA analyses. However, further validation, especially against separate effect tests, was recommended. Some important separate effects topics that would need further validation were identified as: condensation on wall surface, condensate film flow on the walls and its effects on heat transfer, convection heat transfer between atmos-phere and structures, pool surface evaporation and condensation, surface temperature of water pool, spray modelling in specific situations, clearing time of suppression pool vents, heat transfer between liquid water and structure, ice melting rate, and hydrogen deflagration (Figure 2).

EXPERIMENT	STUDIED PHENOMENON	REMARKS
TOSQAN ISP-47 or TOSQAN condensation tests	- Condensation rate on wall condenser - Pressure - Gas temperatures - Steam and helium concentrations - Stratification	Main focus is on condensation calculation. The gas stratification field should be calculated (adjusted) sufficiently well to enable the validation of condensation calculation.
Some separate effect test for convection heat transfer	- Convection heat transfer	No suitable test found yet.
TOSQAN sump test	- Pool surface evaporation and condensation	
Test on surface pool temperature	- Pool surface temperature in condensation and evaporation cases.	No suitable test found yet.
AECL-SP Dousing test no. 1	- Heat removal by dousing (spray)	
VICTORIA no.	- Ice melting rate	Re-calculation with the latest code

Figure 2. 22 cases were recommended for further validation [5] (only a part of the table is shown).

Validation analyses based on the assessment reports

Several experiments have been calculated based on the findings of validation assessment reports and these are listed in Table 1.

Table 1. Tests with separate effects calculated in 2015-2018.

Experiment or case	Phenomenon or scenario	Used code
19-rod bundle experiments [6]	bundle heat transfer and friction	Apros
ACHILLES ISP-25 [7]	core reflood	Apros
Becker burnout experiments [8]	critical heat flux	Apros
ERSEC ISP-7 [9]	core reflood	Apros
FLECHT SEASET test 31302 [10] FLECHT SEASET test 32013 [10]	core reflood	Apros
LOTUS [6]	friction and phase separation in annular flow	Apros
RBHT reflooding experiments 937, 945 and 1143 [11]	core reflood	Apros
NEPTUN experiments 5050 and 5052 [12]	core reflood	TRACE
HYMERES/PANDA natural circulation test HP6_1 [13]	natural circulation, stratification	Apros containment
TOSQAN ISP-47 [14]	wall condensation	Apros containment
TOSQAN spray test 101 [15]	spray	Apros containment
TOSQAN test T201 [16]	wall condensation, sump evaporation	Apros containment

One of the simulated cases was the ISP-7 case of the tubular ERSEC reflooding experiments [9] (Figure 3). Some years ago at VTT the phenomena related to core reflooding were identified as high priority and a development project was started in order to improve the code capability. In this development project a mechanism for an automatically adapting nodalisation of the channel wall heat structures was created. The new adapting nodalisation mechanism refined the calculation grid in the vicinity of the quench front in reflooding scenarios, so that the very steep axial temperature gradients in the wall can be captured. This is essential in order to be able to accurately simulate the progression of the quench front, as the heat conduction in the channel wall as well as a reflooding-specific heat flux model are dependent on the axial wall temperature gradient. In addition to the adapting nodalisation mechanism, a few smaller improvements were implemented into the reflooding models of Apros, which improved Apros' predictive capability to some extent.

In order to verify the functionality of the adapting nodalisation scheme, assess the effect of other improvements made into the code, and to help identifying aspects in the code that would still need improvement, the ISP-7 case was recalculated in

COVA with the current development version of Apros. As the improvement were still on-going, the gained results reflected only the current unfinished status of the work.

The simulations confirmed the need to use a very fine nodalisation for the channel wall heat structures in the case of reflooding simulations. The adapting nodalisation mechanism was verified to work as expected and give results very close to a fixed fine nodalisation. Consequently, it was recommended to carry out any future validation simulations related to reflooding scenarios by using the adapting nodalisation together with a coarse thermal-hydraulic nodalisation. Similar nodalisation strategy was then recommended to be applied also in real life safety analysis simulations. Despite the improvements, it was still seen that the results demonstrated a need to further improve the physical models affecting the outcome of reflooding situations.

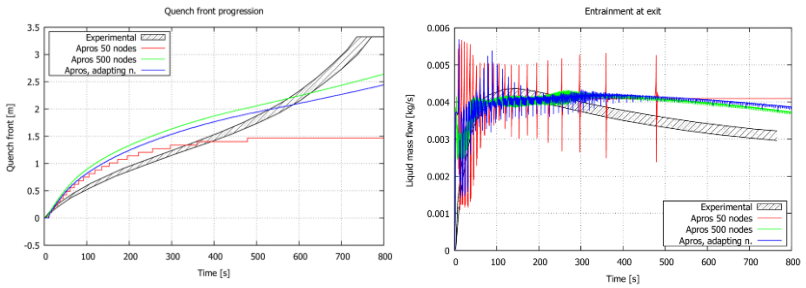

(a) (b)

Figure 3. (a) Quench front progression and (b) entrainment at heated channel exit in ISP-7 calculation [9].

Simulation of new experiments

Apart from the work guided mainly by the validation matrix assessments, an integral part of COVA have also been the analyses of new experiments and benchmark exercises. In years 2015-2018 such cases included for example the OECD/NEA's ATLAS SBLOCA and FONESYS critical flow benchmarks and simulation of OECD/NEA HYMERES experiments. The calculated cases are listed in Table 2.

Table 2. Benchmarks and new experiments calculated in 2015-2016.

Experiment or case	Used code
ATLAS A5.1 benchmark [17]	Apros
ATLAS A5.1 post-test calculation [18]	Apros
ATLAS A5.2 pre-test calculation [19]	Apros
BNL critical flow experiments [20]	Apros
Boivin critical flow experiments [21]	Apros
FONESYS critical flow benchmark [22]	Apros
FONESYS extended critical flow benchmark [23]	Apros
PKL IIIi NC-flowmap test [24]	Apros
PKL4 i2.2 run3 benchmark [25]	Apros
HYMERES HM 2-1 and 3-2 calculations [26]	Apros containment
HYMERES HP6 scoping calculations [27]	Apros containment
PASI characterizing experiments [28]	Apros & Apros containment

Two of the cases were the HM2-1 and HM3-2 HYMERES MISTRA experiments, calculated with Apros containment. MISTRA is a large experimental facility belonging to the CEA and located at Saclay nuclear research centre, devoted to containment thermal-hydraulics and hydrogen risk. The containment is a stainless-steel cylindrical vessel with an internal volume of 97.6 m^3 and comprises two shells, a flat cap and a bottom, which are joined by twin flanges. The outer dimensions of the facility correspond to a linear length scale ratio of 0.1 in relation to a typical French PWR containment. Three so-called condensers are inserted into the MISTRA vessel along the vertical walls. The inner compartment consists of a vertical cylinder, which is closed at the bottom, and is fitted with a ring plate [29]. The facility is shown in Figure 4.

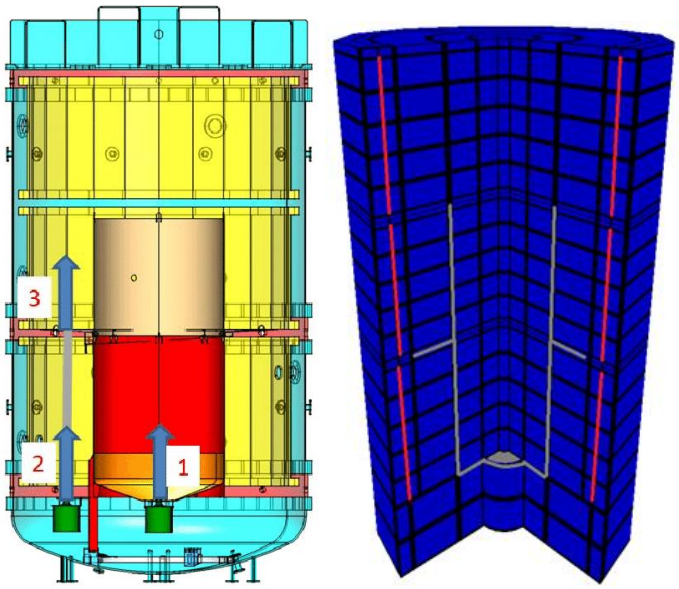

(a) (b)

Figure 4. (a) MISTRA facility [29] and (b) Apros containment nodalization [26].

HM2-1 and HM3-2 experiments study helium distribution in the compartmented volume of the MISTRA facility. In the experiments a stratified dry atmosphere is first created and then helium injection is started to the inner compartment. After this, depending on the test, one or two heat sources that simulate passive autocatalytic recombiners (PARs) are introduced to the upper part of the facility.

The Apros containment model of the MISTRA facility is divided into 22 vertical levels to make it possible to capture the stratification of the gases. The model has 208 containment nodes. The two bottom levels are divided into 6 horizontal nodes, the levels 3-20 are divided into 10 horizontal nodes and the two top levels are divided into 8 horizontal nodes. The outer shell of the MISTRA facility is modelled with 34 heat structures, the inner cylinder with 57 heat structures and the condenser plates are modelled with 5 heat structures each. The model doesn't contain water sumps because the experiments were done in a dry air-helium gas atmosphere.

The heaters used in the experiments (PARs) are modelled with two nodes each. The area of the heater module is modelled with a node that represents the total volume of gas space between the heater plates of the mock-up PAR. The rest of the heater was modelled with the second node. The housing of the heater was not modelled. [26]

Previous analysis of the HM2-1 experiment at VTT [20] had shown that the model under predicted temperatures in the bottom part of the inner compartment during the whole experiment. This was believed to be caused by the lack of radiation heat transfer and heat conduction in the vertical direction of the inner compartment wall.

For the new simulations the model was improved. This was done by adding radiation heat transfer between the outer wall of the inner compartment and the middle and bottom condenser plates. Also radiation heat transfer was taken into account inside the inner compartment and vertical heat conduction was added to the heat structures. The HM2-1 and HM3-2 experiments were then calculated using this improved model. The new results were significantly better than the old ones. Improvement was especially seen in gas temperatures near the bottom of the facility (Figure 5).

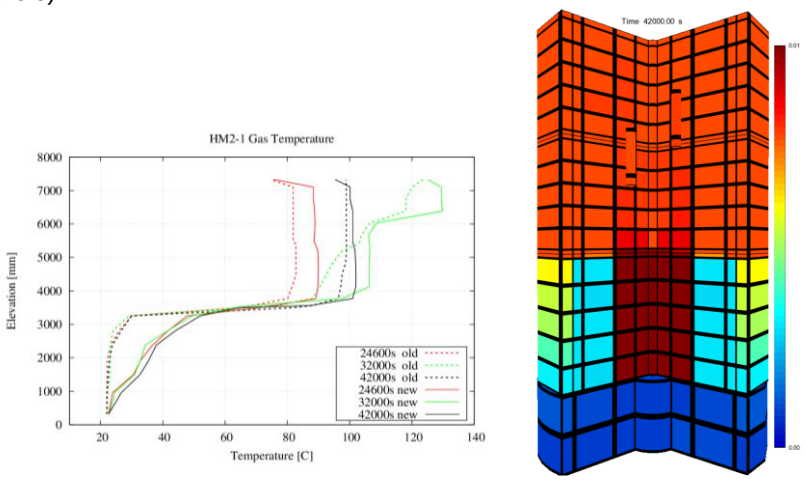

(a) (b)

Figure 5. (a) HM2-1 calculated gas temperatures and (b) HM3-2 helium fraction at the end of simulation.

As an example of interest in domestic test facilities and cooperation in the project, in 2018 a model (Figure 6) was created of the PASI facility [30], located in Lappeenranta University of Technology (LUT). This recently completed facility will be used to study fundamentals and operation modes of a passive heat removal loop closely resembling the AES-2006 PHRS-C passive containment heat removal system. The facility comprises of a heat exchanger located in a pressurizable vessel, connecting gravity driven coolant lines and water tank which acts as a heat sink.

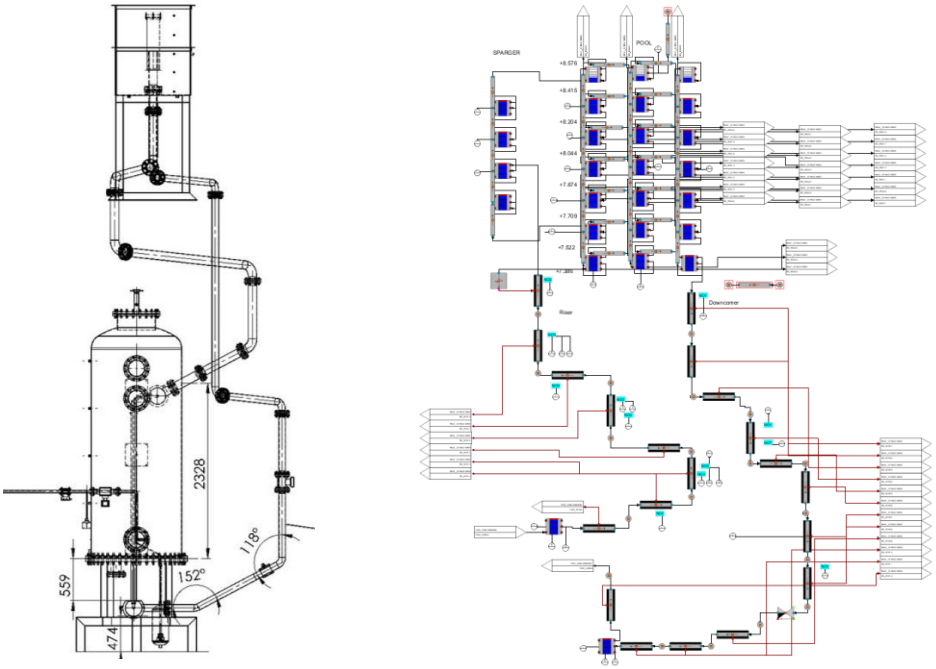

(a) (b)

Figure 6. (a) PASI test facility [30] and (b) the created Apros model [28].

Heat loss, pressure loss and natural circulation pressure characterizing experiments have been simulated with the model with good results. The model creation and simulation of characterizing experiments have created a base which allows simulation of experiments which are expected to realize in 2020. As LUT has prioritized TRACE modelling regarding this facility, they were given access also to the created Apros model. This allows pre-analyzing the planned experiments using two independent codes.

International cooperation

Participation in international research projects related to nuclear safety research in the field of thermal hydraulics has formed an essential part of the project: experimental data produced in these activities was directly utilized in the validation work carried out within COVA, and on the other hand, these validation activities supported conduction of the experiments, in addition to promoting international cooperation and networking in the field of nuclear safety research. Additionally participation fees of some of these programmes were channeled through COVA. In years 2015-2018 the following research programs were participated:

- OECD/NEA ATLAS (Advanced Thermal-hydraulic test Loop for Accident Simulation) project (2014-2017) was aimed at topics of high safety relevance for both current and future power plants. VTT had program review group (PRG) representation in the project.
- OECD/NEA HYMERES (Hydrogen Mitigation Experiments for Reactor Safety) project (2013-2016) objective was to improve the understanding of the hydrogen risk phenomenology in containment in order to enhance its modelling in safety assessments. VTT had program review group (PRG) representation in the project.
- OECD/NEA HYMERES-2 (Hydrogen Mitigation Experiments for Reactor Safety Project Phase 2) project (2017-2021) aims for detailed analysis of the containment phenomenology during postulated severe accidents with the release and distribution of hydrogen. VTT has program review group (PRG) representation in the project.
- OECD/NEA PKL-3 (Primary Coolant Loop Test Facility) programme (2012-2016) was investigating safety issues relevant for current pressurized water plants as well as new PWR concepts. VTT had program review group (PRG) representation in the project.
- OECD/NEA PKL-4 (Primary Coolant Loop Test Facility) test programme (2016-2020) is investigating safety issues relevant for current pressurised water reactor (PWR) plants as well as for new PWR design concepts and focuses on complex heat transfer mechanisms under two-phase flow, boron dilution and precipitation and on cool-down procedures
- OECD/NEA CSNI WGAMA (Working Group on Analysis and Management of Accidents) aims to advance the current understanding of the physical processes related to reactor safety. Mr. Ismo Karppinen from VTT has been appointed as one of the two country representatives of Finland in the task group.
- U.S. NRC CAMP (Code Application and Maintenance Program) is formed to exchange information on thermal-hydraulic safety related issues between U.S. NRC and its international partners. TRACE, PARCS, RELAP5 codes and graphical interface SNAP are made available through this program. Mr. Seppo Hillberg from VTT represents Finland in the program.
- FONESYS Network (Forum & Network of System Thermal-Hydraulics Codes in Nuclear Reactor Thermal-Hydraulics) is an international network of system-thermal hydraulic code developers. It has been created to promote the use of system thermal-hydraulic codes and application of best estimate plus uncertainty (BEPU) approaches, to establish acceptable and recognized procedures and thresholds for verification and validation, and

to create a common ground for discussing envisaged improvements in system codes. VTT has participated in FONESYS since its formation in 2010 as developer of the Apros simulation code.

References

[1] N. Aksan, F. D'Auria, H. Glaeser, R. Pochard, C. Richards and A. Sjöberg. 1993. Separate Effect Test Matrix for Thermal-hydraulic Code Validation, Volume 1, Phenomena Characterisation and Selection of Facilities and Tests. NEA/CSNI/R(93)14/Part.1/Rev., OECD/GD(94)82.

[2] N. Aksan, F. D'Auria, H. Glaeser, R. Pochard, C. Richards and A. Sjöberg. 1993. Separate Effect Test Matrix for Thermal-hydraulic Code Validation, Volume 2, Facility and Experiment Characteristics. NEA/CSNI/R(93)14/Part.2/Rev., OECD/GD(94)83.

[3] OECD/NEA CSNI. 2014. Containment Code Validation Matrix. NEA/CSNI/R(2014)3.

[4] Karppinen, I. 2016. Assessment of Apros thermal hydraulic models with separate effect tests. VTT, Espoo. VTT-R-06020-15

[5] Silde, A. 2016. Assessment of Apros containment software. VTT, Espoo. VTT-R-04560-15.

[6] Lauerma, S., Skripnikov, D., Hovi, T. 2016. Friction and heat transfer experiment simulations with Apros. VTT, Espoo. VTT-R-06266-15.

[7] Leskinen, J. 2017. Assessment of Apros reflood models against the ACHILLES natural reflood experiment. VTT, Espoo. VTT-R-00138-17.

[8] Szogradi, M. 2018. Validation of Apros 6.08 with Becker's burnout experiments. Espoo, VTT. VTT-R-05067-18

[9] Kurki, J. 2017. Simulation of the ISP-7 reflooding experiment with Apros. VTT, Espoo. VTT-R-00359-17.

[10] Dorval, E. 2017. A re-evaluation of FLECHT SEASET test 32013 with Apros. VTT-R-03993-16.

[11] Airaksinen, R. 2018. RBHT Reflooding Heat Transfer Experiments with Apros. Espoo, VTT. VTT-R-03931-18

[12] Hillberg, S. Assessment of NEPTUN reflooding experiments 5050 and 5052 with TRACE V5.0 Patch 5. [NUREG-IA series report which has not yet been published]

[13] Silde, A. 2018. Calculation of the HYMERES/PANDA natural circulation test HP6_1 with Apros containment software. Espoo, VTT. VTT-R-06500-17

[14] Kolehmainen, J. 2018. Simulation of the ISP-47 TOSQAN Experiment with containment package of Apros 6.07. Espoo, VTT. VTT-R-06716-17

[15] Silde, A. 2019. Calculation of TOSQAN spray test 101 using the multi-size spray droplet model of the Apros containment code. Espoo, VTT. VTT-R-00081-19

[16] Silde, A. 2017. Simulations of wall condensation and sump evaporation TOSQAN test T201 using the Apros containment code. VTT, Espoo. VTT-R-05557-16.

[17] Hillberg, S. 2016. Simulation of the ATLAS A5.1 benchmark in blind phase with Apros. VTT, Espoo. VTT-R-06347-15.

[18] Hillberg, S. 2016. Simulation of the ATLAS A5.1 SBLOCA benchmark in post-test phase with Apros. VTT, Espoo. VTT-R-02390-16.

[19] Hillberg, S. 2016. ATLAS A5.2 IBLOCA pre-test calculation with Apros. VTT, Espoo. VTT-R-03700-16.

[20] Hillberg, S. 2019. BNL critical flow experiments with Apros. Espoo, VTT. VTT-R-05798-18

[21] Hillberg, S. 2018. Simulation of Boivin critical flow experiments with Apros 6.07. Espoo, VTT. VTT-R-01059-18

[22] Kurki, J., Alku, T., Karppinen, I. 2016. Simulation of the FONESYS FO-02 Critical flow benchmark with Apros. VTT, Espoo. VTT-R-06071-15.

[23] Hillberg, S. 2017. Simulation of the extended FONESYS FO-02 critical flow benchmark with Apros. VTT, Espoo. VTT-R-00034-17.

[24] Szogradi, M. 2018. Analysis of PKL IIIi NC-flowmap test with Apros 6.07.33.03. Espoo, VTT. VTT-R-00011-18.

[25] Szogradi, M. 2018. Analysis of PKL4 i2.2 run3 benchmark with Apros 6.07. Espoo, VTT. VTT-R-02244-18.

[26] Kolehmainen, J. 2015. Simulation of the HYMERES MISTRA HM 2-1 and HM 3-2 experiments with containment package of Apros 5.14.09. VTT, Espoo. VTT-R-05463-15.

[27] Kolehmainen, J. HYMERES HP6 scoping calculations with Apros 6.05. VTT, Espoo. VTT-R-04125-16.

[28] Kolehmainen, J. 2018. Apros simulations of the PASI characterizing experiments. Espoo, VTT. VTT-R-04602-18

[29] OECD/NEA. 2016. NEA Hydrogen Mitigation Experiments for Reactor Safety (HYMERES) Project. Retrieved from https://www.oecd-nea.org/jointproj/hymeres.html.

[30] Telkkä, J., Kouhia, V., Partanen, H., Räsänen, A., Kauppinen, O-P., Kotro, E., Saure, I., 2017. INTEGRA 5/2018 General description of the PASI test facility. Lappeenranta University of Technology School of Energy Systems Nuclear Engineering.

5.2 Integral and separate effects tests on thermal-hydraulic problems in reactors (INTEGRA)

Vesa Riikonen, Virpi Kouhia, Otso-Pekka Kauppinen, Joonas Telkkä

LUT University
P.O. Box 20, FI-53851 Lappeenranta, Finland

Abstract

The objective of the SAFIR2018 INTEGRA project was to improve the understanding of thermal-hydraulic system behavior by performing integral and separate effects tests with the PWR PACTEL and PASI facilities, in particular regarding the impact of non-condensable gases on core cooling and reliability of natural circulation loop decay heat removal. Carefully designed experiments are the most reliable way to obtain fundamental understanding and reliable data of the phenomena. The data is available also for the development and validation of computer codes for the safety analyses of nuclear power plants. Performing experiments not only requires the hardware and programs controlling the devices and gathering data, but also the knowledge of the system behavior. Computer analyses with system and CFD codes are needed in the planning of the experiments as well as in post analyses to help understanding the physics in the experiments.

Introduction

The objective of the SAFIR2018 INTEGRA project was to improve the understanding of thermal-hydraulic system behavior by performing integral and separate effects tests with the PWR PACTEL (Kouhia et al., 2014) and PASI (Kouhia et al., 2018c) facilities. The focus of the studies was on the impact of non-condensable gases on core cooling (Riikonen et al., 2018c) and reliability of natural circulation loop decay heat removal. The data from the experiments is available for further analyses as well as for the development and validation of computer codes for the safety analyses of nuclear power plants.

A part of the international efforts in enhancing the reactor safety is the OECD projects. Finland participated in the OECD/NEA PKL Phase 3 project (OECD/NEA, 2019a) with PWR PACTEL experiments (Riikonen et al., 2013; Riikonen et al., 2014; Riikonen et al., 2015) as a part of the SAFIR2018 INTEGRA project. The most of the OECD countries using nuclear power participated in the project, which was set to investigate safety issues related to beyond design basis accident transients with significant core heat-up, i.e. station blackout scenarios or loss-of-coolant accidents

(LOCA) in connection with a failure of safety systems. The OECD/NEA PKL Phase 3 project ended in April 2016.

The OECD/NEA PKL Phase 4 project (OECD/NEA, 2019b) began in 2016. The OECD/NEA PKL Phase 4 experiments investigate safety issues relevant for current PWR plants as well as for new PWR design concepts by means of systematic parameter studies on thermal-hydraulic phenomena and transient tests under postulated accident scenarios. Finland is participating in the project with impact of nitrogen on cool-down/heat removal experiments (Riikonen et al., 2018a) with PWR PACTEL in the SAFIR2018 INTEGRA project. The OECD/NEA PKL 4 project continues to the end of June 2020.

Most of the organizations participating in the OECD PKL Phase 4 Project are doing analytical work with thermal-hydraulic codes. It would be beneficial for LUT also to participate in the analytical work of the experiments with the PKL facility. In LUT, a TRACE simulation model of the PKL test facility was made and tested against the characterizing tests of the facility for that as a master's thesis (Tahvola, 2018).

Non-condensable gases, if present in the reactor cooling system, affect the coolability of the nuclear reactor core. In LOCA, nitrogen from hydroaccumulators could enter the reactor system and can temporarily alter the water level in the core by a piston effect. The piston effect on the downcomer side can increase water level in the core and improve core cooling. The accumulator nitrogen discharge to the primary system has been studied with the UPTF and BETHSY test facilities. In UPTF the pressure rise in the loop was observed, but the impact on the core cooling could not be assesses due to the restrictions of the facility (Damerell and Simons, 1993). Tests with the BETHSY facility confirmed the potentially significant impact of nitrogen gas injection from the accumulators on the core cooling in a large break LOCA (Barbier et al., 1996). In the SAFIR2018 INTEGRA project, the effect of nitrogen in LOCA situations was studied experimentally with the PWR PACTEL facility (Riikonen et al., 2018c). The main goal of this testing was to independently verify whether the claimed positive effect of nitrogen on the core cooling can be reproduced and to generate data for the development and validation of thermal-hydraulic system codes.

With the PWR PACTEL experiments, the asymmetric flow in the loops was studied simulating a case where one of the reactor coolant pumps trips (Riikonen et al., 2018b). Tripping of a reactor coolant pump causes asymmetric flow conditions in primary loops as well as in a reactor core if the isolation of the loop is not possible.

System code analyses are usually needed in the planning of the PWR PACTEL experiments as well as in post analyses to help understanding the physics in the experiments (Kauppinen et al., 2015a; Kouhia & Kauppinen, 2017). The flow reversal phenomena in the PWR PACTEL steam generator U-tubes was further studied and analyzed (Kauppinen et al., 2015b) in the SAFIR2018 INTEGRA project.

Many currently marketed LWR designs feature varying numbers of naturally circulating decay heat removal loops. Large diversity of design configurations is available. A review on system characteristics of passive heat removal was written in LUT (Kouhia & Kauppinen, 2016). An open natural circulation heat removal system was

selected to be studied experimentally with the new PASI test facility (Kouhia et al., 2018c). The reference system for this facility is the containment passive heat removal system designed for the AES-2006 type power plant.

PWR PACTEL nitrogen experiments

Non-condensable gases, if present in the reactor cooling system, affect the coolability of the nuclear reactor core. The driving force of the accumulator injection is the pressurized nitrogen volume at the top of the accumulator tanks. In some plants, the release of gaseous nitrogen to the primary side is prevented with an automatic closure of the accumulator injection line at the end of the discharge. If the automatic closure system fails, nitrogen can flow to the reactor cooling system after the accumulators are empty of water. Nitrogen can temporarily increase the water level in the core by the piston effect and have a positive effect on core cooling (Figure 1).

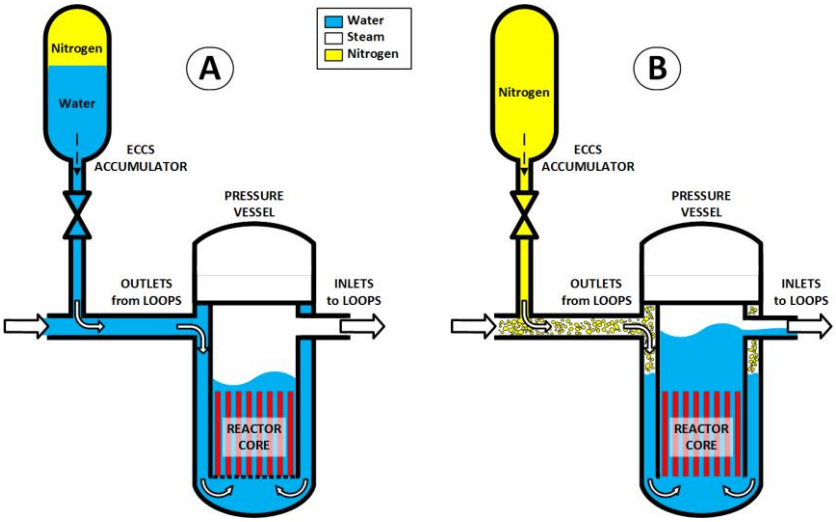

Figure 1. Anticipated behavior of the reactor cooling system during LOCA when nitrogen is injected from the accumulator.

The effect of nitrogen in LOCA situations was studied experimentally (Riikonen et al., 2018c, Riikonen et al., 2016) with the PWR PACTEL facility. The main goal was to verify independently whether the claimed positive effect of nitrogen on the core cooling can be reproduced and to generate data for the development and validation of thermal-hydraulic system codes.

The series of the nitrogen experiments included six experiments. Three of them were reference experiments where nitrogen was not released to the primary system. In four experiments, the accumulator injection was located in a cold leg as in the EPR power plant. In two of those four experiments, the break location was in a cold

leg and in the others in a hot leg. In the last two experiments, the accumulator injection location was in the upper plenum like in the VVER and AES type power plants and the break location was in a cold leg.

A connection line with an orifice plate between the downcomer top part and the upper plenum was constructed into the PWR PACTEL facility to present the analogous flow path in the EPR type power plant. This connection line was open in the first four experiments. As this type flow path is not present in a VVER type power plant, the bypass line valve was closed in the last two experiments.

Each experiment was performed under natural circulation conditions. The experiments began from steady-state natural circulation conditions by opening the break. The used safety functions were the accumulator water injection and the secondary side depressurization. The accumulator water and nitrogen volumes were chosen to represent the volumes of the EPR type accumulators.

After the accumulator water mass was injected to the primary side, the accumulator injection line valve was closed. In the nitrogen release experiments, the nitrogen release line valve was opened immediately after the water injection line closure. To protect the facility from overheating, the core power reduction system was available during the experiments.

With the cold leg break, the injection of the accumulator nitrogen into the primary side did not cause a pressure rise in the cold leg and the downcomer with respect to the upper plenum. However, the core level depletion was delayed and the core heatup postponed few minutes with the nitrogen injection. This was a consequence of the break location. The break location in the cold leg was quite close to the downcomer and allowed the injected accumulator water and nitrogen to escape easily from the system. The nitrogen discharge via the break reduced water loss from the cooling system leaving more water in the system for the core cooling and hence provided a positive impact on the core cooling. The results might be different if the break location was near the steam generator. This will be studied in the PWR PACTEL experiments in the OECD/NEA PKL Phase 4 project.

With the hot leg break, the injection of the accumulator nitrogen into the primary side had a clear negative impact on the core cooling. Nitrogen injected into the cold leg entered the upper plenum and flowed with the steam to the steam generators. In the steam generators, the steam and nitrogen mixture entered the heat exchange tubes where steam condensed, and nitrogen was enriched. Nitrogen in the heat exchange tubes blocked part of the heat exchange area, decreasing the condensation heat transfer in the steam generator U-tubes. The depressurization in the primary side stopped, keeping the accumulator and primary side pressures constant until the temperature of the core started to increase. The experiments show that the accumulator nitrogen can stop the primary side depressurization and cause a core heatup at reactor pressure above or very close to a typical low pressure safety injection shut-off head. More testing would be needed to map the full range of the pressures at which the decoupling of the primary and secondary side pressures takes place, as a function of the number of the accumulators injecting (nitrogen mass) and the number of the steam generators participating in the secondary side

depressurization (volume available for nitrogen). These tests will be proposed in the SAFIR2022 PATE project for 2020 – 2022.

In the upper plenum injection experiments, the effect of non-condensable gases on natural circulation during a SBLOCA was studied and experiment data especially for the APROS validation was generated. In these experiments, the connection line between the upper plenum and the downcomer was closed. The goal to study the effect of non-condensable gases on natural circulation during a SBLOCA was not achieved. That would require at the same time measurable flow rates in the loops, the water level in the core below the hot leg entrance, adequate core cooling to prevent the core heat up, and enough nitrogen in the loops to stop the loop flow. It is not possible to achieve all the required conditions at the same time. Nevertheless, these experiments gave useful data for the code validation especially because there are only few experiments available where the accumulator injects to the upper plenum, which is a special feature of the VVER and AES type reactors.

PWR PACTEL pump trip experiments

With the PWR PACTEL experiments, the asymmetric flow in the loops was studied simulating a case where one of the reactor coolant pumps trips (Riikonen et al., 2018b). In a power plant, the tripping of a reactor coolant pump causes asymmetric flow conditions in the primary loops as well as in the reactor core if the isolation of the loop is not possible. A flow reversal occurs in the affected loop due to the reversal of the pressure distribution in the loop caused by the other running pumps. The final flow conditions are characterized by a slight overflow in the intact loops and a backflow in the loop with the idle reactor coolant pump.

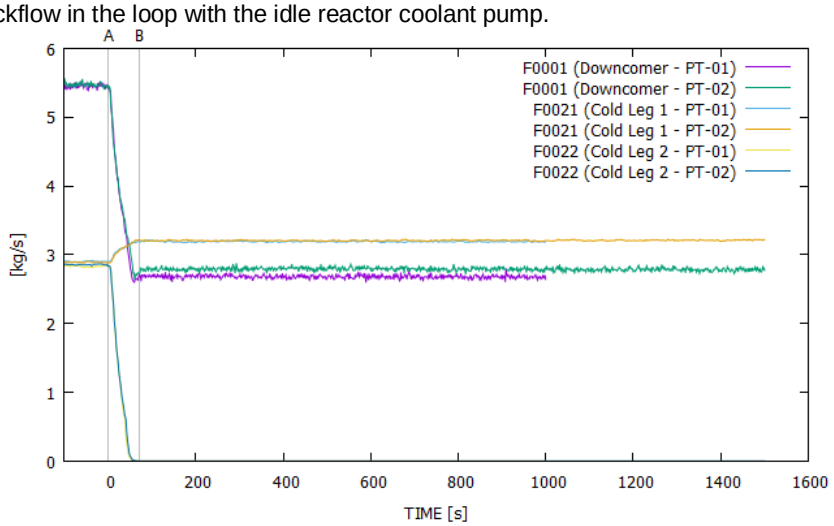

Figure 2. Mass flow rates in the downcomer and the loops in the PWR PACTEL pump trip experiments PT-01 and PT-02. The flow meters cannot measure reverse flows. A = pump trip, B = flow reversal.

Two experiments were carried out. The experiments were otherwise similar to each other but the core power levels after the pump trip were different. The asymmetric flow in the loops was observed in the experiments (Figure 2). The effect of the pump trip on the core was not possible to study with the PWR PACTEL experiments. The facility cannot simulate well enough 3D phenomena, as the parts of the facility are narrow. According to the PWR PACTEL experiments, the pump trip does not weaken the safe operation of the plant. The system stabilizes soon to a new steady state. The effect of the flow reversal in the loop on the pump, for example on the pump cooling, was not studied.

Simulations of PWR PACTEL experiments

The APROS and TRACE system codes were utilized within the SAFIR2018 INTEGRA project to support the planning of the PWR PACTEL experiments in LUT. The codes have been used in pre-test and post-test analyses. The main purpose of the pre-test simulations in the project was to assist in defining test parameters, to obtain a tentative insight on possible conditions to be expected during the actual experiments, and observe beforehand possible issues compromising the safe operation of the facility. Hence, typically parameters and geometrics used in the pre-test analyses have been somewhat different from the final conditions in the experiments. Where feasible, to improve the performance of the simulation models the models were tested with post-test cases, using the final experiment conditions and parameters.

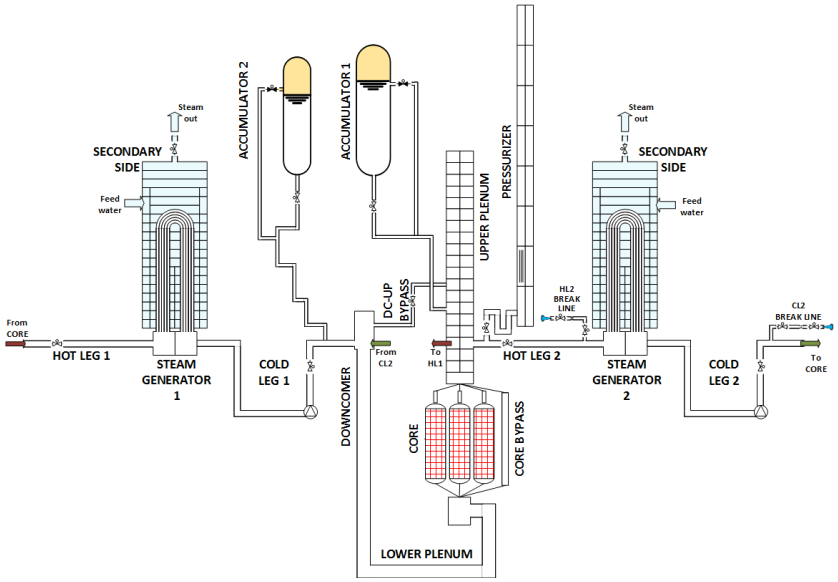

Figure 3. Schematic view of the PWR PACTEL simulation model for the APROS code.

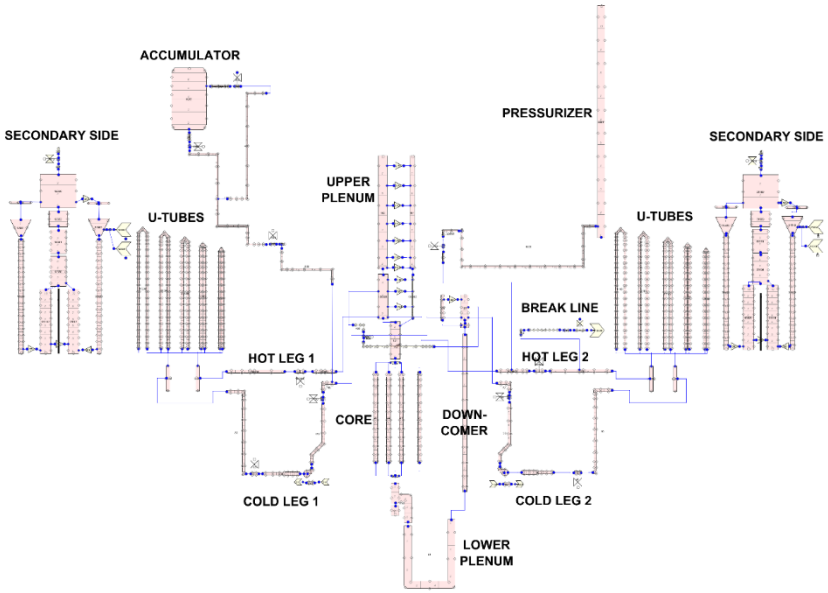

Figure 4. The PWR PACTEL simulation model for the TRACE code.

The APROS and TRACE simulation models of the PWR PACTEL facility have been built with similar principals. The facility is modelled in details, including the complete primary side, the secondary sides of the steam generators and the emergency core cooling systems as needed. The geometry is modelled fairly detailed and the measurement elevations of the facility are taken into account in the nodalizations. In both simulation models the 51 heat exchange U-tubes of the PWR PACTEL steam generators are lumped together into 5 parallel pipe components according to the different main lengths of the U-tubes. For the simulation of the PWR PACTEL nitrogen experiments, the models required some modifications. The accumulator lines for nitrogen injection and the connection line between the upper plenum and downcomer top were added in both models. The general scheme of the simulation models are presented in Figure 3 and Figure 4.

In the SAFIR2018 INTEGRA project, two experiments with the nitrogen injection performed with the PWR PACTEL facility were chosen for the post-test simulations; the hot leg break experiment with the accumulator injection to the cold leg (NCG-13) and the cold leg break experiment with the accumulator injection to the upper plenum (NCG-15) (Kouhia & Kauppinen, 2017).

In these post-test simulations, the codes were able to calculate the nitrogen experiments moderately well, considering the ability to capture main phenomena and conditions in both transient cases. In the NCG-13 simulations of the TRACE code, the hot leg break flow rate and the accumulator water reduction followed the experiment references during the accumulator water injection period exemplary. In the APROS simulation, the accumulator water injection period continued longer com-

pared to experiment. In both simulations, the stop of the primary side depressurization during the nitrogen injection period was not as clear as in the NCG-13 experiment. In the APROS simulation, the accumulator and primary side pressures decreased slowly and steadily in the beginning of this period. After that, the primary side pressure started to increase and the accumulator pressure stabilized to a constant value as the check valve in the accumulator line closed. In the TRACE simulation, the primary side pressure decreased slowly almost all the time and nitrogen was flowing to the primary side. Nitrogen was not able to pressurize the upper plenum as much as in the experiment. In both simulations, the core heatup occurred later than in the experiment. In the APROS simulation, the duration of the nitrogen injection period before the core heat up was relatively well predicted but the longer accumulator water injection period caused the nitrogen injection period to start later than in the experiment and postponed the core heat up. In the TRACE simulation, the water draining from the steam generator U-tubes slowed down the water level decrease in the core during the nitrogen injection period. This prolonged the nitrogen injection period and delayed the core heat up.

In the NCG-15 simulations, the accumulator water injection ended slightly faster than in the experiment. For this reason, the accumulator nitrogen line valve also opened earlier than in the experiment. Despite the early starting time of the accumulator nitrogen injection period, the nitrogen actually started to enter the primary side after several hundred seconds after the initiation of the nitrogen injection system. There was a manometric cyclic behavior in the experiment during the accumulator water injection period, notable from several parameters. The TRACE simulation model predicted the cyclic behavior also but in the APROS simulation that was not so evident. The loop seal clearing strongly affected the conditions in the simulations of the NCG-15 experiment, i.e. in the redistributing the water amounts along the facility and contributing the core cooling capacities. Already during the accumulator water injection period the simulations experienced the core heat-up periods, that were settled either with the loop seal clearings (TRACE, APROS) or with also a core protection system (APROS). The heat-up periods appeared also during the accumulator nitrogen injection period, once settled with the loop seal clearing and finally with clearings along with core protection system. The experiment had also a small core heat-up during the accumulator water injection period, which was halted presumably by the accumulator water injection. In both simulations, the final core heat-up occurred later than in the experiment.

The experiment results do not include any specific clear indication on the nitrogen distributions in the primary side during the transients. The total amounts of nitrogen that were able to enter the primary side in these transients according to the simulation observations and estimations on the experiments vary from hundreds of grams to several kilograms. As the total duration of the simulations and experiments were different, the nitrogen amounts entering the primary side varied and are not necessarily comparable.

Due to the discrepancies in the results of the NCG-13 simulations, modifications to the calculation models of the PWR PACTEL were made and the NCG-13 exper-

iment was simulated again. In the APROS model, the accumulator model was modified by boosting the heat transfer efficiency between the phases and some nodal connections were adjusted in the upper plenum elevations. In the TRACE model, the correlation constant of the Wallis CCFL model at the ends of the steam generator U-tubes were adjusted. With these modifications, the general behavior of the transient and the timing of the main events match better with the experiment results. In both simulations the stop of the primary side depressurization and the timing of the core heat up were predicted satisfactory (Figure 5). In spite of the well predicted general behavior of the transient, in both simulations the amount of nitrogen released from the accumulator were overpredicted. This indicates that both codes underestimate the adverse effect of nitrogen on core coolability. The results of these NCG-13 simulations are offered to be published in a scientific journal.

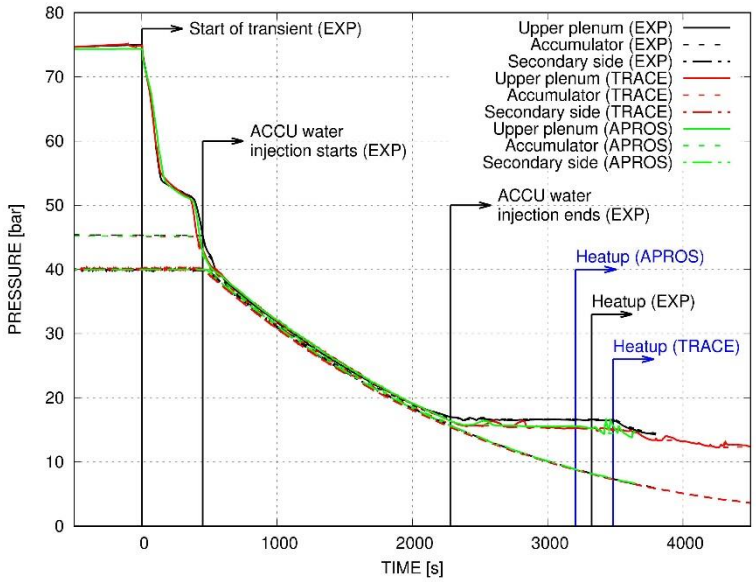

Figure 5. Primary, accumulator and secondary side pressures in the simulations and experiment NCG-13.

The PWR PACTEL pump trip experiment PT-01 was simulated with the APROS code (Kouhia, 2018a). The tripping of the pump in the loop 2 caused asymmetric flow conditions between the loops as the flow in the affected loop reversed. The comparison of the simulation and experiment results showed that the model is capable to simulate the experiment with reasonable accuracy. The differences were detected between the temperature measurements inside the core and steam generator tube areas, caused from the simplified modelling technique utilized (lumped modelling). Figure 6 shows the mass flow rates in the downcomer and both loops in the experiment and simulation. The cold leg 2 measured mass flow rate value

showed zero, as the measurement device could not measure reversed flow. As the other two simulated mass flow rates (downcomer and cold leg 1) were close to the measured ones, it can be assumed that also the cold leg 2 simulated mass flow rate should be close to the real value, i.e. the flow of the cold leg 2 in the experiment also reversed though the measurement was not able to show that directly. The simulation of the PT-01 experiment showed still needs to check the validity of the simulation model, i.e. pressure losses in the loops, the pressurizer surge line and the connection line as well as the heat losses in the upper plenum volumes (latter slightly problematic as the net of reference measurement devices on these parts is fairly limited).

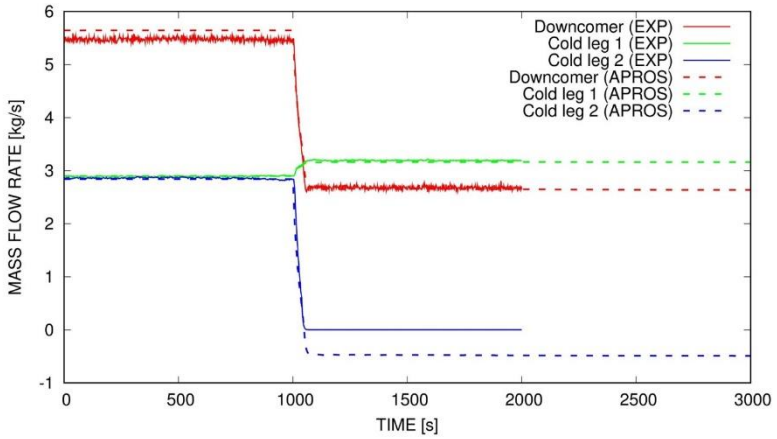

Figure 6. Mass flow rates in the downcomer and loops in the experiment PT-01 and APROS simulation.

In the SAFIR2018 INTEGRA project, a TRACE calculation model of the PKL test facility was built (Tahvola, 2018). The pressure and heat losses in the model were determined according to the pressure and heat loss experiments of the PKL facility. In addition, the model was tested by simulating the natural circulation conditions of one PKL experiment. The natural circulation case showed good accuracy, but more studies should be carried out to test the model with different accident scenarios.

Facility for research on passive heat removal

The SAFIR2018 INTEGRA project introduced a completely new facility, PASI (Kouhia et al., 2018c), for the studies of a passive containment heat removal system. The facility was constructed in 2017 and the first experiments were performed in 2018. The reference system for the PASI test facility is the passive containment heat removal system of the AES-2006 type pressurized water reactor. The design

height scale is 1:2 considering the riser and downcomer pipelines and the heat exchanger.

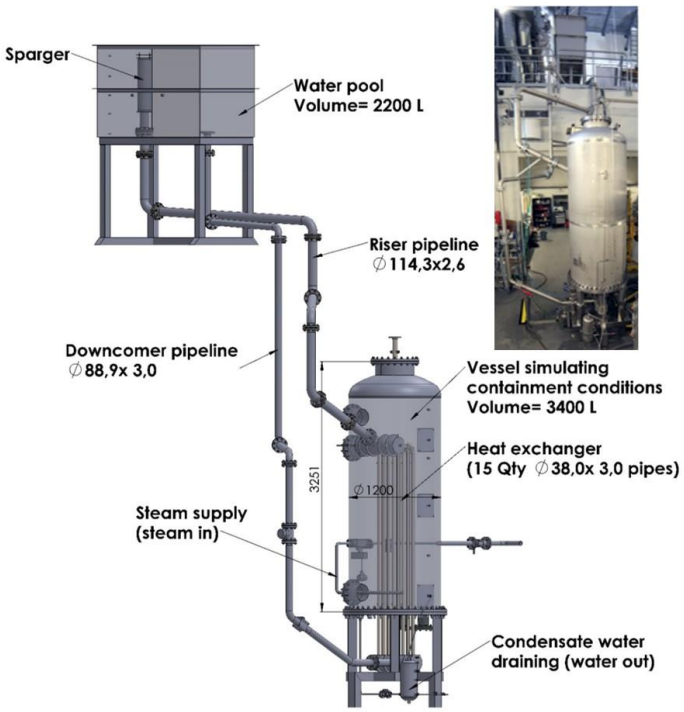

Figure 7. General view of the PASI test loop.

Figure 8. Heat exchanger of the PASI test loop.

Figure 9. A pressure vessel of the PASI test loop simulating containment conditions.

The PASI facility (Figure 7) is a one loop model of an open passive containment cooling system. The system has one heat exchanger with a tube bundle and two

collectors (Figure 8) as well as riser and downcomer pipelines with connections to a water pool forming a heat removal loop. A pressure vessel around the heat exchanger (Figure 9) provides containment environment and the water pool acts as a water reservoir for the natural circulating system.

Additional systems are included to provide steam to the vessel simulating containment conditions and collect condensate water from the vessel. The water pool includes possibilities to remove steam and inject feedwater. An aerosol injection system can be added to the system in future. In addition, the facility includes capillary piping to house fiber-optic transducers for longitudinal temperature distribution measurements when needed.

With the PASI facility, the goal is to conduct tests to measure system performance characteristics, and to detect issues that could disturb the operation of a passive system or prevent it from functioning as designed. Characterizing experiments were performed to analyze, verify and study characteristics that describe this passive heat removal loop (Kouhia & Riikonen, 2018b). The pressure losses were determined for normal and reverse directions. A heat up and cool down method was used to calculate integral heat losses and heat capacities of the facility over a range of fluid temperatures. The uncertainties of the heat losses and heat capacities are relatively high. There is not any single source for the uncertainties. Mostly those are rising from the approximations made for the analysis and from the uncertainties in the measurements.

A natural circulation experiment was performed to study the normal behavior of the PASI facility and the capability to remove heat (Kouhia & Riikonen, 2018b). The natural circulation experiment started from atmospheric pressure and low temperature in the vessel. The PASI facility was operating as expected, transferring heat to the water pool efficiently. The natural circulation in the loop initiated soon after the steam supply to the vessel simulating containment conditions began. The single-phase period showed steady and smooth operation of the heat removal loop, lasting about 2.5 hours. The oscillation phase started as the hot loop side reached saturation conditions and the single-phase flow turned into two-phase flow. This period was characterized by the strong oscillation of the loop mass flow rate (Figure 10).

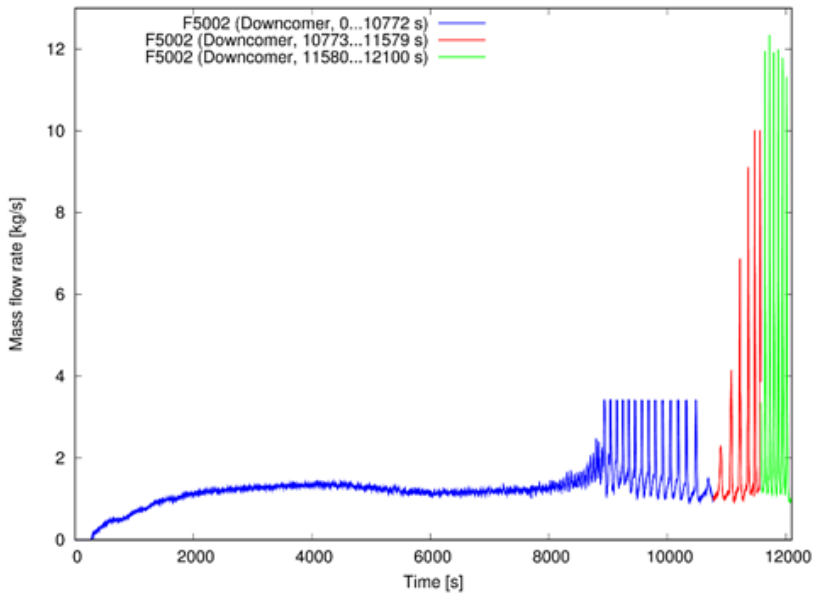

Figure 10. Loop mass flow rate in the natural circulation experiment. At the end of the experiment, the measuring range of the flow meter had to be changed twice because the peak values of the natural circulation mass flow rates exceeded the maximum value of the flow meter measurement range.

Acknowledgement

The Finnish Research Program on Nuclear Power Plant Safety 2015–2018 (SAFIR2018) and the Finnish power companies Teollisuuden Voima Oy (TVO) and Fennovoima Oy have provided funding for the SAFIR2018 INTEGRA project. The OECD/NEA PKL Phase 3 and 4 projects were performed with the financial support of the Finnish Research Programme on Nuclear Power Plant Safety (SAFIR2014 and SAFIR2018), the Finnish power company Teollisuuden Voima Oy (TVO), and the partners participating in the OECD/NEA PKL Phase 3 and 4 projects.

The authors are grateful for their support to all the financiers of this research task, OECD Nuclear Energy Agency (NEA), the members of the SAFIR2014 and SAFIR2018 Reference Group 4, and the members of the Program Review Group and the Management Board of the OECD/NEA PKL Phase 3 and 4 projects. The data from the experiments in the OECD/NEA PKL Phase 3 and 4 projects are available to the NEA member countries via their CSNI representative organizations three years after the end of the project.

References

Barbier, J.C., Clement, P.A., Deruaz, R.L., 1996. A hot leg break accident with HPIS failure and nitrogen injection by the accumulators in the BETHSY facility. ICONE-4, Proceedings, Volume 3.

Damerell, P.S., Simons, J.W., (Eds.), 1993. Reactor Safety Issues Resolved by the 2D/3D Program, NUREG/IA-0127, GRS–101, MPR–1346, July. https://www.nrc.gov/reading-rm/doc-collections/nuregs/agreement/ia0127/.

Kauppinen, O.-P., Kouhia, V., Riikonen, V., Hyvärinen, J. & Sjövall, H. 2015a. Computer analyses on loop seal clearing experiment at PWR PACTEL. Annals of Nuclear Energy, Volume 85, 2015, Elsevier, pp. 47-57.

Kauppinen, O.-P., Riikonen, V., Kouhia, V. & Hyvärinen, J. 2015b. Analysis of reverse flow in low-rise inverted U-tube steam generator of PWR PACTEL facility. The 16th International Topical Meeting on Nuclear Reactor Thermal Hydraulics, NURETH-16, Chicago, USA, August 30-September 4, 2015.

Kouhia, V., Riikonen V., Partanen, H., Räsänen, A., Kauppinen, O.-P., Telkkä, J. & Pyy, L. 2014. General Description of the PWR PACTEL test facility - third edition. Technical report, PAX 2/2014, Lappeenranta University of Technology, Nuclear Safety Research Unit, Lappeenranta, 2014, pp. 28 + 118.

Kouhia, V. & Kauppinen, O.-P. 2016. Review on factors affecting the operation of passive heat removal circuits. Research report, INTEGRA 2/2015, Lappeenranta University of Technology, Nuclear Engineering, Lappeenranta, 2016, pp. 58.

Kouhia, V. & Kauppinen, O.-P. 2017. Simulations of PWR PACTEL nitrogen experiments, INTEGRA 2/2016, Lappeenranta University of Technology, Nuclear Engineering, Lappeenranta, 2017, pp. 64 + 4.

Kouhia, V. 2018a. Simulation of PWR PACTEL Pump Trip Experiment with APROS code. INTEGRA 4/2018, Lappeenranta University of Technology, Nuclear Engineering. Lappeenranta, 2018, pp. 24 + 1.

Kouhia, V. & Riikonen, V. 2018b. PASI facility – characterizing experiments. Research Report, INTEGRA 3/2018, Lappeenranta University of Technology, Nuclear Engineering. Lappeenranta, 2018, pp. 43 + 7.

Kouhia, V., Riikonen, V., Telkkä, J., Partanen, H., Räsänen, A., Kauppinen, O.-P., Kotro, E., Saure, I., Tielinen, K. & Karppinen, J. 2018c. General description of the PASI test facility, second edition. Technical Report, INTEGRA

5/2018, Lappeenranta-Lahti University of Technology LUT, Nuclear Engineering, Lappeenranta, 2018, pp 22 + 32.

OECD/NEA. 2019a. NEA Joint Projects, Completed projects, NEA Primary Coolant Loop Test Facility (PKL-3). Project WWW-pages at URL: https://www.oecd-nea.org/jointproj/pkl-3.html (retrieved February 2019).

OECD/NEA. 2019b. NEA Joint Projects, Ongoing experimental projects, NEA Primary Coolant Loop Test Facility (PKL-4). Project WWW-pages at URL: WWW-pages: https://www.oecd-nea.org/jointproj/pkl-4.html (retrieved February 2019).

Riikonen, V., Kouhia, V. & Kauppinen, O.-P. 2013. Cool down under Natural Circulation Conditions in Presence of Secondary side Isolated Steam Generators. Research Report, PAX 1/2013, Lappeenranta University of Technology, Nuclear Safety Research Unit, Lappeenranta, 2013, pp. 17 + 3.

Riikonen, V., Kouhia, V. & Kauppinen, O.-P. 2014. Station blackout experiments. Research Report, PAX 1/2014, Lappeenranta University of Technology, Nuclear Safety Research Unit, Lappeenranta, 2014, pp. 20 + 18.

Riikonen, V., Kouhia, V. & Kauppinen, O.-P. 2015. PWR PACTEL flow reversal experiments. Research Report, INTEGRA 1/2015, Lappeenranta University of Technology, Nuclear Engineering, Lappeenranta, 2015, pp. 10 + 3.

Riikonen, V., Kouhia, V. & Kauppinen, O.-P. 2016. PWR PACTEL nitrogen experiments. Research Report, INTEGRA 1/2016, Lappeenranta University of Technology, Nuclear Engineering, Lappeenranta, 2016, pp. 23 + 17.

Riikonen, V. 2018a. Quick look report of the PWR PACTEL nitrogen reference experiment in the OECD/NEA PKL Phase 4 project, Research report, INTEGRA 2/2018, Lappeenranta University of Technology, Nuclear Engineering, Lappeenranta, 2018, pp. 10 + 10.

Riikonen, V., Kouhia, V. & Kauppinen, O.-P. 2018b. PWR PACTEL pump trip experiments. Research report, INTEGRA 1/2018, Lappeenranta University of Technology, Nuclear Engineering, Lappeenranta, 2018, pp. 8 + 4.

Riikonen, V., Kouhia, V., Kauppinen, O.-P., Hyvärinen, J. 2018c. Experimental observation of adverse and beneficial effects of nitrogen on reactor core cooling. Nuclear Engineering and Design, vol. 332 (2018), Elsevier, pp. 111-118.

Tahvola Ilkka, Modelling of PKL test facility with TRACE code, Lappeenranta University of Technology, 2018.

5.3 Couplings and instabilities in reactor systems (INSTAB)

Markku Puustinen, Jani Laine, Antti Räsänen, Lauri Pyy, Vesa Tanskanen, Elina Hujala, Eetu Kotro, Kimmo Tielinen, Giteshkumar Patel

Lappeenranta-Lahti University of Technology LUT
School of Energy Systems
Nuclear Engineering
P.O. Box 20, FI-53851 Lappeenranta

Abstract

In the INSTAB project, mechanisms and efficiency of mixing with different subsystems in the pressure suppression pool have been investigated experimentally in the PPOOLEX facility. The tests with a model of a safety relief valve sparger verified that mixing of a thermally stratified water pool could happen also through an erosion process in addition to internal circulation, if suitable flow conditions prevail. The wetwell spray tests in PPOOLEX revealed that mixing of a thermally stratified pool with the help of spray injection from above is possible. The separate effect tests conducted in the SEF-POOL facility to study the details of direct contact condensation, while steam is discharged through a model of a sparger, provided valuable data for the development and validation of the EMS and EHS models done by KTH.

Introduction

A boiling water reactor (BWR) containment is a complex system that includes such typical elements as a pressure suppression pool (PSP), spray and containment venting systems for containment pressure control, blowdown pipes for rapid steam condensation in case of loss-of-coolant-accident (LOCA), spargers for the pressure vessel safety relief valves (SRV), strainers for water supply to emergency core cooling (ECC) and spray systems, nozzles and strainers of the residual heat removal (RHR) system, vacuum breakers, etc. There are several scenarios of safety importance where containment pressure suppression function and pressure suppression pool operation are affected by (i) stratification and mixing phenomena, (ii) interactions with ECC, spray, RHR and filtered containment venting (FCV) systems, (iii) overall water balance in the containment compartments, and (iv) interplay between pool behaviour, diagnostics and procedures. Those scenarios include, for example, different LOCAs (steam line break inside the radiation shield, broken blowdown pipes, leaking safety relief valves), station blackouts and severe accidents. There is a need for validated tools for simulation of realistic accident scenarios with interplay between phenomena, safety systems, operational procedures, and overall containment performance.

The INSTAB project has increased understanding of the phenomena related to BWR pressure suppression function and has enhanced capabilities to analyse Nordic BWR containments under transient and accident conditions. Information has been gathered particularly on the effects of the SRV spargers, RHR nozzles and spray system on mixing and stratification of the wetwell pool. Furthermore, details of direct contact condensation (DCC), while steam is discharged through a model of a sparger, have been studied with separate effect tests.

A combined experimental/analytical/computational program has been carried out. With experiments in the PPOOLEX test facility a database for the development, improvement and validation of numerical simulation models has been generated. Sophisticated, high frequency measurement instrumentation, high-speed video cameras and a PIV system have been used in order to get detailed enough data.

The Effective Heat Source (EHS) and Effective Momentum Source (EMS) models for steam injection through blowdown pipes have been successfully developed, validated and implemented to the GOTHIC and ANSYS Fluent codes by KTH with the help of the experiment results of the previous SAFIR and NKS projects [Li et al., 2014, Villanueva et al., 2015, Li et al., 2018, Gallego-Marcos et al., 2018a]. The experiments carried out in the INSTAB project have helped further extend the concepts of the EHS and EMS models to spargers, RHR system nozzles and containment sprays [Gallego-Marcos et al., 2018b].

PPOOLEX and SEF-POOL test facilities

The PPOOLEX facility models a BWR containment and consists of a wetwell compartment (condensation pool), drywell compartment, inlet plenum and steam line piping [Puustinen et al. 2006]. An intermediate floor separates the compartments from each other but a route for steam flow to the wetwell is created by a vertical blowdown/sparger pipe attached underneath the floor.

The main component of the facility is the ~31 m^3 cylindrical test vessel, 7.45 m in height and 2.4 m in diameter. The test facility is able to withstand considerable structural loads caused by rapid condensation of steam. A sketch of the test vessel is shown in Figure 1. Steam needed in the experiments is produced with the nearby PACTEL test facility, which has a core section with 1 MW heating power and three horizontal steam generators [Tuunanen et al., 1998].

The reference system for the SEF-POOL facility is a SRV sparger pipe of a BWR plant. Hence, the facility is designed in such a way that discharge of steam through injection holes at the sparger lower end into sub-cooled pool water can be simulated representatively [Tielinen et al., 2018]. The goal in the tests is to define the effective momentum for a given steam condensation regime, particularly for the oscillatory bubble regime. For this purpose the design of the test facility is such that the effective momentum (liquid force carried by the condensate liquid) can be directly measured with a force sensor or it can calculated on the basis of measured steam momentum (steam force at the injection hole) (Figure 1).

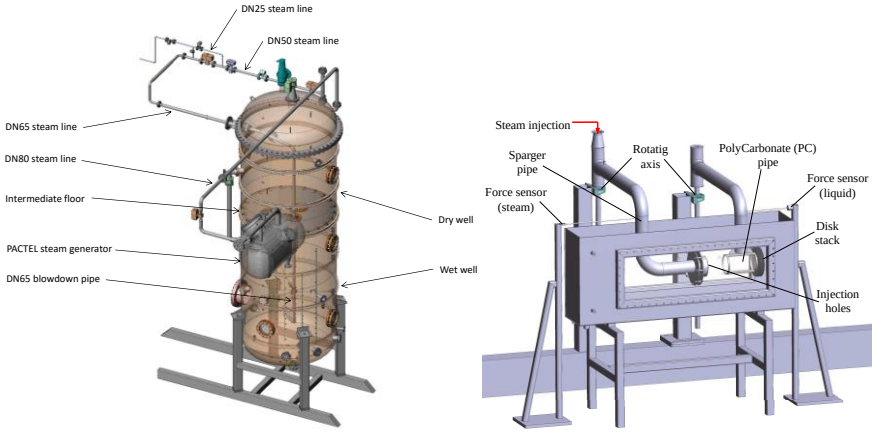

(b) (b)

Figure 1. (a) PPOOLEX test facility. (b) SEF-POOL test facility.

Mixing and erosion of thermal stratification during sparger injection

SRV sparger tests on the mixing phenomenon and on the behaviour of a thermocline have been carried out in the PPOOLEX facility in 2015-2018 to obtain data for the development of the EMS and EHS models done by KTH [Puustinen et al., 2016, Puustinen et al., 2017a, Puustinen et al., 2019]. The test parameters have been selected together with KTH based on pre-test simulations and analysis of the results of the earlier tests in PPOOLEX.

In the 2015 tests, only one row of horizontally oriented injection holes at the sparger head or the eight vertically downwards oriented holes of the load reduction ring (LRR) were used for steam injection. The transition region, where the shift from cold to warm pool water occurred, was practically just below the sparger elevation when steam injection was through the sparger head. When the steam injection was vertically downwards from the LRR, the transition region was deeper in the pool.

Complete mixing was achieved with both tested cases. Figure 2 shows the progression of mixing in the pool water when injection direction was downwards from the LRR of the sparger. In the earlier tests with all the 32 injection holes of the sparger head open a considerably larger steam flow rate was not enough to mix the pool. The flow mode was then different and not enough momentum and internal circulation were created for complete mixing to happen. Mixing was observed only above and a short distance below the sparger head outlet elevation.

These sparger tests in the PPOOLEX facility verified that the existing flow mode of injected steam is a crucial factor in the success of the mixing process of a thermally stratified water pool. Mixing with a larger absolute flow rate can be less successful than with a smaller flow rate if the flow mode after dividing the flow to smaller jets in a sparger head holes is such that not enough momentum and internal circulation is created in the pool for complete mixing to take place.

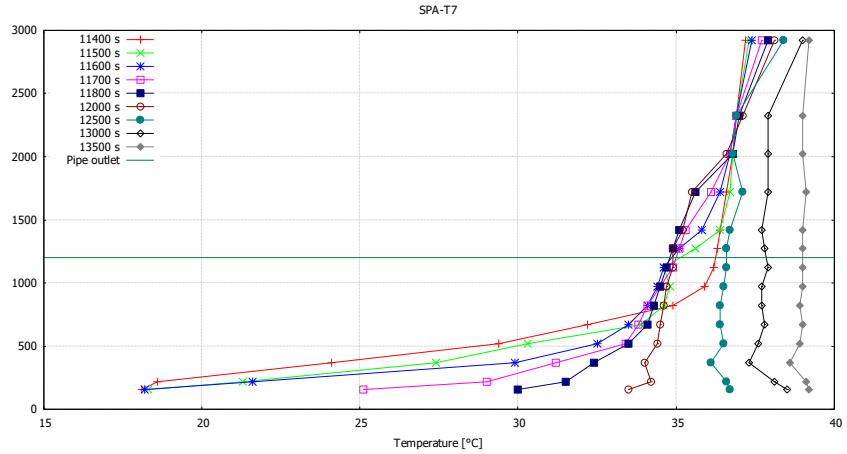

Figure 2. Progression of mixing in pool water when injection direction is downwards from the load reduction ring of the sparger.

In 2016, the first test was done with all the 32 injection holes at the sparger head open whereas the second one was done with only the eight holes in the bottom row open. Particularly the behaviour of the thermocline between the cold and warm water volumes and the progression of the erosion process was of interest. For this purpose, also PIV measurements were tried during the tests.

In both tests the initial uniform temperature profile first changed to a stratified situation and eventually back to a uniform and mixed situation. Along the tests, the thermocline moved downwards. Complete mixing of the water pool through an erosion process was achieved with quite a small steam mass flow rate in the test with most of the injection holes blocked (Figure 3).

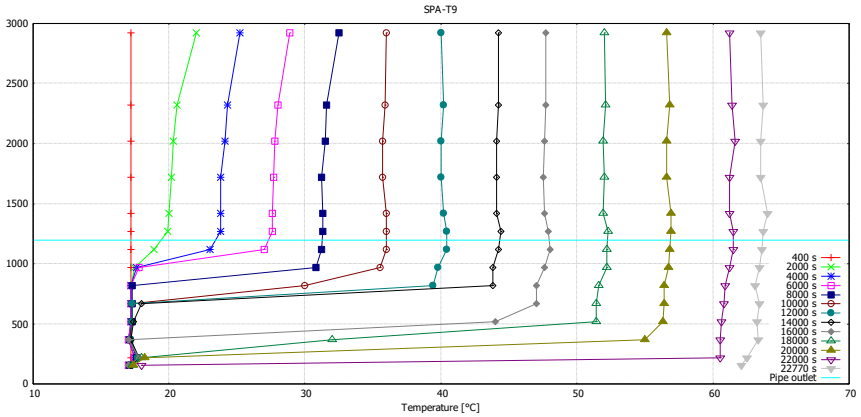

Figure 3. Development of vertical temperature profile of pool water in a test with part of the injection holes blocked.

The PIV measurements of the 2016 tests indicate that some kind of swirls exist around the elevation of the thermocline. The flow direction just under the thermocline can also be opposite to that just above the thermocline. Figure 4 shows a velocity vector field averaged over such a 5.7 second period where the flow patterns were constant enough for the PIV measurement to succeed. Generally, the chaotic nature of the investigated phenomenon created problems when measuring with a slow-speed PIV system and therefore definitive conclusions on the detailed behaviour of the flow fields near the thermocline cannot be made.

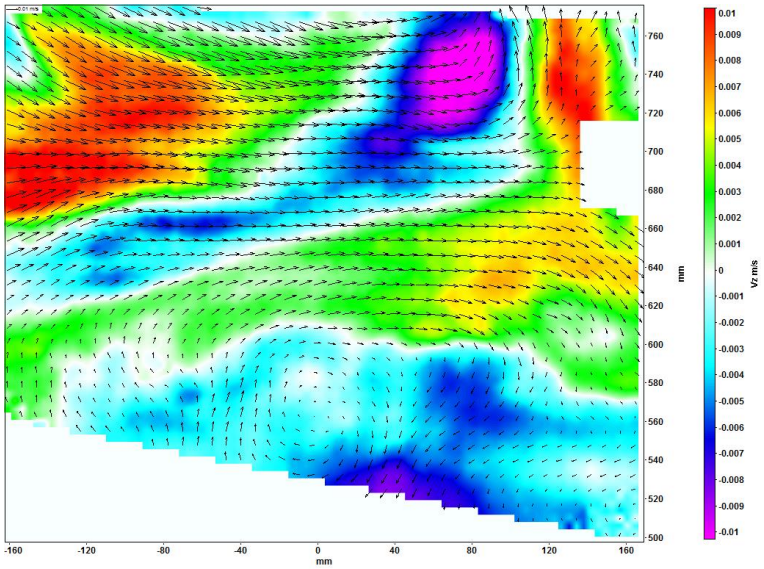

Figure 4. Averaged velocity vector field over a 5.7 second period from the vicinity of the thermocline.

In the 2016 tests, the layers of cold water slowly eroded rather than mixed through internal circulation as has been the case in most of the tests carried out before (either with a straight blowdown pipe or with a sparger pipe). The thermocline region shifted slowly downwards as the erosion process proceeded. These tests in PPOOLEX verified that mixing of a thermally stratified water pool could happen through an erosion process instead of internal circulation if suitable flow conditions in the pool created by steam jets at the injection holes of the sparger prevail.

For the 2017 and 2018 tests, the sparger pipe was moved to the centre of the pool. Earlier sparger tests in PPOOLEX had been done with the sparger pipe in off-the-centre position. In addition, the sparger head was moved up and the pool water level was increased in order to increase the thickness of the cold stratified layer in the 2018 test.

According to the direct contact condensation mode map for pure steam discharge of Chan and Lee, the dominant flow mode in the 2017 and 2018 tests and in the earlier reference test was oscillatory bubble, Figure 5 [Chan et al., 1982].

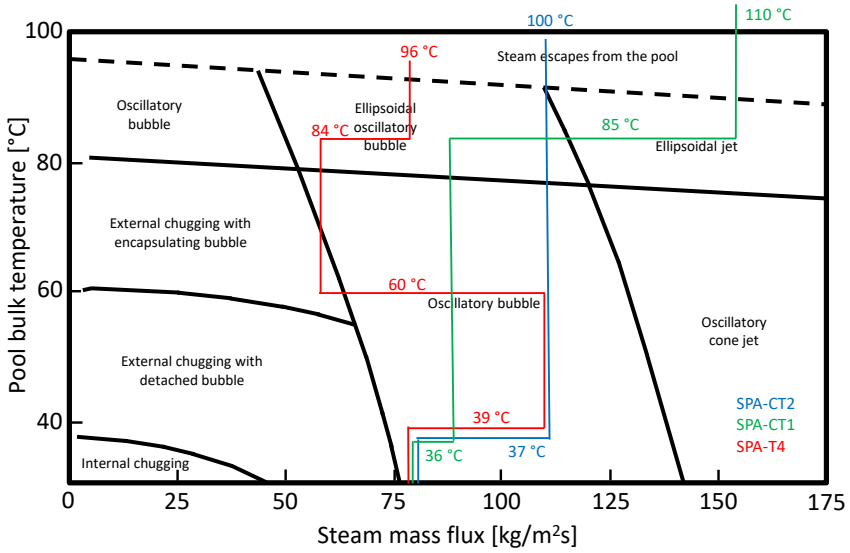

Figure 5. Paths of the SPA-CT2, SPA-CT1 and SPA-T4 tests marked on the direct condensation mode map for pure steam discharge of Chan and Lee.

During the erosion phase, the elevation of the thermocline shifts slowly downwards. However, complete mixing is not achieved and eventually the erosion process slows down and some kind of equilibrium situation develops for a while. Then, a new stratification process seems to start although the steam mass flow rate is kept constant, see Figure 6.

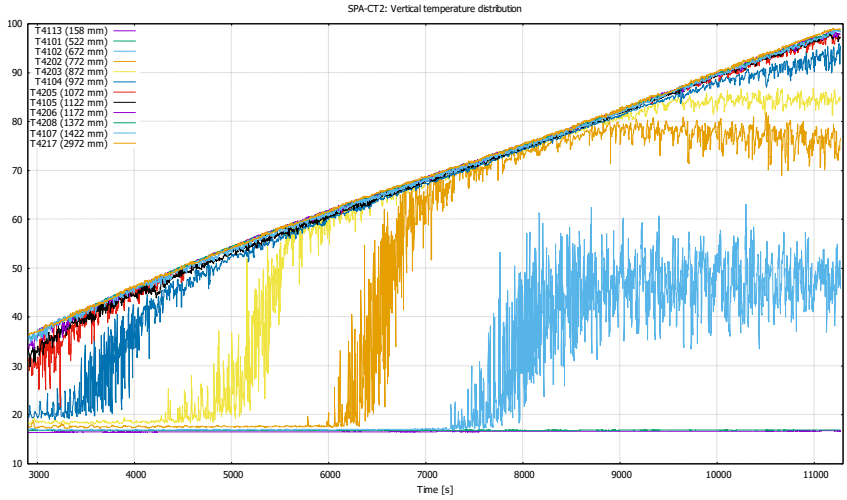

Figure 6. Vertical temperature distribution in the wetwell pool during the erosion phase (2940-11200 s) in the SPA-CT2 test with the sparger in the centre position.

Separate effect tests

In BWRs, the development of thermal stratification or mixing during steam injection through spargers can affect the performance of the suppression pool. Prediction of the effective momentum induced by the oscillatory bubble regime is necessary for the modelling of the pool behaviour. To directly measure the effective momentum an extensive test series has been run in the SEF-POOL facility at LUT [Puustinen et al., 2019, Gallego-Marcos et al., 2018c]. Data of the characteristics of small-scale phenomena affecting the effective heat and momentum sources have been provided. This data is used in the validation of the simplified EHS/EMS models by KTH. The SEF-POOL tests also support the validation effort of the DCC and interfacial area models of CFD codes for steam injection through spargers at VTT and LUT.

Steam mass flux, sub-cooling and injection hole diameter are the variables affecting the condensation regime, which have been analysed during the tests. Momentum has been measured with force sensors and high-speed video clips of the DCC phenomenon of steam have been recorded. Oscillatory bubble, partly the oscillatory cone jet and partly the stable jet regimes are the covered flow modes.

All sub-sonic regimes present a strong dependency of measured forces with the sub-cooling, whereas this effect is practically negligible in stable jet regimes occurring above 300 kg/m^{2}s. However, force sensors start to indicate a clear decreasing trend after the pool water temperature exceeds 80 °C (Figure 7). This behaviour can be attributed to the flow mode change to ellipsoidal jet regime.

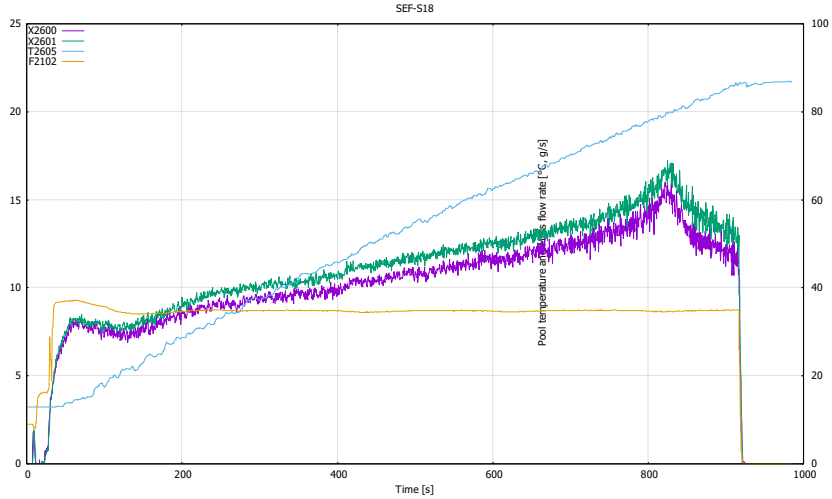

Figure 7. Measured forces (X2600, X2601), flow rate (F2102) and pool temperature (T2605) in a SEF-POOL test.

Analysis by KTH of the forces measured in the SEF tests show a regime transition between 125-175 kg/m^{2}s. Correlations for effective momentum in each regime has been provided by KTH. Further experimental data should be obtained to determine the adequacy of the proposed smoothing function between the two regimes.

Qualitative analysis of video images show that the oscillatory motion of the steam bubbles can be divided into three parts. That is, the bubble begins to grow attached to the injection holes, detaches when the force balance becomes positive in the direction of the steam injection, and collapses as the neck connecting the bubble to the injection hole reduces the steam flow into the bubble (Figure 8). At low subcoolings, detached bubbles can move a large enough distance from the injection holes and allow the formation of a new bubble before their collapse.

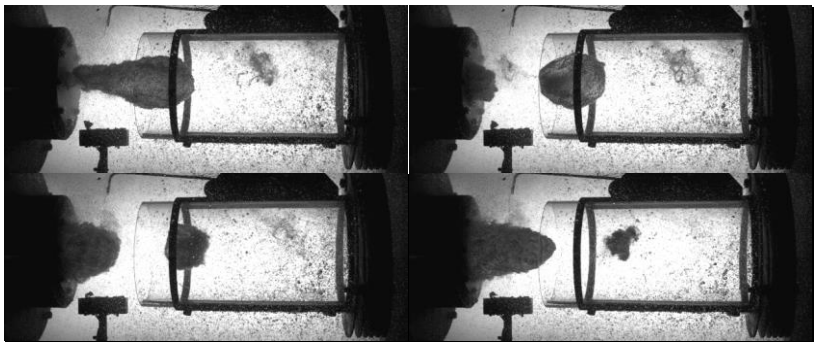

Figure 8. Video frames from a SEF-POOL test (steam mass flux 174 kg/m^{2}s, pool water temperature about 85 °C, injection hole diameter 16 mm, Δt=4285,68 μs).

Bubble parameters, which have been estimated through image processing of the high-speed videos by KTH, include for example the collapse and bubble life frequencies, maximum bubble radius and bubble velocities. Figure 9 presents examples of the obtained bubble collapsing frequencies and radiuses. The collapsing frequencies present a quasi-linear dependency with the sub-cooling. In the low steam mass flux tests S10 and S14, the frequency stabilizes when the sub-cooling is above ~60 °C.

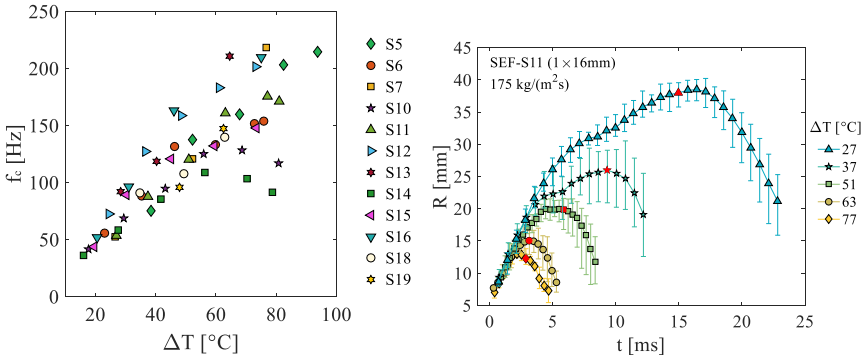

(a) (b)

Figure 9. (a) Bubble collapsing frequencies and (b) time evolution of the bubble radius as a function of the sub-cooling in the SEF-POOL tests.

Spray tests in PPOOLEX

For the spray tests, the PPOOLEX facility was equipped with a model of a wetwell spray system having four spray nozzles (B1/2HH-40 FULLJET, 6.2 mm orifice). The used flow rate of spray injection in the tests was about 30.5-32.0 l/min per nozzle.

Mixing of a thermally stratified pool with the help of spray injection from above was studied in the tests [Pyy et al., 2018]. PIV measurements were conducted in order to produce velocity field data for improving simulation models related to spray operation in CFD and system codes as well as to contribute to the development of the EMS and EHS models for sprays by KTH.

In the beginning, there was a 200 mm layer of warm water on top of the volume of cold water. A downwards penetrating mixing process takes place after the spray injection is started (Figure 10). The cold spray water first cools the topmost layers and then the internal circulation induced by density differences starts to mix the pool deeper and deeper. The TC close to the pool bottom (T4113) remains at its original temperature thus verifying that complete mixing was not achieved during the test.

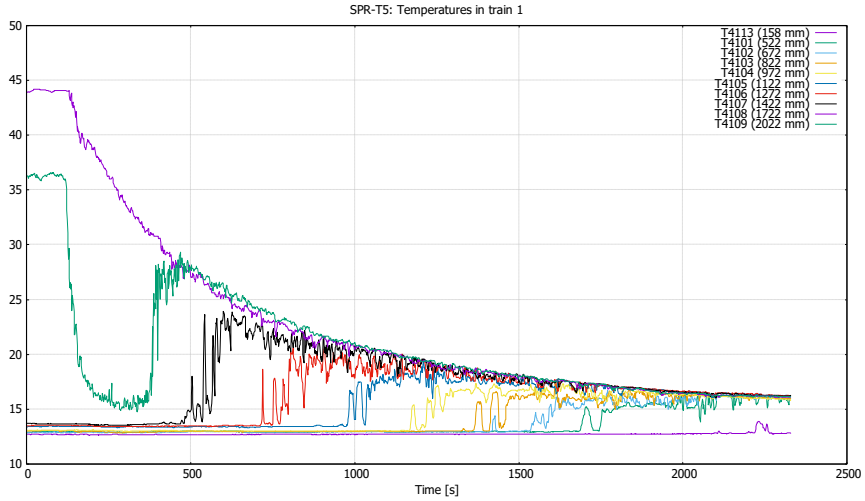

Figure 10. Temperature distribution in the pool in a PPOOLEX spray test.

In all the spray tests, there was a period in the middle when the optical environment was very poor for the PIV measurements to succeed. Results were only obtained from the beginning and at the end of the tests. Furthermore, the dynamic characteristics of the flow makes the analysis of the results difficult and ambiguous. The PIV measurement plane is also small compared to the PPOOLEX wetwell pool and therefore development of large internal circulations in the pool cannot be captured with PIV. When inspecting the instantaneous vector field it was noticed that velocities were in the same range but randomly spread to all directions. It is thus more beneficial to focus on turbulence intensity than on averaged velocity fields. Figure 11 and 12 present the averaged velocity vector field and the corresponding turbulence intensity field for 500 image pairs from a spray test.

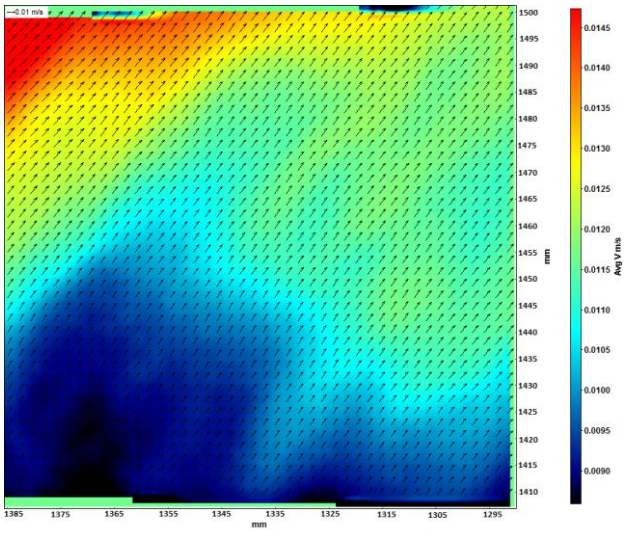

Figure 11. Averaged velocity vector field of PIV measurement sequence from a spray test.

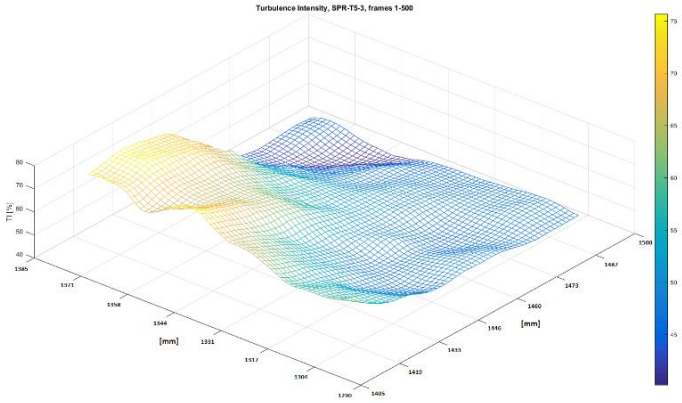

Figure 12. The turbulence intensity field of PIV measurement sequence from a spray test.

Summary and conclusions

Thermal hydraulic tests in the INSTAB project have focused on generating a large database on suppression pool phenomena to be used for the validation of CFD and system codes used for safety analysis of nuclear power plants. The results of the tests on the efficiency of mixing of a thermally stratified pool have been utilized particularly in the development work of the EMS and EHS models for blowdown pipes, SRV spargers and RHR nozzles by KTH. These models have been implemented to the GOTHIC and ANSYS Fluent codes but they will be available to users of other codes as well. The tests with a model of a SRV sparger in the PPOOLEX facility

verified that mixing of a thermally stratified water pool could happen also through an erosion process in addition to internal circulation, if suitable flow conditions prevail.

The tests with the SEF-POOL facility on sparger behaviour have produced data of the characteristics of small-scale phenomena, which affect the effective heat and momentum sources. This information will then provide closures for the simplified EMS/EHS model development work for spargers by KTH. Furthermore, the SEF-POOL tests support the validation effort of the DCC and interfacial area models of CFD codes for steam injection through spargers at VTT and LUT.

The wetwell spray tests in the PPOOLEX facility revealed that mixing of a thermally stratified pool with the help of spray injection from above is possible. The cold spray water first cools the topmost layers and then the internal circulation induced by density differences starts to mix the pool deeper and deeper. PIV measurements were conducted in the spray tests in order to obtain detailed velocity field data for improving simulation models related to spray operation in CFD and system codes. However, the optical environment was very poor for the PIV measurements to succeed and results were only obtained from the beginning and at the end of the tests.

References

Li, H., Villanueva, W., Puustinen, M., Laine, J., Kudinov, P. 2014. Validation of effective models for simulation of thermal stratification and mixing induced by steam injection into a large pool of water. Science and Technology of Nuclear Installations (Vol. 2014), http://dx.doi.org/10.1155/2014/752597.

Villanueva, W., Li, H., Puustinen, M., Kudinov, P. 2015. Generalization of experimental data on amplitude and frequency of oscillations induced by steam injection into a subcooled pool. Nuclear Engineering and Design 295 (2015), http://dx.doi.org/10.1016/j.nucengdes.2015.08.031.

Li, H., Villanueva, W., Puustinen, M., Laine, J., Kudinov, P., 2018. Thermal Stratification and Mixing in a Suppression Pool Induced by Direct Steam Injection. Annals of Nuclear Energy 111 (2018), https://doi.org/10.1016/j.anucene.2017.09.014.

Gallego-Marcos, I., Villanueva, W., Kudinov, P., 2018a. Modelling of Pool Stratification and Mixing Induced by Steam Injection through Blowdown Pipes. Annals of Nuclear Energy 112 (2018), https://doi.org/10.1016/j.anucene.2017.10.019.

Gallego-Marcos, I., Kudinov, P., Villanueva, W., Kapulla, R., Paranjape, S., Paladino, D., Laine, J., Puustinen, M., Räsänen, A., Pyy, L., Kotro, E., 2018b. Pool Stratification and Mixing Induced by Steam Injection through Spargers; Analysis of the PPOOLEX and PANDA Experiments. Nuclear Engineering and Design 337 (2018), https://doi.org/10.1016/j.nucengdes.2018.07.004.

Puustinen, M., Partanen, H., Räsänen, A., Purhonen, H. 2007. PPOOLEX Facility Description. Lappeenranta: Lappeenranta University of Technology. Technical Report POOLEX 3/2006.

Tuunanen, J., Kouhia, J., Purhonen, H., Riikonen, V., Puustinen, M., Semken, R. S., Partanen, H., Saure, I. & Pylkkö, H. 1998. General Description of the PACTEL Test Facility. Espoo: VTT. VTT Research Notes 1929. ISBN 951-38-5338-1.

Tielinen, K., Räsänen, A., Kotro, E., Saure, I., 2018. General description of SEF-POOL test rig. Lappeenranta University of Technology, School of Energy Systems, Nuclear Engineering, Research Report INSTAB 2/2017.

Puustinen, M., Laine, J., Räsänen, A. 2016. Additional Sparger Tests in PPOOLEX with Reduced Number of Injection Holes. Lappeenranta: Lappeenranta University of Technology. School of Energy Systems. Nuclear Engineering. Research Report INSTAB 1/2015.

Puustinen, M., Pyy, L., Laine, J., Räsänen, A. 2017a. Sparger Tests in PPOOLEX on the Behaviour of Thermocline. Lappeenranta: Lappeenranta University of Technology. School of Energy Systems. Nuclear Engineering. Research Report INSTAB 1/2016.

Puustinen, M., Laine, J., Räsänen, A., Kotro, E., Tielinen, K., 2019. Erosion of Thermal Stratification in PPOOLEX Test with Sparger. Lappeenranta: Lappeenranta-Lahti University of Technology LUT. School of Energy Systems. Nuclear Engineering. Research Report INSTAB 2/2018.

Chan, C. K., Lee, C. K. B., 1982. A Regime Map for Direct Contact Condensation. Int. J. Multiphase Flow. 1982.

Puustinen, M., Laine, J., Räsänen, A., Kotro, E., Tielinen, K., 2019. SEF-POOL Tests. Lappeenranta: Lappeenranta-Lahti University of Technology LUT. School of Energy Systems. Nuclear Engineering. Research Report INSTAB 1/2018.

Gallego-Marcos, I., Kudinov, P., Villanueva, W., Puustinen, M., Räsänen, A., Tielinen, K., Kotro, E., 2018c. Effective Momentum Induced by Steam Injection in the Oscillatory Bubble Regime. Submitted for review to Nuclear Engineering and Design.

Pyy, L., Hovi, T., Puustinen, M., Räsänen, A., Kotro, E., 2018. PPOOLEX Spray Tests on Mixing Effects in Condensation Pool. Lappeenranta: Lappeenranta University of Technology. School of Energy Systems. Nuclear Engineering. Research Report INSTAB 4/2017.

5.4 Development and validation of CFD methods for nuclear reactor safety assessment (NURESA)

Timo Pättikangas[1], Ville Hovi[1], Ismo Karppinen[1], Joonas Kättö[3], Giteshkumar Patel[2], Juho Peltola[1], Tommi Rämä[3], Vesa Tanskanen[2], Timo Toppila[3]

[1]VTT Technical Research Centre of Finland Ltd
P.O. Box 1000, FI-02044 Espoo

[2]Lappeenranta University of Technology
P.O. Box 20, FI-53851 Lappeenranta, Finland

[3]Fortum Power and Heat Oy
P.O. Box 100, FI-00048 FORTUM

Abstract

Computational Fluid Dynamics (CFD) methods have been developed and validated for the identified most important topics in nuclear reactor safety assessment. International single-phase mixing benchmarks were participated and spray experiments performed at LUT were modelled in co-operation with Swedish partners. Models for the departure from nucleate boiling (DNB) have been developed for the OpenFOAM code and co-simulations of NPP components with CFD code and Apros system code have been performed.

Introduction

The NURESA project consisted of four Work Packages (WP), where Computational Fluid Dynamics (CFD) methods were developed and validated for nuclear reactor safety assessment.

In WP 1, the international blind benchmark in the Hydrogen Mitigation Experiments for REactor Safety (HYMERES) programme was participated. The benchmark exercise focussed on the hydrogen stratification and erosion of density layer by turbulent mixing processes.

In WP 2, spray and stratification experiments performed with the PPOOLEX facility at LUT was modelled with CFD simulations. In addition, separate effect condensation experiment performed with the SEFPOOL facility at LUT was calculated with ANSYS Fluent and OpenFOAM codes. In the experiment, horizontal steam jets are injected into water pool, where direct-contact condensation of steam occurs.

In WP 3, OpenFOAM CFD solver was developed and validated for nuclear reactor safety assessment. At VTT, subcooled nucleate boiling and wall heat transfer

models were integrated into the Eulerian two-phase solvers of the official OpenFOAM release. In addition, size distribution model of bubbles was implemented in co-operation with Helmholtz-Zentrum Dresden-Rossendorf (HZDR). At LUT, OpenFOAM simulations of POOLEX and PPOOLEX chugging experiments were done and models for direct-contact condensation were developed.

In WP 4, coupled simulation of VVER-440 steam generator with ANSYS Fluent and Apros 6 has been performed. In addition, coupled simulation of VVER-440 pressurizer was performed, where CFD model of the pressurizer was coupled with generic model of VVER-440 nuclear power plant.

In the following, some of the results of the project are reviewed.

Modelling of condensation and thermal stratification in pressure suppression pools

In boiling water reactors (BWR), the analysis of thermal stratification of the pressure suppression pool is important, when hypothetical accident scenarios are investigated. In the INSTAB project of LUT, separate effect test facility SEFPOOL has been constructed for detailed direct-contact condensation studies of spargers of the pressure suppression pools. The test facility has been designed in co-operation with KTH by Puustinen and Kudinov (2017). In the test facility, stream is injected horizontally into water pool through small orifices.

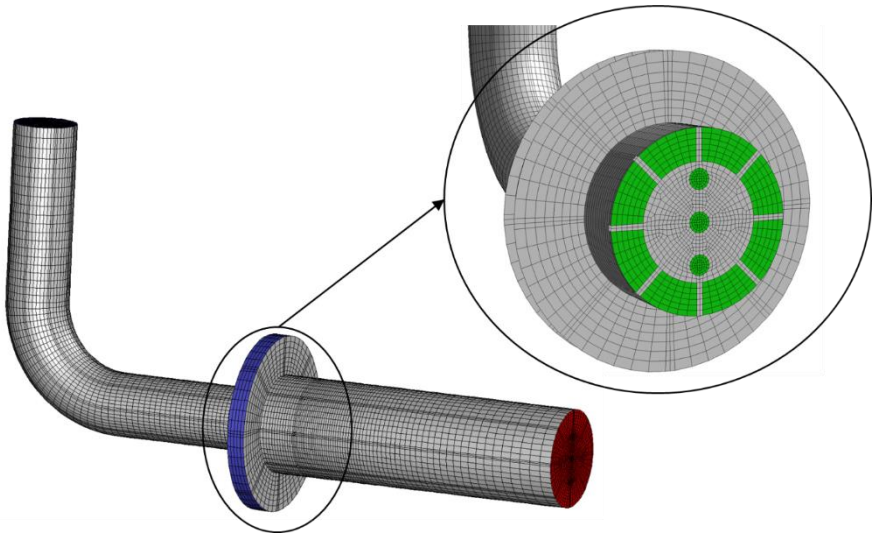

Figure 1. Surface mesh of the CFD model for the SEFPOOL separate effect test facility of LUT. Steam is injected downwards through the pipe, which has a plate with three orifices in the horizontal section of the pipe.

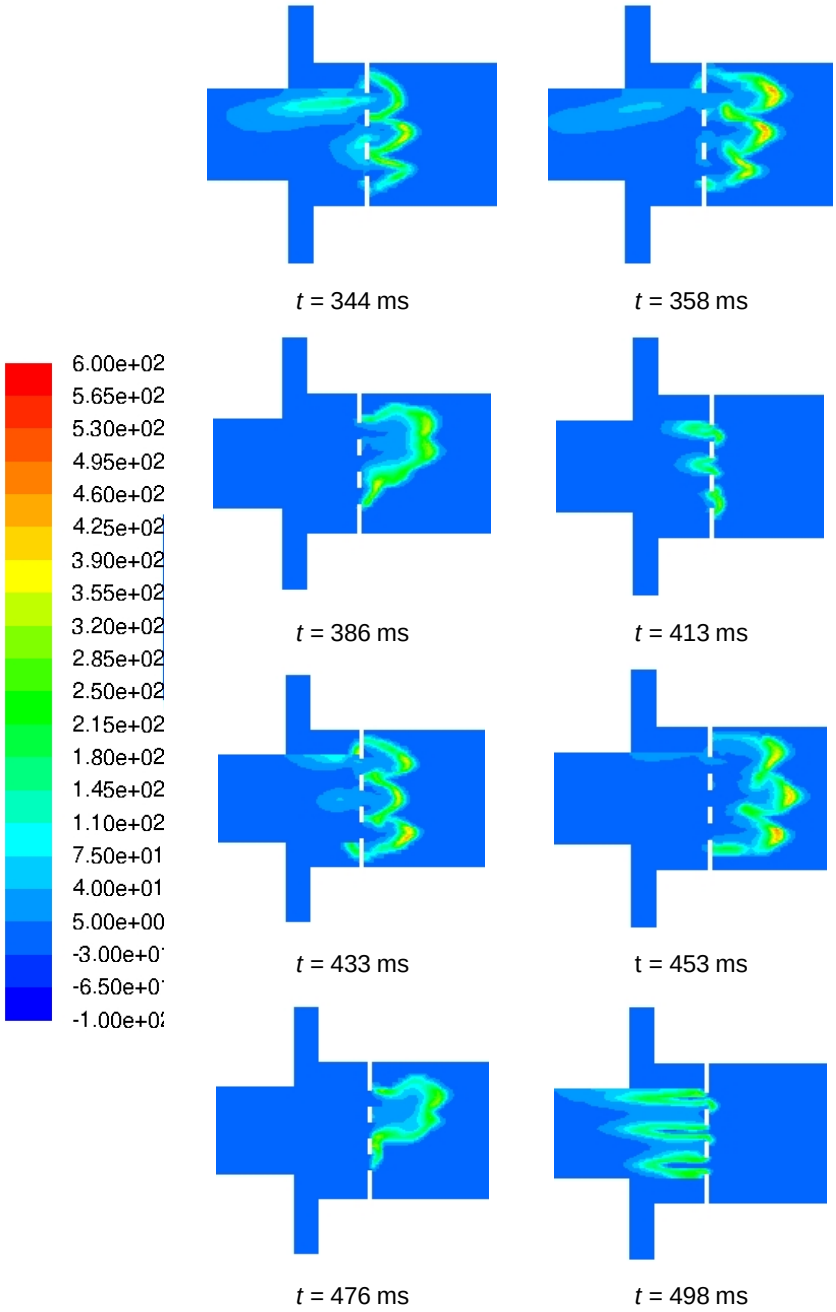

Figure 2. Condensation rate of steam (kg/m^{3}s) in the vertical center plane of the test facility during chugging oscillation.

The CFD model of the separate effect test facility is shown in Figure 1. In the model, steam is injected downwards into the vertical pipe, which bends to horizontal direction. A steel plate with three orifices (∅16mm) is located at the end of the horizontal section. Steam flows through the orifices into the plexiglas tube. The tube is submerged in a box filled with water.

In the following, the simulation results of the SEFPOOL pre-test SEF-T000 are discussed. The simulation parameters were chosen to correspond time t = 353 s of the experiment. The mass flow rate of saturated vapour was 14.8 g/s, which corresponds to mass flux of 24.5 kg/m^{2}s. The temperature of water in the pool was about 67 °C. These parameters are in the transition region between chugging and condensation oscillations.

The calculations were performed by using the Euler-Euler two-phase model of ANSYS Fluent version 18.2. The condensation was calculated by using the two-resistance model, where the Ranz-Marshall model for heat transfer was assumed on the liquid side. On the vapour side, zero resistance was assumed. Evaporation-condensation model of Fluent was used.

In Figure 2, the condensation rate of steam is shown during two periods of chugging oscillation. At time t = 344 ms, steam flowing from left has penetrated through three orifices into the water pool on the right-hand side of the plate. The steam bubbles can be seen to grow until rapid condensation of steam occurs at time t = 413 ms, and liquid water flows through the orifices to the left-hand side of the plate. At time t = 433 ms, new steam bubbles are growing in the water pool until they collapse at time t = 498 ms. This cyclic behaviour is called chugging.

OpenFOAM solver for boiling and condensation

In commercial CFD software, the source code and the implementation of the numerical methods are not openly available. Thus, the possibilities to modify the solver or to include new models are limited. In addition, the license policy prevents effective utilization of parallel computer resources. The use of open-source software in the nuclear safety analysis would increase transparency and improve opportunities for co-operation. The cost of parallel computing capacity has continuously been decreasing and the lack of licensing fees would allow this capacity to be utilized more effectively. This would improve the accuracy and reliability of modelling and increase the number of situations where CFD methods can be utilized.

Our long-term goal is to develop a general-purpose two-phase CFD solver for NRS assessment in co-operation with international partners. Close cooperation with the OpenFOAM Foundation makes possible to include the basic functionality needed in two-phase NRS application into the OpenFOAM Foundation releases. This provides a transparent and publicly available software platform that allows efficient international co-operation. According to the experiences obtained during the SAFIR2014 programme, inclusion of the main features of the developed models in the upstream releases is important for cost-effective and sustainable progress in model development.

Boiling with breakup and coalescence models for bubbles

At VTT, the boiling and condensation models previously developed in the SAFIR program were in 2015 included in the two-phase solvers of the public OpenFOAM 3 release in co-operation with the OpenFOAM Foundation. The goal was to avoid excessive maintenance of a separate solver code that structurally differs from the official OpenFOAM release. The commonly available code also allows efficient co-operation with OpenFOAM developers and other international partners.

In 2016, the wall boiling models were extended to high void fractions and a framework was implemented for runtime selectable heat flux partitioning and wall boiling submodels. The boiling and condensation models were coupled to the Interfacial Area Transport Equation model (IATE) that allows modelling of bubble coalescence and break-up. The models are available in OpenFOAM 5 and more recent releases.

The behaviour of the high void fraction partitioning function was tested in simulations CHF experiment carried out in the Large Water Loop (LWL) facility at the Nuclear Machinery Plant, Skoda, Plzen Ltd. LWL is a 19-rod hexagonal bundle in pressurized water with thermal parameters similar to PWR reactors. Rods are heated electrically and the heated length is 3.5 m. In the present simulation, spacer grids were neglected and symmetry was used to reduce to the computational domain to 1/12th of the full bundle. Figure 3 shows an example of calculated void fraction and liquid temperature in three simulations with different heating powers. The 100% simulation corresponds to the critical heat flux observed in the experiment.

In 2017 and 2018, the focus was on modelling of polydisperse flows and refinement of the platform and implementation. The thermal phase change models were extended from two-phase simulations to n-phase simulations and inhomogeneous class method population balance model developed at Helmholz-Zentrum Dresden-Rossendorf (HZDR) was integrated to the platform in co-operation between VTT, HZDR and CFD Direct Ltd.

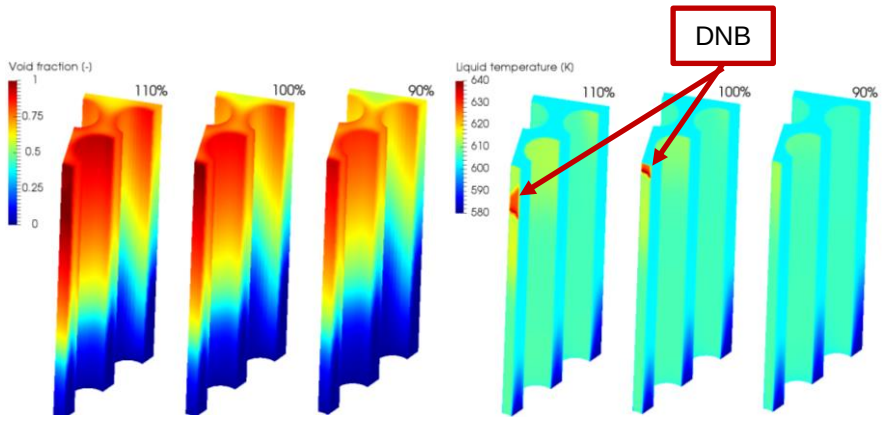

Figure 3. Void fraction (a) and bubble diameter (b) contours from a Large Water Loop simulation. The geometry has been scaled down vertically 1:50 for visualization.

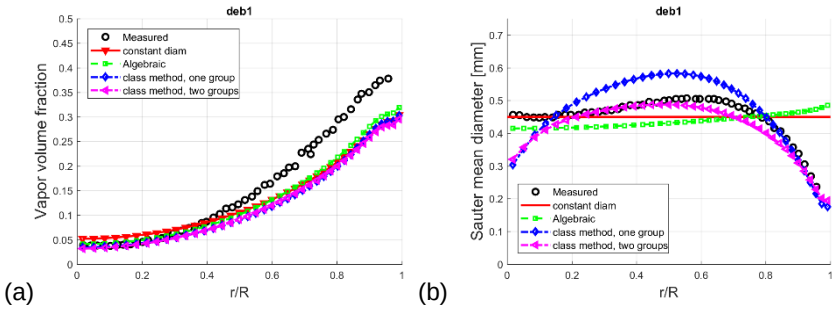

Figure 4. (a) Radial void fraction and (b) bubble Sauter mean diameter profiles of a DEBORA simulation.

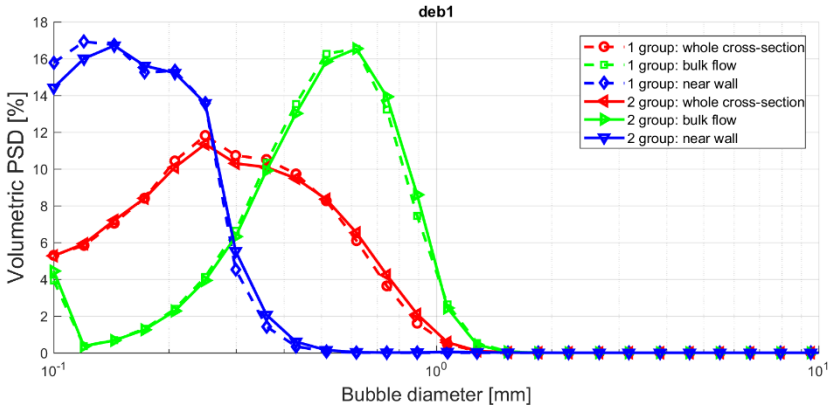

Figure 5. Predicted near wall and bulk flow volumetric bubble size distributions in single and two group class method simulations.

The implemented models can be used by installing OpenFOAM 6 or newer release. The thermal phase change and wall boiling support are included in a general-purpose multiphase framework called reactingEulerFoam which includes two- and n-phase solvers. The thermal phase change models consist of a two-resistance interfacial heat transfer formulation with user selectable heat transfer correlations and a thermal diffusivity wall function that implements a version of the RPI wall-boiling model. There are also user selectable correlations for the partitioning of the wall heat flux between the phases, which allows implementation of correlations that attempt to predict Departure from Nucleate Boiling (DNB).

Figure 4 shows a comparison of results obtained with different size distribution modelling approaches in a data set the DEBORA experiment. This is a vertical boiling high pressure pipe flow with R12 as the fluid. The results shown are the radial Sauter mean diameter of vapour bubbles and the void fraction profiles at the end of the 3.5 m heated section. It should be noted that in this case the diameter profiles at the measurement point were known in advance and parameters of the constant and algebraic model were chosen accordingly.

In the class method simulations, 27 vapour bubble size groups spanning from 0.1 mm to 10 mm diameters were used. Coalescence and breakup models for the bubbles were Prince & Blanch (1990) and Lehr et al. (2002), respectively. Class method submodels were also active to account for interfacial phase change, wall boiling and density changes. The constant and algebraic models overpredict the bubble diameter near the wall as they are not coupled to the bubble departure diameter of the wall boiling model. This decreases the condensation rate of the bubbles as they depart the heated wall and leads to elevated void fraction in the near-wall cells compared to the class method solutions.

With the class method the diameter information is not limited to the mean diameter of bubbles, but in each computational cell there is a distribution of different bubble sizes. Figure 5 shows a comparison of bubble size distributions over the whole pipe cross section at the end of the heated section and separately for the near wall and bulk flow regions. Near the wall, the bubble population consists mostly of bubbles near departure diameter and smaller, while in the bulk flow bubble size grows due to coalescence and disappearance of smaller bubbles due to condensation. In this case the difference between the one and two size group simulations is small because only a small portion of the bubbles are large enough to be affected by the lift force reversal that occurs when Eötvos number is high enough.

Direct-contact condensation in water pool

At LUT, simulations of direct-contact condensation (DCC) were performed during 2015–2016. The chugging mode of DCC was studied in situations relevant to the pressure suppression pool of boiling water reactor (BWR). The simulations were performed by using the Eulerian-Eulerian compressible two-fluid approach of the OpenFOAM. The achieved numerical results were compared to earlier NEPTUNE_CFD simulations of Tanskanen (2012) and to POOLEX experiments of LUT.

The POOLEX STB-28 experiment was studied, which consist of one long steam blowdown into water pool. The purpose of this experiment was to analyse the formation and condensation of steam bubbles at the blowdown pipe outlet as a function of pool water temperature. In the experiment, high-speed and standard video cameras were used to monitor the formation and condensation of steam bubbles.

The STB-28 experiment was simulated both with 2D-axisymmetric and 3D computational geometries. The interfacial heat transfer between steam and water was modelled by using surface renewal theory based condensation model. The k-ε turbulence model was used to solve flow turbulence. Results showed that the implemented compressible two-phase solver of OpenFOAM was able to invoke chugging phenomenon of open-top condensation pool (Figure 6).

The calculated averaged condensation rate and chugging frequency in OpenFOAM simulations were higher than the NEPTUNE_CFD results of Tanskanen (2012). However, regardless of qualitative differences (bubble shapes and sizes) between OpenFOAM and NEPTUNE_CFD, it was concluded that the compressible two-phase solver of OpenFOAM is sufficient to invoke chugging phenomenon.

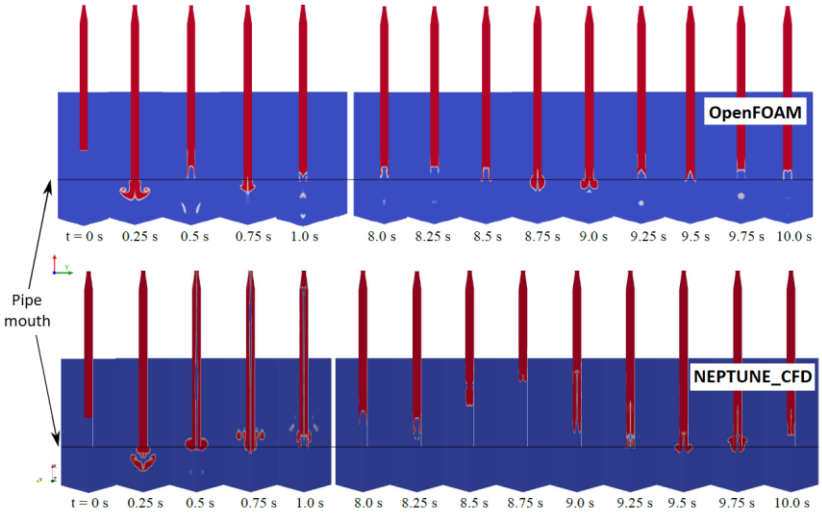

Figure 6. Volume fraction of steam calculated with the 2D-axisymmetric OpenFOAM and NEPTUNE_CFD models for the STB-28-4 chugging experiment.

Simulations were also performed for the pressurized PPOOLEX drywell-wetwell facility of LUT, where the DCC-05 experiment was selected as the reference. In the DCC-05 experiment multi-camera high-speed video data of blowdown event was available, which could be used in the development of pattern recognition algorithms.

Various modelling issues, e.g., the performance of different DCC models, the turbulence modelling, interfacial momentum transfer, geometry and interface initialization were briefly studied both with NEPTUNE_CFD and OpenFOAM. The bubble volume and the chugging frequency during the blowdown were obtained from the experimental data by using the pattern recognition algorithm of Hujala (2013).

The Rayleigh-Taylor Interfacial (RTI) area model of Pellegrini et al. (2015) was included in NEPTUNE_CFD and OpenFOAM. In NEPTUNE_CFD simulations, chugging and natural oscillation occurred with the RTI model at realistic frequencies. This demonstrated that the increase of the interfacial area predicted by the model was of correct order of magnitude and therefore the DCC rate increased favourably. The predicted power spectrum of the bubble volume with the RTI modelling corresponded well to the experiments. In the OpenFOAM simulation, the interfacial area enlarged and condensation rate increased significantly (Figure 7).

The Fast Fourier Transform from the recognized bubble volume showed that the OpenFOAM simulations were able to predict the chugging frequencies in the range 0.5 Hz to 3 Hz both without and with the RTI model. However, OpenFOAM predicted strong interface oscillations at higher frequencies, which did not correspond either to the experiment or to the NEPTUNE_CFD simulations (Figure 8).

During 2017–18, experiments were carried out with the SEFPOOL sparger separate effect test facility in the INSTAB project of LUT. The SEF-INF2 experiment has been considered as the first reference case for simulations with NEPTUNE_CFD and OpenFOAM.

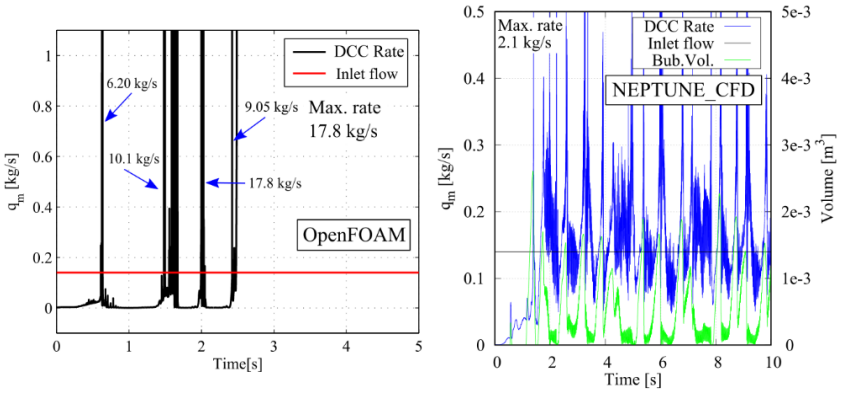

Figure 7. Condensation mass flow rate and bubble volume in the 2D-axisymmetric OpenFOAM and NEPTUNE_CFD simulations of the PPOOLEX DCC-05-4 experiment.

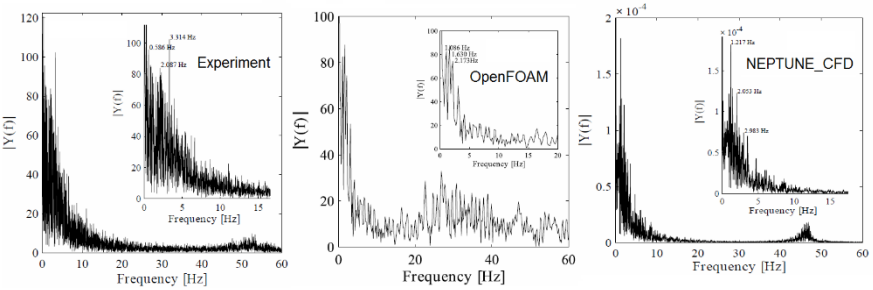

Figure 8. FFT from the recognized bubble volume in the PPOOLEX DCC-05-4 experiment, and in the corresponding 2D-axisymmetric OpenFOAM and NEPTUNE_CFD simulations.

The same methods which were used in the earlier successful suppression pool simulations, have been used in the SEFPOOL simulations. The main focus is in the large interface condensation and interfacial area models for spargers. Preliminary simulations of the SEF-INF2 experiment faced some numerical difficulties. The simulation results of the steam-liquid interface differed clearly from the experiments. Therefore, more work is needed for the successful simulation of these experiments.

Coupled CFD-Apros simulations of VVER-440 pressurizer

CFD model for VVER-440 pressurizer was developed and coupled to an Apros model of a generic VVER-440 plant, by using coupling tool of Apros 6 developed previously by VTT and Fortum.

The CFD model of the pressurizer is presented in Figure 9. The pressurizer was modelled by using the Euler-Euler multiphase model of ANSYS Fluent 18.2. In addition, user-defined functions were implemented for the modelling of evaporation and condensation.

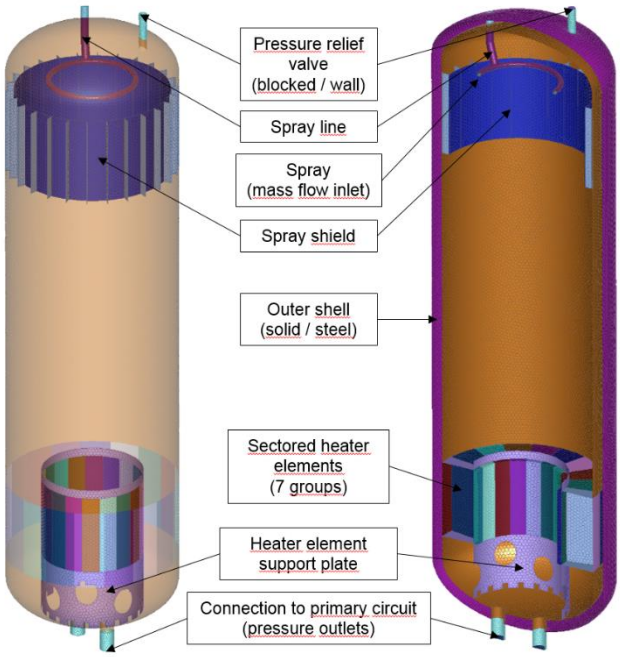

Figure 9. Geometric model and computational mesh of the VVER-440 pressurizer.

In 2017, stand-alone pressure rise and pressure drop simulation of the CFD pressurizer were performed and compared against Apros pressurizer model. In 2018, the pressurizer in the Apros plant model was replaced with detailed 3D CFD model. Flow coupling boundaries between the CFD and Apros models were spray line at the top of the pressurizer and surge line at the bottom of the pressurizer. Liquid level measurement and heater control were configured via Fluent scheme language couplings.

Finally a loss-of-feedwater transient was simulated with coupled CFD-Apros model and the results were compared against Apros VVER-440 plant model results. Pressure comparison of the results of the coupled and stand-alone Apros models are presented in Figure 10.

In Figure 11 mass transfer rate and velocity vectors of the pressurizer during pressure decrease (spray initiated) and pressure increase (heater elements activated) is presented.

Slight time-gap in the behaviour of the cases occurs, but all in all the results of the simulations were very similar considering the compared quantities. More detailed information of the pressurizer flow field can be attained from the coupled model, whereas significantly slower simulation time is the main drawback.

Coupled simulation was robust, no divergence due to the coupling was encountered. The results of the coupled simulation are considered reliable.

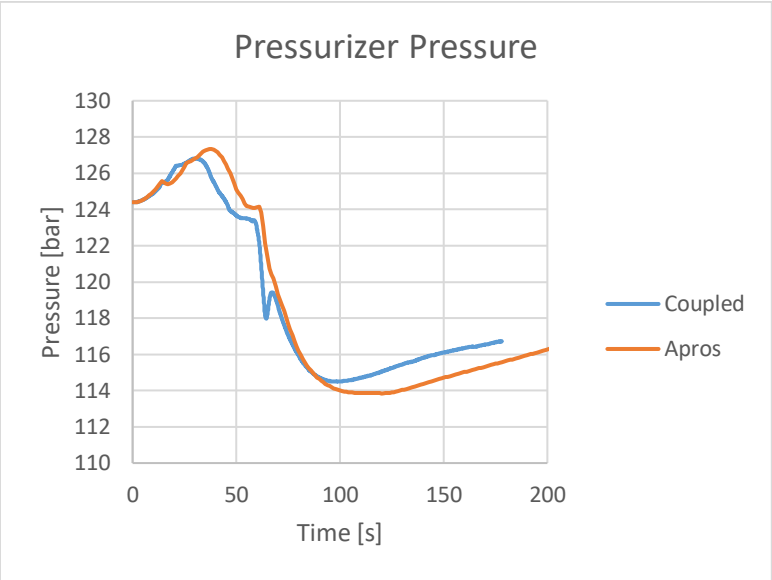

Figure 10. Pressure behaviour comparison.

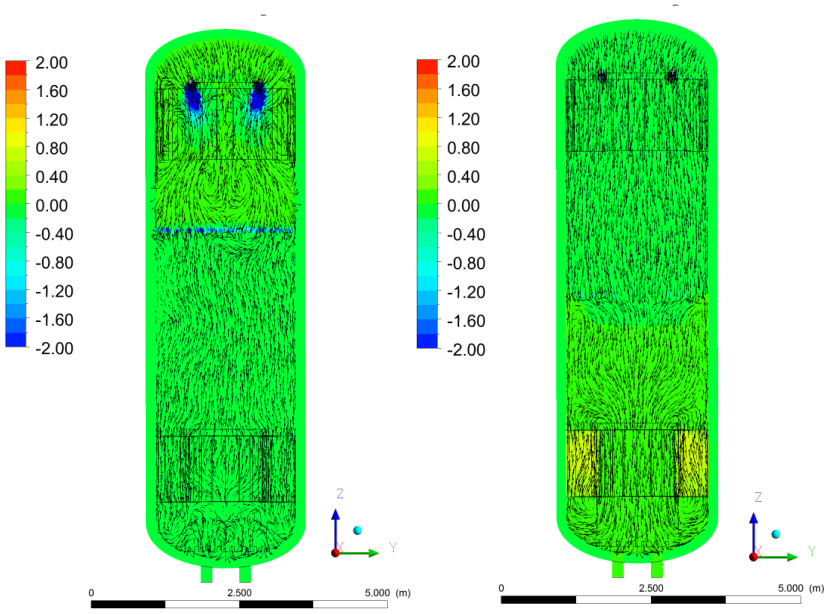

Figure 11. Mass transfer rate [kg/m^3·s] and velocity vectors during pressure decrease (left) and pressure increase (right). Negative value is condensation and positive evaporization. Values below -2 are coloured blue and values above 2 red.

References

Hujala, E., 2013. Evaluation of Bubble Formation and Break Up in Suppression Pools by Using Pattern Recognition Methods. Master thesis. Lappeenranta University of Technology. LUT Energy, Lappeenranta, Finland.

Nariai, H., and Aya, I., 1986. Fluid and pressure oscillations occurring at direct contact condensation of steam flow with cold water, Nuclear Engineering and Design 95, 35–45.

Pellegrini, M., Naitoh, M., Josey, C., Baglietto, E., 2015. Modeling of rayleightaylor instability for steam direct contact condensation, in: The 16th International Topical Meeting on Nuclear Reactor Thermal Hydraulics (NURETH-16), Chicago, IL, August 30-September 4, pp. 1-15.

Puustinen, M. and Kudinov, P., 2017. Design of the separate effect test facility for condensation studies. Private communication.

Pättikangas, T., Ala-Juusela, J., Hovi, V., Huhtanen, R., et al., 2017. Development and validation of CFD methods for nuclear reactor safety assessment (NURESA), in SAFIR2018 – The Finnish Research Programme on Nuclear Power Plant Safety 2015–2018, Interim Report, Hämäläinen, J. and Suolanen, V. (eds), VTT Technology 294, Espoo. p. 253.

Tanskanen, V. 2012. CFD modelling of direct contact condensation in suppression pools by applying condensation models of separated flow. Acta Universitatis Lappeenrantaensis 472, Lappeenranta University of Technology. ISBN 978-952-265-221-8, ISBN 978-952-265-222-5 (PDF), ISSN 1456-4491.

6. Structural Integrity

6.1 Condition monitoring, thermal and radiation degradation of polymers inside NPP containments (COMRADE)

Konsta Sipilä[1], Jukka Vaari[1], Anna Jansson[2], Anna Bondeson[2];

[1]VTT Technical Research Centre of Finland Ltd
P.O. Box 1000, FI-02044 Espoo

[2]RISE Research Institutes of Sweden
P.O. Box 857, 501 15 Borås, Sweden

Abstract

In COMRADE project several ageing related issues in NPP environment were studied, including setting acceptance criterion for O-rings, use of real components in ageing studies, combined effects of radiation and heat and dose rate effect. As a result, several end-of-life criteria was suggested for EPDM O-rings based on the functional property of the O-ring. FE-simulations were conducted to estimate how O-rings endured in a realistic environment. Feasable ways to acquire polymeric materials from running plants and plants underdecomissioning were evaluated. MD-simulations were applied in explaining the mechanisms governing the reverse temperature effect. As part of studying the synergistic effects of radiation and heat, two different kind of behaviour were observed with EPDM and Lipalon cable jacket material in combined high temperature-radiation environments. Also, it was shown that the used sequence in ageing treatments do matter in case of EPDM. Finally the use of semi-empirical models were estimated in the use of predicting dose rate effect and it seems that they require lot of experimental data to provide reliable predictions.

Introduction

Different polymer based materials are widely used in various applications in nuclear power plants and inside containments, e.g. cable jacketing/insulators, sealants, paint coatings, lubricants and greases. As any other material or component, polymers are susceptible to ageing. Elevated temperature, ionizing radiation and moisture are considered to be the most important ageing stressors and they tend to interact with the polymer structure in different ways. In addition to these ageing stressors, the properties of polymer blend, e.g. crystallinity degree, amount of fillers and antioxidants, has an effect to the ageing behaviour. Thus the degradation mechanism can be quite complex.

COMRADE was developed based on input from a feasibility studies from Energiforsk AB and STUK and through discussions between VTT, SP and the Nordic NPPs through Energiforsk. When developing COMRADE it was understood that there are three topics that research efforts could be concentrated. Firstly, there are gaps in knowledge for setting functional based acceptance criteria at the nuclear power plants. Secondly, a study for acquiring polymeric components from the NPPs was in COMRADE. Thirdly, research on ageing of polymers in thermal-irradiative environments were considered to be important, e.g. dose rate effect and synergistic effects of radiation and heat. Three work packages were constructed around these topics and their content is presented below.

Development of condition monitoring methods for polymeric components including low dose rate radiation exposure

The goal was to find functional based acceptance criteria for polymer materials at the nuclear power plants and to find robust test methods for condition monitoring. Acceptance criteria was also calculated through FEM modelling. Furthermore there is a also need to better understand how a polymeric component reacts to different levels of low dose ionizing radiation and synergistic effects between thermo-oxidative and radiation degradation.

All samples in the study were exposed to both gamma irradiation and thermo-oxidative ageing at elevated temperatures in heating cabinets according to the scheme in Figure 1 below. The ageing was completed in two parallel sequences, one using irradiation – heat – irradiation – heat and one with only heat. The ageing temperatures used were chosen based on the heat resistance of the rubber materials (Table 1) and the total dose was 14-18 kGy at a dose rate of approximately 29 Gy/h.

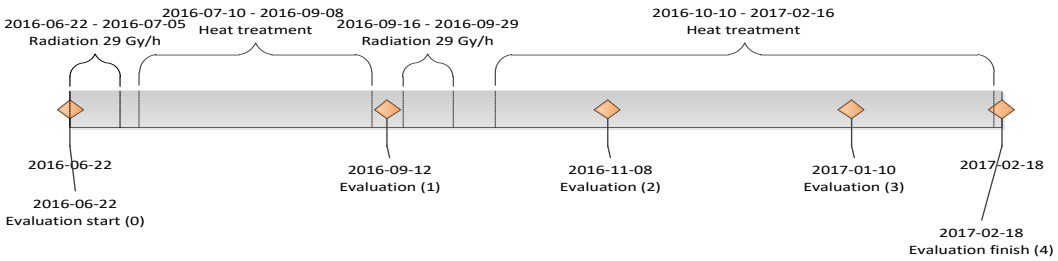

Figure 1. Exposure schedule for the first EPDM ageing treatment; radiation-ageing-radiation-ageing

Three different O-ring rubber materials, supplied by James Walker Ltd, were exposed to three different ageing temperatures each (Table 1). The degradation was followed by measuring deterioration of different material properties as a function of

ageing time, for example elongation at break, compression set and hardness. The end of life criteria was set by measuring leakage in a specially designed test rig, see Figure 2. The end of life (leakage) was correlated to the value of the measured material properties. The test data from the two EPDM O-rings was also used in FEM modelling.

Table 1. Materials studied in WP1.

Material	Grade name	Ageing temperatures (°C)	O-ring dimension (mm)
EPDM	LR 9444	90-120-140	2,99
EPDM	LR 9444	90-120-140	6
FKM	FR 10/70	160-180-195	2,99
Nitrile	NM27/70	60-80-100	6

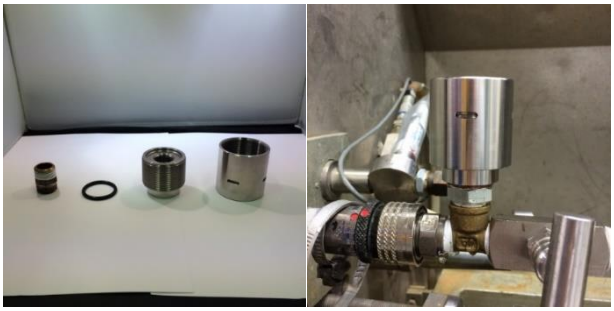

Figure 2. The test rig for leakage measurements, to the left before mounting the O-ring and to the right mounted for leakage test. Leakage was detected at the hole in the cylinder. O-rings were exposed to radiation and heat mounted inside the test rigs.

Table 2 shows end of life criteria for EPDM correlated to material properties. The test values designated “End of life” were measured after 6 months of ageing at 140°C. At this point leakage was also indicated. No leakage was detected at the two lower ageing temperatures.

In Figure 3 compression set is plotted versus the ageing time. The results with and without radiation is very similar indicating that the radiation did not affect the EPDM material significantly. Samples exposed to 140°C for around 150 and 200 days leaked and hence end of life is reached. Compression set is close to or even above 100% when leakage is observed and therefor difficult to use as end of life property.

Table 2. End of life material proerties in comparison to initial values.

Property	End of life	Initial value
Compression set	105%	4,9%
Hardness	80 IRHD-m	72,3 IRHD-m
Elongation at break	50%	182%
Tensile strength	7,5 MPa	12,8 MPa

Stress relaxation is similar to compression set but the force from a compressed O-ring is measured instead of deformation of the O-ring. The force is logged continuously and the method is also more sensitive compared to compression set. The samples are exposed to elevated temperature and measured simultaneously. Because of the sensitivity and amount of test data achieved from stress relaxation theser results were used for FEM calclulations on EPDM rubber.

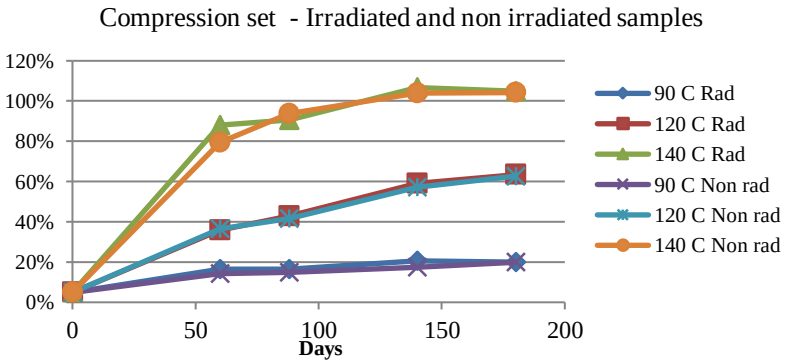

Figure 3. Compression Set Measurements for EPDM O-rings with 2,99 mm diameter.

FKM (Fluorine rubber often known under the trade name Viton) did not show any leakage after terminated exposure and compression set values ended at 90%. FKM materials are known to be very stable at high usage temperatures. FKM was not significantly affected by the radiation.

Finally Nitrile rubber was exposed and analysed. This material became significantly harder upon ageing, and compression set increased. Thermogravimetric analysis showed weight loss starting at approximately 180°C which may explain the increased compression set and hardening of the material when additives evaporate. The effect of higher temperature was significant, but radiation did not seem to affect the material. After initial decreased compression set and hardness the material remained at a rather constant level during ageing.

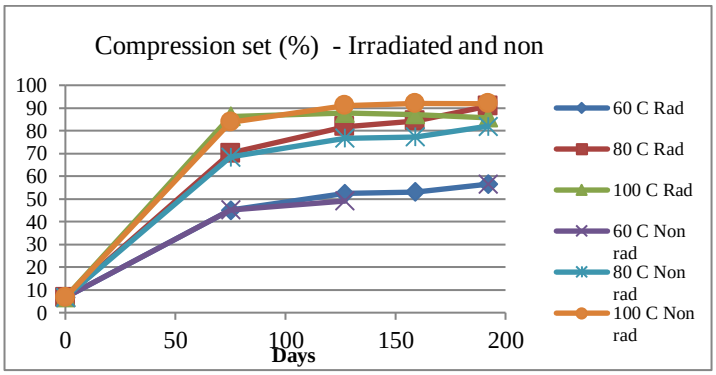

Figure 4. Compression Set for Nitrile Rubber.

Based on the results from three different ageing temperatures activation energies were calculated based on time-temperature superpostion, where curves are shifted along the x-axis, was used to calculate the activation energies and extrapolate service life at 50°C. Degradation rate is dependent on type of polymer, polymer formulation and ageing temperature. Different material properties such as elongation, hardness and compression set are affected differently upon accelerated ageing and as a consequence activation energies varies for different material properties. For EPDM the calculated activation energy is 1,07 eV for compression set whereas the activation energy is only 0,97 eV. In life time prediction it is important to choose a material property relevant for the use of the material, for example compression set for O-rings. By using a low value of activation the service life is not over-estimated. By using activation 0,97 eV activation energy and a end of life value of 50% relaxation the service life for the studied EPDM material at 50°C would be 40 years.

Finite element (FE) simulations of how rubber materials for seals behave over time is performed. A major challenge for the simulations is to find an appropriate material model for the rubber materials and how to calibrate it to experiments. Here is a material model proposed that can include effects like creep, permanent set, and temperature dependence. It is shown how the relaxation tests can be used together with simulations to calibrate rubber material behaviour in seal applications. The visco-elastic (creep) behaviour is the most important in this respect. Compression set data is used in a validation process. A validation process here means that the calibration is done without the validation data. The validation data is instead used to test if the calibrated model can match results from the different validation test. The result is thus a more credible material model.

The effect of temperature is included with calibration of relaxation tests at different temperatures. With this observation the activation energy in Arrhenius equation can be determined. This modelling of the temperature effect is also validated with the compression test data. In the validation, the match between the test and simulated results is reasonable good when considering the rather crude and simple way the

temperature effects calibration is performed. Furthermore, the Arrhenius equation is derived for one well defined chemical reaction while creep in rubbers is a complex process. Considering also this, the thermo-effects modelling seems good. This successful use of the Arrhenius equation for more complex effects is an experience that is often seen in various applications. Although not attempted here, it could also be possible to use the Arrhenius equation for ionizing radiation together with temperature.

The material models are used in an leak and tightness simulation attempt. This work is not fully completed. Although such simulations were successfully used in work such as (6), it does not work to full extent here. Numerical difficulties occur that prevent the simulations to be used to simulate leakage with confidence. From the leak and tightness simulations performed here it is shown that the increased creep for higher ageing temperatures seems to have a detrimental effect on the tightness, although one cannot assure or quantify the effect.

Learn from materials used in plants

Possibilities to analyse materials undergone aging in operating and shut down power plants were studied. This includes Barsebäck but also materials from outages in still operating power plants in the Nordic countries. In a pre-study staff at Barsebäck were interviewed and the result was that no suitable materials could be used for durability studies. Barsebäck plant does not have the ability to give radiological clearance in situ so an external authorized regulator must be engaged, and it is not certain that the equipment that has been in the enclosure can be given radiological clearance at all. If the polymeric material cannot be given radiological clearance the examination must be done in the controlled area. If the investigation will be done in situ the following things must be arranged: admission, training of personnel in handling radioactive materials (2-3 day-course), dosimeters and our equipment will have to be given radiological clearance afterwards. This would increase the cost significant compared to testing at a standard material testing laboratory. Another aspect against using materials from Barsebäck is that after the outtake of the reactors the materials have been stored for many years in different temperatures and atmosphere than the normal service conditions.

Therefore a questionnaire was introduced to NPP polymer material experts via COMRADE industry group to identify the polymeric components that can be available to study. Based on the feasibility study and input from the project team the following components were of interest to investigate and present in the questionnaire:

- O-ring of EPDM, Nitrile, Silicone or Viton
- EPDM seals/gaskets
- Joint sealants / sealants
- Cable transits (e. g. Brattberg cable transit)

- Sealing foam (polyurethane, etc.)
- Cables (Lipalon HHSO-type is previously studied in COMRADE)
- Lubricants and greases
- Paint coatings

The questions regarding the components were on availability of materials, material information, environment and storage conditions.

Several O-rings were obtained from Ringhals and two examples are shown in Figure 5.

Figure 5. Two damaged O-rings from Ringhals to the left no EPDM and to the right no 11 NBR.

The EPDM ring to the left has been in service for three years at 162°C at 12 bar pressure in water/steam. After removal it has been stored for one year at room temperature. The NBR sealing to the left was hard and brittle, hardness was 70 shore A from start and has now around 90 Shore A. Service time and environment is unknown. Hardness was measured on a number of o-rings, beside the example above, and the results varied a lot between the materials. To be able to evaluate components further the information about the materials and their environment in use must be more extensive.

To summarize the main hinders to find material to study were to get clearance of the materials and to find documented information about original material properties and service environment. Moreover, extraction of components from plants about to close and outtakes at running plants need a lot of planning in advance. Based on experience from this project, we would specify component for studies carefully in future projects:

- Type of component, for example O-ring, what dimension.
- Amount of material/component needed.
- Specify relevant tests in advance.
- Decide if additional accelerated ageing should be performed.
- Specification example: ten O-rings of minimum core diameter is needed for hardness and tensile testing and one ageing cycle. In this project we asked for any type of material and tests were performed depending on type and amount of materials achieved.

Polymer ageing mechanisms and effects inside NPP containments

WP3 content can be divided into three different subtasks where the first one focuses on using computational modelling techniques in polymer ageing. In WP3 modelling work related task literature survey was completed in 2016 on the synergistic effects of temperature and radiation in polymer ageing, and on possible ways of considering them in the lifetime prediction of nuclear power plant components. The following topics were looked into in more detail: the proposed mechanisms behind the synergistic effects, material modelling methods feasible for studying ageing and an overview of previous research related to the topic. The mechanisms underlying combined thermal and radiation ageing can be exceedingly complex, involving various chemical and physical processes across multiple structural and time scales. There remains a formidable gap between the present multi-scale materials modelling capabilities and practical lifetime prediction. Currently the most recognized practical lifetime prediction methods are semi-empirical and based on accelerated ageing experiments. Methods applicable to combined thermal and radiation ageing include the superposition of time-dependent data method, and the superposition of dose-to-equivalent-damage data method. The semi-empirical methods are limited in their predictive capability, as they cannot address possible changes in the dominant ageing mechanisms. For this reason, anomalous ageing phenomena such as the reverse temperature effect can render their predictions useless. In 2017-2018 the modelling work inside COMRADE was thus focused on a particular synergistic mechanism or some other relevant detail of the ageing process is feasible, such as the reverse temperature effect.

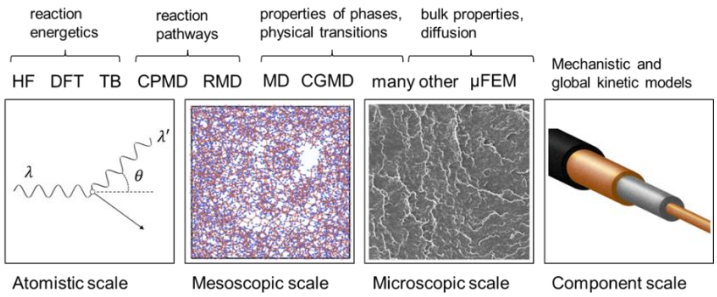

Figure 6. Scales and processes of thermal and radiation ageing coupled with numerical modelling methods.

During 2017 classical molecular dynamics (MD) was used to build united-atom structural models (one particle representing a CH2 or a CH3 unit) for the target material, polyethylene (PE). First, equilibrium structures for fully amorphous polyethylene were created. Then, methods were developed to convert the fully amorphous PE into partially crystalline and/or cross-linked forms. Methods were also

tested for measuring the mechanical properties of PE. In addition, detailed all-atom reactive MD simulations were performed to study the mechanisms of radiation induced damage. The threshold recoil energy (energy required to introduce radiation damage) was estimated to be >20 eV in case of PE. Because MD timescales are significantly shorter than timescales for chemical reactions, the reactions of oxygen and radical species with the polymer will not be treated explicitly in the MD simulations, but will be taken into account in the structural details of the model system. This will require adding a chain scission mechanism to the united-atom PE model during 2018 for a proper description of the aging process.

In 2018, the modelling work of WP3 was started by performing an extensive set of simulations on the crystallisation of cross-linked PE. The main finding was that after crystallisation, cross-links were found exclusively in the amorphous regions. A method was developed and tested for simulated aging of XLPE structures, which involves both bond scission and cross-link formation. Simulations of the tensile test were carried out for PE systems with varying chain length and varying cross-link density. A method to include stretch-induced bond breaking was developed for the united-atom description. According to results, the mechanical strength of polyethylene decreased with decreasing chain length until the material became fragile. Conversely, an increasing cross-link density first improved the mechanical strength, but at high cross-link densities the material became increasingly brittle, as evidenced by a decrease in the elongation at break. These results were in qualitative agreement with the experimentally observed reverse temperature effect, as originally reported by Celina et al (Radiat. Phys. Chem. 48 (1996) 613).

The first goal in the experimental task was to study synergistic effects yielding from radiation and heat on EPDM and CSM rubbers. The samples were aged at three different temperatures and irradiated with three different absorbed doses. Based on the elongation at break results obtained with EPDM samples (Figure 2), it can be stated that moderate increase (ca. 75-125°C) in temperature during exposure to ionizing radiation hinders the degradation process. In addition, plane thermal ageing (equivalent to the thermal ageing component during simultaneous ageing) did not result in any changes in elongation at break. CSM (Lipalon) seemed to be more susceptible to both irradiation and thermally induced ageing and only small synergistic effects rising from simultaneous exposure to radiation and heat could be observed when simultaneous radiation and thermal ageing data was compared to plane thermal ageing data. Thermal ageing at 125°C resulted in clear decrease in elongation at break. Only slightly larger decrease was observed at 125°C when irradiation was conducted simultaneously. Simultaneous exposure to increasing temperature with irradiation resulted in increasing degradation. This behaviour was opposite to what was observed on EPDM samples.

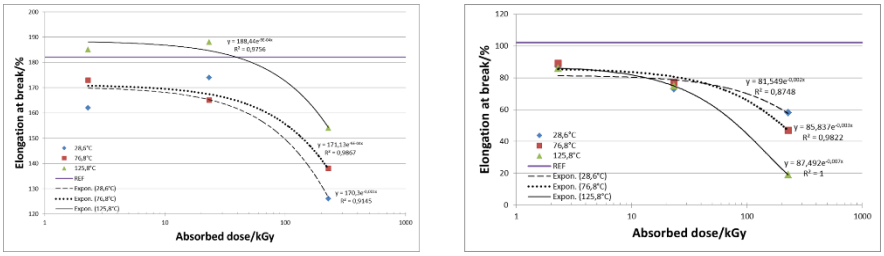

Figure 7. Decrease of elongation at break as function of absorbed dose at different temperatures for EPDM (left) and CSM (right).

In addition the role of aequence in ageing was estimated. In Figure 8 EaB data is presented after three different ageing procedures. The first ageing procedure included thermal ageing at 125°C for three weeks first and then irradiation at room temperature up to 200 kGy dose (blue column in Figure 8). The second ageing procedure (orange column in Figure 8) had the exact same thermal and irradiation ageing's, but their sequence was changed so that at first came the irradiation ageing and then the thermal ageing. In the third ageing procedure, both thermal and irradiation ageing were conducted simultaneously (grey column in Figure 8). The results indicate that the sequence does matter as simultaneous ageing and irradiation-thermal-sequence are compared.

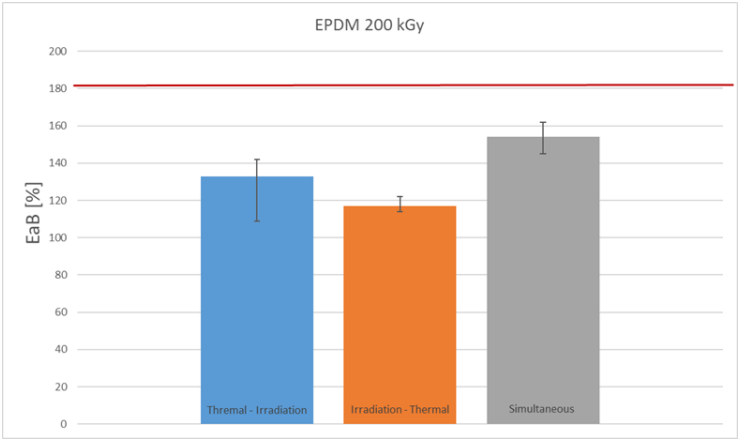

Figure 8. Comparison of sequence of ageing on EPDM samples. Blue column describes the decrease in EaB when sequence is thermal-irradiation, orange column irradiation-thermal and grey column simultaneous thermal and irradiation ageing.

The second goal in the experimental task was evaluating applicability of different techniques on measuring the oxidation profile created on EPDM samples during accelerated ageing and evaluate whether the measured oxidation profile could be

correlated to mechanical properties of the sample material. Studied techniques included differential scanning calorimetry (DSC), time of flight secondary ion mass spectroscopy analysis (ToF SIMS) and Fourier transmission electron microscopy (FTIR). The studied material was sulphur and peroxide cured EPDM rubber and it was aged to three different conditions: thermally aged, gamma radiated and simultaneously (peroxide cured EPDM sequentially) thermally and gamma radiated. The overall condition of samples was evaluated by tensile testing (i.e. tensile strength, elongation at break and modulus at 100% strain). Based on the results obtained with ToF-SIMS (see Figure 9), it can clearly detect the oxidation occurring in the vicinity of surfaces of the aged samples. However, careful sample preparation is required since the method is sensitive to surface roughness and other contaminations. The other two methods had limitations on the sample material and resolution when creating an oxidation profile from surface towards the bulk.

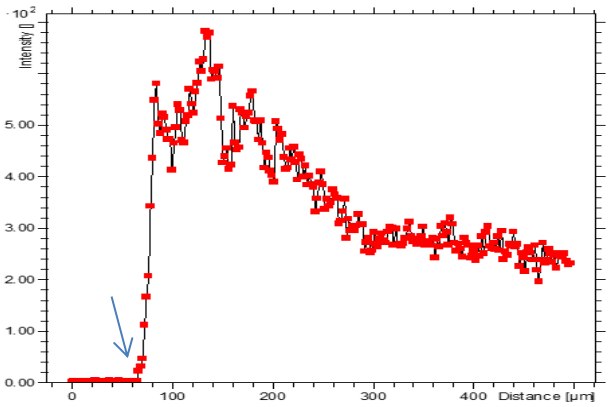

Figure 9. ToF SIMS measurement on EPDM where oxidation (O^- signal intensity) is presented as function of distance from the sample surface-air interface (shown with an arrow) towards bulk material. In this case the ca. 200 µm thick surface layer has oxidized more than the bulk material.

The third goal focused on evaluating different methods that could be used in evaluating dose rate effect, i.e. whether the used irradiation dose rate have an effect to the amount of degradation as the absorbed dose is kept as constant. The applicability semi-empirical power law and superposition models were evaluated whether they could be used in estimating the severity of dose rate effect. In case of the superposition model it was noted that the experimental data obtained was insufficient to make any reliable predictions. With power law model, more reliable results were obtained. However, EPDM showed good radiation resistance which yielded in uncertainty in predictions of dose rate effect when the power law model was applied. In case of Lipalon the dose rate had and an effect to the DED values, as can be seen from Figure 10, but more experimental data from low dose rate irradiations would be required in order to confirm this observation. Overall, it should be stated

that the used dose rates during the irradiations were relatively high and homogeneity of oxidation could not be confirmed which would ease the examination of the data quality. For Lipalon material, the activation energy value (69 kJ/mol) could be calculated from the thermal ageing data, which would mean that in 50°C and 25°C the remaining lifetimes would be 680 days and 16 years, respectively.

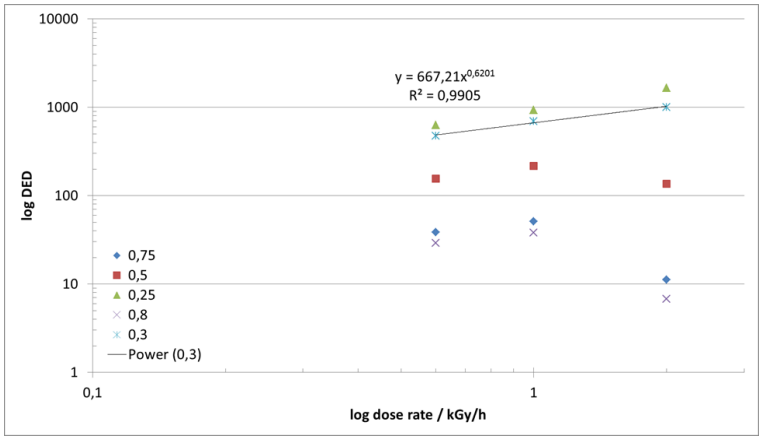

Figure 10. Extrapolation of end-point dose to lower dose rates for Lipalon.

Summary

Several polymer ageing related topics relevant in NPP environments were studied in COMRADE. The most interesting results obtained within the project include:

- An acceptance criterion based on functionality of O-rings can be set for several O-ring material
- Sufficient amount of information is required on material, service and storage environment if they are tended to use in ageing studies
- The simulated changes in crosslink density of the material was shown to be in qualitative agreement with the experimentally observed reverse temperature effect
- EPDM and Lipalon react differently to simultaneous exposure to elevated temperature and irradiation
- The sequence in ageing does matter when EPDM samples are aged
- When semi-empirical methods are used in predicting the severity of dose rate effect, sufficient amount of experimental data is needed

Acknowledgement

The Nuclear Waste Management Fund of Finland VYR, VTT Technical Research Centre of Finland Ltd, the Swedish Radiation Safety Authority SSM and Energiforsk AB are greatly acknowledged for funding this work.

6.2 Analysis of fatigue and other cumulative ageing to extend lifetime (FOUND)

Juha Kuutti[1], Otso Cronvall[1], Ahti Oinonen[1], Tommi Seppänen[1], Antti Timperi[1], Tero Tyrväinen[1], Iikka Virkkunen[2]

[1]VTT Technical Research Centre of Finland Ltd
P.O. Box 1000, FI-02044 Espoo

[2]Aalto University
P.O. Box 11000, FI-00076 AALTO

Abstract

A summary of the results obtained in the SAFIR2018 FOUND project is presented. The project is focused in ageing and failure assessment of NPP components. The main results consists in the developments in evaluating the criticality of cracks in NPP components, a dissertation on the ageing of the BWR RPV and its internals, new experimental research on the primary water affected fatigue, improved methods to assess thermally induced cyclic loads and thermal fatigue, novel probabilistic and risk-informed methods to assess piping failures and developments in assessing the dynamic response of piping systems. In addition, novel research on residual stress measurement techniques and results on the residual stresses in NPP piping components that have been in service for decades are presented.

Introduction

The project FOUND concerns cross-disciplinary assessment of ageing mechanisms for safe management and extension of operational plant lifetime. It develops deterministic, probabilistic and risk informed approaches in computational and experimental analyses.

The focus areas are: Remaining lifetime and long term operation of components having defects; Susceptibility of BWR RPV internals to degradation mechanisms; Fatigue usage of primary circuit, with emphasis on environmental effects and transferability; Fatigue and crack growth caused by thermal loads, with emphasis on modelling; Development of RI-ISI methodologies, NPP piping analysis methods; Residual stresses in BWR NPPs. The research performed and the obtained results on each of these is described in the following.

Remaining lifetime and long term operation of components having defects

With the modern developing NDE methods more indications are found year by year. The computational assessment of flaw behavior due to fatigue or stress corrosion cracking under operational loading including residual stresses is important for determining remaining lifetime of components. In the lifetime assessment of components, numerical methods for computing the component stress state, possible welding residual stresses are in practical use. The evaluation of the operational stresses may not be straightforward, for example in case of thermal loads where there might be significant uncertainties in the assessment caused by the complex thermohydraulic phenomena.

Treatment of uncertainties in structural analyses

Often the uncertainties are treated using safety factors. A review of the safety factor assessment practices was performed in the project (Cronvall 2015). This work provided a short introduction for considering the uncertainty and probability effects in typical structural integrity analyses of NPP piping components. It was found that the multitude of different safety factor definitions and a mixture of conservative and best-estimate assumptions makes it difficult, or even impossible, to define what is the total safety margin of a structure or component. Different types of input data have differently determined safety factors which are not compatible with each other. Structural integrity analyses of structures and components would benefit from more specific definitions of the safety factors. Currently the evaluation of the total safety margin values has to be done with probabilistic terms by risk analysis approach. One possible future development would be probabilistic case studies that consider the full analysis chain, from load determination to calculation of the component stresses and evaluation of defect behavior inclusive of sensitivity analyses to determine the conservatism of analysis phases. The harmonization of the safety parameter definitions, such that all factors affecting the final result with equal weight are treated uniformly, is still an open issue. The importance of these issues increases due to plant ageing and a possible lifetime extension. The input data and related safety factors applicable for the design stage may differ from those applicable after e.g. 30 years of plant operation.

Another common approach related to risk analysis is sensitivity analysis with respect to the unknown parameters. For the thermal loads, this uncertainty analysis was performed in the project (Timperi & Cronvall 2016) by utilizing different methods to estimate the stresses due to thermal mixing. There were notable differences between the resulting stresses evaluated using the approaches, but the envelope of the results was covered by the safety factors typically proposed for thermal loads.

Flaw assessment methods

In addition, there is uncertainty concerning how to computationally assess the possible flaw behavior under the complex cyclic, thermal or residual stress loads.

The numerical determination of crack criticality and possible growth is not straightforward due to the limitations of common methods to evaluate the parameters describing the crack loading. The traditional methods and parameters, such as the J-integral, are not directly suited for these cases. For this purpose, an effort was made to extend the J-integral field of applicability to cover cyclic and non-proportional loading cases in (Kuutti 2016).

In straightforward cases, the flaw assessment is performed using standardized engineering tools. For flaws in nuclear components, the ASME Section XI rules and methods are often applied to assess the flaw criticality. The present capabilities for the computation of the time and/or load cycles to reach the maximum allowable crack sizes, as determined by the ASME code, are based mainly on engineering solutions, leading often to conservative results. Other engineering methods such as the R6 or BS7910 methods can be utilized in the NPP component assessments with reasonable justifications. The relation between the different methods is not fully established and a FAD based approach might be beneficial over the ASME XI rules. This aspect was studied in (Kuutti 2018). The results show that, in most cases, the ASME rules and the FAD approach yield to similar results but significant differences may exist in more complex cases. An example comparison between the approaches is shown in Figure 1.

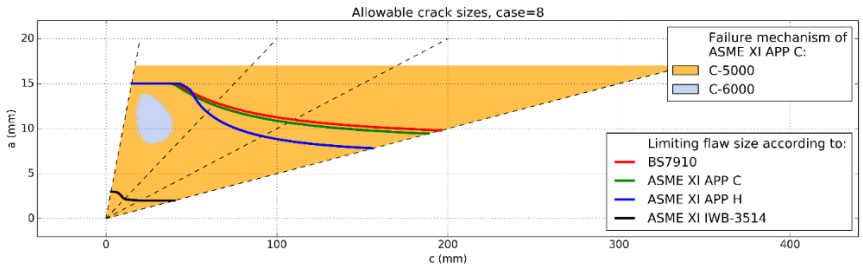

Figure 1. Comparison of allowable flaw sizes determined by the BS 7910 and ASME XI procedures. The studied case is an axial inside surface flaw in a ferritic pipe under internal pressure.

Susceptibility of BWR RPV and its internals to degradation mechanisms

This part of the project concerns the susceptibility of boiling water reactor (BWR) reactor pressure vessel (RPV) and its internals to various degradation mechanisms. This work consists of the following three main parts: (a) literature survey and review; (b) component specific survey on susceptibility to degradation mechanisms; (c) computational analysis approaches, tools and examples. A doctoral dissertation (Cronvall 2018) has been prepared from the work.

The work starts with a literature survey on degradation mechanisms that can/could affect the BWR RPV and/or its internals. This includes an overview and

detailed phenomenological descriptions of these degradation mechanisms. Interaction of degradation mechanisms is considered too. The relevant degradation mechanisms include: irradiation embrittlement (IE), thermal embrittlement (TE), fatigue crack growth (FCG), intergranular stress corrosion cracking (IGSCC), and irradiation accelerated stress corrosion cracking (IASCC). Next, the observed cracking degradation history of BWR RPVs and their internals is described component specifically in more detail with representative examples.

The work then moves on to describe in detail the major practical aspects of the relevant degradation mechanisms that affect the BWR RPV and its internals, and to evaluate the potential significance of their effects on the continued performance of safety functions of the considered components throughout the plant service life.

This is followed with an investigation on the susceptibility of the BWR RPV and its internals to degradation. Of BWR plants, the scope of this work concerns those designed by ABB, focusing on the third generation. The internals determined as significant in TVO report (Lemettinen 2016) and IAEA-TECDOC-1471 (IAEA 2005) were selected to be considered in this work. These components are from TVO units OL1/OL2. Altogether 31 components were selected for more detailed consideration. These components include RPV, Steam separator support legs, Steam outlet nozzles, Feedwater nozzles, Control rods, Core shroud, Core spray nozzles and Control rod guide tubes at the RPV bottom. The summary of the susceptibility of BWR RPV and its internals is presented in Table 1.

Table 1. Summary on component specific susceptibility of BWR RPV and its internals to relevant degradation mechanisms. Here, susceptibility is denoted with "X".

Degradation mechanism	Material types							
	austenitic stainless steels	cast stainless steels	ferritic stainless steels	martensitic stainless steels	high chromium content nickel-base alloys	ferritic and low alloy steels	carbon steels and associated weld metals	low alloy RPV steels
Irradiation embrittlement						X	X	X
Thermal embrittlement		X	X	X	X	X	X	X
Fatigue (i)	X	X	X	X	X	X	X	X
IGSCC	X	X			X			
IASCC	X	X			X			
General corrosion (ii)	X	X	X	X	X	X	X	X
Erosion-corrosion, FAC						X	X	
Mechanical wear	X	X	X	X	X	X	X	X

(i): All metallic materials are in principle susceptible to fatigue, however, in most cases for BWR RPV and its internals the effect is negligible.
(ii): All metallic materials are in principle susceptible to general corrosion, however, for BWR RPV and its internals the effect is negligible.

The loads specific to the BWR RPV and internals are described next. These components experience several kinds of loads. They are in contact with hot and moving liquid coolant during normal plant operations. The coolant saturation temperature corresponding to the system pressure is just below 290 ºC. Internal components located in the vicinity of the core are also exposed to fast neutron fluxes (E > 1.0 MeV) and gamma irradiation. The operating environment inside a BWR RPV generates many loads that are considered to propagate ageing related or time dependent degradation mechanisms. In the top level these can be divided into applied loads, environmental loads and manufacturing induced loads.

The work then moves on to describe the screening process for the considered components. For NPPs the purpose of a screening process is to select the components for further analyses, especially for degradation potential analyses. More specifically, these analyses are here called time limited ageing analyses (TLAAs). The objective of the TLAAs is to identify the degradation mechanisms of components and the increase in failure occurrences, to assess the remaining lifetime of components and to find suitable means to prevent or mitigate the effects of ageing degradation. The applied screening process is based on those by IAEA and EPRI. All considered components were screened.

Computational approaches, tools and analyses are described next. The covered computational approaches apply mainly structural mechanics and fracture mechanics. Temperature distributions, stresses and strains for the analyzed components are computed with general purpose FE codes and/or with analytical equations, where applicable. In most TLAAs, fracture mechanics based analysis code VTTBESIT is used. This code comprises parts developed by VTT and by IWM. Both deterministic and probabilistic crack growth computation procedures are presented. Computational developments are described next. These concern new equations for stresses and strains in multi-metal hollow cylinder as well as new equations for inverse computation of temperatures in bi-metal pipe. The focus of the work is on the TLAAs. Of the 31 considered components, 12 components screened in. Several of these components are assessed to be susceptible to more than one degradation mechanism. These components include all those mentioned above in the connection of susceptibility of BWR RPV and its internals to degradation.

The work then moves on to the TLAAs for the components that screened in. Of the relevant degradation mechanisms, the performed TLAAs concern IE, TE, FCG, IGSCC and IASCC. The maximum component specific number of TLAAs is four, which concerns the Feedwater nozzles, Shutdown cooling nozzles and Core spray nozzles. The TLAAs for the RPV cover 80 years of operational lifetime, whereas those for other components cover 60 years. According to the TLAA results the crack growth is in most cases very slow. In addition, the obtained crack growth results are also conservative. Firstly, it was assumed that initial cracks exist/nucleate from the start of the plant operation, whereas in reality it usually takes several years, even more than a decade, for a crack to nucleate from dormant microscopic size to macroscopic size capable to grow. Secondly, the end-of-life (EOL) crack sizes are computed according to Section XI of the ASME code using safety factors given therein for load induced primary stresses. In a couple of cases the computed crack growth is of significant scale. For instance, according to the TLAA results IGSCC can grow quite rapidly in Core shroud support leg weld. Concerning all performed TLAAs, crack growth is in all cases so slow, that any growing crack would be found in the inspections well before it reaches any critical size. In most cases the resulting crack growth is negligible.

As the main argument of this work concerns the RPV, the TLAA results concerning it are summarized in the following. This component is affected by altogether three degradation mechanisms: IE, TE and FCG. However, the effect of TE is included in the empirical models for IE. According to the IE TLAA results the maximum stress intensity factor values for Appendix G of ASME Section XI reference crack in the RPV shell remain well below the corresponding fracture toughness values that have decreased during 80 years of plant operation. The actual structural integrity margin is considerably larger than what the results show, as the computation procedure includes several conservative assumptions. Thus, even after 80 years of plant operation there is a large structural safety margin for the RPV against IE. The crack growth for FCG in the RPV shell is slow in all cases for 80 years of plant operation, even for the largest initial crack postulate. The maximum crack growth through wall within 80 years is approximately 4.6 mm for this crack postulate with

initial depth and length of 20 and 120 mm, respectively. The crack growth for FCG remains well under maximum EOL crack depth for 80 years of plant operation.

Based on the degradation analysis results, it is concluded that the operational lifetime of the internals of the OL1/OL2 RPV can be safely continued from 40 to at least 60 years. Importantly, it is concluded that the operational lifetime of the OL1/OL2 RPV and connecting main nozzles can be safely continued from 40 to even 80 years. According to the conservative TLAA results, the degradation in terms of crack growth is in most cases very or extremely slow. In the few cases with faster crack growth the cracks would be detected in the inspections well before they grow to any significant size.

The structural risk assessment results for the OL1/OL2 RPV and its internals show that for all components but one the computed risk class is moderate or lower. It is concluded that for the OL1/OL2 RPV and its internals the overall structural risks are small and even in the maximum risk case acceptable

Environmental fatigue of primary circuit

One of the recognized degradation mechanisms of pressure boundary components in nuclear power plants is fatigue. Fatigue damage in NPP pressure vessels and piping originates from mechanical or thermal stresses experienced during transients such as start-up or shut-down. In NPPs, the evaluation of fatigue is based on local strain approach, codified stress analysis and material specific design curves. These design curves are derived from room temperature (RT) strain-controlled low cycle fatigue (LCF) test results and are included in design codes such as Section III of the ASME B&PV Code.

Effects of plant relevant service conditions are however difficult to quantify, challenging the transferability of laboratory data. Experimental work in simulated reactor water has aimed at solving these uncertainties since the 1980's. The current consensus is that reduction in fatigue life in pressurized hot water can be accounted for by using F_{en} reduction factors, described in NUREG report 6909, for example (Chopra & Stevens 2014). F_{en} is defined as the ratio of fatigue life in air to fatigue life in water. For austenitic stainless steels, F_{en} is a function of strain rate, temperature and dissolved oxygen. Decreasing strain rate and/or increasing temperature increase the calculated F_{en}.

Unfortunately, most of the generated data to date has come from non-standard test procedures or specimens to avoid numerous difficulties of performing standard LCF tests in pressurized hot water. In order to generate design compatible data and importantly, to meet the regulatory requirements concerning environmentally assisted fatigue, a miniature fatigue device was first developed at VTT. During SAFIR2010 (Solin et al. 2011), a tailored-for-purpose fatigue device "FaBello" was designed and verified for ASTM E 606 compliant fatigue testing in simulated reactor coolant. In SAFIR2018, FaBello has been used to generate qualified data in support of a new mechanism informed, plastic strain rate based F_{en} model. The aim of this

work is to advance towards an internationally recognized, mechanism-informed scientific model for Fen. It is hypothesized that the new model should emphasize plastic strain rate as a critical parameter, rather than total strain rate. Starting from pioneering works behind the ASME Code, scientific literature suggests such a revision, but this is yet to be proven with valid test results and an appropriate - and code-compatible - model has to be formulated.

Experiments in simulated PWR water

The experimental programme and results are described in detail in Seppänen (2018). Two different stainless steels in solution annealed state were used for the EAF tests. Testing in 2015–2016 was done using stabilized AISI 347, and in 2017–2018 using non-stabilized AISI 304L. Linear strain waveforms were used, but with non-constant strain rate. This was done to represent simplified plant transients and non-realistic mirrored strain waveforms for comparison purposes. The selected strain waveforms were inspired by a typical transient experienced in the primary circuit safety injection system. This waveform was linearized and shortened for testing purposes, as shown in Figure 2. The use of reversed order dual strain rate waveforms for the rising ramp was selected to be able to easily compare effects of plastic strain rate. The equipment makes use of servo-controlled pneumatic bellows, to which one end of the specimen is threaded. The other end is threaded to the rigid load frame. Solid ϕ8 mm specimens are used, and strain is controlled directly from the ϕ8 mm parallel gauge length using calibrated eddy current sensors.

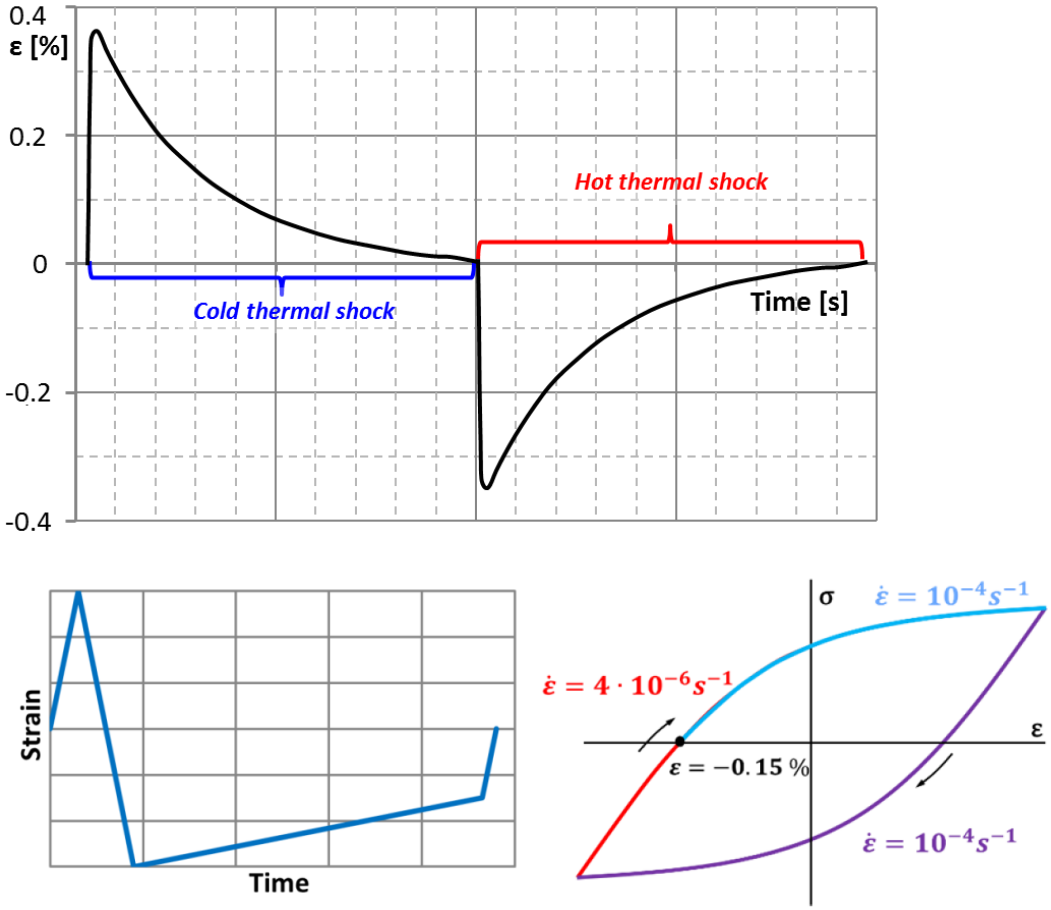

Figure 2. Schematic of a safety injection system transient.

A summary of test results is shown in Table 2 and visualized in Figure 3. The "Actual F_{en}" values are experimental results and "Nominal F_{en}" values are theoretical predictions according to NUREG/CR-6909. Minor deviations can be seen for the realized strain amplitudes and rates, but their effect on the nominal F_{en} prediction is small.

The current tests in water last considerably longer than should be expected based on the existing F_{en} models. Overall there are only four results, in which the experimental F_{en} was above five. All of these were tests using the reversed waveform, which is unrealistic for actual transients and simply applied for maximum contrast. On the other hand, the SIS transient results are generally in the F_{en} range of 4–5, even as low as below three. The design compatibility modification on the elastic modulus further lowers all Fen factors, as it effectively shifts the comparable test strain amplitude up (or the reference curve down).

A clear material difference in the tested specimens is observed if, rather than using the absolute experimental F_{en}, we use the ratio of experimental/predicted. When this is done, it seemingly indicates that the 304L material has superior performance to 347. It would also undermine the procedure of applying a single Fen equation for all stainless steel alloys, because the trend is repeatable over the four test sets. If it is expected that the 304L has improved air fatigue lives over 347, this balances the apparent material differences seen in the results. However, this statement requires caution because the reference curve for 304L is not based on LCF testing at VTT but rather on a scattered set of results. Unfortunately no air testing was possible in this project which leaves a high degree of uncertainty in the conclusions for 304L.

Table 2. Schematic of a safety injection system transient.

Year	Material	FaBello rig	ε_a [%]	Waveform	For rising ramp		$\dot{\varepsilon}$ switch point	Nominal F_{en} [20]	Actual F_{en}
					$\dot{\varepsilon}_1$ [s^{-1}]	$\dot{\varepsilon}_2$ [s^{-1}]			
2015	347	1	0.30	SIS	$3.4 \cdot 10^{-6}$	$8.4 \cdot 10^{-5}$	½ of tensile ramp	9.01	4.80
		2	0.33	SIS	$4.6 \cdot 10^{-6}$	$1.1 \cdot 10^{-4}$		9.02	3.78
		3	0.30	Reverse	$8.7 \cdot 10^{-5}$	$3.5 \cdot 10^{-6}$		9.35	11.21
		4	0.39	Reverse	$1.1 \cdot 10^{-4}$	$4.4 \cdot 10^{-6}$		8.88	5.41
2016		1	0.31	Reverse	$1.0 \cdot 10^{-4}$	$4.1 \cdot 10^{-6}$	¼ of tensile ramp	10.92	8.43
		2	0.32	SIS	$4.4 \cdot 10^{-6}$	$1.1 \cdot 10^{-4}$		7.25	4.44
		3	0.31	Reverse	$1.0 \cdot 10^{-4}$	$4.1 \cdot 10^{-6}$		10.92	12.51
		4	0.31	SIS	$4.2 \cdot 10^{-6}$	$1.0 \cdot 10^{-4}$		7.27	4.84
2017	304L	1	0.31	Reverse	$1.0 \cdot 10^{-4}$	$4.1 \cdot 10^{-6}$	¼ of tensile ramp	10.91	5.56
		2	0.32	SIS	$4.5 \cdot 10^{-6}$	$1.1 \cdot 10^{-4}$		7.23	2.76
		3	0.31	Reverse	$1.0 \cdot 10^{-4}$	$4.1 \cdot 10^{-6}$		10.90	7.75
		4	0.32	SIS	$4.3 \cdot 10^{-6}$	$1.1 \cdot 10^{-4}$		7.23	2.84
2018		1	0.21	Constant $\dot{\varepsilon}$	$6.9 \cdot 10^{-5}$		n/a	6.12	3.70
		2	0.31	SIS	$4.2 \cdot 10^{-6}$	$1.0 \cdot 10^{-4}$	½ of tensile ramp	9.05	3.68
		3	0.31	SIS	$4.1 \cdot 10^{-6}$	$1.0 \cdot 10^{-4}$		9.08	3.97
		4	0.32	SIS	$4.2 \cdot 10^{-6}$	$1.0 \cdot 10^{-4}$		9.03	4.04

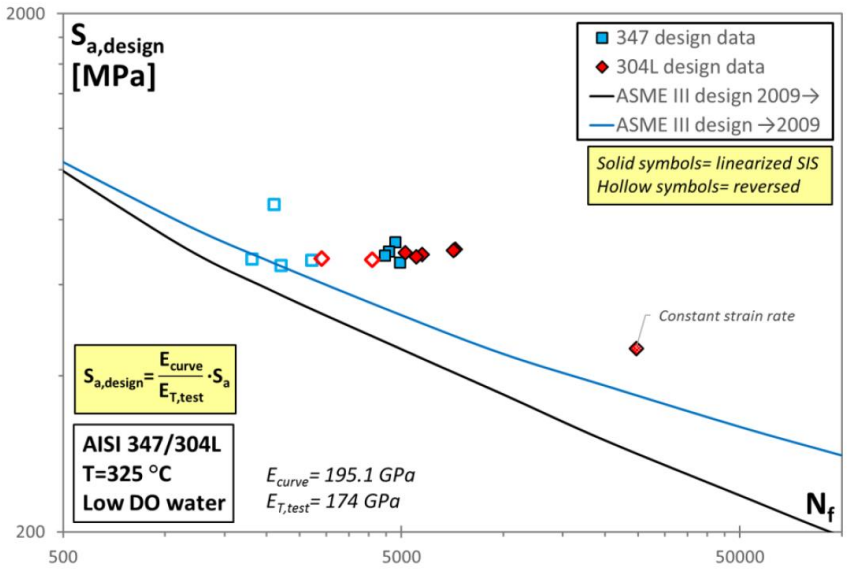

Figure 3. Design compatible test results and ASME fatigue design curves.

VTT approach to modelling EAF

The detailed formulation and reasoning behind the EAF model are given in Seppänen (2018). The starting hypothesis for an improved Fen model is that plasticity is the cause of fatigue damage. From a design point of view plastic strain presents a challenge, but from a mechanistic point of view it is the key to an improved understanding of EAF. Due to cyclic hardening and softening in a total strain-controlled test, plastic strain is not constant between cycles. Within single cycles, the plastic strain rate also varies from essentially zero and approaches the total strain rate as a function of strain. It is understood that in EAF strain rate is inversely proportional to F_{en}, meaning a slow strain rate is more damaging.

The Fen methodology in NUREG/CR-6909 is elegant in form and easy to understand. Therefore the same basic structure is adopted for the improved model proposal with some additions. It is considered essential to use reliable grade specific reference curves, contrary to the NUREG approach of collecting all possible data into a single regression fit. The proposed model includes a temperature effect term, defined as the ratio of fatigue life at RT to the specific temperature, to separate effects caused by temperature alone from those purely caused by reactor coolant. To keep the first model proposal simple in nature, the insensitive strain range concept is included in the model as such to effectively eliminate the range of highly nonlinear plastic strain rate near the valley of a loop. The plastic strain rate in the remaining “Fen effective” part of the loop is obviously dependent on the strain amplitude, but in general is much more linear. For these reasons the total strain rate is

selected as an approximation. In NUREG/CR-6909 the insensitive strain range concept is recognized and basically included in the Fen model. However, its value was fixed based on a strain range of 0.6 %. This was changed into strain amplitude and decreased for mean stress effects and uncertainties, ending with a threshold strain amplitude of 0.10 %. This is an entirely different kind of interpretation as in the proposed model, which applies the range starting from the valley of the hysteresis loop. In the NUREG model, the insensitive strain range is effectively simply a lower threshold strain amplitude for environmental effects and has no influence for the MRA calculation in a non-constant strain rate or temperature situation. A strain amplitude term implemented into the model together with the strain rate term reduces the effective strain rate for a low strain amplitude, while having little influence at higher strain amplitudes. Experimental results and mechanistic understanding of the process suggest more severe F_{en} factors for low strain amplitude. In NUREG/CR-6909 it is noted that the slope of fatigue curves in reactor coolant was somewhat steeper, which is the exact effect the model considers.

The VTT F_{en} in its current form is restricted to the very limited range of variables in which testing has been done (Table 2). Applicability outside this range is not known at the present. In Figure 4, the model applied to the SAFIR2018 test results and earlier research on X6CrNiNb1810mod is compared with the data used in NUREG/CR-6909. The blue data points, representing the VTT model, lie in close proximity to the 1:1 line for experimental/predicted life. The red data points represent the same tests but predicted with the NUREG Fen model. Scatter is in the typical range and as noted earlier the results lie in the conservative direction.

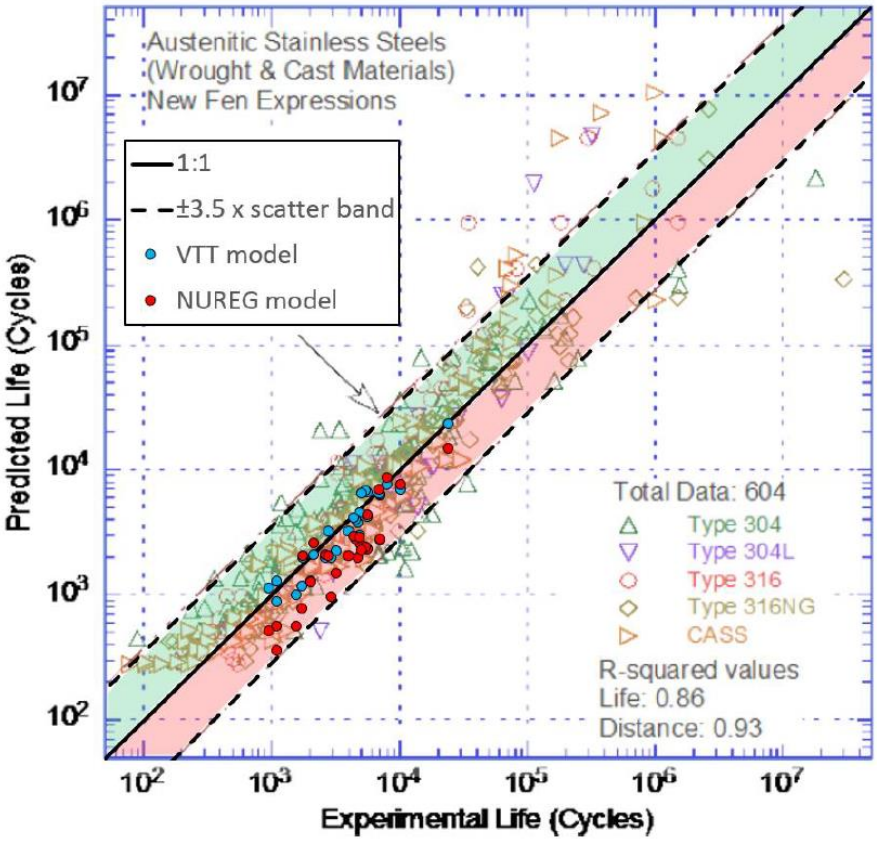

Figure 4. Comparison of results according to NUREG and VTT Fen models alongside all other NUREG data. Underlying figure from NUREG/CR-6909 (Chopra and Stevens 2014).

Modelling of thermal fatigue

This part of the research project focuses in evaluating the fatigue caused by thermal mixing loads both in the high-cycle and low-cycle regimes.

High-cycle thermal fatigue

Techniques to model fluctuating loads due to thermal mixing are developed in Timperi (2016, 2017, 2018a, 2018b). Turbulent mixing of cold and hot fluids can lead to high-cycle thermal fatigue in T-junctions, but modelling of the thermal load induced to the structure is challenging. The spectrum method has been recently proposed as an efficient modelling method, which uses a theoretical turbulence spectrum to represent the fluctuating thermal load (Figure 5).

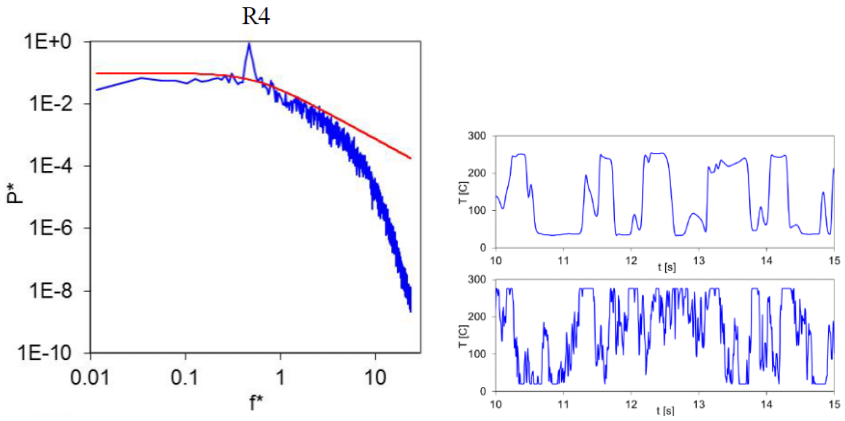

Figure 5. Simulated and model spectra (left) and the temperature signal from CFD (upper right) and the corresponding synthetic signal (lower right).

In this project, further development and application of the method is included. Estimation of the frequency of the largest-scale temperature fluctuations is considered in particular, as this is an essential input parameter for the model spectrum. The method is applied to a T-junction including a mixer pipe and a high temperature difference that induces significant buoyancy effects. The frequency scale of the fluctuations is determined for the flow case based on temperature spectra obtained from a Computational Fluid Dynamics (CFD) simulation. A formula for the frequency scale is proposed, which can be used in approximating the frequency scale for other flow conditions. Fatigue and crack growth analysis of the T-junction wall are carried out by using the spectrum method, and the results are compared with those obtained with sinusoidal and CFD temperature loads. The results (Figure 6) indicate improvement in accuracy over the highly simplified sinusoidal method.

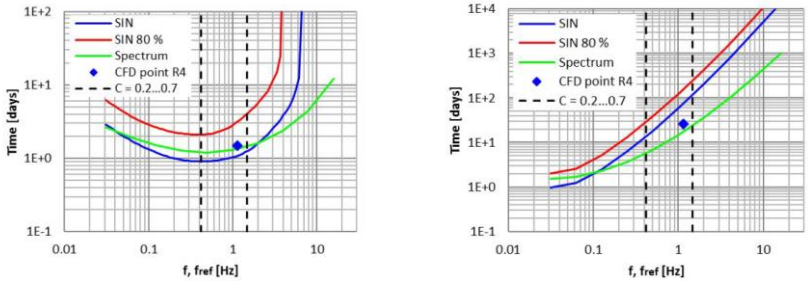

Figure 6. Left: Fatigue time at pipe inner surface for different thermal loads. Right: Crack growth time up to 60 % of wall thickness for different thermal loads.

Low-cycle thermal fatigue

In some cases the thermal cycling causes irreversible deformations in the pipe wall. In these low-cycle thermal fatigue cases, severe cracking may occur at a small number of cycles. This topic is addressed in Kuutti (2017a, 2017b). Due to the cyclic plastic and thermal effects, the traditional fracture mechanical tools are ill-suited to for the evaluation of the susceptibility to cracking and the possible flaw growth rate. In the project, the use of the crack opening displacement as the crack driving force parameter was evaluated through simulations of low-cycle thermal fatigue experiments. The use of the crack tip opening displacement parameter avoids the traditional limitations in the numerical evaluation of the J-integral. The unique relationship between the crack opening displacement and J-integral is derived and the crack driving force is used in a crack growth assessment. The results show that the crack driving force calculated from the uncracked stress distributions overestimates the crack driving force significantly (as compared to values calculated from the crack opening displacement), Figure 7. The crack growth rate calculated with the Paris' law is in good agreement with the experimental results, when the crack driving force is computed from the crack opening displacement. The study highlights the limitations and conservatism of the traditional approaches in lifetime assessment of components under low-cycle thermal loading. The proposed approach appears to be feasible in obtaining more realistic crack growth rate estimates (Figure 8) but is likely too laborious for quick engineering assessments.

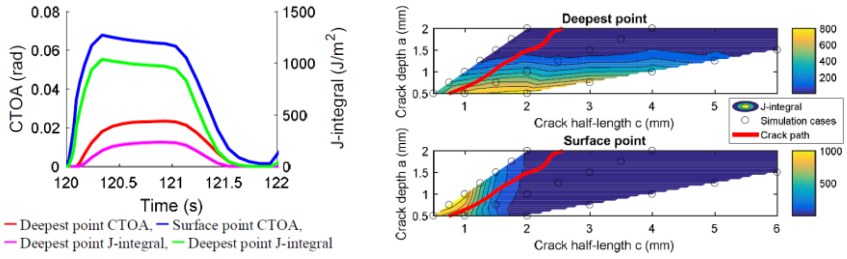

Figure 7. Left: crack behavior during the thermal load cycle. Right: crack growth paths on top of a J-integral contour field.

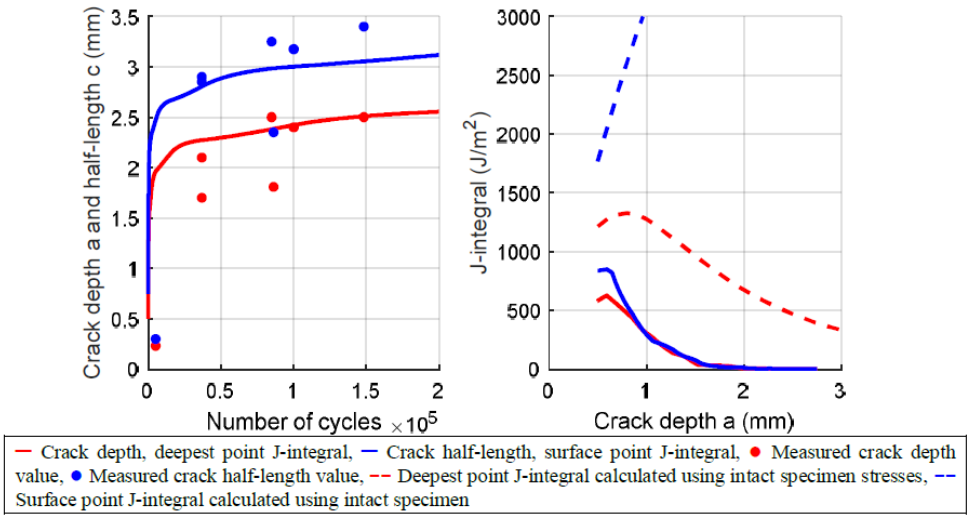

Figure 8. Left: crack depth and length as a function of cycles calculated in the crack growth assessment compared with experimental measurements. Right: J-integrals during crack growth compared the corresponding results calculated using the uncracked stress distributions.

Development of RI-ISI methodologies

The goal of risk informed in-service inspection (RI-ISI) analyses of NPP piping systems is to optimize the inspections so that they are targeted to sites with highest risk. With RI-ISI, the safety of the NPPs can be improved, the irradiation dose to inspection personnel can be decreased, and financial savings can be achieved by removing from the inspection programs sites with small risk but poor approachability. RI-ISI is a multi-disciplinary topic, combining e.g. risk analysis, structural reliability, fracture mechanics and non-destructive inspection techniques. For Finnish NPPs, RI-ISI is a very topical issue. The YVL guidelines state that the piping in-service inspection programme shall be prepared in a risk-informed manner and consequently the NPP licensees are starting to update their RI-ISI programs.

VTT RI-ISI procedure

The VTT RI-ISI procedure (Oinonen 2017) is a combination of deterministic and probabilistic analysis tools for the evaluation of pipe failure possibilities and the risk informed planning of inspections. The procedure allows quantitative evaluation of the influence of different inspection intervals and inspection capability on the leak probability. The procedure combines deterministic fracture mechanical models describing the crack growth with probabilistic methods to evaluate the leak probability and effect of inspections. An example result plot obtained with the VTT RI-ISI procedure is shown in Figure 9.

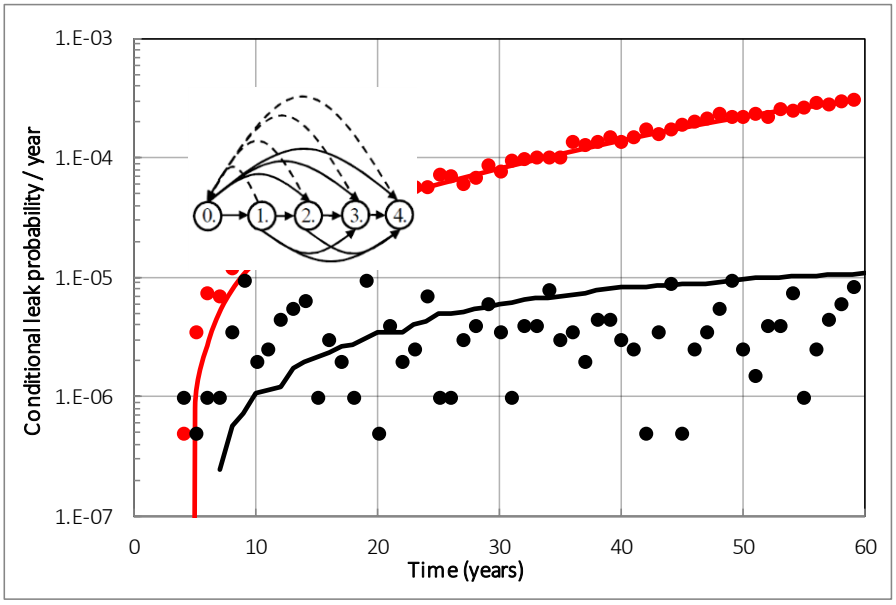

Figure 9. Conditional yearly leak probabilities simulated with the VTT RI-ISI probabilistic fracture mechanics procedure (lines) and Monte-Carlo based procedure (dots). The red line and dots denote cases without in-service inspections (flow of the ageing process along the solid lines in the subfigure) and the black line and dots denote cases with inspections (flow also along the dashed lines in the subfigure).

Recently, the VTT's RI-ISI procedure was enhanced by including LBB capabilities (Oinonen 2018). The latest development version of the VTTBESIMPROB software was applied to crack growth calculations and for stochastic analyses to solve the LBB and break probabilities, along the studied timeline, based on the multiplication rule of probability. For the studied piping elbow, the crack growth calculations involved transitions from the semi-elliptic shape to the slanted through-wall configuration. The LBB argument was based on the approximate crack opening areas that cause detectable leaks and a FAD based procedure was applied to determine the criteria of the allowable crack size for break failures. The results imply that longer initial defects complying with the SCC distribution attain large crack areas before growing through the wall and before causing detectable leaks. Thus, break failures are possible before satisfying the LBB arguments that are in accordance with the applicable standards and guidelines (Figure 10).

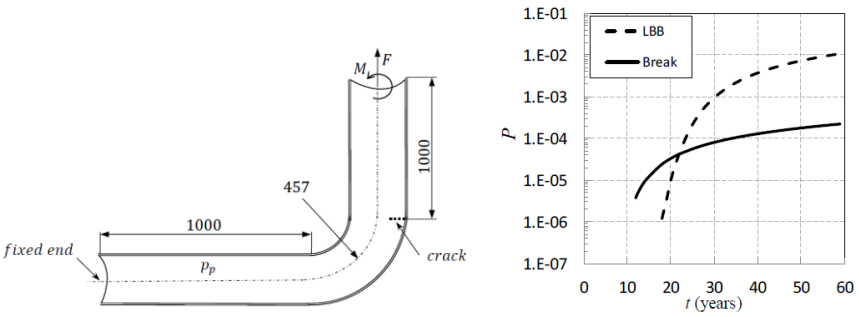

Figure 10. Piping elbow studied in the probabilistic LBB assessment (left) and cumulative probabilities for LBB and break during the component lifetime.

RI-ISI and PRA

Another research topic addresses the connection between RI-ISI and PRA (Tyrväinen 2015, 2016, 2017, 2018). Probabilistic risk assessment (PRA) is used to calculate the quantitative risk of nuclear accident and to analyze the importance of different systems and components. PRA's main purpose is to support risk-informed decision making. PRA also supports RI-ISI analyses by quantifying the consequences of pipe failures, see Figure 11. As identified in the research there is much to be gained from better connection and mutual support between PRA and RI-ISI. One possibility to bring RI-ISI and PRA closer would be to develop a software support for the better integration. Even common analysis software is a possibility. In addition, it would be beneficial to develop an automatic piping failure consequence calculator into the PRA software. Hence, the project introduced a new RI-ISI feature which calculates the conditional core damage probabilities (CCDPs) of piping component failures in the PRA software FinPSA. The work was continued by developing computation of the conditional large early release probabilities (CLERPs) of piping component failures.

Currently, the RI-ISI feature calculates only CCDP and CLERP values, but RI-ISI analyses require also failure probabilities of piping components. It could be possible to add failure probabilities to the RI-ISI table of FinPSA and implement some sort of inspection interval decision rules or optimisation algorithm. However, the approach to determine inspection intervals should be decided first. On the other hand, it is also simple to export CCDP and CLERP values to other applications, where inspection interval optimisation can be performed based on the results.

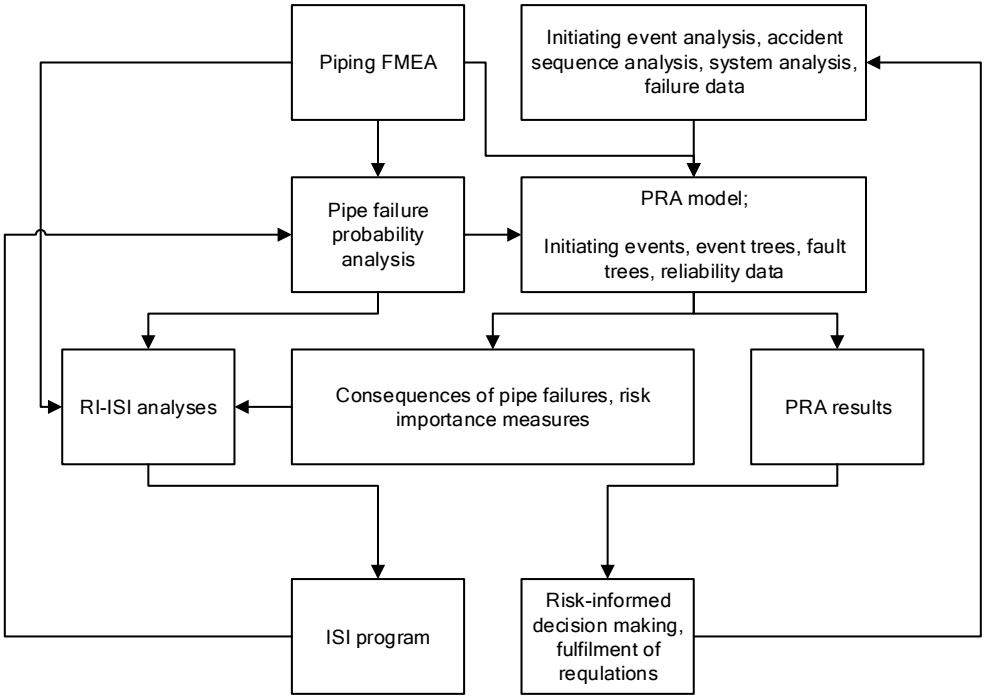

Figure 11. Simplified flowchart of RI-ISI and PRA and their connections.

Research on NPP piping analysis methods

A part of the research focuses in the development of response assessment methods for NPP piping systems. The research performed include a development of a linearization procedure to simplify complex nonlinear piping vibration assessments, development of a method to take into account the fatigue usage of a decaying stress or strain response, evaluation of different methods to combine the results from several dynamic load cases into a resultant suitable for a design standard based assessment, a survey of suitable piping analysis benchmarking tools and evaluation of B_2 stress indices for stress raisers.

Combination of load cases

The ASME III NB-3652 primary stress limit equation requires conservative combination of pipe moments for deterministic analyses. However, the probability of moment maximums of dynamic load cases occurring at the same time may be fairly low. Hence the deterministic approach of applying always the most severe moment combination can be inadequate for risk informed in-service inspection analyses. The probabilistic combination of pipe moments was studied in the project (Timperi 2019). A simplified analysis of the probabilities of the moment peaks overlap was first made. The probability density functions (PDFs) for random moment signals and for

more realistic piping moments signals were then determined. The PDFs and the cumulative distribution functions (CDFs) of the resultant moments of these moment signals were determined. PDFs of the individual moment signals were generally concentrated near zero. Resultant moment distributions from combining all time step combinations showed that most of the values are moderate. However, varying the load case initiation times and searching the maximum resultant moments produced distributions that were clustered closer to the largest possible value. For varying load case initiation times, the 50th and 90th percentile resultant moment ratios $M_i/M_{i,max}$ were in the range 0.33-0.81 and 0.45-0.87, respectively, for various types of moment signals. The algebraic and square root of sum of squares (SRSS) combination methods showed qualitatively fairly similar probability distributions. As the number of combined load cases was increased, the probability of obtaining the highest possible resultant moment decreased. These results are visualized in Figure 12.

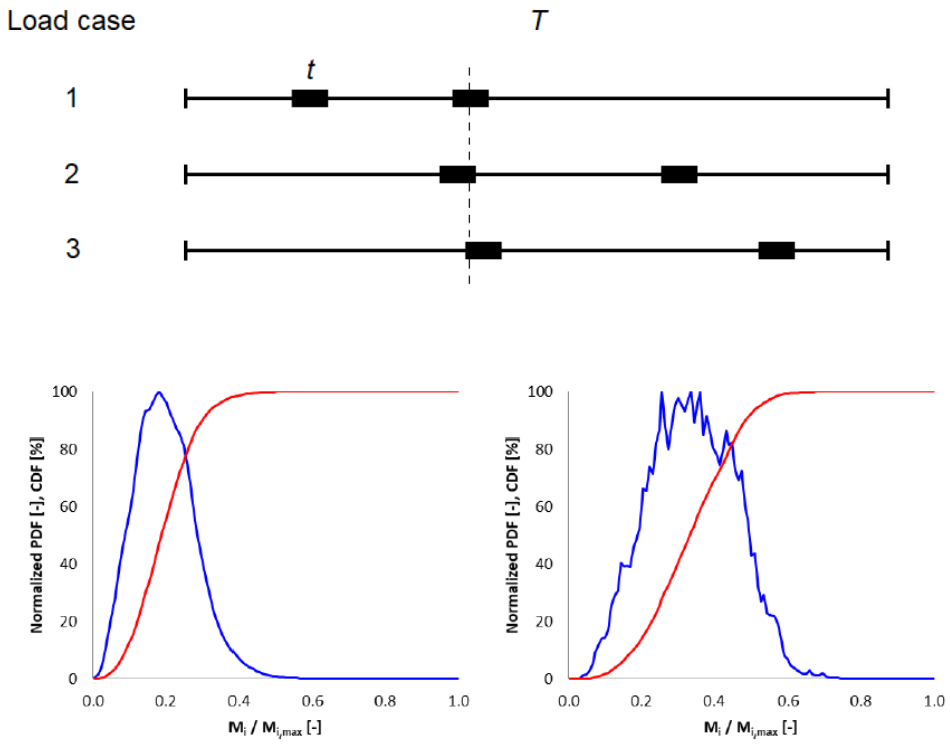

Figure 12. PDF and CDF of the random load signals obtained from combining all possible time step combinations by algebraic (left) and SRSS (right) summation.

B_2 stress indices

The ASME III NB-3652 primary stress limit equation requires stress indices to take into account the effect of component geometry. The stress indices are needed for e.g. piping elbows. The ASME code provides simplified formulae for calculating the stress indices for various components based on geometric parameters. Earlier studies indicate that the code values of the B_2 stress index may be overly conservative.

The B_2 stress index for elbows was studied (Timperi 2018c). A literature survey was first conducted and less conservative B_2 formulae proposed in the literature were reviewed. Geometrically non-linear elastic-plastic finite element calculations were then performed for three different elbows to determine the collapse loads and the corresponding B_2 values. A mesh sensitivity study was first performed, and different ways for determining the B_2 values from the FE results were then considered. The most reliable method seems to be the comparison of collapse loads of the component and of the corresponding straight pipe section. The collapse loads were determined by using the twice-elastic-slope method.

The stress indexes obtained by the FE calculations were compared with the ASME code values and with less conservative correlations proposed in the literature. The FE results showed lower stress indexes compared to the code equation, and the results were in fairly good agreement with previous calculations, Figure 13. When using the collapse load ratio of the elbow and straight pipe, the reduction factors $B_2/B_{2,code}$ were from 0.58 to 0.63. The effect of material data on the B_2 values was about 7% for the considered materials.

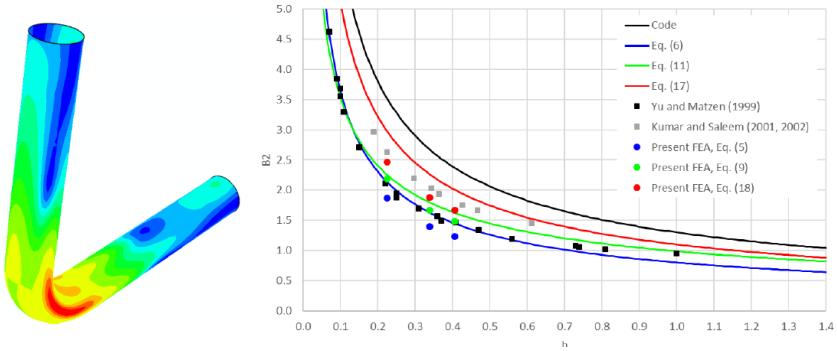

Figure 13. Left: studied piping elbow. Right: comparison of B_2 indices obtained with various FEA and correlations.

Residual stress relaxation in BWR NPPs

Residual stresses play a major role in stress corrosion cracking (SCC), which is identified as significant degradation mechanism for various BWR components. Experience from ageing NPPs shows slower stress corrosion crack growth in many

components than would be expected under currently postulated stresses. Residual stress relaxation decreases the effective loads during the service life and therefore slows down SCC. The effect of residual stress relaxation on SCC is not, in general, considered in crack growth calculations although thermal and mechanical loads are known to relax residual stresses significantly. This is due to insufficient data available on the stress relaxation.

In the project, residual stresses and their relaxation was studied with co-operation of Aalto University and Teollisuuden Voima Oy. Previously used measurement methods are developed further, most notably the Contour method. In addition, residual stresses are measured from pipe sections removed from OL1 and OL2 and compared with other experimental data Virkkunen and Toivonen 2016; Virkkunen 2017a, 2017b).

Contour Method Development

Contour method is an experimental method to measure two dimensional residual stress maps of components. The method was introduced relatively recently (Prime, 2000) and has since found widespread use in various applications.

The contour method is a destructive method. The component to be measured is cut in two. If the sample was initially free from residual stresses, the cut surfaces remains plane. During the cutting, any possible residual stresses on the cut plane and directed perpendicular to the surface are relieved by the introduction of the new free surface. The introduction of the free surface allows displacements on the new surface and thus relieves any possible stresses perpendicular to the cut surface. Consequently, any possible residual stresses on the cut surface are turned to displacements on the newly formed free surface. These displacements cause deviations from planeness of the cut surface and can be measured after the cut and used to compute residual stresses prior to cutting.

The surface measurement is typically done by 3D-coordinate measurement machine, though other measurement devices has also been used. The spatial resolution of the measurement is limited by the resolution of the measurement and subsequent smoothing required. With point-by-point measurements the measurement time increases rapidly with increasing spatial resolution. Measurements in 1 by 1 mm grid are commonly applied.

In current project, the spatial resolution of the contour method was significantly improved by adopting white light interferometry measurement to the cut surface. This development also vastly increased the amount of measurement data to be analyzed, and necessitated significant development of the measurement pipeline.

Residual stress measurements

Residual stress measurements of a modern narrow-gap (with Alloy 52) weld was performed (Virkkunen 2019), Figure 14. The samples were originally prepared for previous project “SINI” and now re-used for residual stress analysis. The narrow gap weld shows an overall good residuals stress structure; the highest tensile stresses are contained within the weld material and the sensitive root area experiences lower stresses. Tensile stresses peak around 420 MPa, which is in-line with

previous measurements on old weld geometries as well as the simulation predictions of the same case.

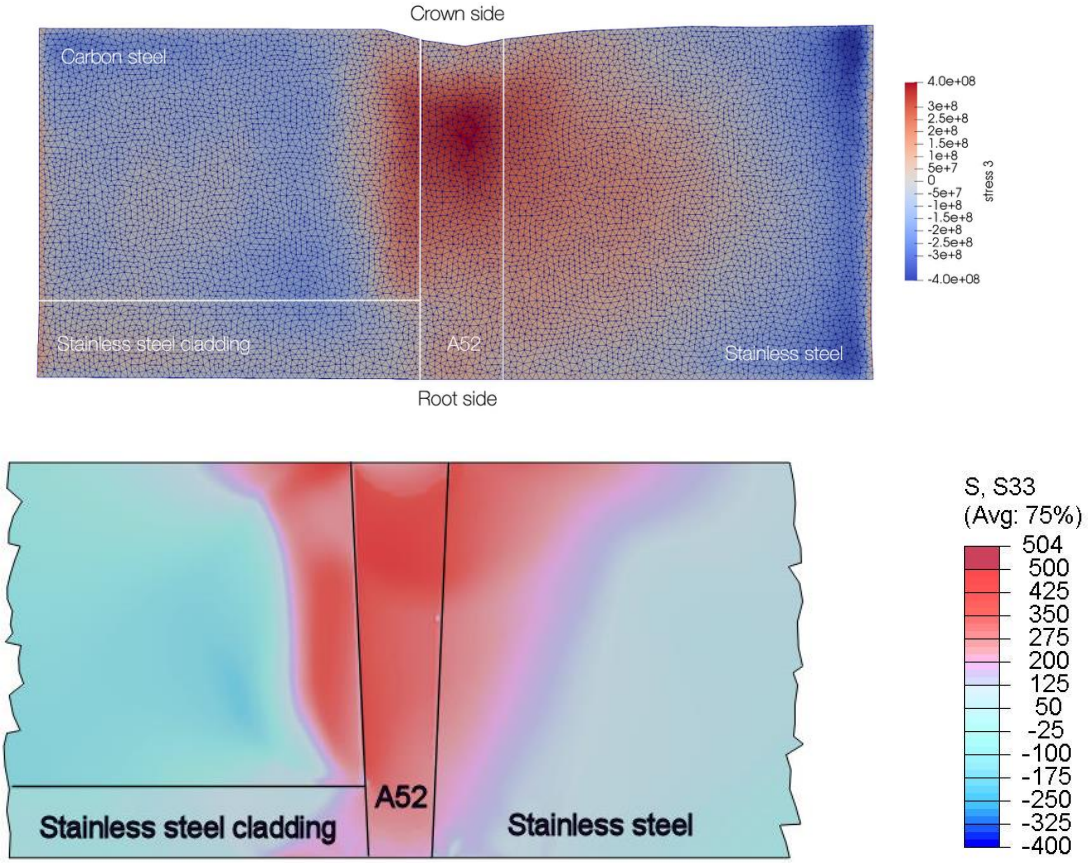

Figure 14. Top: Contour results from Alloy 52 narrow-gap mock-up. The results show largest stresses located in the weld material, with maximum measured stress about 420 MPa. Bottom: Welding residual stress simulation result from the same case.

Teollisuuden Voima provided a removed T-junction for residual stress measurements (Virkkunen 2017a). Prior to measurement, the component had been cut in two. This was done for other investigations, but also provided measurement access to inner surface of the T-junction. The components had also been decontaminated prior to measurement. The sections were measured using X-ray diffraction and the contour method (using white light interferometry and the newly developed measurement pipeline). Contour measurements were completed on four sample surfaces. Typical results are shown in in Figures 15 – 16.

The results indicate, that service loads have caused some relaxation of residual stresses in the weld. The stresses are somewhat lower than were measured for the experimental pipe sections. Also, the tensile stress region is confined more clearly inside the weld and there's a balancing compressive stress in the root area.

The previously developed WLI contour measurement proved invaluable in these measurements. With the numerous disturbances due to decontamination and sample removal, a more traditional contour measurement with lower spatial resolution would have been unable to discern the various effects and thus very limited information would have been obtained about the true residual stress state of the sample. In contrast, with the current measurement, these effects can be separated and accounted for.

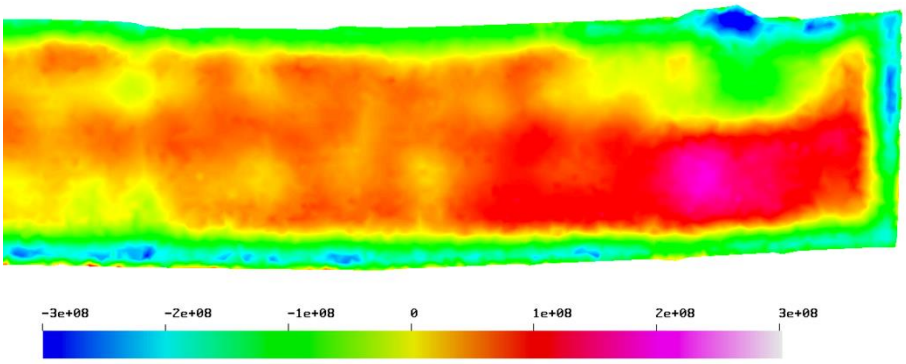

Figure 15. Contour measurements from weld sample A, weld 1 (stress in Pa).

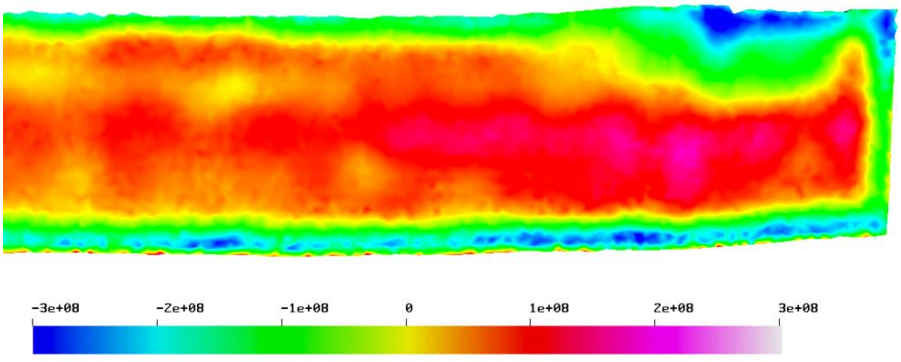

Figure 16. Contour measurements from sample B, weld 1 (stress in Pa).

Concluding remarks

The FOUND project considered different NPP ageing and component failure related aspects as described above. The support from the SAFIR Reference Group 5, Teollisuuden Voima Oyj and the Swedish-Finnish Beräkningsgrupp (BG) is greatly acknowledged.

References

Chopra, O. and Stevens, G.L. 2014. ”Effect of LWR Coolant Environments on the Fatigue Life of Reactor Materials”, NUREG/CR-6909, Rev. 1, ANL-12/60 (Draft), U.S.NRC.

Cronvall, O. 2015. Study on Status of Safety Margins Assessment Practices. VTT Research Report VTT-R-06265-15. Espoo: VTT.

Cronvall, O. 2018. SUSCEPTIBILITY OF BOILING WATER REACTOR PRESSURE VESSEL AND ITS INTERNALS TO DEGRADATION. Doctoral Dissertation, Manuscript draft, 2018. Aalto University.

IAEA 2005. Assessment and management of ageing of major nuclear power plant components important to safety: BWR pressure vessel internals. IAEA-TECDOC-1471, International Atomic Energy Agency (IAEA), Vienna, Austria, 107 p.

Kuutti, J. 2016. A J-integral calculation routine for Abaqus. VTT Research Report VTT-R-05842-16. Espoo: VTT.

Kuutti, J. 2017a. Crack opening displacement as a crack driving force parameter for thermal fatigue simulations. VTT Research Report VTT-R-00087-17. Espoo: VTT.

Kuutti, J. 2017b. USE OF CTOD AS CRACK DRIVING FORCE PARAMETER FOR LOW-CYCLE THERMAL FATIGUE. Transactions, SMiRT-24, BEXCO, Busan, Korea - August 20-25, 2017

Kuutti, J. 2018. Comparison of ASME XI and BS7910 allowable surface flaw size evaluation procedures in piping components. Proceedings of the ASME 2018 Pressure Vessels and Piping Conference PVP2018. July 15-20, Prague, Czech Republic

Lemettinen, P. 2016. OL1/OL2 Power Uprate - Risk Survey for Flow-induced Vibrations of RPV Internals. TVO Report 156094, Teollisuuden Voima Oyj (TVO), Eurajoki, Finland, 15.8.2016. 133 p.

Oinonen, A. 2017. VTTBESIMPROB 0.5 User Manual. VTT Research Report VTT-R-00159-17. Espoo: VTT.

Oinonen, A. 2018. Probabilistic Leak-Before-Break Analysis for a Pipe Elbow. VTT Research Report VTT-R-03118-18. Espoo: VTT.

Prime, M.B. 2000. Cross-Sectional Mapping of Residual Stresses by Measuring the Surface Contour After a Cut. J. Eng. Mater. Technol 123(2), 162-168. doi:10.1115/1.1345526.

Seppänen, T., 2018. Fatigue of AISI 347 and 304L Stainless Steels in PWR Water. VTT Research Report VTT-R-06961-18. Espoo: VTT.

Solin, J. et al. (9 authors) 2011., Fatigue of Primary Circuit Components (FATE), SAFIR2010, The Finnish Research Programme on Nuclear Power Plant Safety 2007–2010, Final Report. VTT Research Notes 2571, p. 368 – 380. [http://www.vtt.fi/inf/pdf/tiedotteet/2011/T2571.pdf]

Timperi, A. & Cronvall O. 2016. Uncertainties in Stresses due to Thermal Mixing Loading. VTT Research Report VTT-R-00063-16. Espoo: VTT.

Timperi, A. 2016. CFD and Structural Calculations of Thermal Mixing in a T-junction. VTT Research Report VTT-R-00221-16. Espoo: VTT.

Timperi, A. 2017. Spectrum Method for Modelling Crack Growth due to Thermal Mixing. VTT Research Report VTT-R-00137-17. Espoo: VTT.

Timperi, A. 2018a. MODELLING OF FATIGUE DUE TO THERMAL MIXING BY USING A SPECTRUM METHOD. Proceedings of the ASME 2018 Pressure Vessels and Piping Conference PVP2018. July 15-20, Prague, Czech Republic

Timperi, A. 2018b. Study on Temperature Spectra for Thermal Fatigue Modelling. VTT Research Report VTT-R-06881-18. Espoo: VTT.

Timperi, A. 2018c. Study of B_2 Stress Indices for Elbows. VTT Research Report VTT-R-06882-18. Espoo: VTT.

Timperi, A. 2019. Study on Probabilistic Combination of Pipe Moments. VTT Research Report VTT-R-00028-19. Espoo: VTT.

Tyrväinen, T. 2015. Connection between PRA and RI-ISI analyses. VTT Research Report VTT-R-04536-15. Espoo: VTT.

Tyrväinen, T. 2016. Computation of consequences of piping component failures in PRA software. VTT Research Report VTT-R-04536-15. Espoo: VTT

Tyrväinen, T. 2017. Computation of conditional large early release probabilities of piping components. VTT Research Report VTT-R-04644-17. Espoo: VTT

Tyrväinen, T. 2018. Computation of consequence measures of piping component failures. VTT Research Report VTT-R-02261-18. Espoo: VTT

Virkkunen, I. and Toivonen, H. 2016. Contour Method Development, FE modeling of Residual Stresses Caused by Cyclic Thermal Loads. Aalto University, Research report, revision 2, 4.2.2016

Virkkunen, I. 2017a. Measurement of residual stresses from BWR welds removed from service. Aalto University, Research report, Revision 1, 13.1.2017.

Virkkunen, I. 2017b. Comparison of test samples and residual stresses from BWR welds removed from service. Aalto University, Research report, Revision 1, 29.1.2017.

Virkkunen 2019. Dissimilar metal weld residual stress measurements using the contour method. Aalto University, Research report, Revision 1, 29.1.2017.

6.3 Long term operation aspects of structural integrity (LOST)

Sebastian Lindqvist[1], Kim Wallin[1], Päivi Karjalainen-Roikonen[1], Heikki Keinänen[1]; Qais Saifi[1], Tommi Seppänen[1], Laura Sirkiä[1], Pentti Arffman[1], Jorma Hietikko[1],

[1]VTT Technical Research Centre of Finland Ltd
P.O. Box 1000, FI-02044 Espoo

Abstract

The main objective for the project long term operation aspects of structural integrity (LOST) is to develop methods and tools for structural safety analysis of primary circuit components, reactor pressure vessel (RPV) and dissimilar metal welds (DMW). The work packages are divided accordingly. Work package 1 focuses on reactor pressure vessel safety; 1) fast fracture in upper shelf region 2) pre-investigations for BREDA. Work package 2 focuses on dissimilar metal welds; 1) residual stresses 2) materials characterisation and 3) numerical simulations. The following was achieved during the four years; 1) the fracture toughness assessment for DMWs is safer than before, 2) the residual stresses in DMWs, also after repair welding, are better understood, 3) the various conditions leading to fast fracture in the upper shelf region have been identified, 4) a new numerical model for predicting ductile crack growth was developed 5) also improvements in RPV surveillance methods were achieved. The work continues in SAFIR2022, AMOS project, to improve analysis and characterisation methods for safety class 1 components.

Advanced structural integrity: Fast fracture in upper shelf region

The YVL guide E.4 requires that the risk for fast fracture is assessed in the upper shelf region. Fast fracture in the upper shelf area can occur by brittle fracture or ductile fracture. In the former case, the material has not been in the actual upper shelf temperature zone. For example, rapid cooling has caused a shift in the ductile-to-brittle regime, and thus, brittle fracture can occur in the upper shelf area. In the latter case, rapid cooling can lower the ductile fracture toughness properties, which can lead to an unstable ductile fracture event. The fracture toughness in the upper shelf area is determined with J-R curves.

Before the project, there was no data, nor predictions, regarding the J-R curve development during a decreasing temperature transient. In LOST, the effect of rapid cooling on tearing resistance (J-R curves) was investigated [1]. The testing was performed in a temperature range above the range covered by the 5 % master curve, identified as the upper shelf region.

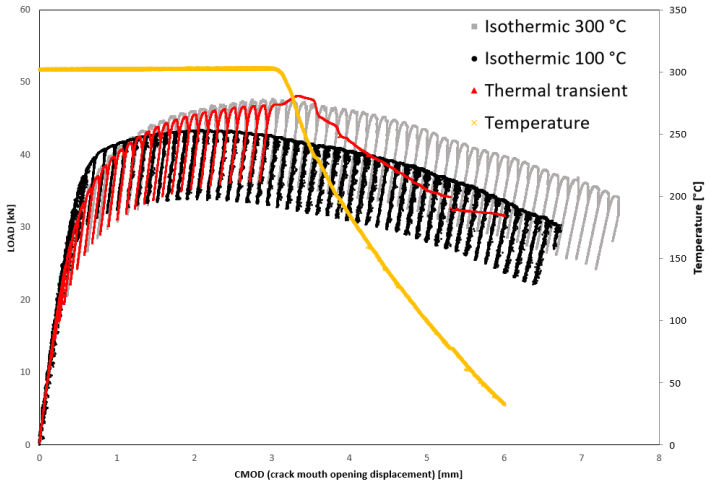

Figure 1. The load under a temperature transient.

Fracture toughness specimens were cooled from 300 °C to the room temperature at a cooling rate of 2 °C/s. The cooling rate of 2 °C/s was determined at the center location of the specimen. The cooling rate is faster close to the surface. The cooling rate was selected to be in the same range as during a loss of coolant accident close to the surface. The following was concluded: For the first time, a testing method was used for characterisation of the effect of cooling rate on fracture toughness in the upper shelf region. No drastic fast fracture in the upper shelf region was observed for the investigated material during a fast cooling transient. However, the conclusion was based on the obtained load-displacement data and further analysis are required. The work continues in SAFIR2022.

The future investigations should focus on 1) the developed method should be applied for an actual RPV steel, since the temperature dependence of the investigated material is not the same as for RPV steels 2) the testing method shall be developed further 3) review the cooling rate during a loss of coolant accident and do a detailed analysis of the applied cooling rate in the thickness direction of the specimen.

[1] Lindqvist, S., Sirkiä, L., Karjalainen-Roikonen, P. 2018. Tearing resistance under isothermic and decreasing thermal transients. Espoo. VTT-R-06958-18. 17 p.

Advanced structural integrity: Miniature-sized specimens and pre-investigation for BREDA

Miniature fracture toughness specimens, 4 mm thick C(T) specimens, were applied in [1] and [2] (figure 1) for characterisation of T_0. The miniature testing techniques are interesting from long term operation perspective, since there is restricted

amount NPP materials available in surveillance programmes. The surveillance programmes are used for following the aging of the RPV and demonstrating the safety. In [1], the initiation location of brittle fracture was characterised and compared to standard sized specimens. The initiation location with respect to mid-plane of miniature C(T) specimens has the same distribution as conventional specimens, and side-grooves did not show a significant effect on the obtained T_0. These results validate the use of miniature C(T) specimens. In addition, miniature sized C(T) specimens were experimentally tested to characterise the ductile-to-brittle transition temperature, T_0, in reference condition for reactor pressure vessel weld of Barsebäck 2. T_0 is -99 °C. The result was in the same range as for thicker specimens, typically used for fracture mechanical testing.

Based on analysis of a large data sets, the T_0 obtained with miniature and thicker C(T) specimens for various materials is in the same range [3]. However, attention should be paid on that macroscopically the same material region is sampled. For example in upcoming SAFIR2022 project BREDA/BRUTE, the fracture toughness of the surveillance specimens is compared to the fracture toughness at ¼ thickness of the RPV, since surveillance specimens are manufactured of the material extracted at ¼ thickness. 9-12 specimens are required for determining a valid T_0 [4].

The goal with experiments carried out in BREDA/BRUTE, SAFIR2022, is to decrease the uncertainty between experimental results from surveillance specimens, and the ageing behaviour of the RPV. In the project the RPV trepan test samples are cut from the decommissioned Barsebäck 2 nuclear power plant. The work done in BREDA is carried out between Royal Institute of Technology-KTH, Stockholm, Chalmers Technical University – CTH, Göteborg and VTT Technical Research Center of Finland, Espoo. VTT is responsible for mechanical testing (tensile, Impact and fracture mechanical testing).

The relevance of the Barsebäck 2 material for the Finnish nuclear power plants was analysed in [5]. The Barsebäck 2 material is investigated in BRUTE, SAFIR2022. The Barsebäck 2 weld has a relatively high Ni content, similarly to Olkiluoto plants and the new Fennovoima plant. The representativity of the material was analysed with a trend curve developed for VVER-1000 materials with a high-Ni content. The trend curve predicts decently the embrittlement behaviour of western high-Ni steels. The irradiation embrittlement of the Barsebäck 2 material is investigated in SAFIR2022 in BRUTE project, in addition to the thermal embrittlement behaviour that can have a dominant effect on the embrittlement behaviour in the low fluence region.

Figure 2. Newest innovation in surveillance specimen test techniques, miniature C(T) specimens. Four miniature C(T) specimens can be extracted from one Charpy-V specimen half.

Finally, previous work on characterisation of decommissioned reactor pressure vessels were reviewed [3]. Based on previous work reported in open literature, the following was concluded: In almost all of the previous investigations, the materials characterisation included chemical, hardness, macrostructure, and fracture toughness analysis in the through-thickness direction. These analyses are necessary to be able to explain the variation of material properties in thickness direction. Yet, the analyses were not comprehensive enough to be able to draw definitive conclusions from the data. A more detailed analysis of the microstructure can be applied for excluding the effect of certain phenomena, such as e.g. the damage observed in the material, and thus, improving the conclusion. The surveillance results were not reported. It is likely that the plants did not even have a surveillance programme. The Barsebäck 2 material investigated in BREDA contains surveillance samples and the material investigation methods are more extensive than in the previous projects.

[1] Wallin, K., Yamamoto, M. & Ehrnstén. U. 2016. Location of initiation sites in fracture toughness testing specimens – the effects of size and side grooves. Proceedings of the ASME 2016 Pressure Vessels and Piping Conference PVP2016.

[2] Lindqvist, S. & Seppänen, T. 2017. BREDA: Fracture toughness measurements with miniature C(T) specimens in reference condition. Espoo: VTT. VTT Technology VTT-R-00140-17. 19 p. + app. 31 p.

[3] Lindqvist, S. 2018. Pre-investigation for BREDA–various aspects related to aging of the reactor pressure vessel. Espoo. VTT-R-06941-18. 29 p.

[4] Kim Wallin, Assessment of Master Curve material inhomogeneity using small data sets, Pressure vessel and piping conference, 2018.

[5] Kim Wallin, Irradiation trend curves for high Nickel steels, VTT-R-00664-18, Espoo, 2017

[6] Lindqvist, S. Boåsen, M. Constraint and fracture toughness. 2018. VTT- R-06942-18. Espoo.

Dissimilar metal welds: Residual stresses

Nickel-base weldments such as Alloy 82/182 dissimilar metal butt welds used in nuclear power plant components have experienced stress corrosion cracking, resulting in the possible need to repair these weldments. Austenitic stainless steel weld overlays have been used extensively on boiling water reactor welds to prevent and tolerate stress corrosion cracking. The axial length and end slope of the weld overlay shall cover the weld and the heat affected zones on each side of the weld. Weld inlay is an alternative mitigation/repair process especially for large bore reactor vessel nozzles. Inlay is a method to limit the direct contact of the primary water to Alloy 82/182 metal. Cladding with alloy 690 weld metals, like alloy 52, is performed at the inner surface groove by using temper-bead welding.
In addition to the weld overlay and inlay, local repair may be needed if flaws or cracks are found. The corresponding material volume is removed and the area is repair welded before applying weld overlay or inlay. In all of the mentioned cases, the remaining residual stresses must be determined to estimate the load bearing capacity and remaining lifetime of the component under operational loading conditions.

In 2016, literature survey concerning inlay welding was performed and stresses due to thick overlay welding were studied [1]0. In the literature survey, the residual stresses and related structural phenomena related to inlay welding were studied.
The goal of the study related to overlay welding was to compute the residual stresses in the dissimilar weld connecting the nozzle and safe-end and to compute the change of residual stresses due to thick overlay welding and combined inlay and overlay welding [2]. The results show that the overlay welding reduces circumferential stresses especially near the inside surface. The decrease of the circumferential stress due to overlay welding is small at larger depths from inner surface. The situation is the same for combined inlay and overlay welding.

In 2017, residual stresses in a case of local repair were studied [3]. The current analysis methods were applied for modelling a local repair welding case performed for a full-scale mock-up. The computational and experimental results were compared. Three-dimensional welding simulation was performed with alternative methods including weld torch movement modelling and weld pass block dumping. The simplified procedure (block dumping) is usually mandatory in real repair cases.

In the case of the girth welding, the comparison of the computed (weld torch movement) and measured residual stresses showed that the stress profiles were similar although the difference between computed and measured results is up to 100 MPa when weld torch movement was modelled. Larger differences exists in the case of the repair welding most probably due to the simplifications made in the computation. Considering the simplified models, the model including both weld pass block dumping and weld torch movement modelling in the last weld passes gave similar results compared to the modelling applying only weld torch movement. The benefit with the simplified model is faster solution times and reduced file size.

In 2018, a mock-up with two girth welds and a weld inlay was studied [4]**Error! Reference source not found.**. The first girth weld was a dissimilar metal weld (DMW). The mock-up resembled a real nozzle. The target was to compare computed and measured stresses.

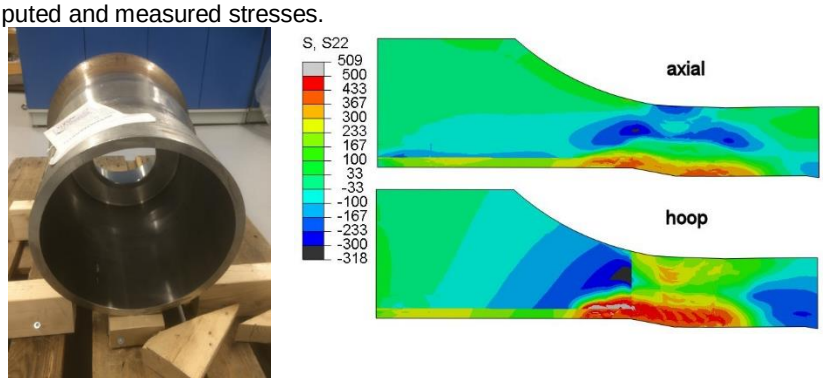

Figure 3. The examined mock-up and computed axial and hoop stress (MPa) after inlay welding and at the RT.

The residual stress finite element computations were performed with axisymmetric models. The computational results showed tensile hoop stresses along the outer surface in the DMW area before inlay welding. The order of magnitude of tensile stresses is 400 MPa. The tensile stresses were reduced due to the inlay welding but the stresses remain tensile (order of magnitude approximately 200 MPa), Figure. The computed axial stresses along the outer surface were tensile after girth welding and change partly to compressive due to inlay welding.

[1] Heikki Keinänen, Inlay welding as a nozzle repair method, literature survey of the residual stress computations, VTT-R-01073-16, Espoo, 2016.

[2] Heikki Keinänen, Stresses due thick overlay welding, Research Report, VTT-R-00374-17, Espoo, 2017.

[3] Heikki Keinänen, Residual stresses in a case of local repair, VTT-R-07120-17, Espoo, 2017.

[4] Heikki Keinänen, Weld repair residual stress simulations and comparison to experimental measurements, VTT-R-01487-18, Espoo, 2018.

Dissimilar metal welds: Materials characterisation

Before the project, there was knowledge gaps related to characterisation of DMWs and use of fracture toughness values in safety analyses for DMWs. The fracture toughness values for DMWs are used as input data for estimation of the largest crack size a component can withstand or as input parameters in probabilistic analyses. Thus, it is important that the values are determined with reliable methods. The problem was that the equations used for determining fracture toughness experimentally are developed for homogeneous materials, and thus, are not necessary applicable for DMWs. In addition, the cracks grow rarely straight in DMWs and there was no method for analyses of the effect of crack path on fracture toughness. Large deviations in crack path can effect the fracture toughness. Thus, the there is a risk that the obtained fracture toughness does not represent a lower boundary value and the safety analysis is affected by this uncertainty.

In LOST, with numerical methods, the applicability of current equations for obtaining fracture toughness of DMWs were investigated [1]. The results showed that the current equations can be used as long as the crack is at the fusion boundary between a hard and soft material, and the resulting plastic field around the hinge point does not extend to two materials with various strength**.** For the investigated DMWs, the fusion boundary is the boundary between hard RPV steel and soft austenitic weld metal. As the distance of the crack to the fusion boundary increases, the equations become less applicable since the plasticity around the hinge point starts to interact with the interface. However, as long as the crack is less than 1 mm from the interface the difference in fracture toughness is insignificant.

The effect of crack path on fracture toughness was investigated for an Alloy 52 DMW in the ductile and brittle regime [3-5]. The results show that the fusion boundary region has the lowest fracture toughness. The size of this region is few micrometers. In the ductile regime, cracks that are further from the fusion boundary deviate to the fusion boundary. Consequently, the fracture toughness is larger. In the brittle regime, the brittle fracture initiates at the fusion boundary, even if the crack is originally further away from the fusion boundary. In addition, a theoretical model was developed to predict the effect of crack location relative to a weak zone on fracture toughness. The model is in line with the experimental data. In future investigations, the applicability of the model should be investigated further. The model provides an economical tool for chacrterisation of lower boundary fracture toughness next to an weak zone. The model can be used for results where the crack has not been located at the weakest location. The purpose is to predict what the fracture toughness would have been if the crack had been on the weakest region.

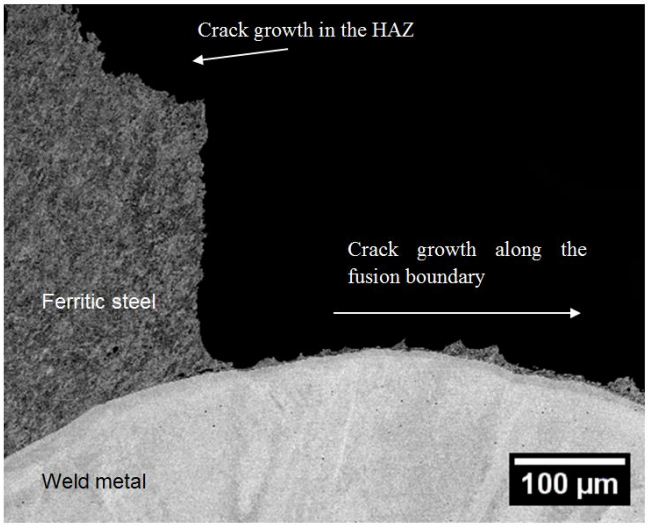

Figure 4. Change in the crack growth path. This variation in crack growth path is typical for cracks in DMWs.

However, the crack does not always deviate towards the weakest location. A VVER DMW that was investigated in LOST had a strength peak at the fusion boundary [6]. The strength peak caused the cracks to deviate away from the fusion boundary, the weakest region. In this case, the model described above is not applicable. Typically, cracks grow towards the material with lower strength.

The effect of specimen configuration on tearing resistance (J-R curves) was also investigated [7]. The results show that the conventional C(T) and SE(B) specimens produce conservative estimates of tearing resistance in comparison to SE(T) specimens. The fracture toughness is 1.4 times higher. Tearing resistance is used to estimate the allowable crack size in the component. Therefore, a greater allowable crack size is obtained with SE(T) specimens. The loading condition ahead of a crack in a SE(T) type specimen is similar to the loading condition in a pipe with a shallow crack. The SE(T) specimen can be used for investigating the transferability of fracture toughness from specimen level to a component level.

[1] Lindqvist, S. & Kuutti, J., Dependence between eta factor and crack location relative to a fusion boundary between hard and soft materials, International Journal of Fracture, Espoo, 2017.

[2] Lindqvist, S. 2015. Plastic η-factors for heterogeneous welds. Research Report. Espoo: VTT. VTT Technology VTT-R-03810-15. 29 p.

[3] Lindqvist, S., A crack-location correction for T0 analysis of an Alloy 52 dissimilar metal weld, Engineering fracture mechanics, Espoo, 2018.

[4] Lindqvist, S. 2017. The effect of crack path on tearing resistance of a narrow-gap Alloy 52 dissimilar metal weld. Engineering fracture mechanics.

[5] Lindqvist, S. 2016. , Dissimilar metal welds – the effect of crack path and specimen configuration on tearing resistance. Espoo: VTT. VTT Technology VTT-R-03998-16. 46 p. + app. 76 p.

[6] Lindqvist, S. 2016. Tearing resistance analysis of a VVER dissimilar metal weld mock-up. Espoo: VTT. VTT Technology VTT-R-03996-16. 24 p. + app. 23 p.

[7] Lindqvist, S., Seppänen, T., Characterization of J-R curves of a HSLA-steel and an Alloy 52 DMW with SE(T) specimens, European Conference on Fracture, Espoo, 2018.

Dissimilar metal welds: Local approach

New elements are developed for taking into account the effect of damage due to excessive plastic deformation and possible ductile crack growth. Strain softening in a ductile material can occur as a result of void nucleation and growth, where material eventually looses its stress carrying capacity. The special elements that are developed here take into account void nucleation at yield point as observed in experiments. The stiffness matrix for these elements is formulated so that it allows the natural growth of the void inside them. Assuming zero stiffness for the region of the special elements surrounded by internal nodes is the main cause for the natural growth of the void [1].

Damage mechanics simulations of specimens or components by this method remarkably reduces the need to use complicated constitutive models with many parameters, where data for most of those parameters are not easily accessible. Instead, the weight of difficulty is put on numerical procedure and computer programming [1].

Special element that have been developed so far and coded with Fortran via user defined subroutine in Abaqus for two-dimensional models is Q16. One special sub-element is developed as well, that being element QS6. For all possible pairs of the main elements and sub-elements, the pair of Q16 and QS6 are programmed first. The number of nodes in the outer edge of Q16 is minimum, and the number of inner nodes is enough to create higher order interpolation functions for accurate prediction of the void growth and shape. On the other hand, one edge of element QS6 has a quadratic shape function, which is suitable for round edges and must be located on the solid void interface. Thus, the pair of Q16 and QS6 reduces the size of the global stiffness matrix and the higher order shape functions are placed around the void, which is the most crucial location [1].

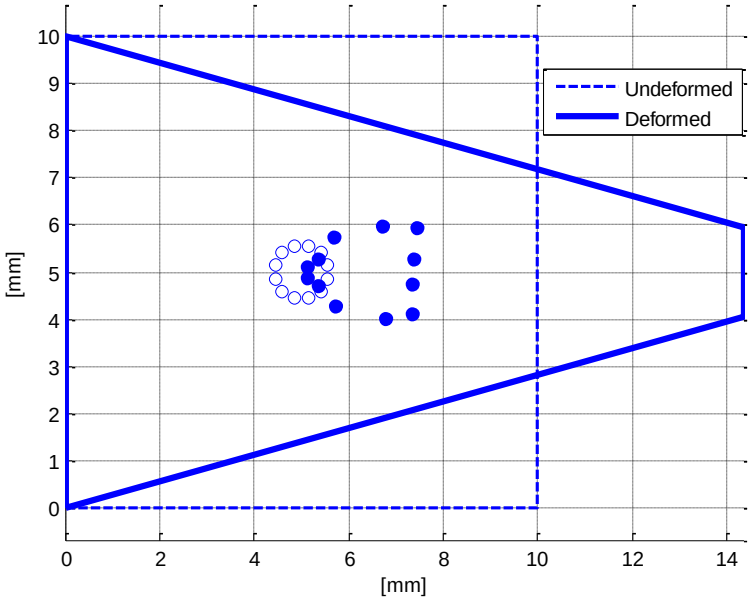

Figure 5. A special element Q16 in deformed and undeformed states [**Error! Reference source not found.**].

[1] Saifi, Q. 2018. Development of special numerical approach for dam-age mechanical analysis with implementation in Abaqus. Research Report. Espoo: VTT. VTT Technology VTT-R-00018-19. 23 p.

[2] Saifi, Q. 2017. Damage mechanics analyses under plastic deformation with special numerical method by local approach, Research Report, VTT-R-00486-18, Espoo,

[3] Saifi, Q. 2015. Crack Growth Computation in Dissimilar Metal Weld Joints by Local Approach. Research Report. Espoo: VTT. VTT Technology VTT-R-04464-16. 20 p.

6.4 Non-destructive examination of NPP primary circuit components and concrete infrastructure (WANDA)

Tuomas Koskinen[1], Esa Leskelä[1], Ari Koskinen[1], Miguel Ferreira[1], Tarja Jäppinen[1*] Iikka VIrkkunen[2]; Fahim Al-Neshawy[2], Teemu Ojala

[1]VTT Technical Research Centre of Finland Ltd
P.O. Box 1000, FI-02044 Espoo

[2]Aalto University of Technology
P.O. Box 11000, FI-00076 AALTO

[*]No longer employed at VTT

Abstract

Passive components in nuclear power plants (NPP)s are monitored through in-service inspections (ISI)s. These passive components consists for example primary cirquit piping, steam generator and safety related concrete infrastructure such as the concrete containment. ISIs are heavily related to monitoring the condition of aging NPPs. WANDA has addressed these issues by focusing on three important aspects of proactive ageing management: early detection of deterioration, monitoring of deterioration, and application of prognostics for the estimation of remaining service life. NDE is one of the recommended tools for the early detection of deterioration of NPP materials.

Work in WANDA was divided into two work packages, in work package one the focus was on early detection deterioration and inspection reliability. These contained research on investigating plausible ways to detect material deteroation and research on efficient ways to evaluate probability of detection curves for ISI. In work package two the focus was on concrete infrastructure. Mainly the goal was to bring concrete NDE research on a par with metal NDE, thus doing foundational work on first concrete containtment mock-up for research purposes and constructing the mock-up itself.

Introduction

The project WANDA – Non-Destructive Examination of Nuclear Power Plant Primary Circuit Components and Concrete Infrastructure, of the SAFIR2018 programme, focuses on the development and understanding of non-destructive examination (NDE) methods in two important nuclear power plant environments: primary circuit component materials and concrete infrastructure. The research work of primary circuit components concentrated on the ultrasonic testing of artificial defects, simulation, probability of detection (POD) and quantitative NDE. The NDE research of concrete infrastructure focused on the evaluation and calibration of the available

NDE methods and monitoring systems for concrete structures. This was achieved through the design and construction of a real-scale reinforced concrete wall mock-up for NDE testing method development and education purposes.

The WANDA project seeks to maintain the high level of expertise of Finnish NDE research with regards to NPP component materials, and to initiate the development of competences directed toward the NDE research of reinforced concrete structures.

NDE for primary circuit components

Topics for the NDE research for components in the primary circuit have been non-destructive testing (NDT) of artificial defects of primary circuit components, simulation, probability of detection (POD), measurement of magnetite in steam generator (SG) with eddy current techniques and preliminary research on quantitative NDE. The development of the NDE techniques is done towards more reliable and efficient ISI to promote the safety of NPP.

Artificial flaws

The study with artificial defects is continued with fatigue cracks which are used as a reference when the performance of an NDT procedure is demonstrated. According to the studies on the artificial defects [Leskelä & Koskinen, 2015] the ultrasonic response varies with the type of the defect and also with the technique used. In the report the inspections were done with three qualified phased array ultrasonic testing procedures using transmit-receive (TR) probes. All the techniques fulfilled the ASME Section XI code requirement for RMSE for length sizing and most techniques fulfilled the code requirement for RMSE for height sizing.

This research confirms the known facts for NDT of NPP ISI that signal-to-noise -ratio between same size defects can vary a lot depending on the defect type, the crack shape and morphology affects the detectability of the defect when skew angle is introduced to the flaw, anisotropic austenitic material affects to the propagation of ultrasonic waves and the high noise level reduces the defect detection and sizing capability. This concludes to that ultrasonic examination and data analysis requires experience and knowledge of various kinds of indications. In Figure 1 the effect of austenitic stainless steel weld to the propagation of the ultrasonic sound.

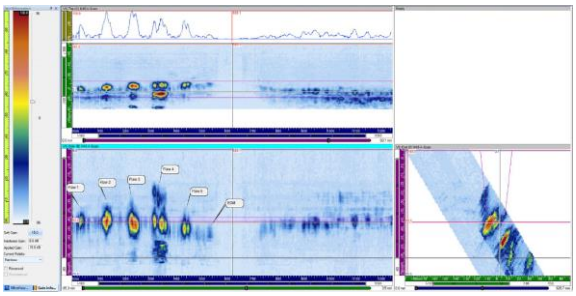

Figure 1. Phased array ultrasonic examination results with TRL technique at 45° longitudinal wave inspected from same of the weld.

NDE reliability

In 2016 assessing NDE reliability with experimental and model assisted probability of detection (POD) for the nuclear industry was started in WANDA Ultrasonic testing is the main tool to inspect the structural integrity of pressurized components in nuclear power plants during in-service inspection. It is important to determine how probable it is to find a certain type and size of a flaw in order to choose to most effective method for different situations. POD curves are used to determine these probabilities. However, these POD curves require a lot of data points in order to be reliable, thus producing these curves is relatively expensive. This is why different simulation tools are used to reduce costs and reduce the amount of physical test pieces.

In present research, new approach to determine POD curve with limited physical training flaws was developed using previously developed eFlaw technology. With this technology, scanned UT-data from single sample was digitally altered and extended to provide unlimited examples of data files for POD determination.

A single weld test piece containing three cracks was used for this study. The test piece was welded austenitic stainless steel pipe representing an actual geometry found in a nuclear power plant primary circuit. Three circumferential straight artificial flaws were produced to the test piece with thermal fatigue by Trueflaw Ltd.

The scanned data was acquired in the UVData file format containing both the raw UT data and the necessary meta-data to interpret the various included signals. The raw UT data was extracted from the file and most interesting channels were selected for this initial study. Figure 2 shows the extracted raw data as B-scan image with the flaw signals marked. In addition to the flaw signal, some locations without flaw signal were marked for removal and re-introduction. This was done to exclude the possibility that the re-introduction itself causes some detectable changes that the inspectors learn to look for.

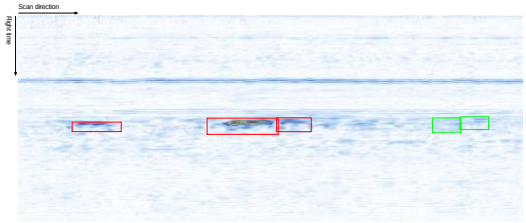

Figure 2. B-scan from the data, as acquired, with the flaw signals marked with red rectangles. Green rectangles show unflawed regions that were removed and re-introduced to study the possibility that the manipulation itself causes detectable changes.

It was taken as a premise, that the signal amplitude is the most significant feature of the crack signal from detection point of view. (Similar premise is used, e.g., in a vs. â POD analysis routinely conducted.) In particular, the crack amplitude (signal) in relation to the noise of the weld would be the most significant feature determining crack detection.

With this technique, it was possible to produce unlimited number of "virtual" data files with different flaw populations for POD determination.

With the ability to create flawed data files on demand, it was possible to gather hit/miss data from various inspectors and to generate POD curves on these data. To facilitate data collection, an online tool was created, which included most basic inspector views (B-view and slider control for data gain) and allowed indication of crack presence by simple click. With this (admittedly simplified) tooling, it was possible to gather quickly the data needed to use conventional statistical tools for POD determination.

Such tooling (albeit currently with limited number of real defects and simplified tooling) enables POD estimation with unprecedented ease and allows use of POD as feedback-tool for inspector training etc.

Even with the very limited number of actual physical cracks, the results were very promising. Inspectors were able to find flaws and generate a plausible POD curve (Fig 3.) with the application even with the lack of an A-scan image and with minimal information.

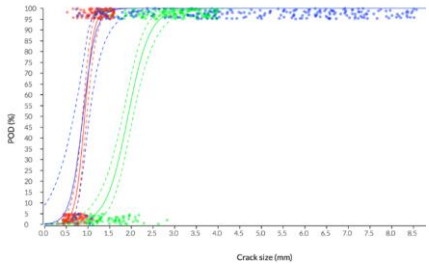

Figure 3. Computed POD curves from combined inspectors and separated in terms of the real crack sizes with points and curves showed in red, green and blue corresponding to original crack sizes of 1.6, 4.0 and 8.6 mm, respectively.

The result indicates it is possible to emulate the amplitude response of a flaw and produce an amplitude response image for an inspector to evaluate. This in turn can be used to generate hit/miss data with real inspector response. [Koskinen et al. 2018a]

The work continued in 2018 and the virtual flaw modification was tested with simulated flaws using CIVA software. The simulated flaws were semi-elliptical flaws with surface roughness implemented in them. The flaws were modified as the thermal fatigue flaws and inspectors reported on the findings through the web app as in previous research and POD curve was formed according to the results.

In the web app, the flaws merge fairly well within the original scan. On cases where the flaw represents a large flaw height the signal response is also quite high, whereas on smaller and lower height of flaws the signal response is lower. When inspectors were shortly interviewed after the test they stated that they were unable to tell on most cases which flaws were simulated, original or modified. One inspector stated that some patterns tended to repeat themselves. On situations where a wide flaw was made to represent a lower height flaw with signal representing almost noise level, which for example in â vs a analysis would have been a clear miss the pattern of a flaw could be distinguished from the noise. However, this is not yet clear weather does this represent a real situation where human eye is able to detect a flaw pattern from the noise or has this similar pattern repeated itself numerous times that the eye has learned to notice this kind of shape. The latter in this case would indicate that more of different shapes of flaws are needed and some way to implement noise partly over the flaw itself.

The POD results proved that the simulated flaws stood out from the POD data while inspectors could not tell weather the flaw they found was originally simulated or thermal fatigue flaw. The comparison of POD results of simulated and thermal fatigue flaws can be seen in figure 4.

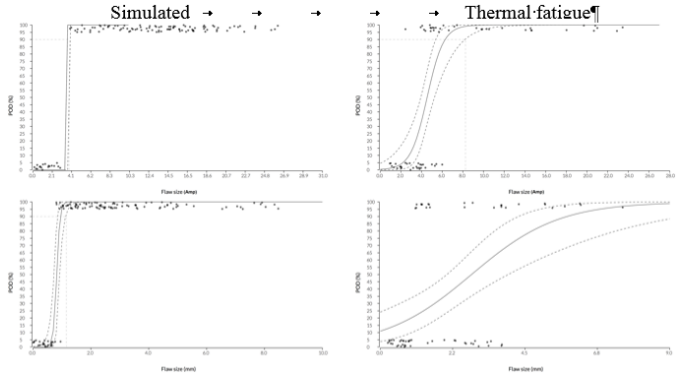

Figure 4. POD vs. amplitude curve (above) POD vs. crack length (below) from a single inspection try. Simulated flaws separated on the left and thermal fatigue flaws on the right.

The POD curve shows that there is a single threshold in which simulated flaws are found which indicates that the simulated flaws do stand out differently than the

thermal fatigue ones. This means that in order to use simulation with virtual flaw setting, simulation needs to be considerable more accurate and represent the physical phenomenon more accurately. The work should contine to investigate the simulation with FEM software. [Koskinen et al. 2018b]

Quantitative NDE

Preliminary research was done in 2018 for evaluation of poison's ratio through non-destrcutively. [Rinta-Aho, 2018] did preliminary report regarding using of Rayleigh waves to determine poisson's ratio by comparing sound speed of Rayleigh wave. The test showed promising results as this could give more comprehensive knowledge on material aging and degradation when monitored during a longer period of time. The results can be seen in table 1

Table 1. Preliminary results. The results are promising: The relative errors of the new Rayleigh wave method are as small as the relative errors of the validation method. Secondly the new Rayleigh method gives same results as the validation method.

	Poisson's ratio	
Material	Rayleigh	Validation
Steel	0.284 ± 0.002	0.285 ± 0.001
Stainless steel 304	0.289 ± 0.002	0.285 ± 0.001
Copper	0.343 ± 0.001	0.343 ± 0.001

The Rayleigh wave scan is conducted in immersion conditions. Therefore, it is possible to use the method to develop a new quantitative scanning ultrasound microscopy (qSAM) method. This new qSAM method would have a huge impact on materials research. This method would make possible to analyze the non-homogeneities of materials and to measure the effects of different material processing methods. The method could be used i.e. to analyze the effects caused by non-uniform heating in welding structures.

NDE for concrete infrastructure

The effects of potential deterioration of NPP concrete structures, systems and components (SSC) must be assessed and managed during both the current operating license period as well as subsequent license renewal periods. Reinforced concrete structures (RCS) differ to the many other mechanical and electrical components, as the replacement of these is impractical. Therefore it is clear that the safety issues related to plant aging and continued service of the concrete structures must become thoroughly resolved [Clayton & Hileman, 2012]. The inspection of NPPs concrete structures present challenges different from those of conventional civil engineering structures. As a result, there is a need for NDE of RCS to be able to undertake

compliance testing, collection of specific data or parameters, condition assessments, and damage assessment.

NPP RCS present a unique challenge for development of performance acceptance criteria because of their large size, limited accessibility in certain locations, the stochastic nature of past and future loads, as well as that of mechanical and durability performance characteristics due to ageing and possibly degradation, and the qualitative nature of many non-destructive evaluation methods. Improved guidelines and acceptance criteria to assist in the interpretation of condition assessment results, including development of probability-based degradation acceptance limits, are required [Ferreira et al., 2016].

Construction of mock-up wall

First part of the project was to focus on the design of the mock-up wall. To determine the design requirements for a NPP mock-up concrete specimen, several meetings were held with the Finnish regulator STUK and operating utilities (TVO and FORTUM), and also with The Finnish Transport Agency who is responsible for the maintenance of Finland's transport system, to roadmap relevant aspects related to NDE of NPP RCS.

Reinforced concrete structures in nuclear power plants (NPP) are deteriorated due to ageing or environmental stress that affect its long term performance over the lifetime of the NPP. To assess the construction quality and long-term performance of the reinforced concrete structures, different non-destructive testing and evaluation (NDT&E) methods are normally employed. Some of the challenges for assessing the performance of these structures are:

a) The assessment of critical structures can only be performed only during the annual overhauls,

b) The accuracy and reliability of the available NDT&E testing devices,

c) The uncertainty of the international uniformity of the methods used for NDT&E tests,

d) The creditability of results and analyses.

To overcome these challenges, a mock-up wall that is representative of a NPP containment concrete cross section was built for the critical investigation of NDT&E methods and techniques. Simulated defects are applied to the mock-up wall. These defects are representative of the most common types of defects in concrete structures such as: dimensional errors; finishing errors; honeycombing; cracking, delamination due to structure stresses or deterioration mechanisms; embedded foreign objects in the concrete; voids adjacent to liner and voids in grouted tendon ducts for the post-tensioned structures.

The mock-up construction was completed on begin of Fall 2018. The reinforced concrete mock-up which simulates a segment of a NPP containment reinforced concrete structure, but without the natural curvature expected. This is considered irrelevant for the main purpose of the wall and does not influence the use of NDT&E.

The mock-up consist of a thick-walled reinforced concrete wall and a reinforced concrete slab base with the dimensions show in figure below. The structure is heavily related to the wall of Olkiluoto 2 and also contains a steel liner. Figure 5 demonstrtes the rough dimensions of the mock-up wall.

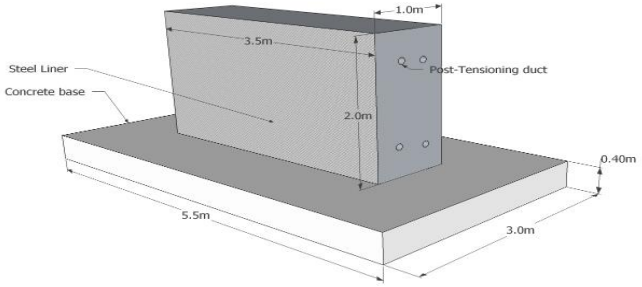

Figure 5. Dimensions of the thick-walled concrete mock-up structure.

Simulated defects were embedded inside the reinforced concrete foundation slab to determine how the current state-of-the-practice NDE techniques will be able to determine various forms of degradation in NPP concrete structures. A honeycomb defect within the slab is show in figure 6.

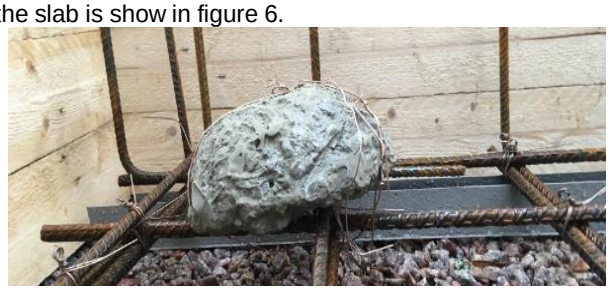

Figure 6. Honeycomb structure prepared in laboratory and sealed with stiff mortar cover to avoid filling of the voids with cement paste from the concrete.

Multiple different representative simulated defects were embedded within the wall structure as well. The defect type and description of the simulation is shown in table 2.

Table 2. List of the simulated defects in the thick-walled concrete mock-up

Defect type	Description
Delamination	Delamination occurs in reinforced concrete structures subject to reinforcement corrosion (0,2 mm plastic sheets, fixed in place)
Honeycomb	Honeycomb (Expanded polystyrene insulation (EPS) 50*200*200 mm3, fixed in vertical direction)
Construction defects	Construction defects (Wooden lumber and gloves, fixed into the reinforcement)

Empty air voids	Air filled voids. (An empty 0.5 l bottle, fixed into the reinforcement)
Water-filled air voids	Water-filled voids. (Water-filled 0.5 l bottle, fixed into the reinforcement)
Duct grouting defects	Styrofoam voids

The flaws described in table two were embedded to the structure before concreting. Embedding of the simulated flaws can be seen in figure 7.

Figure 7. View of the placement of two distinct types of honeycombing – long "sausage" type and flat, round type honeycombing.

The concrete was tested with standardised testing and temperature and relative humidity was monitored trought the process. The picture of the completed mock-up wall can be seen in figure 8. [Ferreira et al. 2019]

Figure 8. Completed wall mock-up.

Assessment of NDE and monitoring methods

The focus has been on this task on existing test methods and the studying availability of new test methods, especially considering the difficulties associated with NPP RCS.

Even though on-site testing of concrete in NPP structures typically only allows for one-sided access, the mock-up is designed to allow for testing access on both sides of the wall with the understanding that the testing on each side of the wall can be treated as an independent measurement. The reinforcement pattern can be similar for both sides of access, allowing evaluation of the effect of different depths using only one defect by comparing results of testing on both sides of the specimen. Although access to both sides would allow for test methods using two-sided access measurements, the testing should focus on one-side per measurement to simulate realistic containment wall access conditions.

Sensor-based monitoring systems can be used to continuously follow the performance of the structures in real-time, mostly over long time periods starting with the manufacturing of the structures. The application of both, NDE methods and monitoring systems, allows for the best performance assessment by generating partly redundant data and using synergetic effects [Bohner et al. 2016].

Since the mock-up is located outdoors, it is beneficial to monitor the state and condition of the wall at the time of NDE testing. Certain NDE methods might utilize this information as input data for data analysis and assessment of the technologies tested. The monitoring plan will address monitoring of relative humidity and temperature; monitoring early age cracking of the mock-up wall.

An important aspect of the mock-up is to allow for continuous long term testing. The intention is for the specimen to be available for a long period of time (i.e.: more than 20 years) which allows for different/new equipment to be assess in a well-documented situation, and to assess in real-time the effects of ageing of RCS. Furthermore, the mock-up will be available for users of NDE equipment to test and calibrate performance accordingly. The education of a new generation of engineers with NDE experience is another goal. The mock-up will allow for the training of young engineers in the use different NDE equipment and in the development of expertise with RCS similar to that of NPPs.

NDE method tested on the wall was a commercially available measuring device of the company Acoustic Control Systems (ACS) with the device name MIRA was used. It is a linear array system (type A1040 MIRA).

The measurement data was generated fort two surfaces of the mock-up wall: the *South main surface*, and the smaller *East surface*. The measuring surfaces had different dimensions. It was once measured once in the horizontal and even in the vertical orientation of the MIRA array system. Preliminary test gave back wall reflection from south side vertical direction shown in figure 9. [Al-Neshawy et al. 2019]

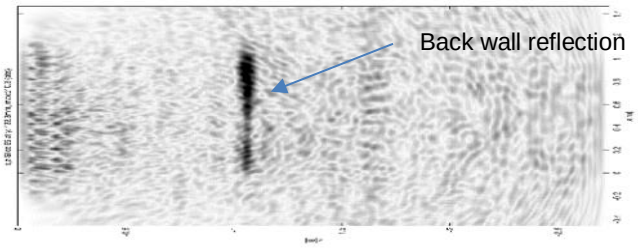

Figure 9. Measurement on the specimen side South, MIRA in the vertical direction.

Summary and conclusions

The Finnish national Research Programme on Nuclear Power Plant Safety (SAFIR2018) is guiding research towards nuclear power plant safety. In the SAFIR2018 research programme, the project NDE of nuclear power plant primary circuit components and concrete infrastructure (WANDA) has focused on the development and understanding of NDE methods, with special focus on reactor internals and more recently concrete infrastructure.

The studies on fatigue cracks were continued with three qualified phased array ultrasonic testing procedures using transmit-receive probes. Shear wave techniques were generally performing well and the use of longitudinal waves is not essential. If scanning is done through the weld both shear wave and longitudinal wave techniques suffer from noise. The tests confirms that signal-to-noise -ratio between same size defects can vary a lot depending on the defect type and mostly anisotropic austenitic material affects to the propagation of ultrasonic waves and the high noise level reduces the defect detection and sizing capability.

In present research, new approach to determine POD curve with limited physical flaws was developed using previously developed eFlaw technology. With this technology, scanned UT-data from single sample was digitally altered and extended to provide unlimited examples of data files for POD determination, with promising results. The research was extended to contain also simulated flaws, but so far the flaws produced with CIVA software proved unreliable when compared to real thermal fatigue flaws. Further research needs to be conducted with FEM modelling.

Quantitative NDE opens possibility to study material properties non-destructively. This is an option to study the effect of heat in welding or other material degradation processes caused by aging.

A study of NDE for detection of defects in NPP reinforced concrete mock-ups is an essential component in defining the most promising techniques and directing the R&D efforts in this field. For the success of such an approach, a realistic containment mock-up is to be built.

The mock-up wall was constructed on fall 2018. The general approach to the reinforcement design for the main wall was loosely based on the cross section design of the containment wall of TVO's NPP Olkiluoto 2. The wall also had steel reinforcement, steel liner and tendon ducts to represent the original containment wall.

During the construction there were numerous simulated defects embedded within the wall and the slab for further NDE research purposes. The properties of the concrete was carefully measured and a monitoring system was installed for assessing the performance of the thick-walled mock up.

The wall enables future research on concrete NDE and opens a possibility for teaching of future experts regarding the NDE of concrete structures.

References

Bohner, E., Kuosa, H., Al-Neshawy, F., Ferreira, M., 2016. NDE of thick-walled reinforced concrete structures – Technologies and systems for performance monitoring. VTT Research Report. VTT-R-00449-16. 63p.

Clayton, D., Hileman, M., 2012. Light Water Reactor Sustainability Nondestructive Evaluation for Concrete Research and Development Roadmap. ORNL/TM-2012/360. OAK Ridge National Laboratory. 72p.

Ferreira, M., Bohner, E., Calonius, K., 2016. Acceptance criteria for maintenance of concrete structures in the nuclear industry - A Preliminary Study. Energiforsk AB. REPORT 2016. 65 p.

Leskelä, E. & Koskinen, A., 2015. Phased array ultrasonic examination of mechanical fatigue cracks in austenitic piping test block. Espoo. VTT research Report. VTT-R-00542-16. 40 p. + app. 86 p.

Koskinen, T. Virkkunen, I. Papula, S. Sarikka, T. Haapalainen, J. Producing a POD curve with emulated signal response data, Insight, Vol 60, No 1, January 2018a

Koskinen, T. & Virkkunen, I. 2018. Hit/Miss POD With Model Assisted and Emulated Flaws. 12th ECNDT, Gothenburg, Sweden, June, 2018b

Rinta-Aho, J. 2018 Non-contact measurement method for Poisson's ratio. Espoo, VTT research Report. VTT-R-06820-18. 5p.

Ferreira, M. Sjöblom, V. Bohner, E. Al-Neshawy, F. Ojala, T. Final Report for the construction of a Non-Destructive Evaluation mock-up. 2019. Espoo, VTT research Report. VTT-R-02769-18. 48p.

Al-Neshawy, F. Ojala, T. Ferreira, M. Sjöblom, V. Evaluation and calibration of NDT/NDE methods. 2019. Espoo, VTT research Report. VTT-R-06833-18. 52p.

6.5 Mitigation of cracking through advanced water chemistry (MOCCA)

Tiina Ikäläinen, Essi Jäppinen, Timo Saario, Konsta Sipilä and Aki Toivonen

VTT Technical Research Centre of Finland Ltd
P.O. Box 1000, FI-02044 Espoo

Abstract

Corrosion problems in the PWR secondary circuit are mostly related to deposition of magnetite particles originating in the feed water line into steam generator (SG) and enrichment of impurities into crevices under these deposits.

In this work, the effect of alternative water chemistry regimes on the feed water line corrosion rate, the tendency of magnetite to deposit into the SG and on the effect of lead (Pb) as a potentially detrimental impurity within the deposits has been studied.

Introduction

About 70% of SG tube failures are attributed to stress corrosion cracking (SCC). SCC is a localized corrosion phenomena, for which the necessary conditions are related to susceptible material, high enough stress level and localized aggressive environment (which can form e.g. within and under deposits due to boiling action). Corrosion problems in the PWR secondary circuit are mostly related to deposition of magnetite particles originating in the feed water line into steam generator (SG) and enrichment of impurities into crevices under these deposits. Different routes are available to minimize the detrimental effect of deposits, e.g. minimization of feed water line corrosion rate, minimization of the tendency of magnetite to deposit into the SG and minimization of the effect of impurities within the existing deposits on SG materials.

An important way to minimise the SG feed water line corrosion is by introducing an oxygen scavenger, hydrazine (N_2H_4), since dissolved oxygen promotes corrosion very effectively. The target is to add enough hydrazine in order to make sure no oxygen is reaching the SG during power operation (typically < 100 ppb). Preservation of SGs during outages requires much higher concentrations (in the range of several thousand ppb) of hydrazine. There is a distinct possibility that, because of the health and environmental risks related to the use of hydrazine, the EU will in the future pass a directive forbidding its use. Already at the moment, the Finnish envi-

ronmental regulations have been tightened so that the use of the highest concentrations of hydrazine during outages is becoming impossible. Thus, there is a need to search for a replacement chemical for hydrazine.

Film forming amines (FFA) have been found efficient in mitigating several of the detrimental aspects related to magnetite deposits. FFAs effectively reduce the source term, i.e. feed water line component corrosion by more than 90% [Betova et al. 2014], even at elevated pH of close to 9.8. In addition, FFAs have been shown to be able to mitigate crevice corrosion, i.e. decrease the aggressiveness of existing crevices within SGs. As FFAs have so far been tried in only a few PWR plants, there is a need for further studies on their application.

Lead has been detected in effectively all tubesheet samples, crevice deposits and surface scales removed from SGs. Typical concentrations are 100 to 500 ppm but in some plants, concentrations as high as 2,000 to 10,000 ppm have been detected [Kim et al. 2009]. The SG tube materials considered to be most resistive towards SCC, i.e. Alloy 600TT, Alloy 800 and Alloy 690 all have been shown to be susceptible to SCC enhanced by presence of lead (PbSCC) [Kim et al. 2005] . However, very little research has been made on the PbSCC susceptibility of the SG body materials, i.e. low alloyed carbon steel, despite the reported wall-through SCC insidences in VVER-440 type SGs in both Russia and Czech republic. There is a clear need on investigation of the susceptibility of low alloyed carbon steel to PbSCC.

Hydrazine replacement

In this project we have studied replacement chemicals for hydrazine under shutdown maintenance periods, i.e. at temperatures up to T = 50ºC and at high concentrations. Based on a literature study [Betova et al. 2016], four chemicals were selected for the experimental studies, carbohydrazine (CBH), iso-ascorbic acid (i-AA), diethyl-hydroxylamine (DEHA) and methyl-ethyl-ketoxime (MEKO). The selection criteria were 1) oxygen scavenger effectiveness, 2) temperature stability, 3) corrosion risks, 4) impact on secondary chemistry, 5) toxicity and 6) environmental impact.

A comparison of the oxygen removal rate by i-AA and MEKO is shown as an example in Figure 1. Based on quantitative evaluation of the data [Betova et al. 2018], the following ranking of the studied compounds by oxygen scavenging ability at 50 °C and pH 9.2 can be proposed: hydrazine > iso-ascorbic acid > carbohydrazide >> DEHA > MEKO, Table 1. This is the same ranking found earlier at 21ºC [Betova et al. 2017]. The rate of oxygen removal by hydrazine was about twice higher than that of i-AA and CBH, and about seven and fifteen times higher than that of DEHA and MEKO, respectively.

The effect of the investigated additives on the corrosion of 22K carbon steel in borate buffer solution at 50 °C was also studied [Betova et al. 2018]. Based on the data it can be concluded that all the additives increase the general corrosion rate of

22K steel (by stabilising Fe_3O_4 over FeOOH and Fe_2O_3) with respect to that in pure buffer solution, hydrazine having the strongest effect.

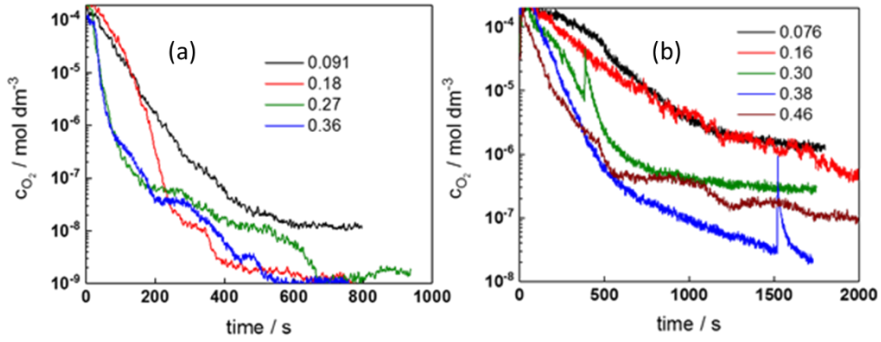

Figure 1. Evolution of the dissolved oxygen concentration with time in a borate buffer solution with the addition of different concentrations (in mmol dm^{-3}) of (a) i-AA and (b) DEHA at 50 °C. The rate of decrease of oxygen is clearly faster with i-AA than with DEHA.

Table 1. Oxygen removal rate at the highest initial scavenger concentration in mmol dm^{-3} (in parentheses).

Scavenger	Oxygen removal rate at T = 50°C / mmol dm^{-3} s^{-1}
Carbohydrazide	0.020 (0.034)
DEHA	0.0054 (0.46)
MEKO	0.0028 (0.75)
Iso-ascorbic acid	0.025 (0.45)
Hydrazine	0.043 (0.32)

Octadecylamine (ODA)

One common way to mitigate deposition of magnetite is to adjust pH in the range of minimal carbon steel corrosion rates (i.e. 9.6 to 9.8) so that the formation of magnetite particles is minimized. Another way is to alter the surface charge of such particles to match the sign of the corresponding charge of SG surfaces, so that particle tendency for deposition is decreased by the resulting repulsive forces. This can be achieved with different amines, such as morpholine and ethanolamine, which are simultaneously used in pH adjustment. However, there is another possible mitigation method consisting of the secondary side water treatment with film-forming amines (FFA). The most commonly used FFA in conventional power industry is octadecylamine (ODA), currently being widely studied for use in nuclear power plant secondary side as well.

In the current project we studied the effect of ammonia, morpholine, ethanolamine and ODA on the surface charge of magnetite particles, and the effect of ODA on the passivation of carbon steel (the main material of feed water line components), [Jäppinen et al. 2017]. The surface charge of magnetite, measured as zeta-potential, was found to be negative at low temperatures and to approach zero at temperatures corresponding to the feed water line entrance to the SG, Figure 2. In case of ODA, however, the surface charge remained close to zero irrespective of temperature. A close to zero surface charge indicates there can be very little attractive electric force driving the deposition of magnetite into the SG.

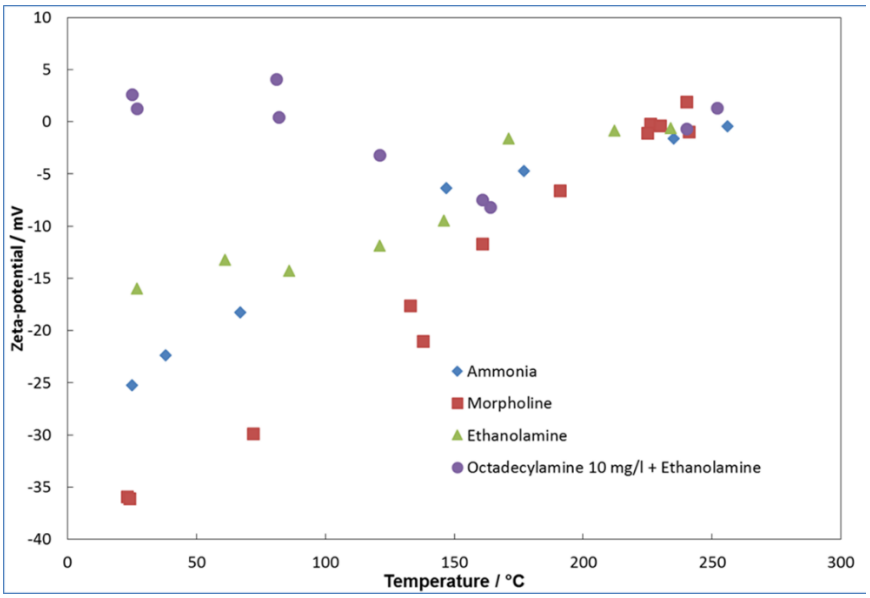

Figure 2. The effect of different additives on surface charge (zeta potential) of magnetite as a function of temperature.

Lead assisted stress corrosion cracking (PbSCC)

In this work, susceptibility of carbon steel 22K (body material of steam generator) to PbSCC was studied in both acidic and alkaline crevice chemistries at T = 278°C [Bojinov et al. 2019]. The main research method was the slow strain rate technique (SSRT) producing a stress-strain curve, in which a decrease of fracture strain (in comparison ot that in air at the same temperature) is a sign of stress corrosion cracking (SCC). The susceptibility to SCC is normally further confirmed by examining the fracture surface with scanning electron microscope (SEM). In SEM pictures, the SCC susceptibility is seen as a fracture morphology clearly differing from that typical of ductile failure (dimple morphology). Electrochemical techniques such as

current density - voltage (CV) -curves and electrochemical impedance spectroscopy were additionally used to study the effect of lead.

The presence of an acidic crevice chemistry (without lead) was found to decrease the fracture strain from about 30% in air to about 21% in the crevice environment, Figure 3, indicating a rather strong susceptibility to SCC. Addition of lead at a concentration of 100 ppm (mg/l) resulted in a fracture strain of about 28%, clearly higher than that for the crevice environment without lead. This result indicates that addition of lead actually decreased the susceptibility to SCC in this case. This result was further corroborated by examining the fracture surfaces, Figure 4, which revealed that the ductile proportion of the surface (not affected by SCC) increased from 43% to 86% when lead was added to the crevice environment. The susceptibility of the carbon steel 22K to SCC was found to be clearly less under the alkaline than the acidic crevice conditions without lead, while the effect of lead was found to be beneficial in both cases.

An oxygen in-leakage into SG affects strongly the corrosion behaviour of SG materials, typically accelerating the corrosion processes. In this work, the effect of oxygen was simulated experimentally under the acidic crevice conditions by increasing the electrochemical potential (ECP). The stress-strain -curves showed that increasing the ECP by a mere 0.1 to 0.2 V resulted in a drastic decrease of the fracture strain down to 10% or even less, indicating a dramatic increase in the susceptibility to SCC.

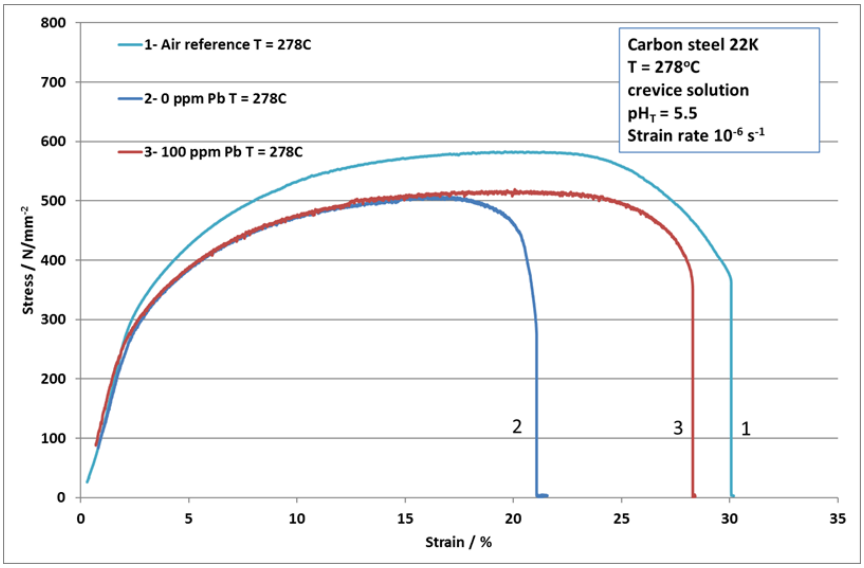

Figure 3. Effect of crevice environment and 100 ppm (mg/l) lead (Pb) on stress-strain curves of carbon steel (body material of steam generator).

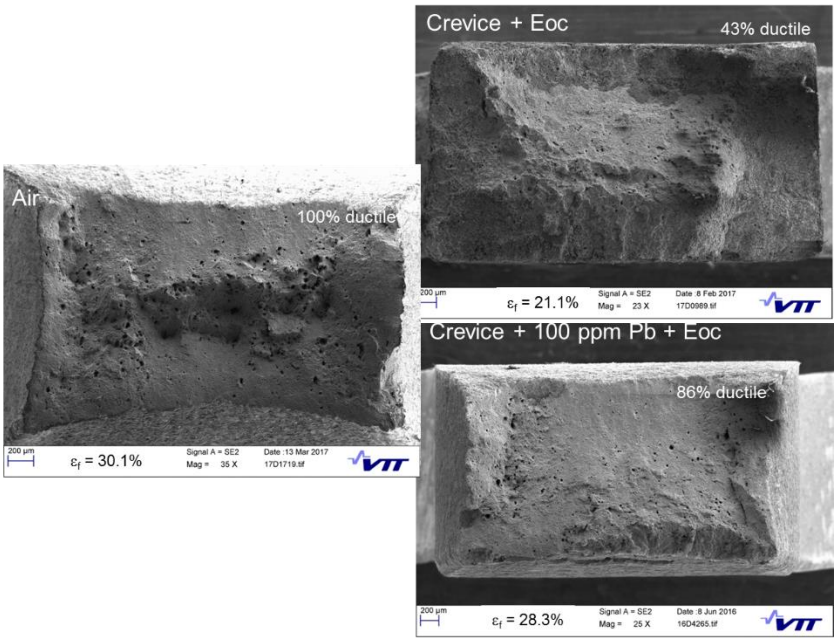

Figure 4. Fracture surfaces of samples tested in a) air, b) in crevice environment without lead (Pb) and c) in crevice environment with 100 ppm (mg/l) lead.

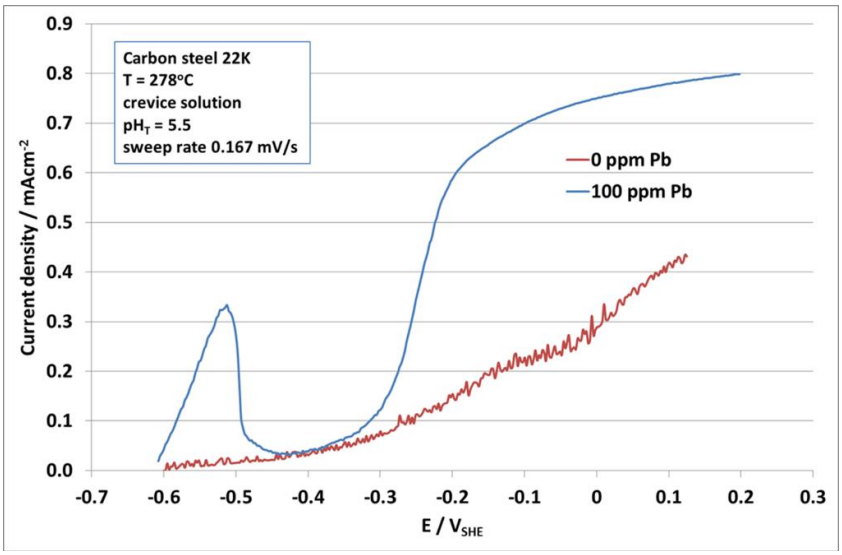

Figure 5. Comparison of current density - voltage -curves for carbon steel in acidic crevice environment without lead (Pb), red line and with 100 ppm (mg/l) of Pb, blue line.

The current density - voltage -curve in the acidic crevice environment without lead showed a slowly increasing trend as a function of potential, indicating a passive surface, Figure 5. The rate of increase goes slightly up above -0.35 V_{SHE}, at which potential Fe_3O_4 (magnetite) is expected to transform to Fe_2O_3 (heamatite). The curve in the presence of Pb, on the other hand, shows an active peak around -0.52 V_{SHE}, followed by passivation and another increase in current density for potentials higher than -0.35 V_{SHE}. Based on these results and E-pH diagrams, Figure 6, it can be assumed that close to the corrosion potential (-0.6 V_{SHE}) Pb^{2+} ions are reduced on the steel to metallic Pb. At potentials more positive than the corrosion potential, Pb starts to dissolve as $PbCl^+$ accounting for the active peak in the current density - potential -curve in Figure 5. The dissolution of lead is most probably accompanied with Fe dissolution leading to an unstable passivation of the surface. The reduction in the SCC susceptibility in presence of Pb is proposed to result from this unstable passivation, which at lest partially prevents localisation of corrosion necessary for SCC to occur.

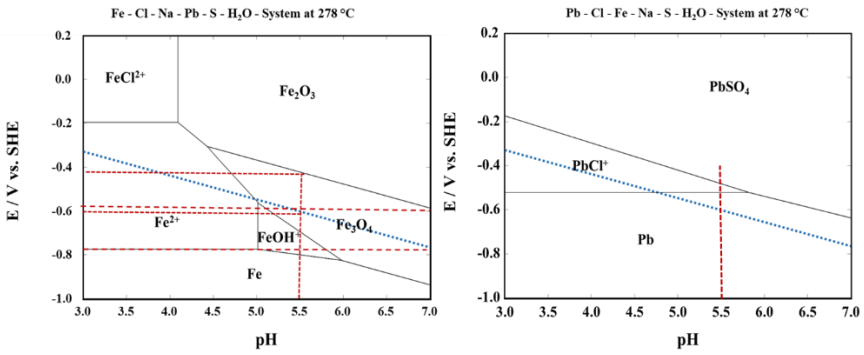

Figure 6. Potential – pH diagrams for Fe (left) and Pb (right) at 278 °C in the crevice solutions. The red dashed lines mark the pH of the solution (vertical line) and the equilibrium potentials (horizontal lines) of Fe_3O_4 /Fe_2O_3 and H_2/H^+.

Summary and conclusions

In this work, means to mitigate corrosion phenomena affecting the integrity of the secondary side of a PWR plant have been studied.

Hydrazine is routinely used in PWRs as an oxygen scavenger, and has been found to be harmful for the environment and potentially cancerous, which may lead to banning the use of it worldwide in the future. Two best candidates to replace hydrazine in steam generator preservation during outages (at T = 50°C) were found to be carbohydrazine and iso-ascorbic acid. However, their efficiency as oxygen scavengers was less than that of hydrazine by a factor of about x2. This means that

larger concentrations of the replacement chemicals would be needed than those typically used with hydrazine.

Alternative water chemistry regimes involving amines have been thought to possibly enable, in addition to adjusting the PWR secondary side circulation pH, to affect the surface charge of magnetite particles so that their deposition into steam generators would be mitigated. The results from this work suggest that the effects of different amines on surface charge of magnetite at the SG temperatures is rather small, and that the surface charge approaches zero. Thus, the surface charge per se is suggested to play an insignificant role in the magnetite deposition process.

The body of the steam generator is made of carbon steel. Due to some wall through cracking insidents in VVER plants in Russia and Czech Republic, a concern has been raised on the possible effect of lead as a promoter of stress corrosion cracking (SCC) of carbon steel. In this work, the effect of an addition of 100 ppm of lead was shown to be beneficial to carbon steel under both acidic and alkaline crevice conditions. Without the addition of lead, carbon steel was found to be much more susceptible to SCC under the acidic than the alkaline crevice conditions. Thus, the plant secondary side chemistry should be preferably maintained so that the crevice conditions remain neutral or slightly alkaline.

References

Betova, I., Bojinov, M. & Saario, T. 2014, Film-Forming Amines in Steam/Water Cycles – structure, properties, and influence on corrosion and deposition processes. VTT Research Report VTT-R-03234-14.

Kim U., Kim, K. & Lee, E. 2009, Oxide investigation formed on Alloy 600 in leaded aqueous solutions. 14th International Conference on Environmental Degradation of Materials in Nuclear Power Systems.Virginia Beach, Virginia, USA, August 23-27, 2009.

Kim, U., Kim, K. & Lee, E. 2005, Effects of chemical compounds on stress corrosion cracking of steam generator tubing materials in caustic solution. Journal of Nuclear Materials 341,169-174.

Betova, I., Bojinov, M. & Saario, T. 2016. Hydrazine replacement in nuclear power plants – alternative substances and techniques. VTT Research Report VTT-R-03426-16, 33 p.

Betova, I., Bojinov, M. & Saario, T. 2017.Kinetics of oxygen removal by hydrazine alternatives in conditions of steam generator preservation during outage. VTT Research Report VTT-R-05209-17, 22 p.

Betova, I., Bojinov, M. & Saario, T. 2018. Hydrazine alternatives as oxygen scavengers and passivation agents in steam generator preservation conditions. VTT Research Report VTT-R-01908-18, 35 p.

Jäppinen, E., Ikäläinen, T., Järvimäki, S., Saario, T., Sipilä, K. and Bojinov, M. 2016. Corrosion behavior of carbon steel coated with octadecylamine in the secondary circuit of a pressurized water reactor. Journal of Materials Engineering and Performance, December 2017, Volume 26, Issue 12, pp 6037–6046.

Bojinov, M., Jäppinen, E., Saario, T., Sipilä, K. & Toivonen, A. 2019. Effect of lead and applied potential on corrosion of carbon steel in acidic and alkaline steam generator crevice solutions. 27 p. Presented for publication in Corrosion Science journal.

6.6 Thermal ageing and EAC research for plant life management (THELMA)

Ulla Ehrnstén[1], Matias Ahonen[1], Mykola Ivanchenko[1], Caitlin Huotilainen[1], Jari Lydman[1,] Aki Toivonen[1], Unto Tapper[1], Roman Mouginot[2], Hannu Hänninen[3]

[1]VTT Technical Research Centre of Finland Ltd
P.O. Box 1000, FI-02044 Espoo

[2]FemtoTools AG, Switzerland

[3]Aalto University
P.O. Box 11000, FI-00076 Aalto

Abstract

The project THELMA, Thermal ageing and EAC research for plant life management, deals with nuclear materials behaviour in light water reactor environments. The development of thermal ageing of stainless steels, both welds in wrought material and cast material, have been investigated. The increase in hardness of the ferrite phase is a good indicator of ageing, while application of electrochemical measurement method double loop electrochemical potentiokinetic reactivation is not straightforward for materials aged in operation. It is, though, a feasible method when ageing has been performed at higher (~400°C) temperature. Thermal ageing of Alloy 690 cause intergranular carbide precipitation, lattice contraction and increased hardness, indicative of ordering reaction. This may affect the long-term primary water stress corrosion cracking resistance of pressurized water reactor (PWR) components. Detailed microstructural investigations of mechanical test specimens made from Barsebäck 2 pressure vessel steel weld metal show e.g. a correlation between a low fracture toughness and brittle fracture initiation at large secondary particles. The detailed results form a basis for similar investigations to be performed on irradiated reactor pressure vessel materials. The research increase the knowledge on materials behaviour in nuclear power plant environments which is needed to assist the safety authority STUK, licensees and other stakeholders in questions concerning plant life management, material degradation assessment and failure analysis. Advanced knowledge must exist in advance, and cannot be built in e.g. failure analysis work, which typically require a short through-put time.

Introduction

The project THELMA, Thermal ageing and EAC (environmentally assisted cracking) research for plant life management, deals with nuclear materials behaviour in light water reactor (LWR) environments with special focus on determination of thermal

ageing in austenitic primary circuit materials, i.e. stainless steel weld and cast materials and nickel-based Alloy 690. Further, precursors for environmentally assisted cracking initiation are studied in co-operation with the EU-MEACTOS (Mitigation of EAV though optimisation of surfaces) project and irradiated stainless steels are characterised for the OECD HALDEN project. THELMA also acts as the national forum for the EU-INCEFA+ (Increasing Safety in NPPs by Covering gaps in Environmental Fatigue Assessment) project, aiming at an improved corrosion fatigue assessment for stainless steels in pressurized water reactor (PWR) environment (Huotilainen, 2018) and for MEACTOS, aiming at mitigating environmentally assisted cracking through surface treatments (Ehrnstén, 2018). Pressure vessel steel materials are characterised to improve the knowledge on factors affecting brittle fracture. A selection of results is presented in the following, focusing on achievement from the later part of the project. The early results have been summarised in the midterm report (Hämäläinen and Suolanen (eds.), 2017). The research increase the knowledge on materials behaviour in nuclear power plant (NPP) environments which is needed to assist the safety authority STUK, licensees and other stakeholders in questions concerning plant life management, material degradation assessment and failure analysis. Advanced knowledge must exist in advance, and cannot be built in e.g. failure analysis work, which typically require a short through-put time.

Thermal ageing of cast stainless steel

Thermal ageing of stainless steel weld metals and cast materials, both having a two phase microstructure comprising of austenite and ferrite, is known to occur in LWR conditions through spinodal decomposition and G-phase formation in the ferrite phase. This results in reduction of ductility and toughness, and in an increased EAC crack growth rate. In THELMA, thermal ageing of Type 316 stainless steel weld metals and of in-service aged cast stainless steel (CASS), type CF8M has been investigated. The results from the investigations on the weld materials were reported in the SAFIR2018 interim report (Hämäläinen and Suolanen (eds.), 2017). The material for the investigations on cast stainless steel is sections from a steam generator inlet (called the hot leg, HL) and from the cross-over leg (called the cold leg, CL) of the Ringhals 2 steam generator (SG), both made from CF8M cast stainless steel. CF8M is one of the two most common cast stainless steels used in NPPs. CF8M contains Mo, which is known to promote thermal ageing, and is therefore, e.g., not used in Class 1 components in OL3. The HL experienced an in-service ageing of approximately 70kh at 325°C and 22kh at 303°C, while the temperatures for the CL were 293°C and 274°C, respectively. This has resulted in degradation of the fracture toughness. The objective of the investigations in THELMA was to evaluate whether electrochemical measurements can be used for determination of the degree of the thermal aging. DL-EPR was developed, and is still routinely used, for measurement

of sensitisation in stainless steel, and is sensitive to chromium depletion. It has, though, been successfully applied on both weld and casts stainless steels aged at higher temperatures.

The microstructure was characterised using light optical microscopy (LOM) and scanning electron microscopy (SEM). The chemical composition of the two-phased material, comprised of austenite and ferrite, was measured using semi-quantitative energy dispersive x-ray spectrosocpy (EDS). Hardness measurements were performed using Vickers hardness numbers and also nanoindentation, H_{IT}. The double loop electrochemical potentiokinetic reactivation (DL-EPR) method was used for the electrochemical measurements. Both standard and stronger than standard solutions were used, as well as different scan rates, similar to earlier investigations on weld metals. Small pieces were also subjected to solution annealing, to obtain a reference material condition (Huotilainen et al., 2018).

The microstructure of the cast stainless steel is depicted in Figure 1. The amount of ferrite vary locally in the HL and CL materials. The nanoindentation measurements showed an increase in the hardness with thermal ageing, Figure 2, in correlation with other data. The results from the DL-EPR measurements were, however, not straightforward, Figure 3. The reactivation ratio percentage i_r/i_a *(%)*, which is reported to correlate to thermal ageing in literature, is more pronounced in the CL than in the HL material, Table 1. Based upon these results it would seem as though DL-EPR is not a suitable technique for quantifying thermal ageing effects in CASS aged at operating temperature range of NPPs. The changes in mechanical properties are due to both spinodal decomposition and G-phase formation. As G-phase is a Ni-silicide, it should not alone have a significant influence on the corrosion properties, and thus not either on DL-EPR response. In this case it is possible, that the decomposition at nanoscale has not yet evolved to a level strong enough to give a clear DL-EPR response.

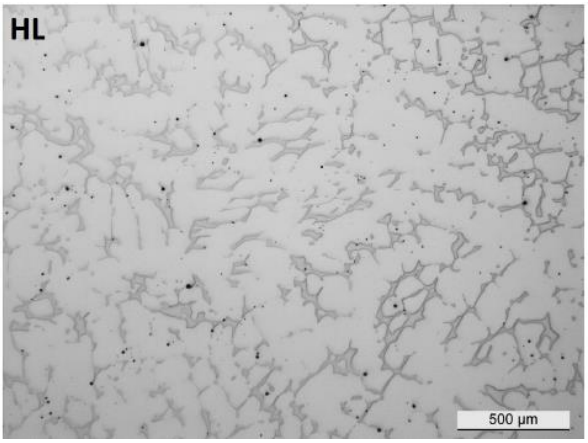

Figure 1. Microstructure of cast stainless steel, showing a two phase structure comprising of austenite (lighter) and ferrite (darker).

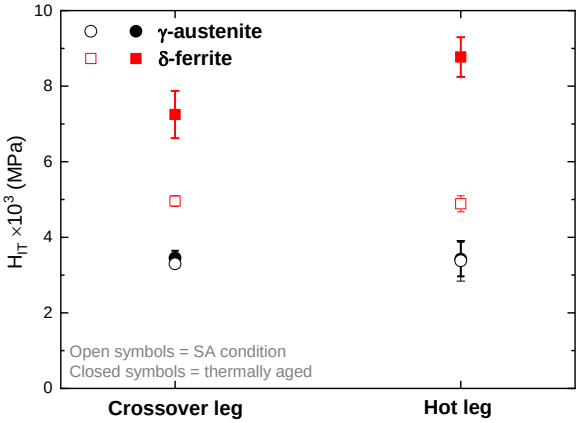

(a)

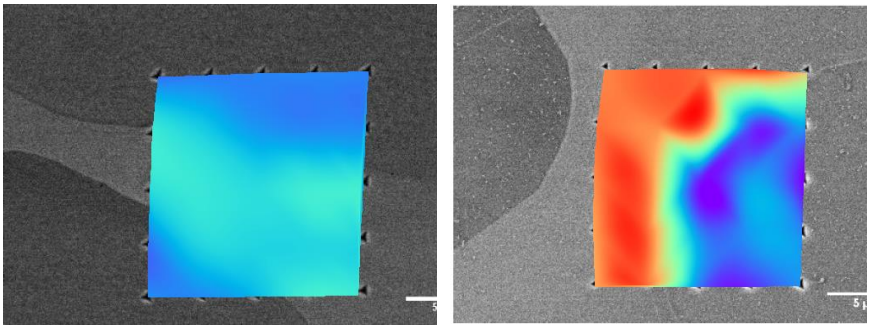

(b) (c)

Figure 2. H_{IT} (MPa) results for CL and HL (a) and SEM image H_{IT} correlation for solution annealed (b) and thermally aged HL material (c).

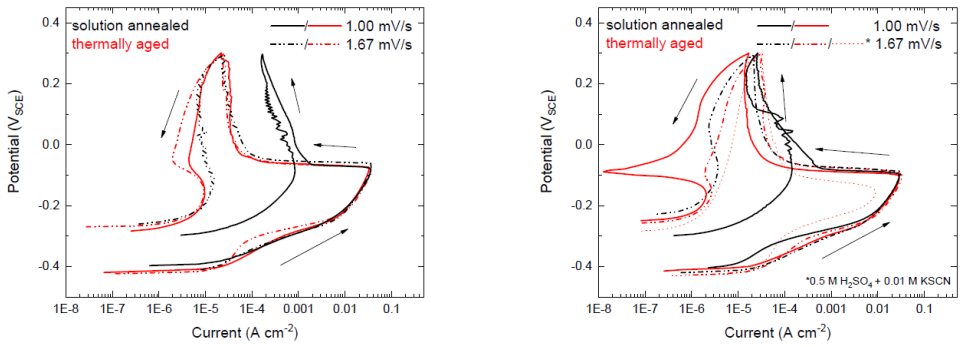

Figure 3. DLEPR curves for (a) HL and (b) CL for different scan rates. The black curve represent the SA condition and the red curves the thermally aged conditions.

The results shows the complexity of thermal ageing, which is affected by several simultaneous changes in the microstructure, which both temperature and time dependent. The results also show that although the DL-EPR method can be used for evaluation of the degree of thermal ageing in materials aged at higher than operational temperatures, but it may not be useful for plant aged materials. More work is needed to develop a method to determine the degree of thermal ageing from plant components without the need to dismantle the component. Recently transient granting (TG) spectroscopy has been developed at MIT, US, and the method is promising. The very preliminary results are in line with the DL-EPR observations showing a stronger “ageing response” in the CL material compared to the HL material.

Table 1. *i_r/i_a (%)* values for solution annealed and thermally aged CL and HL materials.

Material	Condition	Scan rate ($\mathrm{mV\,s^{-1}}$)	i_r/i_a (%)
CL	SA	1.00	2.3
	SA	1.67	4.3×10^{-2}
	TA	1.00	3.0×10^{-2}
	TA	1.67	2.6×10^{-2}
HL	SA	1.00	0.5
	SA	1.67	1.2×10^{-2}
	TA	1.00	0.7×10^{-2}
	TA	1.67	0.8×10^{-2}

Thermal ageing and short range ordering of Alloy 690

Alloy 690 (Ni-30Cr-10Fe) is a nickel-base alloy which has been used to replace Alloy 600 since the 90s in order to improve the primary water stress corrosion cracking (PWSCC) resistance of components in pressurized water reactors. It is mostly used in the thermally treated (TT) condition Alloy 690 TT. Knowing the long-term behaviour of Alloy 690 components is of high importance to assure nuclear energy production, as they are used in critical applications such as the steam generator U-tubes and the reactor pressure vessel head penetrations. As with many other commercial nickel-base alloys, Alloy 690 is subject to an ordering reaction during thermal ageing at temperatures under 550 °C. The main consequence of ordering is lattice contraction, which leads to increased hardness, ductility loss, change in the fracture mode from ductile to intergranular and heterogeneous planar slip. Most manufacturer data showing an excellent Alloy 690 long-term stability has been obtained at 565 °C and higher, but there is a strong probability that ordering can affect the long-term SCC resistance of Alloy 690 at lower temperatures, as an intrinsic driving force or as an additional factor. Thermal ageing of Alloy 690 has been studied in the SAFIR2014 ENVIS project, and continued in the SAFIR2018 THELMA project. A doctoral thesis on the subject was finalised in 2017. The main results were summarised in the SAFIR2018 interim report (Hämäläinen and Suolanen (eds.), 2017) showing that short range ordering (SRO) occurs in the investigated Alloy 690 material. The work has since continued with further microstructural characterisation using atom force microscopy and nanoindentation (Mouginot et al., 2018, Mouginot et al., 2019) and with investigations on the effect of hydrogen on thermally aged Alloy 690 (Hurley et al., 2018).

One of the conclusion from the extensive investigations reported in the thesis (Mouginot, 2017), was that the temperature for the maximum effect of short range ordering is dependent on the iron content of the material. Many investigations reported in the open literature has not taken this into account. For the material in this investigation, having an iron content of 9.2 wt.-%, this temperature is 420°C.

The Alloy 690 material was investigated in 7 conditions, as presented in Table 2. For the additional microstructural characterisation the following methods were used. Intergranular carbide precipitation was characterised using scanning electron microscopy, and the number of precipitates was assessed using ImageJ software. Hardness measurements were performed using increasing load to analyse the effect of increasing interaction volume. Vickers hardness, nanoindentation and atomic force microscopy were used. The nanoindentation hardness increase with increasing ageing temperature up to the expected critical ordering temperature of 420°C, after which it decreases with further increase in ageing temperature, Figures 4 and 5. Notably, the hardness level at 420°C is on average higher than that of Alloy 690 with 20% cold work. The results are in good agreement with earlier results showing a peak in lattice contraction at 420°C ageing (Mouginot, 2017).

The results show a clear influence of SRO on the hardness, with a good reproducibility of the results and good correlation with the literature and previous lattice

parameter measurements. The combination of intergranular (IG) carbide precipitation and growth in combination with SRO is deemed detrimental to PWSCC resistance, and would deserve continued investigations on more commercial Alloy 690 materials, with long ageing times combined with characterisation and PWSCC tests in autoclave environments (Hänninen et al., 2018).

Table 2. Summary of the 7 conditions investigated.

Condition	Code
Solution annealed +WQ	SA
SA+ 17 h at 700°C	TT
TT+10 000 h at 350°C	TT350
TT+10 000 h at 420°C	TT420
TT+10 000 h at 475°C	TT475
TT+10 000 h at 550°C	TT550
TT+20% cold-worked by rolling	TTCW

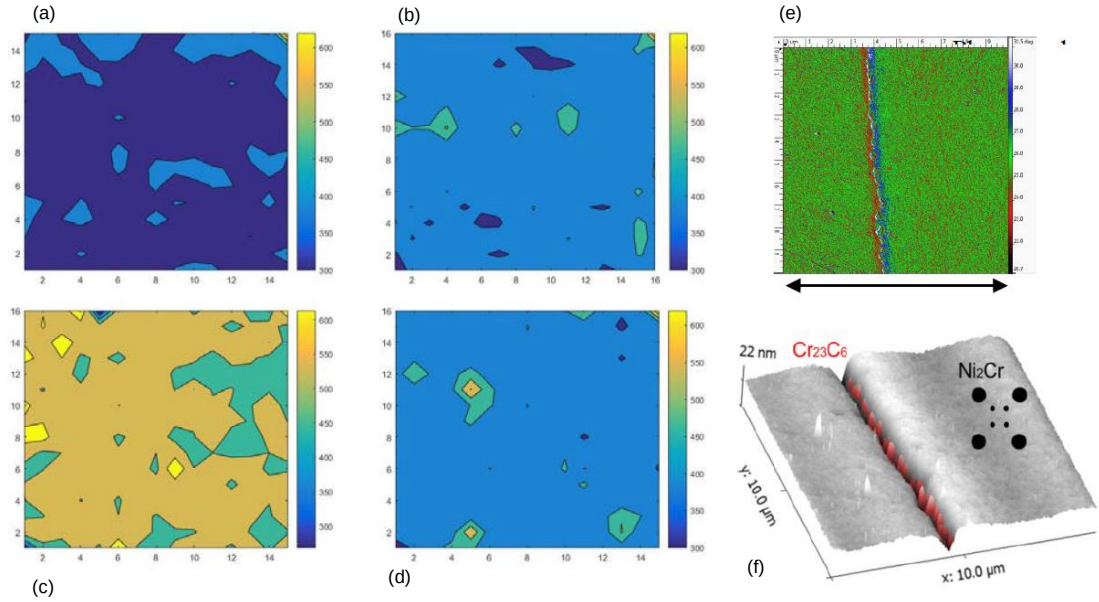

Figure 4. Hardness mapping of Alloy 690 a) SA, b) TT, c) TT420 and d) TT550. A clear increase of the average hardness throughout the matrix is visible in TT420. The AFM of TT420 give a higher special resolution, with e) a phase angle mapping over a grain boundary and f) a 3D topographic map highlighting the location of the IG carbides.

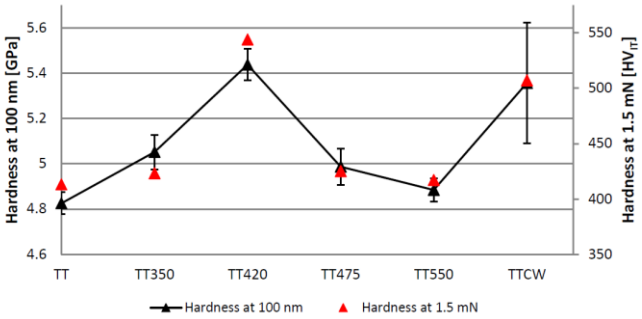

Figure 5. Summary of hardness measurements comparing nanoindentation mapping at 100 nm penetration depth (about 1.6 mN) and using 1.5 mN.

The effect of hydrogen on the thermally aged Alloy 690 material was investigated using thermal desorption spectroscopy (TDS) and mechanical loss spectroscopy (MLS). MLS results are not presented in this summary. Both as-aged and hydrogen

charged specimens were analysed (Hurley et al., 2018). The TDS spectra are shown in Figure 6. The SA specimen present a well-defined desorption peak between about 500 and 800 K accompanied by a desorption shoulder at about 700 K. The TA420°C and TA550°C specimens show peaks at approximately the same temperature, but the peaks are weaker. However, the unaged TT specimen produces the most distinct peak. The hydrogen content of the TT specimen is also highest, being 470 at. ppm H, while that of the SA and TA specimens is about 100 at. ppm H. The TT material has the smallest grain size and thus the most significant grain boundary volume fraction. The grain boundary carbides may act as hydrogen traps, and may explain the highest H-content in this material. H-charging resulted in significant, but varied total hydrogen uptake, depending on the material condition. The peaks of the TDS spectra correlate with the hydrogen uptake. The results indicate that carbides and grain boundaries may act as hydrogen traps and may retain non-negligible amount of hydrogen even before exposure to hydrogenated PWR environment.

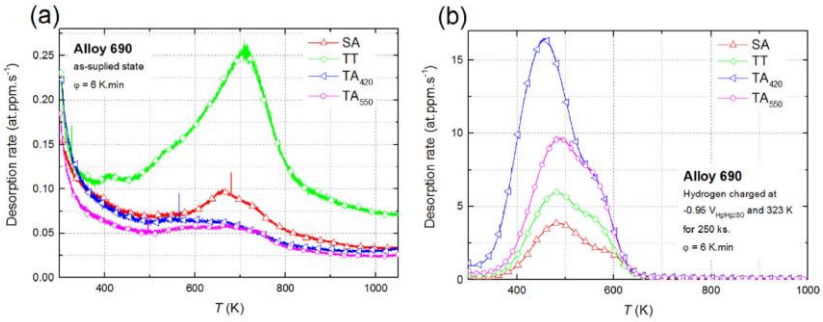

Figure 6. Thermal desorption rate with respect to temperature for (a) non-charged and (b) H-charged specimens.

Improved understanding of RPV weld brittle fracture initiation

The structural integrity of the reactor pressure vessel (RPV) in a NPP is of outmost importance as the RPV is the most important component for safe NPP operation. The neutrons from the core fission reaction affects the properties of the RPV, and especially of the weld metal. These changes are followed in surveillance programs, where mechanical test specimens are located inside the RPV at a location where they accumulate a higher dose than the RPV. Based on the results from the mechanical tests on these specimens, a prediction curve is established, as a basis for life time management. It is known that irradiation causes formation of agglomerates,

that brittle fracture initiation typically occur at secondary particles, and that mechanical test results show some scatter. However, a detailed understanding on the relationship between the mechanical properties, the observed scatter and microstructural characteristics is missing, although it has lately become the focus of several projects, including the ongoing EU-SOTERIA project. Most Nordic RPVs have been manufactured to the same specifications and using the same, high Ni (1.5 wt.%) weld metal.

Unirradiated specimens from Barsebäck 2 weld metal has been subjected to detailed microstructural investigations on mechanical test specimens tested in the SAFIR2018 LOST project. The brittle fracture initiation sites were identified and classified. Cross-sections as close as possible to the initiation site were investigated using LOM and SEM/EDS (Lydman et al., 2019) and the secondary particles were investigated using transmission electron microscopy (TEM).

The results show that the initiation site locations are close to the centre of the specimen, Figure 7(a). 50 % rank probability (P_{rank}) is achieved at 10 % distance from the centre, and the distribution is similar to other results on RPV materials. All but three specimens had an M-value below 30, showing that these specimens fulfils the size requirements, while the three specimen with an M-value above 30 may not do so. This value can be used to further analyse the validity of the results, in addition to the requirements set in the testing standards. Initiation occurs typically at secondary particles, Figure 7(b) with a size between 0.5 µm and 2 µm, and initiation at large particles (1.5 - 2 µm) correlate with low fracture toughness values. Further, the brittle fracture initiation is mostly at the deepest point of the pre-fatigue crack, or very close to it. When this is not the case, the fracture toughness is typically lower than when the initiation is at the deepest point. The microstructure of a weld metal is complex due to the multiple heat transients during welding, and comprise of as-welded areas intersected by re-heated zones from welding of subsequence weld beads, Figure 8(a). Specimens, where the initiation occurred in the re-heated weld metal showed typically lower fracture toughness values compared to those, where brittle fracture initiated in the as-welded microstructure. The initiation area of the WM specimens typically have more grain boundary ferrite and/or polygonal ferrite than the surrounding, Figure 8 (b).

The results have increased the knowledge of the relationship between fracture toughness properties, brittle fracture initiation and microstructure, and shown that these investigations also can be used for further analyses of the mechanical test results to distinguish between intrinsic scatter (data range) and scatter due to testing issues.

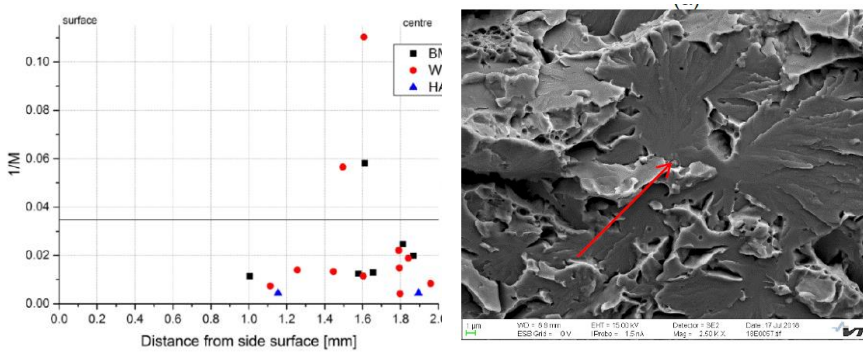

(a) (b)

Figure 7. (a) Initiation site distances from the specimen side surface towards the centre. (b) Initiation of brittle fracture at a secondary particle.

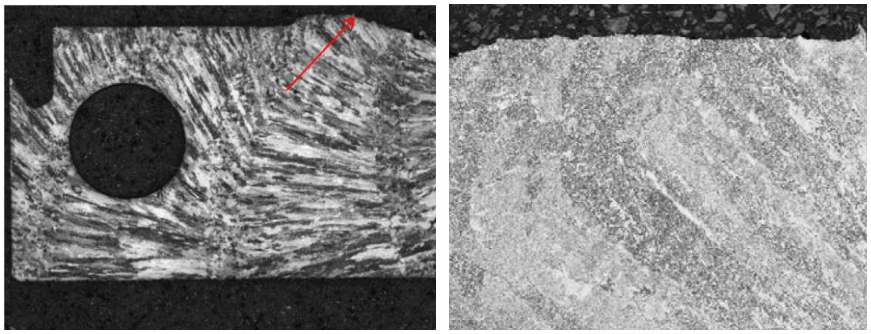

(a) (b)

Figure 8. Macrostructure of a weld metal specimen (a) and the microstructure at higher magnification (b) showing a higher amount of grain boundary ferrite (with light appearance in the picture) next to the initiation site.

The TEM results showed that the weld metal has three main categories of secondary particles (Tapper, 2019), i.e., 1) large oxide particles, with a size larger than 100 nm, whose composition is dominated by O, Al and Mn, 2) and 3) small Mo- or Mn-rich particles with a size less than ~150 nm and 4) elongated Cr-rich particle that were location near or in the grain boundaries. One example of particles in a weld metal specimen is shown in Figure 9. The secondary particle mean size was 257 nm with 154 nm standard deviation, and the size distribution indicated a non-lognormal distribution.

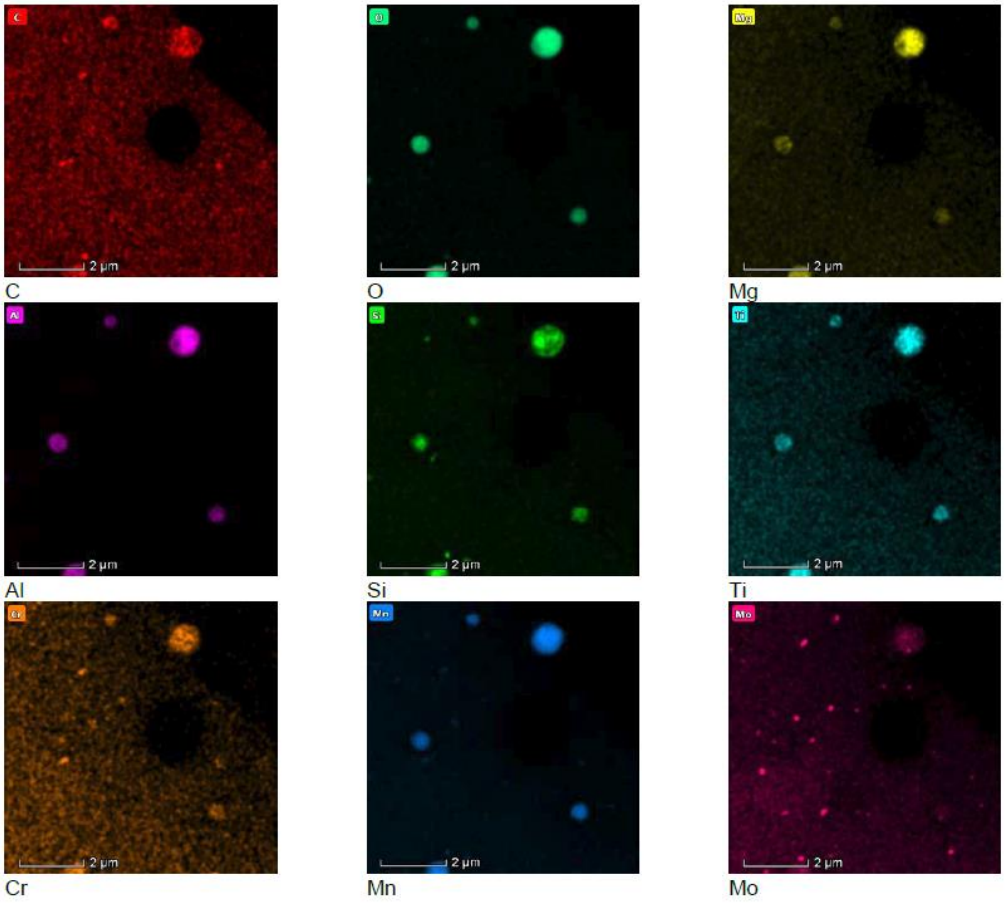

Figure 9. Elemental maps showing two types of particles, i.e., larger oxides and smaller Mo-rich particles.

Characterisation of irradiated stainless steel materials

Structural materials in light water reactors are subject to irradiation-assisted stress corrosion cracking (IASCC). The initiation and propagation of IASCC cracks require a tensile stress, a corrosive environment and a susceptible material. Type 316 and 304 stainless steel are used as structural materials and are susceptible to IASCC. During reactor operation the neutron flux results in irradiation creep or irradiation stress relaxation. Hence, the initial stresses in structural components will vary during reactor operation. If the stresses decrease to zero due to irradiation stress re-

laxation, additional IASCC cannot occur thereafter. VTT has performed the characterisation of selected materials from the Halden program as part of the SAFIR programme. The main objective is to couple the crack growth rates during in-pile IASCC tests with the microstructure to understand the affecting parameters.

The latest investigations were made on three stainless steels of type 316L irradiated to 4 dpa, 304L (5.9 dpa) and cold worked (CW) 316 (9 dpa). The investigations showed the presence of ε-martensite in the 304L material, which is in accordance to expectations, being the least stable stainless steel material. Clear channels were observed in all materials, but the degree of localisation of deformation was different in the materials, being most pronounced in the 9 dpa CW 316 material. That clear channels are produced during deformation of irradiated stainless steels, and that clear channels facilitate further dislocation movement, is a commonly accepted mechanism, but catching them in TEM is less common, as this is challenging (Ivanchenko, 2018a and b). The results gives further insight to the IASCC issues, e.g. for baffle bolts, and other components, suffering from IASCC in both BWRs and PWRs.

A unique opportunity was opened in connection to another project dealing with a VVER 400 absorber made from high-B stainless steel. Very little, if any, publically available information is found on the microstructure of this material. Material from an irradiated absorber will be made available later, and the opportunity was therefore taken to investigate the material in non-irradiated condition.

Boron is alloyed into absorber materials for its good neutron absorbing properties. The ability of the material to absorb neutrons decay, however, as boron is transformed to helium due to interaction with neutrons. This will not only change the absorbing properties of the material, but also the mechanical properties, and possibly cause swelling. The results from this investigation are planned to be used, in addition to e.g., measurement of the He-content, in the planned investigations on the irradiated material. As the material is highly radioactive, it is more than reasonable to evaluate the difference investigation and specimen preparation techniques using a non-irradiated material.

The material is a boron alloyed cast stainless steel, with addition of about 1.2 wt.-% boron. A material with such high boron content is not used in the western NPP designs, although SS with lower boron content is used as absorber material e.g. in spent fuel pools. As the solubility of boron in austenite is very low, it is expected that most of the B is in ferrite phase is in the form of borides. The main objective of this investigation was evaluate the sensibility of different characterisation techniques as preparation for the investigations on irradiated absorber material. The material was characterised using SEM/EDS and with the wavelength dispersive X-ray analyser, SEM/WDS, which is more sensitive than EDS, especially for light elements like B, and with scanning (S)TEM/EDS and also EELS, which is especially useful for light elements such as B (Ivanchenko, 2018c).

The absorber material is a two-phase material comprising of mainly austenite and ferrite, Figure 10. The presence of boron could already be affirmed through careful SEM/EDS analyses, although carbon contamination affects the results. However,

using SEM/WDS, the presence of B in the phase within the ferrite, could be confirmed with high confidence, Figure 11. Preparation of specimens for STEM/EDS proved to be challenging due to the large difference in composition, resulting in uneven electrolytic polishing of the different phases. This resulted in sample where the matrix had almost completely dissolved, while the boron containing phase was still thick, Figure 12. Nevertheless, a few areas with appropriate thickness for analytical TEM were identified and investigated. TEM/EDS mapping showed that the borides have different sizes, and they do contain B, Figure 13. EELS, which is the most challenging technique of all used, proved very useful for detection of B, Figure 14.

The results show that different techniques give complementary results, and the optimum results is obtained by using all of the above mentioned techniques. SEM/EDS could be omitted for detection of boron, but SEM is useful to get an overview of the microstructure and the different phases. For the irradiated material, additional methods, e.g. He-measurement, will be used.

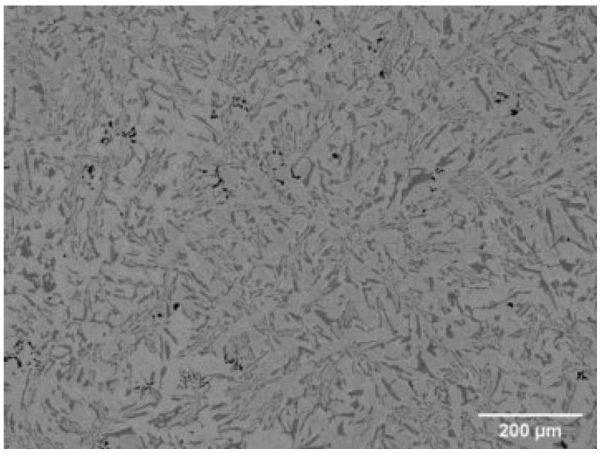

Figure 10. SEM micrograph of the absorber material illustrating presence of two phased, and numerous cast cavities.

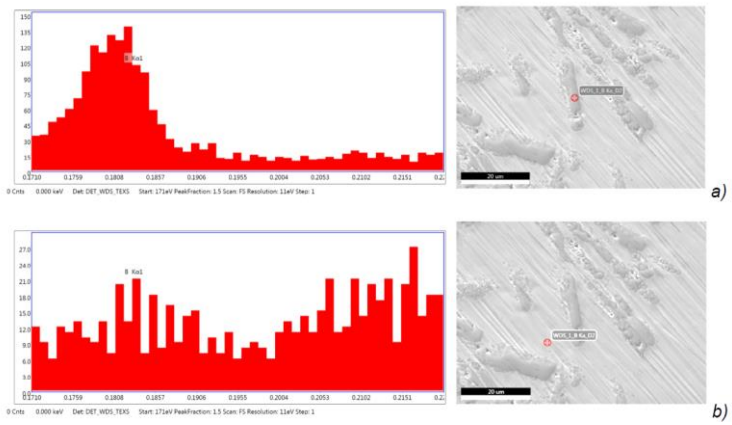

Figure 11. WDS spectra and micrographs for the Fe and Cr-rich phase (a), and the matrix (b).

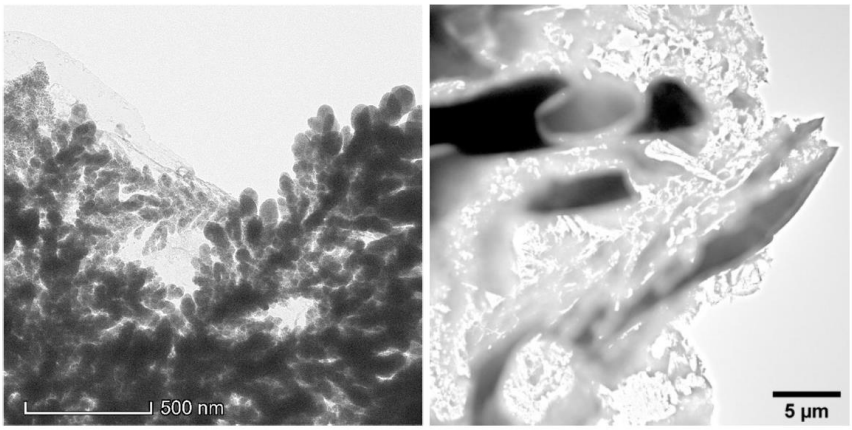

Figure 12. TEM micrograph showing the uneven polishing of the different phase with different composition.

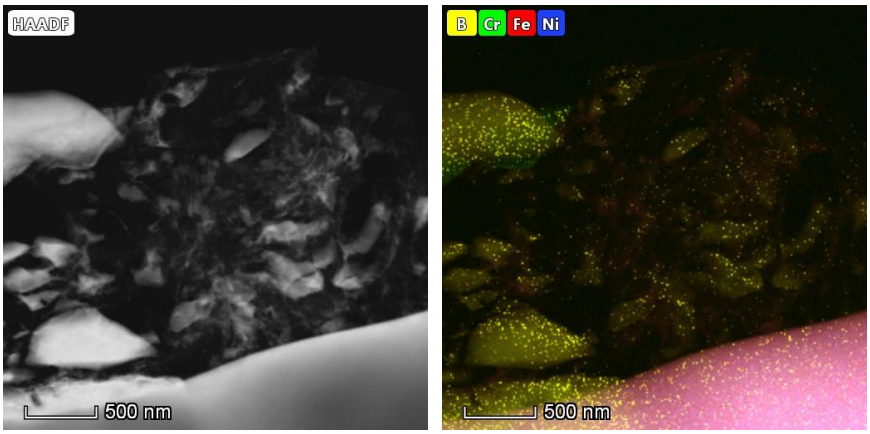

(a) (b)

Figure 13. STEM micrograph (a) and corresponding EDS elemental map (b) showing B in the finely dispersed phase.

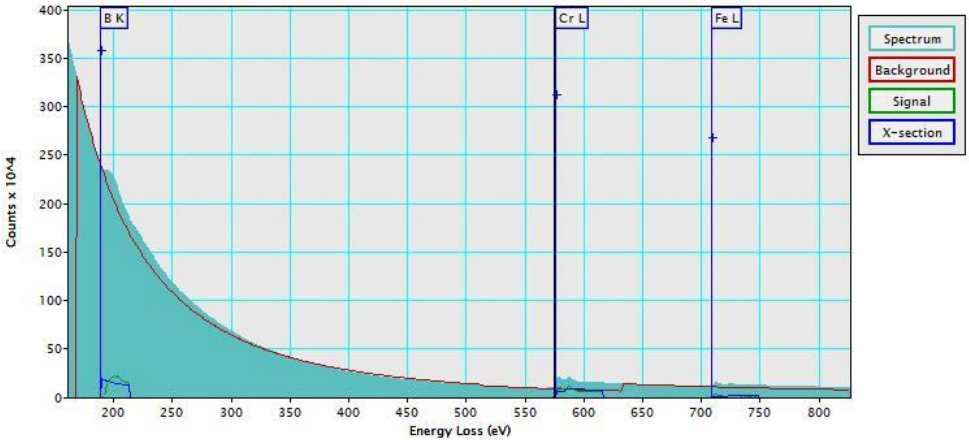

Figure 14. EELS spectrum from a B-containing particle in Figure 9, showing a B-peak.

Acknowledgement

The plant aged cast stainless steel and the B2 RPV material was provided by Ringhals Ab, Sweden. The Alloy 690 samples were aged and provided by the Korean Atomic Energy Research Institute (KAERI). The irradiated stainless steel material was provided by IFE, Norway, and the absorber material by Fortum P&H. To have access to real NPP materials, and especially after long operation times, is of outmost importance for research made in THELMA. The access to real NPP material is very highly appreciated, as is the funding from VYR, VTT Ltd, Halden, NKS and

Aalto University. Mike Short, MIT, is acknowledged for fruitful co-operation, including the willingness to measure the CASS specimens using their newest technique.

References

Ehrnstén, U. Progress report on EU-MEACTOS project in 2018. VTT-R-06699-18, 29.11.2018, 12 p.

Hurley, C., Yagodzinskyy, Y., Mouginot, R., Malitckii, E., Hänninen, H., 2018. Combined effect of thermal ageing and hydrogen. 3rd international conference on metals & hydrogen. 29-31.5.2018, Ghent, Belgium.

Huotilainen, C., 2018. Progress report on EU-INCEFA+ for SAFIR2018 - THELMA. VTT-R- 06855-18.

Huotilainen, C., Ivanchenko, M., Ehrnstén, U., Efsing, P., 2018. Electrochemical investigation of in-service thermal ageing and G-phase precipitation of two CF8M cast stainless steels. Submitted to Materials Science and Engineering A.

Hämäläinen, J and Suolanen, V (eds.), 2017. SAFIR 2018 – The Finnish research programme on nuclear power plant safety 2015 – 2018. Interim report. VTT Technology 294. Pp. 319 – 330.

Hänninen, H. On the mechanisms of EAC of Alloys 690 and 52 in pressurized water reactor applications. Presentation at the 2018 Eurocorr conference, September, 9-13, 2018, ICE Krakow, Poland.

Ivanchenko, M., 2018a Microstructural characterization of in-reactor tested stainless steels: 4 dpa CW 316 Ti SS, 5.9 dpa 304L SS and 9 dpa CW 316 SS. VTT-R-00158-18, 7.2.2018.

Ivanchenko, M., 2018b Microstructural characterization of in-reactor tested stainless steels: 4 dpa CW 316 Ti SS, 5.9 dpa 304L SS and 9 dpa CW 316 SS. VTT-R-00158-18, 7.2.2018.

Ivanchenko, M., 2018c Analytical electron microscopy of unirradiated boron alloyed stainless steel absorber sleeve material. VTT-R- 06938-18.

Lydman, J., Nevasmaa, P. Ehrnstén, U. Microstructural characterization of non-irradiated Barsebäck RPV material. VTT-R- 05554-17, 7.12.2017. 116 p.

Mouginot R., 2017. Effect of thermal ageing on Alloy 690 and 52 in pressurized water reactor applications. Aalto University publications series doctoral dissertations 81/2017. https://aaltodoc.aalto.fi/handle/123456789/25405

Mouginot, R. et al. Development of short-range order and intergranular carbide precipitation in Alloy 690 TT upon thermal ageing. The Minerals, Metals & Materials Society 2018. J.H. Jackson et al. (eds.), Proceedings of the 18th International Conference on Environmental Degradation of Materials in Nuclear Power Systems – Water Reactors, The Minerals, Metals & Materials Series. https://doi.org/10.1007/978-3-319-67244-1_21

Mouginot, R et al., 2019. Nanoindentation study on short-range ordering. Materials Research Express, January 2019.

Tapper, U. Microstructural characterisation of non-irradiated Barsebäck RPV material: Transmission Electron Microscopy study. VTT-R-00041-19, 11.1.2019, 16p.

6.7 Evolving the Fennoscandian GMPEs (EVOGY)

Ludovic Fülöp[1], Vilho Jussila[1], Riina Aapasuo[2], Tommi Vuorinen[2], Päivi Mäntyniemi[2]

[1]VTT Technical Research Centre of Finland Ltd
P.O. Box 1000, FI-02044 Espoo

[2]Institute of Seismology, University of Helsinki
P.O. Box 68, FI-00014 Univ Helsinki

Abstract

Evolving the Fennoscandian GMPEs (EVOGY) project was targeted at proposing an updated ground motion prediction equation (GMPE) for probabilistic seismic-hazard analyses of Finnish nuclear installations. We collected and archived the available recordings of earthquakes in Fennoscandia and created a database with all spectral components important for engineering evaluation.

For developing the GMPE, we used the backbone curves of the G16 equation proposed by Graizer (2016) for central and eastern North America. We adjusted the peak ground acceleration (PGA) prediction of G16 to cover lower magnitudes and very hard-rock conditions of Fennoscandia, but keep it unchanged for magnitudes above M_w4. We adjust the normalized spectral shape prediction of G16 using combined Fennoscandian and NGA-East data for very hard rock.

We evaluated the mean prediction and error using the calibration data, and compared the adjusted GMPE to the subset of hard-rock recordings from the NGA-East database. We used a set of synthetic ground motions created using a hybrid modeling method to confirm the prediction in the near field.

We conclude that the adjusted G16 formulation is adequate for predicting ground motions in Fennoscandia. Due to the compatibility with the original G16 backbone curve and additional comparisons, we estimate that the validity of the proposed formulation is up to the range of $2.0 \leq M_w \leq 6.5$ and $0 \leq R_{rup} \leq 300$km for the hard-rock conditions.

Introduction

The purpose of a Ground Motion Prediction Equation (GMPE) is to determine the expected ground motion at the target site due to a suite of earthquake scenarios. GMPEs are instrumental for seismic-hazard analyses; in continental interiors, however, the apparent versatility of available GMPEs reduces rapidly.

We aim at proposing a GMPE for probabilistic seismic-hazard analyses of Finnish nuclear installations. To extend the GMPE beyond the available magnitude ranges recorded in Finland, we use the backbone curves of the G16 equation proposed by Graizer (2016) for central and eastern North America. We adjust the peak ground acceleration prediction (PGA) of the G16 model to cover lower magnitudes and very hard-rock conditions using Fennoscandian data, but do not change it at the higher magnitudes. We also adjust the normalized spectral shape prediction of G16 using Fennoscandian and NGA-East spectra from very-hard rock. After the calibration of the adjusted GMPE, we evaluate the mean prediction and error. We also compare the adjusted GMPE to the hard-rock recordings in the NGA-East database. Finally, we use a set of synthetic ground motions created using the hybrid modeling method proposed by Fülöp *et al.* (2017) to confirm the prediction in the near field.

The G16 background data and formulation for hard rock

A total of 5026 data points from NGA-East dataset (Goulet *et al.* 2014) were used to calibrate the G16 model proposed by Graizer (2016). Their magnitudes were in the range $3.75 \leq M_w < 6$ with additional three data points from the 1985 M_w6.8 Nahanni earthquake. The average shear-wave velocity V_{s30} was 640 m/s and the highest 2000 m/s. The prediction was extended to the hard-rock definition of V_{S30}=2800 m/s suitable for Fennoscandia.

The G16 formulation for the mean PGA is:

$$PGA_{G16} = G_1 \times G_2 \times G_3 \times C_{mean} \quad (1)$$

On the hard-rock conditions (V_{S30}=2800 m/s), we have:

$$PGA_{2800} = PGA_{G16} \times G_4 \quad (2)$$

or, including the error term in log space:

$$ln(PGA_{2800}) = ln(PGA_{G16}) + ln(G_4) + \epsilon_Y \quad (3)$$

Where:

- PGA_{G16} is the peak ground acceleration predicted by G16;
- PGA_{2800} is the peak ground acceleration predicted by G16 for sites with shear-wave velocity V_{S30}=2800 m/s;
- G_1 is magnitude scaling filter $= [c_1 \times \arctan(M + c_2) + c_3] \times F$;
- G_2 is the distance attenuation filter $= \frac{1}{\sqrt{\left[\left(1-\frac{Rrup}{c_4 \times M + c_5}\right)^2 + 4 \times {D_2}^2 \times \frac{Rrup}{c_4 \times M + c_5}\right]}}$;
- G_3 is anelastic attenuation filter $= \exp(-\frac{c_{11}+c_{12}\times M}{Q_0} \times R_{rup})$;
- G_4 is the site correction filter taking into account the local shear-wave profile. For V_{S30}=2800 m/s, G_4 is constant (=0.57534).
- C_{mean} is a legacy coefficient for the conversion from maximum horizontal component to average horizontal component (=0.89758).
- ε_y is the random error term, modelled as log distribution with a zero mean and the standard deviation σ. The standard deviation of the G16 model is σ=0.848 in natural logarithm units.

Graizer (2016) gave the following constants for the G16: c_1=0.4, c_2=-6.25, c_3=0.55, c_4=2.237, c_5=-7.542, c_{11}=3.9, c_{12}=-0.3445, F=2.232, D_2=0.7 and Q_0=650.

The prediction of G16 for spectra is:

$$SA(T)_{cor,2800} = PGA_{G16} \times SA_{norm} \times \frac{LinAmp_{Vs30=2800}}{LinAmp_{Vs30=640}} \times \frac{1}{Res(T)} \quad (4)$$

Where:

- *T* is the spectra period T=1/*f*, with *f* the spectra frequency;
- SA_{norm} is the shape of the normalised spectra ,
- $LinAmp_{vs30=2800}$ is the site amplification to V_{s30}=2800 m/s relative to the hard-rock conditions. Since the hard-rock definition in G16 is V_{s30}=2800 m/s, $LinAmp_{vs30=2800}$=1;
- $LinAmp_{vs30=640}$ is the site amplification to V_{s30}=640 m/s, the mean shear wave velocity of the G16 calibration dataset;
- Res(T) is a correction factor for residuals for 15 periods in the spectra;

The normalized spectral shape is determined as the sum of two factors:

$$SA_{norm} = I \times \exp\left[-0.5 \times \left(\frac{\ln(T)+\mu}{S}\right)^2\right] + \frac{1}{\sqrt{\left(1-\left(\frac{T}{T_{sp,0}}\right)^{\xi}\right)^2 + 4\times {D_{sp}}^2 \times \left(\frac{T}{T_{sp,0}}\right)^{\xi}}} \quad (5)$$

Where:

- *T* is the spectra period T=1/*f*, with *f* the spectra frequency;
- *I*=1.4 is a constant controlling the spectral amplification;
- μ is controlling the frequency of amplification peak $= m_1 \times RR + m_2 \times MM + m_3$. *RR* and *MM* are different from R_{rup} and M_w, as it will be explained.
- $T_{sp,0}$ is also controlling the peak amplification frequency $= t_1 \times RR + t_2 \times MM + t_3$;
- *S* is controlling the breadth of the spectra $= s_1 \times RR - (s_2 \times MM + s_3)$;
- ξ is controlling the slope of the spectra at low frequencies $= a_1 \times {M_w}^2 + a_2 \times M_w + a_3$;

The distance *RR* used in the above formulas is $=R_{rup}$ for R_{rup}<600km. For 600≤R_{rup}≤1000km, $RR = 600 + 0.5 \times (R_{rup} - 600)$. This latest distance range is not relevant to our considerations. The magnitude *MM* is the equal to the moment magnitude M_w for 5.25<M_w<7.5 and it is $= 5.25 - 0.4 \times (5.25 - M_w)$ for M_w≤5.25 and is $= 7.5 + 0.5 \times (M_w - 7.5)$ for M_w≥7.5.

The following constants were calibrated for SA_{norm} by Graizer (2016): m_1=-0.002, m_2=-0.12, m_3=3.0, t_1=0.0008, t_2=0.16, t_3=-0.4875, s_1=0.0, s_2=0.077, s_3=0.3251, a_1=0.0347, a_2=-0.5542, a_3=3.694, D_{sp}=0.75. Finally:

$$LinAmp_{Vs30} = 1 + \frac{k_{Vs30}}{\sqrt{\left(1-\frac{f_{Vs30}}{f}\right)^2 + 1.96\times\frac{f_{Vs30}}{f}}} \quad (6)$$

With, $k_{Vs30} = -0.5 \times \ln\left(\frac{V_{S30}}{2800}\right)$, and $f_{Vs30} = \frac{V_{S30}}{120} - 1.6$. For the hard-rock conditions $LinAmp_{2800} = 1$ and *f* is the calculated frequency in the spectra.

The expressions for Res(T) can be found in Grazier (2016). They were abandoned from our GMPE adaptation, so they are not reproduced here.

The formulations above show that for a high frequency in the spectra ($f \rightarrow \infty$), corresponding approximately to the PGA, we have $1/f=T \rightarrow 0$, $SA_{norm} \rightarrow 1$ and $LinAmp_{Vs30=2800}/LinAmp_{Vs30=640}=0.57534$ ($=G_4$) from Equation 2: the SA prediction (Eq. 3) for hard-rock at PGA is identical to the direct PGA prediction (Eq. 2).

Data used for adjustments of G16

We assembled the recordings of 185 Fennoscandian earthquakes ($1.5 \leq M_L \leq 4.1$). The spectra of the components (E- east-west, N- north-south, Z- vertical), the geometric mean spectra (GM) and two rotation-independent spectra (RotD50, RotD100; Boore *et al.*, 2006) were calculated. Both the GM and RotD50 spectra can be considered average components. For the final analysis, we selected 77 events of magnitude ≥2. They have 281 recordings with at least a 100-Hz sampling rate and $R_{hyp} \leq 300$ km (Table 1). Due to its Swedish epicentre, the largest earthquake (M_L4.2) has only two recordings at distances of 236 km and 271 km (with a 50-Hz sampling rate) and 100-Hz recordings at the distance of 337 km and above. These recordings were not included in the selection. To the Fennoscandian data we added the hard-rock subset of the NGA-East dataset from Canada (Table 1).

Table 1. Recordings in Fennoscandia and NGA-East spectra selected for the adjustment of the G16

Magnitude bin	No. of events (Fenno+NGA)	Depth ranges (km)	No. of Fenno recordings	No. of NGA recordings
2-2.5	56+1	1.9-36.9	147	5
2.51-3	13+7	1.5-30	59	34
3.01-3.5	7+6	7.5-36.7	60	24+12
3.51-4	0+10	11.4-30	-	32+40
4.01-4.5	1+3	5-28	15	12+7
4.51-5	0+1	13.5	-	22
5.01-6.76	0+5	6-29	-	15+14
Totals:	**110**		**281**	**217**

Formulation of the adjusted Fennoscandian G16 GMPE for PGA

For the low-magnitude events with a very small rupture area $R_{hyp} \sim R_{rup}$. The M_{cat} ~ moment magnitude (M_w). The estimated magnitude error in the dataset is ±0.2 units.

The magnitude scaling filter G1, together with the constants C_{mean} and G4, controls the level of the PGA_{2800} at small rupture distances. The original proposal in G16 is based on the *arctan* function resulting in saturation for high and slower decay

for low magnitudes. At M_w~1.2 the expression predicts non-physical PGA at R=0 km. We compare the PGA scaling of G16 with the Fennoscandian data at distances of 19-50 km (Fig 1). In addition, we plot the PGA from induced earthquakes in southern Finland, with magnitudes 1.4-1.7 recorded in the epicentre (R_{hyp}=6 km, depth 5.5…5.8 km) and from a modelled earthquake of M_w4.3 at a rupture distance of 2 km (Fig. 1). The PGA scaling of G16 appears reasonable for smaller magnitudes.

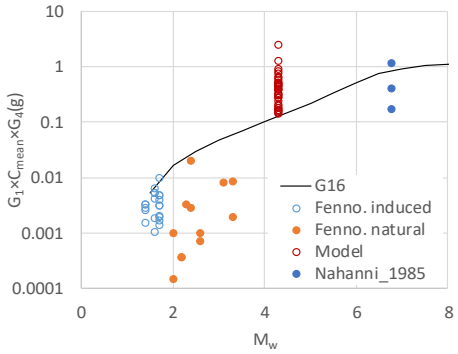

Figure 1. PGA scaling of G16 for V_{s30}=2800 m/s to the Fennoscandian datasets.

The distance attenuation factor G2 controls the extent of the PGA plateau. The plateau reduces with magnitude by the corner distance $c_4 \times M + c_5$. A threshold magnitude, M_{min}, is introduced in the $c_4 \times M + c_5$ term, preventing the decrease of the corner distance for small magnitudes, with c_4, c_5 and M_{min} calibrated against the available data.

The anelastic filter G3 is controlled by the quality factor Q_0 that describes the decay of amplitude of seismic waves with distance at 1 Hz. The G16 prediction with the original parameters including Q_0=650 is higher compared to the Fennoscandian data, the mean prediction being shifted by 0.2459 in log space (Fig. 2a). Data points up to 1000km from the national and the local OBF network are plotted. The optimal for a good mean prediction would be Q_0=991.64, with residual conforming to a log distribution with σ=0.1881 in log10 units (Fig. 2b). For compatibility with G16, we use the given Q_0 and accept a higher error.

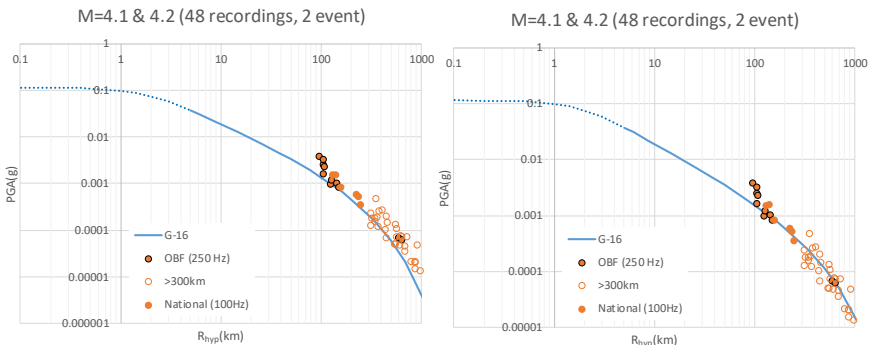

Figure 2. Comparison of the G16 prediction with Fennoscandian recordings within its validity range, using (a) the initial parameters and (b) an optimized Q_0.

Hence, the G16 PGA scaling for 2800 m/s site conditions ($G_1 \times C_{mean} \times G_4$) fits the data reasonably well. We optimize c_4=3,8648, c_5=-12,32 and M_{min}=3.3927, for a good prediction of the mean PGA of the calibration recordings. The comparisons are given in Figure 3.

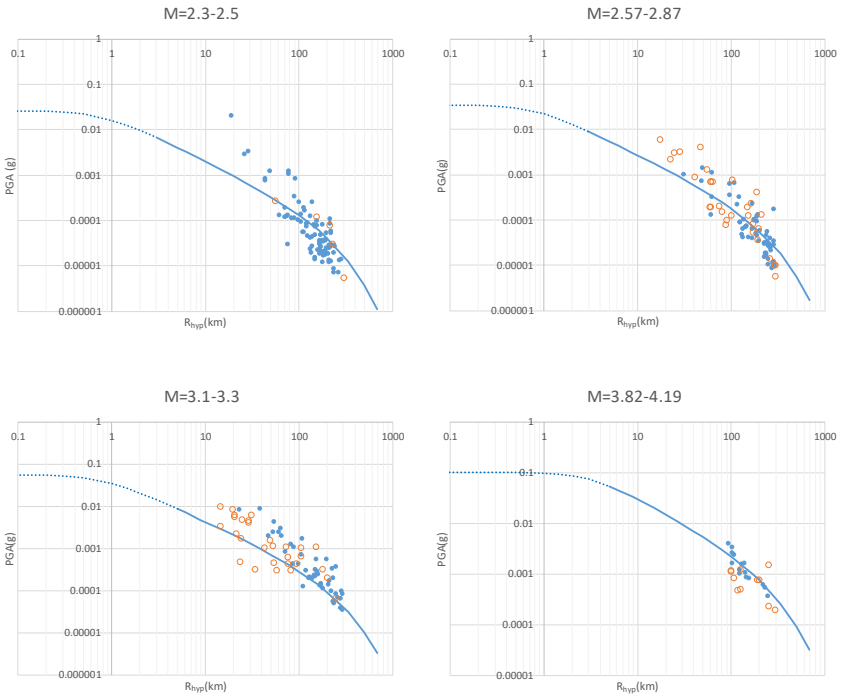

Figure 3. Comparison of the G16 prediction against the 281 calibration recordings. The blue line is the G16 prediction, the dashed segment is the part of the curve with unrealistic R_{hyp} due to focal depths.

The residuals of the prediction can be modelled as a log distribution centred on the mean prediction with σ=0.37075 in log10 units. The error is reasonable for all magnitudes and distances (Fig. 4).

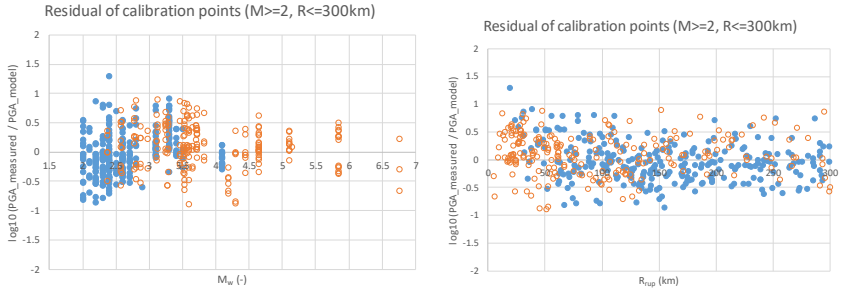

Figure 4. Distribution of the error with M_w and R_{hyp} (blue Fenno., orange NGA)

Formulation of the adjusted Fennoscandian GMPE for spectra

Separating the PGA prediction from that of the spectral shape brings some cumulative errors when PGA is multiplied with SA_{norm}. The G16 spectral shape does not fit well the Fennoscandian data if we try to keep the original residual correction term Res(T) in Eg. 4. Abandoning the residual correction for $M_w<4$ but keeping it for $M_w\geq4$ would result in an undesired discontinuity in the spectral shape at $M_w=4$.

Hence, we choose to recalibrate the spectral shape parameters for the mixed set of Fennoscandian data (Fig. 5a) and the NGA-East subset for hard rock (Fig. 5b). The bulk of the Fennoscandian data were sampled at 100 Hz, the highest at 250 Hz. Each spectrum was used up to the value of sampling frequency divided by 2.5. Some Fennoscandian spectra have a peculiar feature at 0.1 Hz-1 Hz, which we take to be artificial. Also, two Fennoscandian spectra were omitted after visual checking. The NGA-East subset consists of data with V_{s30}=2000 m/s. In addition, we included the spectra of the Nahanni earthquake of 1985-12-23 (V_{s30}=1700m/s), because of the large magnitude and short-distance recordings.

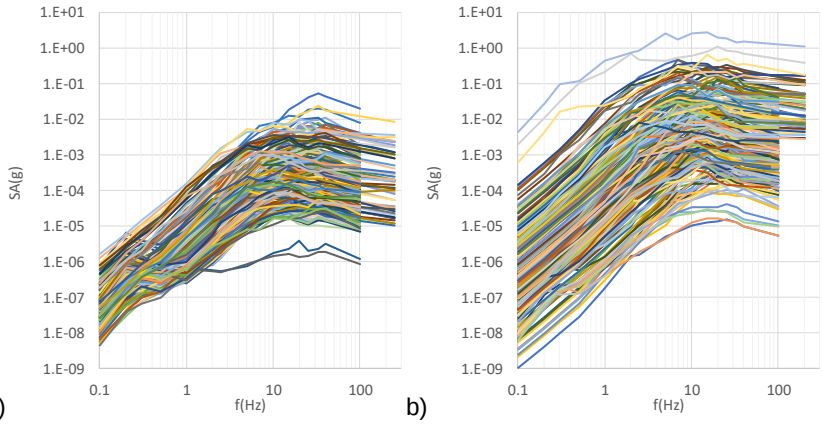

Figure 5. Acceleration spectra (RotD50) of the (a) Fennoscandian dataset and (b) NGA-East subset selected to recalibrate the normalized spectral shape (SA_{norm}).

The parameters used in G16 for controlling the spectral shape are shown in Figure 6. The amplification factor (SA_{max} / PGA) is in the range of 2-4 with mean value around 3 (6a,b). No important trend is visible with magnitude or distance. The location of the amplification peak has higher randomness (c, d). The highest frequency considered reliable is 100 Hz/2.5=40 Hz corresponding to the location of some peaks and making it unclear if the spectra peaks at 40 Hz naturally. The SA peak location frequency decreases with increasing magnitude (c), but is remarkably stable with distance (d). The slope of the spectra at low frequencies in log-log plane was calculated between 1 Hz and 2.5 Hz to eliminate the anomaly below 1 Hz (Fig. 5). The slope factor varies between 1.5-3, with a mean at about 2 (6e,f).

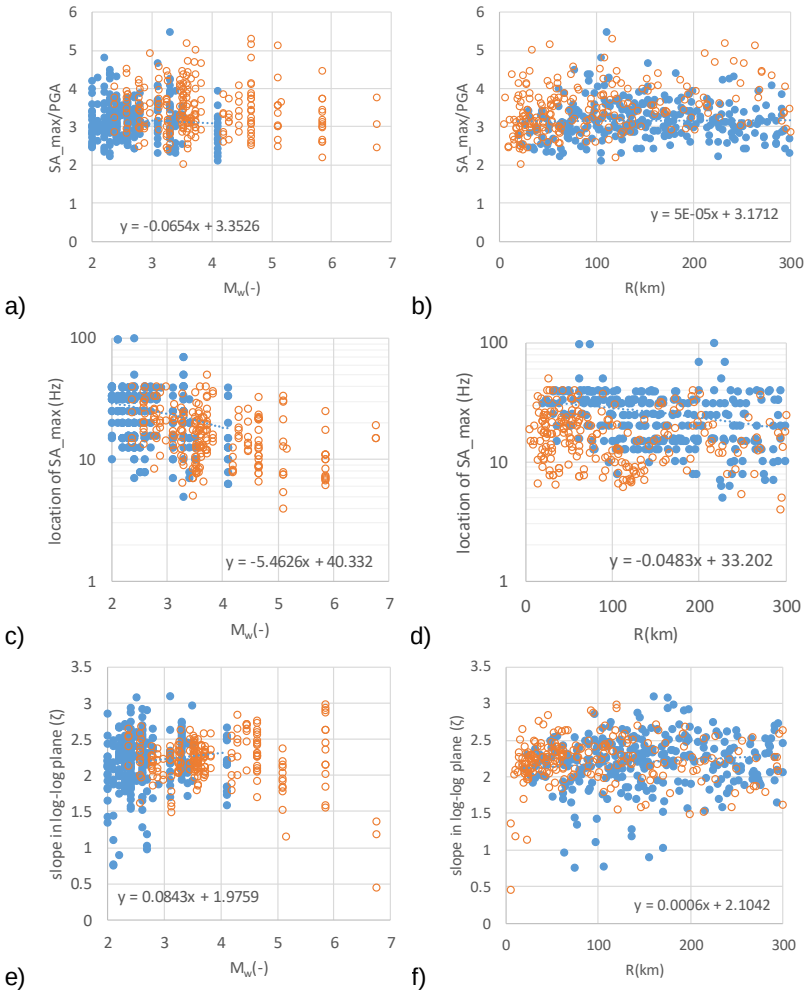

Figure 6. The main control parameters characterising the shape of the acceleration spectra of the Fennoscandian dataset (blue circles) and NGA subset (orange circles). (a,b) amplification (SA_{max}/PGA); (c,d) the frequency of the spectra peak (SA_{max}); (e,f) the slope of the spectra decreasing at lower frequencies.

Adaptation of the G16 spectral shape

MM, an adjusted magnitude in G16, influences μ and $T_{sp,0}$ that define the position of the spectral peak. *MM* also influences *S*, the breadth of the spectra. The *MM* adjusts the lower and upper extremes of the range in magnitudes.

We assessed the fit of the Fennoscandian data to the original G16 prediction using *MM* extended to M2. However, the predicted spectra peak was always located at a too low frequency, since at M_w=2 the value of *MM*=3.95 controls the position.

To adjust G16 to low magnitudes the *MM* is eliminated for $M_w \leq 5.25$. This influences somewhat the precision of G16 in the range $4 \leq M_w < 5.25$. We believe this influence is not significant, but there is no way to estimate the loss of precision. The terms summed in Eq.5 define the shape of the spectra and both μ and $T_{sp,0}$ affect it. When we extend the formulation of *MM*, and partly adjust it in the range of $4 < M_w < 5.24$ the shape of the spectra is influenced (Fig. 7).

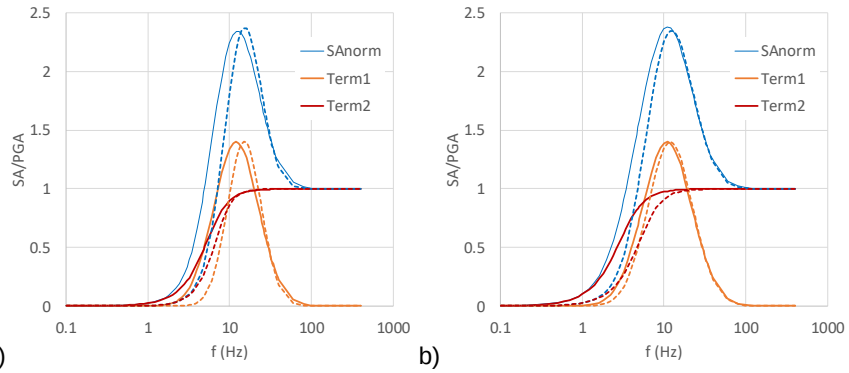

Figure 7. SA_{norm} of G16 from Eq. 5 (a) for M_w=2, RR=20 km and (b) M_w=4, RR=20 km. Continuous lines are the original values while dotted lines are the proposal.

The adaptation of SA_{norm} is achieved by redefining *MM* for low magnitudes and introducing the lower threshold for $T_{sp,0} \geq 2 \times \exp(-\mu)$. This is needed because the original formulation of $T_{sp,0}$ would break down at magnitudes lower than ~3.1 for short distances. For the parameter controlling the slope of the spectra (ξ), G16 used the polynomial function $\xi = a_1 \times {M_w}^2 + a_2 \times M_w + a_3$, with factors calibrated up to M_w4. In our case, slopes are reasonably constant for the data, with a mean of ~2.

The last element of the adaptation is to better describe the location of the spectral peak. The analysis of the spectra has shown that the peak occurs at high frequencies, even at 40 Hz. On the other hand, the peak position is not strongly correlated with magnitude or distance (Fig. 6c.d) and the spectra is characterised by a more extended plateau region (Fig. 5). Due to this plateau it might be that the we can accept less precise forecasting of the peak location, without introducing significant error in the prediction.

In the G16 formulation, the position of the spectra peak is mostly controlled by the factor $\mu = m_1 \times RR + m_2 \times MM + m_3$. We plotted the approximate position of the peak expressed by $1/\exp(-\mu)$ for selected events (Fig. 8). With the original parameters peak location is severely underestimated for smaller magnitudes.

The proposed adaptation results from the observation that the prediction of the spectral shape become worst if the LinAmp and Res(T) correction are applied in Eq. 4. If we compare the control parameters of the spectra from the Fennoscandian dataset and the NGA-East datasets subset, they are very similar. SA_{max}/PGA is in the range of about three, characterised by slight variation both with magnitude and distance. Log-log plane slope of about two. The main difference is in the location of

the peak spectral accelerations: the Fennoscandian data systematically show a higher frequency for the peak than the NGA-East subset.

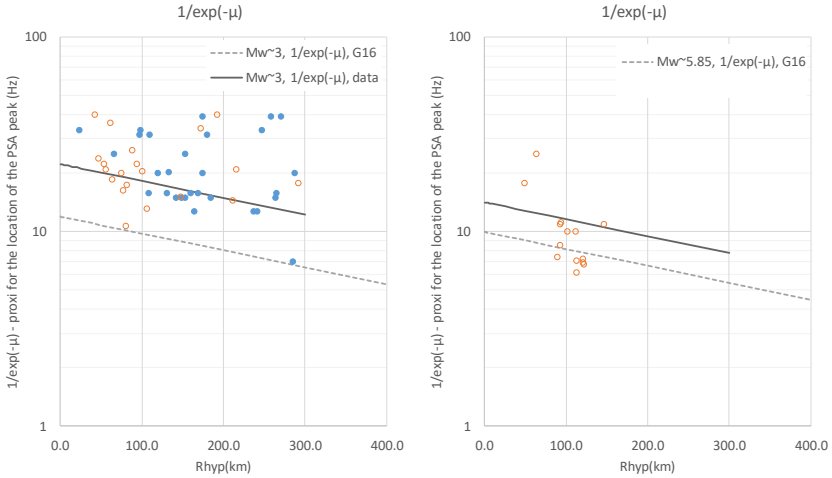

Figure 8. Position of the spectral peak in terms of frequency for selected magnitudes. The original G16 formulation, hypothetically extended to M2 is the lighter grey line. The Fennoscandian values are full circles, the NGA values orange circles. The proposal formulation follows the dark grey line.

We formulate the prediction for spectral shape using the combined set of spectra. We obtained a prediction with the mean residual ($Res=PSA_{prediction}/PSA_{data}$) shown in Table 2. The adapted version of G16 follows the spectra in the range 0.1-40 Hz. We fitted normal distribution to log10(*Res*) for each frequency. Within the range of 1-40 Hz, the largest value is 0.37 gradually decreasing for higher frequencies. The increasing errors below 1 Hz are not relevant (Fig. 5). Examples of the spectral shapes and the predicted spectra for Fennoscandia and Canada are shown in Figure 9. The cumulative errors of the PGA and SA prediction are given in Table 3.

Table 2. Median of *Res* and standard deviation of log10(*Res*) of the spectra prediction for the proposed adaptation of G16

0.1	**0.3**	**0.5**	**1**	**2**	**5**	**10**	**15**	**20**	**25**	**33.3**	**40**
-0.28	-0.35	-0.10	0.006	-0.04	-0.03	0.07	0.08	0.07	0.04	-0.05	-0.07
0.61	0.66	0.45	0.35	0.35	0.29	0.20	0.15	0.13	0.13	0.14	0.16

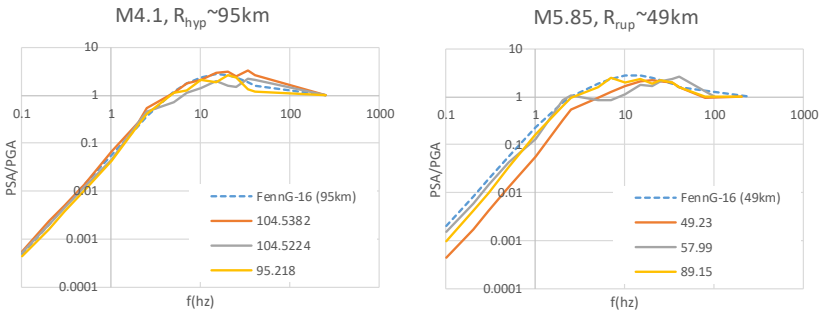

Figure 9. Comparison with selected spectra for the a) Gulf of Bothnia event of 2016-03-19 depth=23.5km and b) NGA-East Saguenay of 1988-11-25.

Table 3. Mean residual and standard deviation of log10(Res) the log10 scale of the proposed adaptation of G16

0.1	0.3	0.5	1	2	5	10	15	20	25	33.3	40
-0.31	-0.38	-0.13	-0.02	-0.07	-0.06	0.04	0.05	0.04	0.005	-0.09	-0.12
0.53	0.55	0.37	0.34	0.34	0.34	0.34	0.36	0.38	0.39	0.37	0.37

Conclusions

We propose an adaptation of the G16 GMPE by Graizer (2016) for Fennoscandia, synthetically presented in Table 4.

Table 4. List of proposed adaptations for G16

Original G16	Proposed adaptation
$SA(T)_{cor,2800} = PGA_{G16} \times SA_{norm} \times \frac{LinAmp_{Vs30=2800}}{LinAmp_{Vs30=640}} \times \frac{1}{Res(T)}$	$SA(T)_{FennG16} = PGA_{Fenn-G16} \times SA_{norm}$, SA_{norm} has identical formulation, but: $I = 1.8186$
$MM = \begin{cases} 5.25 - 0.4 \cdot (5.25 - M_w), M_w \leq 5.25 \\ M_w, 5.25 < M_w < 7.5 \\ 7.5 + 0.5 \cdot (M_w - 7.5), M_w \geq 7.5 \end{cases}$	$MM = \begin{cases} M_w, M_w < 7.5 \\ 7.5 + 0.5 \cdot (M_w - 7.5), M_w \geq 7.5 \end{cases}$
$\xi = a_1 \times {M_w}^3 + a_2 \times M_w + a_3$	$\xi = 2.05$
$T_{sp,0} = t_1 \times RR + t_2 \times MM + t_3$	$T_{sp,0} = \max(t_1 \times RR + t_2 \times MM + t_3, T_{sp,0,max})$ $T_{sp,0,max} = 2 \cdot \exp(-\mu)$
$\mu = m_1 \times RR + m_2 \times MM + m_3$	$\mu = m_1 \times RR + (-0.1584) \times MM + 3.5756$
LinAmp correction in Eq. 4	Eliminated
Residual correction in Eq. 4	Eliminated

It follows the original G16 philosophy by separating the PGA and the spectral shape (SA_{norm}) predictions. The cumulative error is reasonable (Table 3). We prefer to keep the PGA and SA_{norm} separated and the GMPE modular, because the SA_{norm} prediction is remarkably good.

There are two additional outcomes of this investigation. Firstly, we show that the Fennoscandian and NGA-East (mostly Canadian) spectra on hard rock are largely compatible. This is proof on this scale for the first time. We also show that two sets of spectra differ the most in the position of the spectral peak: Fennoscandian spectra peak at a higher frequency.

Secondly, we show that a remarkably good prediction can be achieved for the standard spectra (SA_{norm}), for very hard-rock sites and for the distance range of interest in Finland. This eliminates the need to predict the spectral amplitude at independent frequencies, removing some of the difficulties there were with Fennoscandian spectra at the low frequency ranges.

As a continuation of this study, we plan to compare the result with other GMPE formulations used in Finnish PSHA studies (Varpasuo *et al.* 2001, Vuorinen, 2015). We also intend to develop this GMPE proposal by re-thinking the PGA prediction.

References

Boore, D.M., Watson-Lamprey, J., Abrahamson, N.A., 2006. Orientation-independent measures of ground motion. Bulletin of the Seismological Society of America 96, 1502–1511. https://doi.org/10.1785/0120050209

Fülöp, L., Jussila, V., Lund, B., Fälth, B., Voss, P., Puttonen, J., Saari, J., Heikkinen, P., 2017. Modelling as a tool to augment ground motion data in regions of diffuse seismicity - Final report. NKS Nordic Nuclear Safety Research.

Goulet, C., Kishida, T., Ancheta, T., Cramer, C., Darragh, R., Silva, W., Hashash, Y., Harmon, J., Stewart, J., Wooddell, K. Youngs, R., 2014, PEER NGA-East Database, PEER 2014/17, Pacific Earthquake Engineering Research Center, Berkeley

Graizer, V., 2016. Ground-Motion Prediction Equations for Central and Eastern North America. Bulletin of the Seismological Society of America 106, 1600–1612. https://doi.org/10.1785/0120150374

Varpasuo, P., Saari, J., Nikkari, Y., 2001. Seismic Hazard and Ground Motion for Leningrad NPP site, in: ResearchGate. Presented at the Transactions of the 16th International Conference on Structural Mechanics in Reactor Technology (SMiRT16), Washington DC, USA.

Vuorinen, T., 2015. New Fennoscandian Empirical Ground Motion Characterization Models. MSc thesis, Department of Physics, University of Helsinki, Helsinki, Finland.

7. Research Infrastructure

7.1 Barsebäck RPV material used for true evaluation of embrittlement (BRUTE)

Ehrnstén, Ulla[1], Lindqvist, Sebastian[1], Tähtinen, Seppo[1], Pentti Arffman[1], Jari Lydman[1], Boåsen, Magnus[2]

[1]VTT Technical Research Centre of Finland Ltd
P.O. Box 1000, FI-02044 Espoo

[2]Royal Institute of Technology (KTH), Department of Solid Mechanics,
SE-100 44 Stockholm Sweden

Abstract

The BRUTE project has two corner stones, i.e. 1) pioneering the new hot cell infrastructure at the Centre for Nuclear Safety, VTT and 2) performing mechanical testing and microstructural investigations of Barsebäck 2 reactor pressure vessel (RPV) material. BRUTE is part of a larger entity, the Barsebäck REsearch&Development Arena, BREDA. BRUTE started in 2018 with preparatory work for mechanical testing and microstructural investigations, which will be performed in the SAFIR2022 BRUTE project. One of the main objectives of the BREDA and BRUTE projects is to investigate the correlation between fracture toughness properties of the RPV and the surveillance specimens.

In the BREDA project, cylindrical trepans á ~40 kg, with a diameter of ~200 mm were extracted from B2 RPV beltline welds, subjected to a neutron irradiation, as well as RPV head welds, which are not subjected to irradiation, but to thermal loading. In BRUTE2018, the rationale for the investigations were fine-tuned, plans for microstructural investigations were made and a preliminary test matrix, comprising of more than 1500 mechanical test specimens was developed.

Qualification and verification of test methods is of very high importance to obtain reliable results with small scatter. Most of the selected testing techniques for mechanical tests and microstructural investigation were validated using the new infrastructure, in co-operation with the SAFIR2018 RADLAB project.

The seminar “Reactor pressure vessel embrittlement seminar for the BREDA - BRUTE project” gathered >30 participants from Finland and Sweden, and the state the art was presented, and launched the formation of a Nordic knowledge pool on RPV embrittlement including three doctoral students in three different universities.

Introduction

Ensuring safe operation and the durability of the reactor pressure vessel (RPV) is one of the most important tasks for nuclear power plants (NPP's). Neutron irradiation cause embrittlement of the RPV materials, which affect the mechanical properties of the materials. The effect is typically more pronounced for the weld metal compared to the base material. The embrittlement is monitored through a surveillance program, in which mechanical test specimens are placed in the reactor (inside the RPV) at a position with higher dose rate, i.e., with a lead factor, than the pressure vessel. A prognosis of the RPV behaviour is made based on the mechanical test results obtained from these specimens. The prognosis is one of the key elements for the operation license.

A unique opportunity to determine the mechanical and microstructural characteristics of material removed from the decommissioned Barsebäck 2 (B2) RPV opened with the launch of the BREDA project. In the Nordic nuclear power plant (NPP) fleet the NPPs B1-2, O2-3, R3-4, F1-3 and Ol1-2 have RPV´s that are manufactured by the same supplier, Uddcomb. A high Ni weld metal is used for the welds. Material from the surveillance programme, as well as material, irradiated to a level corresponding to more than 60 year life-time of a boiling water reactor (BWR) and corresponding to typical fluence of a pressurised water reactor (PWR) is also available, as is data from surveillance programs and other testing campaigns. One of the main objectives of the BREDA and BRUTE projects is to investigate the correlation between fracture toughness properties of the RPV and the surveillance specimens.

The new CNS hot cells were installed in 2017 and granted approval for operation by STUK in spring 2018. The SAFIR 2012 RADLAB and SAFIR2018 REHOT projects managed the development, installation and functionality testing of the infrastructure, and this continues in the SAFIR2022 LABWAST project and in VTT-funded projects. The new infrastructure, with versatile equipment for mechanical testing and microstructural investigations, is pioneered in the BRUTE project. Qualification and validation of all test methods to be used in BRUTE is mandatory to ensure reliable and high-quality results, and is a main objective for BRUTE2018. Another objective is to fine-tune the rationale for all investigations, plan all investigations including developing a test matrix for the mechanical tests.

Mechanical tests on unirradiated B2 reference material has been performed in the SAFIR2018 LOST project, and subjected to microstructural investigations in the SAFIR2018 THELMA project. This has given important basis information on the B2 base material and weld metal.

Objectives of the BREDA - BRUTE project

The main part of the investigations on the B2 material will be performed in the SAFIR2022 BRUTE project. To enable a better understanding of the objectives for the work done in BRUTE2018, the objectives of the BREDA and BRUTE projects

are shortly summarised below. The main objectives of the BREDA project are (Boåsen, 2017):

- Investigating the comparability between the fracture toughness properties of the RPV and the surveillance test specimens.
- Understanding the effect of flux and fluence on the shift in ductile-to-brittle (DBTT) transition temperature.
- Understanding the effect of irradiation embrittlement on the fracture mechanical crack tip constraint.
- Identifying the factors affecting the fracture toughness properties in thickness direction.
- Determining the shift in DBTT due to thermal embrittlement versus the shift due to the combined effect of thermal embrittlement and irradiation.

These BREDA objectives govern the mechanical tests and microstructural investigations in the BRUTE project. All methods used in BRUTE need to be verified and practised before using them on B2 material and this was a main objective for BRUTE2018. Another main objective is to fine-tune the rationale for the investigations. BRUTE has also the objective of building a Nordic network and knowledge cluster for RPV embrittlement issues, and to educate new experts.

Materials

Totally fourteen (14) trepans have been removed from the B2 RPV as part of the BREDA project, Figure 1. The RPV is made from plates, and contain thus both horizontal and vertical welds, and trepans were cut from both weld types, and additionally from the RPV head. Four trepans from the beltline region and four from the RPV head region will be transported to CNS for investigations, after the inner surface stainless steel cladding has been removed at the Ringhals plant. The whole cutting including preparation and execution is in-kind work to BRUTE.

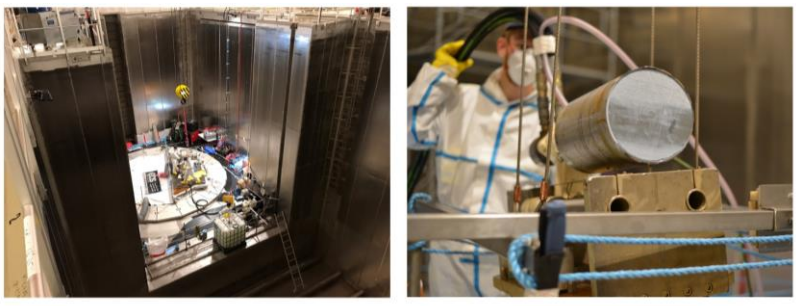

Figure 1. Pictures from the cutting of the trepans at the B2 plant. A drilled trepan from the non-irradiated RPV head is seen on the right-hand side inside the drill.

Three types of materials are investigated, i.e., B2 trepans, surveillance material and material, which has been irradiated in an accelerated manner to high fluence, mimicking more than 300 years of BWR operation. This fluence is in the same order of magnitude as the fluence PWR RPVs achieve during normal operation.

The B2 RPV is manufactured from plates made from SA 533 Gr B Cl. 1 material and welded using a high Ni-weld metal, Table 1.

Table 1. Chemical composition of B2 weld metal (wt-%).

C	Si	Mn	P	S	Cr	Mo	Ni	Cu	Co
0.084	0.22	1.53	0.011	0.004	0.13	0.45	1.47	0.064	0.008

The diameter of the trepans is 197 mm, and the thickness vary between about 70 and 130 mm, depending on the location of the trepan. All trepans are through wall, but the wall thickness is smaller at the RPV head compared to the beltline region. A trepan from the beltline region weigh about 40 kg.

The RPV weld is an X-weld, which has been welded from both sides of the RPV wall, Figure 2. The diameter of the trepan is much larger than the width of the weld, but when cutting is done in plant conditions, it is necessary to have a good margin ascertain that the weld is fully embodied in the trepan. The other two materials are in the form of 10x10x55 mm normal size Charpy V notch specimens, Figure 3, three from the surveillance program and three from the accelerated irradiation campaign. Miniature compact tension C(T) specimens will be used for mechanical testing, enabling up to twelve C(T) specimen from each ChV specimen.

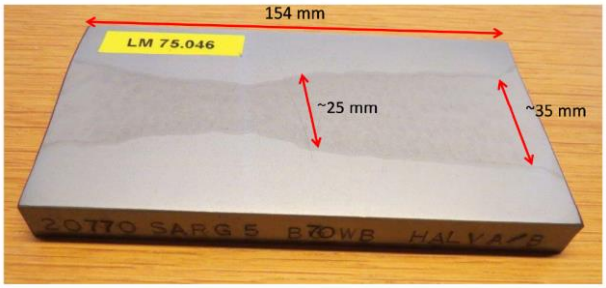

Figure 2. A macrograph of a weld specimen showing the size and shape of the X-weld in the B2 RPV (Boåsen, 2017).

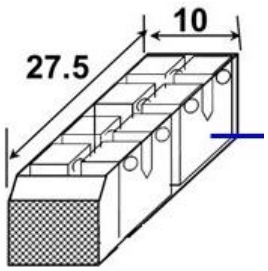

Figure 3. Schematic picture of one half of a 10x10x55 mm Charpy V notch specimen, from which miniature C(T) specimens are cut for mechanical testing (Boåsen, 2019).

Preparatory work for handling trepans

The size of the trepans exceed the design basis for the hot cells, and therefore an evaluation was made on whether full trepans can be accepted and handled at CNS. Dummy trepans, i.e., shaft pieces with similar dimensions as the trepans were purchased, and their handling using magnetic lifters was tested in the reception cell and in the Electric Discharge Machine (EDM) cell. Figure 4 shows a dummy trepan being handled using a magnetic lifter in the reception cell, where the first steps of handling are done. The trials were successful.

The second step is handling of the trepans in the EDM cell. The design of CNS relies on cutting using EDM, which is an accurate and versatile cutting method. However, the large weight of the trepans require a special jig for moving the trepan on the EDM working table. The jig was designed, manufactured, assembled and functionality tested, Figure 5. The performance of the jig is good, and the decision was made to accept full trepans at CNS.

Localisation of the weld in the trepans with high accuracy is important to assure that precise cutting plans can be made resulting in mechanical test specimens and specimens for microstructural characterisation from intended locations. The stainless steel cladding on the inner surface of the trepans is removed by Ringhals Ab at the Ringhals site. This will reduce the activity of the trepans remarkably. Preliminary trials at Ringhals indicate that the weld can be made clearly visible by etching the trepan, facilitating marking of the weld location before transportation to CNS. Plans for a second option were developed in BRUTE2018, i.e., etching of the trepans at CNS.

Numerous additional preparatory actions where undertaken in BRUTE2018, including evaluation of the surface quality needed for hardness measurements (Ehrnstén, 2018), procurement of equipment for microstructural characterisation, training using the equipment etc. This work will continue in 2019.

Figure 4. Testing manoeuvrability of a 40 kg dummy trepan as part of the evaluation if full trepans can be used for the investigations. The trials were successful.

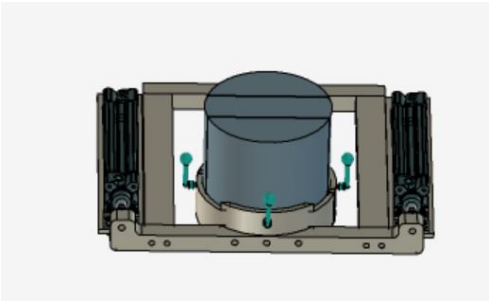

Figure 5. Jig for moving the trepan under the EDM wire. The weld is in the mid-part of the trepan.

Mechanical testing

A report reviewing the methods associated with the planned fracture mechanical testing of the B2 material was written, including the procedure for validation of the C(T) testing using miniature C(T) specimens (Planman, 2018). The steps described in the report have been applied in BRUTE2018.

A report on a preliminary test matrix was written based on BREDA plans, additional discussions with stakeholders and key experts as well as modelling (Boåsen, 2019). The word preliminary is used to highlight the possible need for adjustments of the test matrix based on first results. The performed modelling of the constraint

effect in different types of specimens, as part of the doctoral thesis by M. Boåsen, KTH, and the results are utilised in BRUTE. The matrix comprise of miniature C(T) and single edge notched SE(B) specimen for cleavage, ductile fracture and constraint testing, Charpy-V notch specimens for impact testing, tensile specimens for mechanical properties determination in addition to slide-slabs for hardness and microstructural investigation. More than 1500 specimens can be manufactured from the trepans alone, and prioritisation is needed to optimise the available material and resources.

Most of the mechanical test methods have been validated in co-operation with the RADLAB project, and this work will be finalised in BRUTE2019.

A key issue in the current test matrix is to gain insight into the similarity between the surveillance program and the B2 RPV. Specimens are removed from the same depth of the RPV as the surveillance specimens. Improved insight in the correlation between impact and fracture toughness test results is also a foreseen result.

Cleavage or brittle fracture is a key issue in the assessment of RPV-integrity. The reference temperature, T_0, which characterizes the fracture toughness of ferritic steels in the ductile-to-brittle transition region will be determined using miniature C(T) specimens. The T_0 temperature increase with increasing fluence, as depicted in Figure 6, and assuring a margin between the minimum temperature during operation and T_0 is a key issue. Miniature C(T) specimen testing technique has been developed to meet the challenge that many power plants encounter when planning for life extension, connected to a need to utilise existing material as efficient as possible. The method facilitates testing of up to 12 specimens from one standard 10x10x55 mm Charpy V notch specimen. The testing is in BRUTE done on specimens from different depth of the RPV wall, thereby giving data as a function of fluence.

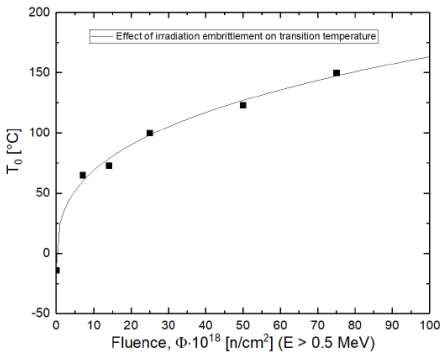

Figure 6. Example of T_0 as function of fluence for a RPV steel (Lindqvist, 2018).

Constraint describes the concentration of stresses or deformation at a crack tip and this is dependent on the configuration, as schematically shown in Figure 7. A large component such as a RPV has a low constraint, while the specimens used for determination of the properties have larger constraint. The effect of constraint is determined using SEN(B) specimens with different crack sizes both for thermally aged and irradiated material.

Ductile fracture testing is planned to determine the fracture resistance curve, J-R curve and fracture toughness at ductile fracture onset, J_{IC}.

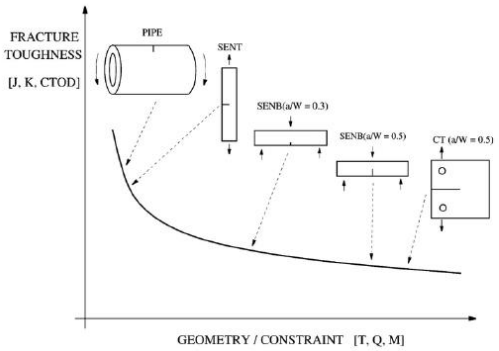

Figure 7. Schematic picture showing the effect of constraint on the fracture toughness in different specimens and components (Boåsen, 2018).

Microstructural characterisation

The microstructural characterisation comprise of hardness measurements, fractographic investigations of the test specimens and microstructural investigations of the weld metal and of mechanical test specimens (Lydman, 2018). All investigations are done from macro- to microscale. Atomic scale investigations are done at Chalmers University as part of the BREDA project using Atom Probe Tomography, APT.

One objective of the microstructural investigations is to explore possible reasons for observed scatter in mechanical test results. Investigations performed on non-irradiated, reference B2 material (SAFIR2018 THELMA, Lydman, 2019) is used as basis for the investigation in BRUTE. The results show that initiation mainly occur at secondary particles, that larger particles is correlated with lower fracture toughness and that initiation seem to favour the re-heated microstructure of the weld, Figure 8.

Atom probe investigations show that both thermal ageing and irradiation cause formation of cluster, which increase the hardness and decrease in the fracture toughness. The clusters have, though, different characteristics (Lindgren, 2018). This observation is very important for BRUTE. As the change in fracture toughness properties may be small due to the rather low fluence in the B2 RPV, it is important to be able to distinguish between the effects from thermal ageing and those from irradiation.

Hardness measurements are performed through wall, and give information about macroscopical (mechanical) changes from the attenuation of fluence through the RPV wall, and on a local scale on changes from microstructural features.

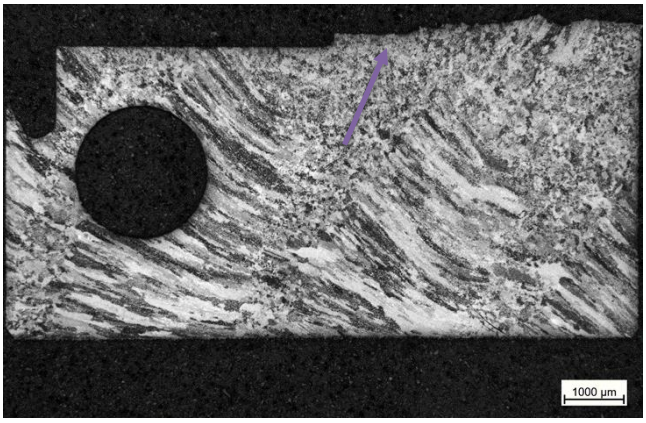

Figure 8. Micrograph of a cross-section from a miniature C(T) specimen made of un-irradiated B2 material. The primary initiation site is in the reheated weld metal (Lydman, 2018).

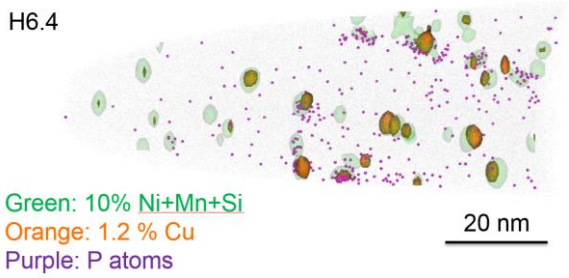

Figure 8. Clusters in high Ni weld metal as analysed using APT. (Lindgren, 2018).

Summary and conclusions

BRUTE2018 focussed on preparatory work for mechanical and microstructural investigations on B2 material, including unique trepan material from the reactor pressure vessel. The work continues in SAFIR2022 BRUTE and in BREDA. BRUTE is a part of a large entity with the goal of comparing surveillance data to data from a real pressure vessel. To confirm the correlation is highly important. The other main objective is pioneering the CNS hot cell infrastructure.

The preparatory work comprised fine-tuning the rationale for the investigations to meet the set goals, and on planning and verification of mechanical tests and microstructural methods to be used. Training to use new equipment, learning from this, and taking the lessons learned into account in the subsequent further development of the methods has highlighted the amount of details connected to each method. A seamless co-operation with RADLAB, LOST and THELMA has been essential to accomplish the set objectives.

Acknowledgement

The Swedish and Finnish stakeholders are acknowledged for launching the BREDA project under the leadership of Energiforsk, and for making the B2 RPV and other materials available to BRUTE. MEAE is acknowledged for support to BRUTE in the form of a letter of intent. The funding from VTT, VYR and NKS is highly appreciated.

References

Boåsen, M. et al. Underlag för materialuttag ur Barsebäck 2. Bilaga 2 till BREDA projekt plan, 2017. 12 p.

Boåsen, M. Ageing and constraint effects of low alloy steels. BRUTE seminar presentation, 31.10.2018, CNS,VTT, 32 p.

Boåsen, M. et al. Preliminary mechanical test matrix for the BREDA/NRUTE project. VTT Research Report VTT-R-06849-18, 10.01.2019, 24 p.

Ehrnstén, U. Evaluation of surface requirement for hardness measurements in BRUTE. VTT Research Report VTT-R-06879-18, 12.12.2018, 13 p.

Lindgren, K. *Effects of Irradiation and Thermal Ageing on the nanoscale chemistry of steel welds.* Chalmers University Doctoral thesis, ISBN 978-91-7597-825-3, No 4506, 2018.

Lindqvist, S. Effect of constraint on fracture toughness and size effects for fracture. BRUTE seminar presentation, 31.10.2018, CNS, VTT. 24 p.

Lydman, J. Characterisation plan for Barsebäck 2 trepan – BRUTE 2018 deliverable 2.1. VTT Research report VTT R-01423-18, 6.4.2018, 19 p.

Lydman, J. Microstructural characterization of non-irradiated Barsebäck RPV base material and weld metal. VTT-R-05125-18, 11.1.2019, 155 p.

Planman, T. Background and overview of mechanical testing methods to be used in BREDA. VTT Research Report VTT-R-02227-18, 25.5.2018, 13 p.

7.2 JHR Collaboration & Melodie follow-up (JHR)

Ville Tulkki[1], Caitlin Huotilainen[1], Santtu Huotilainen[1], Petri Kinnunen[1]

[1]VTT Technical Research Centre of Finland Ltd
P.O. Box 1000, FI-02044 Espoo

Abstract

Jules Horowitz Reactor (JHR), a new European material testing reactor (MTR), is currently under construction at CEA Cadarache research centre in France. The JHR consortium has set up three working groups (WG) to determine experimental needs and plan future experiments. After gathering information on the topics of interest for the first experiments from the JHR consortium members, and creating the ranking grids for the selection of the topics, the WGs agreed on fuel and material irradiation experiments, which would become the first experiments planned and performed by the international JHR consortium. The position paper, which describes these pre-JHR experiments proposed by the WGs, was drafted and delivered to the JHR governing board in 2016, with preparatory work on-going afterwards. The Melodie, Mechanical Loading Device for Irradiation Experiments, delivered to CEA in 2012 as a part of the Finnish in-kind contribution to the international JHR project, is a device for the study of the irradiation creep of a Zircaloy-4 fuel cladding tube specimen. The instrumented test device has the capability to control the biaxial loading and to measure the biaxial strain of the specimen online. The Melodie in-core experiment started in May 2015 and lasted for six reactor cycles. The LVDT5, measuring the axial strain, produced consistent low-noise data in just one week, making it possible to analyse the value of the axial creep strain. The behaviour of the loading frame, the gas management system and the data acquisition system was reliable throughout the experiment, which indicates the potential of the technology considering future experiments.

Introduction

Jules Horowitz Reactor (JHR), a new European material testing reactor (MTR), is currently under construction at CEA Cadarache research centre in France. Finland is participating in the construction with a 2 % in-kind contribution, which includes Underwater Gamma spectrometry and X-ray radiography (UGXR) and Hot-cell Gamma spectrometry and X-ray radiography (HGXR) systems as well as a Mechanical Loading Device for Irradiation Experiments (MeLoDIE). With this in-kind contribution, Finland will have the possibility of utilising the new JHR research infrastructure dedicated to nuclear safety related research. Furthermore, the in-kind contribution enables access to the results of the future experiments.

JHR will offer modern irradiation experimental capabilities to study material & fuel behaviour under irradiation. JHR will be a flexible experimental infrastructure to meet industrial and public needs within the European Union related to present and future Nuclear Power Reactors. JHR is designed to provide a high neutron flux (twice as large as the maximum available today in MTRs), to run highly instrumented experiments to support advanced modelling giving prediction beyond experimental points, and to operate experimental devices giving environmental conditions such as pressure, temperature, flux, and coolant chemistry relevant for example for water reactors, for gas cooled thermal or fast reactors, and for sodium fast reactors. These objectives require representative tests of structural materials and fuel components, as well as in-depth investigations with separate-effect experiments, coupled with advanced modelling.

According to the consortium agreement, JHR is aimed to become an international user facility with the model of the Halden Reactor Project with multinational projects and proprietary experiments. Consequently, CEA is preparing, with the support of the OECD/NEA, a joint programme, which has the strategic scope to address fuel and material issues of common interest that are key for operating and future NPPs (mainly focused on LWR).

The JHR consortium has set up three working groups (WG) to determine experimental needs and plan future experiments. To have our national interests brought forward and to be able to follow and participate in the planning of the experiments, VTT has named participants to each of the three WGs. The WGs hold meetings twice a year, and in spring an annual JHR Technical Seminar is held, where the outcomes of the WG meetings and the progress of in-kind work are presented.

The Melodie, Mechanical Loading Device for Irradiation Experiments, was delivered to CEA in 2012 as a part of the Finnish in-kind contribution to the international Jules Horowitz Reactor (JHR) construction project. It is a device for the study of the irradiation creep of a Zircaloy-4 fuel cladding tube specimen. The instrumented test device has the capability to control the biaxial loading and to measure the biaxial strain of the specimen online.

After the delivery of the Melodie sample holder, the experimental setup was completed with the addition of a glove box containing a gas management system and a safety box to allow the independent operation of the setup. After some modifications and extensive preliminary testing, the experimental setup was finally ready to be transferred to the Osiris reactor building in the end of March 2015.

The in-core experiment was started on 7 May, 2015. With the final shutdown of the Osiris reactor taking place at the end of 2015, a total of six reactor cycles of irradiation were planned for Melodie. Because of the definitive time limit, some of the original experimental objectives had to be condensed or omitted. However, the main objectives were retained.

JHR collaboration progress

The planning of the future experiments in JHR has been launched within three working groups (WG), namely Fuel WG (FWG), Materials WG (MWG), and Technology WG (TWG). The objective of these working groups is to advise the Governing Board (GB) on potential scientific topics of interest for future R&D programs in JHR, through proposal of joint international programs or multi-lateral programs. This is done by determining experimental needs, planning future experiments, and developing experimental devices and infrastructure. Some of the experimental devices are based on existing technologies, but also new types of devices are being developed, extending the experimental capabilities and bringing new information on the subjects studied.

To fulfil the objective set for the WGs, the participants have identified open issues in the field of nuclear fuel and nuclear materials development and qualification, elaborated shared criteria to define the ranking grids to identify issues of common interests for participants taking into account their potential scientific and/or industrial interests, assessed the grid and selected a first set of potential joint or multilateral experiments in JHR, with special attention to programs which could fulfil the needs of both FWG and MWG. Furthermore, the WGs have defined initial technical specifications for the first experimental program (irradiation and PIE), and considered the feasibility of these first programs, in particular the possible role of existing MTRs associated with hot labs as support for qualification and/or benchmarking experiments and the added value offered by the JHR.

Another outcome of the WG meetings was to investigate the opportunity to define an experimental program of common interest to be eventually performed within one of the operating research reactors according to the priorities set by the WGs and with regard to the preparation of future irradiation programs in JHR. In addition to the scientific and technical aspects, such consensus on JHR validation/qualification experiments will enhance the way of working together within the consortium as well as the preparation of being efficient together once the JHR is in operation.

In 2016, the specifications for potential first experimental campaigns were formulated. The goal of the structural materials experiment formulated then was to study the effect of the neutron spectrum on the irradiation damage production and the mechanical behaviour of the material. Therefore, it was planned to irradiate specimens in two different spectra to same doses. The material selected for the irradiation experiment was decided to be stainless steel, but a more specific selection of the material was not made. It was pointed out that the specimens must all be from the same material heat, and in addition to the specimens prepared for the irradiation experiment also non-irradiated specimens must be available for comparison in the post-irradiation examination. For the fuel experiment, a power transient or ramp experiment had been determined to be the most appropriate type of an experiment, given the experimental devices available in the start-up of JHR. A twin experiment with sibling rods to demonstrate JHR capabilities was considered to be of both technical and scientific value. First sibling rod would be irradiated in BR2 and second in JHR. The test would be a stepwise ramp experiment to a very high power in order

to observe the fuel microstructural changes while at the same time ensuring the integrity of the fuel rod. For reference, the xM3 experiment performed at Studsvik R2 reactor in 2005 had experienced central melting of the fuel while maintaining rod integrity.

In the second WG meeting of 2016, which was organised by SCK.CEN in Mol, Belgium, the participants discussed the FIJHOP (Foundation for future International Jules HOrowitz experimental Programs) project proposal submitted in the H2020 October call. The main general objective of the 5-year project, with a total of 20 partners including the 12 JHR consortium members, is to prepare for the future joint international experimental programs performed in JHR by utilising the existing European material testing reactors (MTR), namely BR2, HFR and LVR-15 reactors. The FIJHOP project would essentially include the pre-JHR experiments initially discussed in the previous WG meeting.

FIJHOP proposal was submitted to EC Horizon2020 call in 2016, however it did not receive funding. The planning for experimental campaign continued based on the initial plan for FIJHOP. Eventually, fuel and materials experiments were separated, with materials experiments being arranged in a in-kind work supported by DINAMIC proposal to H2020 in 2018 (not funded) and fuel proposal turning into a CEA/SCK.CEN/EdF proposal for OECD/NEA joint program P2M to kickstart international collaboration after Halden reactor shutdown in summer 2018.

Results of the JHR collaboration

The synthesis document describing the work carried out by the WGs and the objectives for the future was distributed to the WGs for review in mid-December 2015. After a review round, a revised version of the document was delivered by the WGs to the JHR governing board in early 2016.

After gathering the information about the potential topics of interest for the first experiments from the JHR consortium members, and subsequently creating the ranking grids for the evaluation and selection of the topics, the WGs agreed on a fuel irradiation experiment and a material irradiation experiment, which wouold become the first experiments planned and performed by the international JHR consortium. The position paper, which describes these pre-JHR experiments proposed by the WGs, was drafted and delivered to the governing board in 2016.

Based on the work carried out by the WGs and described in the synthesis document and the position paper, a project proposal was drafted during the summer 2016 and submitted to the European Commission H2020 October call on the 5th of October 2016. While FIJHOP was not funded the planning for experimental campaign continued based on the initial plan. Eventually, fuel and materials experiments were separated, with materials experiments being arranged in a in-kind work supported by DINAMIC proposal to H2020 in 2018 (not funded) and fuel proposal turning into a CEA/SCK.CEN/EdF proposal for OECD/NEA joint program P2M to kickstart international collaboration after Halden reactor shutdown in summer 2018.

Melodie follow-up

The Melodie, Mechanical Loading Device for Irradiation Experiments, was delivered to CEA in 2012 as a part of the Finnish in-kind contribution to the international Jules Horowitz Reactor (JHR) construction project. It is a device for the study of the irradiation creep of a Zircaloy-4 fuel cladding tube specimen. The instrumented test device has the capability to control the biaxial loading and to measure the biaxial strain of the specimen online.

The Melodie experimental setup includes a sample holder, a Chouca irradiation capsule, a glove box containing a gas management system and a safety box for the sample holder, another glove box for the Chouca capsule, above-water lines and underwater lines for connecting the pneumatic and electrical lines between the glove box and the sample holder, and a Moog standalone servo controller for the control of the experimental pneumatic lines and for data acquisition.

The upper part of the Melodie sample holder, with the interface to the Chouca capsule and to the underwater lines, was manufactured by Soterem (Toulouse, France) according to the French RCC-MX nuclear construction code. The Chouca capsule is a material irradiation device used by CEA in the Osiris reactor. It has a double wall tube structure with electrical heaters on the level of the reactor core for controlling the temperature profile. The gas management system is based on a system previously used with pneumatic loading devices at VTT, with the addition of a standalone pressurisation loop. The safety box is an interface between the gas management system and the sample holder, and it also connects the Melodie experimental system to the Osiris safety systems.

The main goal of the Melodie in-core experiment was to act as a prototype for future instrumented material experiments in the JHR. Therefore, the instrumentation in the Melodie sample holder, including the pneumatic mechanical loading units and LVDT (Linear Variable Differential Transducer) sensors, had to be tested and their operation validated in reactor environment.

Zircaloy-4 was chosen as the material of the specimen, because it is well known and the results of the experiment can be compared to data already available. Potentially it was also possible to produce new creep data, especially to study the performance of the cladding in the early stages of creep or in transient situations, because of the online control and measurement.

Being delayed from the original scheduled start of the irradiation, and the shutdown of the Osiris reactor nearing, the experimental objectives were revised and the plan was to test all possible features and capabilities of the device in a short amount of time. Typically, creep is a slow deformation process under stress and temperature over a relatively long time period. In this case, however, the original plan of performing an irradiation creep test by keeping constant irradiation and stress conditions during one or more reactor cycles without changes was abandoned. Instead, the stress levels were varied within a single reactor cycle to be able to test the performance of the device efficiently.

The Melodie sample holder was placed in the position 24NE of the Osiris reactor core, with an average fast neutron flux of 1.2×10^{14} n/cm^{2}s. The target temperature

for the Zy-4 specimen was 350 °C. The temperature of the specimen could be controlled to some extent with the electrical heaters of the Chouca to have as flat a temperature profile as possible.

In-core experiments are divided into cycles based on the reactor operating schedule. In Osiris, each cycle was 18 to 25 days long, and between the cycles there were outages of about 10 days each. From August to September, a longer maintenance outage was scheduled, and there was no irradiation cycle. Therefore, the Melodie experiment, started in May 2015, had six cycles of reactor time before the shutdown of Osiris at the end of 2015.

During the in-core experiment, the Melodie sample holder was inserted into the Chouca capsule. The bottom part of the sample holder was submerged in NaK, which prevented oxidation and acted as a thermal conductor. The rest of the Chouca was filled with helium gas. Helium was also used in the pneumatic loading units and the mover because of its low activation under irradiation. The pneumatic and electrical lines of the sample holder were connected to the gas management system and the Moog controller. The Moog controller was used together with the glove box for adjusting the pressure in the four experimental pressure lines. LVDT and pressure sensor signals were recorded with a selected acquisition rate, and the recorded files were transferred to a computer during operation. Data was recorded also to the Osiris database via the local network. The Osiris database contains the data from the same experimental signals as the Moog, plus data from all 12 thermocouples, the reactor linear power, and the control rod positions.

Results of the Melodie in-core experiment

The first cycle of the Melodie in-core experiment started on 7 May, 2015. The goal was to first ensure the instrumentation is working the same way as out-of-pile. During the first diameter scans with the DG after the start of the cycle it was immediately observed that the DG does not show similar behaviour as out-of-pile. The signal had a lot of disturbance and was not consistent between the scans. It was concluded that the disturbance was most probably due to temperature changes in the sensor. The tests with the DG continued throughout the reactor cycle with varying scanning speeds. Because of the lack of repeatability in the measurement the problem was difficult to analyse more closely. The temperature profile was also adjusted with the electrical heaters in the Chouca to see if it had any influence on the DG signal, but it was found not to mitigate the problem.

After discovering the problems with the online measurement capability of the DG, the second reactor cycle was dedicated to axial strain measurement. During the preliminary tests and also the first reactor cycle the focus had been on the diameter measurement, and little emphasis had been put on the behaviour and tuning of the LVDT5. Therefore, the interpretation of the axial strain measurement was not as straightforward as expected. The LVDT5 signal was working, but taking into account the thermal expansions and elastic deformations of the loading frame was difficult. It was decided to continue gathering data and simultaneously trying to perform initial

analysis on it to be able to conclude whether the measurement was producing rational results or not. This work continued in the third cycle.

The axial strain measurements continued, and early in the third cycle the LVDT5 produced consistent low-noise data making it possible to analyse reliably the value of creep in one week. The stress level was changed twice, and the creep rate with stress levels of 60 MPa, 110 MPa and 60 MPa was measured during the third reactor cycle. However, in the end of the cycle the strains measured during the cycle were compared to those measured in room temperature before and after the cycle, and there was a discrepancy between the measurements, indicating that further analysis was needed.

During the long summer outage after the third cycle, it was discovered in out-of-pile measurements that the impedances of the LVDT5 coils were strongly drifting, suggesting some degree of damage in the sensor. In the DG, however, there was no noticeable change in the electrical signals compared to the measurements before the start of irradiation, and the scanning diameter measurement seemed to be working fine out-of-pile.

The fourth cycle was dedicated to offline hoop strain measurement. The diameter was measured before and after the cycle to have an integrated measurement over the cycle. These offline measurements were repeated later after each of the remaining cycles.

In the fifth cycle the focus was back on the axial strain measurement. The goal was to repeat the measurement carried out in the third cycle. After the fifth cycle the Melodie device was brought to the hot cells in the Osiris reactor building for changing the Chouca. The sample holder was extracted from the original Chouca and inserted into a new one. The new Chouca has a slightly different design in terms of the gas gap between the two tubes, which has an effect on the temperature profile on the core level. The change of the Chouca was planned already after the first cycle, when the behaviour of the system was found not to be satisfying with regard to the DG measurement. However, it was not carried out until the last outage because of the other tests performed during the reactor cycles and also because of the preparations needed for the change procedure.

In the sixth and last reactor cycle the goal was to test the behaviour of the DG in the new Chouca. The behaviour was not very different from the first cycle, which confirmed the assumption formed after the first cycle that the inherent performance of the sensor is too sensitive to the harsh environment of the Osiris reactor and the solution is beyond our reach during the time frame of this experiment. The remaining days of the last cycle were again dedicated to the axial strain measurement.

After the Melodie experiment was finished that part of the Finnish in-kind is considered delivered.

References

Al-Mazouzi, Abderrahim, Marek Miklos, and Petri Kinnunen. “Synthesis Document.” Memo, Fuel, Materials and Technology Working Groups, JHR Consortium, 2015.

Bignan, Gilles, Abderrahim Al-Mazouzi, Marek Miklos, and Petri Kinnunen. “Position Paper.” Position Paper, Fuel, Materials and Technology Working Groups, JHR Consortium, 2016.

Bignan, Gilles, and Jérôme Estrade. “The Jules Horowitz Reactor: A new high performance MTR (Material Testing Reactor) working as an international user facility in support to nuclear industry, public bodies and research institutes.” *16th Meeting of the International Group On Research Reactors (IGORR).* Bariloche, 2014.

Bignan, Gilles, and Nicolas Waeckel. “The key-role of material testing reactors in support to nuclear industry: Example of JHR and of the ICERR scheme.” *IAEA International Conference on Research Reactors: Safe Management and Effective Utilization.* Vienna: IAEA, 2015.

Guimbal, Philippe, et al. “Status of the MeLoDIE experiment, an advanced device for online biaxial study of the irradiation creep of LWR cladding.” *3rd International Conference on Advancements in Nuclear Instrumentation, Measurement Methods and their Applications (ANIMMA).* Marseille, 2013.

Huotilainen, Santtu. *Development and 3D design of an in-reactor material creep test device.* Master's thesis, Espoo: Aalto University, 2010.

Huotilainen, Santtu. *Progress report on JHR collaboration.* Espoo: VTT-R-06014-15, 2015.

Huotilainen, Santtu. *Technical report on the Melodie in-core experiment.* Espoo: VTT-R-06016-15, 2015.

Tähtinen, Seppo. *Melodie sample holder - development and performance.* Espoo: VTT-R-00516-13, 2013.

7.3 Development of thermal-hydraulic infrastructure at LUT (INFRAL)

Joonas Telkkä[1], Elina Hujala[1], Lauri Pyy[1]

[1]LUT University
P.O. Box 20, FI-53851 Lappeenranta, Finland

Abstract

The aim of the INFRAL project was to develop the thermal hydraulic measurement infrastructure of the LUT University nuclear safety research laboratory, to secure the operability of the existing test facilities and to launch a study on the new large-scale integral test facility. During the SAFIR2018 research programme, the advanced measurement techniques, i.e. particle image velocimetry (PIV), wire-mesh sensors (WMSs) and high-speed cameras (HSCs) were versatilely used in different research projects. The expertise on these measurement systems, as well as on the related data processing procedures, took big leaps forward. The study on the new modular integral test facility, titled MOTEL (MOdular TEst Loop), was launched in 2016. The survey of the research based requirements for the new test facility was conducted on the national level to ensure that the needs of Finnish stakeholders will be fulfilled. Further, the modularity based requirements for the MOTEL facility were studied, and the first configuration of the test facility was introduced. International co-operation with other top-level universities and research institutes continued during SAFIR2018, and thus LUT has formed valuable connections to research institutes such as Paul Scherrer Institute, University of Michigan and Helmholtz-Zentrum Dresden-Rossendorf.

Introduction

In the SAFIR2014 research programme, the research project ELAINE was launched for the enhancement of measurement instrumentation available for the thermal hydraulic experiments in LUT University. Significant milestones in the project were the acquisitions of a particle image velocimetry (PIV) measurement system, wire-mesh sensor (WMS) electronics and a system of three modern high-speed cameras (HSC). In addition to acquisitions of experimental hardware, a new data storage system for the experimental data (EDS) was developed and taken into active use. In addition, one important task in the project was the maintenance of the (PWR) PACTEL test facility in order to secure its operability and availability for the experiments.

In the SAFIR2018 programme, the INFRAL project was launched in 2015, and it aimed for the further development of the techniques related to the advanced measurement techniques and their applications. The goal was to build good in-house expertise in the use of the acquired techniques to facilitate the needs of computational modellers in the future experiments in the best way technically possible. The CFD grade measurements can give new insights into the physics behind the different flow phenomena that may ultimately lead to improvements in the safety of nuclear power plants. Further, the goal of the INFRAL project was to secure the operability of the PACTEL test facilities and to launch a study on the new major test facility to prepare for the post-PACTEL era.

During the SAFIR2018 programme, the INFRAL project was divided into four different work packages. The first work package (Advanced measurement techniques) included activities that were related to the use of advanced measurement techniques in LUT. Part of the work was to develop analytical tools to extract the needed data from the measurements. The other part was to study the applicability of the techniques for different flow problems and to develop new measurement solutions. The second work package (Maintenance and equipment) aimed on the maintenance of (PWR) PACTEL and other test facilities, and it comprised the yearly inspections, calibrations and other maintenance actions.

The third work package (Modular Integral Test Facility (MOTEL)) aimed on designing and constructing a new large-scale integral test facility in the LUT laboratory. The fourth work package (Project management, international co-operation and publications) included the tasks related to the project management and participation to the reference group meetings and seminars. Also, international co-operation actions, such as research visits to different research institutions, were part of the work package.

Advanced measurement techniques

The work package 1 of the INFRAL project consisted of research topics that are related to the study and application of the so-called advanced measurement techniques: particle image velocimetry (PIV), wire-mesh sensors (WMSs) and high-speed cameras (HSCs). The measurement systems were acquired to LUT already during the previous project (ELAINE) in 2011–2014. During the SAFIR2018 research programme, the advanced measurement systems were developed further and used in various applications. Some of the application targets of the systems were also related to non-SAFIR projects. The PIV measurement system, in particular, was versatilely used in many different projects during 2015–2018. The tasks in the work package 1 were the following:

- Advanced and combined use of PIV/WMS/3D Cam systems (T1.1)
- Evolutionary WMS applications (T1.2)
- Improvement of 3D High-Speed Camera data analysis (T1.3)

- New applications of advanced measuring techniques (T1.4)

The task 1.1 supported the use of advanced measurements techniques in LUT University. In 2015, the particle image velocimetry system was upgraded for shadowgraphy use with add-on components (software+hardware). Therefore, no conventional PIV measurements were performed in 2015. Shadowgraphy is used to size water droplets with the help of bright backlight that creates a measurable edge of the particle's cross section. The end result is a droplet distribution from the measurement area, which can be used to determine the spread parameter for Rosin-Rammler distribution used commonly for droplet mass fraction frequency distributions. A test facility with easy-to-control environment was created and successfully tested during 2015. The work done with the shadowgraphy system was also related to the INSTAB project (Pyy, 2015).

In 2016, the PIV system was mainly utilized in contract measurement schemes. In December 2016 PIV was applied within the SPA-T8R and SPA-T9 test series where thermally separated layers of water were mixed with a sparger using different amounts of outlets open within the sparger. The test series was a part of the INSTAB project. As it had been found out before in case of condensation, the optical aberrations created too challenging environment for successful PIV measurements. Another downside with the existing PIV system is the low frequency of the laser and the cameras. Hence they don't work well with the fluctuating water phase even without any optical aberrations, causing problems with time-averaging. Preliminary qualitative inspection of SPA-T8R and SPA-T9 results showed that similar flow structures appeared roughly for few seconds, and with a low-speed PIV system only 2–40 image pairs can be measured. One possibility to achieve better velocity data would be to update the laser for one with kilohertz range in order to capture hundreds of image pairs. This would improve the reliability of the time-averaged velocity fields, or make possible to execute time-resolved PIV (TR-PIV) when the phenomenon is very short and unrepeatable. Naturally, optical aberrations would still appear when condensation of steam occurs near the field-of-view (FOV), between cameras and the FOV or in the laser sheet line. With higher water temperatures the fluorescent tracer particles also fall to the bottom of the PPOOLEX vessel, creating yet another problem for PIV measurements, as the seeding density gets lower with the elevating temperature.

In December 2016, a new set of sCMOS cameras were acquired to update the PIV measurement system. This update doubled the measurement frequency to 15 Hz (7 Hz before) making the laser unit the limiting component frequency-wise. The biggest advantage of the sCMOS cameras is the better chip design compared to the former ImagerX Pro cameras. The chip can withstand more reflection making it easier to apply in the challenging measurement environments as well as better overall performance for shadowgraphy measurements. The new cameras were taken into operation in 2017.

The contract measurements with PIV involved three different measurement schemes in 2016, where the most challenging scheme was the measurement of 8 MW gas burner in a chamber. Measurement experience was also gathered from a

simple airflow (stereo-PIV) and water flow within a channel (planar-PIV), which were more traditional measurements with more easily controlled and optically sturdier environments.

The shadowgraphy extension of the PIV system was not utilized in 2016 for measurement activities, but a master's thesis "Spray Droplet Size Distribution Measurement" by Dmitry Skripnikov was finalized in September 2016 (Skripnikov, 2016). The thesis emphasized in handling of shadowgraphy droplet distribution data and ways to validate CFD (ANSYS Fluent) results with droplet mass fraction frequency distribution by providing correct spread diameter for Rosin-Rammler droplet number and volume distributions. The thesis was graded 4 (very good).

In 2017, the PIV system was actively used in the LUT laboratory. In the first half of 2017, an ambitious measuring scheme for a contract measurement was executed. All in all, almost quarter of million raw images were captured and analysed. The measurements were conducted in a planar-PIV mode and part of the measurements with added second camera measuring with a camera endoscope. In this measurement scheme, the camera endoscope was utilized in the measurements for the first time. The measurements were focused on water flow within a rectangular channel. Considerable amount of experience was achieved in this commercial project in physical arrangements for PIV as well as in data processing schemes.

The PIV system was also used in the INSTAB project in 2017 in SPR-4, SPR-5, SPR-6 and SPR-7 tests. In these tests, the PPOOLEX test facility was layered with cold water in the bottom and hot water on the top. PPOOLEX was filled with 1800 mm of water in which 200 mm was hot water on the top (SPR-T6 1500 mm of water and 200 mm of hot water on the top). The hot layer was approximately 50 °C, and the cold water temperature was approximately 12 °C. Four spray nozzles situated on the top of the wet well of PPOOLEX were used to spray cold water on the top of the hot water layer. The main motivation was to test out the optical environment and its suitability to PIV measurements. Unfortunately, the optical environment was not ideal for PIV. The cases were measurable only before the hot layer or the mixing zone enters the measurement area creating aberrations. There were indications that the time before the hot layer or mixing layer enter the measurement area, the flow is highly turbulent. After the measurement area is clear of aberrations, the flow is more consistent with less turbulence intensity.

In 2017, the PIV system was also updated with external Programmable Timing Unit allowing the use of up to eight cameras in the future. The addition will also allow additional light source to be used with laser. This allows timing of PIV cameras, laser, high-speed cameras and their light source in synchronous manner if needed. New hard drives for the system computer and a new DaVis10 software that is compatible with the Windows10 operating system were acquired during 2017.

In 2018, the PIV measurement system was utilized for contract measurements exclusively. The follow-up to water flow in a rectangular channel was executed during the first half of 2018. A new method of seeding the flow with natural convection flow next to a heated wall was designed and executed successfully. The PIV system in action is presented in Figure 1. In addition, PIV was used in wind tunnel measurements. These measurements focused on the drag reduction by small groove

riblets on surface of a wing. The measurements were conducted together with the Laboratory of Fluid Dynamics at LUT University. New experience considering seeding of gaseous flows was gathered. In addition, data from Constant Temperature Anemometry (CTA) was gathered for velocity comparison, and a publication from the results is in the making. In 2018, there were no hardware or software updates for the PIV system.

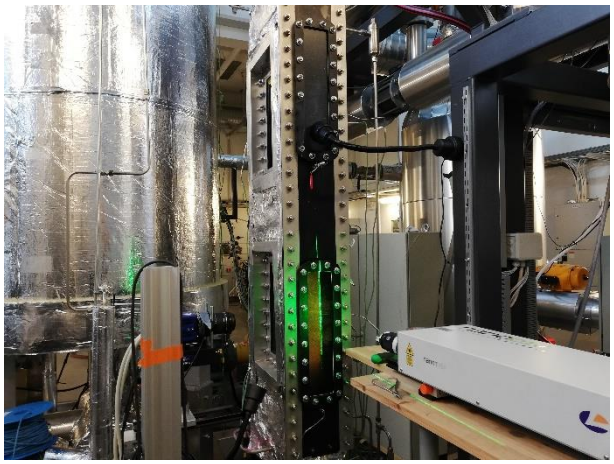

Figure 1. PIV system in action in planar-PIV mode with new sCMOS cameras.

PIV has been found out to be an effective tool in velocity measurements where it is applicable. PIV has been applied multiple times with success in many projects, but studies within SAFIR programme have been challenging stated with the reasons mentioned before. However, a lot of important user experience has been gathered within SAFIR-related studies. All in all, the usability of the PIV system has improved substantially during INFRAL. PIV will remain an important part of the LUT thermal hydraulic measurement infrastructure in the future.

Within the task 1.2, the advanced applications for the wire-mesh sensor technique were actively studied in LUT. The axial sensor design, named AXE, was designed and constructed in the previous ELAINE project in the SAFIR2014 programme to tackle the problems related to the measurement of the axial flow behavior. Like the name of the sensor states, it is installed axially into the centreline of the flow channel to study the axial flow dynamics of the two-phase flow. The sensor has 16 x 128 wires placed with the 3 mm x 3 mm spatial resolution over the area of 45 x 381 mm^2.

In 2015, the applicability of the AXE sensor was studied under various flow conditions in the HIPE (Horizontal and Inclined Pipe Experiments) test facility. The first measurement results were presented in the NURETH-16 conference (September 2015, Chicago, U.S.) (Ylönen & Hyvärinen, 2015).

The results from the axial WMS measurements were also presented in the SWINTH-2016 workshop in June 2016 (Ylönen et al., 2016). The participation to the workshop also supported the use of all kinds of advanced measurement techniques as the workshop was intended for researchers who are developing and applying these techniques in practice. The paper presented in the SWINTH workshop was later chosen to be published in Nuclear Engineering and Design. The paper was then modified and later published in NED (Telkkä et al., 2018).

It can be stated, based on the conducted measurements that the axial sensor design has advantages and drawbacks. The sensor can be applied to study the axial behavior of the two-phase flow. However, the sensor itself has noticeable effects on the flow velocities as the comparative experiments with the traditional WMSs revealed. In 2016, the axial WMS technique was studied further. Two separate swirling devices with different blade angles (30 ° and 60 °) were designed and manufactured. The swirling devices were applied to the HIPE test facility to create a swirling two-phase flow. Two identical series of experiments were aimed to be conducted separately with both swirling devices using both axial and radial sensors under swirling two-phase flow conditions. The set-up of the experiments is presented in Figure 2. The test matrix of these experiments, i.e. the pipe inclinations and superficial water and air flow rates, was the same as in the previous experiments without the swirling devices.

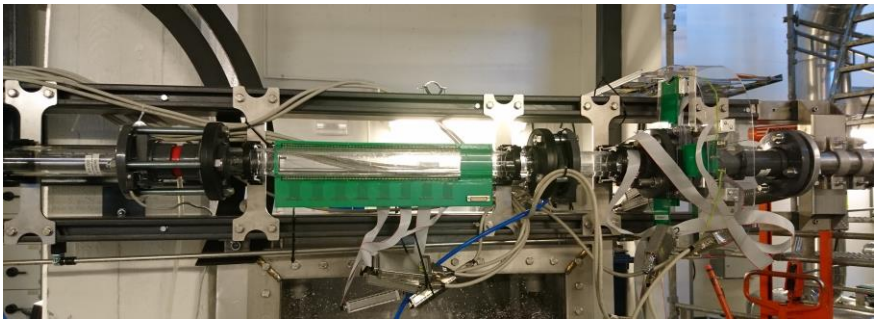

Figure 2. Set-up of the WMS measurements with a swirling device (horizontal flow case). The swirling device is on the left (red color), the axial sensor in the middle, and the two radial sensors are on the right.

The measurements were postponed to 2017 for the reason that the air mass flow meter of the HIPE test facility was broken. The reason for the importance of the air mass flow meter to the measurements was the aim of using the same superficial velocities as in the previous measurements without the swirling devices. During the first half of 2017, some swirling flow measurements were conducted, until the WMS electronics unit itself was broken and it had to be sent for repair. The unit was received back to LUT in August. The rest of the tests were conducted in December 2017. In 2017, it was also decided that a new WMS data analysing software, WMS Framework, will be purchased from Helmholtz-Zentrum Dresden-Rossendorf

(HZDR), and it will be used for the analysis instead of MATLAB codes. The idea for the procurement of the software came during a research visit to HZDR. The visit took place between 14th and 17th of August with two researchers from LUT attending. The WMS Framework software offers relatively fast data analyzing capabilities compared to the old method by using MATLAB codes. A bachelor's thesis was written in 2017-2018 regarding the implementation of the new software and the data analysis of the swirling flow WMS measurements.

In addition to developing own WMSs in the LUT laboratory, the development of the so-called high temperature and high pressure WMS technique at ETH Zurich and Helmholtz-Zentrum Dresden-Rossendorf (HZDR) has been followed. The new design of the sensor was developed (Kickhofel, 2015) in order to simplify the manufacturing process compared to the previously developed one (Pietruske & Prasser, 2007). The high temperature/high pressure WMS technique was also presented in the SWINTH-2016 workshop where good knowledge of it was acquired (Kickhofel et al., 2016). The sensors can operate at temperatures potentially up to 350 °C and pressures up to 22 MPa (Kickhofel et al., 2016).

The technique has already been used at HZDR, and there has been communication between LUT and HZDR/ETH Zurich regarding this issue. HZDR has already gained some promising results from the conducted measurements, and hence in principle the functioning of the high temperature/high pressure WMS technique has been confirmed. There have been preliminary plans of applying this technique to the forthcoming modular integral test facility, MOTEL. The temperature and pressure levels will be so high in the test facility that the traditional WMSs cannot be applied to it. High temperature/high pressure WMSs could offer a novel means of void fraction measuring in challenging circumstances. Characteristics, restrictions, economic requirements etc. of the HT/HP WMS technique were discussed during the above-mentioned research visit to HZDR. During the research visit, there were also valuable discussions related to possible applications of the "traditional" wire-mesh sensors.

In 2018, the swirling two-phase flow WMS measurement results were further analyzed, and a conference paper was prepared concerning the results. An abstract titled "*Defining Void Fraction with Axial Wire-Mesh Sensor in a Swirling Two-Phase Flow*" was sent to SWINTH-2019 (Specialists Workshop on Advanced Instrumentation and Measurement Techniques for Experiments Related to Nuclear Reactor Thermal Hydraulics and Severe Accidents, 22–25 October 2019, Livorno, Italy). The abstract was accepted in September. The full paper was prepared during late 2018, and it will be finalized during the first half of 2019. The main focus of the paper is to evaluate the performance of the axial sensor under swirling flow conditions, particularly the AXE sensor's ability to determine void fraction distributions compared to traditional radial sensors.

Example of the results is presented in Figure 3. The figure presents the one-dimensional averaged void fraction distribution at the 106th receiver wire of AXE measured with the traditional radial (TRAD) and axial (AXE) sensors using the 30° swirl generator. The figure visualizes the void fraction measurement accuracy of

AXE compared to that of radial sensor. The void fraction distributions along the diameter of the flow channel are obtained from the traditional sensor data by taking the average value of two middle wires and comparing it to the corresponding receiver wire of the axial sensor. Three different superficial airflow rates are presented (0.2 m/s, 0.4 m/s and 0.6 m/s), the superficial waterflow rate being 0.8 m/s in all measurements.

In the figure, the x-axis describes the distance from the centerline of the flow channel. It can be seen from the figure that the void fractions measured with the radial sensor are significantly higher than those measured with the axial sensor. The difference becomes smaller, as the superficial airflow rate is increased. The increased airflow rate not only increases the measured void fraction values, but also spreads it out more along the diameter of the flow channel. The widening can be seen mostly in the traditional sensor data. The swirling air phase in the middle of the flow channel clearly becomes wider. In the AXE data, the distribution is wider than in the TRAD data in every case. It is probable that the upstream edge of the AXE sensor scatters the focused air swirl over the whole volume of the flow channel. Thus, void fraction values measured with the axial sensor stay lower.

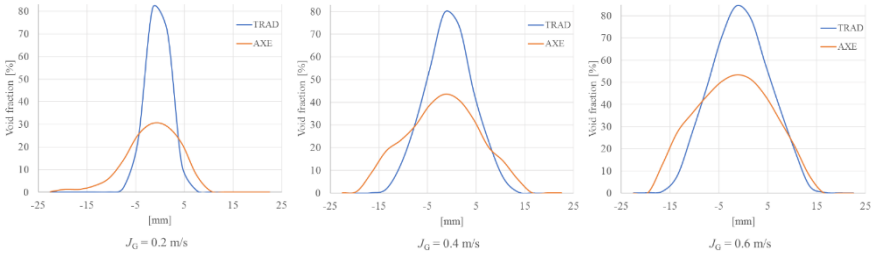

Figure 3. Averaged void fractions at the 106th receiver wire of AXE measured with the 30° swirl generator.

The conclusion of the analysis of the measurement results is that because of the intrusive structure of the axial sensor design, it cannot measure void fraction distributions very accurately. Especially in the case of swirling flow, the upstream edge of the sensor breaks the flow and affects the void fraction results. Thus, initial design for a new kind of sensor has started in the LUT laboratory. Changing the structure of the axial sensor in a way that the intrusive edge would be eliminated completely and adding the distance between the sensor wires either with insulation material or by using different thickness circuit boards have been considered.

The actions in task 1.3 are related to the improvement of high-speed camera data analysis procedures using the experimental data from the PPOOLEX blowdown pipe experiments. During 2015, the pattern recognition algorithm was improved to be more accurate. The challenge was to combine all three video directions together due to a large amount of swarm of small bubbles especially on the bottom and the right side cameras. Most of the evaluations and calculations were made by using the left side camera only, but other cameras were used for the confirmation of the

results. The evaluations of the volume and the surface area of the bubbles were performed too. From the bottom camera images, the form of the bubbles were evaluated symmetrical. From the left side image, the 3D model was produced, and the volume and the area of the bubble calculated. Error of the volume and the area estimation is less than 15 percent for the pure sphere. Also the accelerations and the velocities of the bubbles were evaluated. The chugging frequencies were evaluated by using the pattern recognition algorithm.

In 2016, only analysis of the old experiments was made, and there were no new measurements with high-speed cameras concerning pattern recognition. During 2016, the pattern recognition algorithm made for the DCC-05 experiments was improved, and the data analysis methods were added. The old challenges, with combining all three video directions together due to a large amount of small bubbles especially on the bottom and the right side cameras, still occurred. Hence, most of the evaluations and calculations were made using the left side camera only, and other cameras were used for the confirmation of the results. The evaluations of the volume and the surface area of the bubbles were performed. From the bottom camera images, the form of the bubbles were evaluated symmetrical. From the left side image, the 3D model was produced, and the volume and the area of the bubble calculated. Calculation methods were enhanced. Error of the volume and the area estimation was less than 10 percent for the pure sphere. Also the accelerations and the velocities of the bubbles were evaluated. The full DCC-05 part 4 video material was analyzed and the different frequencies were assessed at separate phases of the bubbles. The preliminary results were published in 2017 (Patel et al., 2017).

The TRA-04 (transparent blowdown pipe) experiments pattern recognition procedure and data analysis was done in 2016-2017. The chugging frequencies were estimated by using Fast Fourier Transform (FFT) to the bubble volume data obtained with pattern recognition. Wavelet Transform analysis was also used in denoising of the signal.

In 2017, HSC data and the developed pattern recognition were used for inscription of one peer-reviewed article and a conference paper in the NURETH-17 conference. The journal article "*Pattern recognition algorithm for analysis of chugging direct contact condensation*" was submitted to Nuclear Engineering and Design in July 2017, and it was published in 2018 (Hujala et al., 2018a).

The NURETH-17 conference paper "*Frequency Analysis of Chugging Condensation in Pressure Suppression Pool System with Pattern Recognition*" concentrated on the DCC-05-4 experiments (Hujala et al., 2017). The frequency analysis showed that the experiment consisted of three different bubble modes named A, B, and C. Type A bubble cycle is the simplest one. The bubble grows in two parts, as a fluctuating part where the bubble builds up oscillating and the rapid growth part, where the fluctuating bubble grows fast and then condensates completely very rapidly. Type B bubble cycle consists of multiple oscillating parts of which the final one grows faster and breaks up rapidly. The volume in the preceding fluctuating parts does not fall to zero at any time. Type C bubble consists one or multiple fluctuating parts. The bubble oscillates, grows, and breaks up with comparable rates without having a rapidly collapsing volume period.

In 2017, the HSC system was also used in new steam momentum experiments within a separate effect pool test facility (SEF-POOL) where steam is injected through an inlet.

In 2018, the NURETH-17 conference paper was invited to the special issue of Nuclear Engineering and Design and it was published in December 2018 (Hujala et al., 2018b). In 2018, SEF-POOL tests continued. Two tests were conducted for the development of the pattern recognition algorithm. In these tests, a steam jet was horizontally directed through a sparger into a water pool, where the steam condensed by a direct contact condensation (DCC). The SEF-INF1 experiment was operated within the condensation oscillations (CO) mode and the SEF-INF2 was operated within the bubbling condensation oscillation (BCO) mode according to the condensation regime map of Song et al. (2012) presented in Figure 4.

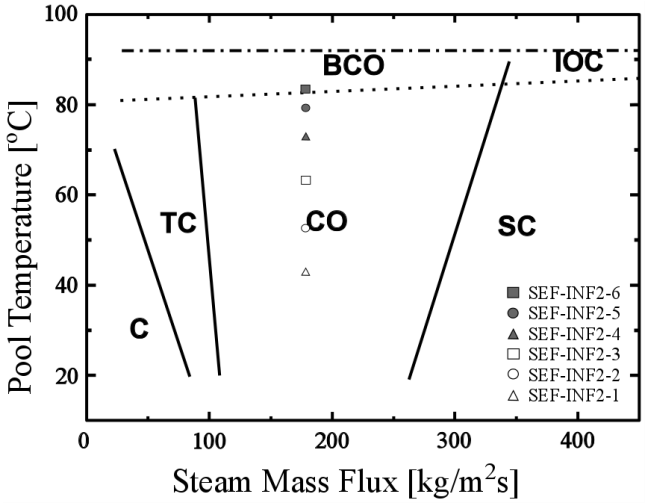

Figure 4. Regime map of Song et al. (2012). C=chugging, TC=transitional chugging, CO=condensation oscillation, BCO=bubbling condensation oscillation, SC=stable condensation, ICO=interfacial condensation oscillations.

The SEF-INF2 was chosen as the first reference case for the pattern recognition algorithm development and CFD simulations. Snapshots of the SEF-INF2 tests 1-6 are presented in Figure 5. SEF-INF2-6 experiment was chosen as the most interesting case due to its larger bubbles and BCO mode.

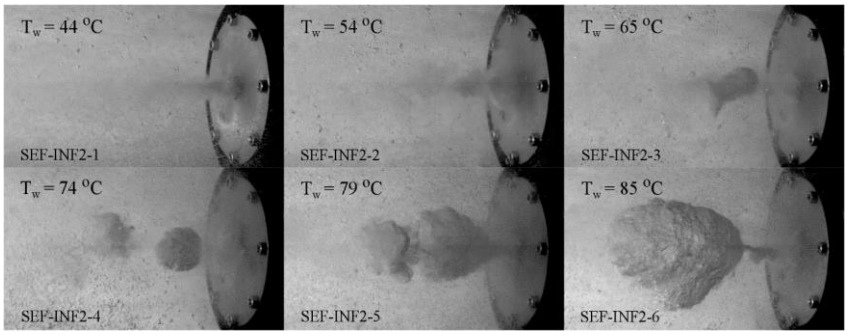

Figure 5. SEF-INF2-1…SEF-INF2-6 experiments. Steam mass flux was hold constant (180 kg/(m^2s)), meanwhile the temperature of the condensation pool water T_w increased from the initial temperature of 12 °C to the SEF-INF2-6 tests 85 °C. It can be seen that SEF-INF2-1…SEF-INF2-3 tests are in condensation oscillation mode (T_w = 44 °C… 65 °C), SEF-INF2-4 and SEF-INF2-5 tests are near bubbling condensation oscillation mode (T_w =74 °C and 79 °C respectively) and SEF-INF2-6 in pure bubbling condensation oscillation mode mode (T_w = 85 °C).

Results of the image and data analysis and CFD simulations of the SEF-INF2 test will be presented in the NURETH-18 conference at Portland, USA in August 2019. An abstract titled *"Analysis of Bubbling Mode Condensation Oscillation in Horizontal Sparger"* was submitted and accepted, and the full paper will be written in early 2019.

The goal of the task 1.4 was to follow the state-of-the-art of advanced measurement techniques and their applications in experimental thermal hydraulic research in universities and research institutes across the world. The task was comprised of following the journal articles and conference papers on the field, communication with other experts, as well as participating in conferences/seminars and doing research visits to other universities/research institutes. The followed measurement techniques include also other techniques and systems than those in use in the LUT laboratory, such as tomography measurement systems. Also completely new advanced measurement techniques have been surveyed. One example of recently developed measurement techniques is the distributed temperature sensor (DTS) based on Rayleigh-backscatter phenomenon. The technique utilizes optic fibers, and it enables the measurement of temperature distribution in high detail in different geometries, such as a slab or a rod (Gerardi et al, 2015).

The distributed temperature sensor technique was presented also in the SWINTH-2016 workshop, where more information concerning it was acquired. Regarding the characteristics of the DTS technique, temperatures up to 850 degrees Celsius can be measured. The technique can measure the temperature profile along the length of the fibre at an accuracy comparable to thermocouples and sampling rates < 1 Hz. Obtaining a full profile, instead of a few point values, would represent a major advance in providing temperature data for understanding of physics

and validation of codes. Point resolution and temperature resolution in DTSs are mutually exclusive to some degree. If accurate temperature measurement is preferred, the spatial resolution suffers. And the other way around, if spatial resolution is of importance, the measurement accuracy weakens. (Lomperski et al., 2016)

In 2017, the DTS technique was introduced at LUT by the manufacturer, and the electronic hardware was purchased in the same year. The functioning of the technique was planned to be conducted in 2018. The testing was originally planned to be conducted in the new passive heat removal test facility, PASI, within the INTEGRA project as one of the characterization experiments of PASI. However, the testing was dropped out from INTEGRA. The problem was, also, that the firmware of the electronics was not capable to handle temperature measurement. Thus, the testing of the optic fibers was postponed to 2019. The technique will be applied to heat exchanger tubes of PASI, in order to gain information on the temperatures and flow behavior inside the heat exchanger tubes. One intended target of application for the technique is also the forthcoming modular integral test facility, MOTEL, which has been designed in 2018, and will be erected in the laboratory during 2019. The optic fibers are intended to be used e.g. to measure temperature distributions in the core section of MOTEL.

In addition to optic fibers, ultrasonic flow measurement devices have been purchased to LUT laboratory, and they will be tested in 2019. They will be used to measure flowrate from single heat exchanger tubes of the PASI facility. The structure of the facility is designed in a way that the flow measuring from single tubes is enabled. Later on, the ultrasonic flow measurement devices will be applied to the MOTEL test facility to measure flow from the annular downcomer space of MOTEL. However, measuring flowrate from an annular flow channel with this technique requires testing.

In addition, the development of different tomography measurement systems has been followed during SAFIR2018. The research visit to University of Michigan (UMICH), which took place in September–October 2016, provided lots of important information concerning tomography systems and their characteristics, such as technical and economic requirements. Two researchers from LUT attended the research visit, and during the visit the tomography measurement systems of UMICH Nuclear Engineering and Radiological Sciences department were introduced. Tomography systems, which could enhance e.g. void fraction measuring possibilities, are among the potential advanced measurement systems to be applied in the LUT laboratory at some point in the future.

Maintenance and equipment

The second work package of INFRAL aimed on the maintenance of (PWR) PACTEL and other test facilities in the LUT laboratory. The maintenance actions ensure the availability of the facilities for the thermal hydraulic experiments conducted in other research projects, such as INTEGRA and INSTAB.

The periodical inspections of the pressure vessels are performed in accordance to the legislation regarding pressure vessels and equipment. Aged components in the facilities are replaced and the operability of the systems is ensured by purchasing spare parts to replace broken ones. Typically, these parts include moving parts such as valve and automation components, but also parts for control and data acquisition systems.

Due to the upgrades in the power grid automation operated by the local power utility, the use of the PACTEL test facility has raised concerns as the unbalanced phase control system used in the core simulator trips the utility's phase trip alarms. In 2015, the replacement of the core simulator power control equipment was evaluated. The hardware was purchased in 2016. Also the power measurement system of PACTEL has been renewed.

In 2015, the procurement process of a computer for the post-processing of computational and experimental data was started, and the computer was taken into operation in 2016.

During the SAFIR2018 research programme, the upgrade of power transformers has been prepared to increase the electrical power available for the thermal hydraulic experiments (1 MW → appr. 2.5 MW). The upgrade will enable higher heating power to be available for new experimental facilities, such as MOTEL. The higher heating power enables new research topics such as more realistic critical heat flux studies with different fuel geometries. However, the power transformer upgrade process has been postponed, and the options for the upgrade are being studied in the many organizations involved. In addition to the three affected laboratories of LUT School of Energy Systems, also Suomen Yliopistokiinteistöt as the owner of the buildings, Lappeenranta Energia as the power provider, as well as electrical system design consultants are part of the process.

The general maintenance of the PACTEL facilities has continued as planned during SAFIR2018. The yearly calibrations and inspections have been carried out, and some of the components, such as pressure and pressure difference gauges, have been renewed. In 2018, the heating element of the PACTEL pressurizer was renewed because one of the heaters was broken. As the heating element was replaced, the pressurizer heating power was increased to 21 kW from the previous power of 13 kW.

Modular Integral Test Facility (MOTEL)

The work package 3 of the INFRAL project aimed on surveying different possibilities to construct an integral test facility as a successor of (PWR) PACTEL. Within INFRAL, background research regarding the forthcoming test facility was conducted, the purpose of which was to support the actual design of the facility. The design and the construction of the facility are done with a funding from the Academy of Finland.

In 2015, a project proposal was submitted to the Academy of Finland on the topic. The work package started in 2016 with the study of the research based requirements for the new test facility, titled MOTEL (MOdular TEst Loop). The survey of the research based requirements for the new modular integral test facility was conducted on the national level to ensure that the needs of Finnish stakeholders will be fulfilled. In addition, international trends and needs for the thermal hydraulic experimental research were studied to enable participation to various joint international projects in the future.

In 2016, a research report concerning the research based requirements for the new facility was written (Telkkä & Hyvärinen, 2016). The key design feature of the test facility is modularity, which means that the facility will be built of interchangeable parts that enable easy modifications of the facility. Hence, the facility will be able to represent widely different types of nuclear power plants, VVERs, PWRs, BWRs and SMRs (Small Modular Reactors), in contrast to traditional large scale thermal hydraulic test facilities that refer to only one plant design.

The facility is intended to allow study of both local phenomena and system level behavior. The purpose of the experiments to be conducted is to gather data, which can be used as such but also for computer code validation. In 2016, the actual design process of MOTEL started with a survey of the options for the first heater element.

In 2017, modularity based requirements of the MOTEL facility were studied, and a research report on the issue was written (Telkkä et al., 2017). The report introduced the modularity based requirements of MOTEL, i.e. the principles on how the modularity will be executed. In addition, the physical scaling principles of the facility were introduced. The scaling of MOTEL is based on the two-tiered hierarchical scaling methodology (H2TS).

In 2018, as the actual design of the facility was finalized, a report describing the first configuration of the MOTEL facility was written (Telkkä & Karppinen, 2018). The first MOTEL version represents NuScale's SMR design, which has a unique helical coil steam generator. The behavior of this type of steam generator will be one of the main interests regarding the experiments with the first MOTEL configuration. MOTEL will be built in the LUT laboratory during 2019. The facility will evolve in the future, and it can be upgraded with e.g. horizontal steam generators and/or an SMR containment. The first MOTEL configuration is presented in Figure 6.

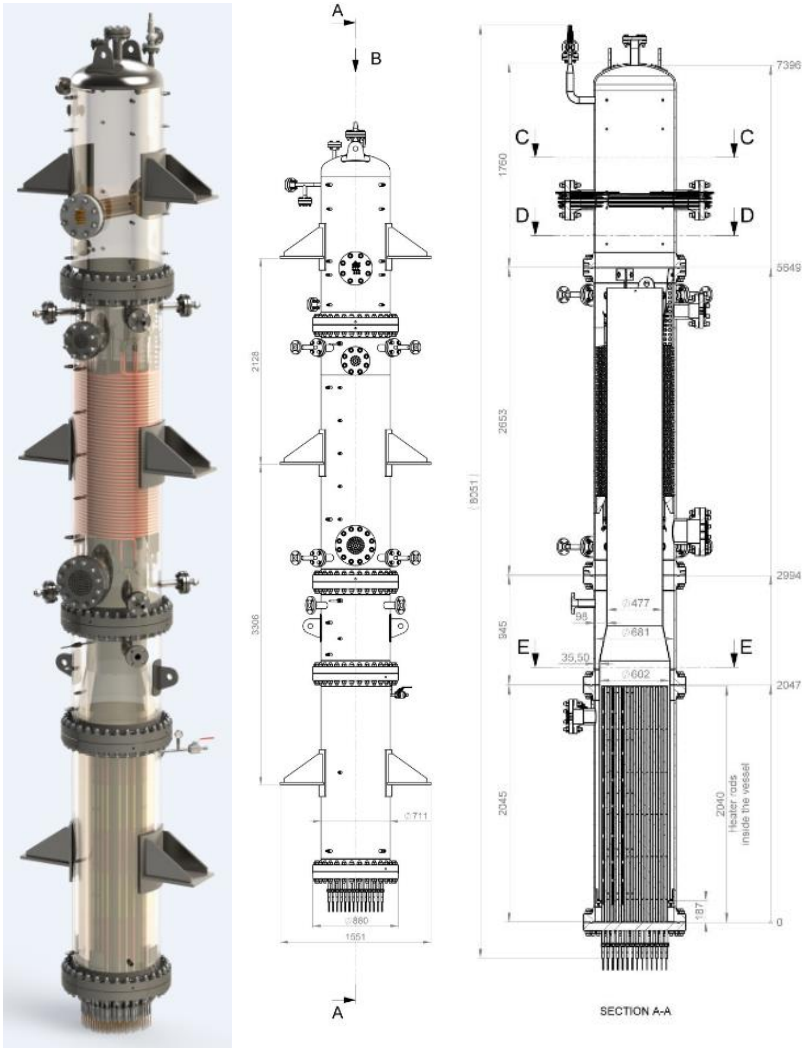

Figure 6. An overall view and the dimensions of the first configuration of the MOTEL test facility. The three changeable modules can be detected: core module, steam generator and pressurizer.

Project management, international co-operation and publications

The work package 4 included the tasks related to the project management and participation to the reference group meetings and seminars. Also, international co-operation activities were a part of the work package.

The building of expertise on the advanced measurement techniques requires collaboration and networking with other research institutes that are using the same techniques for thermal hydraulic studies. The exchange of experiences on advanced measurements have continued with institutes such as Paul Scherrer Institute (PSI, Switzerland), ETH Zurich, Helmholtz-Zentrum Dresden-Rossendorf (HZDR) and University of Michigan (UMICH).

In September–October 2016 two researchers from LUT made a research visit to University of Michigan. The first visit to UMICH took place in November 2014, and since then the thermal hydraulic measurement infrastructure at UMICH had developed significantly. The purpose of the visit was to get familiar with some of the measurement systems that don't exist at LUT laboratory, for example the LDV (laser doppler velocimetry) system and the tomography systems, deepen the knowledge and know-how on PIV and WMS measurement techniques and data processing procedures, as well as to network with other experts on the field and enhance the good connections with UMICH.

In August 2017, two researchers from LUT attended a research visit to HZDR. During the visit, laboratories, test facilities and measurement techniques of HZDR were introduced. Characteristics, restrictions, economic requirements etc. of the high temperature/pressure wire-mesh sensor technique were discussed. During the research visit, there were also valuable discussions related to possible applications of the "traditional" wire-mesh sensors. In addition, the WMS data analysing software WMS Framework was introduced, and it was decided to be purchased to the LUT laboratory.

In February 2018, two researchers attended the Short Courses on Multiphase Flows at ETH Zurich, Switzerland. Profound syllabus of multiphase flows was gained. The occasion also served as a good opportunity to network with other experts on the field.

References

Gerardi, C., Bremer, N., Lisowski, D. & Lomperski, S. 2015. Distributed Temperature Sensor testing in Liquid Sodium. Proceedings of the 16th International Topical Meeting on Nuclear Reactor Thermal Hydraulics (NURETH-16), Chicago, U.S., August 30–September 4, 2015. 10 p.

Hujala, E., Tanskanen, V. & Hyvärinen, J. 2017. Frequency Analysis of Chugging Condensation in Pressure Suppression Pool System with Pattern Recognition. Proceedings of the 17th International Topical Meeting on Nuclear Reactor Thermal Hydraulics (NURETH-17), Xi'an, China, September 3-8, 2017. 13 p.

Hujala, E., Tanskanen, V. & Hyvärinen, J. 2018a. Pattern recognition algorithm for analysis of chugging direct contact condensation. Nuclear Engineering and Design 332 (2018), 202-212. 11 p.

Hujala, E., Tanskanen, V. & Hyvärinen, J. 2018b. Frequency analysis of chugging condensation in pressure suppression pool system with pattern recognition. Nuclear Engineering and Design 339 (2018), 244-252. 9 p.

Kickhofel, J. 2015. Wire Mesh Sensor for High Temperature High Pressure Applications. Proceedings of the 16th International Topical Meeting on Nuclear Reactor Thermal Hydraulics (NURETH-16), Chicago, U.S., August 30–September 4, 2015. 12 p.

Kickhofel, J., Yang J. & Prasser, H.-M. 2016. Designing a High Temperature High Pressure Mesh Sensor. Proceedings of the Specialist Workshop on Advanced Instrumentation and Measurement Techniques for Nuclear Reactor Thermal Hydraulics (SWINTH-2016), Livorno, Italy, June 15–17, 2016. 12 p.

Lomperski, S., Bremer, N., Gerardi, C. & Lisowski, D. 2016. Performance Assessment of a 50 m-long Fiber Optic Distributed Temperature Sensor in a Fluid Dynamics Experiment. Proceedings of the Specialist Workshop on Advanced Instrumentation and Measurement Techniques for Nuclear Reactor Thermal Hydraulics (SWINTH-2016), Livorno, Italy, June 15–17, 2016. 11 p.

Patel, G., Tanskanen, V. Hujala E. & Hyvärinen, J. 2017. Direct contact condensation modeling in pressure suppression pool system. Nuclear Engineering and Design 321 (2017), 328-342. 15 p.

Pietruske, H. & Prasser, H.-M. 2007. Wire-mesh sensors for high-resolving two-phase flow studies at high pressures and temperatures. Flow Measurement and Instrumentation 18 (2007), 87–94. 8 p.

Pyy, L. 2015. Single spray nozzle tests. Research Report INSTAB 2/2015, Lappeenranta University of Technology. 25 p.

Skripnikov, D. 2016. Spray Droplet Size Distribution Measurements. Master's Thesis, Lappeenranta University of Technolgy. 69 p.

Song, C.H., Cho, S. & Kang, H.S. 2012. Steam Jet Condensation in a Pool: From Fundamental Understanding to Engineering Scale Analysis. Journal of Heat Transfer 134(3) (2012). 15 p.

Telkkä, J. & Hyvärinen, J. 2016. Research based requirements of MOTEL. Research Report INFRAL 1/2016, Lappenranta University of Technology. 22 p.

Telkkä, J., Hyvärinen, J. & Kauppinen, O.-P. 2017. Modularity based requirements of MOTEL. Research report INFRAL 1/2017, Lappeenranta University of Technology. 19 p.

Telkkä, J., Ylönen, A., Hyvärinen, J. and Varju, T. 2018. Estimation of velocity fields from the axial wire-mesh sensor data. Nuclear Engineering and Design 336 (2018), 34-44. 11 p.

Telkkä, J. & Karppinen, J. 2018. Modular Test Loop (MOTEL). Research report INFRAL 1/2018, LUT University. 18 p.

Ylönen, A. & Hyvärinen, J. 2015. Study of Two-Phase Pipe Flow using the Axial Wire-Mesh Sensor. Proceedings of the 16th International Topical Meeting on Nuclear Reactor Thermal Hydraulics (NURETH-16), Chicago, U.S., August 30–September 4, 2015. 10 p.

Ylönen, A., Varju, T. & Hyvärinen. J. 2016. Estimation of Velocity Fields from the Axial Wire-Mesh Sensor Data. Proceedings of the Specialist Workshop on Advanced Instrumentation and Measurement Techniques for Nuclear Reactor Thermal Hydraulics (SWINTH-2016), Livorno, Italy, June 15–17, 2016. 15 p.

7.4 Radiological laboratory commissioning (RADLAB)

Wade Karlsen[1]

[1]VTT Technical Research Centre of Finland Ltd
P.O. Box 1000, FI-02044 Espoo

Abstract

The RADLAB project executes the renewal of the radiological research infrastructure hosted by VTT, embodied in the new VTT Centre for Nuclear Safety. At the core of the new facility are the hot cells for testing and characterization of activated reactor structural materials in support of safe, long-term nuclear power plant operation. In the first half of the SAFIR2018 program (see Interim Report), the project oversaw the design and fabrication of the new hot cells, while in the second half of the program the focus has been on the on-site installation and bringing them into full operation. Simultaneously the project has executed the procurement of key hot laboratory equipment, the purchase cost of which has been supported by the investment aid mechanism financed through the complementary RADINFRA project. Additional activities have included the design, fabrication and installation of self-built research facilities and materials and waste-handling and storage facilities, as well as the full laboratory infrastructure commissioning and ramp-up of operations for both reactor safety and final repository research.

Introduction

The VTT CNS and its hot cell facility is a national infrastructure hosted by VTT, and is considered an important element in fulfilling the national requirements for independent competencies for domestic nuclear power generation. As such, from 2016 onward, the Finnish State Nuclear Waste Management Fund (VYR) has supported the renewal of the radiological laboratory research infrastructure via three instruments: 1) the research and infrastructure instrument, generally comprised mainly of personnel, travel and associated research execution expenses; 2) a special allocation for supporting the VTT Ltd. Centre for Nuclear Safety radiological laboratory facility expense, and 3) a special allocation for supporting the VTT Ltd. Centre for Nuclear Safety radiological laboratory equipment investment expenses as investment aid. All three instruments are jointly supported by the SAFIR2018 (nuclear power plant safety) and KYT2018 (nuclear waste management) research programs.

VTT has been hosting the Finnish national hot laboratory infrastructure since the first nuclear power plants were constructed in Finland in the 1970's. Historically the principle radioactive materials handling has been for the testing of reactor pressure vessel steels as part of the surveillance programs of the power plants, but over time

the activities have broadened to outgrow both the capacity and capabilities of the existing facilities. As such, a decision was made in 2011 to build a whole new facility, with the additional goal of gathering most of the VTT Nuclear Safety research personnel currently scattered around the Otaniemi campus, into a single, compact facility called the VTT Centre for Nuclear Safety (CNS). The facility houses new radiological laboratories with contemporary hot cells.

As described in a paper in the HOTLAB 2014 conference [Karlsen, 2014), the new VTT CNS includes an office wing and a radiological laboratory wing. The office wing is comprised of a ground floor conference center above which are three floors of office space, to accommodate 150 VTT research scientists engaged in various aspect of nuclear energy expertise, from nuclear core computations to thermal hydraulic modelling, and from severe accident phenomena to power plant safety reviews. The laboratory activities include research involving radiochemistry, nuclear waste management, dosimetry, failure analysis as well as mechanical and microstructural characterization of structural materials. Its diverse portfolio of modern research devices is essential for a broad range of applications in support of the safe operation of nuclear power plants and safe nuclear waste management. Already during the last two years of the 2018 program, several SAFIR and KYT projects have carried out experimental research utilizing the new laboratories, including studying the structural performance of nuclear power plant materials (THELMA and BRUTE), studying the chemistry and transport of fission products (CATFIS), studying C-14 release from metallic decommissioning waste (HIILI-14), and studying the behavior of swelling clay barriers for nuclear waste management (THEBES).

The hot cells of the VTT CNS

The core of the hot laboratory is the hot cell facilities that enable safe handling of radioactive materials. The new hot cells are aimed at the mechanical testing and microstructural characterization of beta- and gamma-emitting materials of nuclear power plant structures. These shielding facilities are located in the high bay of the VTT CNS, which was designed specifically to accommodate them. The design, construction and installation of the hot cells was carried out on a turn-key contract by Isotope Technologies Dresden GmbH (ITD).

As was described in a paper in the HOTLAB 2015 conference [Karlsen & Butze, 2015), and shown in Figure 1, the hot cell design includes a suite of six hot cells on the main floor, located above a utility cell in the basement, as well as a shielded glove-box/warm cell. A separate cell located in the basement has a series of alpha-numerically indexed silos for the orderly storing of radioactive specimens. Several special features were incorporated into the design for VTT's particular needs. Several large pieces of equipment that were already existing at VTT needed to be accommodated into the design of some of the cells, and were also moved in as a part of the hot cell installation. A shielded, enclosed conveyor connects the two upstairs cell rows, and features a lift to transport test specimens from the basement utility cell to this shielded conveyor, with the primary purpose of conveniently transporting

specimens between the basement and the two upstairs cell rows in a shielded manner. The utility cell features a two-directional transport cask docking system, enabling safe and secure docking of transport casks of different size and orientations (horizontal as well as vertical), with weight as high as 10 metric tons. For directly transporting bulky specimens to the main hot cells, each cell line also has a bottom-port matched to two different casks used for transports within the facility. As visible in Figure 2, the main floor hot cells are arranged in two rows with a closed access space between the rows, from which the interiors of individual cells can be accessed.

The ventilation for the high bay is designed such that the hot cells operate at a 200 Pa under-pressure with respect to the surrounding air, and thereby a portion of the high bay air is exhausted by way of the hot cells, which are equipped with HEPA filters on both intake and exhaust lines. This ensures that any radioactive contamination can be contained within the hot cells, which in turn minimizes the likelihood for contamination in the workspace around the hot cells.

The RADLAB summary in the SAFIR2018 Interim Report gave a comprehensive description of the types of equipment that have been procured for installation in the VTT CNS and its hot cells [Karlsen, 2017]. Therefore, this paper focuses on the construction and installation of the new hot cells and their equipment, which represent the culmination of the four year effort between 2015 and 2018.

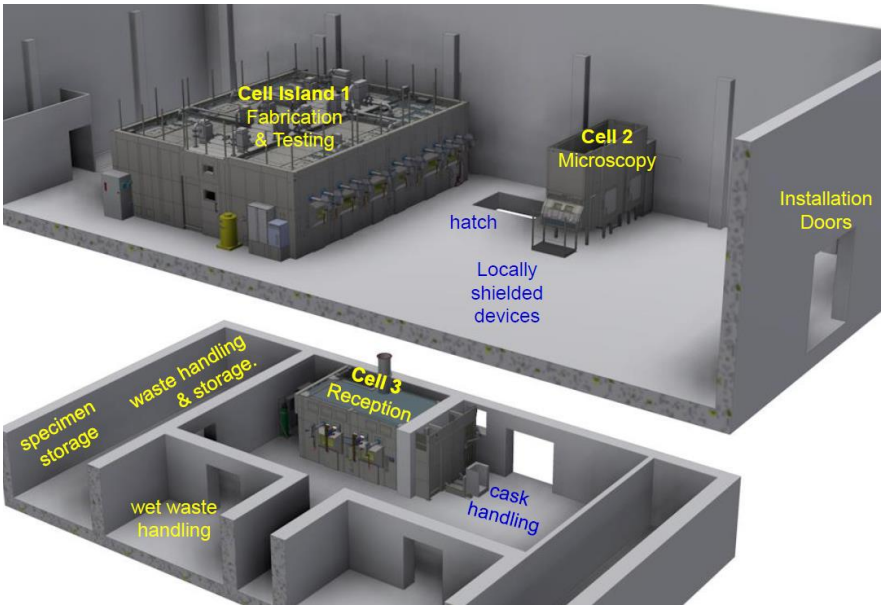

Figure 1. Layout of the hot cells with main working cells located on the main floor, connected to the utility/reception cell in the basement.

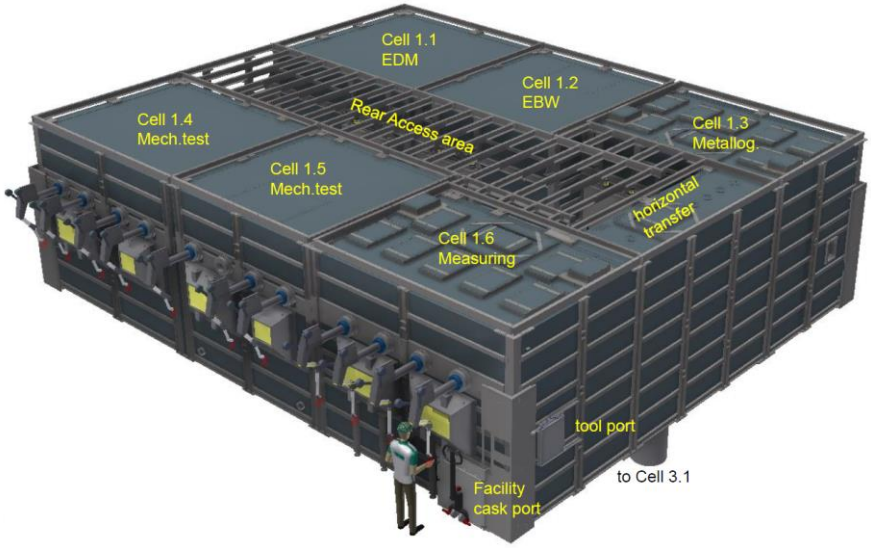

Figure 2. Layout of the main hot cells, numbered 1.1 through 1.7.

Hot cell manufacturing and installation

The hot cells are constructed of three main constituents: stainless steel containments where the radioactive sources are handled, inserted within gamma shielding realized by lead blocks and leaded glass windows, supported by a structure of bolted steel beams and frames. Following manufacturing in Germany, the on-site installation of the hot cells began in January 2017, and was completed in August of the same year [Karlsen & Rahnfeld, 2017).

Several large pieces of equipment that already existed at VTT needed to be accommodated in the design of some of the cells, and were then moved in as a part of the hot cell installation. These included an electric discharge machine (in Cell 1.1), an electron beam welder (in Cell 1.2), and a hydraulic mechanical testing device (in Cell 1.5). Additionally, two new mechanical testing devices were procured by VTT and integrated into Cell 1.4 by ITD as a part of the turn-key contract.

A shielded, enclosed conveyor connects the two upstairs cell rows (called Cell 1.7), and features a lift to transport test specimens from the basement utility cell, to this shielded conveyor, with the primary purpose of conveniently transporting specimens between the basement and the two upstairs cell rows in a shielded manner. For directly transporting bulky specimens to the main hot cells, each cell line also has a bottom-port matched to two different casks used for transports within the facility. The separate, free-standing set of lighter cells (2.1, 2.2 and 2.3) are dedicated to microscopy-related activities. Manufacturing and installation of the hot cells was executed as a series of modules, as described in the following sections.

Module 1A: Cells 1.3-1.7-1.6

Cells 1.3 and 1.6 are essentially mirror images of each other, and both are intended for various small, table-top devices such as a dimension-measuring microscope, hardness tester, fractography macroscope, metallography specimen mounting press, etc. The horizontal transport track of Cell 1.7 also emerges into each of those cells. The principle challenge with this module was the need to manage the air-tightness and the functionality of the containment with conveyor connections horizontally between Cells 1.3 and 1.6, as well as vertically between Cell 1.7 on the main floor and Cell 3.1 in the basement. This arrangement is shown in Figure 3.

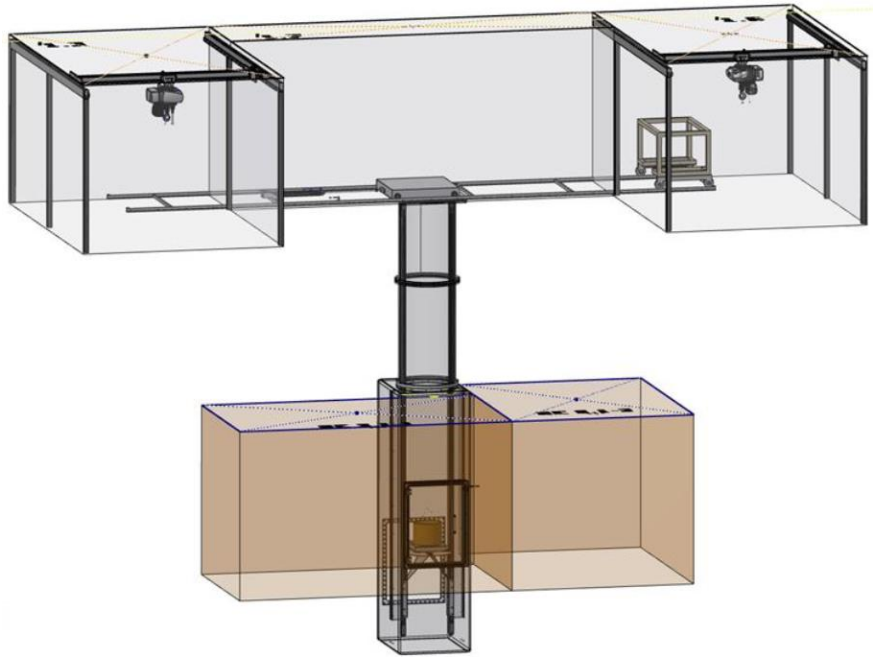

Figure 3. A shielded conveyor system can transport horizontally between Cells 1.3 and 1.6 via Cell 1.7, and vertically between Cell 3.1 and 1.7.

The co-location of Module 1A on the main floor with Module 3 located in the basement was a crucial parameter accommodated already in the design and construction phase of the building itself, manifested as a large, round opening in the floor of the high bay. While the opening's location was blocked out with forms during the original concrete pour, the accuracy required to accommodate the hot cells meant that it was subsequently more precisely bored to 700 mm diameter, with tighter dimension control also placed on its exact location. The rest of the hot cell modules were then aligned according to this precise reference point. For that reason the installation in VTT's premises also began with Module 1A.

While most of the other cells can be isolated from their neighboring cells, Module 1A is a single, common air space, which enables the conveyor running the length of Cell 1.7 to travel between cells 1.3 and 1.6 without any additional doors to navigate. On the other hand, the elevator running between cells 1.7 and 3.1 features airtight doors at the bottom and top, enabling the elevator shaft itself to serve as an airlock to allow isolation of Module 3.

Due to its large volume, the containment for Module 1A posed a manufacturing challenge. As with all the other containments, it was manufactured by cutting and welding of heavy gauge stainless steel sheets, strengthened as required by stainless steel stiffeners, stainless steel frameworks around cutouts, etc., as shown in Figure 4.

Module 3: Cell 3.1

Module 3 is the transport reception cell, and therefore it has the greatest lead shielding wall thickness (25 cm), features the transport cask reception system with two different docking ports, and includes the vertical conveyor system connecting to Cell 1.7 above. A further design challenge was that the basement location of that cell has a ceiling height of only about 3 meters, although the 75 cm thickness of the concrete in the ceiling offered significant gamma shielding to the space above. Because of the conveyor system, on-site installation of Module 3 was carried out simultaneously with Module 1A.

Figure 4. Example of a section of the containment box from Module 1A.

Although the design began as two different cells, 3.1 and 3.2, ultimately the functionality of the module was improved by combining them into a single, large air space about five meters long. To facilitate manufacture of the containments, they were still designed as two different containments of different dimensions, which were then connected on their common open side. To flexibly accommodate casks of different sizes and loading/unloading orientations, the docking system includes both horizontally- and vertically-oriented ports, which in turn required a convex step, or pop-in, to be incorporated into the right-hand end of the containment box, as illustrated in Figure 5.

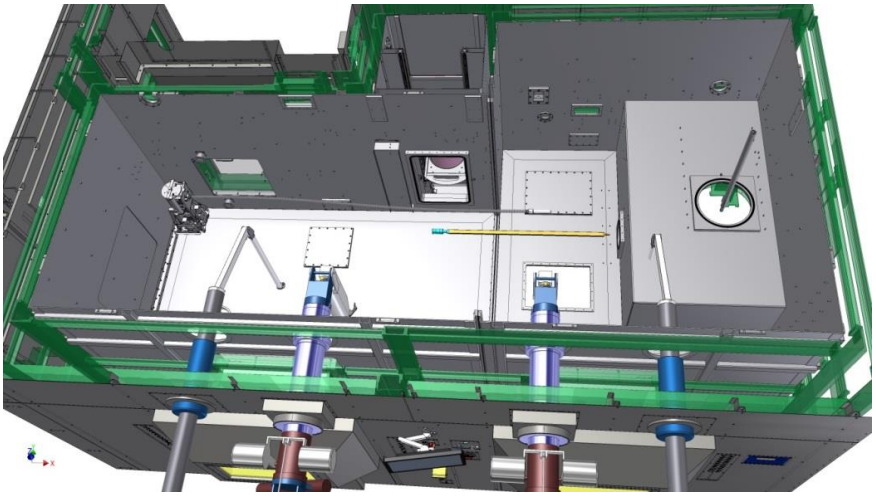

Figure 5. To accommodate casks of different sizes and loading/unloading orientations, the docking system includes both horizontally- and vertically-oriented ports, which in turn required a convex step, or pop-in, to be incorporated into the right-hand end of the containment box.

Since casks for road transport of radioactive materials can be quite heavy, the docking system functionality was specified to accommodate casks weighing up to 10 metric tons. For maneuvering casks into position in a safe, accurate and controlled manner, a special platform was designed to be operated by a powered pallet truck, matched with special guide rails aligning it to the docking port, and meshing with a screw-powered lifting system located beneath the pop-in of the containment box. Different adapters are then fitted onto the base pallet for accommodating casks of different diameter, heights and loading orientation. Optical and mechanical sensors and switches help to ensure that the heavy casks cannot be driven against the port, while hand-screws are incorporated to gently move the casks the final millimeters to accurately position against the docking port, and ensure an air-tight interface. Site acceptance testing of the system carried out with a mock-up of VTT's existing vertically-oriented transport cask demonstrated good functionality of the solution (Figure 6).

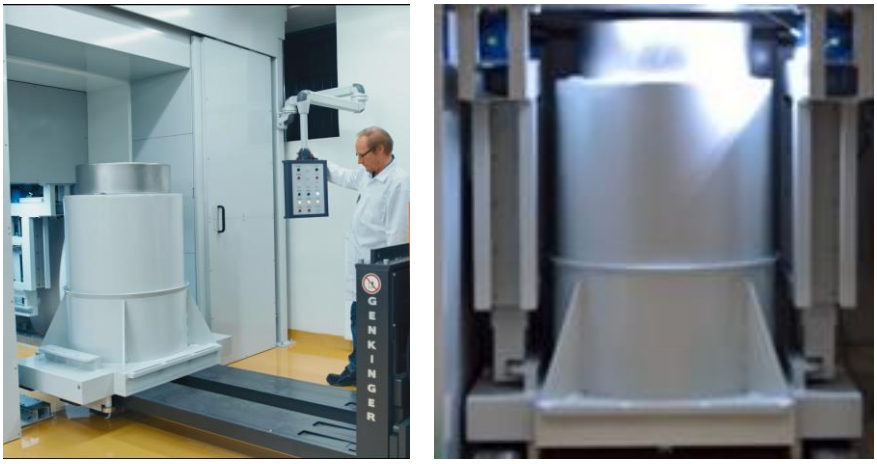

Figure 6. Site acceptance testing of the cask docking port of Cell 3.1 was carried out with a mock-up of VTT's existing vertically-oriented transport cask, and demonstrated good functionality of the system.

The vertical conveyor system was fabricated as part of Module 3, since all motors and actuators are located in the maintenance space behind the Module 3 containment. The elevator itself is located within a < 700 mm diameter tube fitted to the opening in the floor of the main high bay. Testing of the functionality of this part of the conveyor was first carried out in the factory. This included demonstration of the air-tight doors located at the top and bottom of the conveyor, of the belt-driven movement of the elevator module along the length of the tube, of the sliding tray that is manually drawn into Cell 3.1 for placing of the boxes or pails containing specimens to be transported, as well as the safety interlocks that prevent e.g. the top door from opening before the bottom door is closed, or driving of the elevator module into the top door when it is closed.

Because of the need for the vertical conveyor system to function integral with the horizontal conveyor, full testing of the system was carried out on-site once all containments were in place, electricals were connected, etc. The fully installed system can be operated from cells 1.3, 1.6, 1.7 and 3.1, but for safety, interlocks require transports sent from one location to first be accepted by the next location before the carrier actually moves. Likewise, movement is not enabled before any manipulators that could potentially be in the pathway of the carrier, are first parked in a safety position containing an interlock (Figure 7).

The installation of Modules 1A and 3 not only enabled testing of the full functionality of the conveyor system, but also connection of the units to the facility ventilation system for the first time. Once connected, the leak-tightness of the containments in their as-installed condition was successfully demonstrated.

Figure 7. The horizontal conveyor (right) and vertical conveyor (left) work integrally to transport a pail or box containing radioactive specimens between Cells 1.3, 1.6 and 3.1 via Cell 1.7. It has air-tight doors at the top and bottom, so it functions as an airlock between 1.7 and 3.1.

Module 1B: Cells 1.1-1.2

Cells 1.1 and 1.2 feature large devices that VTT had purchased earlier as industrial-grade instruments, and already used in the old radiological facilities; the electric discharge machine (EDM) and electron beam welder (EBW), respectively. Both devices posed their own challenges that had to be accommodated in the design, fabrication and installation of the hot cells.

As described in more detail in a separate report [Karlsen & Moilanen, 2018], the EDM is a valuable device for cutting radioactive materials, mainly to make specimens for either mechanical testing or microstructural analysis. Its computer numerical control can enable rather complex cutting paths, and the resulting as-machined surface finish is often sufficient for purpose without any further treatment. The EBW is a key device used for joining two materials with a high quality fusion zone, relatively narrow heat affected zone, and clean, slag-free result. Deployed in the hot cell, the main application of the EBW at VTT is in the fabrication of additional test specimens from small pieces of irradiated material welded to a larger volume of non-irradiated material [Karlsen & Jokipii, 2018]. For Charpy impact type specimens this involves adding extensions on each side of small piece of hot material, while for a compact-tension (CT) type of specimen this can involve inserting a small cube of hot material into a pre-machined CT specimen blank. Because the EDM cutting and EBW joining steps are often used consecutively over a few iterations, those two cells are located next to each other. However, since the EDM is more susceptible to contamination while the EBW should be kept quite clean, the devices are located in separate cells connected by an air-tight double-door pass through. To make it possible for heavier pieces needing cutting to be brought directly to the EDM, the cell containing the EDM has a bottom port to accommodate both sizes of facility cask. The arrangement of these cells is shown in Figure 8.

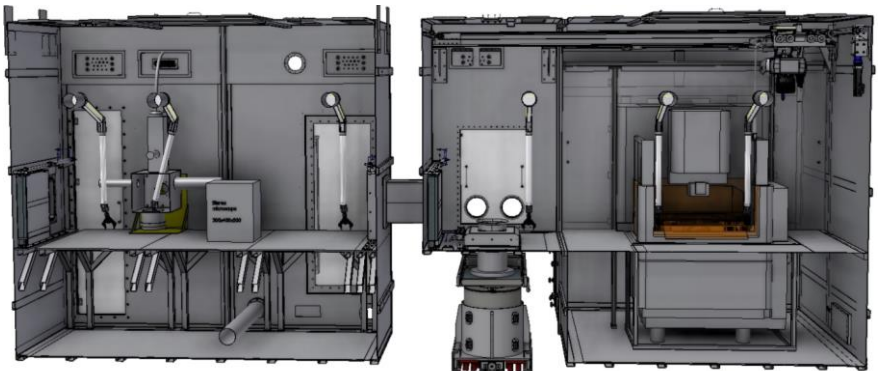

Figure 8. Module 1B contains the EBW in Cell 1.2 (left) and the EDM in Cell 1.1 (right). Only the portion of the devices where radioactive materials handling is required are located within the containments of each cell. The containments are connected by a double-door pass-through.

EDM Cell 1.1

The standard version of the Agie Charmilles CUT 200 mS EDM is shown in Figure 9. The device was special-ordered by VTT such that the control system (on right-hand side of device) could to be separated from the main pool/cutting head unit so that only the main portion would be installed inside the containment of the hot cell.

Besides its large size, one feature posing both a challenge and an opportunity, is the EDM's use of a recirculating pool of water as a conducting medium for the localized electric discharge produced on the work-piece to achieve the erosive cutting action. When machining radioactive materials, the cutting debris can become suspended in the water, and then be carried to other parts of the device, as well as into the water circuit itself. VTT has developed a particle separation circuit that can recover the radioactive debris from the water, and in this way utilize the problem to a benefit, to capture the debris before it enters the ion exchange filters.

This particle separation circuit is located in a separate room in the basement of the facility (Figure 9), so a rectangular opening was incorporated into the concrete floor of the main hot cell high bay to enable the required connections between the EDM in Cell 1.1, and that basement room. This feedthrough location formed another fixed point (in addition to the vertical conveyor system) that had to be incorporated into the overall hot cell layout, and also incorporated into the design and manufacture of the Cell 1.1 containment. Due to the large size of the EDM device, and the importance of ensuring proper feedthrough alignment of the cell structures and containment, the device was positioned inside the cell already during on-site installation. Once the device was in place, the feedthrough tubes to the basement were accurately positioned in the opening in the high bay floor, and then the opening was sealed off with a castable fire-resistant compound required for fire compartmentalization in the facility. Ultimately installation of the device into the cell was achieved and alignment was proved to be successful, as shown in Figure 10.

Figure 9. The EDM device (left) was special-ordered from the manufacturer such that the control panel could be separated from the cutting head and pool. At VTT the cutting unit is installed in Cell 1.1, and a special water circuit is deployed in the basement to enable separation of the radioactive cutting debris from the process water (right).

EBW Cell 1.2

The welding heat source of the EBW is a high power electron beam. The welding takes place in a vacuum chamber that is about the size of a small microwave oven, located at the bottom of the electron beam column. The handling of radioactive specimens occurs in and around this vacuum chamber. However, the EBW also includes a large power supply and vacuum pumping system, contained in a rather large box attached to the vacuum chamber (blue box in photo in Figure 11), and requires a water circuit to cool the lenses of the electron beam column. The power supply itself is also a significant source of thermal load into the surroundings, but for pumping efficiency, it is disadvantageous to locate the electron beam column and vacuum chamber very far from the vacuum pumping system. To accommodate the EBW in Cell 1.2, the containment was designed to accommodate the vacuum chamber and electron beam column, with the rest of the device located in the rear service area of the cell. Nonetheless, the gamma shielding was implemented as a full cell aligned with the walls of the neighboring cells. As a consequence, the box containing the power supply, vacuum systems, etc. was still located within the gamma shielding of that cell, but any personnel accessing this cell maintenance area is in that way still protected from any sources in the adjacent cells. That decision also allows the cell to be adapted later for other types of equipment, by merely modifying the containment, without significantly affecting the main cell structures or shielding walls.

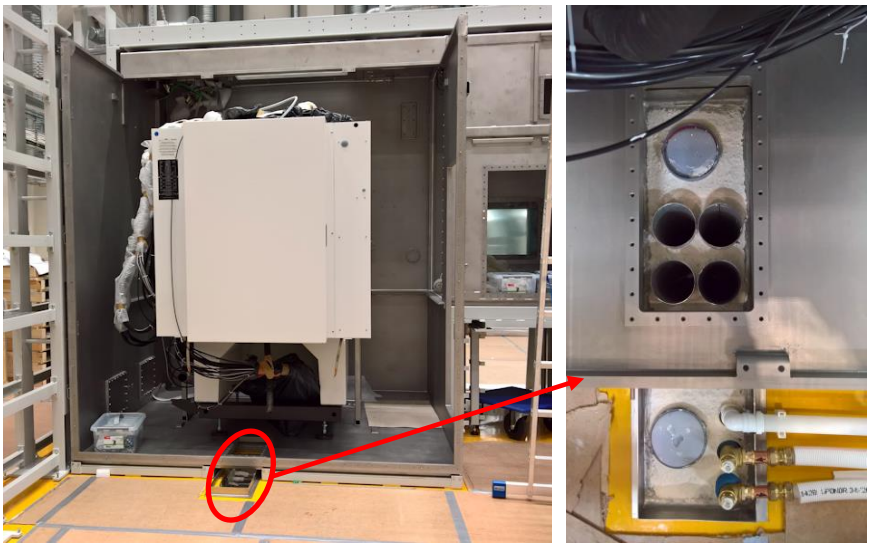

Figure 10. The EDM was installed during on-site installation of hot cell Module 1B. The feedthrough tubes to the basement water handling system were then positioned and cast in the floor to secure them and provide the fire compartmentalization required of the building.

Location of the power supply in the rear part of the cell also meant that the high thermal load released by the power supply was mainly confined to that rear maintenance area as well. To handle that additional heat load, the cell design included an air-to-water heat exchanger mounted inside that rear area. Those water lines ran parallel to the separate water lines accommodated for the cooling of the EBW column itself, but both water circuits were then connected to the building's centralized water chilling circuit.

To facilitate the containment approach, the EBW device itself was slightly modified by extending the tube connecting the vacuum chamber to the power supply box, and incorporating a feedthrough in the back wall of the containment that separated the chamber from the power supply box. Other nuclearization modifications made to the EBW included rotating the electron beam column by a quarter turn to enable changing of the electron beam source filament by hand from the side by the containment access door, and incorporating a self-cleaning system for the in-chamber camera's lens that is subject to contamination by the deposition of welding vapors.

Because of the size of the EBW device, it was also installed in the hot cells during the on-site construction. However, unlike the EDM, the device had already been in use for some time with activated materials, so thorough decontamination of the components had to be carried out before the device could be moved out of the old facilities and into the new hot cells. This too was ultimately successful, as shown in Figure 11. The device and its functionality testing are described in more detail in a separate report [Karlsen & Jokipii, 2018].

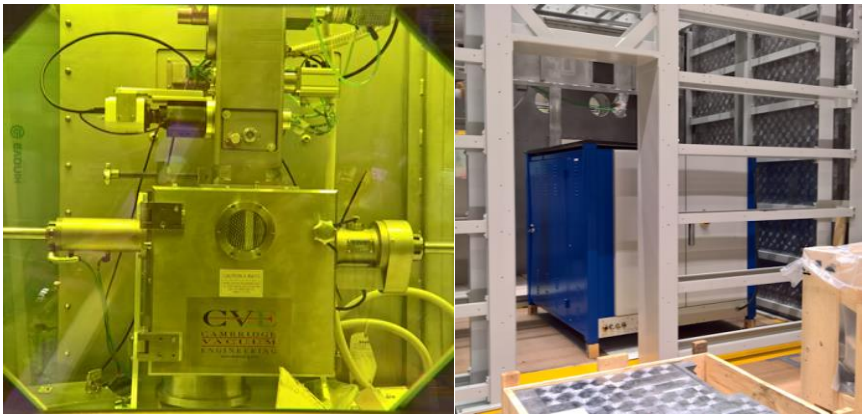

Figure 11. Since the electron beam welding takes place in a relatively small chamber (left), the large blue box containing the power supply and vacuum system was located in the rear of the cell in the new facilities (right), with only the e-beam column and vacuum chamber located inside the containment.

Module 1C: Cells 1.4-1.5

The final module of the main hot cell block contains the mechanical testing devices (Figure 12). Surveillance testing of RPV materials involves mechanically testing the neutron irradiated specimens by impact testing, fracture toughness testing, tensile testing, or combinations thereof. When testing is carried out within fully shielded cells, the use of semi-automatic systems is advantageous.

Cells 1.4 and 1.5 contain a selection of mechanical testing devices, which were accommodated in the design, fabrication and installation of the cells. The devices specified by VTT for Cell 1.5 included an existing MTS servo-hydraulic tensile testing device that was used in the old facilities, and a table-top fatigue pre-cracking device that VTT purchased new for the new hot cell.

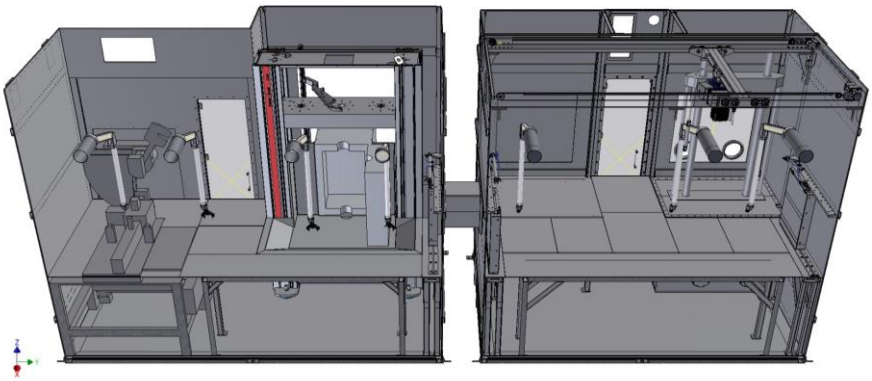

Figure 12. Module 1C contains the mechanical testing devices, with the Zwick devices in Cell 1.4 (left) and MTS device and space for a Piezomatic fatigue pre-cracking device in Cell 1.5 (right).

As a part of the turn-key contract, a Zwick HIT50 impact testing device and Zwick Z250SW electromechanical tensile testing device were integrated into Cell 1.4. Both devices utilize liquid nitrogen for achieving the lower test temperatures, and electric resistance elements for achieving the higher temperatures. Therefore, integration of the devices into the cells required accommodating all the feedthrough connections, specimen handling actions, and access for device maintenance and calibration activities.

As with the other cells, the main strategy for mechanical device integration in Module 1C involved sophisticated containments enabling handling of the radioactive material within a robust under-pressure, while still allowing reasonable hands-on access to the devices through the rear maintenance area of the cell. The liquid nitrogen supply is also located outside of the containment.

The integration of the Zwick devices into the cells was executed mainly as a joint action between ITD and Zwick personnel, with VTT participating as the device purchaser and ultimate end-user. This successful collaboration was initiated already in the design phase of the hot cells, and continued even during the manufacturing phase as small details were worked out to ensure functionality according to VTT's needs. After VTT conducted the factory acceptance tests of the Zwick devices at their German factories, the devices were delivered to ITD's factory for integration into Cell 1.4. After VTT conducted the FAT of the integrated result at the factory, all the components were shipped to VTT for final on-site installation. Integrated installation of both Zwick devices was accomplished as a part of the on-site installation of Module 1C, as shown in Figure 13.

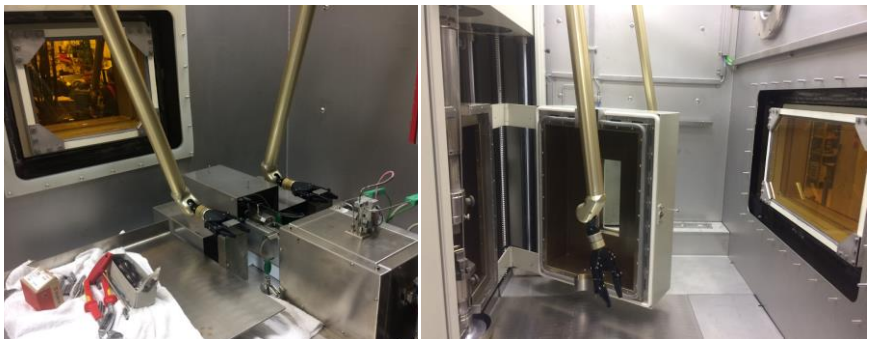

Figure 13. A Zwick HIT50 impact testing device (left) and Zwick Z250SW electro-mechanical tensile testing device (right) were fully integrated into Cell 1.4, including safety interlocks to prevent the impact hammer from accidently hitting a stray manipulator (left).

Module 2: Cells 2.1-2.2-2.3

This module is a series of lighter cells dedicated to microscopy-related activities. As shown in Figure 14, they are comprised of an isolated cell for a light-optical metallography microscope, a main cell for preparing cross-sections and carrying out downsizing steps for scanning electron microscopy (SEM) and transmission electron microscopy (TEM) specimens, and a lightly shielded glovebox for final preparation of TEM foils and other activities requiring the dexterity offered by (gloved) fingers. A bottom port is accommodated in the main cell, and a small horizontal port is included in one end of the shielded glove box.

In the early design stages, the main cell of Module 2 would have been equipped only with three ball-tongs for manipulation, but upon further design iteration, a pair of manipulators was selected instead, since they offer greater functionality. Ball tongs remain in the cell housing the light microscope, while the glove box on the end has three hand ports with shielded covers, intended to enable a pair of gloves to be used at a time, while the third port remains closed.

Because the light cells of Module 2 involve only small, table-top devices, the cells are all table height, and accessibility to the interiors is facilitated merely by a heavy shielding door in the back of each cell, behind which there is a translucent window containing glove ports to maintain containment during small hand operations. To change out equipment, the cell interior is first emptied of sources and cleaned up, and then the containment window is simply removed to allow access.

Because it is a self-contained and relatively straightforward set of cells, Module 2 was the last one to be completed at the factory, and also the last to be installed on-site.

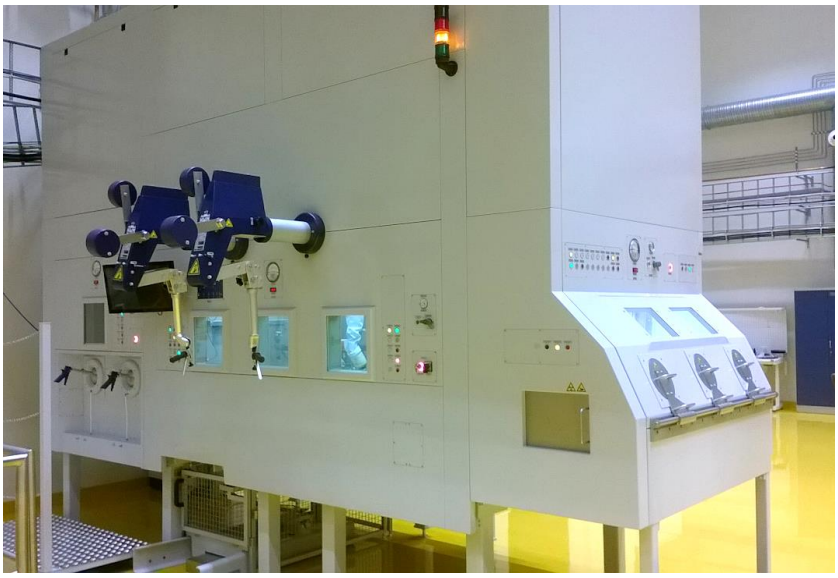

Figure 14. Module 2 is mainly for microscopy, and is comprised of three main compartments: LOM on left, specimen prep cell in middle, glove box on right end.

Shielded specimen storage

To ensure safe and orderly interim storage of radioactive test materials, a separate cell was procured on a subcontract with ITD. The location chosen for the storage facility was the far corner of the basement, to take advantage of natural shielding offered by the surrounding granite base-rock.

The system consists of both a shielded collection of alphanumerically organized silos, and the means for safely and orderly picking and placing of the radioactive materials and examining them for identifying features. The completed facility is shown in Figure 15.

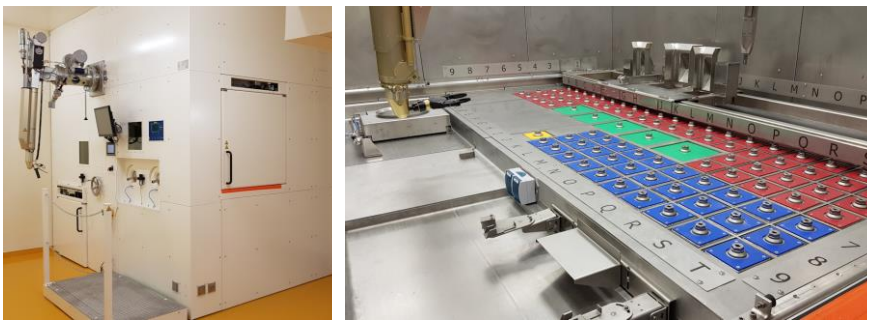

Figure 15. Alphanumerically arranged storage silos inside a handling cell was fabricated on a subcontract and installed in a corner of the basement against the granite bedrock for temporary storage of radioactive specimens.

Hot cell technical commissioning

Once the main hot cells and their integrated equipment were installed in 2017, most of 2018 was spent with installing remaining in-cell equipment and testing in-cell equipment for functionality in the hot cell setting. Two such devices are located in hot cell 1.6 for table-top equipment: an optical dimensioning microscope, and a microhardness tester. They are shown in the cell in Figure 16.

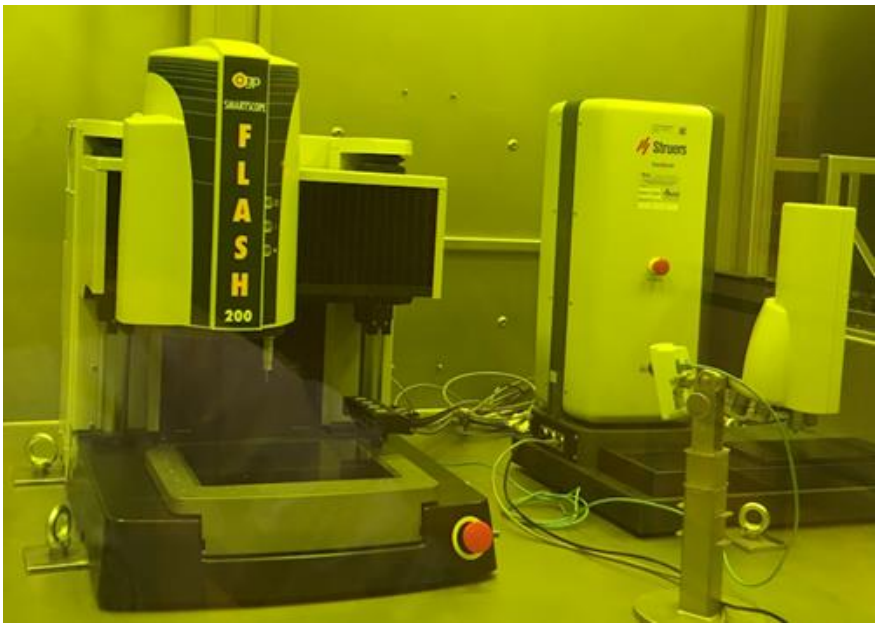

Figure 16. An OGP Smartscope CNC200 “Flash” table-top digital optical dimensioning microscope (left) and a Struers DuraScan-80 table-top microhardness testing device (right) are installed in Cell 1.6.

Optical dimensioning microscope (Cell 1.6)

Dimensional measurement is one of the most important processes in mechanical testing, and also has applicability in failure analyses and other research and testing processes in which geometry determination or confirmation is important. The measurement of test specimen geometries e.g. dimensions, notch depth/geometry, lateral expansion, reduction of area, etc. before and after mechanical testing is important for accurately determining the properties of the material being tested.

An OGP Smartscope CNC200 “Flash” table-top digital optical dimensioning microscope was installed in hot cell 1.6 for dimensional measurement of radioactive specimens. It is an automatic dimensional measurement system that was specially designed for remote operation. The device has both a touch probe and a laser

pointer, and it is equipped with high-speed video technology and a variety of illumination options. With a motorized x-y-z stage, the measurement area is 200 x 200 x 150 mm, which is suitable for all mechanical test types and most macrograph cross-sections.

To enable remote operation in the hot cell, several modifications were made to the device and its manner of installation, while incorporation of tweezer grips for the manipulators and utilization of a modular jig construction kit facilitate the reliable handling of specimens.

When the optical dimensioning microscope is used for measuring dimensions of a sample with optical or touch probe measurement, it can produce immediate results displayed on the screen, reports comparing the results to dimensional requirements, and can be used for making a DXF-format CAD-drawing, or for taking images of the sample and its surface.

As reported in a separate report [Karlsen & Jokipii, 2018], the device was been shown to be fully functional for its intended purposes, it has been calibrated, and therefore it is ready for use in research and testing work.

Microhardness tester (Cell 1.6)

Measurement of a material's hardness can give some insight into its mechanical properties and performance in some conditions. When materials are neutron irradiated, a clear increase in hardness can also be measured, and therefore the extent of mechanical property changes can be indicated without needing a full-size mechanical test specimen.

A Struers DuraScan-80 table-top microhardness testing device was also installed in hot cell 1.6, for use in measuring radioactive materials. The device is capable of standardized testing in accordance with ASTM E384: "Standard Test Method for Knoop and Vickers Hardness of Materials" and ISO 6507-1: "Metallic materials – Vickers hardness test." To enable remote operation in the hot cell, several modifications were made to the device and its manner of installation, while the utilization of a modular jig construction kit facilitates the reliable handling of specimens.

Participation in a round-robin of HV1 and HV10 hardness ranges revealed that VTT's hot cell microhardness tester is quite accurate, giving measurements very similar to the average of all of the measurements of the 17 participants. Therefore, the device has been shown to be fully functional for its intended purposes, it has been calibrated, and therefore it is ready for use in research and testing work.

In-cell EDM (Cell 1.1)

As elaborated in the separate report [Karlsen & Moilanen, 2018], the cutting performance of the installed EDM device was tested and shown to work well. During functionality testing, a PEPS CAD/CAM program was employed to specifically cut a set of tensile test specimens from a piece of RPV material, demonstrating the process of go-ing from a 3-D model of the object to be produced, through to CNC cutting of the material by the EDM. With a mock-up of a 40kg RPV trepan, it was shown

that using an electromagnet on the in-cell hoist for vertical lifting in conjunction with an actuated fixing device for the necessary horizontal translation, heavy work-pieces can be brought to the EDM and accurately placed between the cutting heads for subsequent sawing. These are illustrated in Figure 17. While the external cleaning circuit was made sufficiently functional for operation of the EDM for sawing tests, the circuit will still need to be refined before it can be deployed in its final form.

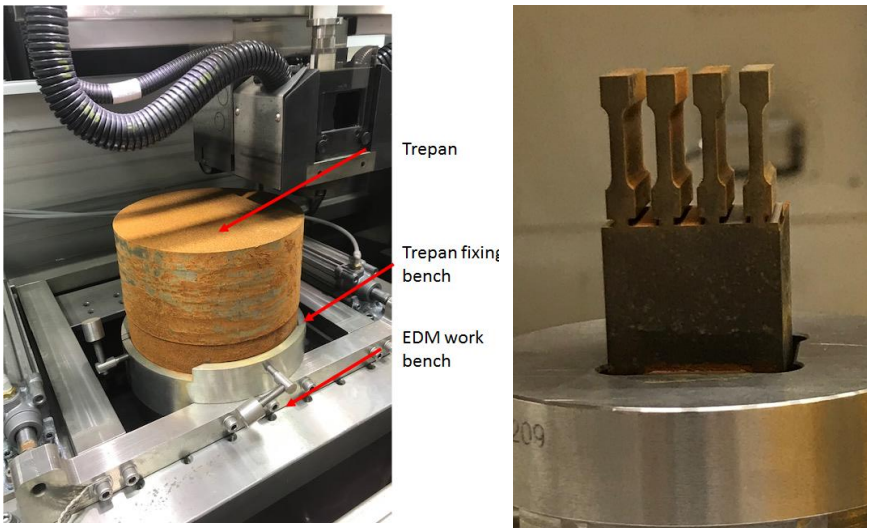

Figure 17. The functionality of the installed in-cell EDM was demonstrated by achieving accurate positioning of a large RPV trepan mock-up (left), as well as by executing cutting routines for items like tensile specimens (right).

In-cell CNC milling machine (Cell 3.1)

Since the EDM is capable of most material cutting needs, the main requirement for conventional in-cell machining operations, is the ability to open the surveillance capsules utilized in the aging management programs of reactor pressure vessels (RPV). Such capsules contain the test specimens in a compact, organized fashion, protect them from exposure to the reactor water, but still allow sufficient neutron penetration into the specimens to enable them to adequately represent the neutron effects on the RPV itself. The welded surveillance capsules have different geometries, depending on the design of the particular nuclear reactor in which the capsules have been irradiated. At present the domestic reactors in Finland are known to employ four different capsule geometries, with somewhat varying dimensions. The capsules are fabricated by welding of relatively thin-walled stainless steel pieces. The actual test specimens are merely contained within this capsule, so testing first requires opening of this capsule in a manner that allow recovery of the specimens without damaging them in any way.

As was described in a separate report [Tähtinen, 2017), the requirements and restrictions set by the hot cell environment when it comes to remotely-operated milling operations are such that a custom-designed CNC machine is the best alternative for a fixed in-cell machining device. In 2018 a tender was carried out for the design and fabrication of a custom in-cell CNC milling machine. The contract awarded to Metecno Oy. The device, shown in Figure 18, is to be delivered in March 2019 for installation in the receiving cell 3.1

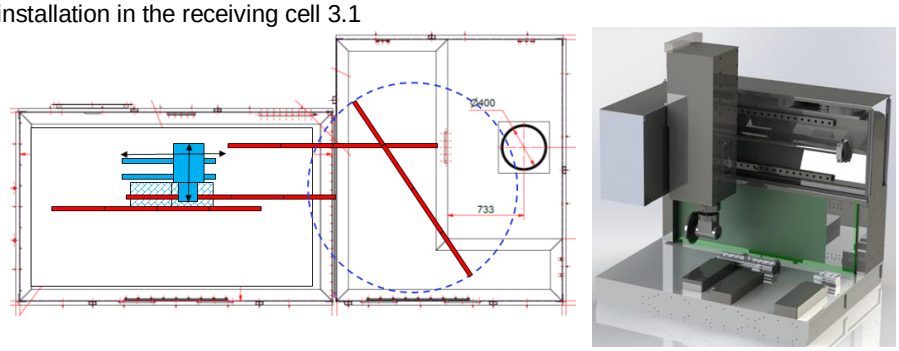

Figure 18. Remotely operated CNC mill (right) modelled in the handling space within Cell 3.1 (in blue on left), with a monolithic type RPV surveillance capsule (long red object).

In-cell mechanical testing devices (Cells 1.4 & 1.5)

The knowledge on tensile and fracture toughness properties of any material is the basis for all structural integrity analysis. In the new hot cells, the mechanical testing is mainly carried out by the material testing machines installed in Cell 1.4. The HIT50 device is a light impact hammer of 50 J capacity for small Charpy V-notched specimens, and is equipped with a tempering furnace for testing temperatures between -180 – 600°C integrated with a RoboTest I semiautomatic feeding unit. The Z250 has a capacity up to 250kN and is equipped with an environmental chamber for testing temperatures between -150 – 400°C, and accommodates a laser extensometer. The device has been designed for use in a radioactive environment in a shielded hot cell, e.g., the electronics and control boxes have been separated from the equipment, and installed outside the hot cell shielding walls where feasible.

As elaborated in a separate report, efforts to bring the Zwick Z250SW device to full functionality after installation have included the needed calibrations for standardized testing, practice in standard maintenance procedures such as changing of probes and load cells, as well as practice in remote handling of the test specimens. [Tähtinen, 2018]. Successful execution of practice tests with various test specimen morphologies have demonstrated that the device functions in accordance with requirements, and therefore is ready for use in testing campaigns for customers and research projects (Figure 19).

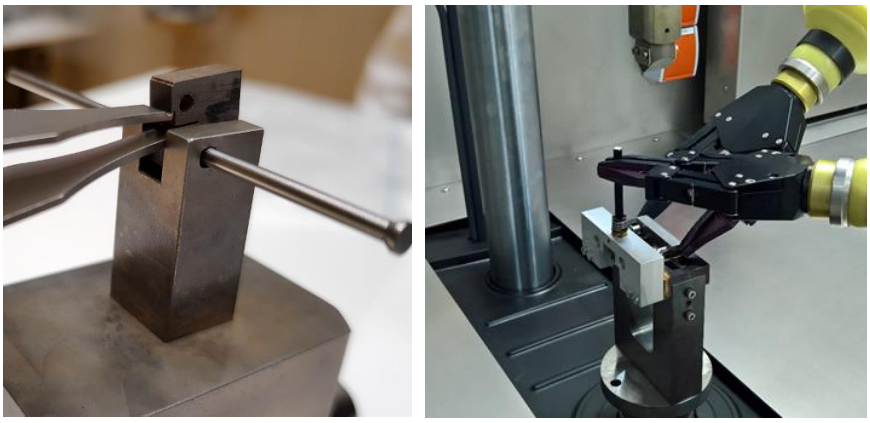

Figure 19. Functionality testing of the mechanical test devices included demonstrating the capability to handle the precise manipulation tasks involved when loading test specimens into the device (right) and installing extensometers (left).

Fracture toughness tests on notched specimens of either Charpy morphology or compact tension specimens are preceded by a fatigue pre-cracking phase, which is carried out by the devices in Cell 1.5, shown in Figure 20. The existing MTS 370.10 mechanical testing device is a free-standing instrument having a 100 kN capacity, which has been used for fatigue pre-cracking of fracture toughness test specimens by cyclic loading, as well as subsequent fracture toughness testing of the specimens. The device is also capable of being equipped with an environmental chamber for testing at both low and elevated temperatures, or with a high-temperature furnace for things like creep testing. Depending on specimen morphology, the fixtures/grips must generally be changed by hand between the different test types. For that reason, a separate Piezomatic dedicated fatigue pre-cracking device was ordered from SCK-CEN, which enables semi-automatically pre-cracking of up to 10 Charpy-type SEN(B) specimens in series (Schuurmans & Scibetta, 2014). While the Piezomatic device is employed only for three point bend SEN(B) type specimens and the MTS primarily for compact tension C(T) type specimens, the MTS is also suitable for SEN(B) specimens.

As described in a separate report, following exercises conducted with both devices, including their use remotely with the aid of manipulators, it can be stated that both devices function in accordance with requirements, and therefore are ready for use in testing campaigns for customers and research projects. [Tähtinen, 2019).

Figure 20. The Piezomatic (left) and the MTS (right) are both installed in Cell 1.5, and their functionality for fatigue pre-cracking of fracture toughness specimens has been demonstrated.

Hot cell radiological commissioning

With the installation of the new hot cells, the operating license for the radiological facility was expanded to also include them. That license was granted by STUK in early May 2018, enabling full operation of the hot cells and the rest of the A-class area for hot work to be initiated. The A-class area includes the room containing the analytical scanning electron microscope, the main hot-cell hall, and the basement rooms.

At the end of May 2018 the first delivery of hot specimens to the hot cells was successfully executed. The specimens were a batch of O-ring specimens made from Ringhals flux thimble tube, for conducting autoclave tests and microscopy for the EU SOTERIA project on IASCC. The reported activity of the load was 28.9 GBq Co-60. While inside the cell the radiation field was about 1300 microSv/hr at a distance of about 3,5 meters away, thanks to the shielding and manipulators offered by the reception cell 3.1, the whole transport cask unloading operation was executed with no personnel dose.

Locally shielded devices

In addition to the hot cells, some devices in the A-class radiological facilities are locally shielded. Simultaneous to the hot cell installation and technical commissioning in the last two years of the 2018 program, progress has also been made on taking into use the large instrumented impact testing device, the autoclave and water circuit simulating reactor primary circuit conditions, and the wet waste handling. Localized shielding strategies have also been designed and implemented to various degrees.

Instrumented impact hammer

The Charpy impact test is a staple test method for measuring irradiated RPV material properties. The test, in which a pendulum hammer is swung at a specimen, is still a common method to determine fracture toughness. VTT procured a Zwick RKP 450 impact test machine for installation in the new facilities with local shielding (Figure 21). As described in more detail in a separate report, it is a 450J device with an instrumented impactor [Arffman, 2018]. The instrumented impactor can record force-displacement information, which give some further insight into the fracture properties of the material tested. To facilitate testing of irradiated materials, it is a semi-automatic test machine, which can be remotely operated once the specimens have been loaded to the feeding line in a magazine. This reduces the dose of the user. The temperature control chamber has a working temperature range from -180°C to 300°C, achieved by a combination of either heating by electrical resistance coils, or cooling by liquid nitrogen injection. When the chamber reaches the first desired temperature, the specimens that will be tested in that temperature are fed one by one into the chamber automatically.

Due to the size of the machine, it is to be locally shielded instead of being located inside the hot cells. The design for the shielding consists of three concrete walls and a mobile lead screen. With this shielding the machine can be operated without concern of excess irradiation for personnel.

The RKP 450 has been installed and its functionality has been tested with specimens of ferritic steels prepared for that purpose. The impact hammer has been calibrated by VTT External Services, and therefore is in principle ready for conducting impact testing of all materials. To achieve full accreditation of the impact test method with the new device, round-robin testing has started in December 2018.

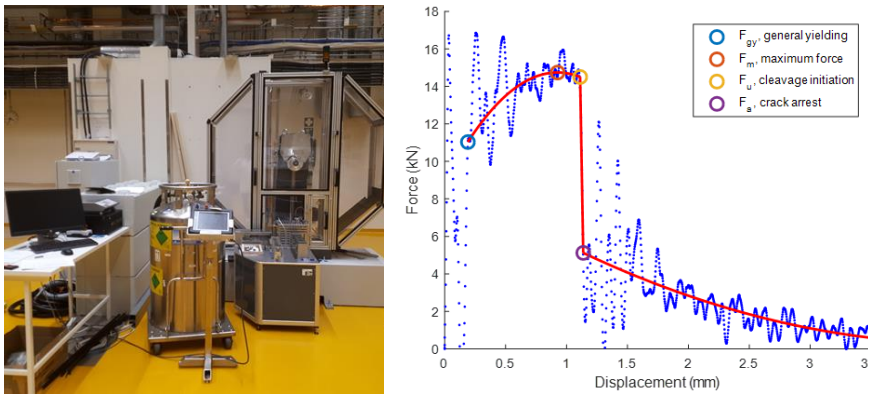

Figure 21. The Zwick RKP 450 has been installed in a locally-shielded position in the main hot cell hall (left), and the functionality of its performance has been tested, including e.g. of the instrumented impact hammer (right).

Local shielding for mechanical test devices

Besides the large instrumented impact hammer, two older tensile devices moved from the old facilities are also set up in the main hot cell hall for use with local shielding. Those devices are an MTS 810 and an Instron 5869. To enable their use in testing low-activity radioactive specimens, modular walls have been designed, and a prototype has been fabricated. They are comprised of steel frames on heavy-duty castors, which are then filled with lead shielding bricks. The utilization of the walls around the two different devices is shown in Figure 22. In addition, Plexiglas containments designed to be lowered over the devices have also been designed, through which airflow can be drawn with a slight under-pressure to minimize the spread of any potential particulate contamination that may occur when fracturing test specimens [Palosuo et al, 2018].

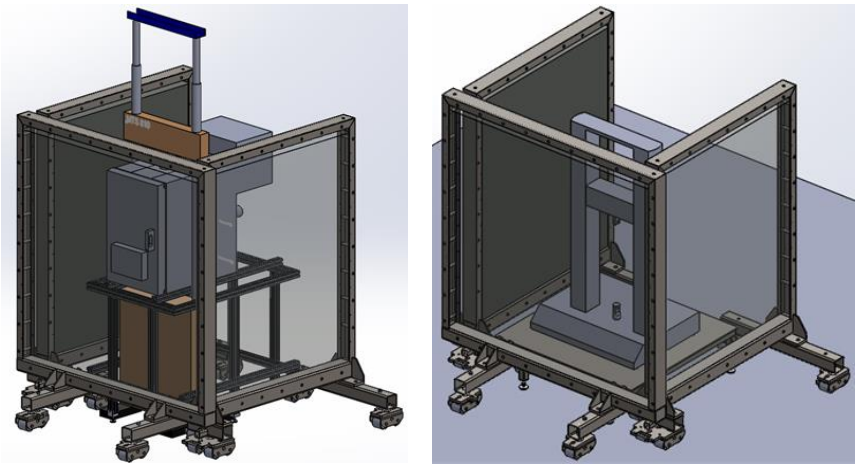

Figure 22. Modular shielding walls fabricated of steel frames on castors, to be filled with lead shielding bricks, are dimensioned for use with either the MTS (left) or the Instron device (right).

Autoclave and water circuit

Hot autoclaves enable safe mechanical testing of radioactive materials in well-controlled, simulated power plant water environments. Reactor materials are tested in simulated reactor coolant chemistries in order to determine stress corrosion crack growth rates for safety analysis, to select optimal materials for components (i.e. benchmarking of materials with respect to stress corrosion cracking susceptibility or oxidation resistance), to study the stress corrosion cracking mechanisms, etc. The main use for such facilities currently is in assessing the susceptibility of stainless steel internals component materials to irradiation assisted stress corrosion cracking (IASCC), generally as a function of material irradiation condition, loading scenario, and water chemistry [Toivonen et al., 2018].

By the conclusion of the 2018 program, one autoclave and one water recirculation loop are operational (Figure 23). The functionality, regarding mechanical testing performance and water chemistry/temperature adjustment, can be concluded to fill the expectations. The local shielding and remote handling for radioactive test specimens has been designed and will be completed in early 2019.

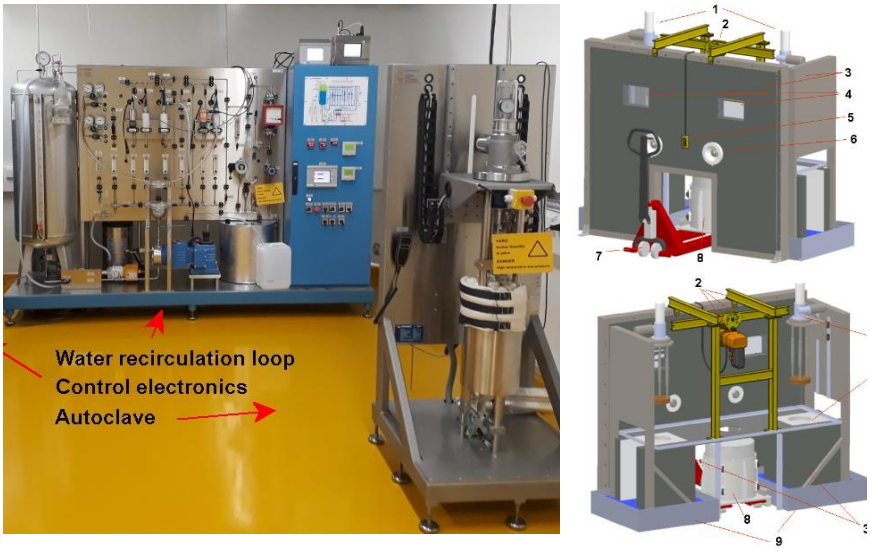

Figure 23. By the end of the 2018 program, one hot autoclave and one water recirculation loop are operational (left), enabling testing of irradiated materials in simulated primary circuit conditions. Shielding will be ready in early 2019 (right).

Wet waste handling cabinet

Several processes in the radiological facilities involve water and/or chemicals, which can subsequently become activated suspensions or solutions. Such wet waste is handled by three main routes: evaporation (for volatiles and water), ion exchange resins (for activated liquid solutions), and solidification (for residues and concentrates).

For executing those steps, a custom evaporation and re-condensation cabinet was procured on a subcontract with Platom Oy. As shown in Figure 24, the device is comprised of two gloved work-stations; one on the left is for docking a 200 liter barrel that can be heated by the application of thermal bands to facilitate evaporation of water, and the one on the right being a table-top with a mixer for cementation and space for setting up an ion-exchange resin filter tower. On the far left of the photo can be seen a condenser which can drain into another barrel, and in that way enable the capturing the condensate to check that it is non-active, while also drying the exhaust air before the HEPA filter. The system and its operation are described in more detail in a separate report [Siivinen, 2018].

Figure 24. The wet-waste handling cabinet is comprised of two gloved work-stations; the one on the left is for docking a 200 liter barrel that can be heated by the application of thermal bands to facilitate evaporation of water, and the one on the right is a table-top with a mixer for cementation, and space for setting up an ion-exchange resin filter tower.

Summary

The hot cells were successfully installed in VTT's new Centre for Nuclear Safety radiological research and testing facility in 2017 and 2018. The new hot cells are aimed at the mechanical testing and microstructural characterization of beta- and gamma-emitting materials of nuclear power plant structures. Several unique features were incorporated into the hot cells for VTT's particular needs, including the accommodation of several large pieces of equipment that were already existing at VTT, a special shielded, enclosed conveyor for transporting test specimens between the main cell lines, and special transport cask docking system to accommodate transport casks of different sizes and orientations. The final installed result is of high quality and can be expected to serve VTT's needs for many decades to come.

Additional equipment was installed into the completed hot cells, and the functionality of all the in-cell devices was tested, demonstrating their level of readiness for use with irradiated materials. Likewise, the functionality of locally shielded devices were also tested, and the local shielding solutions designed and advanced to various degrees. The license for operation of the facilities with radiological materials

was granted by STUK in May 2018, and the first shipment of hot specimens was received that same month.

Acknowledgment

VTT wishes to acknowledge the important support of the Finnish Nuclear Waste Management Fund, VYR for making the infrastructure renewal financially possible.

References

Arffman, P., Functionality report of RKP450 impact test device with semi-automatic tempering and specimen feed, VTT Report VTT-R-06917-18, 2018, 13p.

Karlsen, W. & Jokipii, M., Functionality report of in-cell optical dimensioning microscope, VTT Report VTT-R-06640-18, 2018, 18p.

Karlsen, W. & Mattila, M., Functionality report of the in-cell hardness testing device, VTT Report VTT-R-06639-18, 2018, 8p.

Karlsen, W. & Moilanen, P., Functionality report of in-cell Electric Discharge Machine, VTT Report VTT-R-06874-18, 2018, 20p.

Karlsen, W. & Jokipii, M., Functionality report of in-cell Electron Beam Welder, VTT Report VTT-R-06637-18, 2018, 13p.

Karlsen, W., "The new VTT Centre for Nuclear Safety," Proceedings of the 52nd HOTLAB meeting, Baden, Switzerland, September 21-25, 2014, SCK-CEN (2014), 18p.

Karlsen, W. & Butze, F. "The new VTT hot cells" Proceedings of 52nd HOTLAB meeting, 27 September - 1 October 2015, Leuven, Belgium Proceedings. http://hotlab.sckcen.be/en/Proceedings, SCK-CEN (2015), 11 p.

Karlsen, W. "Radiological laboratory commissioning (RADLAB)" in SAFIR2018 – The Finnish Research Programme on Nuclear Power Plant Safety 2015–2018 Interim Report, J. Hämäläinen & Vesa Suolanen (eds.) (URL: http://www.vttresearch.com/impact/publications) ISBN 978-951-38-8524-3, VTT Technology 294, ISSN-L 2242-1211, ISSN 2242-122X (Online) http://urn.fi/URN:ISBN:978-951-38-8524-3, Copyright © VTT (2017), pp. 362-387.

Karlsen, W. & Rahnfeld, C. "Fabrication and Installation of VTT's new hot cells," in Proceedings of the 54th Annual Meeting of the Hot Laboratories and Remote Handling Working Group, HOTLAB 2017, September 17-22, 2017, Mito, Japan, 14p. http://hotlab.sckcen.be/en/Proceedings

Palosuo, I., Arffman, P., Karlsen, W., VTT:n Ydinturvallisuustalon paikallissuojattavat testauslaitteet, VTT Report VTT-R-06971-17, 2018, 12 p.

Schuurmans, J. & Scibetta, M. “Cost-effective precracking of Charpy V-notch specimens for frature toughness testing using a piezo-electri actuator,” Proceedings of the 52nd HOTLAB meeting, Baden, Switzerland, September 21-25, 2014, SCK-CEN (2014), 9 p.

Siivinen, J., VTT:n Ydinturvallisuustalon jatteiden kasittely, VTT Report VTT-R-06888-17, 2018, 23 p.

Siivinen, J., VTT:n Ydinturvallisuustalon jätteiden käsittely - laitteiston toimintakuvaus, VTT Report VTT-R-06831-18, 2018, 17p.

Toivonen, A., Jokipii, M., Väisänen, P., Functionality report of hot autoclaves, VTT Report VTT-R-03555-18, 2018, 12p.

Tähtinen, S. Background study on machining options in the VTT hot cells, VTT Report VTT-R-03878-17, 2017, 26 p.

Tähtinen, S., VTT Ydinturvallisuustalon kuumakammioiden toimintaperiaate, VTT Report VTT-R-00485-18, 2018, 18 p.

Tähtinen, S. Saarinen, J., Arffman, P. Functionality report of in-cell 250kN material testing machine, VTT Report VTT-R-05557-18, 2018, 26p.

Tähtinen, S., Functionality report of the in-cell fatigue precracking devices, VTT Report VTT-R-00048-19, 2019, 20p.

Series title and number

VTT Technology 349

Title	**SAFIR2018 - The Finnish Research Programme on Nuclear Power Plant Safety 2015-2018** Final Report
Author(s)	Jari Hämäläinen & Vesa Suolanen (eds.)
Abstract	The Finnish Research Programme on Nuclear Power Plant Safety 2015–2018, SAFIR2018, continues a series of Finnish national research programmes in nuclear energy that started in 1989. The programmes were initially carried out separately in the fields of operational aspects of safety (YKÄ 1990–1994, RETU 1995–1998) and structural safety (RATU 1990–1994, RATU2 1995–1998, OHA 1995–1998), and then in combined programmes (FINNUS 1999–2002, SAFIR2003–2006, SAFIR2010 2007-2010, SAFIR2014 2011-2014). Simultaneously research has been carried out in the national nuclear waste management programmes (KYT2018 in parallel with SAFIR2018). SAFIR2018 consisted of four main research areas: (1) Plant safety and systems engineering; (2) Reactor safety; (3) Structural safety and materials; and (4) Research infrastructure. Research was carried out annually in around 30 projects that were guided by six reference groups. The research results of the projects have been published in scientific journals, conference papers and research reports. The programme management structure consisted of the Management Board, four steering groups managing the research areas, six reference groups, and programme administration. SAFIR2018 Management Board had representatives of the Radiation and Nuclear Safety Authority (STUK), the Ministry of Economic Affairs and Employment (MEAE), Fennovoima Oy, Fortum, Teollisuuden Voima Oyj (TVO), VTT Technical Research Centre of Finland Ltd (VTT), Aalto University (Aalto), Lappeenranta University of Technology (LUT), the Finnish Funding Agency for Innovation (Tekes), and the Swedish Radiation Safety Authority (SSM). The research in the programme was carried out by VTT, LUT, Aalto, University of Oulu, Finnish Meteorological Institute (FMI), Finnish Institute of Occupational Health (FIOH), University of Helsinki (Institute of Seismology, ISUH), University of Jyväskylä, RISE Research Institute of Sweden, Risk Pilot AB, Finnish Software Measurement Association FISMA and IntoWorks. A few subcontractors also contributed to the work in the projects. This report has been prepared by the programme management in cooperation with the project leaders and project staff. More information about SAFIR2018 can be found on the programme website http://safir2018.vtt.fi/. Finnish national research on nuclear power plant safety continues in SAFIR2022 programme for the years 2019–2022, see http://safir2022.vtt.fi/.
ISBN, ISSN, URN	ISBN 978-951-38-8682-0 ISSN-L 2242-1211 ISSN 2242-122X (Online) DOI: 10.32040/2242-122X.2019.T349
Date	March 2019
Language	English
Pages	498 p. + app. 0 p.
Name of the project	The Finnish Nuclear Power Plant Safety Research Programme 2015-2018, SAFIR2018
Commissioned by	MEAE
Keywords	nuclear safety, safety management, nuclear power plants, human factors, safety culture, automation systems, control room, nuclear fuels, reactor physics, core transient analysis, thermal hydraulics, modelling, severe accidents, structural safety, construction safety, risk assessment, research infrastructure
Publisher	VTT Technical Research Centre of Finland Ltd P.O. Box 1000, FI-02044 VTT, Finland, Tel. 020 722 111, https://www.vttresearch.com

SAFIR2018 - The Finnish Research Programme on Nuclear Power Plant Safety 2015-2018

Final Report

ISBN 978-951-38-8682-0
ISSN-L 2242-1211
ISSN 2242-122X (Online)
DOI: 10.32040/2242-122X.2019.T349

VTT beyond the obvious